ANNUAL REVIEW

INSTITUTE FOR MOLECULAR SCIENCE

1995

ANNUAL REVIEW

INSTITUTE FOR MOLECULAR SCIENCE

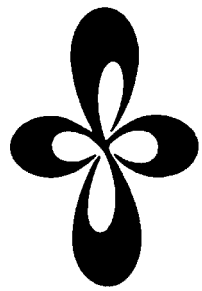

1995

Published by
Institute for Molecular Science
Okazaki National Research Institutes
Myodaiji, Okazaki 444, Japan
Phone 0564-55-7418 (Secretary room)
Telex 4537-475 KOKKEN J
Fax 0564-54-2254

IMS 1995

In 1993, all the research groups in IMS were critically reviewed by a panel of distinguished molecular scientists; their evaluations and comments were reported in IMS Report 93. The review has also been extended to the six research facilities in IMS by specialists in the respective fields. Based on these critical reviews, all the staffs in IMS worked very hard last year to provide a future plan for the institute. The plan has been reported in IMS Report 94 published in March of this year. Among many proposals given in the report, the most important one is a drastic scraping and building plan for the research facilities. Two research development centers which are strongly associated with the research groups should be newly established by reorganization and unification of the present three research facilities. The establishment of the new research development centers is very important in keeping our leadership role in molecular science research for the coming 21st century.

A new laboratory – Theoretical Studies IV – has been added this year to Department of Theoretical Studies. Physical Organic Chemistry Laboratory which has been operated by faculty members transferred with their positions from other universities has been closed by accomplishment of its mission. Instead, we are planning to establish a new laboratory of Molecular Clusters next year. I am very pleased to announce that IMS was authorized by the Ministry of Education, Science and Culture as a center of excellence. We are expecting a special support to IMS by this authorization. As usual, there had been a high turnover of personnel during the past year. Professor Y. Maruyama and Professor A. Nakamura retired from IMS and were appointed to professorship positions at Housei University and Osaka University, respectively. Successors of the two retired professors are Professor H. Kobayashi from Toho University and Professor M. Shionoya from Hiroshima University. Professor Y. Watanabe of Kyoto University was appointed as a professor of the Department of Applied Molecular Science. Associate Professor K. Isobe of the same department moved to Osaka City University as a full professor. We have appointed four young associate professors. They are Dr. T. Tahara of the Department of Vacuum UV photoscience, Drs. T. Kinoshita and H. Hama of the Ultraviolet Synchrotron Orbital Radiation (UVSOR) Facility and Dr. Y. Okamoto of the Department of Theoretical Studies. Professor T. Ibuki and Associate Professor H. Hosono took positions in the Interface Molecular Science Laboratory by transferring their positions at Kyoto University of Education and Tokyo Institute of Technology, respectively. We also had a high turnover of research associates and technical associates.

Professor E. W. Schlag of Technische Universitat Munchen was appointed as a foreign councilor to succeed Professor P. Day. Professor H. Inokuchi who are the immediate past President of Okazaki National Research Institutes and also a former Director-General of IMS has agreed to serve as a Distinguished Research Consultant. Professor Inokuchi was honored as Person of Cultural Merit. Professor S. Nagakura who is a Distinguished Research Consultant and ex-Director General of IMS received the Highest National Honor from the Emperor. The Chemical Society of Japan Award for Technical Achievements was awarded to Mr. K. Sakai, technical section chief of UVSOR. I would like to congratulate these distinguished persons for their achievements.

Twenty years have passed since the establishment of IMS in 1975. A commemorative ceremony was held on May 12, 1995 in the presence of many participants. This was a very good occasion to trace the history of IMS and to set our goals for the new development in the research of molecular science toward the 21st century.

September, 1995

Mitsuo Ito

Mitsuo Ito
Director-General

CONTENTS

IMS 1995 ..... Mitsuo Ito iii
CONTENTS v
ORGANIZATION AND STAFF 1
COUNCIL 10
BUILDINGS AND CAMPUS 11
RESEARCH ACTIVITIES I
DEPARTMENT OF THEORETICAL STUDIES 13
A. Development of New Theoretical and Numerical Techniques in the Study of Molecular Electronic Structures 13
1. Three-Center Expansion of Electron Repulsion Integrals with Linear Combination of Atomic Electron Distributions 13
2. Theoretical Calculations of Nonlinear Electrical Susceptibilities and Raman Scattering Intensity 13
B. Structures, Spectra and Dynamics of Water Cluster Complexes with Some Ions and with Some Organic Molecules 13
1. Theoretical Studies of Boron-Water Cluster Ions $B^+ (H_2O)_n$ and Aluminum-Water Cluster Ions $Al^+ (H_2O)_n$: Isomers and Intra-Cluster Reactions 13
2. Molecular Orbital Studies of the Structures and Reactions of Singly Charged Calcium Ion with Water Clusters, $Ca^+ (H_2O)_n$ 13
3. Theoretical Study of Entropy Effects on the Intra Cluster Reactions: Ab Initio Monte Carlo Simulations of $Mg^+ (H_2O)_n$ Clusters 14
4. Theoretical Studies of the Infra-Red Spectra of the Phenol-Water Clusters 14
5. Spectroscopic Study of 7-Azaindole-$(H_2O)_n$ (n=1-3) Complexes and its Dimer 14
C. Theoretical Studies of Excited and Ionic States of Ammonia Clusters and Ammonium Radical 15
1. Theoretical Studies of Dissociation Reactions of Ammonium Radical and Intra-Cluster Reactions of Ammonia Clusters 15
D. Geometric and Electronic Structures of Binary Element Clusters 15
1. Photoionization Electronic Spectroscopy of AlNa 15
2. Photoelectron Spectroscopy of $Al_nS_1^-$ Clusters (n=1-9) 15
3. Electronic Properties of Silicon-M Binary Clusters (M = C & Na) 15
4. Photoelectron Spectroscopy of Silicon-Carbon Cluster Anions ($Si_n C_m^-$) 16
5. Theoretical Study of Carbon Doped Small Silicon Clusters : Electron Affinities of Sin C (n=2-5) 16
6. Ab Initio Studies on the Structures, Vertical Electron Detachment Energies and Fragmentation Energies of C_nN^- Clusters 16
E. Structures and Reaction Dynamics in the Ground and Excited States of Argon Cluster Ions Ar_n^+ 16
1. Theoretical Study on the Photoabsorption Spectra of Argon Cluster Ions 16
F. Potential Energy Surfaces of Photoabsorption Spectra of Some Triatomic Molecules 17
1. Systematic Theoretical Studies of mono- and di-hydrides of Early Transition Metals 17
2. Theoretical Studies of Potential Energy Surfaces and Vibronic States of Low-Lying States of CS_2 17
G. Ab initio MO studies of Energy Rich Ring NO_x and HNO_x 17
1. Prediction of Unusual Cyclic Radicals NO_x (x=2-6) 17
2. Theoretical Study of the Cyclic Isomers of HNO_x 17
H. Electronic Structure of Electron-Donor-Acceptor Complexes 18
1. An ab initio MO Study of κ-$ET_2Cu[N(CN)_2]Br$ 18
2. Molecular Orbital Studies of Structure of Tetrathiofluvalene Cation Dimer $(TTF^+)_2$ and Dimer Cation $(TTF)_2^+$ and the IR Intensity Induced by Charge-Transfer Interaction 18
I. Theoretical Studies of State and Isomer Dependence of Internal Rotation Barriers 18
1.Theoretical Study of the Double Internal Rotation of Methyl Groups in o- and m-xylenes and their Cations 18
J. Ab Initio MO Studies of the Reaction Intermediates 19
1. Ab Initio Studies on Structures of the Hexa-Coordinate Phosphorus Intermediate for the Phosphoryl Ester Exchange and N→O Migration Reactions of Dimethyloxyphosphoryl-Threonine 19
K. Prediction of Protein Tertiary Structures from the First Principles 19
1. Thermodynamics of Helix-Coil Transitions Studied by Multicanonical Algorithms 19
L. Developing a New Method for Diagonalization of Large Hermitian Matrices 19
1. Calculating the Eigenvalues of Large Hermitian Matrices by Difference Equations 19
M. Semiclassical Theory of Chaotic Systems 19
1. Complex Classical Trajectories and Chaotic Tunneling 19
2. Toward the Classical Understandings of Quantum Chaological Phenomena: Dynamical Localization and Chaotic Tunneling 19
3. Pruning Trees of Tunneling Paths with Principle of Exponential Dominance 20

4. Semiclassical Quantization and Periodic Orbits of Dispersing Billiards 20
5. Statistical Properties of Eigenfunctions for Quantum Billiards with and without Positive Lyapunov Exponent .. 20
6. Polygonal Billiards: Correspondence between Classical and Trajectories and Quantum Eigenstates 20
7. Level Statistics and Semiclassical Periodic-Orbit Expansion for Polygonal Billiards 20
8. Statistical Properties of Spectra of Pseudointegrable System 21
N. Theoretical Studies of Chemical Reaction Dynamics 21
1. Quantum Dynamics of the Mu + H_2 and Mu + D_2 Reactions 21
2. Accurate Quantum Dynamics of Light Atom Transfer ChemicalReaction: O + HCl → OH + Cl 21
3. Quantum Dynamics of the Mu + H_2 (HD,D_2) and H + MuH (MuD) Reactions 21
4. Effects of Vibrational Excitation on Multidimensional Tunneling: General Study and Proton Tunneling in Tropolone 22
5. Overlapping-Resonance Scattering and Statistical Theory of Unimolecular Decomposition 22
6. Competition between Intramolecular Vibrational Energy Redistribution and Unimolecular Dissociation: A Scattering Theoretical Point of View 22
O. Theory of Nonadiabatic Transition due to Curve Crossing 22
1. Theory of Nonadiabatic Transition for General Two-state Curve Crossing Problems. I. Nonadiabatic Tunneling Case. 22
2. Theory of Nonadiabatic Transition for General Two-state Curve Crossing Problems. II. Landau-Zener Case ... 23
3. Semiclassical Analysis of Resonance States Induced by Conical Intersection 23
P. Theoretical Studies of Characteristics and Dynamics of Superexcited States of Molecules 23
1. Characteristics and Dynamics of Superexcited States of Molecules 23
2. Characteristics and Dynamics of Superexcited States of CO 23
Q. New Molecular Switching Mechanism 23
R. Laser Assisted Surface Ion Neutralization 24
S. Theoretical Studies of Nonlinear Optical Spectroscopy of Molecules in the Condensed Phase 24
1. Femtosecond Pump-Probe Spectroscopy of Intermolecular Vibrations in Molecular Dimers 24
2. Field-Theoretical Approach to Vibrational Modes of Molecules in the Condense Phase 24
T. Dissipation, Tunneling, Nonadiabatic Transition for Curve Crossing Problems in the Condensed Phase ... 25
1. Electronic Dephasing in Femtosecond Curve Crossing Spectroscopy 25
2. Relation between Electronic Coupling and Energy Splitting for Electron Transfer Reactions in the Superexchange Case 25
U. Theoretical Studies of a Strongly Correlated Electron System 25
1. Resonating Hartree-Fock Approach to Electron Correlations in ab initio MO Calculations 25
2. A Systematic Analysis of the Magnetic Susceptibility in the Itinerant Electron Model 25
3. The SDW-CDW Phase Transition in the One Dimensional Extended Hubbard Model 25
V. Theoretical Studies of Adsorption Reactions on Solid Surfaces by Molecular-Orbital Cluster Models 26
1. The Cluster Model Calculations for Li KVV Transitions on Cu surface 26
2. Molecular-Orbital Study of Li and LiOH Adsorbed on a Cu (001) Surface. II. A Cluster Model Including Image Charges 26
3. Model Potentials for Main-Element Atoms and their Application to Molecular Calculations 26
W. Spin-Orbit CI Studies on Heavy Atomic Systems 26
1. Spin-Orbit CI Studies on Non-Adiabatic Interactions in Excited States of ICl Molecule 27
2. Spin-Orbit CI Studies on the Photo-Detachment Spectra of IHI^- and $BrHI^-$ 27
X. Structures and Dynamics of Condensed Molecular Systems 27
1. Growth and Collapse of Structural Patterns in the Hydrogen Bond Network in Liquid Water 27
2. Conformation, Energy and Folding Ability of Selected Amino Acid Sequences 27

RESEARCH ACTIVITIES II

DEPARTMENT OF MOLECULAR STRUCTURE 29

A. Laboratory and Astronomical Spectroscopy of Transient Molecules 29
1. Microwave Spectrum of the NiO Radical in the $X\,^3\Sigma^-$ Ground Electronic State 29
2. Microwave Spectrum of the TiN Radical in the $^2\Sigma^+$ Ground Electronic State 29
3. Microwave Spectrum of the NCl Radical in the Electronically Excited State, $^1\Delta$ 29
4. Microwave Spectrum of the Isotopomers of HCS^+ and its Substitution Structure 30
5. Renner-Teller Effect of a Linear Molecule Having Two Bending Modes 30
6. Microwave Spectrum of the CHF_2 Radical (X^2A') 30
7. Microwave Spectrum of a New Phosphorus-Containing Free Radical $H_2PO(X^2A')$ 30
8. Microwave Spectrum of the FS_2 Radical in the X^2A'' Ground Electronic State 31
9. NH_2D in Dark Cloud Cores and Dust-Related Interstellar Chemistry 31
B. Development of a Mt. Fuji Submillimeter-Wave Telescope 31
1. Development of Wide-Band Acousto Optical Spectrometers(AOS) for the Mt. Fuji Telescope 32
C. Laser Investigation of Antiproton-Helium Compounds 32
1. A New Laser Induced Resonant Transition at 470.724 nm in the $v = n - l - 1 = 2$ Cascade of Metastable Antiprotonic Helium Atoms 32
2. Laser-Induced Resonant Transitions at 593.39 and 463.95 nm in the $v = n - l - 1 = 2$ and 3 Metastable

Cascades of Antiprotonic Helium-3 Atoms 33
D. Laser Cooling and Trapping of Neutral Atoms 33
1. Measurement of Penning Ionization Rates in Ultracold Collisions between Excited Helium Atoms in a Magneto-Optical Trap 33
E. Molecular Science of Biomolecules 34
1. Time-Resolved Resonance Raman Evidence for Tight Coupling between Electron Transfer and Proton Pumping of Cytochrome *c* Oxidase upon the Change in Heme Oxidation State from Fe^{V}=O to Fe^{IV}=O 34
2. Microcirculating System for Simultaneous Determination of Raman and Absorption Spectra of Enzymatic Reaction Intermediates and its Application to the Reaction of Cytochrome *c* Oxidase with Hydrogen Peroxide 35
3. Resonance Raman/Absorption Characterization of the Oxo-intermediates of Cytochrome *c* Oxidase Generated in its Reaction with Hydrogen Peroxide: pH and H_2O_2 Concentration Dependence 35
4. Ultraviolet Resonance Raman Studies of Hemoglobin Quaternary Structure Using a Tyrosine-α42 Mutant: Changes of $\alpha_1\beta_2$ Subunit Interface upon the T → R Transition 36
5. Resonance Raman Study on Axial Ligands of Heme Irons in Cytochrome *bd*-Type Ubiquinol Oxidase from *Escherichia coli* 36
6. Molecular Structure of Redox Metal Centers of the Cytochrome *bo* Complex from *Escherichia Coli:* Spectroscopic Characterization of the Subunit I Histidine Mutant Oxidases 36
7. Unusual Conformational Behavior of Oligomeric Poly(oxyethylene) Chains in Dilute Aqueous Solution: A Raman Spectroscopic Study 36
8. Synthesis, Characterization and Reversible Oxygenation of μ-Alkoxo-diiron(II) Complexes with a Dinucleating Ligand, N,N,N',N'-Tetrakis {2-(6-methylpyridyl)methyl}-1,3-diaminopropan-2-olate 37
9. Observation of Multiple CN-Isotope-Sensitive Raman Bands for CN-Adducts of Hemoglobin, Myoglobin and Cytochrome *c* Oxidase; Evidence for Vibrational Coupling between the Fe-C-N Bending and Porphyrin in-Plane Modes 37
F. Vibrational Spectroscopy of Molecules in Transient States 38
1. Time-Resolved Resonance Raman Spectra of Meso-Substituted Copper Porphyrins in the T_1 State: Implication for the Solvent Dependent Red-Shift of Emission Spectra 38
2. Time-Resolved Resonance Raman Spectra of Octaethylporphinato Copper(II) in the Lowest Excited Triplet State 38
3. Time-Resolved Stokes/Anti-Stokes Raman Study of Primary Photoprocesses in Ni-porphyrin Complexes in Solution 38
4. Time-Resolved Resonance Raman Studies of Photoinduced Binding/Release of Axial Ligands by Porphyrin Complexes with Transition Metals 39
5. SRS-based Tunable Source of 3-ps, 1-kHz Pulses with Micro-Joule Energies for Ultrafast Time-Resolved Spectroscopy 39
G. Molecular and Electronic Structures of Metallofullerenes and the Fullerene Radical Anions 39
1. Electronic Structure of Crystallized C_{60}^- (C_{60} Anion) 39
2. ESR Measurements on Spin Multiplet States of Metallofullerenes 39
3. ESR Study on the Reactivity of Two Isomers of LaC_{82} with the Disilirane 40
4. Chemical Reactivity of a Metallofullerene: EPR Study of Diphenylmethano-La@C_{82} Radicals 40
H. Site Selective Spectroscopy in Solid Crystals 40
1. Heterodyne Detection of Optical Magnetic Double-Resonance 40

RESEARCH ACTIVITIES III
DEPARTMENT OF ELECTRONIC STRUCTURE 41
A. Ultrafast Intermolecular Electron Transfer 41
1. Dynamical Aspects of Ultrafast Intermolecular Electron Transfer Faster than Solvation Process: Substituent Effects and Energy Gap Dependence 41
2. Deuterium Isotope Effect on the Solvation Dynamics 41
3. Effects of Vibrations in Chemical Dynamics: High-Frequency Vibrational and Low-Frequency Solvent Dynamical Effects on Intermolecular Electron Transfer 42
B. Liquid Dynamics Studied by Higher Order Nonlinear Spectroscopy 43
1. Fifth Order Optical Response of Liquid CS_2 Observed by Ultrafast Non-Resonant Six-Wave Mixing 43
2. Temporally Two-Dimensional Raman Spectroscopy of Liquids by Six-Wave Mixing with Ultrashort Pulses 43
3. Time-Resolved Higher Order Nonlinear Spectroscopy in Liquids: Overtone Vibrational Dephasing 43
C. Development of Ultrafast Spectroscopic Methods 43
1. Femtosecond Laser System Based on Chromium-Doped Forsterite Crystal 44
2. Cavity-Dumped Femtosecond Kerr-Lens Mode-Locking in Chromium-Doped Forsterite Laser 44
D. Development of Femtosecond UV-Pump and UV-Probe Spectroscopy and its Application to Small Molecule Reaction in Condensed Phase 44
1. Construction of Femtosecond Transient Absorption System Using Regeneratively Amplified Ti:Sapphire Laser 45
2. Study of Bimolecular Reaction in Neat CH_3I by Femstosecond Transient Absorption Spectroscopy 45
E. Photoinduced Primary Processes in Natural and Artificial Photosynthetic Systems 46

1. Spontaneous Emission Measurements on Photosystem Two Reaction Centres by Subpicosecond Fluorescence Up-Conversion ····· 46
2. Photoinduced Electron Transfers between Porphyrin and Quinone Connected via Multipoint Hydrogen Bondings ····· 47
F. Dynamic Behavior of Electronic Excited States ····· 47
1. One- and Two-Photon Fluorescence Excitation Spectra of the 2^1Ag States of Linear Tetraenes in Free Jet Expansions ····· 48
2. Excited State Enol-Keto Tautomerization in Salicylic Acid: A Supersonic Free Jet Study ····· 48
3. Exciton Behavior of J-Aggregates of Carbocyanine Dye at Low Temperatures ····· 48
G. Photochemistry on Well-Defined Surfaces ····· 49
1. Angular Distributions of N_2 in Photodissociation of N_2O Adsorbed on a Partially Oxidized Si(100) Surface at 95K ····· 49
2. NEXAFS Study on the Adsorption Structure of N_2O on a Si(100) Surface ····· 49
H. Activation of Methane ····· 50
1. Laser-Induced Photochemistry of Methane Adsorbed on a Pt(111) Surface ····· 50
2. Photochemistry of Methane on Deuterium-Covered Pt(111) Surfaces ····· 51
I. Dynamic Processes in Electronically -and/or Vibrationally-Excited Molecules ····· 51
1. Stimulated-Emission-Pumping Laser-Induced-Fluorescence Spectroscopy of Phenol and Anisole ····· 51
2. The C=O Stretching Frequency in the $S_1(\pi^* - n)$ State of Acetaldehyde and its Deuterated Derivatives Determined with the Photofragment Excitation Spectroscopy ····· 52
3. Geometry and Torsional Potential of *2,2'*-Bithiophene in a Supersonic Jet ····· 52
4. Internal Rotation of the Methyl Group in the *m*-Tolinitrile·Rare Gas Complexes ····· 53
5. Photodissociation of $N_2O{\cdot}H_2O$ in a Supersonic Jet ····· 53
6. Development of Methodology to Detect Product in a Quantum State with Translational Energy Measurements ····· 54
7. Translational Energy Measurements of CH_3 upon Dissociation of CH_3CHO after Irradiation the UV Photons ····· 54
8. Dissociation Rate Measurements of CH_3CHO upon Irradiation of UV Photons ····· 55
9. Nascent State Distributions of OH Radicals Produced in the Reaction of $O(^1D)$ with H_2O ····· 55
J. Self-Organization in Chemical Reactions ····· 55
1. Photo-Response of Chemical Oscillators ····· 55
2. Oxidation of Thiocyanate by Bromate is Not an Oscillatory Reaction in a Batch Reactor ····· 56
3. Photo-Induced Disproportionation of Iodomalonic Acid ····· 56
4. The Role of the Dushman Reaction and the Ferricyanide Ion in the Oscillatory $IO_3^- - SO_3^{2-} - Fe(CN)_6^{4-}$ Reaction ····· 56
5. Frequency-Multiplying Bifurcation in the Oscillatory Belousov-Zhabotinsky Reaction Proceeding in Interacting Water Droplets of Reverse Microemulsion of Aerosol OT in Octane ····· 57
6. The pH Dependence of the Belousov-Zhabotinsky Reaction in Water-in-Oil Reverse Microemulsion of AOT in Octane ····· 57
7. Molecular Dynamics Simulations of Nonequilibrium Spatial Correlations in a Reaction Diffusion System ····· 58
8. The Effect of the Light Irradiation for the Subsystem of the Ferrocyanide-Bromate-Sulfite System under the Batch Condition ····· 58
9. Photo-Induced Bifurcation in the Ferrocyanide-Bromate-Sulfite System under the Flow Condition ····· 58
10. Photoinduced Bifurcation and Multistability in the Oscillatory Briggs-Rauscher Reaction ····· 59
11. Photoinduced Bifurcation in the Starch-Added Briggs-Rauscher Reaction ····· 59
K. Laser Investigation of Molecular Photodissociation Dynamics ····· 60
1. UV Photodissociation of Dichloroethylenes: Cl Elimination Processes ····· 60
2. Br Elimination by 193 nm Excitation of Vinylbromide ····· 60
3. Semiclassical and Quantal Analyses on 2D Imaging of Photofragment Vector Correlation ····· 61
4. Photodissociation Dynamics of N_2O at 193 nm: Analysis of Vector Correlation in $O(^1D)$ Fragment ····· 61
5. 223 nm Photodissociation of OCS: Velocity Distribution of $S(^1D$ and $^3P)$ Atoms ····· 61
6. State-Dependence in the Predissociation of C_2H_2 in $\tilde{A}\ ^1A_u$ state Studied by H-Atom Action Spectroscopy ····· 62
L. Laser Investigation of Bimolecular Reactions ····· 62
1. Construction of Molecular Beam Diagnostics Chamber ····· 62
2. Construction and Characterization of Photolytic Hydrogen Beam ····· 62
M. Laser Ablation-Molecular Beam Method. Competitive Solvation of Monopositive Metal Ions in the Gas Phase ····· 63
1. Magic-Number-like Behavior of Ammonia Ligands in Mixed-Ligand Metal Complexes $M^+(NH_3)_m(CH_3OH)_n$. Preferred Coordination of Ammonia Ligands in the First Coordination Sphere ····· 63
2. Highly Selective Solvation of Monopositive Metal Ions in the Gas Phase as Revealed by the Laser Ablation-Molecular Beam Method Using Ammonia-Water Binary Clusters ····· 63
3. Reactions of Monopositive Metal Ions (M^+) with Mixed Molecular Clusters like $(NH_3)_m(H_2O)_n$ As Studied by Laser Ablation-Molecular Beam (LAMB) Method. Preferred or Nonspecific Coordination ····· 63
4. Laser Ablation-Molecular Beam (LAMB) Method. Coordination (Solvation) Chemistry of Monopositive Metal Ions in the Gas Phase ····· 63

N. Laser Chemistry of Polymers: Laser Ablation/Multiphoton-Mass Spectrometry Detection of Fragments, Reconstruction of Polymer Films from Laser-Ablated Fragments, Surface Treatment of Polymers with Pulsed Lasers, and CVD-like Preparation of Polymer Films from Monomers 64
1. Laser Ablation of Polymethylmethacrylate and Polystyrene at 308 nm: Demonstration of Thermal and Photothermal Mechanisms by a Time-of-Flight Mass Spectroscopic Study 64
2. Multiphoton Ionization-Mass Spectrometric Study on Laser Ablation of Polymethylmethacrylate and Polystyrene at 308 nm 64
3. Preparation of Reorganized Films of Polyacrylonitrile by Ablation with an Excimer Laser 64
O. Raman/IR Spectroscopy of Azacrown Ether Complexes 64
1. Stoichiometry and Conformation of Azacrown Moiety in Sodium Complexes of Azacrown Ethers. A Raman/IR Spectroscopic Study. Part I. Complexes of 4,13-Diaza-18-Crown-6 65
2. Stoichiometry and Conformation of Azacrown Moiety in Sodium Complexes of Azacrown Ethers. A Raman/IR Spectroscopic Study. Part II. Complexes of 4,13-Diaza-15-Crown-5 65
P. External Magnetic Field Effects upon Chemical Reactions 65
1. Magnetic Field and Magnetic Isotope Effects upon Biradical Photochemistry 65
Q. Magnetic Behavior of Stable Radical Crystals and ElectronicStructures of Organic High-Spin Molecules 66
1. Ferro- and Antiferromagnetic Behaviors of Stable Free Radical Crystals of *N*-(Arylthio)-2,4,6-triarylphenylaminyls 66
2. Pulsed- and cw ESR Study of Exchange Interaction, Spin Relaxation and Spin Dynamics on Low-Dimensional Organic Magnetic Materials 66
3. Spin Alignment and Spin Density Distributions of Organic High-Spin Molecules 66

RESEARCH ACTIVITIES IV

DEPARTMENT OF MOLECULAR ASSEMBLIES 67
A. Solid State Properties of Phthalocyanine Salts and Related Compounds 67
1. Pressure-Induced Charge Transfer in One-Dimensional Phthalocyanine Conductor, NiPc $(AsF_6)_{0.5}$ 67
2. Pressure-Induced d-π Charge Transfer in One-Dimensional Phthalocyanine Conductors, $NiPc(AsF_6)_{0.5}$ and $CoPc(AsF_6)_{0.5}$ 67
3. The 130 K Transition in Bi Oxides Heavily Doped by Iron Phthalocyanine: Superconductivity versus Magnetism 68
B. Structure and Properties of Organic Conductors 68
1. Spectroscopic Study of Solid BDNT and its Monocation and Dication Salts 68
2. Electronic and Vibronic Structure of Non-planar Organic Charge-Transfer Salt, *m*-BDNT-PF_6 68
3. Resonant Raman Scattering in Single Crystals of BDNT, $BDNT^+$, and $BDNT^{2+}$ 68
4. Crystal Structures of $BDNT^{2+}$ Salts, BDNT-$(ClO_4)_2$-CH_2Cl_2 and BDNT-$(SbF_6)_2$ 69
5. Superconductivity in Conducting Polymer-Fullerene Composite Doped by Alkali Metal 69
6. Alkali-Metal Doping of Fullerene-Conducting Polymer Composite: Evolution of Conductivity and ESR 69
7. Granular Superconductivity in "Conducting Polymer-Fullerene-Alkali Metal" Composite 69
8. Photoconductivity of Poly(2,5-diheptyloxy-p-phenylenevinylene) in Air Atmosphere. Magnetic Field Effect and Mechanism of Generation and Recombination of Charge Carriers 69
9. Optical Properties of High-Pressure Phases of C_{60} Fullerene 70
C. NMR Study of Organic Conductors and Superconductors 70
1. ^{13}C NMR Study of Layered Organic Superconductors Based on BEDT-TTF Molecules 70
2. Antiferromagnetic Ordering and Spin Structure in the Organic Conductor,κ-$(BEDT\text{-}TTF)_2Cu[N(CN)_2]Cl$ 70
3. NMR Relaxation Rate in the Superconducting State of the Organic Conductor, κ-$(BEDT\text{-}TTF)_2Cu[N(CN)_2]Br$ 71
4. Electron Correlation in κ-Phase Family of BEDT-TTF Compounds Studied by ^{13}C-NMR, where BEDT-TTF is bis(ethylenedithio)-tetrathiafulvalene 71
5. Systematic Study of the Electronic States Around the Metal-Insulator Transition of κ-$(BEDT\text{-}TTF)_2X$ Salts by ^{13}C-NMR 72
6. Strong Electron Correlation and Metal-Insulator Transition in (BEDT-TTF) (TCNQ) 72
7. ^{13}C-NMR Study on the Organic Superconductor, β_L-$(BEDT\text{-}TTF)_2I_3$ 72
8. Effect of Annealing on the Electronic State of β-$(BEDT\text{-}TTF)_2I_3$ 73
D. Electron Transport and Magnetic Study of Anisotropic Superconductors 73
1. Extremely Large Penetration Depth in α-$(BEDT\text{-}TTF)_2NH_4Hg(SCN)_4$ 73
2. Construction of an AC Susceptibility Measurement System Combined with DC Magnetic Fields 74
3. Superconductivity of ZrRuSi Prepared at High Pressure 74
E. Thermodynamic Study of Organic Conductors 74
1. Construction of Low-Temperature Specific Heat Apparatus of Themal Relaxation Method 74
2. Characterization of Low-Temperature Electronic States of Organic Conductors, α-$(BEDT\text{-}TTF)_2MHg(SCN)_4$ [M=K, Rb, and NH_4], by Specific Heat Measurements 75
3. Specific Heat Around the Superconductive Transition of α- $(BEDT\text{-}TTF)_2NH_4Hg(SCN)_4$ 75
4. Electronic Specific Heat Coefficient of κ-$(BEDT\text{-}TTF)_2Cu[N(CN)_2]Cl$ 75

F. Novel Electronic States of d-π System of $(DCNQI)_2M$ ····· 76
1. ^{15}N and ^{13}C NMR Shift in $(DMe\text{-}DCNQI)_2M$ [M=Li and Cu] ····· 76
2. Electronic States of $(DI\text{-}DCNQI)_2M$ (M=Li, Cu, Ag) ····· 76
3. Carrier Doping to One-Dimensional Conductors, $(DCNQI)_2Li$ ····· 77
G. Ultra-Thin Organic Film Systems Prepared by Molecular Beam Epitaxy (MBE) Technique ····· 77
1. Spectral Dependence of the Anisotropy of $\chi^{(3)}$ of Epitaxially Grown Vanadyl Phthalocyanine Film ····· 77
2. Nonliniar Optical Characteristics of MBE-Grown Phthalcyanine Thin Films ····· 77
3. Nonlinear Optical Characteristics of Vanadyl Phthalocyanine Thin Film Grown by Molecular-Beam-Epitaxial Method ····· 77
H. Novel Molecular System C_{60}: Fullerites and Fullerides ····· 78
1. Laser Pulse Induced Transient Photoconductivity of C_{70} Single Crystal ····· 78
2. Delayed Generation of Free Charge Carriers in C_{70} Single crystals ····· 78
3. Transport Property of C_{60} and C_{70} Single Crystals ····· 78
4. Magnetic and Electrical Behaviors of C_{60} (TDAE) Single Crystals ····· 78
I. Development of New Organic Superconductors and Novel Molecular Metals ····· 79
1. New Organic Superconductors, λ-$BETS_2GaX_{4-x}Y_x$ (BETS= bis(ethylenedithio) tetraselenafulvalene) ····· 79
2. New BETS Conductors with Magnetic Anions ····· 79
J. Low-Temperature Crystal Structures and Phase Transitions of Molecular Conducting Systems ····· 79
1. Electronic Band Structure and Superconducting Transition of κ-$(BEDT\text{-}TTF)_2I_3$ ····· 80
K. Development of Pulsed Field Gradient NMR Spectroscopy ····· 80
1. New Pulsed Field Gradient NMR Spectrometer for Solids and Liquid Crystals ····· 80
2. Measurement of Anisotropic Self-Diffusion Coefficient Tensor in Smectic Liquid Crystalline CBOOA ····· 81
L. Phase Transitions and Dynamical Ordering in Liquid Crystals ····· 81
1. ^{13}C NMR Study on the Orientations and Motions of Alkyl Chains in Antiferroelectric Liquid Crystal MHPOBC ····· 82
M. Two-Dimensional Electronic Systems ····· 82
1. NMR Study of Sodium-Hydrogen-Graphite Ternary Intercalation Compound ····· 82
2. Preparation of Organic Charge Transfer Complexes with Two-Dimensional Conduction Layers and their Electronic Properties ····· 83
N. Synchrotron Radiation Excited Surface Reaction ····· 83
1. Synchrotron Radiation Excited Etching of Diamond ····· 83
O. New Physical Properties and Electronic Structures of Quasi-One-Dimensional Halogen-Bridged Mixed-Valence Metal Complexes (MX Chains) ····· 84
1. Photogeneration of Solitons and Polalons in MX Chains ····· 84
2. d-π Interaction in MX Chains ····· 84
3. Electronic Structure of Quasi-One-Dimensional Halogen-Bridged Nickel(III) Complexes: Model Compounds for High-T_c Superconductors ? ····· 85
4. Electronic Structures and Physical Properties of Quasi-One-Dimensional Halogen-Bridged Binuclear Metal Compounds (MMX Chains) ····· 85
P. Low-Dimensional Charge Transfer Metal Complexes Connected with Hydrogen-Bonds ····· 86
1. Synthesis and Physical Properties of Charge Transfer Metal Complexes Connected with Hydrogen-Bonds, $[Pt(H_2dag)(Hdag)]$ $[Ni(dmit)_2]$.solvent ····· 86
Q. Low-Dimensional Magnetic Systems with S=1/2, 1, 3/2 , 2 ····· 86
1. New Haldane Gap System with S=1: Syntheses, Crystal Structures, and Magnetic Properties of Linear-Chain Azido-Bridged Nickel(II) Complexes ····· 86
R. Ultraviolet Photoelectron Spectroscopy and X-rayAbsorption Near Edge Structure Spectroscopy of Organic Solids ····· 87
1. Angle-Resolved Photoemission from Oriented Thin Films of Naphthacene:Comparison with Theoretical Spectra ····· 87
2. UPS Study of $NiPS_3$ and $FePS_3$ Crystals Using Synchrotron Radiation ····· 87
3. Photoelectron Angular Distribution of Thin Films of Copper Phthalocyanine on MoS_2 Surfaces: Quantitative Determination of Molecular Orientation ····· 88
4. Ultraviolet Photoelectron Spectroscopy of Poly(pyridine-2,5-diyl), Poly(2,2'-bipyridine-5,5'-diyl), and their K-doped States ····· 88
5. Ultraviolet Photoelectron Spectroscopy of Alkaline-Metal Doped Polyacetylene ····· 88
6. UV Photoemission Study of Amorphous n-$C_{36}H_{74}$ Films and Their Annealing Process ····· 88
7. Ultraviolet Photoelectron Spectra of C_{78} and C_{96} ····· 89
8. Molecular Orientation and Electronic Structure of Evaporated Porphyrin Films ····· 89
S. Electrical Conductions and its Related Properties of Organic Solids ····· 89
1. New Low-Dimensional Organic Metals of $(BEDT\text{-}ATD)_2X(THF)$ ($X=PF_6$, AsF_6) Stable at Low Temperature ····· 89
2. Preparation and Properties of Lithium-Doped C_{60} by Lithium Azide ····· 90
3. X-ray Photoelectron Spectroscopy Characteristics of a Novel Organic Semiconductor BTQBT and its Derivatives ····· 90
4. Electronic Structure of the Quasi One-Dimensional Organic Conductors DCNQI

(N, N dicyanoquinonediimine)-Cu Salts ····· 90
5. Thermal Expansion of Tetrakis (alkylthio)tetrathiafulvalenes ····· 91
RESEARCH ACTIVITIES V
DEPARTMENT OF APPLIED MOLECULAR SCIENCE ····· 92
A. Highly Oxidized Iron Porphyrin Complexes ····· 92
1. Acylperoxo-Iron(III) Porphyrin Complexes: A New Entry of Potent Oxidants for the Alkene Epoxidation ····· 92
2. High Valent Fe Porphyrin Complexes. O=Fe^{IV} Porphyrin π-Cation Radical vs. O=Fe^{V} Porphyrins ····· 92
3. Preparation and Characterization of Oxoiron(IV) Chlorin Complexes as the First Models for a Reaction Intermediate in the Catalytic Cycle of Cytochrome *d* ····· 92
4. Resonance Raman Characterization of Iron(III) Porphyrin *N*-Oxide: Evidence for an Fe-O-N Bridged Structure ····· 93
B. Model Studies on Nitrite Reductase ····· 93
1. Model Studies of Nitrosyl Intermediates in the Catalytic Cycle of Dissimilatory Nitrite Reductases ····· 93
C. Alteration of Biological Functions of Heme Enzymes by Site-Directed Mutagenesis ····· 93
1. Putative Hydrogen Bond Network in Distal Site of Horseradish Peroxidase ····· 93
2. Rolls of Amino Acid Residues in Heme Vicinity on the Oxygen Activation ····· 94
D. Transition Metal Sulfide Clusters ····· 94
1. A Unique Three-Step Cyclic Reaction Sequence of Heterotrimetallic Sulfide Clusters. Structures and Properties of $[\{Cp^*RhP(OEt)_3(\mu\text{-}WS_4)(CuCl)Cu\}_2(\mu\text{-}Cl)_2]$ ($Cp^* = \eta^5\text{-}C_5Me_5$) with a Branched Structure and $[\{Cp^*RhP(OEt)_3(\mu\text{-}WOS_3)(CuCl)Cu\}_2(m\text{-}Cl)_2]$ with a Linked Incomplete Cubane-Type Structure ····· 94
2. Synthesis and Property of Pentanuclear (Cu^{I}-Rh^{III}_2-W^{VI}_2) Heterometallic Sulfide Cluster Ion Predicted by Fast Atom Bombardment Mass Spectrometry ····· 94
E. Helical Arrays ····· 95
1. Drastic Structural Change in Silver(I) Complexes with Alteration of the Optical Activity of a Pyridine Derivative Ligand: Helical Arrays with Extended Structure and an Optically Inactive Dinuclear Complex ····· 95
2. A Novel Synthesis of Optically Active *C2*-Symmetric Pyridine Derivatives. Efficient Reaction of Chiral Triflates with 2-Picolyllithium Reagents ····· 95
F. Strong Correlation Effects in Organic Conductors ····· 95
1. On the Phase Transition of α-$(ET)_2I_3$ ····· 95
2. Electronic States of Conducting Organic κ-$(BEDT\text{-}TTF)_2X$ ····· 95
3. Intereationship of Electronic States among α-$(ET)_2I_3$, $(ET)_2MHg(SCN)_4$ and κ-$(ET)_2X$ ····· 96
G. Syntheses, Crystal Structures and Solid State Properties of Halogen-Bridged Metal Complexes with Linear Chain Structures ····· 96
1. Electrochemical Synthesis and Crystal Structure of a Novel One-Dimensional Halogen-Bridged Nickel(III) Complex ····· 96
2. Electrocrystallization, Crystal Structure and Solid State Properties of Halogen-Bridged One-Dimensional Compound, $\{[Ni(en)_2Br](ClO_4)_2\}_\infty$, Having an Elongated Ni···Ni Distance ····· 97
H. Modeling Reaction of Metalloenzyme Active Center ····· 97
1. Oxygen Evolution by Water Oxidation with Manganese Porphyrin Dimers ····· 97
2. Importance of Mn-Mn Separation and their Relative Arrangement on the Development of High Catalase Activity in Manganese Porphyrin Dimer Catalysts ····· 97
3. How Do Nitrogen Bases Accelerate Decomposition of H_2O_2 in a Manganese Porphyrin Dimer ? Quantitative Evaluation of the Effect by Its Axial Ligation *vs.* General-base Catalysis ····· 97
4. Preparation of a 1,8-Anthracene-Linked Manganese(IV) Porphyrin Dimer and its Reduction with H_2O_2. The O_2 Evolution Stage by the Reduction of the $Mn(IV)_2$ Complex is Not a Rate-Determining Step in the Catalytic Disproportionation of H_2O_2 ····· 98
5. Siteselective Oxidation of Olefins by Menas of Lipophilic Metalloporphyrin Catalysts in Liposome Membranes ····· 99
6. New and Efficient Synthesis of Oligomeric Porphyrins *via* Stepwise Nucleophilic Substitution of Aminoporphyrins to Cyanuric Chloride ····· 99
7. Formation and Characterization of $Pz_3Cu(II)$-Fe(III) Porphyrin Complex as Structural Model of Cytochrome *c* Oxidase ····· 100
8. Preparation of Tricatecole Fe-Quinone Complexes and its Electrochemical Study ····· 100
I. Design, Properties and Reactivity of New Organometallic Compounds ····· 101
1. Synthesis of Boron Carriers for Neutron Capture Therapy and the Studies of Activated Imines ····· 101
2. Synthesis and Biological Properties of Water-Soluble *p*-Boronophenylalanine Derivatives. Relationship between Water Solubility, Cytotoxicity and Cellar Uptake ····· 101
3. Synthesis of Netropsin and Destamycin Analogues Bearing Ortho-Carborane and their DNA Recognition ····· 101
4. Synthesis of All Carboxylate-free DTPA Derivatives via Palladium Catalyzed Carbon-Carbon Bond Formation Reaction ····· 101
5. Highly Stereocontrolled and Concise Asymmetric Synthesis of the b-Lactam Framework via a TCC Method ····· 101
RESEARCH ACTIVITIES VI
DEPARTMENT OF VACUUM UV PHOTOSCIENCE ····· 102

A. Electronic Structure and Decay Mechanism of Inner-Shell Excited Molecules 102
1. Angular Distribution of Fragment Ions Following the C 1s Photoexcitation of C_2H_2 102
2. Molecular Symmetries and Angular Distribution of Fragment Ions Following the S 1s Excited SO_2 102
3. Electronic States of Gaseous and Adsorbed Thiophene C_4H_4S Studied by the S 1s Photoabsorption Spectra 102
4. Angular Distribution of 1sσ Photoelectrons from Fixed-in-Space N_2 Molecules 103
5. Angular Distribution of 1s Photoelectrons from Spatially Aligned CO Using Angle-Resolved PEPICO 103
6. Electron Impact Core Excitation of SF_6: S 2p, S 2s and F 1s Spectroscopy 103
7. Dissociation Dynamics of Core-Excited BF_3 Probed by the Photoelectron-Photoion-Photoion Coincidence 103
8. Rydberg-Valence Mixing in the C 1s Excited States of CH_4 Probed by Electron Spectroscopy 103
B. Soft X-ray Photoelectron-Photoabsorption Spectroscopy and Electronic Structure of Transition Metal Compounds 104
1. Resonant Ni 3p and 3s Photoelectron Spectra Following the Ni 2p Excitation in NiO 104
2. Ni $L_{2,3}MM$ Resonant Auger Spectra of $K_2Ni(CN)_4$ Following the Ni 2p Excitation 104
C. Studies of Photochemical Reactions using Ultrafast Laser and Synchrotron Radiation 105
1. Time-Domain Approach to the Solute-Solvent Interactions in Photochemical Reactions 105
2. Application of Broadband Incoherent Light to Femtosecond Time-Resolved Spectroscopy 105
3. Construction of an Optical Cell for Spectroscopic Studies on Supercritical Fluids 105
D. Synchrotron Radiation Stimulated Surface Reactions 106
1. *In Situ* Detection of Surface SiH_n in Synchrotron-Radiation-Induced Chemical Vapor Deposition of a-Si on a SiO_2 Substrate 106
2. Infrared Reflection Absorption Spectra for Trimethyl Aluminum and Dimethyl Aluminum Hydride Condensed Layer on SiO_2 Surface with Buried Metal Layer 106
3. Design of Double Multilayer Monochromator for Surface Photochemical Reactions Induced by Synchrotron Radiation 107
4. Development of Electron-Ion Coincidence Spectroscopy for Study of Surface Dynamics 107
5. Auger Electron-Ion Coincidence Study for H_2O Condenced on SiO_2/Si(111) 107
6. Synchrotron Radiation Assisted Surface Processes of Diethylzinc on GaAs(100) 108
7. Adsorption and Thermal Decomposition of Diethyltellurium on GaAs(100) 108
E. Photoionization Dynamics Studied by Electron Spectroscopy Combined with a Continuous Synchrotron Radiation Source 108
1. Autoionizing Resonance in Photoionization from the $1\pi_u$ Level of Acetylene 108
2. Autoionization of Acetylene Studied by Two-Dimensional Photoelectron Spectroscopy 109
3. Autoionization of NO in an Excited Valence State Affected by Perturbations of Valence-Rydberg Mixing 109
4. Autoionization of Nitrogen Atoms Produced by Dissociation of Superexcited NO Moleules 109
F. Rebuilding the Monochromator on the Beam Line BL2B2 in UVSOR 110
1. Tentative Design of an 18m Spherical Grating Monochromator 110
2. Evaluation of the Resolving Power and Photon Flux of the 18m SGM by Ray Tracing 110
G. Desorption Induced by Electronic Transitions on the Solid Surface of Condensed Gases 111
1. Angular and Kinetic Energy Distributions of the Desorption of Ne Metastable Induced by Excitons at the Surface of Solid Ne 111
2. Photon Stimulated Desorption of O^- from O_2 Condensed on an Ar Film 111
H. Elucidation of Ion-Solid Chemistry in Ion-Implanted Amorphous SiO_2 and Creation of Novel Materials by Implantation 112
1. Optical and Electrical Properties of Proton-Implanted Amorphous SiO_2, GeO_2-SiO_2, MgO-P_2O_5 and Nanocrystalline $MgIn_2O_4$: Novel Materials by Proton Implantation 112
2. Chemical Interaction in Ion-Implanted Amorphous SiO_2 and Application to Formation and Modification of Nanosize Colloid Particles 112
I. Electronic Structure Design of Wide Gap Conductors and Control of their Conduction Behavior 112
1. Generation of Electron Carriers in Insulating Thin Film of $MgIn_2O_4$ Spinel by Li^+ Implantation 112
2. Preparation of Electroconductive and Transparent Thin Films of $AgSbO_3$ 113
3. Novel Transparent and Electroconductive Amorphous Semiconductor: Amorphous $AgSbO_3$ Film 113
4. Photoemission Studies on Valence Band Structure of $AgSbO_3$ 113
J. Absolute Photoabsorption Cross Section and Breakdown Pathways of Molecules Containing *d*-Electrons 113
1. Absolute Photoabsorption of BrCN in the Valence Shell and the Bromine M, Carbon K and Nitrogen K Shell Regions (5-450 eV) 113
2. Ionic Photofragmentation (11.5-100 eV) and PIPICO Spectroscopy (40-130 eV) of BrCN in the Valence Shell and Bromine 3*d* Regions 114
K. Electronic States and Dissociative Channels of Valence Shell Excited Molecules 114
1. Radiative Dissociation of C_2H_2, C_2HD and C_2D_2 Superexcited at 50-90 nm Region 114
2. Photoabsorption and Fluorescence Cross Sections of $SiCl_4$ in the Region of 6.2-31 eV 114
L. Growth and Characterization of II-VI Compound Semiconductor Thin Film Using Metalorganic Sources 115
1. Phown by Photo-Assisted Metalorganic Vapor Phase Epitaxy 115
2. Synchrotron Radiation Excited Growth of ZnTe Using Metalorganic Sources 115

3. Construction of a System for Novel Low-Temperature Growth of II-VI Compound Semiconductors Using Synchrotron Radiation ····· 115
4. Synchrotron-Radiation-Excited Growth of ZnTe by Alternating Gas Supply Using Metalorganic Sources ···· 115
5. Low Temperature Deposition of II-VI Compound Semiconductors by Synchrotron Radiation Using Metalorganic Sources ····· 115
6. Growth of High-Quality ZnTe Layers by MOVPE ····· 116
7. Aluminum Doping of ZnTe Grown by MOVPE ····· 116
M. Electronic Structures of Organic/Inorganic Interfaces Studied by UV Photoemission ····· 117
1. The Electronic Structure and Energy Level Alignment of Porphyrin/Metal Interfaces Studied by Ultraviolet Photoelectron Spectroscopy ····· 117
2. The Electronic Structure of 8-Hydroxyquinoline Aluminum/Metal Interfaces Studied by Ultraviolet Photoelectron Spectroscopy ····· 117
RESEARCH ACTIVITIES VII
COORDINATION CHEMISTRY LABORATORIES ····· 118
A. Stereochemistry of Coordination Compounds and Adsorption Phenomena of Various Gases on Inorganic Solids ····· 118
1. Stereochemistry of Six-Coordinated Silicon(IV) Complexes ····· 118
2. Photochemistry of Cobalt(III) Complexes Containing a Sulfinate-*S* Ligand. Linkage and Geometrical Isomerization ····· 118
3. Force Field Calculation of Metal Complex Systems Including Antitumor Platinum(II) Complexes ····· 119
4. Manganese(III) Complexes Containing Optically-Active Tetradentate Schiff-Base Ligands. The Effect of Phenyl Substituents ····· 119
5. Dielectric Behaviors in the Inorganic Solid-H_2O Systems ····· 120
6. Stabilization of Copper Metal Clusters in Mordenite Nanopores: Water Treatment of Evacuated Copper-Ion-Exchanged Mordenite at 300 K ····· 120
7. Solid-State Circular Dichroism Spectra of *trans*-Diamminetetranitrocobalt(III) Salts and *mer*-Triamminetrinitrocobalt(III) ····· 121
8. Polymeric and Monomeric Structures of a Schiff-Base Oxovanadium(IV) Complex: Orange and Green Forms of [VO{sal-(*RR*)-stien}] and Interconversion between these Species ····· 121
B. Creation of Complexes Containing New Types of Bonds between a Transition Metal and a Phosphorus ····· 122
1. Cationic Phosphenium Complexes of Group 6 Transition Metals: Reactivity, Isomerization, and X-ray Structures ····· 122
2. Migratory Insertion of a Phosphorus Ligand into a Transition Metal-Alkyl Bond ····· 122
3. Reactivity of Cationic Transition-Metal Phosphenium Complexes ····· 122
4. Conversion of Transition-Metal Complexes with Stannyl and Phosphenium Ligands into those with Stannylene and Phosphine Ligands by Alkyl Migration from Sn to P ····· 123
5. P-C Bond Cleavage of Phosphorus Bridged [1]Ferrocenophane Coordinating to $[Cp(CO)_2Fe]^+$ Fragment ···· 123
6. Synthesis and Stereochemistry of Transition-Metal Complexes with Tetraphosphamaclocycle ····· 123
7. Synthesis and Structure of Poly (pyrazolyl)borate Complexes of Zirconium (IV) ····· 123
C. Metal Complexes as Targeting Agents for Nucleic Acids ····· 124
1. Three-Point Recognition of Thymine Base by a Zn^{II}-Cyclen Complex ····· 124
2. Multipoint Recognition of Nucleobases by a Zn^{II} Complex of Acridine-Pendant Cyclen ····· 124
3. Inhibition of Polynucleotide Hybridization and *in vitro* Poly(Phe) Synthesis by a Zn^{II}-Cyclen Complex ····· 125
D. Organometallic Chemistry of Early Transition Metals ····· 125
1. Polyethylene with Extremely Narrow Polydispersity Obtained from the New Catalyst Systems $Nb(C_5Me_5)(diene)Cl_2$-MAO and $Nb(C_5Me_5)(diene)_2$-MAO ····· 125
2. Diene Complex of Lanthanum: The Crystal Structure of a Diene-bridged Dilanthanum Complex, $[LaI_2(thf)_3(\mu\text{-}\eta^4 : \eta^4\text{-}PhCH{=}CH\text{-}CH{=}CH\text{-}Ph)LaI_2(thf)_3]$ ····· 125
E. Studies on Mixed Ligand Complexes ····· 126
1. 4- and 5-Coordinate Dinuclear Copper(II) Complexes with the Tetraacetylethanediide and an N-Alkylated Diamine or a Triamine ····· 126
2. Thermo-analytical and X-Ray Diffractometoric Observations of a Plastically Crystalline Phase in Molecular Mixed Ligand Complex ····· 126
3. Copper(II) Mixed Ligand Complex with an N-alkylated Diamine and a New β-Diketonate ····· 126
4. Electronic Structure and Electronic Transitions of (Catecholate)(1,10-phenanthroline) copper (II): Intramolecular Interligand Electronic Interaction ····· 126
5. d-f Matal Ion Interaction through Fe-CN-Ln Bridge between Dicyanobis (1,10-phenanthroline) iron (II) Complex and $LnCl_3$ ····· 127
F. Activation of Carbon Dioxide by Metal Complexes ····· 127
1. Ruthenium Formyl Complexes as the Branch Point in Two- and Multi-Electron Reduction of CO_2 ····· 127
2. Multi-Step CO_2 Reduction Catalyzed by $[Ru(bpy)_2(CO)]^{2+}$ (bpy = 2,2'-bipyridine, qu = quinoline). Double Methylation of Carbonyl Moiety Resulting from Reductive Disproportionation of CO_2 ····· 127
3. Catalytic Formation Ketones by Double Alkylation of CO Formed by Reductive Disproportionation of

CO_2 on a Ruthenium Complex ····· 128
4. Comparison of Ru-C Bond Characters Involved in Successive Reduction of Ru-CO_2 to Ru-CO_2OH ····· 128
5. Crystal Structure of $[Ru(bpy)_2(CO)(\eta^1\text{-}C(O)OH)]^+$ as a Key Intermediate in CO_2/CO Conversion ····· 128
6. Oxalate Formation in Electrochemical CO_2 Reduction Catalyzed by a Rhodium-Sulfur Cluster ····· 129
7. Remarkable Decrease in Overpotential of Oxalate Formation in Electrochemical CO_2 Reduction by a Metal- Sulfide Cluster ····· 129
8. Control of Coordination Mode of η^{1-} and η^{2-} 1,8-Naphthyridine Ligated to Ru(II)-bis(bipyridine) Complexes ····· 129
G. Development of Highly Selective Reactions Using Early Transition Metal Complexes ····· 130
1. Intramolecular Coupling of Alkynyl Groups of Bis(alkynyl)silane Mediated by Zirconocene Compounds: Formation of Silacyclobutene Derivatives ····· 130
2. A Vinylzirconation Reaction of Alkynes ····· 131
3. Oxidative Addition of 2-Haloalkene to Zirconocene ····· 131
4. Highly Selective and Practical Alkyne-Alkyne Cross Coupling Reaction Using Cp_2ZrBu_2 and Ethylene ····· 131
5. Reaction of Zirconocene Ethylene Complex with Diynes: Formation of Bridged Zirconacyclopentenes ····· 132
6. Cycloaddition of Zirconacyclopentadienes to Alkynes Using Copper Salts: Formation of Benzene Derivatives ····· 132
7. Practical and Selective Method for Preparation and Reactions of Cp_2HfRCl and Cp_2HfRR' ····· 132
8. Formation of a Five-Membered Carbocyclic Ring by Reaction of Zirconacyclopentane with RCOCl ····· 132
9. Zirconium Mediated or Catalyzed Highly Stereoselective Cyclization of 1,4,7-Trienes ····· 132
10. Chemoselective Carbon-Carbon Bond Formation Reaction of Zirconacyclopentenes with Allylic Compounds ····· 133
H. Building of Two and Three-Dimensional Coordination Polymers Possessing Potential High Electrical Conductivity, Novel Host Metal Complexes and Polynuclear Complexes ····· 133
1. Building of 2D Sheet of Tetrakis (methylthio)tetrathiafulvalenes Coordinating to Copper(I) Halides with Zigzag and Helical Frames and the 3D Network through the S···S Contacts ····· 133
2. Syntheses, Structures and Properties of Copper(I) Coordination Polymers with Bridging Phenazine: Construction of One- and Two-dimensional Structures with π-π Stacking of Phenazine ····· 133
3. Synthesis and Structures of Tetranuclear and Hexanuclear Copper(I) Complexes with Iminomethanethiolate Bridges Derived from Isothiocyanate ····· 134
4. Syntheses and Characterization of One- and Two-Dimensional Copper(I) Coordination Polymers with Tetrakis (ethylthio)tetrathiafulvalene and the Properties of their Iodine-doped Compounds ····· 134
5. Syntheses, Structures and Properties of a Linear Copper(I) Coordination Polymers with Tetrakis(ethylthio)tetrathiafulvalene ····· 134
6. Synthesis and Crystal Structure of Three-Dimensional Lanthanum(III) Coordination Polymer with Mellitate, $\{La_2[C_6(COO)_6](H_2O)_9\}\cdot 2H_2O$ ····· 135
7. Crystal Structure and Magnetic Properties of Manganese(II) Mellitate, $[Mn_2\{C_6(COO)_6\}(H_2O)_6][Mn(H_2O)_6]\cdot 2H_2O$ with Two-Dimensional Layer Structure and Three-Dimensional Hydrogen Bonding Networks ····· 135
8. Synthesis and Structural Characterization of Crown Thioether Complexes of Silver(I) and Copper(II) ····· 136
9. A Molecular Cavity for Tetrahedral and Y-Shaped Anions. Synthetic and Structural Studies of Macrocyclic Dicopper(I) and Disilver(I) Compounds of 1,6-Bis(diphenylphosphino)hexane ····· 136
10. Cooperative Metal Ions Binding by Metal-Organized Crown Ether ····· 136
11. Formation of a Metallocycle by Dimerization of Acrylonitrile. Crystal Structure of the Hexakis {(1,4-dicyanobutene-1,4-diyl)-nickel(II)} Complex ····· 137
12. Synthesis and Crystal Structure of a Mono- and Dinuclear Nickel(0) Ethylene Complex with 4,4'-Bipyridine (bpy); $\{[Ni(bpy)(C_2H_4)]_2\ [Ni_2(bpy)(C_2H_4)_4]\}$ ····· 137
13. Co-ordinative Versatility of Pyrazole Derivative Ligand 3,5-Bis(2-Pyridyl)Pyrazole (Hbpypz) in Silver and Copper Compounds. Synthesis, Characterization and Crystal Structures of $[Ag_2(Hbpypz)_4](ClO_4)_2\text{-}2(CH_3)_2CO$, $\{[Ag(Hbpypz)]\ (ClO_4)\}_\infty$ and $[Cu_4(bpypz)_4(ClO_4)_4]\text{-}2H_2O$ ····· 137
I. Design, Synthesis, and Property of Metal-Complex Based Magnetic Materials ····· 138
1. Complexes Derived from the Reaction of Manganese(III) Schiff Base Complexes and Hexacyanoferrate(III): Syntheses, Multi-Dimensional Network Structures, and Magnetic Properties ····· 138
2. Metamagnetic Property of Cyano(N,N-ethylenebis(salicylideneamino))manganese(III) ····· 140
J. Interconversion between Monomeric and its Self-assembled Oligomeric Metal Complexes ····· 140
1. Proton Promoted Interconversion between Monomer and Self-Assembled Cyclic Oligomer of Cu(II) and Pd(II) Complexes with 2-(4-imidazolyl)-ethylimino-6-methylpyridine ····· 140
2. B-N Bond Formation by the Reaction of (N-3-Methoxysalicylidene-N'-(imidazol-4-ylmethylene)-1,3-propanediamino)copper(II) Perchlorate and Sodium Tetraphenylborate ····· 141
K. Study of Metallomesogens ····· 141
1. Synthesis and Characterization of Alkoxo-oxygen Bridged Copper(II) Complexes Exhibiting Disk-Like and Rod-Like Shapes ····· 141
RESEARCH ACTIVITIES VIII
COMPUTER CENTER ····· 143

A. Theoretical Studies of Highly Excited Vibrational States in Polyatomic Molecules 143
1. Semiclassical Study of Avoided Crossings 143
2. Rotation Induced Vibrational Mixing in Highly Excited Vibrational States of Formaldehyde II 143
3. Wave Packet Dynamics of CaNC/CaCN 143
CHEMICAL MATERIALS CENTER 144
B. Preparation and Properties of Novel Heterocyclic Compounds 144
1. Benzobis(thiadiazole)s Containing Hypervalent Sulfur Atoms: Novel Heterocycles with High Electron Affinity and Short Intermolecular Contacts between Heteroatoms 144
2. Synthesis and Properties of Tetrathiafulvalene Derivatives Containing Quinoid Structures: Novel Electron Donors of Organic Conductors 144
3. Preparation and Properties of Tris(1,3-dithiole) Donors Containing Thiophene Spacer Units 144
4. Organic Metals Based on Butterfly-Shaped Donor Molecules 145
5. Preparation and Properties of Bis[5-(6-methyl-1,4-dithiafulven-6-yl)-2-thienyl]methanes Affording Near-Infrared Absorbing Cations by Oxidation 145
6. New Narrow-Bandgap Polymer Composed of Benzobis(1,2,5-thiadiazole) and Thiophenes 145
7. Synthesis and Properties of 5,7-Di(2-pyrrolyl)[1,2,5]thiadiazolo[3,4-b]thieno[3,4-e]pyrazine: A New Monomer Candidate for Intrinsically Conducting Polymer 146
8. Syntheses and Properties of Novel Conducting Dithiolato-Metal Complexes Having Peripheral Heteroatoms and Extended p-Conjugated Systems 146
9. Structures and Physical Properties of Cation-Radical Salts of Unsymmetrical Tetrathiafulvalene Derivatives Fused with a 1,2,5-Thiadiazole Ring 147
INSTRUMENT CENTER 148
C. Studies of Solvated Metal Clusters 148
1. Photodissociation Spectra of $Ca^+(H_2O)_n$ (n=1-9) 148
2. Photoelectron Spectroscopy of Mass-Selected $Na^-(NH_3)_n$ Ions 148
3. Photoelectron Spectroscopy of Mass-Selected $Li^-(NH_3)_n$ Ions 149
D. Studies on Hypervalent Molecular Clusters 151
1. Ultrafast Photochemistry of Ammonia Clusters: Formation of Hypervalent Molecular Clusters Containing the NH_4 Radical 151
2. Stability of Hypervalent Molecular Clusters Containing the NH_4 Radical 151
3. Construction of a New Reaction Cell for the Study of Metastable Dissociation Dynamics 152
E. Studies of Ultrafine Particles 153
1. New Preparation Technique to Synthesis Metal Carbide System 153
2. Isolation and Agglomeration of Zinc Nanocolloids Observed by ESR Spectroscopy 153
F. Studies of Nanoscale Carbons 153
1. Concentration of Single-Wall Carbon Nanotubes 153
2. Raman Scattering from Single Wall Carbon Nanotubes Concentrated by Centrifugation 153
3. Magnetic Properties of Carbon Nanostructures Studied by ESR and Magnetic Susceptibility 154
4. Structural Characterization of Multiwall Carbon Nanotubes by Electron Diffraction 154
G. Solid State NMR 155
1. Simulation of Homonuclear Two Spin-1/2 Systems under Sample Spinning. Effects of Jump Motions on NMR Line Shapes 155
2. Spinning Sideband Superposition for Quadrupole MAS NMR Spectra Using a Magic-Angle-Turning Technique 155
EQUIPMENT DEVELOPMENT CENTER 156
H. Activities of Division of "IMS Machines" 156
1. Broad-Band Infra-Red Window for Ultra-High-Vacuum Apparatus 156
2. Time-of-Flight-Type Mass-Spectrometer for High-Mass Materials 157
I. Development of Experimental Devices 157
1. 16-Channel Programmable Pulse Generator for NMR 157
ULTRAVIOLET SYNCHROTRON ORBITAL RADIATION FACILITY 158
J. Development of the UVSOR Light Source 158
1. Study of Radiation Properties from a Helical Optical Klystron for the UV Free Electron Laser on the UVSOR 158
K. Development of Beam Lines and Equipment for UVSOR 158
1. Construction of a Photoelectron Spectroscopy and Microscopy System 158
L. Researches by the Use of UVSOR 159
1. Dynamics of Photon-Stimulated Desorption of Excited-State Alkali Atoms from Alkali Halides 159
2. Effect of Quenching Process on the Decay of the Fast Luminescence from Barium Fluoride Excited by VUV Synchrotron Radiation 159
3. Optical and Photoelectrical Studies of Electronic Structure of $R_3Au_3Sb_4$ (R=La, Ce and Pr) 159
4. The Investigation of Well-Defined NaCl Surface 159
RESEARCH FACILITIES 161
Computer Center 161

Chemical Materials Center 161
Instrument Center 161
Low-Temperature Center 161
Equipment Development Center 161
Division of IMS Machines 162
Ultraviolet Synchrotron Orbital Radiation Facility 162
SPECIAL RESEARCH PROJECTS 163
(1). Development and Evaluation of Molecular Synergistic Systems and their Application to Chemical Energy Conversion 163
Development of High-Sensitivity Submillimeter-Wave to Far Infrared Spectroscopic System for the Study of Transient Molecules 163
Studies on Laser Cooling and Trapping of Neutral Atoms 163
Mechanism of Oxygen Activation by Heme-Copper Terminal Oxidase Superfamily 164
Laser Raman Beat Detection of Magnetic Resonance 164
Liquid Dynamics Studied by New Ultrafast Nonlinear Spectroscopies 164
Studies of Laser-Induced Photochemistry on Solid Surfaces 164
Light Sesitivity of the Self-Organizing Chemical Systems 165
Spectroscopy of Polyatomic Molecules with a Combination of Ultraviolet Laser and Synchrotron Radiation 165
Electronic Structure and Reaction Dynamics of Solvated Metal Ions 165
Organic Conductors Based on Novel Heterocyclic Compounds 166
(2). Materials Science on Molecular Devices 166
π-d Interaction in Molecular Metals 166
Fabrication of Novel Organic Molecular Assemblies with the Use of the Molecular Beam Epitaxy Technique 166
Study on the Solid State Properties of Fullerenes 166
NMR Studies on the Dynamical Properties of Condensed Matter Systems 166
(3). Material Control in Multi-Reaction Centers 167
Chemical Modification of Home Enzymes 167
Specific Feature of Copper-Ion-Exchanged Mordenite for Dinitrogen Adsorption at Room Temperature 167
Migration Reactions of a Transition-Metal Fragment to the Cyclopentadienyl Ring with Bond Cleavage between Transition Metals 167
Metal Complexes as Targeting Agents for Nucleic Acids 168
Activation of Carbon Dioxide by Metal Complexes Directed Toward Carbon-Carbon Bond Formation 168
Novel Type of Carbozirconation Reaction of Alkynes 168
(4). Development of Microscopic Environments with Functionality and Quantum Steering for Reactions 169
Structures, Reactions and Spectroscopy of Molecules and Molecular Clusters 169
Prediction of Protein Tertiary Structures by Multicanonical Algorithms 169
Quantum Mechanical and Semiclassical Studies of Chemical Reaction Dynamics 169
Multi-State Quantum Fokker-Planck Approach to Nonlinear Optical Spectroscopy of Displaced Morse Oscillators System 169
Dynamics and Design of Chemical Reactions in Liquid Water 170
Ultrafast Chemical Reactions in Condensed Phase 170
Laser Investigation of Photodissociation and Bimolecular Reactions 170
In Situ Observation of Silicon Hydrides on Si(100) Surfaces during Synchrotron-Radiation-Stimulated Si_2H_6 Gas Source Molecular Beam Epitaxy 170
New Apparatus for Studying Reaction Dynamics of Inner Core Excited Molecules 171
Multi-Purpose Testing Equipment in Ultra-High-Vacuum 171
Study for High Brilliant Radiation Using the UVSOR Electron Storage Ring 171
(5). Study of Molecular Solid Toward Molecular Electronics 171
Search for Negative-*U* Materials in Molecular Solid 171
Toward Comprehensive Understanding of Various Electronic Phases in Molecular Conductors; Control of Metal-Insulator Transition 172
The Electronic Structure and Energy Level Alignment of Porphyrin/Metal Interfaces Studied by Ultraviolet Photoelectron Spectroscopy 172
OKAZAKI CONFERENCES 174
JOINT STUDIES PROGRAMS 177
1. Special Projects 177
2. Research Symposia 178
3. Cooperative Research 178
4. Use of Facilities 179
5. UVSOR 179
FOREIGN SCHOLARS 181
AWARDS 184

LIST OF PUBLICATIONS 185
REVIEW ARTICLES AND TEXTBOOKS 197
AUTHOR INDEX-RESEARCH ACTIVITIES AND SPECIAL RESEARCH PROJECTS .. 199

ORGANIZATION AND STAFF

Organization

The Institute for Molecular Science compromises twenty three research laboratories each staffed by a professor, an associate professor, two research associates and several technical associates, two research laboratories with foreign visiting professors, and six research facilities. The laboratories are grouped into six departments and one facility for coordination chemistry:

Department of Theoretical Studies	Theoretical Studies I
	Theoretical Studies II
	Theoretical Studies III[1)]
	Theoretical Studies IV (April '95–)
Department of Molecular Structure	Molecular Structure I
	Molecular Structure II[1)]
	Molecular Dynamics
Department of Electronic Structure	Excited State Chemistry
	Excited State Dynamics
	Electronic Structure[1)]
	Molecular Energy Conversion[2)]
Department of Molecular Assemblies	Solid State Chemistry
	Molecular Dynamics Assemblies
	Molecular Assemblies[1)]
Department of Applied Molecular Science	Applied Molecular Science I
	Applied Molecular Science II[1)]
	Physical Organic Chemistry[3)]
Department of Vacuum UV Photoscience	Photochemistry
	Chemical Dynamics
	Interface Molecular Science[3)]
	Synchrotron Radiation Research[2)]
Coordination Chemistry Laboratories	Synthetic Coordination Chemistry[3)]
	Complex Catalysis
	Fundamental Coordination Chemistry
	Coordination Bond[1)]
Research Facilities are:	Computer Center
	Chemical Materials Center
	Intrument Center
	Low-Temperature Center
	Equipment Development Center
	UVSOR (Ultraviolet Synchrotron Orbital Radiation) Facility

1) Professors and associate professors are adjunct professors from other universities.
2) Research Laboratories with foreign visiting professors.
3) Professors, associate professors, and research associates, along with their positions, are transferred from other universities.

Scientific Staff

Mitsuo ITO	**Professor, Director-General**

Emeritus Professors

Saburo NAGAKURA	President, The Kanagawa Academy of Science and Technology
Eiji HIROTA	President, The Graduate University for Advanced Studies
Katsumi KIMURA	Professor, Japan Advanced Institute of Science and Technology
Keiji MOROKUMA	Professor, Emory University, U.S.A.
Hiroo INOKUCHI	Distinguished Research Consultant, Institute for Molecular Science
Yusei MARUYAMA	Professor, Hosei University

Department of Theoretical Studies

Theoretical Studies I

Suehiro IWATA	Professor
Yuko OKAMOTO	Associate Professor (April '95–)
Tsutomu IKEGAMI	Research Associate
Akira SHUDO	Research Associate
Takeshi TSURUSAWA	Technical Associate (April '95–)
Toshio ASADA	IMS Fellow (June '95–)
Toshiaki FUJII	Graduate Student
Hidekazu WATANABE	Graduate Student
Chang Guo-Zhan	Visiting JSPS Ronpaku Fellow from Central China Normal University, China (May '95–August '95)
Jong Keun Park	Visiting Research Fellow ; KOSEF Fellow (May '95–)
Yumin Li	JSPS Post-Doctoral Fellow (June '95–)
Duckhwan Lee	Visiting Scientist from Sogang University, Korea (July '95–August '95)
Simon MATHIEU	Visiting Professor from Universite Paul Sabatier, France (August '95–)
Fernando Rei ORNELLAS	Visiting Professor from Institute of Chemistry, University of São Paulo, Brazil (August '95–)

Theoretical Studies II

Hiroki NAKAMURA	Professor
Yoshitaka TANIMURA	Associate Professor
Chaoyuan ZHU	Research Associate
Ko OKUMURA	Research Associate (October '94–)
Shoji TAKADA	Technical Associate (–April '95)[1]
Norikazu TOMITA	IMS Fellow
Akira OKADA	IMS Fellow (June '95–)
Kengo MORIBAYASHI	JSPS Post-Doctoral Fellow (–April '95)[2]
Ken-ichiro TSUDA	Graduate Student (–March '95)[3]
Yuji MICHIHIRO	Graduate Student (–December '94)[4]
Miyabi HIYAMA	Graduate Student
Yutaka MARUYAMA	Graduate Student (April '95–)
Evgueni E. NIKITIN	Visiting Professor from Technion Israel Institute of Technology, Israel (August '94–October '94)
Frank O. GOODMAN	Visiting Professor from University of Waterloo, Canada (November '94–)
Seung C. PARK	Visiting Professor from Sung Kyun Kwan University, Korea (March '95–April '95)
Abraham BEN-REUVEN	Visiting Professor from Tel Aviv University, Israel (August '95–)

Theoretical Studies III

Yukikazu ICHIKAWA	Adjunct Professor from The Institute of Space Astronautical Science (–March '95)
Eisaku MIYOSHI	Adjunct Professor from Kyushu University (April '95–)
Satoshi YABUSHITA	Adjunct Associate Professor from Chiba University (–March '95)[5]
Michio SASAI	Adjunct Associate Professor from Nagoya University (April '95–)
Kiyoshi SOMEDA	Research Associate (–March '95)[6]
Seiichiro TEN-NO	Research Associate

Theoretical Studies IV

Department of Molecular Structure

Molecular Structure I

Shuji SAITO	Professor
Norio MORITA	Associate Professor
Shuro TAKANO	Research Associate
Yoshiki MORIWAKI	Research Associate
Mitsutaka KUMAKURA	Technical Associate
Kaori KOBAYASHI	Technical Associate (April '95–)
Hideo FUJIWARA	IMS Fellow (June '95–)
Axel H. SALECK	JSPS Post-Doctoral Fellow (–May '95)[7]
Takeshi OKUBO	Research Fellow (–March '95)[8]
Masahiro GOTO	Graduate Student from Nagoya University* (–March '95)[9]
Jian TANG	Graduate Student
Tsuyoshi HIRAO	Graduate Student
Kei-ichi NAMIKI	Graduate Student
Naomi INADA	Graduate Student from Hiroshima University*

Molecular Structure II

Tadaoki MITANI	Adjunct Professor from Japan Advanced Institute of Science and Technology (–March '95)
Isao MORISHIMA	Adjunct Professor from Kyoto University (April '95–)
Masao KITANO	Adjunct Associate Professor from Kyoto University
Takashi OGURA	Research Associate
Hiroyuki OZEKI	Research Associate

Molecular Dynamics

Teizo KITAGAWA	Professor
Tatsuhisa KATO	Associate Professor
Michio MATSUSHITA	Research Associate
Yasuhisa MIZUTANI	Research Associate
Masahiro MUKAI	Research Associate
Naoki HAYASHI	Technical Associate
Shun HIROTA	Graduate Student (–March '95); JSPS Post-Doctoral Fellow (April '95–)
Jörg MATYSIK	JSPS Post-Doctoral Fellow (July '95–)
Xiaojie ZHAO	Research Student (October '94–)
Denis A. PROSHLYAKOV	Graduate Student
Takeshi KODAMA	Graduate Student
Tadashi IWASE	Graduate Student (April '95–)
Takeshi TOMITA	Graduate Student (April '95–)
Yuki UESUGI	Graduate Student (April '95–)

Department of Electronic Structure

Excited State Chemistry

Keitaro YOSHIHARA	Professor
Yoshiyasu MATSUMOTO	Associate Professor
Kyoichi SAWABE	Research Associate
Keisuke TOMINAGA	Research Associate
Shigeichi KUMAZAKI	Technical Associate
Kazuo WATANABE	Technical Associate
Yuri A. GRUZDKOV	JSPS Post-Doctoral Fellow (–February '95)[10]
Toshihisa ANAZAWA	IMS Fellow (June '95–)
Ikuo KINOSITA	Visiting Research Fellow (April '95–)[11]
Hiroyuki KATO	Graduate Student
Ken-ichi SAITOW	Graduate Student
Hideaki SHIROTA	Graduate Student (April '95–)
Kaoru OHTA	Graduate Student from Kyoto University* (April '95–)
Haridas PAL	JSPS Visiting Scientist from Bhabha Atomic Research Center, India
Jangseok MA	Post-Doctoral Fellow (November '94–)
Eugene V. SLOBODCHIKOV	JSPS Visiting Scientist from Institute of Chemical Physics, Russian Academy of Science, Russia (April '95–August '95)
Valey F. KAMALOV	JSPS Visiting Scientist from Institute of Chemical Physics, Russian Academy of Science, Russia (–January '95)
Gary P. KEOGH	Visiting Graduate Student from Imperial College of Science, Technology, and Medicine, UK (–September '94)
D. Melissa JOSEPH	Visiting Graduate Student from Imperial College of Science, Technology, and Medicine, UK (September '94–December '94)

Excited State Dynamics

Ichiro HANAZAKI	Professor
Toshinori SUZUKI	Associate Professor
Masao TAKAYANAGI	Research Associate (–March '95)[12]
Kenichi TONOKURA	Research Associate
Suketu R. GANDHI	JSPS Post-Doctoral Fellow (–May '95); Research Associate (June '95–)
Hideki KATAYANAGI	Technical Associate
Akiko KAMINAGA	Technical Associate
Lizla S. BONTUYAN	JSPS Post-Doctoral Fellow (–May '95)[13]
Nobuaki YONEKURA	IMS Fellow
Yuxiang MO	Visiting Research Fellow (October '94–)
Noriaki OKAZAKI	Graduate Student (–March '95); JSPS Post-Doctoral Fellow (April '95–)
Nobuhisa HASHIMOTO	Graduate Student
Takeshi SHIBATA	Graduate Student (April '95–)

Electronic Structure

Hiroyasu SATO	Adjunct Professor from Mie University
Ryoichi NAKAGAKI	Adjunct Associate Professor from Kanazawa University (–March '95)
Yoshio TEKI	Adjunct Associate Professor from Osaka City University (April '95–)
Yoshihito MORI	Research Associate (–March '95)[14]
Takamichi KOBAYASHI	Research Associate (–January '95)[15]
Nobuaki TANAKA	Research Associate (April '95–)
Yukito NAITOH	JSPS Post-Doctoral Fellow (–May '95); Research Associate (June '95–)

Molecular Energy Conversion

Fernando RULL-PEREZ	Visiting Professor from University of Valladlid, Spain (–November '94)
Gyula RÁBAI	Visiting Associate Professor from Kossuth Lajos University, Hungary (–September '94)
Ming C. LIN	Visiting Professor from Emory University, USA (January '95–August '95)
Valey A. IVANOV	Visiting Professor from Bilkent University, Turkey (–November '94); Visiting Research Fellow (December '94–March '95)[16]

Department of Molecular Assemblies

Solid State Chemistry

Kyuya YAKUSHI	Professor
Kazushi KANODA	Associate Professor
Akito UGAWA	Research Associate
Yasuhiro NAKAZAWA	Research Associate
Ken-ichi IMAEDA	Technical Associate
Kazuya MIYAGAWA	Technical Associate
Mikio URUICHI	Technical Associate
Takafumi MIYAZAKI	JSPS Post-Doctoral Fellow
Makoto INOKUCHI	JSPS Post-Doctoral Fellow (April '95–)
Toshihiro HIEJIMA	Graduate Student
Jian DONG	Graduate Student
Hiromi TANIGUCHI	Graduate Student
Ko-ichi HIRAKI	Graduate Student
Akiko SHIMIZU	Graduate Student from Nagoya University* (–March '95)
Mikhail KOZLOV	Visiting Research Fellow (September '94–January '95)[17]
Anvar A. ZAKHIDOV	Visiting Scientist from Uzbek Academy of Science (October '94 – March '95)
Jingui QIN	Visiting Scientist from Wuhan University, China (July '95–)
Christopher J. NUTTALL	Visiting Graduate Student from Royal Institute of Great Britain (July–August '95)

Molecular Assemblies Dynamics

Yusei MARUYAMA	Professor (–March '95)[18]
Hayao KOBAYASHI	Professor (July '95–)
Seiichi MIYAJIMA	Associate Professor
Toshiyasu SUZUKI	Research Associate (–December '94)[19]
Hironori OGATA	Research Associate

Osamu OISHI	Technical Associate
Noriko YAMAMURO	IMS Fellow (–October '94)[20]
Toshihito NAKAI	IMS Fellow (December '94–)
Takeshi ARAI	JSPS Post-Doctoral Fellow (–March '95)[21]
Jonas V. Kröber	JSPS Post-Doctoral Fellow (September '94–)
Shaoli FANG	Graduate Student (–September '94)[22]
Atsushi SUZUKI	Graduate Student (–March '95)[23]
Naomi MIYAJIMA	Visiting Scientist from Hokkaido Univ. (–February '95)
Eugene FRANKEVICH	Visiting Scientist (February–March '95)
Jong-Jean KIM	Visiting Scientist from Korean Advanced Institute of Science and Technology (August '95–)
Chikako NAKANO	Visiting Research Fellow
Zhang BIN	Visiting Research Fellow (October '94–January '95)
Wang PING	Visiting Research Fellow (September '94–February '95)

Molecular Assemblies

Kosuke SHOBATAKE	Adjunct Professor from Nagoya University
Yukio OUCHI	Adjunct Associate Professor from Nagoya University (–March '95)
Masahiro YAMASHITA	Adjunct Associate Professor from Nagoya University (April '95–)
Shinji HASEGAWA	Research Associate
Tomoyuki MOCHIDA	Research Associate (November '94–)

Department of Applied Molecular Science

Applied Molecular Science I

Yoshihito WATANABE	Professor (October '94–)
Kiyoshi ISOBE	Associate Professor (–September '94)[24]
Masaaki ABE	Research Associate
Shin-ichi OZAKI	Research Associate (April '95–)
Makoto TADOKORO	Research Associate (–September '94)[24]
Takanori NISHIOKA	Technical Associate (–March '95)[24]
Senji WADA	IMS Fellow (May '95–)
Hiroshi SHIMOMURA	IMS Fellow (–November '94)[25]
Seiji OGO	Graduate Student
Toshitaka MATSUI	Graduate Student (April '95–)
Yoshio GOTO	Graduate Student from Kyoto University (April '95–)
Kunio HATANAKA	Graduate Student
Tetsuji ITO	Graduate Student
Minoru MITSUMI	Graduate Student
Koichi TAMAKI	Graduate Student
Md. Badruz ZAMAN	Graduate Student
Rimo XI	Graduate Student (–November '94)[26]

Applied Molecular Science II

Hidetoshi FUKUYAMA	Adjunct Professor from Tokyo University
Koshiro TORIUMI	Adjunct Associate Professor from Himeji Inst. Tech.
Yasuhiro AOYAMA	Adjunct Professor from Nagaoka University of Technology (–March '95)
Takahiro HOSOKAWA	Adjunct Associate Professor from Osaka University (–March '95)
Jiro TOYODA	Research Associate (–April '95)[27]
Takayoshi SUZUKI	Research Associate (–May '95)[27]

Physical Organic Chemistry (–March '95)

Yoshinori NARUTA	Associate Professor (–March '95)[28]
Hisao NEMOTO	Associate Professor (–March '95)[29]
Naoki ASAO	Research Associate (–March '95)[30]
Satoshi USUI	Research Associate (–March '95)[31]
Jianping CAI	Post-doctoral Fellow (–March '95)
Masaoki GOTO	Graduate Student from Kyoto University (–March '95)
Kanako ICHIHARA	Graduate Student from Kyoto University (–March '95)
Mari ICHIMURA	Graduate Student from Kyoto University (–March '95)
Takao SASAKI	Graduate Student from Kyoto University (–March '95)
Masa-aki SASAYAMA	Graduate Student from Kyoto University (–March '95)

Department of Vacuum UV Photoscience

Photochemistry

Nobuhiro KOSUGI	Professor
Tahei TAHARA	Associate Professor (January '95–)
Yasutaka TAKATA	Research Associate
Satoshi TAKEUCHI	Research Associate (May '95–)

Haruhiko OHASHI	Technical Associate
Jun-ichi ADACHI	Technical Associate
Motohiko NAKAMURA	IMS Fellow
Shigeki MATSUO	IMS Fellow (May '95–)
Mitsuhiko KONO	Graduate Student
Misa KAYAMA	Graduate Student (April '95–)

Chemical Dynamics

Tsuneo URISU	Professor
Koichiro MITSUKE	Associate Professor
Kazuhiko MASE	Research Associate
Hiroaki YOSHIDA	Research Associate
Yoshiyuki TSUSAKA	Research Associate
Hideo HATTORI	Technical Associate
Mitsuru NAGASONO	Technical Associate
Masakazu MIZUTANI	IMS Fellow (June '95–)
Takayuki MIYAMAE	JSPS Post-Doctral Fellow (April '95–)
Hiroshi YOSHIKAWA	Research Fellow (–May '95)
Akitaka YOSHIGOE	Graduate Student
Shinya HIRANO	Graduate Student (April '95–)
Minoru KANNO	Graduate Student (–March '95)
Yoshiaki IMAIZUMI	Graduate Student
Yasumasa HIKOSAKA	Graduate Student from Tokyo Institute of Technology*
Syed Irfan GHEYAS	Graduate Student from Saga Univ.*

Interface Molecular Science

Hiroshi KAWAZOE	Professor (–March '95)[32]
Norio IBUKI	Professor (April '95–)
Mitsuhiro NISHIO	Associate Professor (–March '95)[33]
Hideo HOSONO	Associate Professor (April '95–)
Koji HAYASHI	Research Associate (–March '95)[34]
Naoyuki UEDA	Research Associate
Hisao ISHII	Research Associate (April '95–)
Toshihiro OGATA	Graduate Student from Saga Univ.* (–March '95)
Hiroshi MIZOGUCHI	Graduate Student from Tokyo Institute of Technology* (–March '95)

Synchrotron Radiation Research

Valery A. IVANOV	Visiting Professor from Bilkent Univ. Ankara, Turkey (–November '94)
Frank O. GOODMAN	Visiting Professor from Univ. of Waterloo, Waterloo, Canada (December '94–)
Sergei KROUGLIK	Visiting Associate Professor from Academy of Science of Belarus, Minsk, Republic of Belarus (February–August '95)

Coordination Chemistry Laboratories

Koji TANAKA	Director (April '95–)

Synthetic Coordination Chemistry

Yuzo YOSHIKAWA	Professor
Hiroshi NAKAZAWA	Associate Professor
Yasushige KURODA	Research Associate
Tsutomu MIZUTA	Research Associate
Takashi FUJIHARA	IMS Fellow (June '95–)
Yasuharu OHMORI	Graduate Student from Okayama Univ. *
Yoshitaka YAMAGUCHI	Graduate Student from Hiroshima Univ. *
Masakazu HIROTSU	Graduate Student from Okayama Univ. * (–March '95)
Koji YUTOH	Graduate Student from Okayama Univ. * (–May '95); Visiting Research Fellow (April '95–)
Yuri MIZUNO	Graduate Student from Nara Women's Univ. *
Etsuko KONDO	Graduate Student from Okayama Univ. * (–March '95)
Rei ITOH	Graduate Student from Hiroshima Univ. * (–March '95)
Michiyo KOKKA	Graduate Student from Hiroshima Univ. * (–March '95)
Tomoaki YAMASAKI	Graduate Student from Hiroshima Univ. * (–March '95)
Daisuke KATAOKA	Graduate Student from Okayama Univ. * (–March '95)
Motoyuki TASAKA	Graduate Student from Okayama Univ. * (–March '95)
Hong Ling LIU	Graduate Student from Okayama Univ. * (–March '95)
Koichiro TOYOTA	Graduate Student from Hiroshima Univ. * (–March '95)
Kazuhiko ITOH	Graduate Student from Hiroshima Univ. * (April '95–)

Kazumori KAWAMURA	Graduate Student from Hiroshima Univ. * (April '95–)
Toshinori MORI	Graduate Student from Okayama Univ. * (April '95–)
Mitsuru KISHISHITA	Graduate Student from Hiroshima Univ. * (April '95–)
Katsuya YAMAMOTO	Graduate Student from Hiroshima Univ. * (April '95–)
Tamas RADNAIT	Visiting Professor (May–August '95)

Complex Catalysis

Akira NAKAMURA	Professor (–March '95)[35]
Mitsuhiko SHIONOYA	Professor (June '95–)
Yutaka FUKUDA	Adjunct Professor from Ochanomizu Women's Univ.
Junichiro SETSUNE	Adjunct Professor from Kobe Univ.
Thomas DANIEL	Research Associate (–April '95)[36]
Rainer HARN	Visiting Research Fellow (–April '95)[37]
Nathalie LAVAUD	Visiting Research Fellow (–April '95)

Functional Coordination Chemistry

Koji TANAKA	Professor
Tamotsu TAKAHASHI	Associate Professor (–September '95)[38]
Hirotaka NAGAO	Research Associate (–March '95)[39]
Noriyuki SUZUKI	Research Associate
Kiyoshi TSUGE	Research Associate (May '95–)
Ryuichiro HARA	Technical Associate
Tetsunori MIZUKAWA	Technical Associate
Toyohisa ISHIDA	IMS Fellow (–March '95)[40]
Masato KURIHARA	IMS Fellow (June '95–)
Martin KOTORA	Visiting Research Fellow (–May '95)[41]
Koichiro AOYAGI	Graduate Student (–March '95)[42]
Yoshinori KUSHI	Graduate Student (–September '95)[43]
Hiroshi NAKAJIMA	Graduate Student
Kiyotsuna TOYOHARA	Graduate Student
Kayoko KASAI	Graduate Student
Zhenfeng XI	Graduate Student
Yasushi NISHIHARA	Graduate Student
Reinald FISCHER	Visiting Associate Professor from Friedrich-Schiller Univ. Jena (December '94–)
Philippe DROGNAT LANDRÉ	Visiting Research Fellow (March '95–)
Shou-Quan HUO	Visiting Research Fellow (May '95–)
Mathew LEESE	Visiting Research Fellow (July–October '95)

Coordination Bond

Kazuko MATSUMOTO	Adjunct Professor from Waseda Univ. (–March '95)[44]
Akira NAGASAWA	Adjunct Professor from Saitama Univ. (–March '95)[45]
Megumu MUNAKATA	Adjunct Professor from Kinki Univ. (April '95–)
Naohide MATSUMOTO	Adjunct Professor from Kyushu Univ. (April '95–)

Research Facilities

Computer Center

Suehiro IWATA	Director
Mutsumi AOYAGI	Associate Professor
Shinkoh NANBU	Research Associate
Toshiya TAKAMI	Research Associate
Satoshi MINAMINO	Technical Associate
Kouichi MOGI	IMS Fellow (May '95–)

Chemical Materials Center

Ichiro HANAZAKI	Director (–May '95)
Yoshito WATANABE	Director (June '95–)
Yoshiro YAMASHITA	Associate Professor
Shoji TANAKA	Research Associate
Masaaki TOMURA	Technical Associate
Katsuhiko ONO	Graduate Student (–March '95); JSPS Post-Doctoral Fellow (April '95–)
Chitoshi KITAMURA	Graduate Student
Akira OHTA	Graduate Student

Instrument Center

Shuji SAITO	Director
Kiyokazu FUKE	Associate Professor (–Jun '95)[46]
Shunji BANDOW	Research Associate
Fuminori MISAIZU	Research Associate (–March '95)[47]

Daisuke KUWAHARA	Research Associate
Masaomi SANEKATA	Graduate Student (–March '95)[48]
Ryozo TAKASU	Graduate Student

Low-Temperature Center

Yusei MARUYAMA	Director (–March '95)[18]
Kyuya YAKUSHI	Director (April '95–)

Equipment Development Center

Teizo KITAGAWA	Director
Michio WATANABE	Associate Professor
Shuji ASAKA	Research Associate
Jeung Sun AHN	Research Associate (–October '94)[49]

Ultraviolet Synchrotron Orbital Radiation Facility

Nobuhiro KOSUGI	Director
Masao KAMADA	Associate Professor
Toyohiko KINOSHITA	Associate Professor (October '94–)
Hiroyuki HAMA	Research Associate (–January '95); Associate Professor (January '95–)
Kazumichi NAKAGAWA	Adjunct Associate Professor from Kobe Univ. (–March '95)
Kazutoshi FUKUI	Adjunct Associate Professor from Fukui Univ. (April '95–)
Atsunari HIRAYA	Research Associate
Shin-ichiro TANAKA	Research Associate
Shin-ichi KIMURA	Research Associate
Yong Q. CAI	JSPS Foreign Research Fellow (January '95–)
Sayumi HIROSE	JSPS Research Fellow
Shinya YAGI	IMS Fellow (April '95–)
Naoshi TAKAHASHI	Graduate Student
Kazuhiko KIMURA	Graduate Student

Technical Staff

Akira UCHIDA	Technical Division Head
Osamu MATSUDO	Technical Section Chief
Keiichi HAYASAKA	Technical Section Chief (–March '95)
Kiyonori KATO	Technical Section Chief
Kusuo SAKAI	Technical Section Chief
Fumio NISHIMOTO	Technical Section Chief
Fumiyasu MIZUTANI	Computer Center (April '95–)
Kunihiko TANAKA	Computer Center (–December '94)[50]
Fumitsuna TESHIMA	Computer Center
Shigeki NAITO	Computer Center (April '95–)
Masaaki NAGATA	Chemical Materials Center (Unit Chief)
Sachiyo NOMURA	Chemical Materials Center
Takaya YAMANAKA	Instrument Center (Unit Chief)
Masahiro SAKAI	Instrument Center
Hisashi YOSHIDA	Low-Temperature Center (Unit Chief)
Takashi TAKAYAMA	Low-Temperature Center
Toshio KINOSHITA	Electronic Structure (Unit Chief)
Toshio HORIGOME	Equipment Development Center (Unit Chief)
Mitsukazu SUZUI	Vacuum UV Photoscience (Unit Chief)
Shinji KATO	Equipment Development Center
Nobuo MIZUTANI	Equipment Development Center
Kouichi UCHIYAMA	Equipment Development Center
Tomonori TOYODA	Equipment Development Center
Takayuki YANO	Equipment Development Center (April '95–)
Masami HASUMOTO	UVSOR Facility
Jun-ichiro YAMAZAKI	UVSOR Facility
Eiken NAKAMURA	UVSOR Facility

* Carries out graduate research of IMS on Cooperative Education Program of IMS with graduate schools.

1) Present Address: Department of Chemistry, University of Illinois, Noyes Laboratory, Box 32-1,505 South Mathews Avenue, Urbana, Illinois 61801, U.S.A.
2) Present Address: Data and Planning Center, National Institute for Fusion Science, Chikusa-ku, Nagoya, 464-01
3) Present Address: Exploratory Research Laboratory, Fundamental Research Laboratories, NEC Corporation, 34 Miyukigaoka, Tsukuba, Ibaraki 305
4) Present Address: New Technology Communications Co., Ltd, 2-16-13 Hyakunin-cho, Shinjuku-ku, Tokyo 169
5) Present Address: Department of Chemistry, Faculty of Science and Technology, Keio University, 3-14-1 Hiyoshi, Kohoku-ku,Yokohama 223
6) Present Address: Department of Pure and Applied Sciences, Graduate School of Arts and Sciences, University of Tokyo, 3-8-1, Komaba, Meguro-ku, Tokyo 153
7) Present Address: Physikalisches Institut, Universität zu Köln, D-50937 Cologne, Germany
8) Present Address: Souken Kagaku Co., 3-29-5 Takada, Toshima-ku, Tokyo 171
9) Present Address: National Industrial Research Institute of Nagoya, Hirate-cho, Kita-ku, Nagoya 462
10) Present Address: Shock Dynamics Center, Washington State University, Pullman, WA 99164-2814, USA
11) Permanent Address: Yokohama City University, 22-2 Seto, Kanazawa-ku, Yokohama 236
12) Present Address: Graduate School of Bio-Applications and System Engineering, Tokyo University of Agriculture and Technology, 3-5-8 Saiwaicho, Fuchu, Tokyo 183
13) Present Address: 462 e. Northwood Ave Apt G, Columbus, OH 43201, USA
14) Present Address: Department of Applied Chemistry, Nagoya Institute of Technology, Showa-ku, Nagoya 466
15) Present Address: National Institute of Research in Inorganic Materials, 1-1 Namiki, Tsukuba, Ibaraki 305
16) Present Address: N. S. Kurnakov Inst. General and Inorganic Chemistry of the Russian Academy of Sciences, 31 Leninskii prospekt, GSP-1, Moscow 117907, Russia
17) Present Address: National Institute of Materials and Chemical Research, Higashi 1-1, Tsukuba, Ibaraki 305.
18) Present Address: Dept.of Material Chemistry, Hosei University, Kajino-machi, Koganei, Tokyo 184.
19) Present Address: Basic Research Laboratory, NEC Corporation, Miyukigaoka 34, Tsukuba, Ibaraki 305.
20) Present Address: Institute of Chemistry, Tsukuba University, Tennodai, Tsukuba, Ibaraki 305.
21) Present Address: Dept. of Physics, Kyushu University, Hakozaki, Higashi-ku, Fukuoka 812.
22) Present Address: Center for Applied Energy Research, University of Kentucky, 3572 Iron Works Pike Lexington, KY 40511-8433, USA.
23) Present Address: Dept.of Material Chemistry, Hosei University, Kajino-machi, Koganei,Tokyo 184.
24) Present Address: Osaka City University, 3-3-138 Sugimoto, Sumiyoshi, Osaka 558
25) Present Address: Department of Chemistry & Biochemistry, University of Notre Dame, Notre Dame, Indiana 46556, U.S.A.
26) Present Address: Department of Chemistry, University of Chicago, 5735 South Ellis Avenue, Chicago, Illinois, 60637, U.S.A.
27) Present Address: Osaka University, 1-1 Machikaneyama-cho, Osaka 560
28) Present Address: Kyushu University, 6-10-1 Hakozaki, Higashi-ku, Fukuoka, 812
29) Present Address: Tokushima University, 1-78 Shoumachi, Tokushima, 770
30) Present Address: Tohoku University, Aramaki Aza Aoba, Sendai, 980
31) Present Address: Kumamoto University, 2-39-1 Kurokami, Kumamoto, 862
32) Present Address: Research Laboratory of Engineering Materials, Tokyo Institute of Technology, Nagatsuta, Midori-ku Yokohama 227
33) Present Address: Department of Electronic Engineering, Saga University, 1 Honjou, Saga 840
34) Present Address: Center of Cooperative Research, Gifu University, Gifu 501-11
35) Present Address: Dept. of Macromolecular Science, Faculty of Science, Osaka Univ., Toyonaka, Osaka 560
36) Present Address: Berliner Str. 4, 36119 Nevhof, Germany
37) Present Address: Baumgartenstr. 96, D-34130 Kassel, Germany
38) Present Address: Catalysis Research Center, Hokkaido Univ., Kita-ku, Sapporo 060
39) Present Address: Dept. of Chemistry, Faculty of Science, Sophia Univ., 7-1 Kioi, Chiyoda, Tokyo 102
40) Present Address: Asahi Denka Kogyo K. K., 5-2-13 Shirahata, Urawa, Saitama 336
41) Present Address: Dept. of Chemistry, Purdue Univ., West Lafayette, Indiana 47907, USA
42) Present Address: Noyori Molecular Catalysis Project, ERATO, Research Development Corporation of Japan, Aichi Inst. of Tech., 1247 Yachigusa, Yakusa, Toyota 470-03
43) Present Address: Nippon Paint, Co. Ltd., Research Inst. for Chemicals and Macromolecules, 19-17 Ikeda-naka, Neyagawa, Osaka 572
44) Present Address: Dept. of Chemistry, School of Science and Engineering, Waseda Univ., 3-4-1 Ohkubo, Shinjuku, Tokyo 160
45) Present Address: Dept. of Chemistry, Faculty of Science, Saitama Univ., 255 Shimo-Okubo, Urawa, Saitama 338
46) Present Address: Dept. of Chemistry, Faculty of Science, Kobe University, Turukou, Nada-ku, Kobe 657
47) Present Address: Dept. of Chemistry, Fac. of Science, Tohoku University, Aoba, Aoba-ku, Sendai 980
48) Present Address: Dept . of Physics, Fac. of Science, Nihon University, Sakuragamimizu, Setagaya-ku 156
49) Present Address: Japan Advanced Inst. of Science and Technology, Hokuriku Tatsunokuchi, Nomi, Ishikawa 923-12
50) Present Address: Computer Center, Aichi University, 1-1 Machihata-cho, Machihata, Toyohashi-shi 441

COUNCIL

Mitsuo ITO — **Director-General**

Councilors

Chairman	Yukio HORI	Vice President, Kanazawa Institute of Technology
Vice-Chairman	Mitsuo TASUMI	Professor, The University of Tokyo
	Schunichi AKIMOTO	Professor Emeritus, The University of Tokyo
	Yoshikazu ITO	Chairman of The Board, Toray Industries, Inc.
	Hiizu IWAMURA	Professor, Kyusyu University
	Nobuo KATO	President, Nagoya University
	Haruo KURODA	Professor, Science University of Tokyo
	Kazuhiro MARUYAMA	President, Kyoto Institute of Technology
	Noboru MATAGA	Division Head, Institute for Laser Technology Professor Emeritus, Osaka University
	Yoshio MATSUNAGA	Professor, Kanagawa University
	Hidetake MORIMOTO	Adviser, Toyota Central Research & Development Laboratories, Inc.
	Toru MORIYA	Professor, Science University of Tokyo
	Hitoshi OHTAKI	Professor, Ritsumeikan University
	Shinichi SASAKI	President, Toyohashi University of Technology
	Ryoichi SHIMIZU	Director, The Institute of Statistical Mathematics
	Hiroshi SHIONO	Professor, Seikei University
	Hisashi TANAKA	Professor Emeritus, Kyoto University
	Soji TSUCHIYA	Professor, Japan Women's University
	Edward William SCHLAG	Director, Institute for Physical Chemistry, Technical University of Munchen
	Mostafa A. EL-SAYED	Professor, Georgia Institute of Technology

The Council is the advisory board for the Director-General. Two of the councilors are slected among distinguishied foreign scientists.

Distinguished Research Consultants

Hiroaki BABA	Professor Emeritus, Hokkaido University
Kenichi FUKUI	President, Institute for Fundamental Chemistry
Hiroo INOKUCHI	Professor Emeritus, Institute for Molecular Science
Saburo NAGAKURA	President, The Kanagawa Academy of Science and Technology
Ikuzo TANAKA	President, National Institute for Academic Degrees

Administration Bureau

Mikio HASHIMOTO	Director-General, Administration Bureau
Nobuaki SHIMIZU	Director, General Affairs Department (–March '95)
Akihiro SHIBASAKI	Director, General Affairs Department (April '95–)
Mutsuo MIYAZAKI	Director, Finance and Facilities Department (–March '95)
Kenji KANDA	Director, Finance and Facilities Department (April '95–)
Isao FUJII	Head, Personnel Division
Ryouichi KUWABARA	Head, Personnel Division
Shigeaki AIHARA	Head, Research Cooperation and International Affairs Division
Yoshiji SHIMA	Head, Budget Division (–March '95)
Takashi KODAMA	Head, Budget Division (April '95–)
Masayuki JINNO	Head, Accounts Division (–March '95)
Kenzo OZEKI	Head, Accounts Division (April '95–)
Takashi SUZUKI	Head, Construction Division
Yoshiaki KAMACHI	Head, Equipment Division

BUILDINGS AND CAMPUS

The IMS campus covering 62,343 m^2 is located on a low hill in the middle of Okazaki City. The inequality in the surface of the hill and growing trees are preserved as much as possible, and low-storied buildings are adopted for conservation of the environment. The buildings of IMS are separated according to their functions as shown in the map. The Research Office Building and all Research Facilities except for the Computer Center are linked organically to the Main Laboratory Building by corridors. Computer Center, Library and Administration Buildings are situated between IMS and the neighboring National Institute for Basic Biology and National Institute for Physiological Sciences, because the latter two facilities are common to these three institutes.

The lodging facility of IMS called Yamate Lodge, located within ten minutes' walk, has sleeping accommodations for 15 guests and two families. Mishima Lodge, located within four minutes' walk east of IMS can accommodate 74 guests and 20 families. Scientists who visit IMS as well as two other institutes can make use of these facilities. Foreign visiting scientists can also live at these lodgings with their families during their stays.

After the publication of the last Annual Review of IMS (1994), annexes of the Computer Center and the Mishima Lodge have been built.

The Institute for Molecular Science

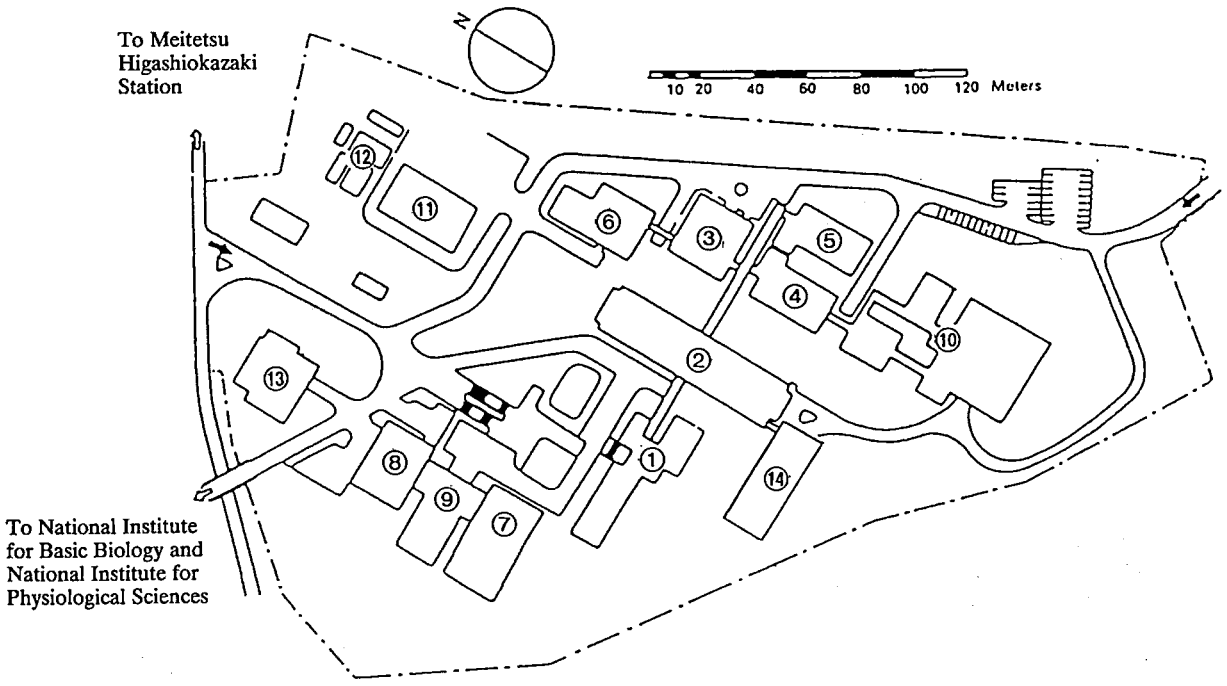

1. Research Office Building
2. Main Laboratory Building
3. Equipment Development Center
4. Instrument Center
5. Chemical Materials Center
6. Low-Temperature Center
7. Computer Center
8. Library
9. Central Administration
10. UVSOR Facility
11. Power Station
12. Waste-Water Disposition Facilities
13. Faculty Club
14. South Laboratory Building

Okazaki (population 300,000) is 260 km west of Tokyo, and can be reached by train in about 3 hours from Tokyo via New Tokaido Line (Shinkansen) and Meitetsu Line. The nearest large city is Nagoya, about 40 km northwest of Okazaki.

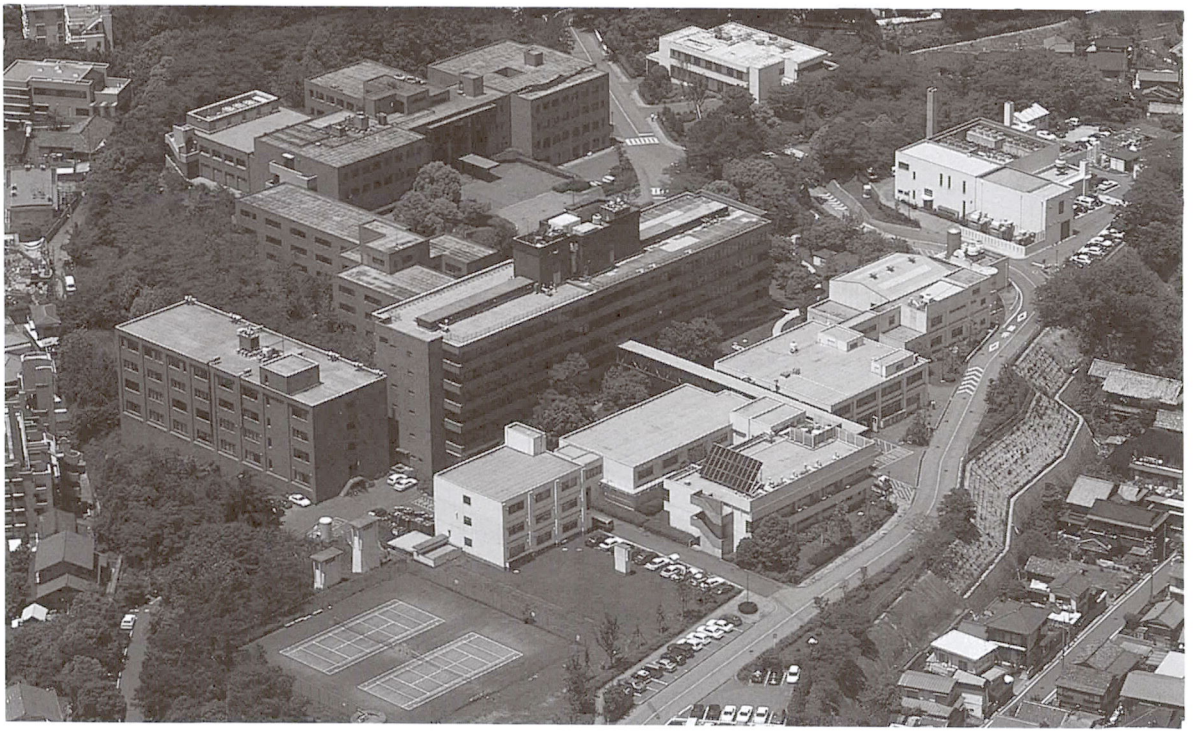

RESEARCH ACTIVITIES I
Department of Theoretical Studies

I-A Development of New Theoretical and Numerical Techniques in the Study of Molecular Electronic Structures

I-A-1 Three-Center Expansion of Electron Repulsion Integrals with Linear Combination of Atomic Electron Distributions

Seiichiro TEN-NO and Suehiro IWATA

[Chem. Phys. Letters **240**, 578 (1995)]

A new systematic way to construct the auxiliary basis functions in approximating the evaluation of electron repulsion integrals is proposed and applied to the SCF and MCSCF wave function calculations. In the approximation, the one-electron density is expanded in terms of a linear combination of atomic electron distributions (LCAD) and the four-center two-electron repulsion integrals are reduced to the three- and two-center quantities. This results in a high-accuracy approximation as well as a large reduction in disk storage and input/output requirement; proportional to N^3 rather than N^4, N being the number of basis functions. Numerical results indicate that the error causing from the present approximation decreases as the size of molecular basis functions increases and that the LCAD version of MCSCF calculation requires only a fractional amount of the CPU time required in the conventional procedure without loss of accuracy.

I-A-2 Theoretical Calculations of Nonlinear Electrical Susceptibilities and Raman Scattering Intensity

Duckhwan LEE, Seiichiro TEN-NO and Suehiro IWATA

Nonlinear optical interaction has provided valuable experimental tools for probing quantum mechanical structures and dynamical informations on molecular systems. Theoretically nonlinear interactions are often described in terms of nonlinear electrical susceptibilities. Although quantum chemical evaluations of nonlinear susceptibilities are crucial for complete understanding of such interactions, such computation has not been an easy task mainly due to the difficult sum over complete set of intermediate states. Most quantum chemical softwares deal only with the static limit which is hardly meaningful for usual experiments. Calculation of Raman intensity becomes further complicated because one has to know in detail how the electronic wavefunctions depend on nuclear motions. In this study, the frequency dependent moment method (FDMM) employing CI wavefunctions will be examined for calculating various nonlinear susceptibilities and Raman scattering intensity. In this method, directly dealing with the dynamic properties, the cumbersome sum over states is entirely replaced by a set of simultaneous equations which then can be solved readily. The nuclear coordinate dependency can also be included analytically for nonlinear processes with Raman-type vibrational resonance such as ordinary Raman and coherent Raman scattering. Furthermore, the FDMM can be applicable not only for any CI wavefunctions but also for semi-empirical CI wavefunctions which are more practical to obtain.

I-B Structures, Spectra and Dynamics of Water Cluster Complexes with Some Ions and with Some Organic Molecules

I-B-1 Theoretical Studies of Boron-Water Cluster Ions $B^+ (H_2O)_n$ and Aluminum-Water Cluster Ions $Al^+ (H_2O)_n$: Isomers and Intra-Cluster Reactions

Hidekazu WATANABE *(Graduate university for advanced studies)* **and Suehiro IWATA**

[*J. Phys. Chem,* in Press]

With *ab initio* molecular orbital calculations, structures of the singly positive charged boron-water clusters $B^+ (H_2O)_n$ and aluminum-water clusters $Al^+ (H_2O)_n$ are determined. The insertion reaction products $HBOH^+ (H_2O)_{n-1}$ and $HAlOH^+ (H_2O)_{n-1}$ are also investigated. Structures of the dimer-core clusters $[M^+ (H_2O)_2](H_2O)_{n-2}$ are similar to each other for M=B and Al. In contrast, the stability and structures of $[B^+ (H_2O)] (H_2O)_{n-1}$ and $Al^+ (H_2O) (H_2O)_{n-1}$, are quite different. The monomer-core boron clusters $[B^+(H_2O)](H_2O)_{n-1}$ do not have stable local minima; the spontaneous proton transfer reaction takes place to form $BOH(H_3O)^+ (H_2O)_{n-2}$. In other words, the acid-basis reaction takes place in such small clusters. In the larger clusters, the reaction further proceeds and the clusters isomerize to the linear type $HBOH (H_2O)_{n-1}$. On the other hand, in the clusters $Al^+ (H_2O) (H_2O)_{n-1}$, no such reaction takes place. The cis-form hydrated products of the insertion reaction $HMOH^+ (H_2O)_{n-1}$ are more reactive and the acid-base reaction is seen in both M=B and Al.

I-B-2 Molecular Orbital Studies of the Structures and Reactions of Singly Charged Calcium Ion with Water Clusters, $Ca^+ (H_2O)_n$

Hidekazu WATANABE *(Graduate university for advanced studies)* **and Suehiro IWATA**

The structures of the hydrated singly positive charged calcium clusters $Ca^+ (H_2O)_n$ and their hydrogen-eliminated products $(CaOH)^+ (H_2O)_{n-1}$ are optimized with the ab initio molecular orbital method and are compared with the magnesium cation-water clusters which were

investigated previously. For n > 2 , structures of $Ca^+(H_2O)_n$ are different from structures of $Mg^+(H_2O)_n$. In the clusters $Mg^+(H_2O)_n$, the angle of O-Mg-O is near 90°. In contrast, the cluster $Ca^+(H_2O)_n$ forms the square planar structure. Structures of $(CaOH)^+(H_2O)_{n-1}$ are also different from those of $(MgOH)^+(H_2O)_{n-1}$. The structural differences are attributed to the d orbitals of Ca ion. The molecular ion $(CaOH)^+$ in the hydrogen-eliminated products $(CaOH)^+(H_2O)_{n-1}$ is very similar to the $(MgOH)^+$ ion. A positive charge in $CaOH^+$ is strongly localized on a Ca ion as $Ca^{2+}\ O^-\ H$, which is similar to that in $MgOH^+$. Consequently, the hydration energies of the $(CaOH)^+(H_2O)_n$ are much larger than those of $Ca^+(H_2O)_n$. The internal energy change of the hydrogen elimination of $Ca^+(H_2O)_n$ is positive for n=1-4, but becomes negative for n > 5 , which is in good agreement with the product switching in the TOF spectrum reported by Fuke group. The effect of the isotope substitution and equilibrium constants of hydrogen (deuterium) elimination reaction and difference from the magnesium cation-water clusters observed in their experiment can be explained qualitatively.

I-B-3 Theoretical Study of Entropy Effects on the Intra Cluster Reactions: Ab Initio Monte Carlo Simulations of $Mg^+(H_2O)_n$ Clusters

Toshio ASADA and Suehiro IWATA

Recent years, the intra-cluster reactions such as hydrogen-eliminated reactions probably have been the most important topics in the cluster chemistry. Although a relatively large number of studies have been made on singly charged $Mg^+(H_2O)_n$ clusters, little is known about phenomena in a thermal equilibrium condition. Thus, we perform Monte Carlo simulations of small clusters consisting of a Mg^+ ion and some water molecules to investigate thermodynamic effects on the intra-cluster reaction.

For energy evaluations, without assuming the analytical forms of conventional inter-molecular potential functions, we directly calculate the total energy of the system with ab initio molecular orbital methods. The superior points of this method lie in the following. Many body interactions are explicitly taken into consideration. In addition water molecules can be freely deformed and reorganized by the change of circumstances.

Entropy effects may play an important role for the reactions of $Mg^+(H_2O)_n$ clusters. Analysis of the mole fraction of isomers, thermodynamic quantities, charge distributions and spin fluctuations are now under way according to the procedure.

I-B-4 Theoretical Studies of the Infra-Red Spectra of the Phenol-Water Clusters

Hidekazu WATANABE *(Graduate university for advanced studies)* **and Suehiro IWATA**

Very recently, infra-red (IR) absorption spectra of the phenol-water clusters, phenol-$(H_2O)_n$ (n≤4), are reported by Mikami and Ebata group. In the experimental infra-red spectra of phenol-$(H_2O)_n$ clusters for n≤3 have "window regions", which are the transparent region between the symmetric and antisymmetric stretching bands of water molecules. To identify these absorption bands, the structures of the phenol-$(H_2O)_n$ (n≤4) are determined with ab initio molecular orbital method and calculated their IR spectra. The calculated IR spectra of the simple ring structures, which are formed through the hydrogen bonds of the -OH group of the phenol and water molecules, well reproduce the transparent window regions and they are in good agreement with the observed IR bands both in position and in relative intensity. For n=4 , two kinds of spectra are found in the experiment; one has a window region and the other has several bands in the same energy region. The formers are identified with an isomer of a simple ring structure and the latters are identified with mixtures of several isomers which consist of a small ring and branches of waters.

I-B-5 Spectroscopic Study of 7-Azaindole-$(H_2O)_n$ (n=1-3) Complexes and its Dimer

Atsushi NAKAJIMA *(Keio Univ.)*, **M. HIRANO** *(Keio Univ.)*, **Ryouji HASUMI** *(Keio Univ.)*, **Hidekazu WATANABE** *(Graduate university for advanced studies)*, **C. C. CARTER** *(Ohaio state Univ.)*, **J. M. WILLIAMSON** *(Ohaio state Univ.)*, **T. A. MILLER** *(Ohaio State Univ.)* **and Koji KAYA** *(Keio Univ.)*

In a dimer of the 7-azaindole, it is known that the proton transfer reaction takes place in its electronic excitation state through the hydrogen bonds between two molecules. To determine structures of the dimer of 7-azaindole and the 7-azaindole-$(H_2O)_n$ n≤3 complexes, their high resolution laser induced fluorescence (LIF) spectra are measured and simulated using the structures determined with the ab initio method. From the ab initio calculations, the most stable isomers of the 7-azaindole$(H_2O)_n$ have a ring structure, in which the water molecules are bonded to both N and NH. The simulated LIF spectra with the most stable structures are in very good agreement with the experimental. The most stable isomer of the dimer of the 7-azaindole is planar; the ab initio structure suggests that the proton transfer can take place easily. The second stable isomer is also planar, but in this isomer the proton transfer can hardly proceed.

I-C Theoretical Studies of Excited and Ionic States of Ammonia Clusters and Ammonium Radical

I-C-1 Theoretical Studies of Dissociation Reactions of Ammonium Radical and Intra-Cluster Reactions of Ammonia Clusters

Jong Keun PARK, Seiichiro TEN-NO and Suehiro IWATA

Recently, there are extensive studies for protonated and unprotonated ammonia clusters and ammonium radical (NH_4)-ammonium cluster. A detailed understanding of intra-cluster reactions requires a state-to-state correlation diagram of a ground and excited state surfaces between the reactants and the products

In the ground state surface from NH_4 radical to NH_3 + H and NH_2 + H_2 , the Rydberg character of the singly occupied orbital of NH_4 is changed to the valence character along the NH bond rupture. Particularly, the ground state of NH_4 correlates with the first excited state of NH_2 ($^2A_1$) + H_2 . In correlation diagrams for the hydrogen transfer surface of ammonia complexes (NH_4···NH_2) → (NH_3 ···NH_3), there is no stable intermediate (NH_3···NH_3) from a complex (NH_4 ···NH_2) to asymptote (NH_3+NH_3), that is, the local minimum potential well does not exist. The binding energy between the complex (NH_4···NH_2) and separated molecules (NH_4 + NH_2) is 4.88 eV. This value is much higher than that of $(NH_3)_2$.

I-D Geometric and Electronic Structures of Binary Element Clusters

I-D-1 Photoionization Electronic Spectroscopy of AlNa

Atsushi NAKAJIMA *(Keio Univ. and RIKEN)*, **Kuniyoshi HOSHINO** *(Keio Univ.)*, **Katsura WATANABE** *(Keio Univ.)*, **Yuji KONISHI** *(Keio Univ.)*, **Tsuyoshi KURIKAWA** *(Keio Univ.)*, **Suehiro IWATA** *(Keio Univ. and IMS)* **and Koji KAYA** *(Keio Univ. and RIKEN)*

[*Chem.Phys.Letters,* **222**, 353-357 (1994)]

Two electronic transitions are observed for a new heteronuclear dimer, AlNa, using two-color two-photon ionization spectroscopy (2R2PI). The combination of the analysis of vibronic structure and ab initio calculation enables us to assign the two transitions as D $^1\Pi \leftarrow X\ ^1\Sigma^+$ and C $^1\Sigma^+ \leftarrow X\ ^1\Sigma^+$; the origins of the D and C states are located at 16427 and 15422 cm^{-1} and the vibrational frequencies being 151 cm^{-1} in the D state, 115 cm^{-1} in the C state and 186^{-1} in the X state, respectively.

I-D-2 Photoelectron Spectroscopy of $Al_nS_1^-$ Clusters (n=1-9)

Atsushi NAKAJIMA *(Keio Univ. and RIKEN)*, **Tetsuya TAGUWA** *(Keio Univ.)*, **Kojiro NAKAO** *(Keio Univ.)*, **Kuniyoshi HOSHINO** *(Keio Univ.)*, **Suehiro IWATA** *(Keio Univ. and IMS)* **and Koji KAYA** *(Keio Univ. and RIKEN)*

[*J.Chem.Phys.* **102**, 660-665 (1995)]

Photoelectron spectra of $Al_nS_1^-$ (1< n < 9) cluster anions were measured at the photon energies of 3.49 and 4.66 eV, using a magnetic bottle electron spectrometer having 60 meV resolution. AlS$^-$ has an electron affinity of as large as 2.6 eV, attributed to large stability by six bonding electrons. A new electronic state, A' $^2\Pi$, was found 0.4 eV above the AlS ground state, which is in agreement with theoretical calculations. $Al_nS_1^-$ cluster anions are produced efficiently up to n=5, but the production of larger cluster sizes is found difficult. The mass distribution of $Al_nS_1^-$ cluster anions and electron binding energy can be explained by a geometric structure obtained by theoretical calculation.

I-D-3 Electronic Properties of Silicon-M Binary Clusters (M = C & Na)

Atsushi NAKAJIMA *(Keio Univ. and RIKEN)*, **Kojiro NAKAO** *(Keio Univ.)*, **Motoki GOMEI** *(Keio Univ.)*, **Reiko KISHI** *(Keio Univ.)*, **Suehiro IWATA and Koji KAYA** *(Keio Univ. and RIKEN)*

[*Mat. Res.Soc.Sym.Proc.* **358**, 61-66 (1995)]

Elctronic properties of silicon-carbon and silicon-sodium binary clusters, produced by laser vaporization, were investigated by photoelectron spectroscopic or photoionization spectroscopic method. The photoelectron spectra of the $C_1Si^-_{m-1}$ clusters are similar to those of pure Si_m^- clusters in the peak positions and their envelopes, which is attributed to the similar electronic structure of Si and C atoms, leading to a similar geometry. In contrast, the similarity in the photoelectron spectra is not observed between C_n^- and $C_{n-1}Si_1^-$ clusters, which is attributed to a change in their geometry; from chain to ring. The ionization energies (Ei) of the $Si_n\ Na_m$ clusters ($1 \le n \le 15$) were determined from the threshold energy of their ionization energy of their ionization efficiency curves. The clear parallelism between the ionization energy of Sin Na and the electron affinity (EA) of Sin is found; $Al_nS_1^-$there are three local minima at n=4, 7 and 10. This implies the facts that (1) the structure of the Sin Na clusters keeps the frame of the corresponding Sin cluster unchanged and that (2) the parentage of singly occupied molecular orbital (SOMO) of Sin Na is the LUMO of Si_n . Furthermore, the Eas of Sin Na ($4 \le n \le 7$) were determined from the threshold energy in the photoelectron spectra of Sin Na - . When the EAs of Si_n Na are compared with those of Sin , the EAs decrease at n=4-6, but the EA increases at n=7. The results of ab initio calculation show that the Na atom

is bound by two Si atoms (bridge site) at n=4-6, whereas it is bound by one Si atom (apex site) at n=7.

I-D-4 Photoelectron Spectroscopy of Silicon-Carbon Cluster Anions ($Si_n C_m^-$)

Atsushi NAKAJIMA *(Keio Univ. and RIKEN)*, **Tetsuya TAGUWA** *(Keio Univ.)*, **Kojiro NAKAO** *(Keio Univ.)*, **Motoki GOMEI** *(Keio Univ.)*, **Reiko KISHI** *(Keio Univ.)*, **Suehiro IWATA and Koji KAYA** *(Keio Univ. and RIKEN)*

[*J.Chem.Phys.* in press]

Photoelectron spectra of $Si_n C_m^-$ cluster anions ($1 \le n \le 7$ and $1 \le m \le 5$) were measured at the photon energies of 3.49 eV, by using a magnetic bottle electron spectrometer. Then C_m^- clusters were produced either by a laser vaporization of a silicon-carbon mixed rod or by two laser vaporizations of carbon and silicon rods in a He carrier gas. The spectra of $Si_n C_1^-$ ($3 \le n \le 7$) clusters are similar to those of pure Si_{n+1} clusters in the peak positions and their envelops, which is attributed to the isovalent electronic structure of Si and C atoms as well as to the similar geometric structure. In contrast, the similarity in the photoelectron spectra is not observed between C_{m+1}^- and $Si_1C_m^-$ ($2 \le m \le 5$) clusters, which is attributed to a change in their geometry ; from chain to ring. These experimental conclusions are discussed with the results of our theoretical calculations.

I-D-5 Theoretical Study of Carbon Doped Small Silicon Clusters : Electron Affinities of Sin C (n=2-5)

Reiko KISHI *(Keio Univ.)*, **Motoki GOMEI** *(Keio Univ.)*, **Atsushi NAKAJIMA** *(Keio Univ.)*, **Suehiro IWATA and Koji KAYA** *(Keio Univ.)*

The geometries and energies of Si_nC and Si_nC^- (n=2-5) were investigated with ab initio MO calculations including electron correlation effects. For neutral Si_n C clusters, the most stable isomer takes the structure in which the Si atom having the highest ratio of hybridization in Si_{n+1} cluster is exchanged with a C atom. For its anion, another Si atom is substituted for a C atom in Si_{n+1}^- cluster because of the high electronegativity of the C atom. The adiabatic and vertical electron affinities of Sin C were evaluated and they reproduced the trends found in the observed photoelectron spectra of Si_nC^-.

I-D-6 Ab Initio Studies on the Structures, Vertical Electron Detachment Energies and Fragmentation Energies of C_nN^- Clusters

Chang-Guo ZHAN (*Central China Normal Univ. and IMS)* **and Suehiro IWATA**

[*J. Chem. Phys.*, submitted (1995)]

In a recently published report on the time-of-flight mass spectrometry studies and *ab initio* RHF/3-21G calculations of the C_nN^- clusters (n=1 to 13), Wang, Huang, Liu and Zhang claimed that all the C_nN^- clusters (n=1 to 13) should be linear chains. In the present work, we report new results obtained from a series of *ab initio* calculations on the ground states of the C_nN^- cluster anions. The results calculated at different approximation levels reveal that the geometries of the C_nN^- determined at the levels without using the polarization functions is qualitatively incorrect and that the diffuse functions of the two atoms at the two end-points of the C_nN^- chains and the higher-order electron correlation correction are important in evaluating the vertical electron detachment energies (VDEs) of the C_nN^- anions. It is concluded from the calculated results that for the singlet ground states, only the linear structures of CN^-, C_2N^-, C_3N^- and C_5N^- are stable and the linear structures of the other C_nN^- (n=4 and 6 to 13) are not at the local minima on the potential energy surfaces. The VDEs and fragmentation energies of C_nN^- (n=1 to 7) in their ground states are evaluated with the MP4SDTQ method at the MP2 geometry, using 6-31G(d) except for two end atoms of each chain, to which a diffuse sp functions are augmented. The calculated VDEs and fragmentation energies all show that the C_nN^- clusters with odd n are more stable than those with even n, which is consistent with the observed even-odd alternation of the TOF signal intensities.

I-E Structures and Reaction Dynamics in the Ground and Excited States of Argon Cluster Ions Ar_n^+

I-E-1 Theoretical Study on the Photoabsorption Spectra of Argon Cluster Ions

Tsutomu IKEGAMI and Suehiro IWATA

A method to calculate the photoabsorption cross section from the classical trajectory is developed and applied to the visible spectra of the argon cluster ions under finite temperature.

A cluster is characterized by vast amount of isomers and their floppy structures. Those structures are all located near in energy, but their electronic properties have a wide variation.The photoabsorption cross section is sensitive to the electronic properties, so that the proper treatment of the distribution over isomers and the thermal motion of nuclei are indispensable for the calculation of the realistic spectra.

Here, the photoabsorption spectra of the argon cluster ions Ar_n^+ are calculated under the finite temperature condition. The motion of the nuclei and the several isomers are accounted for through the classical trajectory calculations on the electronic ground state. The potential energy surface for the trajectory calculation is obtained from the diatomics-in-molecules (DIM) Hamiltonian. The electronic excited states, which are necessary to calculate the absorption spectra, are also calculated from the DIM

Hamiltonian.The calculated spectra show the red shift as the cluster size is increased.If the thermal motion is ignored, the shift occurs from n=15 to n=18. At 10 K, however, the shift occurs at n=8 and n=14 in a two-step manner, in agreement with an experimental observation.The red shift of Ar_n^+ is due to a strongly anisotropic solvent effect on the Ar_3^+ ion core and the thermal motion of the solvent atoms induces the early red shift at n=8 .Therefore, the spectral shift at n=8 can be attributed to the dynamical red shift, whereas the red shift at n=14 is the static one.

I-F Potential Energy Surfaces of Photoabsorption Spectra of Some Triatomic Molecules

I-F-1 Systematic Theoretical Studies of mono- and di-hydrides of Early Transition Metals

Toshiaki FUJII and Suehiro IWATA

The ground and low-lying excited states of MH and MH_2 (M=Ca, Sc, V, Ti, Cr and Mn) are systematically examined with the SA(state-averaged) CAS(chemically-active space) SCF(self-consistent field) method. The state average is taken over all states correlated to the highest multiplet state of the electron configuration $(3d)^n$ $(4s)^2$ of the metal. The molecular states from this electron configuration are described by $(\sigma)^2$ $(\delta_+, \delta_-, \pi_{d+}, \pi_{d-}, \sigma_d)^n$ $(\sigma^*)^1$ for MH and $(\sigma_g)^2$ $(\sigma_u)^2$ $(\delta_+, \delta_-, \pi_{d+}, \pi_{d-}, \sigma_d)^n$ for MH_2 with an obvious notation. The calculated potential energy surfaces and the atomization energies are all insensible to the occupation number (n) of the 3d orbitals and the way of occupation in them. In other words, the MH bond is formed by 4s and 4p atomic orbitals of the metal and 1s orbital(s) of hydrogen; the 3d orbitals do not barely participate the bonding and the 3d electrons behave as spectators. The state ordering among the states is understood by the orbital ordering, $\delta < \pi < \sigma$.

I-F-2 Theoretical Studies of Potential Energy Surfaces and Vibronic States of Low-Lying States of CS_2

Kazutoshi OKADA *(Kobe Univ.)*, **Hajime KATO** *(Kobe Univ.)* **and Suehiro IWATA**

There are numerous experimental studies for near-UV absorption and emission spectra of CS_2 . In the present work, the accurate ab initio calculations are carried out for the lowest three singlet and four triplet excited states. The basis sets used are [5111/2111/11] for C and [5311/5111/11] for S. The type of the CI calculations is the multi- reference POL CI. The potential surfaces of 1^1A_2 (which originates from $^1\Sigma^-$) and $1\ ^1B_2$ (which does from a component of $^1\Delta$) are intermingled each other and both states are bent. These two states become A" and A' symmetries, respectively, in the asymmetric CS stretching. Thus, two states are mixed only through the rotational coupling. In the same energy region, three triplet states are closely lying and crossed with the singlet states. The perturbations among these singlet and triplet states are key factors in understanding the spectroscopies and the dynamics of the excited states of CS_2 .

I-G Ab Initio MO Studies of Energy Rich Ring NO_x and HNO_x

I-G-1 Prediction of Unusual Cyclic Radicals NO_x (x=2-6)

Yumin LI and Suehiro IWATA

In environment science the molecular form NO_x stands for a family of nitrogen oxides and their properties and structures have attracted a great deal of interest among theoretical chemists as well as experimental chemists. But for $x \geq 4$ almost no theoretical and experimental studies are reported. In this work ab initio MO calculations at the UHF and MP2 levels with 6-31G* basis set are carried out to examine the stability and the structure of a series of NO_x (x=2-6) radicals. We have located a series of stable radicals with a ring comprised of one nitrogen atom and two to six oxygen atoms. The true stability is confirmed by evaluating the harmonic frequencies at both levels. The bonds in the cyclic radicals are discussed by comparing with the related known molecules in both distance and bond stretching vibrational frequencies. The reaction energy for $NO_x \rightarrow NO_2 + (x-2)/2\ O_2$ is evaluated with the MP4SDTQ approximation and it is shown that the cyclic NO_x is a new type of energy-rich molecules.

I-G-2 Theoretical Study of the Cyclic Isomers of HNO_x

Yumin LI and Suehiro IWATA

A series of cyclic isomers of HNO_x (x=2-6) are examined with ab initio SCF MO method. All of these cyclic isomers have a ring comprised of one nitrogen atom and two to five oxygen atoms. They are classified under the following three types.

Type A : NO_x ring with an exo hydrogen bonded to nitrogen

Type B : NO_x ring with an exo OH bonded to nitrogen

Type C : NO_x ring with an exo OOH bonded to nitrogen

The geometry optimizations are carried out at the HF and MP2 levels with the 6-31G** basis set and the energies are evaluated at the MP4SDTQ level. The calculated harmonic vibrational frequencies for HNO_x are all real to

confirm the true stability of the molecules. We have failed to locate a five-membered ring HNO_x at the MP2 level. The geometries, vibrational frequencies and IR intensities are discussed by comparing with the related known data. The conformational preferences among the isomers are interpreted in terms of an intramolecular, bifurcated hydrogen bond.

I-H Electronic Structure of Electron-Donor-Acceptor Complexes

I-H-1 An ab initio MO study of κ-$ET_2Cu[N(CN)_2]Br$

Seiichiro TEN-NO, Norikazu TOMITA, Suehiro IWATA and Yoshitaka TANIMURA

An ab initio MO study of structure and stability of an organic superconductor κ-$ET_2Cu[N(CN)_2]Br$ has been performed. Preliminarily, we have optimized the geometrical parameters of ET, $ET^{+1/2}$ and ET^+ molecules at RHF (ROHF)/DZd level using C_{2h} symmetry. The obtained theoretical parameters are very close to those of experiment and the observed geometrical change in detaching an electron is small, i.e. within 0.02Å in bond length and 1.3° in bond angle, except for the main C=C bond, 0.7Å. In order to obtain complete crystalline parameters in Pnma, the monomer geometry of $ET^{+1/2}$ is fitted to the X-ray diffraction data of κ-$ET_2Cu[N(CN)_2]Br$ such that the root-mean square deviation is minimized. Using the geometrical parameters, $ET_2Cu[N(CN)_2]Br$ and ET_2^+ for the nearest pairs are calculated at UHF and ROHF level with Stevens/Basch/Krauss/Jasien/Cundari basis set for their effective core potentials. In both of the results, spin densities are localized in one of ET molecules. This indicates that reorganization of non-conducting electrons and on-site Coulombic interactions dominate the electronic structure of this complex. From these observations, we can conclude that (1) the true wave functions are well described by superpositions of the spin-localized nonorthogonal determinants; and (2) the electron correlations among dimer units play important roles to the bulk systems.

I-H-2 Molecular Orbital Studies of Structure of Tetrathiofluvalene Cation Dimer $(TTF^+)_2$ and Dimer Cation $(TTF)_2^+$ and the IR Intensity Induced by Charge-Transfer Interaction

Hidenori MATSUZAWA *(Chiba Inst. Tech.)* **and Suehiro IWATA**

The geometric structures of TTF radical cation dimer $(TTF^+)_2$ and dimer cation $(TTF)_2^+$ are determined with ab initio molecular orbital methods. The harmonic frequencies and infra-red absorption intensities are also evaluated and the change by dimerization is examined. In the dimer cation at the equilibrium structure, $(TTF)_2^+$, a positive charge (an odd electron) is localized on one of TTF's in the present approximation and two TTF molecules are displaced to the molecular axis. On the other hand, in the cation dimer, $(TTF^+)_2$, two ions are completely overlapped to each other. The optimized structures are compared with those in crystals of various salts.

The enhancement of the IR intensity in some of the normal modes is found in the calculated spectrum and it is analyzed in terms of the modulation of the charge-transfer interaction by the intramolecular vibration, which is often called the electron-molecular vibration (emv) coupling. Based on the ab initio calculations, a new model Hamiltonian is derived for the change of the IR bands in $(TTF)_2^+$ and $(TTF^+)_2$.

I-I Theoretical Studies of State and Isomer Dependence of Internal Rotation Barriers

I-I-1Theoretical Study of the Double Internal Rotation of Methyl Groups in o- and m-xylenes and their Cations

Tadayoshi SUZUKI *(Waseda Univ.)*, **Masaaki FUJII** *(Waseda Univ.)* **and Suehiro IWATA**

The recent experimental studies suggest that the potential energy curves of the internal methyl rotation in xylenes depend on the electronic states as well as the isomers. In the present study, the ab initio MO calculations are carried out with the GAUSSIAN92 package, on the workstation clusters of the computer center at IMS. The two levels of theory employed are Hatree-Fock(HF) for closed-shell S_0 state of neutral molecules; and unrestricted Hatree-Fock(UHF) for open shell (doublet) cation ground state. The basis set used is 6-31G. Assume methyl-A is at the left side of methyl-B. The methyl rotor angles A, B are defined equal to zero when one CH bond lies in the plane of the benzene ring on the right-hand side. The potential energy surfaces of two methyl rotations are drawn while optimizing all other geometric parameters at each step. In the ground state and ionic ground state of o-xylene, when A is equal to 0 and B is equal to 60 (where a hydrogen atom of methyl-A faces a hydrogen atom of methyl-B),the barrier is highest and then both methyls are rotated 60, o-xylene takes the most stable structure. Although no barrier is found in the ground state of the m-xylene, the barrier appears in the ionic ground state. In o-xylene, the reverse direction of two methyl rotation (a kind of gear motion) is much easier than the same direction of rotation.

I-J Ab Initio MO Studies of the Reaction Intermediates

I-J-1 Ab Initio Studies on Structures of the Hexa-Coordinate Phosphorus Intermediate for the Phosphoryl Ester Exchange and N→O Migration Reactions of Dimethyloxyphosphoryl-Threonine

Chang-Guo ZHAN *(Central China Normal Univ. and IMS)* **and Suehiro IWATA**

[*Chem. Phys. Lett.*, in press (1995)]

Recently observed unusual chemical reactivities of the N-phosphoryl amino acids reveal that a special hexa-coordinate phosphorus intermediate may exist in the reaction process. It looks unstable and has not been observed directly. In this letter, we report results obtained from *ab initio* calculations on the structures of the dimethyloxyphosphoryl-threonine and the corresponding hexa-coordinate phosphorus intermediate. The calculated results indicate that the hexa-coordinate phosphorus intermediate is stable because it is associated with a local minimum on the potential energy surface, which supports the hypothesis derived from the experimental studies. All the P-O and P-N bonds in the intermediate should be much more active because their bond lengths are much longer than the corresponding single bonds in the reactant and product. By use of the calculated results, it is very easy to understand the reactivities of the dimethyloxyphosphoryl-threonine and other similar dialkyloxyphosphoryl amino acids.

I-K Prediction of Protein Tertiary Structures from the First Principles

I-K-1 Thermodynamics of Helix-Coil Transitions Studied by Multicanonical Algorithms

Yuko OKAMOTO and Ulrich H.E. HANSMANN *(IPS, ETH Zürich, Switzerland)*

[*J. Phys. Chem.* **99**, 11276 (1995)]

Thermodynamics of helix-coil transitions in amino-acid homo-oligomers are studied by the recently proposed multicanonical algorithms. Homo-oligomers of length 10 are considered for three characteristic amino acids, alanine (helix former), valine (helix indifferent) and glycine (helix breaker). For alanine other lengths (15 and 20) are also considered in order to examine the length dependence. From one multicanonical production run with completely random initial conformations, we have obtained the lowest-energy conformations and various thermodynamic quantities (average helicity, Zimm-Bragg S and σ parameters, free energy differences between helix and coil states, etc.) as functions of temperature. The results confirm the fact that alanine is helix-forming, valine is helix-indifferent and glycine is helix-breaking.

I-L Developing a New Method for Diagonalization of Large Hermitian Matrices

I-L-1 Calculating the Eigenvalues of Large Hermitian Matrices by Difference Equations

Toshiaki IITAKA *(Inst. Phys. and Chem. Res.)*, **Ayori MITSUTAKE** *(Nara Women's Univ.)* **and Yuko OKAMOTO**

Diagonalization of Hermitian matrices is required in many fields of science and engineering. When the size of matrices becomes large, however, regular built-in routines are of no use because of the limitations in computer resources (in both memory space and CPU time). Hence, algorithms that are effective for large matrices are in demand. While Lanczos method is one of the well-known methods that is widely used, we developled a new method that is based on the difference equations of Newton equations for a system of harmonic oscillators (Y. Okamoto and H.J. Maris, *Comp. Phys. Comm.* **76**, 191 (1993)). This time a similar method that is based on the difference equations of Schrödinger equations is developed and the effectiveness of the algorithm is tested in the eigenproblem of the Heisenberg antiferromagnetic chain.

I-M Semiclassical Theory of Chaotic Systems

I-M-1 Complex Classical Trajectories and Chaotic Tunneling

Akira SHUDO and Kensuke S. IKEDA *(Yukawa Inst. for Theor. Phys.)*

[*Phys. Rev. Lett.* **74**, 682 (1995)]

Tunneling phenomena in the presence of chaos are investigated. Several remarkable features, which form sharp contrast to the tunneling in the integrable system, can be well understood in terms of the semiclassical theory including complex classical trajectories. In particular, it is found that the dominant contribution to the tunneling regime comes from many complex branches which are not connected with any real manifolds and are linked at caustics to form the bifurcation chains. Chaotic tunneling is proposed as a new class of tunneling phenomena which

originate from complicated nature of the complex dynamical system.

I-M-2 Toward the Classical Understandings of Quantum Chaological Phenomena: Dynamical Localization and Chaotic Tunneling

Akira SHUDO and Kensuke S. IKEDA*(Yukawa Inst. for Theor. Phys.)*

[*Prog. Theor. Phys. Suppl.* **116**, 283 (1994)]

Semiclassical analyses for two typical quantum chaological phenomena, dynamical localization and chaotic tunneling are carried out. It is found that there exists correlation among classical trajectories contributing the semiclassical propagator and it becomes an origin of dynamical localization. The complex semiclassical theory is developed to describe the dynamical tunneling in a system with mixed phase space. Tremendous number of candidates of complex paths contributing the semiclassical propagator are discovered. It is also shown that complicated structures appearing in the tunneling tail are interpreted as a remarkable manifestation of the underlying complex dynamical system.

I-M-3 Pruning Trees of Tunneling Paths with Principle of Exponential Dominance

Akira SHUDO and Kensuke S. IKEDA*(Ritsumeikan Univ.)*

Stokes phenomenon is investigated in the complex semiclassical theory of chaotic tunneling and a rule for locating contributing tunneling paths out of a complicated set of candidates is proposed. According to an *ordering hypothesis*, the candidate tunneling paths are reordered so as to form a tree structure and the *Principle of Exponential Dominance*(PED) recently revised by Adachi is extended to prune non-contributing paths. This rule allows us to reproduce fine details of complicated chaotic tunneling tail. A phenomenon for which PED plays a crucial role in explaining it is also demonstrated.

I-M-4 Semiclassical Quantization and Periodic Orbits of Dispersing Billiards

Takahisa HARAYAMA *(Waseda Univ.)*, **Akira SHUDO and Yasushi SHIMIZU** *(Tokyo Inst. of Tech.)*

[*Prog. Theor. Phys. Suppl.* **116**, 259 (1994)]

Several ideas proposed to resum the absolutely divergent series of periodic-orbit summation as a form of Selberg type zeta function are applied to the semiclassical quantization of a dispersing billiard system consisting of three circular arcs. It is found that Riemann-Siegel lookalike formula and Novel quantization show remarkable agreement with the exact quantum mechanical evaluation. An analysis using several statistical measures reveals that the length spectrum has a universal feature at least for short range correlation property.

I-M-5 Statistical Properties of Eigenfunctions for Quantum Billiards with and without Positive Lyapunov Exponent

Yasushi SHIMIZU *(Tokyo Inst. of Tech.)* **and Akira SHUDO**

[*Prog. Theor. Phys. Suppl.* **116**, 267 (1994)]

Statistical properties of eigenfunctions of quantum polygonal and dispersing billiards are numerically investigated in detail. Residual parameter and skewness, which estimate the deviation of amplitude distribution from the Gaussian form, are evaluated for hundreds of eigenfunctions. Almost all eigenfunctions of the dispersing billiards show random pattern. For polygonal billiards, it is found that the majority shows quite complicated pattern, but some eigenfunctions are highly regular. Among them two types of highly regular patterns are conspicuous and both eigenfunctions are apparently influenced by the vertices. The difference between the origin of irregular eigenfunctions of the dispersing billiards and that of the polygonal billiards is also discussed.

I-M-6 Polygonal Billiards: Correspondence between Classical and Trajectories and Quantum Eigenstates

Yasushi SHIMIZU *(Tokyo Inst. of Tech.)* **and Akira SHUDO**

[*Chaos, Solitons and Fractals(Special issue on Quantum Chaos)*, **5**, 1337 (1995)]

Correspondence between classical trajectories and quantum eigenstates in polygonal billiards is studied. It is shown that level statistics of polygonal billiards are close to GOE-type fluctuation but they depend weakly on the energy. Among the eigenfunctions with quite irregular patterns which cannot be distinguished from typical patterns of classical chaotic billiards, there are regular eigenfunctions each of which is associated with a certain classical counterpart. Moreover, some of regular eigenstates do not seem to correspond to periodic orbits which typically form families in the billiard boundary. The analysis using periodic-orbit quantization and also Fourier transform of the density of states indeed yields evidence that there are certainly contributions from the corner orbits which connect vertices of the boundary.

I-M-7 Level Statistics and Semiclassical Periodic-Orbit Expansion for Polygonal Billiards

Akira SHUDO

[*Advanced Series of Dynamical Systems(Geometry and Analysis in Dynamical Systems)* **14**, 71 (1994)]

Statistical properties of quantum levels and semiclassical analysis for billiards whose boundary is given by a shape of polygon are presented. Although eigenvalue sequences show level reclusion, the nearest neighbor spacing distribution and the spectral rigidity slightly deviate from the prediction of Gaussian Orthogonal Ensemble.

For a particular shape of polygonal billiards(*1/3* π-rhombus), a complete set of length spectrum of classical periodic orbits can be obtained. The framework of the ordinary periodic orbit theory including only the family of periodic orbits is no sufficient to give a full explanation for numerical results of level statistics.

I-M-8 Statistical Properties of Spectra of Pseudo-integrable System

Akira SHUDO, Yasushi SHIMIZU *(Tokyo Inst. of Tech.)*, **Petr ŠEBA** *(Acad. of Science of the Czech Rep.)*, **Jugen STEIN** *(Marburg Univ.)*, **Hand-Jurgen STÖCKMANN** *(Marburg Univ.)* **and Karol ŻYCZKOWSKI** *(Krakow Univ.)*

[*Phys. Rev.* **E49**, 3748 (1994)]

The spectral properties of various quantum pseudointegrable billiards (rhombus, gnomon, deltoid) are analyzed and they are linked to the genus of the invariant surface of the corresponding classical model. Numerical investigations of the quantum billiards are completed by an experimental study of microwave resonators. Absorption spectra of microwaves in "L-shaped" resonators are measured and the distributions of eigenfrequencies are investigated.

I-N Theoretical Studies of Chemical Reaction Dynamics

Accurate quantum dynamics calculations of triatomic chemical reactions have been made possible with use of the hyperspherical coordinates and some interesting features of the dynamics have been revealed.

A new WKB-type of theory has been developed for the energy splitting due to multidimensional tunneling and intriguing effects of vibrational excitation on the tunneling have been found. Unimolecular dissociation and vibrational energy re-distribution have been analyzed by using the approach of the resonant scattering theory.

Our ultimate purposes are to clarify reaction mechanisms and to develop illuminating approximate theories.

I-N-1 Quantum Dynamics of the Mu + H_2 and Mu + D_2 Reactions

Ken-ichiro TSUDA *(Graduate Univ. for Advanced Studies)*, **Kengo MORIBAYASHI and Hiroki NAKAMURA**

[*Chem. Phys. Lett.*, **231**, 439 (1994)]

Quantum mechanically accurate calculations are carried out for the Mu + H_2 and Mu + D_2 reactions using the hyperspherical coordinate approach. The results for the rate constant are in good agreement with experiment. Comparisons are also made with other more approximate calculations. The effect of initial rotational excitation and final rotational state distribution are also analyzed.

I-N-2 Accurate Quantum Dynamics of Light Atom Transfer ChemicalReaction: O + HCl → OH + Cl

Kengo MORIBAYASHI and Hiroki NAKAMURA

[*J.Phys. Chem., in press*]

The hydrogen atom transfer reaction between two heavy atoms, O(^{3}P) + HCl ($v_i = 0, j_i = 0 \sim 2$) → OH (v_f = 0,1, j_f) + Cl, is studied quantum mechanically accurately with use of the hyperspherical coordinate approach, where v_λ and j_λ designate the vibrational and rotational quantum numbers in the λ arrangement channel. The collision energy considered in this study ranges up to ~ 0.7 eV and the total angular momentum J is required up to ~ 120. The potential energy surface employed is the one derived by Koizumi, Schatz and Gordon (KSG) based on *ab initio* data. The effects of the potential energy surface topography on the dynamics are analyzed in terms of the collision energy dependence and the j_i dependence. The effects of the nonlinearity of the transition state of the KSG surface is clearly manifested in these dynamics. Not only the accurate integral cross section and the rate constant are evaluated, but also Ω_i- dependence of the dynamics and final rotational state distribution are analyzed, where Ω_i is the z-component of J in the initial arrangement channel. The j_f -distribution at $E_{coll} \geq 0.5$eV shows an interesting resemblance with the feature recently observed experimentally. The energy-shift approximation is extended so as to cover the general triatomic systems which require a large number of J. This extended CCPA (constant centrifugal potential approximation) is shown to work well.

I-N-3 Quantum Dynamics of the Mu + H_2 (HD,D_2) and H + MuH (MuD) Reactions

Ken-ichiro TSUDA *(Graduate Univ. for Advanced Studies)*, **Kengo MORIBAYASHI and Hiroki NAKAMURA**

[*J.Chem.Phys.*, **103**, 5512 (1995)]

Quantum mechanically accurate calculations are carried out for the following reactions involving muonium atom (Mu) using the hyperspherical coordinate approach: Mu + H_2 → MuH + H , Mu + D_2 → MuD + D , Mu + HD → MuH (MuD) + D (H) , H + MuH → MuH + H and H + MuD → MuH + D. The initial vibrational state is restricted to the ground state ($v_i = 0$) and the collision energies considered are up to ~ 1.2*eV*. The various aspects of the dynamics, such as the isotope effects, the initial rotational state (j_i) dependence and the final rotational state (j_f) distribution are analyzed for a wide range of j_i and j_f. Some of the isotope effects can be interpreted in terms of the variations in reaction barrier and endothermicity. The following two intriguing features are also found: (1) strong enhancement of reaction by initial rotational excitation and (2) oscillation of integral cross section as a function of collision energy in the case of the Mu-transfer

reactions.

I-N-4 Effects of Vibrational Excitation on Multidimensional Tunneling: General Study and Proton Tunneling in Tropolone

Shoji TAKADA and Hiroki NAKAMURA

[*J. Chem. Phys.*, **102**, 3977 (1995)]

Tunneling energy splittings of vibrationally excited states are calculated quantum mechanically using several models of two-dimensional symmetric double well potentials. Various effects of vibrational excitation on tunneling are found to appear, depending on the topography of potential energy surface; the symmetry of the mode coupling plays an essential role. Especially, oscillation of tunneling splitting with respect to vibrational quantum number can occur and is interpreted by a clear physical picture based on the semiclassical theory formulated recently [Takada and Nakamura, *J. Chem. Phys.* **100**, 98 (1994)]. The *mixed tunneling* in the C region found there allows the wave functions to have nodal lines in classically inaccessible region and can cause the suppression of the tunneling. The above analysis is followed by the interpretation of recent experiments of proton tunneling in tropolone. *Ab initio* molecular orbital calculations are carried out for the electronically ground state. A simple three-dimensional model potential is constructed and employed to analyze the proton tunneling dynamics. Some of the experimentally observed intriguing features can be explained by the typical mechanisms discussed above.

I-N-5 Overlapping-Resonance Scattering and Statistical Theory of Unimolecular Decomposition

Kiyohiko SOMEDA, Hiroki NAKAMURA and Frederick H. MIES*(NIST, USA)*

[*Prog. Theor. Phys. Supplement* **116**, 443 (1994)]

A random matrix model of unimolecular decomposition is investigated based on the Feshbach theory of resonant scattering. Energies of zero-th order quasi-bound states are randomly distributed and coupling matrix elements between these quasi-bound states and continua are generated by Gaussian random numbers. The average decay rate of the quasi-bound states exhibits systematic behavior as a function of density of quasi-bound states, average magnitude of the coupling and number of continua. The average decay rate coincides with the one predicted by the statistical theory of unimolecular decomposition (RRKM theory) when the mean spacing of the quasi-bound states is comparable with the average resonance width. Under this condition, the spectrum of the quasi-bound states is most diffuse and we can neither resolve each quasi-bound state nor even distinguish resonant collision from direct one clearly.

I-N-6 Competition Between Intramolecular Vibrational Energy Redistribution and Unimolecular Dissociation: A Scattering Theoretical Point of View

Kiyohiko SOMEDA, Hiroki NAKAMURA and Frederick H.MIES *(NIST, USA)*

[*Laser Chemistry* **15**, 145 (1995)]

Systematic behavior of decay rates of resonances above dissociation threshold is investigated by using the theory of resonance scattering. The condition for the Rice-Ramsperger-Kassel-Marcus (RRKM) rate formula to be valid is clarified by analyzing the random model of unimolecular dissociation. The decay rate averaged over many resonances agrees with the RRKM rate when the mean spacing and the mean width of the resonance states coincide with each other . On the other hand, auto- and mutual-correlation functions of the non-stationary wave functions indicate a rather paradoxical and intriguing phenomenon: In the RRKM regime, insufficient time is left for intramolecular vibrational energy redistribution (IVR) before dissociation.

I-O Theory of Nonadiabatic Transition due to Curve Crossing

The semiclassical theory of the nonadiabatic transition due to curve crossing, pioneered by Landau, Zener and Stukelberg, has been completed in a form very convenient for various applications. For instance, a formula, as simple as but far better than the famous Landau-Zener formula, has been derived. Multilevel and multidimensional problems are now challenged.

I-O-1 Theory of Nonadiabatic Transition for General Two-state Curve Crossing Problems. I. Nonadiabatic Tunneling Case.

Chaoyuan ZHU and Hiroki NAKAMURA

[*J.Chem. Phys* .,**101**,10630 (1994)]

Based on the achievements for the linear potential model, new accurate and compact formulas are established for general two-state nonadiabatic tunneling type curve crossing problems. These can cover practically the whole range of energy and coupling strength and can be directly applied not only to nonadiabatic tunneling itself, but also to the various problems such as inelastic scattering, elastic scattering with resonance and perturbed bound state problem. All the basic potential parameters can be estimated directly from the adiabatic potentials and the nonunique diabatization procedure is not required. Complex contour integrals are not necessary to evaluate the nonadiabatic transition probability and thus the whole theory is very convenient for various applications. The previously proposed simple and compact formula, better than the famous Landau-Zener formula, is shown to be applicable also to general curved potentials. The explicit expressions are derived also for the nonadiabatic tunnel-

ing (transmission) probability. Now, the present theory can present a complete picture of the two-state curve crossing problems.

I-O-2 Theory of Nonadiabatic Transition for General Two-state Curve Crossing Problems. II. Landau-Zener Case

Chaoyuan ZHU and Hiroki NAKAMURA

[*J.Chem. Phys* .,**102**,7448 (1995)]

New accurate and compact formulas are established for general two-state curve crossing problems in the Landau-Zener case, in which the two diabatic potentials cross with the same sign of slopes. These formulas can cover practically the whole range of energy and coupling strength and can be directly applied to various problems involving the curve crossing. All the basic potential parameters can be estimated directly from the adiabatic potentials and nonunique diabatization procedure is not required. Complex contour integrals are not necessary to evaluate the nonadiabatic transition parameter; thus the whole theory is very convenient for various applications. The compact formula for the Landau-Zener transition probability, which is far better than the famous Landau-Zener formula, is proposed. Now, together with the previous paper [Zhu and Nakamura, *J. Chem. Phys.* **101**, 10630 (1994)], the present semiclassical theory can present a complete set of solutions of the two-state curve crossing problems.

I-O-3 Semiclassical Analysis of Resonance States Induced by Conical Intersection

Chaoyuan ZHU, Evgueni E. NIKITIN *(Technion, Israel and IMS)* **and Hiroki NAKAMURA**

The resonance states induced by nonadiabatic coupling in the conical intersection problem are analyzed semiclassically. Not only the general framework but also the explicit analytical expressions of resonance position and width are presented. Interestingly, the nonadiabatic transition schemes are found to be quite different in two representations employed, i.e.,adiabatic and generalized adiabatic (or dynamical state, or post-adiabatic) representations. In the former case the transition is assigned to be the Landau-Zener (LZ) type and the latter case is analyzed by a mixture of LZ- and Rosen-Zener (RZ) -type in the case of $m > 3/2$ and by the nonadiabatic tunneling (NT) type in the case of $m = 1/2$, where m is the angular momentum quantum number. Both of these semiclassical results agree well not only with each other in spite of the very different schemes but also with the exact numerical results in a wide range of energy and angular momentum.

I-P Theoretical Studies of Characteristics and Dynamics of Superexcited States of Molecules

Superexcited states of molecules show various intriguing properties and participate in a variety of dynamic processes. Their characteristics and dynamics are studied by using the quantum chemical methods and the multichannel quantum defect theory. A general theoretical procedure applicable to diatomic molecules is now developed.

I-P-1 Characteristics and Dynamics of Superexcited States of Molecules

Hiroki NAKAMURA

[*J. Chinese Chem. Soc.* **42**, 359 (1995)]

Characteristics and dynamics of superexcited states of molecules are interpreted by emphasizing their significant roles in various molecular dynamic processes. The states are expected to open a new field of physics and chemistry; but because of their complexity, they should be investigated by using the possible multifarious means from the various view points. The interplays between theory and experiment and also between the two theories, dynamics theory and quantum chemistry, are crucial to reveal this world. More systematic studies are required for the superexcited states of polyatomic molecules.

I-P-2 Characteristics and Dynamics of Superexcited States of CO

Miyabi HIYAMA*(Graduate Univ. for Advanced Studies)* **and Hiroki NAKAMURA**

["Dissociative Recombination: Theory, Experiment and Application", World Scientific, in press]

The theoretical framework which is supposed to be the best for diatomic molecule at present is utilized to investigate the various dynamic processes involving superexcited states of CO. The method is composed of quantum chemical calculations of the electronic states, evaluation of the electronic coupling matrix element as a function of electron energy and internuclear distance and of a nonperturbative solution of the K-matrix integral equation. Some preliminary results of quantum chemical calculations are obtained.

I-Q New Molecular Switching Mechanism

Shinkoh NANBU, Frank O.GOODMAN *(Univ. of Waterloo and IMS)* **and Hiroki NAKAMURA**

Based on the intriguing phenomenon of complete reflection in nonadiabatic tunneling potential systems, the following new possibilities were proposed before by one of the authors: [1] (1)bound states in the continuum and (2)switching the transmission in a periodic potential sys-

tem composed of the same N units of potential of the nonadiabatic tunneling type. Direct numerical demonstrations of these phenomena are now made. Wave functions of the localized states in the continuum are directly obtained by solving the coupled Schroedinger equations. Switching of the transmission can be demonstrated by using wave packet propagations.

Reference

1) H. Nakamura, *J.Chem.Phys.* **97**, 256 (1992).

I-R Laser Assisted Surface Ion Neutralization

Frank O.GOODMAN*(Univ. of Waterloo and IMS)* **and Hiroki NAKAMURA**

[*Progress in Surface Science*, in press]

Some aspects of the theory of LASIN (laser assisted surface ion neutralization) are considered, with emphasis on the physical origins of the so-called "double-peak" structures found in some calculations of the charge-transfer (neutralization) probability, P ,as a function of the laser frequency η.[1] We show that these double-peak structures are all special cases of multiple-peak structures which result from quantum interference effects and that, in fact, the *second* peak is to be considered as the main resonance peak. This result is interesting in itself, because it is the *first* peak which has been considered to be the main resonance peak before now. It is sufficient to simplify the discussion to consideration of a two-level model, which represents the solid valence band by a single level at ε_m , because the results in question are qualitatively independent of the number of levels used to represent the band (provided, of course, that at least one level is used). Clarification of the physical reason for the multiple peaks is based on the semiclassical theory [2] of nonadiabatic transition, in which the peaks are due to the phase difference between the two adiabatic paths which result from diagonalization of the hamiltonian of the two-level system: constructive interferences result in peak maxima and destructive interferences result in peak minima (which are in fact zeros). With the "electronic hopping potential" modelled by $V(t) = V_0\mathrm{sech}(\lambda t)$ and the"laser potential" by $W(t) = W_0\mathrm{sech}(\lambda t)\cos(\eta t + \delta)$, in the usual notation, an approximate analytical expression for $P(\eta)$ is presented for the case $|W_0 / V_0| \ll 1$, which covers most of the previous treatments and is shown to give good agreement with the exact results.

References

1). F.O. Goodman, K.W. Sulston, R.I. Lindsay and S.G. Davison, *Phys. Rev.* **B47**, 10685(1993).
2). H. Nakamura, *Int. Rev. Phys. Chem.* **10**, 123 (1991).

I-S Theoretical Studies of Nonlinear Optical Spectroscopy of Molecules in the Condensed Phase

The nonlinear optical response of molecules in the condensed phase subjected to femtosecond laser pulses is studied using various techniques developed in statistical physics and field theory.

I-S-1 Femtosecond Pump-Probe Spectroscopy of Intermolecular Vibrations in Molecular Dimers

Yoshitaka TANIMURA and Shual MUKAMEL *(Univ. of Rochester)*

[*J. Chem. Phys. (communications)* **103**, 1981 (1995)]

The dynamics of intermolecular vibrations in molecular aggregates can be directly monitored by ultrafast spectroscopic techniques. Starting with the third order response function obtained using the path-integral approach, we calculate the pump-probe spectrum of a molecular dimer, taking into account the effects of an intermolecular vibration coupled to the solvent. The various contributions to the signal which represent distinct Liouville space paths are identified and analyzed.

I-S-2 Field-Theoretical Approach to Vibrational Modes of Molecules in the Condense Phase

Ko OKUMURA and Yoshitaka TANIMURA

[*Phys. Rev.* **E53**, January (1996), in presss]

We study various vibrational modes of molecules more precisely due to the recent development of Laser technique. We generalize the quantum Brownian oscillator model, which has been used to study the vibrational mode of molecules, so as to deal with more realistic cases: we have developed a formalism which allows us to systematically calculate experimental observables, including the anharmonicity of the adiabatic potential. By this formulation we can also deal with the nonlinear coupling between molecules and the heat bath and the anharmonic-oscillator heat bath. Application to absorption spectrum, off-resonant Raman spectroscopy and four-wave-mixing spectroscopy are under going. At the present calculation is made perturbatively though we aim to use the current formalism as a starting point for nonperturbative calculation by using Fukuda's Legendre transformation method.

I-T Dissipation, Tunneling, Nonadiabatic Transition for Curve Crossing Problems in the Condensed Phase

The role of dissipation in curve crossing phenomena in condensed phases is studied. Our goal is to clarify the interplay between the quantal nonadiabatic transition and the dissipation processes.

I-T-1 Electronic Dephasing in Femtosecond Curve Crossing Spectroscopy

Yoshitaka TANIMURA and Shual MUKAMEL *(Univ. of Rochester)*

[*Proc. of in. conf. of Raman spectroscopy*, ed. N.-T. Yu and X.-Y. Li, (John Wiley & Sons, 1995) p. 24]

Femtosecond nonlinear optical spectroscopies provide a powerful tool for studying electronic and vibrational dynamics, including nonadiabatic curve crossing and electron transfer processes. We developed a procedure for incorporating microscopically effects of electronic dephasing in coherent spectroscopies involving strong fields. The approach applies to coherent Raman measurements as well as any other four wave mixing including pump-probe spectroscopy. It is based on equations of motion for phase space wavepackets and provides a simple semiclassical picture for these processes.

I-T-2 Relation between Electronic Coupling and Energy Splitting for Electron Transfer Reactions in the Superexchange Case

Akira OKADA

Relation between the electronic coupling and the energy splitting for electron transfer reactions in the superexchange case is investigated. It has been known that the electronic coupling is half of the energy splitting in a quasi degenerate two state system (not in the superexchange case) and this relation has been commonly used to calculate the electronic coupling. We calculate the energy splitting in the superexchange case according to T.Kato (*Prog. Theor. Phys.*,**4**, 154 (1994)) and C.Bloch(*Nuclear Physics*, **6**, 329 (1958)) and show that the electronic coupling is not half of the energy splitting in this case.

I-U Theoretical Studies of a Strongly Correlated Electron System

We study macroscopic and microscopic electronic structures of strongly correlated electron systems. The purpose of this study is to understand the mechanism of conductivity, superconductivity and magnetization of low dimensional electron systems.

I-U-1 Resonating Hartree-Fock Approach to Electron Correlations in ab initio MO Calculations

Norikazu TOMITA, Seiichiro TEN-NO and Yoshitaka TANIMURA

Electronic structures of molecules are studied using the resonating Hartree-Fock (Res-HF) method. This method has been successfully applied to investigations of large quantum fluctuations in one-dimensional electronic systems. In the Res-HF method, the correlated wavefunctions are approximated by superpositions of non-orthogonal Slater determinants (S-dets), where both CI coefficients and orbitals are variationally optimized. In the calculation of carbon mono-oxide, it is found that a Res-HF wavefunction with two generating S-dets can explain a correlation energy to the same extent of a 175CSF-CASSCF wavefunction. Furthermore, the electrostatic field induced by the Res-HF wavefunction is much better than that of CASSCF. This implies that the Res-HF wavefunctions are much more suitable than the conventional MCSCF wavefunctions to treat dynamic correlation effects.

I-U-2 A Systematic Analysis of the Magnetic Susceptibility in the Itinerant Electron Model

Ko OKUMURA

[*J. Magn. Magn. Mater.* **140-141**, 191 (1995); *Phys. Rev.* **B52**, 13358 (1995)]

The self-consistent renormalization theory of the itinerant electron model was the first theory to show that the Curie-Weiss behavior of the magnetic susceptibility is not peculiar to the localized model. But the theory was justified on the basis of physical intuition so that the improvement of the approximation is a hard problem. In this work the susceptibility is studied by the inversion method, in which the way to improve the approximation is always known in principle. The inversion method advances the Stoner theory systematically since the method is a kind of perturbation theory and its first order calculation reproduces the mean-field theory. The second order of the inversion method is applied for the concrete model for the first time. It is possible to realize the Curie-Weiss law and the lowering of the critical temperature T_c as a result.

I-U-3 The SDW-CDW Phase Transition in the One Dimensional Extended Hubbard Model

Norikazu TOMITA, Akira IKAWA *(Kyoto Univ.)* **and Hideo FUKUTOME** *(Kyoto Univ.)*

[*Synth. Met.* **69**, 679 (1995)]

We study SDW-CDW phase transition in the one dimensional extended Hubbard model at a half-filling. A

scaling analysis using the resonating Hartree-Fock method with the numbers of electrons from 8 to 20 strongly suggests that the ground state is many-fold degenerated ($^1A_1^+$, $^1B_1^+$, $^3A_2^-$ and $^3B_2^-$ states) in the SDW region while it is doubly degenerated ($^1A_1^+$ and $^1B_2^-$ states) in the CDW region. Only the $^1A_1^+$ state makes a continuous phase transition from the SDW state to the CDW one. The $^1B_1^+$, $^3A_2^-$ and $^3B_2^-$ states cross the $^1B_2^-$ state around the phase boundary. We show that the continuous phase transition in the $^1A_1^+$ state is brought about by defects connecting the SDW-CDW domains called halfons. The correlation structures of these states are shown to clarify the origin of the degeneracies of the ground states.

I-V Theoretical Studies of Adsorption Reactions on Solid Surfaces by Molecular-Orbital Cluster Models

I-V-1 The Cluster Model Calculations for Li KVV Transitions on Cu Surface

Takeshi NORO *(Hokkaido Univ.)* **and Eisaku MIYOSHI** *(Kyushu Univ. and IMS)*

Recently Tochihara et al. have found in their studies of Li adsorption on Cu(001) surface that there were two features in the Auger spectra at about 50 eV, which features developed with increasing Li desorption time.[1-2] The peak positions of the features were at 46 eV and 49 eV and both were assigned to Li KVV Auger transitions. Since there is only a single peak of Li KVV Auger at 48.7 eV for a Li film when one use soft X-ray excited Auger electron spectroscopy (AES),[3] it is interesting to answer the question: why are there two peaks for Li KVV Auger on Cu surface. Tochihara and Mizuno propose two possible transitions[1]; one is Li(1s) Li(2s) Li(2s) for 49 eV, whose final state is doubly ionized state from s-type bonding orbitals $(s)^{-2}$ and the other is Li(1s) Cu(3d) Cu(3d), whose final state is doubly ionized state from Cu 3d orbitals $(Cu\ 3d)^{-2}$. The purpose of this study is to elucidate the assignment of the Li KVV Auger transitions from computational point of view by using a simple cluster model. We performed MCSCF and MRSDCI calculations. The model used in this study is $LiCu_5$ cluster. The calculations showed that the peak at 49 eV is assigned to doubly ionized states from s-type bonding orbitals $(s)^{-2}$ and the peak at 46 eV to doubly ionized states from s-type bonding orbitals and localized Cu 3d orbitals $(s)^{-1}\ (3d)^{-1}$.

References
1) H. Tochihara and S. Mizuno, *Surf. Sci.* **279**, 89 (1992).
2) S. Mizuno, H. Tochihara and T. Kawamura, *Phys. Rev.* **B50**, 17540 (1994).
3) M. L. Shek, J. Hrbek, T. K. Sham and G.-Q. Xu, *Surf. Sci.* **234**, 324 (1990).

I-V-2 Molecular-Orbital Study of Li and LiOH Adsorbed on a Cu (001) Surface. II. A Cluster Model Including Image Charges

Tomonari SUMI, Yoshiko SAKAI *(Kyushu Univ.)* **and Eisaku MIYOSHI** *(Kyushu Univ. and IMS)*

Using a simple cluster model, Cu4Li,[1] we calculated the equilibrium Li-surface distance and the Li vibrational frequency perpendicular to Cu(001) surface to be 2.01Å and 309 cm^{-1}, which agreed well with experimental values for Li/Cu(001). However, calculated value for the Li-O stretching vibration in the Cu4LiOH cluster was 895 cm^{-1}, which was far from an experimental value of 600cm^{-1} in LiOH/Cu(001).[2] To improve agreement of theoretical and experimental values of the Li-O vibrational frequency, we considered a cluster model which included image charges of the $Li^{+\delta}\ O^{-\delta'}\ H^{+\delta''}$ adsorbate. The values of the image charges were determined self-consistently. The cluster model with image charges considerably improved the agreement of the theoretical and experimental Li-O vibrational frequencies.

References
1) Y. Sakai, E. Miyoshi and S. Katsuki, *Phys. Rev.* **B52**, in press.
2) S. Mizuno et al., *Surf. Sci.* **264**, 103 (1992).

I-V-3 Model Potentials for Main-Element Atoms and their Application to Molecular Calculations

Yoshiko SAKAI *(Kyushu Univ.)*, **Eisaku MIYOSHI** *(Kyushu Univ. and IMS)*, **Tetsuya ICHIKAWA, Yuzo SUDO and Kouji SANEMATSU** *(Kyushu Univ.)*

To save computational efforts by treating only active electrons in large systems such as model clusters for adsorption on surfaces, it is indispensable to develop effective core potentials (ECPs) or model potentials, which are one of ECPs, for atoms. Model potentials for main element atoms Li through Rn were generated systematically. These model potentials were tested for the molecules CsX, BiX (X=F, Cl, Br and I), XeF_2, XeF_4, IF_2^- and IF_4^- at the levels of Hartree-Fock and CI calculations. The calculated values of bond distances, vibrational frequencies, dissociation energies and ionization potentials agreed reasonably well with available experimental values. For As_2, CASSCF and MRSDCI calculations were performed and the results were comparable with all-electron calculations using high-quality basis sets. It was shown that the model potentials work very well for molecular calculations.

I-W Spin-Orbit CI Studies on Heavy Atomic Systems

We have developed an efficient direct spin-orbit (SO) CI program system, employing various aspects of group theory, such as spin-dependent unitary group, time reversal and double point groups. As applications of this method, we have studied on ICl, IHI andBrHI systems.

I-W-1 Spin-Orbit CI Studies on Non-Adiabatic Interactions in Excited States of ICl Molecule

Satoshi YABUSHITA *(Keio Univ. and IMS)*

We have applied the SOCI method to several electronic excited states of ICl to study the non-adiabatic interactions. We have used the RECP's by Christiansen et al. and the SOCI calculations containing more than two million CSF's of singlet and triplet generated in the second-order CI scheme for each irreducible representation of C_{2v} double group. ICl molecule is know to have two absorption maxima at 2.6 and 5.2eV with the similar intensities. With our theoretical vertical energies and transition moments, we assigned the former to the $B^3\Pi_{0+}$(2431) and the latter to a mixture of $^3\Pi_{0+}$(2341) and $^1\Pi_1$ (2341) and to a smaller extent $^3\Sigma^-_{0+}$(2422). This assignment is contradict the previous one by Balasubramanian, but ours seems to be more physically sensible. One justification of this is the good agreement between experimental and theoretical branching ratios of the photodissociation products of I+Cl, I+Cl* and I*+Cl at 240nm, i.e., experimentally 1:2:2 and theoretically 0.18:0.46:0.36. As for the non-adiabatic interactions among excited states with Ω=0+ symmetry, we have found three avoided crossings, Av-A between the 0+(II)/0^+(III), Av-C between the 0^+(III)/0^+(IV) and Av-B between the 0^+(II)/0^+(IV), the last of which was suggested by Tiemann et al. and proved here for the first time. Our result also indicates that the so-called Z1(II) state, which is actually $^1\Pi_1$ (2431), crosses with the B state just inside the Av-B point, supporting the analyses by Gordon and Tiemann et al. These potential curves also yield wavelength dependency of the theoretical branching ratios, I+Cl/I+Cl*, which is in good agreement with the experiment by de Vries et al. at 480-530 nm. These successful results show the applicability of our theoretical method.

I-W-2 Spin-Orbit CI Studies on the Photo-Detachment Spectra of IHI^- and $BrHI^-$

Satoshi YABUSHITA *(Keio Univ. and IMS)*

Although the potential energy surfaces and resonance features around the transition state region of the chemical reaction, IH+I → $IHI^‡$ → I+IH, have been studied intensively by Neumark et al. with the photodetachment spectroscopy of IHI- and by Schatz with the computation of Franck-Condon factors, there are still several unsolved problems, namely what is the electronic state(s) representing the transition state and how many states are involved as the final states of the photodetachment experiment? We have therefore studied the electronic structures of IHI and BrHI to construct their theoretical photodetachment spectra. We used the RECPs by Christiansen et al. and the basis functions of TZP + diffuse sp+df for halogens and TZ+3p2d for H. In order to obtain the final energies, we used the second-order SOCI method with the Davidson correction. The total number of doublet CSF's became more than 10 millions, even though we used efficiently the double group and time reversal symmetry. To manage this many of CSF's, we employed what we call the "contracted SOCI method". It was found that near degeneracy of the $1\pi_u$,$1\pi_g$ and $2\sigma_u$ orbitals (in case of IHI) causes significant second order SO mixing. This SO effect increases the IH bond distance at the saddle point by 0.02Å for the ground $^2\Sigma^+_u$ (Ω=1/2), while it decreases the IH distance by 0.015Å for $^2\Pi_u$ (Ω=1/2) state. This second order SO effect also has an important effect on the barrier height by increasing it from 2.6 to 5.7 kcal/mol. Employing a simple one dimensional Franck-Condon model for the anti-symmetric Q_3 mode, we have successfully simulated the photodetachment spectra and studied particularly the significant SO effect on the spectra and the importance of more than one electronic states of XHI.

I-X Structures and Dynamics of Condensed Molecular Systems

I-X-1 Growth and Collapse of Structural Patterns in the Hydrogen Bond Network in Liquid Water

Eli SHIRATANI *(Nagoya Univ.)* **and Masaki SASAI** *(Nagoya Univ. and IMS)*

[Submitted to *J. Chem. Phys.*]

Intermittent and chaotic motions of the hydrogen bond network are studied with the molecular dynamics simulation. By analyzing the fluctuation in the radial distribution function, it is shown that individual water molecule alternately goes through two different periods; the structured period and the destructured period. During the structured period the local structure around the molecule is developed more than the average. At room temperature the lifetime of each period is hierarchically distributed from a few hundreds fsecs to several psecs. This intermittent structural fluctuation is quantitatively analyzed by defining a new quantity, local structure index (LSI). Molecules which have the large LSI value have tendency to be close to each other to form clusters. Temporal and spatial correlations of the structural order are studied with this new method. The analyses of the structural fluctuation provide a new perspective to study the collective motion of water molecules.

I-X-2 Conformation, Energy and Folding Ability of Selected Amino Acid Sequences

Masaki SASAI *(Nagoya Univ. and IMS)*

[*Proc. Natl. Acad. Sci.* **92**, 8438 (1995)]

Evolutionary selection of sequences is studied with a knowledge-based Hamiltonian to find the design principle to fold to the model protein structure. With sequences selected by the naive energy minimization, the model structure tends to be unstable and the folding ability is low. Sequences with the high folding ability have not only the low energy minimum but also the energy landscape which is similar to that found for the native sequence over

the wide region of the conformation space. Though there is a large fluctuation in foldable sequences, the hydrophobicity pattern and the glycine locations are preserved among them. Implications of the design principle for the molecular mechanism of folding are discussed.

RESEARCH ACTIVITIES II
Department of Molecular Structure

II-A Laboratory and Astronomical Spectroscopy of Transient Molecules

Vast, cold and low-density space environment is a unique laboratory, whose physical and chemical conditions are rarely attained in the laboratory on Earth. The unique space laboratory is favorable to the existence of transient molecules such as molecular ions, free radicals and unstable molecules, most of which are very exotic and non- terrestrial. These exotic transient molecules are generally difficult and challenging problems for laboratory spectroscopy. Laboratory spectroscopy may be enriched by astronomical studies on non-terrestrial transient species which represent new development in high-resolution molecular spectroscopy. On the other hand, detailed knowledge about new transient molecules obtained by laboratory spectroscopy is essential to a deeper understanding of physical and chemical processes in space. We develop a high-sensitivity submillimeter-wave and far-infrared spectrometers suitable for high-resolution spectroscopy of transient molecules of astronomical interest. We expect that our laboratory spectroscopy may accelerate the mutually beneficial aspect between laboratory spectroscopy and astrochemistry and astrophysics.

II-A-1 Microwave Spectrum of the NiO Radical in the X $^3\Sigma^-$ Ground Electronic State

Kei-ichi NAMIKI*(Graduate Univ. for Advanced Studies)* **and Shuji SAITO**

The diatomic oxides of the 3d transition metal have attracted considerable attention of molecular spectroscopists, because they show very complicated electronic spectra, but give a good systematic example of the chemical bonding which depends on the 3d orbital of the metal and the 2p orbital of oxygen. As one of the 3d transition metal oxides, we studied the microwave spectrum of NiO in the ground electronic state X $^3\Sigma^-$ by using a source modulated submillimeter-wave spectrometer. The NiO radical was generated by dc-sputtering of powdered NiO which was distributed over the inner surface of the cathode. Rotational transitions of ^{58}NiO and ^{60}NiO were measured in the region 110-460 GHz and those of ^{58}NiO in the v=1 were measured in the region 240-370 GHz. The measured frequencies of NiO were least-squares analyzed and its precise molecular constants including the rotational constant, centrifugal distortion constants, spin-rotation coupling constants with their centrifugal distortion terms and centrifugal distortion terms for spin-spin coupling constant were precisely determined and are compared with those derived from optical spectroscopic studies[1-3]

References

1) V. I. Srdanov and D. O. Harris, *J. Chem. Phys.*, **89**, 2748 (1988).
2) E. J. Friedman-Hill and R. W. Field, *J. Mol. Spectrosc.*, **155**, 259(1992).
3) R. S. Ram and P. F. Bernath, *J. Mol. Spectrosc.*, **155**, 315 (1992).

II-A-2 Microwave Spectrum of the TiN Radical in the $^2\Sigma^+$ Ground Electronic State

Kei-ichi NAMIKI*(Graduate Univ. for Advanced Studies)*, **Timothy C. STEIMLE***(Arizona State Univ. and IMS)* **and Shuji SAITO**

The nitrides containing 3d transition metals have also deserved much attention of spectroscopists and theoretical chemists. The nitride of the titanium metal TiN is well characterized by optical spectroscopy, but there has been no pure microwave spectroscopic study on TiN.[1-3] We measured pure rotational transitions of TiN in the ground electronic state $^2\Sigma^+$ by using a submillimeter-wave spectrometer. TiN was produced by dc-sputtering of titanocene dichloride powder which was contained in a small glass boat placed in the inside of the cathode. Nine rotational transitions were measured in the region 260-446 GHz. The rotational and fine structure constants of TiN were revised by the least squares method and are compared with those derived by pump/probe microwave-optical double resonance spectroscopy.[3]

References

1) K. Brabaharan, J. A. Coxon and A. B. Yamashita, Can. J. Phys., 63, 997(1985).
2) T. C. Steimle, J. E. Shirley, K. Y. Jung, L. R. Russon and C. T. Scurlock, J. Mol. Spectrosc., 144, 27(1990).
3) D. A. Fletcher, C. T. Scurlock, K. Y. Jung and T. C. Steimle, J. Chem. Phys., 99, 4288(1993).

II-A-3 Microwave Spectrum of the NCl Radical in the Electronically Excited State, $^1\Delta$

Kaori KOBAYASHI, Masahiro GOTO, Satoshi YAMAMOTO *(Univ. of Tokyo)* **and Shuji SAITO**

Molecules in the metastable electronic state are rarely studied by pure microwave spectroscopy in spite of their importance to high resolution spectroscopy as well as to chemical kinetics. This is because even diatomic molecules in the metastable electronic state are less efficiently produced for detection by microwave absorption spectroscopy. Only several examples have been reported so far: SO(a $^1\Delta$, b$^1\Sigma^+$), O_2 (a $^1\Delta_g$), CO(a $^3\Pi$, a' $^3\Sigma^+$) and NF(a $^1\Delta$). We detected the pure rotational transitions of the NCl radical in the first electronically excited state a$^1\Delta$ with a submillimeter-wave spectrometer. NCl(a $^1\Delta$) was generated by a dc-glow discharge in a mixture of N_2 and Cl_2. Seven rotational transitions were observed in the region 162-404 GHz. Since the magnitude of the nuclear spin-orbit coupling constant for each nitrogen and chlorine nucleus is nearly equal, the matrix elements of the Hamiltonian appropriate for the $^1\Delta$ electronic state are formulated by using the coupling scheme of Hund's case a_β: G=I(Cl)+I(N) and F=J+G. Observed spectral lines were analyzed by a least-squares program based on the

matrix elements derived. The detailed molecular constants of NCl($a^1\Delta$) including the rotational constant, centrifugal distortion constant and detailed hyperfine structure constants for the nitrogen and chlorine nuclei were precisely determined for the first time.

References

1) S. Yamamoto and S. Saito, *J. Chem. Phys.*, **86**, 102 (1987).

II-A-4 Microwave Spectrum of the Isotopomers of HCS^+ and its Substitution Structure

Jian TANG *(Graduate Univ. for Advanced Studies)* **and Shuji SAITO**

[*Astrophys. J.*, **451**, L93 (1995)]

The thioformyl ion HCS^+ is one of the fundamental species in the interstellar sulfur chemistry. It was first detected in the Orion Nebula by Thaddeus, Guélin and Link[1],and was confirmed immediately in the laboratory by Gudeman et al.[2] In the present study the rotational transitions of its isotopomers were observed in the range of 72-396 GHz with a source-modulated submillimeter-wave spectrometer. The rotational constant B_0 was determined to be 18018.262(3), 20444.495(3) and 20991.572(4) MHz for DCS^+, $H^{13}CS^+$ and $HC^{34}S^+$, respectively, with 3σ standard deviations in the parentheses. The substitution bond lengths of HCS^+ were derived to be r_s (CH)=1.0789 Å and r_s(CS)=1.4782 Å.

References

1) P. Thaddeus, M. Guelin and R. A. Linke, *Astrophys. J.*, **246**, L41(1981).
2) C. S. Gudeman, N. N. Haese, N. D. Piltch and R. C. Woods, *Astrophys. J.*, **246**, L47(1981).

II-A-5 Renner-Teller Effect of a Linear Molecule Having Two Bending Modes

Jian TANG *(Graduate Univ. for Advanced Studies)* **and Shuji SAITO**

We have reported the microwave spectrum of a linear carbon-chain radical HCCS in the excited states of two bending modes, ν_4 and ν_5.[1] For a further detailed analysis of the observed spectra, we developed a formulation of the Renner-Teller effect for a linear molecule with two bending vibrations. A vibronic interaction term of the two modes is introduced into the Hamiltonian. Although the matrix elements for the excitation of two modes have been given for the case of $\Delta v = \Delta(v_4+v_5) = \pm 2$ by Petelin and Kiselev,[2] we showed that the matrix elements of $\Delta v=0$ are significant between the states of the (v_4, $v_5 \pm 1$) and ($v_4 \pm 1$, v_5). The effect of the new interaction term to the rotational levels of the $^2\Pi$ electronic state is discussed numerically by varying the relative magnitude of two bending modes. The formulation will be applied to the case of HCCS,when the vibronic energies of the bending modes are made clear.

References

1) J. Tang and S. Saito, *Ann. Rev.*, II-A-6(1994).
2) A. N. Petelin and A. A. Kiselev, *Int. J. Quantum Chem.*, **6**, 701 (1972).

II-A-6 Microwave Spectrum of the CHF_2 Radical (X^2A')

Naomi INADA *(Hiroshima Univ. and IMS)*, **Hiroyuki OZEKI, Shuji SAITO, Ko SAITO** *(Hiroshima Univ.)* **and Michiro HAYASHI** *(Hiroshima Univ.)*

Fluoromethyl radicals CH_nF_{3-n} show a systematic tendency in the molecular structure: plane structure of CH_3[1] to pyramidal structure of CF_3.[2] This has attracted much attention to molecular spectroscopists and quantum chemists.We detected the rotational spectral lines of CHF_2 in the ground electronic state X^2A' for the first time with the microwave spectroscopic method. CHF_2 was produced directly in the free space cell by the reaction of CH_2F_2 with microwave discharge products of CF_4. Many b-type R- and Q-branch transitions which showed fine structure due to electron spin and hyperfine structures due to fluorine and hydrogen nucleus spins were measured in the range 100 to 400 GHz. They were analyzed by the least squares method, resulting in a determination of its detailed and precise molecular constants. A negative and large inertia defect derived indicates that the molecule has a pyramidal structure with symmetry of C_s. This result is consistent with that of a recent sophisticated quantum chemical calculation.[3] The structure of CHF_2 was determined from the rotational constants determined.

References

1) C. Yamada, E. Hirota and K. Kawaguchi, *J. Chem. Phys.*, **75**, 5256 (1981).
2) Y. Endo, C. Yamada, S. Saito and E. Hirota, *J. Chem. Phys.*, **77**, 3376(1982).
3) V. Baron, A. Grand, A. Minichino and R. Subra, *J. Chem. Phys.*, **99**, 6787(1993).

II-A-7 Microwave Spectrum of a New Phosphorus-Containing Free Radical $H_2PO(X^2A')$

Tsuyoshi HIRAO *(Graduate Univ. for Advanced Studies)*, **Shuji SAITO and Hiroyuki OZEKI**

When phosphine PH_3 reacts with oxygen, many phospho-hydroxy intermediates are generated in the gas phase. Among them PH,[1] PH_2, PO, PO_2 and HPO[2] were well characterized by high resolution spectroscopy. However, there still remain many phospho-hydroxy intermediates because the phosphorus atom gives various polymorphous species expressed by a general chemical formula $H_mP_nO_l$. We identified another new intermediate $H_2PO(X^2A')$ in the gas phase for the first time with microwave spectroscopy. H_2PO was produced by a dc-glow discharge in a mixture of phosphine and carbon dioxide. The a-type R-branch transitions were observed by every 37 GHz in the region 149-374 GHz, showing K-structure modified with fine structure due to electron spin and hyperfine structure due to phosphorus and hydrogen nuclei. Several hundred observed spectral lines were analyzed by the least squares method to determine detailed molecular constants with high precision. The molecular constants determined show that this molecule has a symmetry of C_s and a pyramidal structure.

References
1) M. Goto and S. Saito, *Chem. Phys. Letters*, **211**, 443(1993).
2) S. Saito, Y. Endo and E. Hirota, *J. Chem. Phys.*, **84**, 1157(1986).

II-A-8 Microwave Spectrum of the FS_2 Radical in the X^2A'' Ground Electronic State

Jian TANG *(Graduate Univ. for Advanced Studies)* **and Shuji SAITO**

The FS_2 radical, belonging to the thiosulfeno(XS_2) group, is an important intermediate in the fluorination reaction of sulfur-bearing molecules. The presence of the FS_2 radical was first shown in the rf discharge of the SF_6 - O_2 mixture by mass spectrometric study,[1] and the optical spectrum of FS_2 was observed by LIF spectroscopy.[2] In the present study, we observed more than a hundred rotational transitions, both a-type and b-type and each split into four fine and hyperfine components, in the range of 125-185 GHz by the dc discharge of SF_6. The rotational constants and the centrifugal distortion constants, the spin-rotation constants with its centrifugal distortion corrections and the hyperfine interaction constants were determined. The accidental resonance of some rotational energy levels made the parameter $(\varepsilon_{ab}+\varepsilon_{ba})/2$ determined well and induced some forbidden transitions for normal asymmetric-rotors to be observed in the spectrum of FS_2.

References
1) R. J. M. M. Snijkers, J. F. Coulon and G. Turban, *J. Phys. D*, **24**, 1098(1991).
2) Q. Zhuo, J. Karolczak and D. J. Clouthier, *J. Chem. Phys.*, **100**, 6113(1994).

II-A-9 NH_2D in Dark Cloud Cores and Dust-Related Interstellar Chemistry

Shuji SAITO, Hiroyuki OZEKI, Masatoshi OHISHI *(National Astronomical Observatory)* **and Satoshi YAMAMOTO** *(Univ. of Tokyo)*

Recently we mapped NH_2D and CH_3OD lines toward Orion-KL with Nobeyama Millimeter-Wave Array and found that NH_2D and CH_3OD are mainly distributed over the peak intensity regions of NH_3 and CH_3OH in Orion A, respectively. We concluded that most of ammonia and methanol in Orion A originate from dust grains.[1] We consider that such dust related phenomenae happen not only in the energy-rich star forming region, but also in dark clouds. We survey the NH_2D spectral line for 15 dark cloud cores with the 45 m radio telescope of Nobeyama Radio Observatory in 1994 and 1995 and detected relatively strong signals of NH_2D for six cores among seven ones associated with IRAS (infared) sources and for two cores among eight ones not associated with IRAS. We think that most of NH_2D detected toward IRAS sources are produced from dust grains by a kind of energy-rich phenomenae. The detection of NH_2D for two cores without IRAS sources is worth discussing in details. Based on a tentative map of NH_2D for L134N (a dark cloud core without IRAS), we think that NH_2D in L134N should be generated from dust grains by an energy-rich phenomena, though within this dark cloud any thermal or photo source have not been suggested observationally so far.

References
1) S. Saito, H. Mikami, S. Yamamoto, Y. Murata and R. Kawabe, *Astron. Soc. Pacific Conf. Series*, **59**, 241(1994).

II-B Development of a Mt. Fuji Submillimeter-Wave Telescope

Shuji SAITO, Hiroyuki OZEKI, Hideo FUJIWARA, Satoshi YAMAMOTO *(Univ. of Tokyo)*, **Yutaro SEKIMOTO** *(Univ. of Tokyo)*, **Junji INATANI** *(National Astronomical Observatory)*, **Masatoshi OHISHI** *(National Astronomical Observatory)* **and Norio KAIFU** *(National Astronomical Observatory)*

In these years the submillimeter-wave to far infrared region has attracted much attention in the field of astronomy, because the initial stage of star-forming activity or, in other words, the final stage of molecular cloud contraction shows various physical and chemical phenomena in the energy region of this wavelength. Several submillimeter-wave telescopes have now been developed to study astrophysics and astrochemistry of the star-forming region through atomic and molecular lines. Since atmospheric attenuation, mainly due to water vapor, becomes high in the submillimeter-wave to far infrared region, astronomical observations should be made at a high-altitude site with cold environment. We plan to build a submillimeter-wave telescope at the summit of Mt. Fuji. The main scientific purpose of our project is (1) a survey of the neutral carbon(C_I) line at 492 GHz and (2) a search for new simple and fundamental molecules, especially related to dust chemistry, which will make us to understand evolutional physical and chemical processes of the molecular cloud as a whole. In these two years we measured atmospheric transmittance at the summit of Mt. Fuji with a home made radiometer operated at 220 GHz under collaboration with the Mt. Fuji weather station of Japan Meteorological Agency. We found that about 45 % of five months, November of 1994 to March of 1995, has atmospheric optical depth less than 0.06, which is suitable for astronomical observation in the submillimeter-wave region. We also found that Mt Fuji showed much better conditions for submillimeter-wave observastions in the mid winter. In the summer of 1994 we sampled soil and rock from 3 m long cores obtained by a boring machine at the telescope site. It was found that scoria soil is frozen below about 85 cm in depth from the surface and the frozen scoria is hard enough to support a heavy telescope building of 200 ton or more. Detailed investigations are now in progress on the design of the telescope, telescope mounting, telescope base,radome, deicing and antisnow accumulation system, 500 and 700 GHz receivers, back-end acousto-optical spectrometer, data processing and remote control.

II-B-1 Development of Wide-Band Acousto Optical Spectrometers(AOS) for the Mt. Fuji Telescope

Hiroyuki OZEKI, Hideo FUJIWARA, Hisashi YOSHIDA and Shuji SAITO

The acousto-optical spectrometer(AOS) constitutes a central part of a back end system of the Mt. Fuji submillimeter-wave telescope, which converts RF signals coming from a receiver system to a spectral image. Construction of our AOS system is one of the developmental items in the project, because a wide-band(over 1 GHz bandwidth) AOS operating in such a severe environment at the summit of Mt. Fuji requires additional efforts to realize a high stability and reliability over a long period. The AOS system consists of a light source, a diffraction cell, imaging optics and a linear photo-diode array(1024 ch. PDA). The diffraction cell is made of lithium niobate crystal and covers the RF frequency range of 1.6 to 2.6 GHz with the number of resolvable spots of over 1000. The resolution bandwidth is expected to be around 1.0 MHz. The electronic unit integrates and stores the imaging data from PDA and monitors the enviromental condition to ensure the stable performance of the spectrometer. The whole system is operated in remote through IEEE-488 bus.

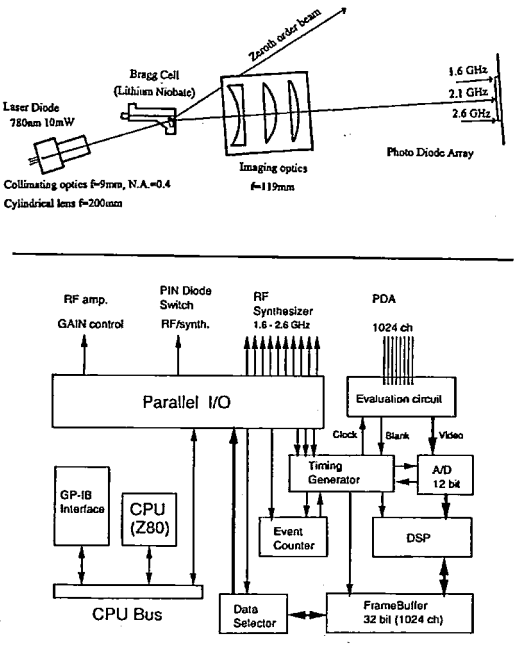

Optics and Electronics designs of the AOS

II-C Laser Investigation of Antiproton-Helium Compounds

A recent discovery of anomalous survival of antiprotons in dense helium media suggested the creation of an antiproton-helium compound ($\bar{p}$ - He^+) . If the creation of such an unusual compound is true, it is the first long-lived exotic atom containing hadrons other than normal protons and neutrons. Moreover, from the viewpoint of atomic and molecular spectroscopy, this new compound is a very attractive object of study, because it has characters of both atoms and molecules; in other words, it is neither an atom nor a molecule, but a completely new entity. Therefore, we started the laser spectroscopic investigation of this compound in order, first, to get a definite evidence of the creation, second, to study its properties and dynamics and finally to explore the possibility of its applications.

II-C-1 A New Laser Induced Resonant Transition at 470.724 nm in the $\upsilon = n - l - 1 = 2$ Cascade of Metastable Antiprotonic Helium Atoms

F.E. MAAS*, R.S. HAYANO*, T. ISHIKAWA*, H. TAMURA*, H.A. TORII* *(*Tokyo Univ.)*, **N. MORITA, T. YAMAZAKI**, I. SUGAI**, K. NAKAYOSHI**** *(**INS, Tokyo Univ.)*, **F.J. HARTMANN†, H. DANIEL†, T. von EGIDY†, B. KETZER†, A. NIESTROJ†, S. SCHMID†, W. SCHMID†** *(†Muchen Tech. Univ.)*, **D. HORVATH** *(KFKI Inst.)*, **J. EADES†† and E. WIDMANN††** *(†† CERN)*

[*Phys. Rev. A* **52**, 1287 (1995)]

With the same observation scheme as was used in our previous experiment, a new laser induced resonant transition in metastable antiprotonic helium atoms has been found. According to theoretical calculations, internal energy levels of the antiprotonic helium atom are classified into two groups; one is a group of metastable states with large principal quantum numbers n and orbital angular momenta l of the antiproton's orbital and the other a group of Auger-dominated short-lived states with smaller l. The antiprotonic helium atoms in metastable states undergo only slow radiative transitions successively, nearly keeping the radial node number $\upsilon = n-l-1$ constant and finally reach Auger-dominated short-lived states that proceed to ionized states ($\bar{p}He^{2+}$) followed by immediate annihilation via the Stark mixing. The last metastable state in each $\upsilon = n-l-1$ cascade can be resonantly deexcited by a laser into the lower Auger-dominated short-lived state, resulting in a sharp peak in the $\bar{p}$-annihilation time spectrum at the laser ignition time. Therefore, by measuring the annihilation counts at this peak as a function of the laser wavelength, we can obtain a resonance profile of the transition. The center wavelength of the new resonance thus observed is 470.724 ± 0.002 nm, which well agrees to theoretical values predicted for the (n=37, l=34)→(36, 33) transition. This fact, along with the previous result on the (39, 35)→(38, 34) transition, provides a clear evidence for the creation of antiprotonic helium atoms. Similar to the previous experiment, we also observed the time dependence of the laser-induced annihilation signals to obtain the decay rate and nascent population in each relevant level, which are summarized in Figure 1 together with those obtained in the previous experiment on the (39, 35)→(38, 34) transition. The decay rates determined in the present experiment are all in good agreement with the theoretical values and this fact also proves the creation of antiprotonic helium atoms. Furthermore, to our surprise, it is seen in Figure 1 that more than 35% of the total metastable population is distributed in the two cascade chains $\upsilon = n-l-1 = 2$ and 3. This fact must have been a good luck

to our success in the observation.

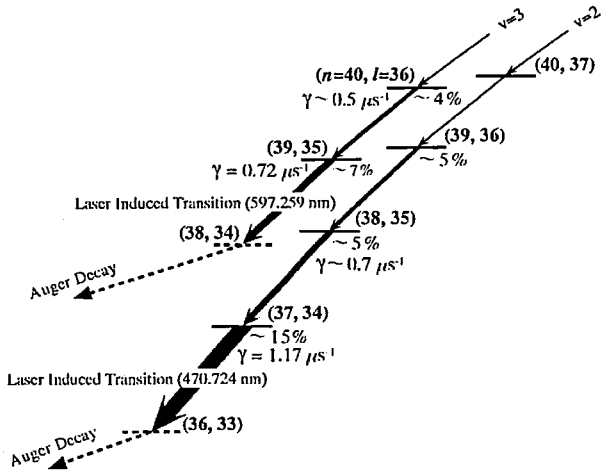

Figure 1. Decay chains of internal energy levels in the antiprotonic helium atom. The experimental decay rate (Υ) and nascent population ratio (in percentage) with respect to the total metastable population are indicated near each level. The thickness of the arrows visualizes the population transferred between each level.

II-C-2 Laser-Induced Resonant Transitions at 593.39 and 463.95 nm in the $v = n - l - 1 = 2$ and 3 Metastable Cascades of Antiprotonic Helium-3 Atoms

H.A. TORII*, M. HORI*, T. ISHIKAWA*, R.S. HAYANO*(*Tokyo Univ.), M. KUMAKURA, N. MORITA, I. SUGAI *(INS, Tokyo Univ.)*, B. KETZER†, F.J. HARTMANN†, H. DANIEL†, T. Von EGIDY†, R. POHL†(†Munchen Tech. Univ.), F.E. MAAS(Mainz Univ.), D. HORVATH *(KFKI Inst.)*, T. YAMAZAKI††, E. WIDMANN†† and J. EADES††(††CERN)

Laser-induced resonant transitions in metastable antiprotonic ^{3}He atoms have been observed with the same experimental scheme as was used for the observation of antiprotonic ^{4}He atoms. In our observation scheme, it is essential that we have some idea beforehand of the location of the metastable/short-lived boundary in the (n, l) plane. For ^{4}He, the Auger-rate calculation by Ohtsuki indicates that metastable $\bar{p}He^+$ levels are those for which the Auger decay requires more than three units of angular momentum change. This led us to the successful observation of two transitions in antiprotonic ^{4}He atoms. No such calculations were available for ^{3}He, but we applied the above principle to the ^{3}He case to obtain the metastable/short-lived boundary and selected the candidates for observable transitions. Despite the lack of Auger lifetime estimates for antiprotonic ^{3}He atoms, high-precision theoretical values for transition wavelengths have recently been calculated. By using a molecular-expansion variational method, Korobov has calculated the transition energies for antiprotonic ^{4}He and ^{3}He atoms. His values for the antiprotonic ^{4}He atoms are 597.23 nm for the (39,35)→(38,34) transition (experimental value 597.259 ± 0.002 nm) and 470.71 nm for the (37,34)→(36,33) transition (experimental value 470.724 ± 0.002 nm), both within 30 ppm of the observed values. These are much more accurate than the theoretical values available to us during our previous experiments, which typically had an accuracy of ~1 nm. We therefore set our scan range to a few hundredths of a nm around Korobov's prediction and succeeded once again in observing resonant transitions. Two transitions were observed and their center wavelengths were determined to be 593.388 and 463.946 nm. These values are both in good agreement with Korobov's theoretical predictions within a discrepancy of 50 ppm. From this agreement with Korobov's values, we can conclude with confidence that the 593 nm resonance is the (38,34)→(37,33) transition in the $v = n$-l-1 = 3 chain and that the 464 nm resonance is the (36,33)→(35,32) transition in the $v = n$-l-1 = 2 chain. If the l-value were changed by one unit for the 593 nm (464 nm) transitions, the measured and predicted wavelengths would disagree by more than 0.3 nm (1.0 nm). The present assignment is also consistent with the aforementioned rule on the Auger decay rates.

II-D Laser Cooling and Trapping of Neutral Atoms

When an atom absorbs or emits a photon, the atom is accelerated or decelerated because a photon has momentum. On the other hand, a strong radiation field modifies the internal energy of an atom, so that an atom in an inhomogeneous radiation field receives a force from the field. The former mechanism allows us to cool the translational temperature of neutral atoms to an extremely low temperature by laser radiation and the latter enables the spatial control of neutral atoms with lasers. As the ranslational temperature goes down to nano kelvin region, the atomic de Broglie wavelength becomes a macroscopic size and macroscopic quantum-mechanical collective motion of atoms can then be expected to occur. The long de Broglie wavelength also enables us to realize an atomic interferometry. On the other hand, the easy control of atomic spatial position and velocity with lasers is expected to open the possibility of various applications. For these reasons, we have been studying the laser cooling and trapping of neutral atoms.

II-D-1 Measurement of Penning Ionization Rates in Ultracold Collisions between Excited Helium Atoms in a Magneto-Optical Trap

Mitsutaka KUMAKURA and Norio MORITA

We have determined Penning ionization rates in ^{4}He*-^{4}He* and ^{3}He*-^{3}He* ultracold collisions in a magneto-optical laser trap. The Penning ionization process is known to be the main loss mechanism in laser traps of rare gas atoms, so that it should be studied and overcome to increase the trap density.

For the He trap at a fixed temperature of about 600 μK, two kinds of measurement were carried out to determine the ionization rate; one was simply to observe the time evolution of fluorescence intensity from the trap after atomic feeding was shut off with the trapping laser continuously kept on. Figure 1 (a) shows a time-resolved fluorescence spectrum thus obtained for the trap of ^{4}He atoms. In this case, we found that the decay rate was line-

arly dependent on the trap density and the rate coefficient was determined to be 3.2×10^{-9} cm $^3s^{-1}$ for the ^{4}He trap and 6.3×10^9 cm^3 s^{-1} for the ^{3}He trap. Since the typical trap density was 4×10^{10} cm^{-3}, the ionization rates at this density were estimated to be 1.3×10^2 s^{-1} and 2.5×10^2s^{-1} for the ^{4}He and ^{3}He traps, respectively. Although these values represent the collisional ionization rates in the real trap, which is always irradiated by the trapping laser resonant with the $2s^3S \rightarrow 2p^3P$ transition, those ionization processes are due to a mixture of 2*s*-2*s*, 2*p*-2*p* and 2*s*-2*p* collisions. We then performed another measurement to obtain the ionization rate only due to the 2*s*-2*s* collision; after atomic feeding was shut off, the trapping laser was alternately on and off with a repetition rate of 10 kHz and a duty ratio of 10%. Figure 1 (b) shows a time-resolved fluorescence spectrum observed with this method in the ^{4}He trap. In this case, since the fluorescence lifetime of the upper level (2*p*) is 97 ns, the trapped atoms spend 90% of the time in the lower level (2*s*). Therefore, the decay rate of the envelope of successive fluorescence peaks at the laser-on periods approximately represents the ionization rate only due to the 2*s*-2*s* collision. However, the ionization rates thus obtained for the ^{4}He and ^{3}He traps, 1.1 s^{-1} and 1.5 s^{-1}, respectively, were both independent of the trap density. This means that the ionization rates due to the 2*s*-2*s* collision were much smaller than those caused by collisions with residual gases in the vacuum chamber used. From these results, we see that the ionization rates due to the 2*s*-2*s* collision are more than two orders of magnitude smaller than those due to the mixed collision processes under the normal trap condition. This fact means that, if we can somehow trap only the 2*s* atoms, it is possible to increase the trap density by more than an order of magnitude. On the other hand, it is also found that the ionization rates for ^{3}He are considerably larger than for ^{4}He. This must be because of the presence of hyperfine structures in ^{3}He and also because of the difference in nuclear exchange symmetry in the collision complex He^*-He^*, though more detailed analysis is still necessary for further discussion.

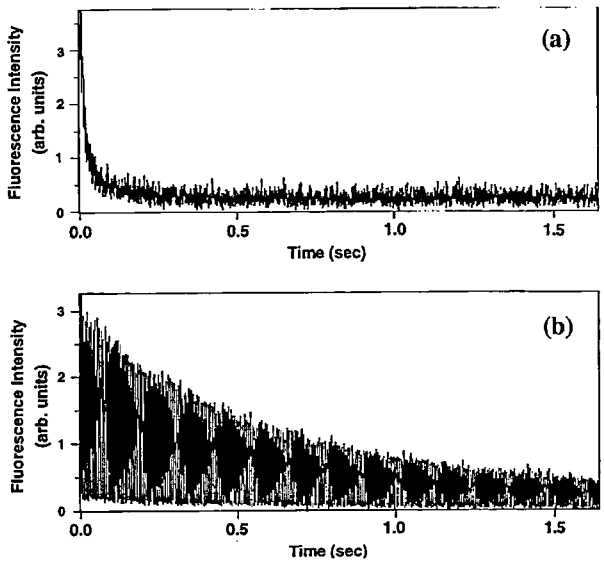

Figure 1. Time evolution of fluorescence from the trap after atomic feeding is shut off with the trapping laser (a) continuously kept on and (b) alternately on and off with a frequency of 10 kHz and a duty ratio of 10%.

II-E Molecular Science of Biomolecules

Elucidation of a structure-function relationship of proteins is a current subject of this group. The primary technique used for this project is the stationary and time-resolved resonance Raman and absorption spectroscopies. The main themes that we want to explore are (1) mechanisms of oxygen activation by enzymes, (2) mechanisms of electron- and proton-transfers through proteins and their coupling in energy transducing membranes, (3) primary processes of photoreceptor proteins and (4) higher order protein structures and their dynamics. In category (1), we have examined stationary complexes of a variety of cytochrome oxidases, cytochrome P-450's and peroxidases and also treated their enzymatic reaction intermediates by using the mixed flow transient Raman apparatus and the Raman/absorption simultaneous measurement device. We recently demonstrated that the so-called "peroxy" and "ferryl" intermediates of cytochrome oxidase in the dioxygen reduction are also generated in the reaction of oxidized cytochrome oxidase with H_2O_2. For (2) we have investigated cytochrome *c* oxidase, while for (3) we treated a bacterial photosynthetic reaction center. For (4), we developed a novel technique for UV Raman measurements based on the combined use of the first/second order dispersions of two gratings in an ordinary double monochromator and applied it successfully to 244-nm-excited RR spectra of several proteins including phytochrome, hemoglobin and viruses. A new spinning cell system developed for UV Raman experiments requires a small amount of samples and therefore, it became possible to determine the UVRR spectra of mutant proteins. We applied this system to β37 and α42 mutant of Hb A and established the Raman spectra of β37 Trp and α42 Tyr of Hb A in the T and R quaternary structures.

II-E-1 Time-Resolved Resonance Raman Evidence for Tight Coupling between Electron Transfer and Proton Pumping of Cytochrome *c* Oxidase upon the Change in Heme Oxidation State from Fe^{V}=O to Fe^{IV}=O

Takashi OGURA, Shun HIROTA, Denis A. PROSHLYAKOV, Kyoko SHINZAWA-ITOH (*Himeji Inst. of Tech*), **Shinya YOSHIKAWA** (*Himeji Inst. of Tech*) **and Teizo KITAGAWA**

Mechanism of dioxygen reduction catalyzed by cytochrome *c* oxidase, the terminal enzyme of the respiration chain of aerobic organisms, has been investigated with time-resolved resonance Raman spectroscopy. Five oxygen-isotope-sensitive bands have been identified for $^{16}O_2$ /$^{18}O_2$ intermediates at 571/544, 804/764, 356/342, 785/750 and 450/425 cm^{-1} in the order of appearance. The first and last ones, which have been assigned to the Fe^{III}-O_2^- and Fe^{III}-OH stretching modes, respectively, are in general consensus, but the remaining three bands are currently under debate. This study establishes that the

804/764 cm^{-1} species is generated prior to the 785/750 cm^{-1} species, although both bands have been assigned to the Fe=O stretching mode and that the reduction rate from the 804/764 to 785/750 cm^{-1} species was distinctly slower in D_2O than in H_2O. Thus, this study suggests that the O-O bond is heterogenically cleaved at the binuclear site to form an Fe^V=O state with the 804/764 cm^{-1} bands and that the electron transfer to the Fe^V=O heme is coupled tightly with the proton translocation.

II-E-2 Microcirculating System for Simultaneous Determination of Raman and Absorption Spectra of Enzymatic Reaction Intermediates and its Application to the Reaction of Cytochrome *c* Oxidase with Hydrogen Peroxide

Denis A. PROSHLYAKOV, Takashi OGURA, Kyoko SHINZAWA-ITOH (*Himeji Inst. of Tech*), **Shinya YOSHIKAWA** (*Himeji Inst. of Tech*) **and Teizo KITAGAWA**

[*Biochemistry* in press]

A new high-performance device for Raman/ absorption simultaneous determination was developed. This was combined with a newly designed microcirculating system of sample and was successfully applied to study intermediates in the reaction of bovine oxidized cytochrome *c* oxidase (CcO) with hydrogen peroxide under steady state conditions at ambient temperatures. Measurements with this device made it possible to directly correlate the species defined in terms of the visible absorption characteristics with specific Raman bands. The "607 nm" form of the enzyme obtained with $H_2{}^{16}O_2$ gave an oxygen-isotope sensitive band at 804 cm^{-1} (769 cm^{-1} with $H_2{}^{18}O_2$) in the Soret excited resonance Raman (RR) spectrum. Its frequency and isotopic frequency shifts are exactly the same as those observed previously with 607 nm excitation for the "607 nm" form, for which the presence of an oxoiron heme was demonstrated. The so-called "580 nm" form of the enzyme obtained with $H_2{}^{16}O_2$ gave the main oxygen-isotope-sensitive band at 785 cm^{-1} (750 cm^{-1} with $H_2{}^{18}O_2$), but appeared to consist of multiple species. This band was assigned to the Fe^{IV}=O stretching mode of ferryloxo heme on the basis of its isotopic frequency shift. Another oxygen-isotope-sensitive band was found at 355 cm^{-1} (340 cm^{-1} for $H_2{}^{18}O_2$) similar to the case of dioxygen reaction. Temporal behavior of this band did not agree with either that of the 804 cm^{-1} band or that of the 785 cm^{-1} band, but seemed to grow between the two species. The RR spectra in the higher frequency region of the "607 nm" and "580 nm" forms excited at 427 nm were quite alike and did not support the formation of a porphyrin π cation radical.

II-E-3 Resonance Raman/Absorption Characterization of the Oxo-intermediates of Cytochrome *c* Oxidase Generated in its Reaction with Hydrogen Peroxide: pH and H_2O_2 Concentration Dependence

Denis A. PROSHLYAKOV, Takashi OGURA, Kyoko SHINZAWA-ITOH (*Himeji Inst. of Tech*), **Shinya YOSHIKAWA** (*Himeji Inst. of Tech*) **and Teizo KITAGAWA**

[*Biochemistry* in press]

The oxo-intermediates of cytochrome *c* oxidase (CcO) derived from the reaction with H_2O_2 have been studied at various pH values and H_2O_2 concentrations, to compare them with intermediates in the dioxygen reduction. Intermediates were maintained in steady states by supplying H_2O_2 at a constant rate and subjected to the high-performance Raman/absorption simultaneous determination technique reported previously (Proshlyakov et al., submitted). The "607 nm" form became less prominent with increasing pH from 7.4 to 10.0 with concomitant increase of the "580 nm" form. At pH 6.0, however, the "607 nm" form disappeared, leaving a peak near 580 nm. The Fe=O stretching ($\nu_{Fe=O}$) frequencies of the oxo-heme of the "607 nm" form, observed at 804/769 cm^{-1} for their $H_2{}^{16}O_2/H_2{}^{18}O_2$ derivatives, were unaltered in the pH range from 7.4 to 10.0 and exhibited D_2O sensitivity even at pH 10.0, indicating that the hydrogen bond between the iron-bound oxygen and some distal residue is retained at pH 10. At neutral pH, two other oxygen-isotope-sensitive Raman bands have been observed at 785/750 cm^{-1} and 355/340 cm^{-1} when the "580 nm" form was dominant. The former and latter Raman difference peaks disappeared above pH 8.5 and 9.0, respectively, under medium concentrations of peroxide inspite of the prominent 580 nm absorption band present. Under the saturating concentrations of peroxide, however, these Raman bands were observed even at pH 10.0 and their frequencies remain unaltered between pH 7.4 and 10.0, although in the absence of peroxide no bands were observed despite of dominance of the "580 nm" form. At high concentrations of H_2O_2, the "607 nm" form was completely replaced with the "580 nm" form and in the absence of H_2O_2, the "580 nm" form was slowly decomposed to the oxidized form. These results indicate that while the "607 nm" form is the detectable primary intermediate for the reaction of oxidized CcO with H_2O_2, both the formation and decomposition of the "580 nm" form requires H_2O_2. While the different pH dependences of the two oxygen-isotope-sensitive Raman bands indicated the presence of two separate species in the name of the "580 nm" form, the disappearance of the isotope labeling of the "580 nm" form means that the exchange of the heme-bound oxygen with that of bulk water surpasses the formation rate of the "580 nm" form at alkaline pH. Such an oxygen exchange with bulk water did not occur in the "607 nm" form. Upon exchange of solvent from H_2O to D_2O, the prominent 607 nm band observed in H_2O significantly decreased in intensity with concomitant increase of the 580 nm band, indicating that the overall reaction rate is limited by a proton transfer reaction step which could be a key step of the redox linked proton pumping in the dioxygen reduction.

II-E-4 Ultraviolet Resonance Raman Studies of Hemoglobin Quaternary Structure Using a Tyrosine-α42 Mutant: Changes of $\alpha_1\beta_2$ Subunit Interface Upon the T → R Transition

Masako NAGAI *(Kanazawa Univ. School of Medicine)*, **Kiyohiro IMAI***(Osaka Univ. School of Medicine)*, **Shouji KAMINAKA** *(Kurume Univ. School of Medicine)*, **Yasuhisa MIZUTANI and Teizo KITAGAWA**

[*J. Mol. Struct.* in press]

Quaternary structure changes between T (tense) and R (relaxed) states of human hemoglobin A (Hb A) and its α42Tyr mutant, obtained through site-directed mutagenesis, were investigated by ultraviolet resonance Raman (UVRR) spectroscopy using 235-nm excitation. Raman excitation at 235 nm enabled us to detect bands of tryptophan (Trp) and tyrosine (Tyr) residues. UVRR spectral contribution of α42Tyr, which is located in the "switch" region of $\alpha_1\beta_2$ interface and forms H-bond with the carboxylate side chain of β99Asp only in the T state, was extracted for each of deoxy- and CO-forms by subtracting the spectra of Hb αY42H from those of Hb A. This demonstrated that α42Tyr is responsible for frequency shifts of Y8a (1619 cm^{-1}) and Y9a (1179 cm^{-1}) of Tyr RR bands of Hb A but other Tyr residues are involved in intensity changes. The UVRR spectral changes of Trp bands upon ligand binding were similar between Hb A and Hb αY42H, indicating that the conformation changes of Trp residues of Hb A and Hb αY42H upon the quaternary structure change are alike. In order to get insight into implications of these changes of Tyr UVRR bands of Hb A between the R and T states, UVRR spectra of free Tyr and *p*-cresol in various solvents were examined with 235-nm excitation. UVRR spectrum of Tyr in Hb A was similar to that of Tyr in an aqueous solution but distinct from that of Tyr in crystalline powders. The ν_{8a} band of *p*-cresol was upshifted and intensified in H-bond forming solvents, irrespective of an H-bond donor or acceptor, compared with that in a non-H-bonding solvent. Accordingly, the frequency shifts of Y8a and Y9a of Hb A upon the T→R transition was ascribed to the H-bond formation of α42Tyr in the T state.

II-E-5 Resonance Raman Study on Axial Ligands of Heme Irons in Cytochrome *bd*-Type Ubiquinol Oxidase from *Escherichia coli*

Shun HIROTA, Takashi OGURA, Yasuhiro ANRAKU *(Univ. of Tokyo)*, **Robert B. GENNIS** *(Univ. of Illinois)* **and Teizo KITAGAWA**

[Biospectroscopy in press]

Resonance Raman spectra of cytochrome *bd* -type ubiquinol oxidase enriched with Fe-isotopes were investigated with excitation at 406.7, 424.0, 441.6 and 647.1 nm. The bands of reduced form at 252 and 400 cm^{-1} were tentatively assigned to ν_{Fe-His} of high-spin b_{595} and ν_{Fe-Met} of low-spin b_{558}, respectively. The ν_{Fe-O2} and δ_{FeOO} bands of heme *d* -O_2 were observed at 568 and 432 cm^{-1}, respectively. The ν_{Fe-CO} frequency of heme *d* -CO was unusually low (477 cm^{-1}) but the ν_4 frequency was not of P-450 type. Therefore, the axial ligand of heme *d* would not be an ordinary histidine or cysteine.

II-E-6 Molecular Structure of Redox Metal Centers of the Cytochrome *bo* Complex from *Escherichia Coli:* Spectroscopic Characterization of the Subunit I Histidine Mutant Oxidases

Motonari TSUBAKI *(Himeji Inst. of Tech.)*, **Tatsushi MOGI** *(Univ. of Tokyo)*, **Hiroshi HORI** *(Osaka Univ.)*, **Shun HIROTA, Takashi OGURA, Teizo KITAGAWA and Yasuhiro ANRAKU** *(Uinv. of Tokyo)*

[*J. Biol. Chem.* **269**, 30861-30868 (1994)]

A site-directed mutagenesis study on the conserved subunit I histidines of the cytochrome *bo* complex in *Escherichia coli* identified ligands of the low-spin heme B and Cu_B centers, although the assignment of the proximal ligand of the high-spin heme O was ambiguous (Minagawa, J., Mogi, T., Gennis, R. B. and Anraku, Y. (1992) *J. Biol. Chem.* **267**, 2096-2104). We have extended this work and characterized the metal centers in the purified histidine mutant oxidases by optical, EPR and resonance Raman spectroscopies and by biochemical analysis. We found that the H284A and H333A oxidases contain two heme B molecules, which exhibit the g_z=2.99 low-spin and cyanide-sensitive $g_\perp$ =6 high-spin EPR signals, while the H419A oxidase contains only low-spin heme B, which shows the g_z component in a considerably higher magnetic field at g=2.92. The Cu_B center was partially retained in the H284A oxidases. Thus, we concluded that His419 is the proximal ligand of the high-spin heme O and that His284 is located at the distal side of the high-spin heme O. His 284 plays an indispensable role in maintaining the structure of the Fe_o-Cu_B binuclear site suitable for the exogenous ligand binding in the reduced state since its substitution eliminated the CO-binding activity. In addition, we found that His106 and His421 are in fact the axial ligands of the low-spin heme B though the H421A mutation perturbed the binuclear metal center seriously. Based upon experimental results with isotopic substitutions on iron in the oxidases, we assigned the Raman band at 208 cm^{-1} to the iron-histidine stretching mode($\nu_{Fe^{2+}-N(His)}$) of the wild-type ferrous cytochrome *o* , which was upshifted slightly by a loss of the Cu_B center in the H333A oxidase. A molecular structure of the metal centers and a possible mechanism of the electron transfer-coupled proton pumping in the cytochrome *bo* complex are proposed on the basis of our present findings.

II-E-7 Unusual Conformational Behavior of Oligomeric Poly(oxyethylene) Chains in Dilute Aqueous Solution: A Raman Spectroscopic Study

Hiroatsu MATSUURA *(Hiroshima Univ.)*,**Sei MASATOKI** *(Hiroshima Univ.)*, **Motomu TAKAMURA** *(Hiroshima Univ.)*, **Keiji KAMOGAWA and Teizo KITAGAWA**

Conformational behavior of oligomeric poly

(oxyethylene) (POE) chains in aqueous solution has been studied by Raman spectroscopy. The spectra of aqueous solutions, with mole fractions down to 0.005, of short POE compound $CH_3(OCH_2CH_2)_mOCH_3$ (m=1-4) were measured with a newly developed multi-reflection cell. The observed spectra show that, with increasing water fraction, the preference of the gauche conformation of the O-CH_2-CH_2-O segment increases, but it decreases on passing a particular composition of the solution. A new structure model of the POE-water system was proposed to explain this unusual conformational behavior. The significant gauche preference of the POE chain in water is associated in large part with the conformational adaptation of the POE segments to the water structure. For concentrations lower than the composition giving maximum gauche population, the stability of the gauche-preferred POE-water structure is diminished owing to the development of a region of water molecules not directly interacting with the POE chain. The important feature of the present model is that the structured network of water with POE chains favorably incorporated is stabilized by interlinking one another without being interrupted by heterogeneous regions such as bulk-link water regions.

II-E-8 Synthesis, Characterization and Reversible Oxygenation of μ-Alkoxo-diiron(II) Complexes with a Dinucleating Ligand, N,N,N',N'-Tetrakis {2-(6-methylpyridyl)methyl}-1,3-diaminopropan-2-olate

Yoshihito HAYASHI *(Kanazawa Univ.)*, **Takayuki KAYATANI** *(Kanazawa Univ.)*, **Hideki SUGIMOTO** *(Kanazawa Univ.)*, **Masatatsu SUZUKI** *(Kanazawa Univ.)*, **Akira UEHARA** *(Kanazawa Univ.)*, **Yasuhisa MIZUTANI, Teizo KITAGAWA and Yonezo MAEDA** *(Kyushu Univ.)*

[*J. Am. Chem. Soc.* in press]

Two new types of dinucleating ligands, symmetric Me_4-tpdp and asymmetric Me_2-tpdp, were synthesized, (Me_4-tpdp=N,N,N',N'-tetrakis {2-(6-methyl-pyridyl) methyl}-1,3-diaminopropan-2-olate and Me_2-tpdp=N,N-bis {2-(6-methylpyridyl)methyl}=N',N'-bis(2-pyridyl-methyl)-1,3-diaminopropan-2-olate). Their μ -alkoxo-diiron (II) complexes [Fe_2(Me_4-tpdp) (C_6H_5COO) (H_2O)](BF_4)$_2$ (**1**), [Fe_2(Me_4-tpdp) (CF_3CO_2)(H_2O)](BF_4)$_2$ (**2**) and [Fe_2(Me_4-tpdp) (CF_3CO_2)](BF_4)$_2$·H_2O (**3**) were synthesized and the structure of complex **1** was determined by X-ray crystallography. Complex **1** crystallizes in monoclinic space group $P2_1/n$ with *a* =19.257 (2) Å, *b* =17.166 (3) Å, *c* =12.558 (2)Å, β=96.55 (1)° and Z=4. The complex has a doubly bridged structure with μ -alkoxo of Me_4-tpdp and μ -benzoate and contains two distinct iron centers: one five-coordinate iron center with N_3O_2 donor set and one six-coordinate iron center with N_3O_3 donor set with an additional coordinated water molecule. Introduction of 6-methyl group in pyridyl group results in an elongation of the Fe-N(pyridyl) bond distances. The Fe-N and Fe-O bond distances in the six-coordinate iron center are substantially longer than those in the five-coordinate iron center except for the Fe-N(tertiary amine) bonds. Mösbauer spectrum of **1** exhibited two sets of quadrupole doublets corresponding to the two distinct iron centers. Electronic spectra of **1** revealed that dissociation of a coordinated water occurs in CH_2Cl_2 to form two five-coordinate iron centers, whereas in DMSO six-coordinate iron centers are predominant due to the coordination of DMSO. Complexes **1** and **2** showed the reversible oxygenation at -40°C, whereas the reversible oxygenation was not observed for complex **3**. The thermal stability of the oxy-complexes against irreversible oxidation are highly dependent on the electron donor ability of ligands; introduction of 6-methyl group in pyridyl group weakens the electron donor ability of pyridyl nitrogen and stabilizes oxy-form against irreversible oxidation. Resonance Raman spectrum of oxy-**1** exhibited two oxygen-isotope sensitive bands in the ν(O-O) region and two bands in the ν(Fe-O) region. The presence of two ν(O-O) Raman bands at 918 and 891 cm^{-1} are interpreted in terms of Fermi-resonance, while the two ν(Fe-O) bands are assigned to the symmetric and anti-symmetric combinations of Fe-O stretching of Fe-O-O-Fe unit. Thus the Raman spectra indicated the formation of μ-peroxo species. The oxygen affinities ($P_{1/2}$) of the complexes were determined for the first time by spectrophotometric methods; those of **1** and **2** in CH_2Cl_2 at -40°C are ca. 6 and ca. 41 Torr, respectively.

II-E-9 Observation of Multiple CN-Isotope-Sensitive Raman Bands for CN-Adducts of Hemoglobin, Myoglobin and Cytochrome *c* Oxidase; Evidence for Vibrational Coupling between the Fe-C-N Bending and Porphyrin In-Plane Modes

Shun HIROTA, Takashi OGURA, Kyoko SHINZAWA-ITOH *(Himeji Inst. of Tech)*, **Shinya YOSHIKAWA** *(Himeji Inst. of Tech)* **and Teizo KITAGAWA**

The CN-isotope-sensitive resonance Raman (RR) bands were investigated for CN^- adducts of hemoglobin (Hb), myoglobin (Mb) and cytochrome *c* oxidase (CcO). All proteins gave the CN-isotope-sensitive bands around 450-480 and 340-440 cm^{-1}. CyanometHb ($HbCN^-$) gave an intense isotope-sensitive band at 452, 448, 447 and 443 cm^{-1} for $^{12}C^{14}N^-$, $^{13}C^{14}N^-$, $^{12}C^{15}N^-$ and $^{13}C^{15}N^-$. CyanometMb ($MbCN^-$) gave them at similar frequencies, but CN-bound resting CcO (CcO_{rest}·CN^-) gave them at distinctly higher frequencies; 478 cm^{-1} ($^{12}C^{14}N^-$), 473 cm^{-1} ($^{13}C^{14}N^-$), 473 cm^{-1} ($^{12}C^{15}N^-$) and 468 cm^{-1} ($^{13}C^{15}N^-$). They are shifted slightly to lower frequencies in the reduced form (CcO_{red}·CN^-); 475 cm^{-1} ($^{12}C^{14}N^-$), 472 cm^{-1} ($^{13}C^{14}N^-$), 472 cm^{-1} ($^{12}C^{15}N^-$) and 465 cm^{-1} ($^{13}C^{15}N^-$). The monotonous feature of the frequency changes against the increase of total mass of CN^- suggest that these bands arise from the Fe-CN^- stretching mode (ν_{Fe-CN^-}). The higher frequency of ν_{Fe-CN^-} for CcO than those for $MbCN^-$ and $HbCN^-$ suggests that the CN^- binding site of CcO has special environments presumably due to the presence of the Cu_B ion. Besides this main band, several weak CN^- -isotope-sensitive bands were observed below 440 cm^{-1}, but the pattern of the isotope-difference spectra were specific to each protein. These low frequency difference peaks were significantly weaker in intensity for ^{15}N isotopes compared with ^{13}C isotopes in common. The band fitting calculations indicated that the Raman intensi-

ties of several porphyrin vibrations are altered by CN-isotopes without changing their frequencies. This suggests that the $FeCN^-$ bending mode (δ_{FeCN^-}) is present around ~380 cm^{-1} and this mode is coupled with more than two porphyrin vibrations which differ among Hb, Mb and CcO. The CN^- stretching (ν_{CN^-}) Raman band was observed for the first time at 2227 cm^{-1} for $MbCN^-$.

II-F Vibrational Spectroscopy of Molecules in Transient States

Raman spectroscopy reveals the vibrational spectrum of a molecule, which is sensitive to geometrical as well as electronic structures. When a wavelength of the probe beam is tuned within the absorption band of the molecule in question, resonance enhancement of Raman intensity takes place and thus makes it possible to detect Raman scattering from an excited molecule or a reaction intermediate even if its population is considerably small. We have taken this advantage of resonance effects to explore the structures of metalloporphyrins and free-base porphyrins in the excited singlet and triplet states. By using various isotope-labeled porphyrins, we established vibrational assignments of excited states. This year we constructed a picosecond pump/probe time-resolved Raman measurement system with the time resolution of 1.7 ps. It was successfully applied to observe RR spectra of vibrationally hot Ni-porphyrin in a dd electronic excited state and to determine the vibrational temperature from the intensity of Stokes/anti-Stokes Raman bands. In order to vary the pump wavelength in a relatively wide range, optical parametric oscillation was introduced successfully.

II-F-1 Time-Resolved Resonance Raman Spectra of Meso-Substituted Copper Porphyrins in the T_1 State: Implication for the Solvent Dependent Red-Shift of Emission Spectra

Motoko ASANO-SOMEDA, Shin-ichiro SATO, Katsuhiro AOYAGI *(Fukushima Natl. College of Tech.)* **and Teizo KITAGAWA**

[*J. Phys. Chem.* **99**, 13800-13807 (1995)]

Time-resolved resonance Raman (TR^3) spectra were obtained with a pump/probe technique using two 7 ns pulsed lasers for Cu(II) complexes of four meso-substituted porphyrins, including tetra-phenylporphin (TPP), tetra (3,4,5-trimethoxyphenyl) porphin ($T_{3,4,5OMe}PP$), tetramesitylporphin(TMP) and tetra-(pentafluorophenyl)porphin($T_{F5}PP$). These copper (II) porphyrins were examined in order to elucidate why emission spectra of (TPP)Cu and ($T_{3,4,5OMe}PP$)Cu are significantly red-shifted in fluid media compared with in rigid media, while those of (TMP)Cu and ($T_{F5}PP$)Cu do not exhibit remarkable shift. All porphyrin skeletal bands are similarly broader in the T_1 state except for an phenyl internal mode. It was unexpected that the ν_2 and ν_{11} bands were shifted to lower frequencies in the T_1 state than those of the ground state irrespective of the symmetry property, a_{1u} or a_{2u}, of HOMO. This is incompatible with the Raman empirical rule that ν_2 band is shifted to lower and higher frequencies upon the formation of the a_{2u} and a_{1u} cation radicals, respectively. The ν_{27} mode (C_m-phenyl out-of-phase stretching) was resonance enhanced and shifted to higher frequencies in the T_1 state. The magnitudes of frequency shifts of ν_2, ν_1 and ν_{27} bands upon excitation to T_1 state changed in the same order as that of the red-shift of the emission spectra in the fluid solution, that is, ($T_{3,4,5OMe}PP$)Cu ≈ (TPP)Cu>(TMP)Cu>($T_{F5}PP$)Cu. Since these vibrations contain C_α-C_m or C_m-phenyl stretching character, the present observation suggests that the red-shift in the fluid solvent is associated with distortions at the methine bridges. The phenyl ν_{8a} band was strongly enhanced in the T_1 state for (TPP)Cu but not for (TMP)Cu and ($T_{3,4,5OMe}PP$)Cu, although their frequencies remain unaltered, suggesting that the $T_n \leftarrow T_1$ excitation involves distortion of the phenyl ring along ν_{8a} coordinate, for (TPP)Cu but not for others.

II-F-2 Time-Resolved Resonance Raman Spectra of Octaethylporphinato Copper(II) in the Lowest Excited Triplet State

Motoko ASANO-SOMEDA, Katsuhiro AOYAGI *(Fukushima Natl. College of Tech.)* **and Teizo KITAGAWA**

Time-resolved resonance Raman spectra were measured with a pump/probe technique using two 7 ns pulsed lasers for Cu(II) octaethylporphyrin(OEP) in the lowest excited triplet state. Raman bands in the excited state were assigned on the basis of polarization ratios and isotope shifts for OEP-meso-d_4 and OEP-^{15}N compounds. All the observed bands were polarized and bandwidths depended on the modes. The skeletal ν_2, ν_3 and ν_4 modes gave broad bands and exhibited downshifts relative to the ground state frequencies. In contrast, peripheral ethyl modes gave sharp band profiles similar to that of the ground state and the frequency changes upon the excitation were smaller than the skeletal modes.

II-F-3 Time-Resolved Stokes/Anti-Stokes Raman Study of Primary Photoprocesses in Ni-porphyrin Complexes in Solution

Sergei KRUGLIK, Yasuhisa MIZUTANI and Teizo KITAGAWA

2-color time-resolved RR spectra of Ni(OEP) in toluene and THF were measured as function of a delay time between pump and probe pulses both in Stokes and anti-Stokes spectral regions with time resolution of 2.5 ps. Optimization of the experimental conditions was made and several experimental schemes were tested, including variation of the excitation geometry, pumping and probing wavelengths and intensities and concentration of samples. Anti-Stokes Raman spectra were recorded in 550-1700 cm^{-1} spectral region and the kinetics of changes in anti-Stokes Raman intensities for the modes ν_4, ν_7 and ν_{15} of the porphyrin macrocycle were found to be quite different. This finding reveals that the relaxation over the vibrational degrees of freedom is not uniform and moreover, is time-dependent. Our data suggest that the intra-molecular vibrational energy redistribution in Ni(OEP) takes place

in several-picosecond rather than in sub-picosecond time scale. Reliable evidence for the conformational changes in the excited state of Ni(OEP) have also been obtained on the basis of the bandshape analysis of the ν_{10} mode. Preliminary analogous time-resolved RR study has been performed for the solution of Ni(TPP) in toluene.

II-F-4 Time-Resolved Resonance Raman Studies of Photoinduced Binding/Release of Axial Ligands by Porphyrin Complexes with Transition Metals

Sergei KRUGLIK, Yasuhisa MIZUTANI and Teizo KITAGAWA

Comprehensive systematic study of the excited (d,d) state has been performed by saturation nanosecond RR technique for 4- and 6-coordinate Ni(OEP) complexes in toluene, THF, pyridine and piperidine solutions, including observation of transient polarized spectra with Soret- and Q-bands excitations. Vibrational frequency map was compiled which included typical ranges for the 10 porphyrin marker frequencies in the $^1A_{1g}$, $^3B_{1g}$ and $^3B_{1g}(L)_2$ electronic states. On the basis of this background, RR study of a photoinduced ligation process for Ni(OEP) in pyridine has been performed which showed that some new long-lived transient state, clearly distinct from the above mentioned states, was formed in the process of photoexcitation relaxation in nanosecond time scale. Picosecond single-color RR study of 6-coordinate Ni(OEP)/piperidine complex revealed appearance, during 2.5-ps pulses irradiation, of transient Raman spectrum which was similar to that in Ni(OEP)/pyridine complex at nanosecond time scale. On the basis of the Raman frequencies, it is possible to suggest that in both cases the non-equilibrated $^1A_{1g}$ ground state of the ligated Ni(OEP) complex is responsible for the appearance of these new transient species. 2-color time-resolved RR studies were performed for Cu(OEP) in benzene-d_6 and THF solutions. In non-coordinating benzene, the excited triplet (π,π^*) state of Cu(OEP) is populated which shows prominent broadening of porphyrin bands and breaking-down the one-to-one analogy between the lines in the ground- and excited-state RR spectra. In THF, the reversible process of axial binding/release of a THF molecule to the central copper atom with participation of the triplet (π,π^*) and (d,d) excited states was checked by time-resolved RR technique with 2.5 ps time resolution. This study confirmed the results of previous picosecond transient absorption and nanosecond RR investigations and showed that the excitation relaxation in Cu(OEP)/THF complex exhibit two-phase character with the characteristic decay times lying in sub-nanosecond time domain.

II-F-5 SRS-based Tunable Source of 3-ps, 1-kHz Pulses with Micro-Joule Energies for Ultrafast Time-Resolved Spectroscopy

Valentin ORLOVICH, Sergei KRUGLIK, Yasuhisa MIZUTANI and Teizo KITAGAWA

Raman shifters based on compressed gases (hydrogen and methane) have been constructed for frequency conversion of the radiation of the second harmonics of Positive Light - Tsunami laser system with 3 ps. 1 kHz, 50-200 μJ pulses in 380-427 nm spectral region. These shifters were optimized and tested for generation of powerful radiation from the 1st and 2nd Stokes components of scattering in methane and from the 1st Stokes component in hydrogen. Statistical characteristics of scattering radiations from the above mentioned sources have also been investigated. The tunable radiation at 427-569 nm spectral region with the conversion efficiency of up to 20% and high energy stability was obtained. The constructed Raman shifters were used in 2-color pump-probe time-resolved RR studies of the solutions of biological molecules and their model compounds.

II-G Molecular and Electronic Structures of Metallofullerenes and the Fullerene Radical Anions

The continued interest in radical ions of fullerenes and metallofullerenes has resulted from the discovery of superconductivity in the CT complexes of alkali metals with fullerenes. Spectroscopic information concerning the electronic structure of C_{60}^- isolated in a single crystal salt has been obtained by EPR, absorption and fluorescence measurements at low temperature. The metallofullerenes are of great interest because they could give rise to new chemical entities with novel properties, such as the superconductivity or the ferromagnetism. However, little is known about the physical and chemical properties. The EPR measurements of the spin multiplet state and chemical reactivities of metallofullerenes have been reported.

II-G-1 Electronic Structure of Crystallized C_{60}^- (C_{60} Anion)

Takeshi KODAMA, Tatsuhisa KATO and Masako KATO *(Nara Women's Univ.)*

The crystal structures of the high quality single crystals of salts of $[(C_6H_5)_4P]_2[C_{60}][X]_x$ (X = Cl, Br, I) are analyzed by the Xray diffraction. The absorption spectrum of the crystal , which is disperced in the KBr perets, mesured at 10 K comfirmes that the C_{60}^- anion are produced in the crystals. The two g-tensors with the almost same magnitude which are oriented at right angles with each other in the single crystal are determined from the angular dependent ESR measurement. The two g-tensors can be explained by the scheme of the distinguishable two D_{2h} J-T distorted structure of C_{60}^- anions fixed in the two different sites in the single crystal. More over the two sites in the single crystal is defined by the C_2 axes with the two orientation at 90° relative to each other in the a-b plane of the lattice.

II-G-2 ESR Measurements on Spin Multiplet States of Metallofullerenes

Tatsuhisa KATO, Toshiyasu SUZUKI and Kazunori YAMAMOTO *(Power Reactor & Nucle. Fuel Development Corp.)*

Gd metal has the electronic structure with the configuration of $4f^75d^16s^2$ and with the spin nonet term. Then it is quite worthwhile to investigate the cage-effect of C_{82} on the spin state of $Gd@C_{82}$. Recently it has been reported by some group that $Gd@C_{82}$ was obtained by an arc-burning of a composite graphite rod and purified by the high performance liquid chromatographic (HPLC) method. We has succeeded in purifying an adequate amount of $Gd@C_{82}$ by the HPLC method and performed ESR measurements of $Gd@C_{82}$ in CS_2 solution below 4K . The spin multiplet term of $Gd@C_{82}$ which is investigated by using the computer simulation is reported.

II-G-3 ESR Study on the Reactivity of Two Isomers of LaC_{82} with the Disilirane

Tatsuhisa KATO, Takeshi AKASAKA *(Univ. of Tsukuba)*, **Kaoru KOBAYASHI** *(Tokyo Metropol. Univ.)*, **Shigeru NAGASE** *(Tokyo Metropol. Univ.)*, **Kazunori YAMAMOTO** *(Power Reactor & Nucle. Fuel Development Corp.)*, **Hideyuki FUNASAKA** *(Power Reactor & Nucle. Fuel Development Corp.)* **and Takeshi TAKAHASHI** *(Power Reactor & Nucle. Fuel Development Corp.)*

We have found the photochemical and thermal addition of the disilirane to the LaC_{82}-A isomer, which give the new ESR active species. The both ESR spectra of the adducts in photo- and thermal reactions are well simulated by at least six octet components and the isotropic La coupling constants and g factors of the six octet components are determined. On the other hand the reaction of the LaC_{82}-B isomer with the disilirane gives no ESR active species. This fact is also verified by the Mass spectroscopic measurement. The different reactivities with the disilirane between the two isomers are not interpreted by a popular view that the two isomers have the different C_{82} cage structure and suggest that the origin of the isomers of metallofullerenes should be re-examined.

II-G-4 Chemical Reactivity of a Metallofullerene: EPR Study of Diphenylmethano-$La@C_{82}$ Radicals

Tatsuhisa KATO, Toshiyasu SUZUKI, Yusei MARUYAMA, Takeshi AKASAKA *(Univ. of Tsukuba)*, **Kaoru KOBAYASHI** *(Tokyo Metropol. Univ.)*, **Shigeru NAGASE** *(Tokyo Metropol. Univ.)*, **Kazunori YAMAMOTO** *(Power Reactor & Nucle. Fuel Development Corp.)*, **Hideyuki FUNASAKA** *(Power Reactor & Nucle. Fuel Development Corp.)* **and Takeshi TAKAHASHI** *(Power Reactor & Nucle. Fuel Development Corp.)*

Reaction of $La@C_{82}$ with diphenyldiazomethane has been studied by EPR. The EPR spectra of the reaction mixture indicate the consumption of the starting radical and the production of new four octets which are probably due to monoaddition regioisomers. The FAB mass spectrum shows peaks due to $La@C_{82}$ and $La@C_{82}(CPh_2)_n$ (n=1 to 3). Broad EPR signals as the background of the sharp octets are probably due to bis- and trisadducts. These EPR changes correcpond to the stepwise additions of diphenyldiazomethane to the C_{82} cage as observed for the reaction of C_{60} with diphenyldiazomethane. Our results suggest that a variety of functionalized metallofullerenes can be produced by modifying the procedures of the C_{60} derivative synthesis.

II-H Site Selective Spectroscopy in Solid Crystals

The line broadening due to the variation of the environment over the some sites in the crystal structure prevents from determining small energy splitting between pair of closely spaced levels with high accuracy. However the broadening effects give a nice probe to investigate the intermolecular interaction in the crystal structure. On the other hand some techniques of the site selective spectroscopy to eliminate the disturbance were proposed. We are applying the technique of the heterodyne detection of optical magnetic double-resonance to some systems of crystal.

II-H-1 Heterodyne Detection of Optical Magnetic Double-Resonance

Michio MATSUSHITA and Tatsuhisa KATO

It is often the case that paramagnetic molecules doped into a crystal does not occupy a single site of unique environment but occupy several sites of different environments. The EPR spectrum of the sample will be a superposition of signals from different sites in the crystal. To study the effect of environments on magnetic properties of the host molecules, one could make use of site-dependence of the optical excitation energy to select individual sites. In order to perform site-selective magnetic resonance by optical-rf double resonance, we have built up the system of Raman heterodyne detection of the double resonance. As a preliminary measurements, zero-field NMR transitions of Pr^{3+} in LaF_3 crystal were measured at 1.5 K. The incident light was tuned to the transition from the ground $^1D_2$ state to the electronically excited $^3H_4$ state (592.6 nm). The NMR transitions of both ground and excited states were observed.

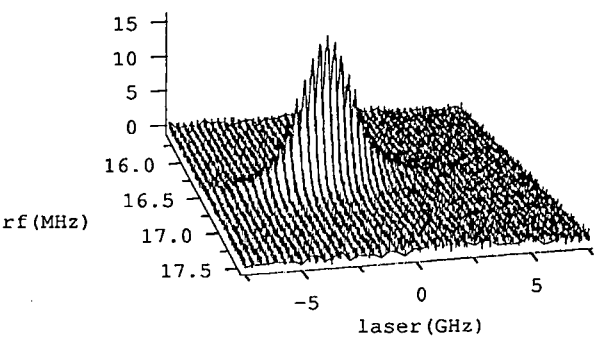

RESEARCH ACTIVITIES III
Department of Electronic Structure

III-A Ultrafast Intermolecular Electron Transfer

We have recently reported ultrafast fluorescence quenching of excited dye molecules in neat electron-donating solvents and attributed this to intermolecular electron transfer (ET). To understand the role of solvent dynamics and intramolecular motion in ET, it is important to study the time dependence of the reaction in detail. Accurate measurements of fluorescence decay were made with xanthenes and coumarins in aniline and N,N-dimethylaniline. We found ET rate in some cases determined directly by nuclear rearrangement and in the other cases by solvent relaxation dynamics. Most interestingly we found deuterium isotope effects on both the electron transfer and solvation dynamics of aniline.

III-A-1 Dynamical Aspects of Ultrafast Intermolecular Electron Transfer Faster Than Solvation Process: Substituent Effects and Energy Gap Dependence

Yutaka NAGASAWA *(Graduate Univ. for Advanced Studies)*, **Arkadiy P. YARTSEV, Keisuke TOMINAGA, Prem B. BISHT, Alan E. JOHNSON and Keitaro YOSHIHARA**

[*J. Phys. Chem.* **99**, 653 (1995)]

We have investigated intermolecular electron transfer (ET) from electron donating solvent (aniline and N,N-dimethylaniline) to coumarins in the excited state by means of the femtosecond fluorescence up-conversion technique. The coumarins we studied have variety of structures with different substituents in the 4- and 7-positions. The ET occurs on a time scale ranging from a few nanoseconds to a couple of hundred femtoseconds depending on the structure of the coumarins and solvent. The origin of this substituent effect is mainly attributed to the variation of the energy gap between the reactant and product states. This is confirmed by theoretical calculations in terms of the extended Sumi-Marcus two-dimensional model. Good agreement between the experiment and calculation shown in Figure 1 indicates that some of the reactions take place from the relaxed vibrational state of reactant to the excited vibrational states of high frequency modes of product states. The simulated population decays for non-equilibrium configuration of solvents agreed well with experimental data. In the steady-state fluorescence spectra was also observed an effect of very fast fluorescence quenching due to ET, i.e., the amount of fluorescence Stokes shift depends on the rate of ET because the excited state is quenched in competition with thermal equilibration of solvent configuration. We regard this spectral shift as the result of "chemical timing" effect in solution.

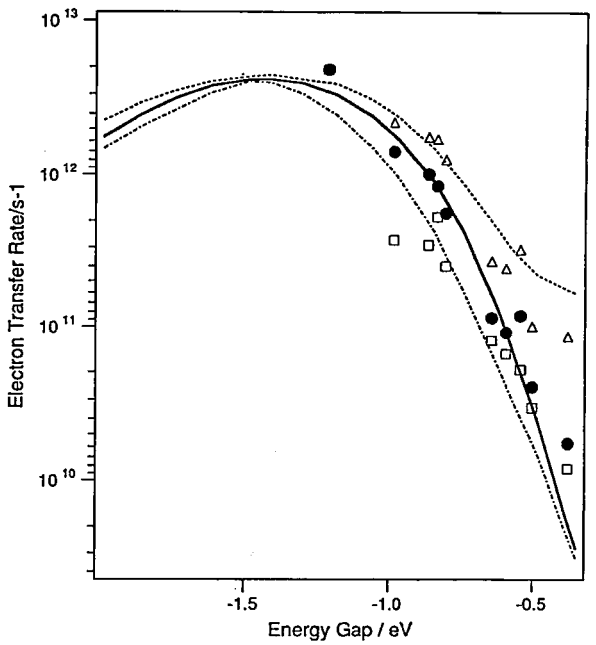

Figure 1. The simulated energy gap dependence based on extended Sumi-Marcus model. The broken line is the simulated time constant of the first component τ_1, the dashed and dotted line is that of the second component τ_2, and the solid line corresponds to their average $< \tau >$. The unfilled triangle, rectangle, and filled circle symbols correspond to the experimentally obtained τ_1, τ_2, and $< \tau >$, respectively.

III-A-2 Deuterium Isotope Effect on the Solvation Dynamics

Haridas PAL, Yutaka NAGASAWA *(Graduate Univ. for Advanced Studies)*, **Keisuke TOMINAGA, Shigeichi KUMAZAKI and Keitaro YOSHIHARA**

[*J. Chem. Phys.* **102**, 7758 (1995)]

In this work we have investigated the solvation dynamics of aniline (AN) and N,N-dimethylaniline (DMA) and their deuterated analogues such as AN-d7 ($C_6D_5ND_2$), AN-d2 ($C_6H_5ND_2$) and DMA-d6 ($C_6H_5N(CD_3)_2$) by dynamic fluorescence Stokes shift method with coumarin-102 as a fluorescence probe. The results of this study are listed in Table 1. The interesting points to be noted from this Table are; (1) For both perdeuterated AN-d7 and amino deuterated AN-d2 the solvation dynamics are slower than that in normal AN. (2) The isotope effect is, however, almost the same for both AN-d7 and AN-d2. (3) With deuterated DMA-d6 there is no isotope effect on the solvation dynamics. Therefore, it is evident that the iso-

tope effect on the solvation dynamics in the present systems is directly related to the presence of the NH_2 group of the solvent molecules. The presence of the NH_2 group makes AN an intermolecularly hydrogen bonded solvent. For reorientation of the solvent molecules they have to break the existing hydrogen bonds and remake those in the new orientation. Substitution of the amino group hydrogens by deuterium is thus expected to slow down the solvation dynamics via a reduction in the dynamics of hydrogen bond breaking and making process (because of the higher mass of D). For D_2O it has been shown that this liquid is more structured and exhibit a stronger hydrogen bonding than the normal water.[1] A similar situation is also expected for deuterated AN. Thus the hydrogen bond breaking process will be less favorable in AN-d2 and AN-d7 in comparison to that in normal AN. This will also in effcet cause a reduction in the solvation dynamics of the deuterated anilines.

Reference

1) G. Nemethy and H.A. Scheraga, *J. Chem. Phys.* **41**, 680 (1964).

Table 1. Solvation times[a] for normal and deuterated AN and DMA.

Solvent	a_1	τ_{s1} (ps)	a_2	τ_{s2} (ps)	$<\tau_s>$ (ps)[b]
AN	0.28	1.2±0.2	0.72	17.8±0.6	13.2±0.5
AN-d7[c]	0.33	1.6±0.2	0.67	20.6±0.6	14.3±0.5
DMA[d]	0.35	3.8±0.3	0.65	22.6±0.6	16.0±0.5

a: $C(t) = a_1 \exp(-t/\tau_{s1}) + a_2 \exp(-t/\tau_{s2})$; $a_1 + a_2 = 1$; C(t) is the spectral shift correlation function.
b: $<\tau_s> = a_1 \tau_{s1} + a_2 \tau_{s2}$
c: solvation dynamics in AN-d2 is similar to that in AN-d7.
d: solvation dynamics in DMA-d6 is similar to that in DMA.

III-A-3 Effects of Vibrations in Chemical Dynamics: High-Frequency Vibrational and Low-Frequency Solvent Dynamical Effects on Intermolecular Electron Transfer

Keitaro YOSHIHARA, Haridas PAL, Hideaki SHIROTA *(Graduate Univ. for Advanced Studies)*, **Yutaka NAGASAWA** *(Graduate Univ. for Advanced Studies)* **and Keisuke TOMINAGA**

[*Time Resolved Vibrational Spectros*copy-7, in press]

We have investigated the substituent and the deuterium isotope effects on the ultrafast intermolecular electron transfer (ET) from electron donating solvents sush as aniline (AN), N-alkyl anilines and N,N-dialkyl anilines to a number of excited (S_1) 4-CF_3 coumarin dyes. It has been observed that; (1) In all the cases the ET dynamics are nonexponential. (2) In many cases the ET process is much faster than the diffusive solvation process. (3) The ET rates are drastically dependent on the substituents of the coumarin dyes (Figure 1). (4) The ET rates drastically depend on the substituents at the amino group of the donor solvents. (5) With AN and N-alkyl anilines, as the amino group hydrogens are substituted by deuterium the ET dynamics become slower (Figure 1). (6) With deuterated N,N-dimethyl aniline (DMA-d6; the N-methyl group hydrogens are substituted by deuterium), however, there is no isotope effect on the ET dynamics. The observed results are analysed within the framework of two dimentional ET theory. The effects of the substituents of both the donor and the acceptor are found to be mostly due to the changes in the reaction exothermicities (ΔG^0). The substition effects of the donors, however, indicate the involvement of some high frequency vibrational modes of the amino group (ring-nitrogen stretching or amino group wagging) to the ET dynamics. Cyclic voltammetric measurements indicate that the solvent structural effects arising from the intermolecular hydrogen bondings cause a reduction in the reaction exothermicity (ΔG^0) on substituting the NH hydrogens of the donors by deuterium and this in turn makes the ET dynamics slower.

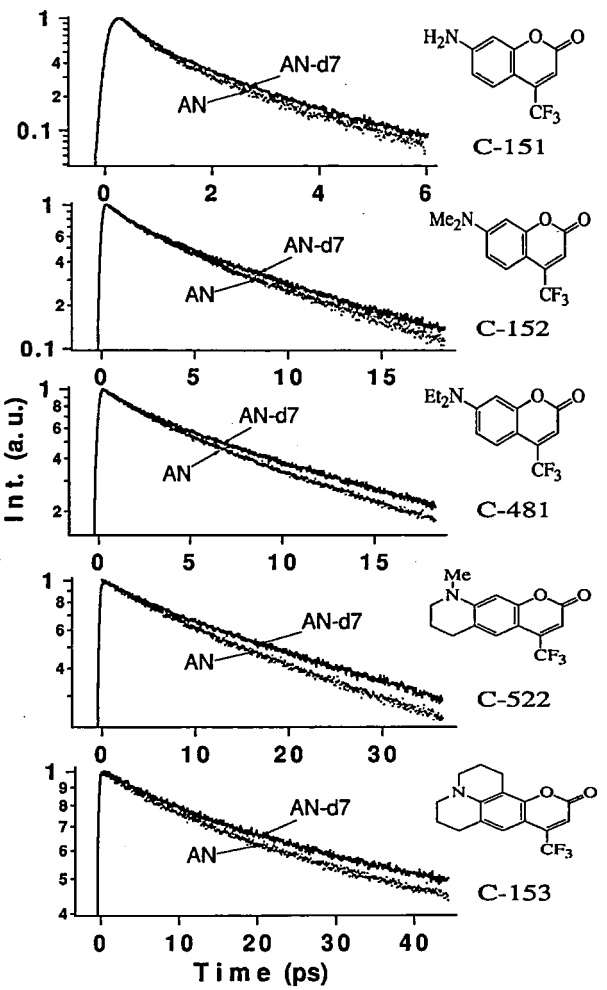

Figure 1. Fluorescence decays of a number of 4-CF_3 coumarin dyes in aniline (AN) and perdeuterated aniline (AN-d7) are shown. Both the substituent effect of the acceptors (coumarins) and the deuterium isotope effect of the solvent donor (AN) on the ET dynamics are indicated.

III-B Liquid Dynamics Studied by Higher Order Nonlinear Spectroscopy

We have developed techniques to observe higher order (fifth and seventh order) nonlinear optical response from liquids to investigate microscopic dynamics and structures of liquids. The experiments include vibrational echo-type experiments for high- and low-frequency modes and overtone dephasing experiments for high-frequency modes. The vibrational echo-type experiments are temporally two-dimensional spectroscopy and can determine the relative importance of inhomogeneity of the spectral broadening. The overtone dephasing experiments allow us to investigate the vibrational quantum number dependencies of the dephasing mechanisms.

III-B-1 Fifth Order Optical Response of Liquid CS_2 Observed by Ultrafast Non-Resonant Six-Wave Mixing

Keisuke TOMINAGA and Keitaro YOSHIHARA

[*Phys. Rev. Lett.* **74**, 3061 (1995)]

The first observation of the fifth order optical response of liquid CS_2 was conducted by ultrafast non-resonant six-wave mixing with five different pulses. The technique allows us to unambiguously distinguish homogeneous and inhomogeneous contributions to spectral broadening of low frequency vibrational modes. The experimental results are reproduced well in terms of one overdamped mode in the homogeneous limit and one underdamped mode with the width of the inhomogeneity less than 2.5 ps^{-1}.

III-B-2 Temporally Two-Dimensional Raman Spectroscopy of Liquids by Six-Wave Mixing with Ultrashort Pulses

Keisuke TOMINAGA, Gary P. KEOGH (*Imperial College and IMS*), **Yukito NAITOH and Keitaro YOSHIHARA**

[*J. Raman Spec.* **26**, 495 (1995)]

A temporally two-dimensional Raman spectroscopy has been developed to observe the fifth order optical response of liquids. Taking advantage of temporal two-dimensionality, this technique can unambiguously distinguish homogeneous and inhomogeneous contributions to the dephasing of low frequency vibrational modes. A femtosecond laser system with a high energy operating at kHz repetition rates was built. A six-wave mixing method with five different pulses has been developed for the first time.

III-B-3 Time-Resolved Higher Order Nonlinear Spectroscopy in Liquids: Overtone Vibrational Dephasing

Keisuke TOMINAGA, Gary P. KEOGH (*Imperial College and IMS*), **Jangseok MA and Keitaro YOSHIHARA**

[*Time-Resolved Vibrational Spectroscopy-7*, in press]

We have developed a technique to observe time profiles of vibrational dephasing of the first overtone (v = 2) as well as the fundamental bands in liquids with a good signal-to-noise ratio under non-resonant conditions using femtosecond pulses. The overtone signal is based on the fifth-order nonlinear phenomena. This method allows one to compare experimental results and theoretical predictions of the vibrational dephasing of both the fundamental and overtone bands in a quantitative level. Examples of the observed overtone dephasing signals are shown in Figure 1.

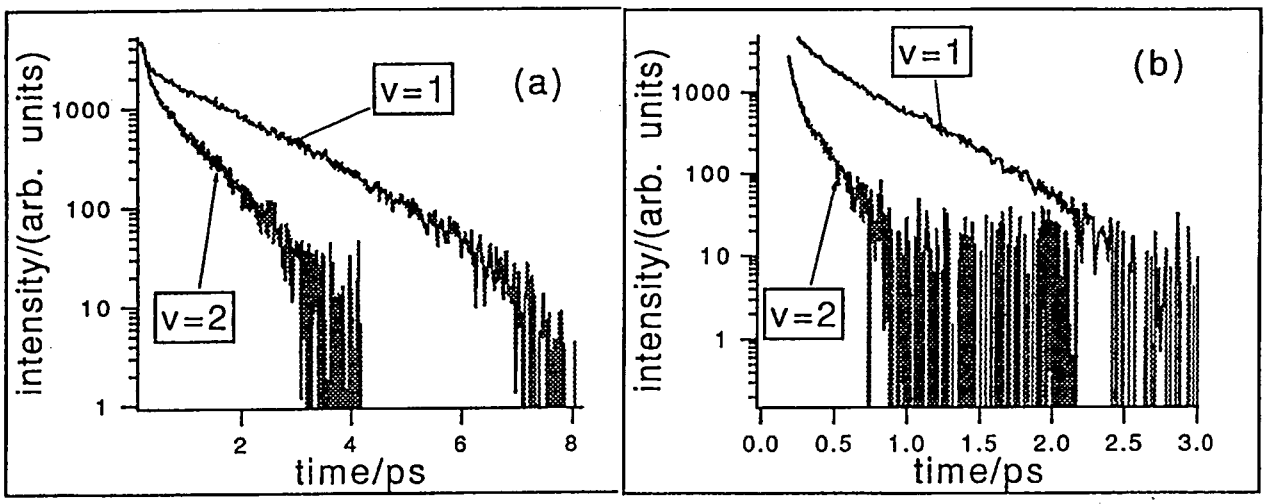

Figure 1. Time profiles of the vibrational dephasing of the first overtone and fundamental bands of (a) the C-D stretching of CD_3I and (b) C=C stretching of $Cl_2C{=}CCl_2$.

III-C Development of Ultrafast Spectroscopic Methods

The discovery of self-mode-locking has recently initiated the rapid development of ultrashort pulse generation in

solid-state laser systems. The Ti:sapphire lasers have been demonstrated to be a reliable light source of producing pulses down to 10 fs regime with either prism pairs or dispersion-controlled multilayer dielectric mirrors. In parallel with the advances of the Ti:sapphire laser system, many ultrabroad band solid-state laser materials have been developed as alternative sources of generating ultrashort laser pulse. One such material is chromium-doped forsterite (Cr^{4+}:Mg_2SiO_4) of which laser generates ultrashort pulse at the near infrared region. We have developed a cavity-dumped femtosecond Cr:forsterite laser. This system will be used to study ultrafast dynamics of intermolecular electron transfer by fluorescence up-conversion technique. In addition to this laser system, we have installed the six-pass dye amplifier system for ultrafast transient absorption studies and higher order nonlinear spectroscopic experiments.

III-C-1 Femtosecond Laser System Based on Chromium-Doped Forsterite Crystal

Eugene V. SLOBODCHIKOV (*Inst. Chem. Phys., Russian Acad. and IMS*), **Jangseok MA, Keisuke TOMINAGA and Keitaro YOSHIHARA**

A solid-state femtosecond laser system based on new laser material (Cr^{4+}:Mg_2SiO_4- chromium-doped forsterite) was build and operated by Kerr-lens self-mode-locking. Two versions of chromium-doped forsterite femtosecond laser system were built. In cw femtosecond operation 3 nJ, 40 fs laser pulses at 1260 nm and 0.2 nJ, 37 fs laser pulses at 630 nm were obtained at frequency of 76 MHz. In cavity-dumped femtosecond operation 30 nJ, 54 fs laser pulses at 1260 nm and 3 nJ, 49 fs laser pulses at 630 nm were obtained at variable repetition rate (400 Hz - 800 kHz).

The femtosecond laser pulses at 630 nm were used as seed pulses for a six-path bow-tie dye amplifier pumped by the second harmonic of the diode-laser-pumped Nd:YLF laser output. The 0.6 μJ, 43 fs laser pulses were obtained at frequency of 4 kHz. The "white light continuum" generation was realized by focusing amplified pulses in 1 mm fused silica plate as shown in Figure 1.

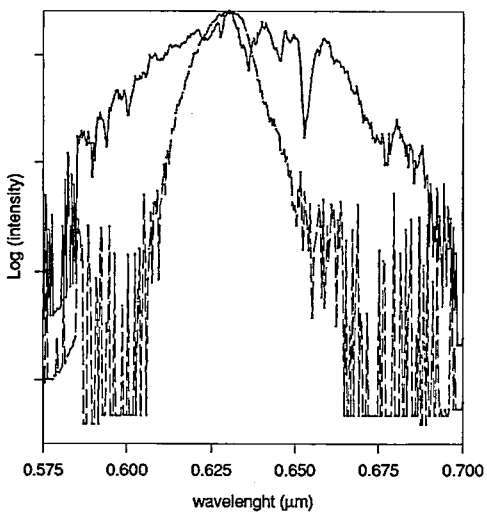

Figure 1. Spectrum of "white light continuum" and spectrum of input amplified laser pulses (central peak).

III-C-2 Cavity-Dumped Femtosecond Kerr-Lens Mode-Locking in Chromium-Doped Forsterite Laser

Eugene V. SLOBODCHIKOV (*Inst. Chem. Phys., Russian Acad. and IMS*), **Jangseok MA, Valey KAMALOV, Keisuke TOMINAGA and Keitaro YOSHIHARA**

[*Opt. Lett.*, submitted]

We have performed what is to our knowledge the first demonstration of the cavity dumping operation in a Kerr-lens mode-locked Cr:forsterite laser. At 1260 nm, the pulse durations as short as 54 fs with pulse energies as high as 30 nJ at variable repetition rates (400 Hz - 4 MHz) were obtained. By frequency doubling in a BBO crystal, the pulse durations as short as 49 fs with conversion efficiencies approaching 10 percent were obtained. The high stability and ultrashort pulse widths with a variable repetition rate in both infrared (1260 nm) and red (630 nm) make this system an attractive tunable light source for ultrafast spectroscopy. The whole system is shown in Figure 1.

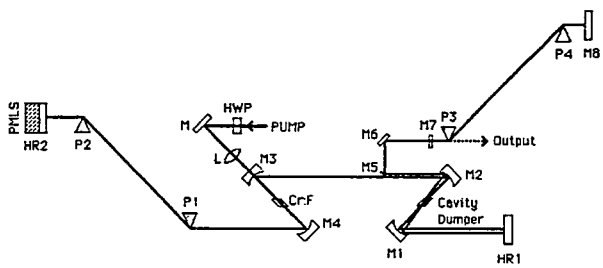

Figure 1. The schematic of the cavity-dumped femtosecond Kerr-lens mode-locked chromium-doped-forsterite laser: pump, mode-locked Nd:YAG laser; HWP, half wave plate; L, f = 9 cm lens; Cr:F, 1.9 cm Cr:forsterite crystal; Cavity Dumper (or Bragg Cell), 3 mm fused-silica acousto-optic modulator; HR1 and HR2, high reflector; M1-M4, R = 5 cm mirrors; M5-M7, high reflectors; M8, gold-coated mirror; P1-P4, SF-6 prisms; PMLS, piezo-electric mode starter.

III-D Development of Femtosecond UV-Pump and UV-Probe Spectroscopy and Its Application to Small Molecule Reaction in Condensed Phase

The primary process of photoexcited molecules in condensed phase has been much influenced through various interactions with environments, which can induce the energy and phase relaxation in the molecular motion and give the final state distribution different from the isolated system. The ultrafast time-resolved spectroscopy has played an important role in the investigation of these processes. In the case of photodissocation in solution, it has been shown in some molecules that, on the way to fragmentation, the geminate recombination occurs due to the cage effect of the solvent and the vibrational relaxation follows. Due to the limited tunability, the femtosecond dye laser restricts objects of study. If we treat

simple small molecules universally, it is possible to understand the characteristic behavior of the photodissociation process in solution in detail by comparison with studies in the isolated system, which have considerably developed in both experiment and theory. The recent development of the femtosecond Ti:sapphire laser can realize this expectation. The advantage of Ti:sapphire laser is a very high stability, wide wavelength tunability and tractability. When we use the third harmonics as a pump source, we can excite these molecules by the femtosecond pulse around 266 nm, which corresponds to the first absorption band. The white light generation by this laser is used to probe the products. On the basis of these considerations, we have constructed a femtosecond transient absorption system using a regeneratively amplified Ti:sapphire laser and studied the basic photoinduced process in solution, such as photodissociation, isomerization, ionization and other chemical reactions.

III-D-1 Construction of Femtosecond Transient Absorption System Using Regeneratively Amplified Ti:sapphire Laser

Yukito NAITOH, Keisuke TOMINAGA, Ken-ichi SAITOW (*Graduate Univ. for Advanced Studies*) **and Keitaro YOSHIHARA**

In order to study the photoinduced dynamical process of simple small molecules in condensed phase, we have constructed a femtosecond transient absorption system, which is schematically shown in Figure 1. As a light source, we use a regeneratively amplified Ti:sapphire laser, which gives femtosecond pulses with 150 fs duration, 750 mJ energy, and 1 kHz repetition around 800 nm. Since the most of simple molecules such as CH_3I and H_2O_2 have a first absorption band in UV region, specially shorter wavelengths than 300 nm, we have produced the third harmonics around 266 nm by the sum frequency mixing between the fundamental and the second harmonics using a BBO crystal (type I). The conversion efficiency is about 10%. The white light continuum, which is generated by the focusing of a portion of either the fundamental or the second harmonics into the water cell, is able to probe the transient species over a wide range from UV to near IR. We have prepared two detection systems. One can bring a time profile of the transient absorption at a given wavelength selecting a part of the white light continuum by the interference filter as shown in Figure 1. The other consists of a monochromator and a multichannnel diode array. We can get transient absorption spectra, which help us to grasp a time-dependent change of absorption wavelength of the products clearly.

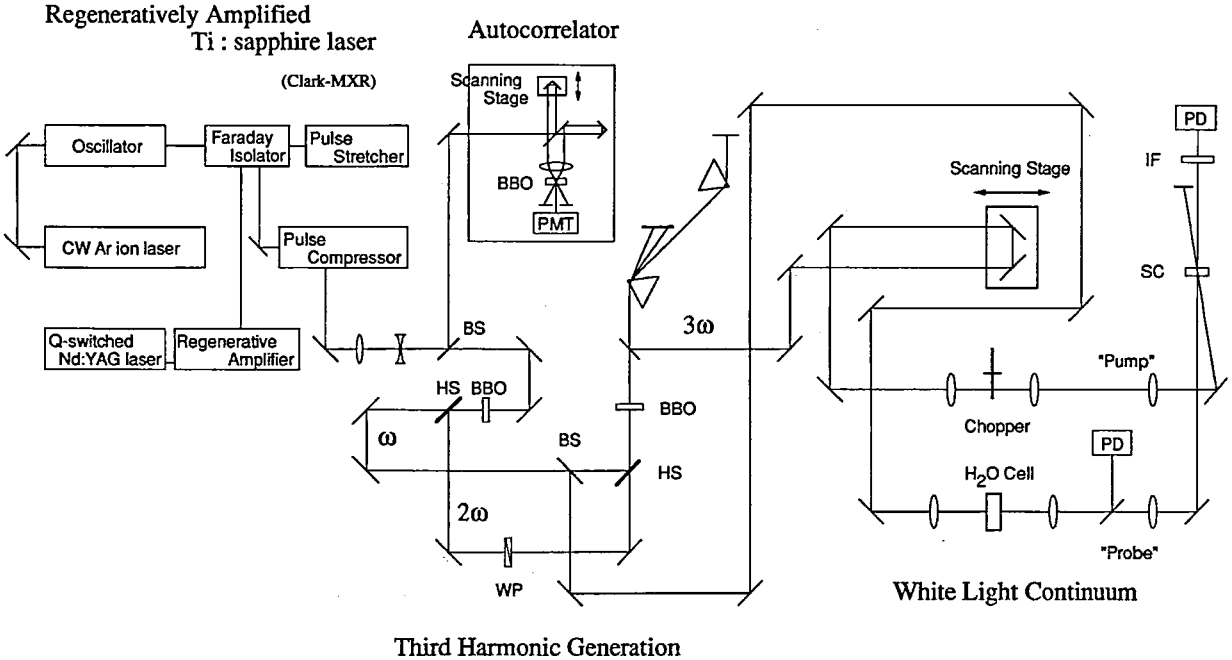

Figure 1. Schematic representation for the femtosecond transient absorption system. The third harmonics and the white light continuum are used as a pump and probe source, respectively. PMT:photomultiplier tube, HS:harmonic separator, BS:beam splitter, WP:$\lambda/2$ waveplate, SC:sample flow cell, IF:interference filter, and PD:photodiode.

III-D-2 Study of Bimolecular Reaction in Neat CH_3I by Femstosecond Transient Absorption Spectroscopy

Yukito NAITOH, Ken-ichi SAITOW (*Graduate Univ. for Advanced Studies*), **Keisuke TOMINAGA and Keitaro YOSHIHARA**

In chemical reactions in solution, the transition state and the neighbor region is expected to be much influenced by solvent molecules different from the isolated system. Though this seems to be the most important process, only a few studies are performed experimentally in this respect. In order to overcome this situation, we have studied a photoinduced reaction in neat CH_3I;

$$I^* + CH_3I \rightarrow I_2 + CH_3, \qquad (1)$$

where $I^*(^2P_{1/2})$ is prepared by photodissociation of CH_3I with UV femtosecond light pulse. One of the characteristic of this reaction is the translational diffusionless attack of the nearest CH_3I by the photofragment I^*. We

observed the femtosecond transient absorption of the reaction product, I_2, by probing the B-X transition at several wavelengths as shown in Figure 1. The results show that there are a rapid rise and a slow decay. This rapid rise can support that the reaction proceeds within the nearest solvent cage. The difference of the first component of the time constant depending on the observed wavelength may indicate the transient behavior from the exit of the transition state to the product I_2. The peak position of the transient absorption spectrum, which is constructed based on the single wavelength measurements, is shifted time-dependently from red to blue corresponding to the static absorption spectrum of I_2 in CH_3I. We also measured the pump laser power dependence of the I_2 signal intensity and ascertained it to be the first order, that is, the reaction is consistent with (1).

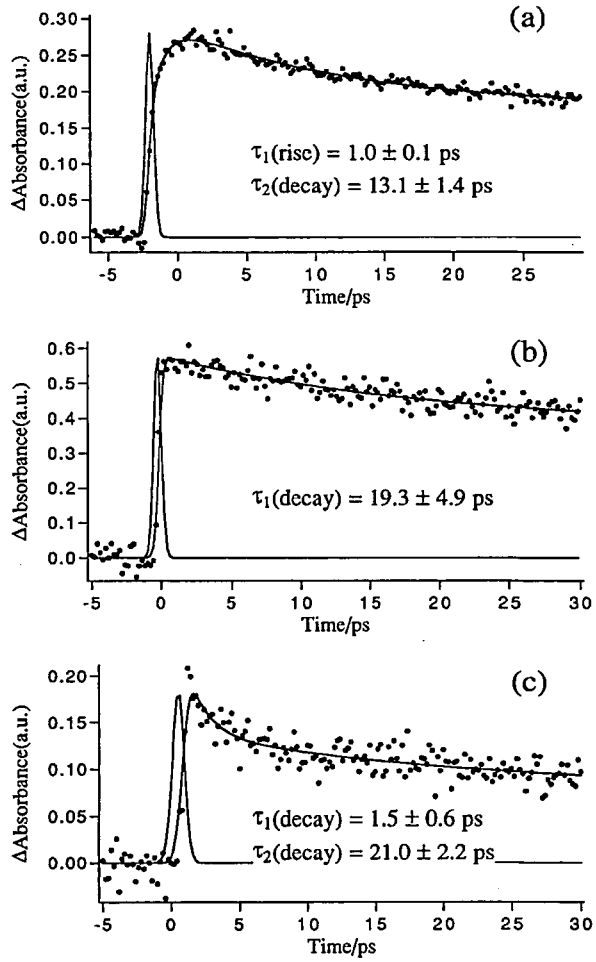

Figure 1. The transient absorption of reaction product I_2 probed at (a) 400 nm, (b) 540 nm, and (c) 700 nm. These measurements indicate that time profiles within the first 5 ps are obviously different. Dots and lines represent data points and fitting curves, respectively. Instrumental functions are described with each profile.

III-E Photoinduced Primary Processes in Natural and Artificial Photosynthetic Systems

The high efficiency of electronic energy transfer and electron transfer in photosynthesis have led researchers to look for ways to study the fundamental chemistry of these processes in simplified systems. One approach to this problem is to investigate isolated reaction center (RC) proteins from photosynthetic organisms. This received a definite momentum after the detailed X-ray structure of the reaction center from purple bacteria *Rhodopseudomonas viridis* was clarified in 1984. There are other approaches to design *de novo* energy and electron transfer systems with features of photosynthetic systems. The vital part of the second method is the synthesis of complex molecular systems, which are often referred to as supramolecular systems. In III-E-1, photosystem II reaction center (PS II RC) pigment-protein complex isolated from pea is studied. The 3D-structure of PS II RC is not known yet, but it is considered to be analogous to those of purple bacteria based on homology of amino acid sequences and stoichiometry. We, however, found that their primary processes are very different. In III-E-2, artificial electron transfer systems are studied, which revealed a unique feature of interaction between donor and acceptor of porphyrin-quinone pairs.

III-E-1 Spontaneous Emission Measurements on Photosystem Two Reaction Centres by Subpicosecond Fluorescence Up-Conversion

Shigeichi KUMAZAKI, D. Melissa JOSEPH*, Ben CRYSTALL*, James R. DURRANT*, James BARBER*, George PORTER*, Keitaro YOSHIHARA and David R. KLUG* (**Imperial College*)

[*Biochemistry*, submitted]

Fluorescence up-conversion experiments were performed on isolated Photosystem Two (PS II) reaction centres (D1/D2/cyt b559 complex) in order to estimate time scale of the primary charge separation. The complex is a minimum unit for light capture and subsequent charge separation. The experiments were conducted with excitation wavelength at 684 nm and an instrument response function of 600 - 800 fs (FWHM), by which primary electron donor chlorophyll(s), P680, is excited and contribution of energy transfer at picosecond time scale to the

overall primary charge separation is avoided. The loss of singlet excited states of reaction center chlorins (chlorophyll *a* and pheophytin *a*) is dominated by ~ 20 ps time constant, although a smaller proportion of the emission was associated with a time constant of ~ 2 ps as shown in Figure 1. These results are quantitatively in agreement with previously published transient absorption data. The up-conversion experiments also revealed a surprisingly high proportion of a longer lived component of a time constant of ~100 ps. These data were confirmed by time-correlated single photon counting measurements.

Reference

1) J.R. Durrant, G. Hastings, D.M. Joseph, J. Barber, G. Porter, and D.R. Klug, *Biochemistry* **32**, 8259 (1993).

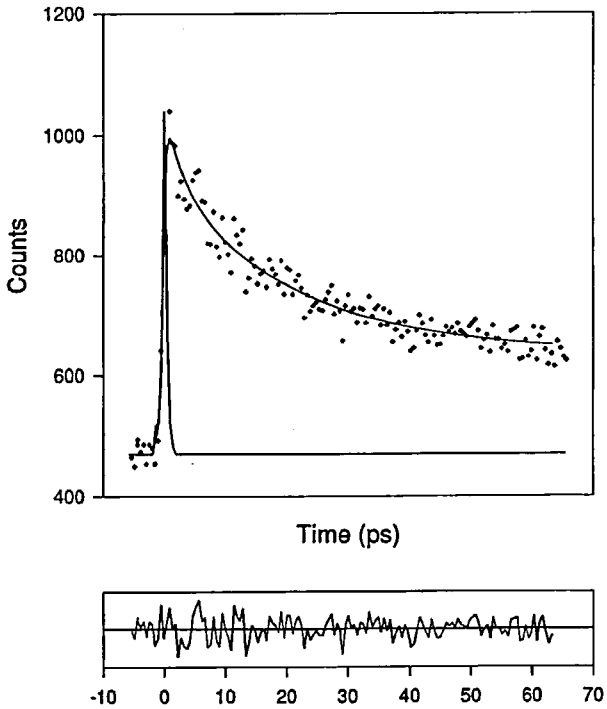

Figure 1. Fluorescence up conversion data with a typical instrumental response function and a biexponential fit to the data.

III-E-2 Photoinduced Electron Transfers between Porphyrin and Quinone Connected via Multipoint Hydrogen Bondings

Takashi HAYASHI*, Takashi MIYAHARA*, Hisanobu OGOSHI*, Shigeichi KUMAZAKI and Keitaro YOSHIHARA (**Kyoto Univ.*)

Electron transfers between porphyrin and quinone after photoexcitation of the porphyrin was studied by transient absorption spectroscopy. Excitation (2-3 ps pulse at 570 nm) of compound **2** (Figure 1) in toluene induces transient spectra in Figure 1(a) (superposition of $S_n \leftarrow S_1$ absorption and stimulated emission of $S_0 \leftarrow S_1$; S_1 lifetime of the porphyrins are a few nanoseconds), in which 650 nm is nearly an isosbestic point. Mixture of **1** or **2** with **3** in toluene shows substantial positive signals at around 650 nm (Figure 1(b)), which is attributed to cation of **1** or **2**. The short-lived radical pair states suggest that the electron transfers are not rate-limited by diffusion process and that the association via hydrogen bondings seem to be stable from excitation to the recovery to the original neutral states. Two types of complexes show surprisingly similar results (Figure 1(b)), in spite of their different porphyrin-ring to benzene-ring distances. Explanation simply based on electronic interaction as $V^2=exp(-\beta R)$ (R is the distance between the donor and acceptor) should demand β value of less than 0.2 $Å^{-1}$, compared to typical β values reported so far (1.4 $Å^{-1}$ in noncovalently bonded biological systems and 0.6 $Å^{-1}$ in convalently bridged synthetic systems in solution).[1] The electronic interaction in our cases may be mediated by the intervening naphthol substitutes, which could make the electron transfer kinetics rather insensitive to change of the distance.

Reference

1) C.C. Moser, J.M. Keske, K. Warncke, R.S. Farid and P.L. Dutton, *Nature* **355**, 796 (1992).

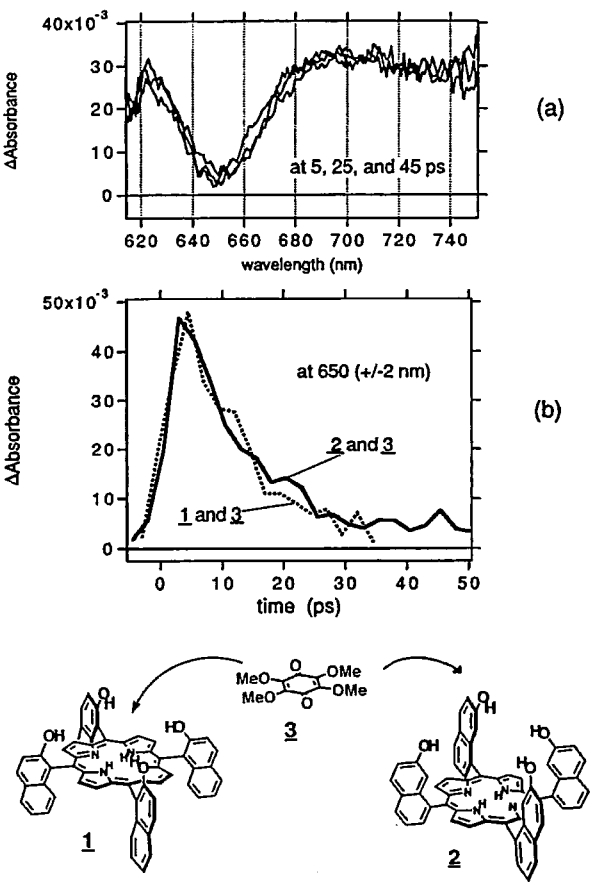

Figure 1. (a) Transient absorption spectra of compound **1** (porphyrin) in toluene at 5, 25, 45 ps after excitation. (b) kinetics of absorbance change for mixture of compounds (**1** and **3**) and (**2** and **3**) in toluene. The structures of componds are shown with the numbering (**1**, **2** and **3**) used.

III-F Dynamic Behavior of Electronic Excited States

Optical excitation of molecules to electronically excited states causes a variety of dynamical behavior, depending upon the nature of electronic structures and environments, such as energy transfer, proton transfer, chemical reaction, radiationless transition, ionization, and others. Most of these processes fall into the nanosecond, picosecond and femto-

second times scales. In this chapter we firstly discuss our observation of the one- and two-photon fluorescence of tetraenes. Secondly we report excited state enol-keto tautomerization in salicylic acid. Thirdly we describe exciton behavior of J-aggregates.

III-F-1 One- and Two-Photon Fluorescence Excitation Spectra of the 2^1Ag States of Linear Tetraenes in Free Jet Expansions

Hrvoje PETEK and rew J. BELL (*Univ. of Southampton and IMS*), **Young S. CHOI** (*Inha Univ. and IMS*), **Keitaro Yoshihara, Brett A. TOUNGE** (*Bowdoin College*) **and Ronald L. CHRISTENSEN** (*Bowdoin College and IMS*)

[*J. Chem. Phys.* **102**, 4726 (1995)]

One- and two-photon fluorescence excitation spectra of $S_1 \leftarrow S_0$ transitions of the all-*trans* isomers of 1,3,5,7-octatetraene, 1,3,5,7-nonatetraene, and 2,4,6,8-decatetraene have been obtained in free jet expansions as shown in Figure 1. Comparison of the one- and two-photon spectra allows the unambiguous identification of electronic and vibronic origins and, for octatetraene and decatetraene, provides clear evidence for molecular inversion symmetry. One-photon spectra show a_g progressions built on Herzberg-Teller, b_u promoting modes, while two-photon spectra are built on progressions of a_g modes starting from the 2^1Ag←1^1Ag electronic origins. In nonatetraene, the absence of inversion symmetry results in an allowed electronic origin in both the one- and two-photon spectra. Fluorescence lifetimes indicate abrupt onsets of nonradiative decay processes (tentatively attributed to *trans*←*cis* isomerization) at ~2100 cm^{-1} excess energy.

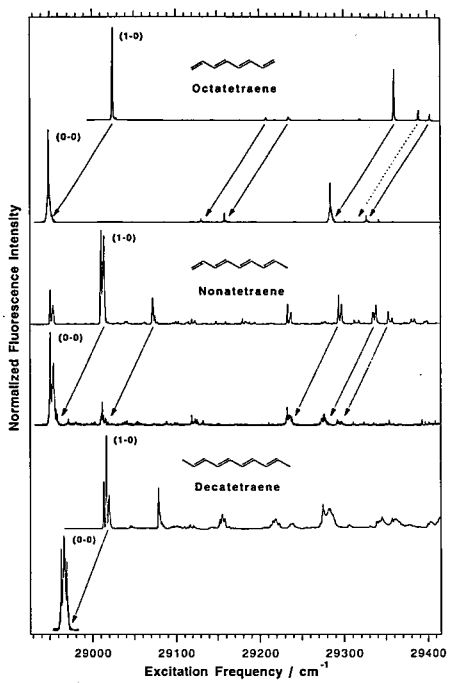

Figure 1. Comparison of the origins of the one- and two-photon $S_1 \leftarrow S_0$ fluorescence excitation spectra of all-*trans*-octatetraene, nonatetraene, and decatetraene. To emphasize that the one- and two-photon spectra of octatetraene and decatetraene do not overlap, the spectra are presented on an absolute energy scale (observed transition energies). Spectra have been normalized to give the same intensities for the electronic and vibronic origins of each molecule. Full arrows indicate bands that build on both electronic and vibronic origins. The broken arrow indicates a b_u band that only is observed in the one-photon spectrum.

III-F-2 Excited State Enol-Keto Tautomerization in Salicylic Acid: A Supersonic Free Jet Study

Prem B. BISHT, Hrvoje PETEK and Keitaro YOSHIHARA

[*J. Chem. Phys.* **103**, 5290 (1995)]

Excited state enol-keto isomerization in salicylic acid (SA) monomer and dimer has been studied in a supersonic free jet expansion. Two carboxylic group rotamers of SA with significantly different photophysical properties are found in the expansion. The rotamer I, the major form of SA in the expansion, has an intramolecular hydrogen bond and can undergo excited state tautomerization reaction. Its S_1 origin is at 335.34 nm. Single vibronic level emission spectra are dominated by progressions in OH stretching (3230 cm^{-1}), and in-plane bending of the carboxylic group (240 cm^{-1}). The spectra appear to consist of two components, normal (UV) and tautomer (BLUE) emissions, even at the origin. The intensity of the BLUE relative to the UV emission depends on the vibronic state, rather than the excess vibrational energy between the origin and 1100 cm^{-1}. The fluorescence decay time profiles for both the emission components of rotamer I are identical within ~1 ns experimental time resolution. A nonradiative decay process with an activation energy of ~1100 cm^{-1} is deduced from an abrupt decrease in fluorescence lifetimes above this energy. The rotamer II cannot undergo excited state tautomerization. Its electronic origin is at 311.52 nm and emits only UV fluorescence.

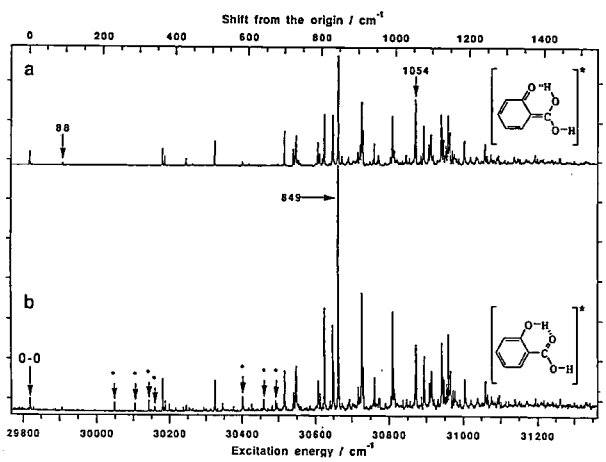

Figure 1. The fluorescence excitation spectra of the isomer I on monitoring (a) BLUE fluorescence, (b) UV fluorescence. Asterisk (*) indicates the bands due to the SA dimer. The spectra are normalized at the origin.

III-F-3 Exciton Behavior of J-Aggregates of Carbocyanine Dye at Low Temperatures

Valey F. KAMALOV, Irina A. STRUGANOVA (*Laser for Photochemistry Ltd.*) **and Keitaro YOSHIHARA**

[*J. Phys. Chem.*, submitted]

Frenkel exciton formed in J-aggregate of carbocyanine dye in the polyvinyl alcohol film was found to have an effective coherent size of 18 molecules at 4K. The exciton emission quantum yield drops four times when temperature increased from 20 to 60 K. The effective coherent exciton size decreases to 4 molecules at T > 100 K, mainly due to thermal population of low frequency intermolecular mode of $30cm^{-1}$ which destroys mutual coherence of dipole moments in the aggregate. Nonradiative relaxation becomes efficient with rise of temperature. The rate constant obeys in accordance with incoherent exciton features at T > 60 K.

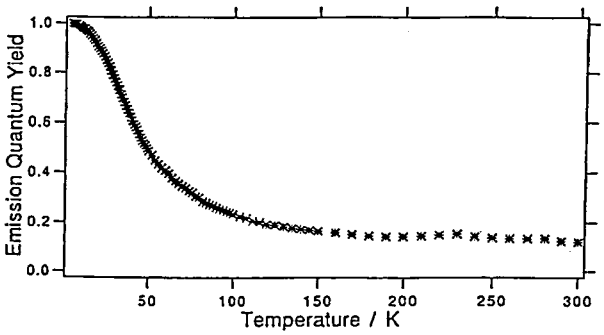

Figure 1. Temperature dependence of the relative quantum yield of BIC J-aggregate emission in the PVA film. Excitation 530 nm.

III-G Photochemistry on Well-Defined Surfaces

Recently, it has been found that upon the irradiation of light from visible to ultraviolet, a number of adsorbed molecules on metal surfaces reveal variety of photochemical processes, including photo-stimulated desorption, rearrangement of adsorbed states, photodissociation, and photo-initiated reactions with coadsorbates. Since photo-initiated reactions can be induced without any thermal activation of reactants, they may provide good opportunities for studying a new class of surface reactions which may not be induced thermally. We have studied photochemistry of various adsorption systems on well-defined metal and semiconductor surfaces mainly by temperature-programmed desorption (TPD), X-ray photoelectron spectroscopy (XPS), work function measurements, Near edge x-ray absorption fine structure (NEXAFS) and angular-resolved time-of-flight (TOF) spectroscopy of photodesorbed species associated with pulsed laser irradiation. Single crystals can be cooled to 40 K by a closed-cycle He refrigerator, which allows us to study physisorbed adsorbates and various combinations of coadsorbates.

III-G-1 Angular Distributions of N_2 in Photodissociation of N_2O Adsorbed on a Partially Oxidized Si(100) Surface at 95K

Jihwa LEE, Hiroyuki KATO *(Graduate Univ. for Advanced Studies)*, **Kyoichi SAWABE and Yoshiyasu MATSUMOTO**

[*Chem. Phys. Lett.* **240**, 417 (1995)]

The time-of-flight distributions of photofragment N_2 produced in UV photodissociation of N_2O adsorbed on a partially oxidized Si(100) surface at 95K have been measured as a function of the desorption angle. Photo-induced electron transfer initiates dissociation of N_2O to produce an adsorbed oxygen atom and energetic N_2 desorbing from the surface. Interestingly, the angular distribution of N_2 originating from chemisorbed N_2O molecules is peaked at ~32° from the surface normal. The observed results are discussed based on the bonding geometry and photodissociation dynamics of N_2O.

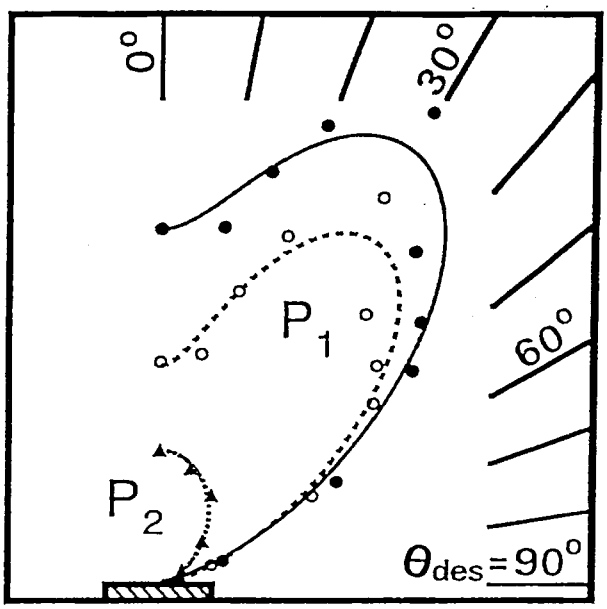

Figure 1. Polar plot for the angular distributions of N_2 obtained by velocity-weighted integration of the TOF distributions. The yields of the total (solid circle), P_1 component (open circles), and P_2 component (solid triangles) are shown together. The solid line shows the distribution of the total desorption yield represented by $0.75[\cos^{8.0}(\theta_{des} - 32°) + \cos^{8.0}(\theta_{des} + 32°)] + 0.25\cos^{2.2}\theta_{des}$, determined from least-squares fits. The fitted results for the P_1 and the P_2 components are also shown with broken and dotted lines, respectively.

III-G-2 NEXAFS Study on the Adsorption Structure of N_2O on a Si(100) Surface

Kyoichi SAWABE, Hiroyuki KATO *(Graduate Univ. for Advanced Studies)*, **Shin-ichiro TANAKA, Masao KAMADA and Yoshiyasu MATSUMOTO**

Angular distributions of photodesorbed species reflect on orientation of adsorbates and dynamics following electronic excitation by photon irradiation. We found that photo-induced dissociation of N_2O on a partially oxidized Si(100) surface shows a peculiar angular distribution; the angular distribution of photofragment N_2 originating from chemisorbed N_2O is peaked at ~32° from the surface normal.[1] In order to examine how initial orientation of the adsorbates is correlated with the angular distribution observed, we performed Near edge x-ray absorption fine structure (NEXAFS) measurements. The measurements have been done with a UHV system of the BL2B1 of the UV-SOR facility. NEXAFS spectra were taken by measuring partial electron yield as a function of incidence angle of light. There are two prominent peaks around the nitrogen K-edge: 401.1 and 404.6 eV. These peaks originate from the transitions from 1s orbitals of terminal and center N atoms of N_2O to the unoccupied π^* molecular orbital, respectively. Figure 1 shows the integrated area of the π^* resonance of the terminal nitrogen atom vs incidence angle of light. We analyzed the data assuming (1) N_2O adsorbates are linear and aligned along the direction of Si dimer bonds, and (2) the direction of the dipole transition moment is perpendicular to the molecular axis. Unfortunately, the accuracy of the tilt angle has larger error, since the dynamic range of π^* resonance around 40° is small. Thus, we estimate that the tilting angle of N_2O on the partially oxidized surface is 40°± 10°. The discrepancy from the observed peak of the N_2 angular distribution suggest that the dissociation dynamics also affects the angular distribution of photofragments.

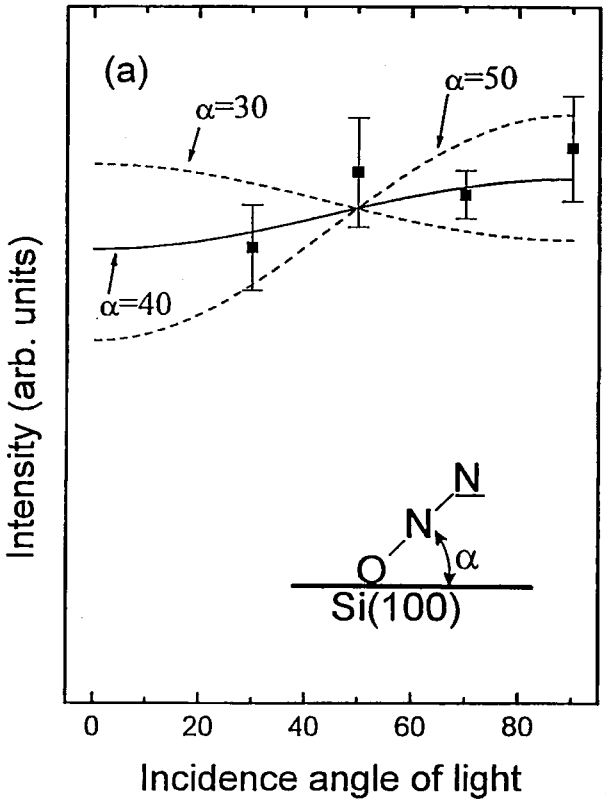

Figure 1. Plot of integrated area of the π^* resonance of terminal N around the nitrogen K-edge as a function of incidence angle of light. Curves are calculated results for tilting angle of 30°, 40°, and 50° from the surface plane.

Reference

1) J.Lee, H.Kato, K.Sawabe, and Y.Matsumoto, Chem. Phys. Lett. **240**, 417(1995).

III-H Activation of Methane

Since methane is the most abundant in natural gas and the least reactive alkane, it is vital to develop new conversion methods directly transforming methane to products such as alcohols and higher hydrocarbons in industry. Furthermore, it is very interesting to understand scientifically how methane is activated. Thus, the issue of "methane conversion" is a great challenge for chemists and now under intense study. Among catalytic processes in methane conversion, C-H bond cleavage on catalyst surfaces, i.e., "C-H bond activation", is generally considered to be the initial and most crucial step. While major efforts for C-H bond activation have been made to search catalysts on which methane dissociatively chemisorbed, we have taken photochemical approach in this study. It is well known that methane in the gas phase is transparent from visible to UV and has a continuous absorption band only in vacuum ultraviolet. Hence, methane dissociation through excitation of the band requires intense VUV photons that are not easily obtainable from conventional light sources and lasers. Thus, utilization of VUV photons for C-H bond activation is costly and not practical. However, in the last year, we have found that methane physisorbed on Pt(111) can be effectively dissociated with the irradiation of 193 nm-photons, yielding chemisorbed CH_3 and adsorbed H adsorbates as products. This year we have extended the study on the UV photodissociation of methane on Pt(111) to explore its excitation mechanism and dissociation and desorption dynamic.

III-H-1 Laser-Induced Photochemistry of Methane Adsorbed on a Pt(111) Surface

Yuri A. GRUZDKOV, Kazuo WATANABE, Kyoichi SAWABE and Yoshiyasu MATSUMOTO

[*J.Chem.Phys.* submitted]

Adsorbed states and photochemistry of methane and deuterated methane adsorbed on a Pt(111) surface have been investigated by temperature-programmed desorption, X-ray photoelectron spectroscopy, and work function measurements before and after irradiation with UV photons. Laser irradiation at 193 nm onto the Pt(111) surface covered with methane at 40 K leads to both desorption and dissociation of methane to methyl and hydrogen adsorbates. This is remarkably different from the photochemistry of methane in the gas phase where photodissociation takes place only at $\lambda \leq 145$ nm. With an extensive irradiation of 193-nm photons the photochemical processes are eventually quenched and the coverages of the photoproducts are saturated. Until the saturation region is reached about one half of the first layer methane is either dissociated or desorbed while the other one half unreacted

and remained on the surface. In contrast to the above findings, no photochemical reactions result from the 193-nm irradiation of methane adsorbed on a Xe/Pt(111) overlayer or from the 248-nm irradiation of methane on the bare Pt surface. These results indicate that under the irradiation of 193-nm photons the photochemical processes occur only for methane in close contact with substrate atoms. Furthermore, the observed photochemical processes suggest that electronic configurations of methane excited states are significantly mixed with substrate electronic states. Photodesorption dynamics has also been studied by measuring angle-resolved time-of-flight distributions as shown in figure1. In addition to the direct photodesorption, methane desorption takes place via associative recombination between a methyl adsorbate and a hydrogen atom produced by the photodissociation of adsorbed methane. Both desorption channels give sharp angular distributions along the surface normal.

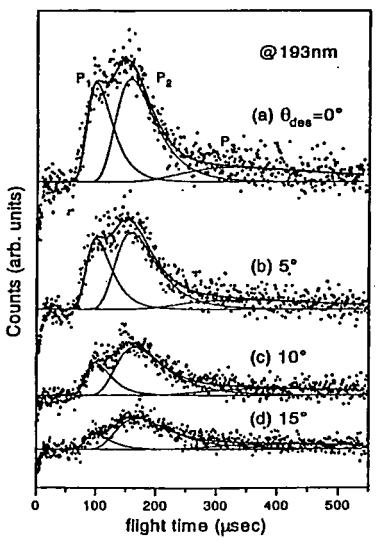

Figure 1. Time-of-flight distributions of CD_4 from Pt(111) as a function of the desorption angle. (a) 0° (along the surface normal), (b) 5°, (c) 10°, (d) 15°. The surface was saturated with CD_4 and irradiated with 193-nm photons. Signals were detected at m/e=20 (CD_4^+).

III-H-2 Photochemistry of Methane on Deuterium-Covered Pt(111) Surfaces

Yuri A. GRUZDKOV, Kazuo WATANABE, Kyoichi SAWABE and Yoshiyasu MATSUMOTO

[*Surf.Sci.* submitted]

Photochemistry of methane adsorbed on deuterium-precovered Pt(111) surfaces has been investigated by temperature-programmed desorption and X-ray photoelectron spectroscopy before and after irradiation with 193-nm photons. Two different deuterium adlayers are used: ordered D(1×1) and disordered D on Pt(111). Methane adsorbates on these D-covered surfaces at 40 K undergo either desorption or dissociation to methyl and hydrogen adsorbates. The H-D exchange reaction to produce CH_3D adsorbates also takes place. This reaction is due to photo-induced recombination between CH_3 photofragments and precovered D adatoms. As has been observed in methane on the bare Pt(111) surface, the photoreactions are quenched when about one half of methane adsorbates is depleted. The total depletion cross sections of methane on the D-covered surfaces are smaller than that on the bare surface. The fraction for the desorption (dissociation) channel increases (decreases) when the surface is congested with deuterium adatoms. When the surface is annealed after the photon irradiation, methyl adsorbates recombine either with photochemically produced H adatoms or pre-adsorbed D adatoms and desorb as CH_4 or CH_3D, respectively. The ratio of the desorption yield of CH_4 to CH_3D is larger than that expected from the kinetic isotope effect of the associative recombination. This result is discussed in terms of the non-uniform distribution of the photo-products and the restricted mobility of H (D) adatoms under the presence of CH_3 adsorbates.

III-I Dynamic Processes in Electronically -and/or Vibrationally-Excited Molecules

Fundamental molecular aspects of chemical reactions and energy transfer processes in the electronically or vibrationally excited states have been studied. Particular interests have been directed to the study of the photochemical reaction dynamics of carbonyl compounds, to the dynamics of vibrationally-excited van der Waals complexes using the stimulated-emission-pumping-laser-induced-fluorescence spectroscopy and the hole-burning spectroscopy, and to the photochemical reaction dynamics of the weakly-coupled complexes such as van der Waals and hydrogen-bonded complexes. Some applications of the stimulated-emission-pumping-laser-induced-fluorescence spectroscopy and the hole-burning spectroscopy are also presented to determine the molecular geometries and the vibronic structures in the excited electronic states.

III-I-1 Stimulated-Emission-Pumping Laser-Induced-Fluorescence Spectroscopy of Phenol and Anisole

Masao TAKAYANAGI and Ichiro HANAZAKI

[*Laser Chem.* **14**, 103 (1994)]

The SEP-LIF (Stimulated emission pumping-laser induced fluorescence) technique was applied to the investigation of dynamical behavior of vibrationally excited phenol and anisole produced in the supersonic expansion. In the SEP-LIF scheme, a molecule excited to a specific vibrational state by SEP is detected by measuring the LIF excitation spectrum with an appropriate delay to probe the vibrational relaxation. Four vibrational states, $6a_1$, $16a_2$, 12_1, and 1_1,, of phenol, and six vibrational states, $16b_1$, $18b_2$, $6a_1$, 12_1, $16a_2$ and 1_1, of anisole were investigated.

For both of phenol and anisole, it is found that the relaxation of the vibrational states below 1,000 cm^{-1} in the ground electronic state is so slow under the collisionless condition that only the transitions from the vibrational states initially prepared by SEP are observed as the SEP-induced bands in the SEP-LIF spectra. The low frequency torsional motion of methyl group in anisole does not accelerate IVR (intramolecular vibrational redistribution) much in this energy region.

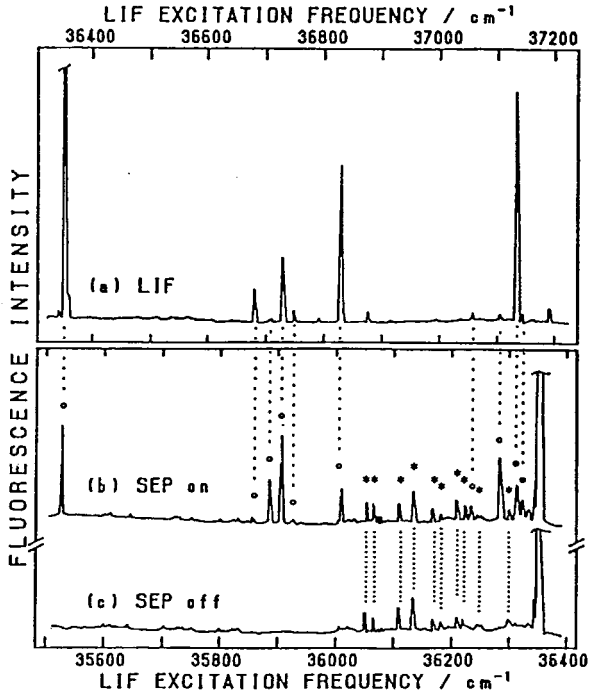

Figure 1. (a) LIF excitation spectrum of phenol (upper scale). (b) SEP-LIF spectrum with the SEP excitation to 12_1 (823 cm^{-1}), and (c) LIF excitation spectrum in the same frequency region as (b). The spectra in (b) and (c) are given with a shift of 823 cm^{-1} to the right with respect to (a). Thus (c) is the same LIF excitation spectrum as (a) which continues to the left end of (a). The bands marked by open circle in (b) appear upon the SEP excitation. Those with asterisk are the background bands observed without SEP.

III-I-2 The C=O Stretching Frequency in the $S_1(\pi^* - n)$ State of Acetaldehyde and its Deuterated Derivatives Determined with the Photofragment Excitation Spectroscopy

Takumi KONO, Masao TAKAYANAGI and Ichiro HANAZAKI

[*Laser Chem.* **15**, 249 (1995)]

The vibrational structure was recorded for the $S_1(\pi^* - n)$ state of acetaldehyde (CH_3CHO) and its deuterated derivatives (CH_3CDO, CD_3CHO and CD_3CDO) up to ~3500 cm^{-1} above the 0-0 bands with the LIF (laser induced fluorescence) and PHOFEX (photofragment excitation) techniques. In the PHOFEX spectroscopy, the yield of the formyl radical, HCO ($\tilde{X}$) or DCO ($\tilde{X}$), produced in the photodissociation of acetaldehyde is measured against the excitation frequency. The yield was determined by monitoring one of the rotational lines in the $\tilde{B} \leftarrow \tilde{X}$ transition of the formyl radical by the LIF technique. This is the first measurement of the vibronic structure of acetadehydes in supersonic jets above the dissociation threshold where they are non-fluorescent. The results have made it possible to locate ν_4 (the C=O stretching) and $2\nu_4$ unequivocally; the ν_4 fundamentals at 1217, 1189, 1210 and 1178 cm^{-1} above the 0-0 band for CH_3CHO, CH_3CDO, CH_3CDO, respectively. The corresponding overtone ($2\nu_4$) bands are observed, respectively, at 2414, 2350, 2399 and 2334 cm^{-1}. All the vibronic bands newly observed in the PHOFEX spectra are found to be interpreted as the combinations of ν_4 with the modes appearing in the lower frequency (< 1200cm^{-1}) region, which consists of ν_{10} (the C-C-O in-plane bending), ν_{14} (the C=O out-of-plane wagging) and ν_{15} (the methyl torsion).

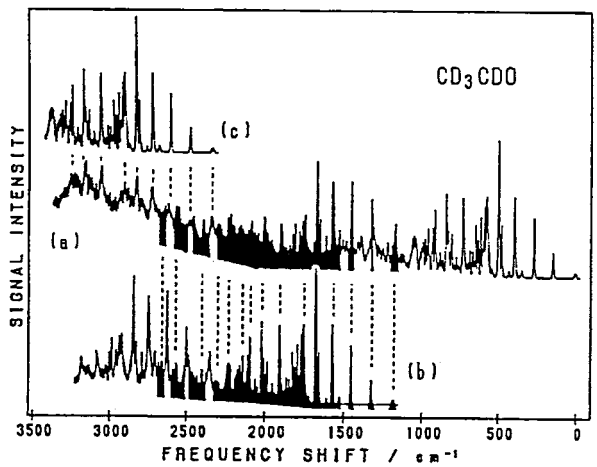

Figure 1. (a) Excitation spectrum of CD_3CDO synthesized from the LIF-excitation and PHOFEX spectra. (b) The same spectrum as (a) shifted by ν_4 (1178 cm^{-1}) to the higher energy. (c) The same spectrum as (a) shifted by $2\nu_4$ (2334 cm^{-1}). Shaded bands in (b) belong to 0_0^0, while those shaded in (a) belong to 4_0^1.

III-I-3 Geometry and Torsional Potential of *2,2'*-Bithiophene in a Supersonic Jet

Masao TAKAYANAGI, Tatsuo GEJO and Ichiro HANAZAKI

[*J. Phys. Chem.* **98**, 12893 (1994)]

Fluorescence-excitation, hole-burning, and dispersed-fluorescence spectra of *2,2'*-bithiophene in a supersonic jet were measured. Two species were identified in the fluorescence-excitation spectra and were distinguished clearly in the hole-burning spectra. These species have the origin bands with the 91.4 cm^{-1} shift to each other and show almost the same vibronic structures. They are assigned to the vibronic bands due to *2,2'*-bithiophene in the ground and low-lying excited vibrational states. Long and harmonic bands due to the torsional vibration in the excited electronic state suggest a substantial change in the torsional angle upon the electronic excitation. The equilibrium structure in the excited electronic state is found to be *trans* planer with a deep, harmonic, and single-minimum torsional potential. In the dispersed-fluorescence spectra, short and anharmonic progressions due to the torsional vibration in the ground electronic state were observed. By simulating the progressions, *2,2'*-bithiophene in the ground electronic state is found to have a double-minimum torsional potential, whose equilibrium

structures are twisted by about 21° from the *trans*-plannar structure. The height of the barrier between the minima is estimated to be about 25 cm^{-1}. Franck-Condon calculations were also performed to examine the observed intensity distributions in the fluorescence-excitation, hole-burning, and dispersed-fluorescence spectra.

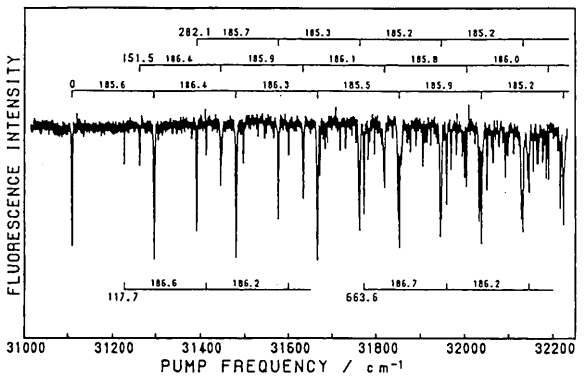

Figure 1. Hole-burning spectrum of *2,2'*-bithiophene measured with the probe laser tuned at ν_0^0, (the origin band of the main component).

III-I-4 Internal Rotation of the Methyl Group in the *m*-Tolinitrile·Rare Gas Complexes

Masao TAKAYANAGI *(Tokyo University of Agriculture and Technology)* **and Ichiro HANAZAKI**

The $S_1 \leftarrow S_0$ excitation spectra of *m*-tolunitrile and its 1:1 complexes with Ne, Ar and Kr were measured under the supersonic jet condition by the laser-induced-fluorescence and hole-burning techniques. The observed torsional frequencies (in units of cm^{-1}) are as follows:

	$3'a_1$	2'e	4'e
monomer	57.1	22.0	81.9
m-tolunitrile·Ne	56.8	24.3	83.5
m-tolunitrile·Ar	58.5	26.7	84.7
m-tolunitrile·Kr	60.2	29.4	86.5

The torsional potentials for the internal rotation of the methyl group in the S_1 state were determined from the observed torsional frequencies. The effect of the complex formation on the torsional potential is discussed.

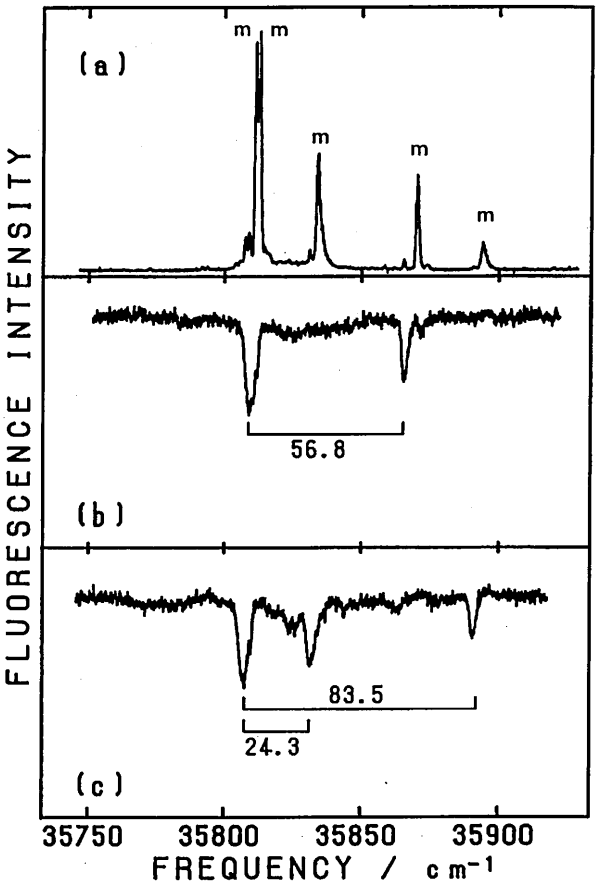

Figure 1. LIF-excitation and hole burning spectra of *m*-tolunitrile seeded in Ne.
(a) LIF-excitation spectrum. The bands due to the monomer are marked with *m*.
(b) Hole burning spectrum of the *m*-tolunitrile·Ne complex measured by probing the $0'a_1 \leftarrow 0''a_1$ band at 35808.4 cm^{-1}.
(c) Hole burning spectrum of the *m*-tolunitrile·Ne complex measured by probing the 1'e ← 1"e band at 35806.9 cm^{-1}. Torsional frequencies are shown in (b) and (c).

III-I-5 Photodissociation of $N_2O \cdot H_2O$ in a Supersonic Jet

Masao TAKAYANAGI *(Tokyo Univ. Agrlic. & Tech.)*, **Nobuaki TANAKA, Hong-Lae KIM** *(Kangweon Natl. Univ. Korea)* **and Ichiro HANAZAKI**

The 193 nm photodissociation of the $N_2O \cdot H_2O$ complex produced in a supersonic jet undergoes a reactant-pair reaction, $N_2O \cdot H_2O + h\nu \rightarrow 2OH + N_2$. It is interesting to use the ^{18}O-labelled water in place of the normal water in this reaction, since in the case of the corresponding bimolecular reaction, $N_2O + h\nu \rightarrow O(^1D) + N_2$, $O(^1D) + H_2O \rightarrow 2OH$, the "new" OH produced by the extraction of one of the water hydrogens by $O(^1D)$ and the "old" OH left after the extraction can be distinguished as ^{16}OH and ^{18}OH, respectively. We have measured the relative populations in various rotational states of the products, ^{16}OH and ^{18}OH, produced in the 193 nm photodissociation of $N_2O \cdot H_2{}^{18}O$ in a supersonic jet. A typical result is shown in Figure 1 in the form of the Boltzmann plot of relative populations measured by the laser-induced-fluorescence technique. It shows clearly that there is no distinction

between the rotational distributions of ^{16}OH and ^{18}OH. This result indicates that the reactant-pair reaction initiated by the photodissociation of the $N_2O{\cdot}H_2O$ complex must proceed through a relatively long-lived intermediate in which rotational energy is randomized over two OH radicals. The intermediate is possibly a hydrogen peroxide type with the life time of at least 100 ps. This is in sharp contrast with the corresponding bimolecular reaction where the "new" OH has a considerably higher rotational temperature than the "old" OH.

$$N_2{}^{16}O{\cdot}H_2{}^{18}O \rightarrow N_2 + {}^{16}OH + {}^{18}OH$$

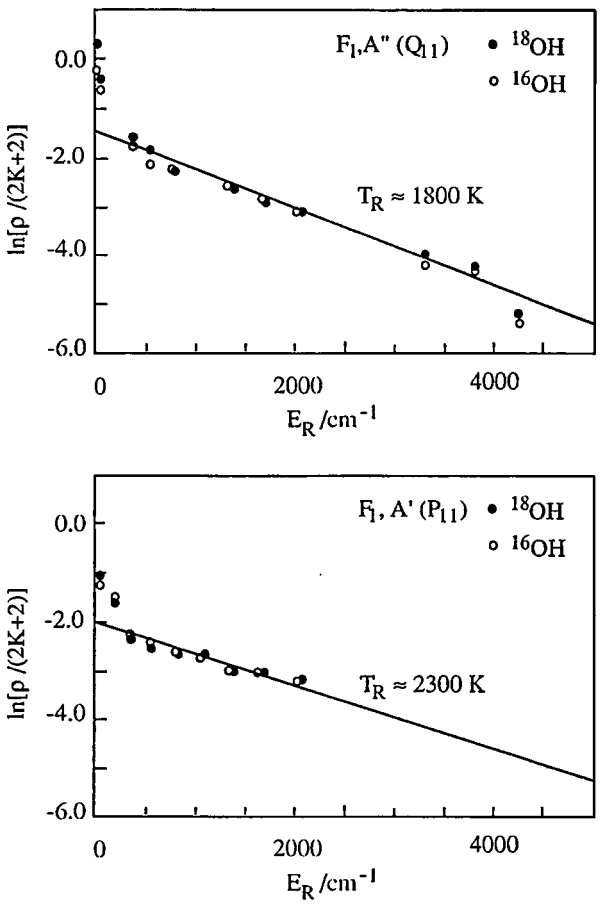

Figure 1. Boltzmann plots for the rotational distibution in ^{16}OH and ^{18}OH produced in the reactant-pair reaction of $N_2O{\cdot}H_2{}^{18}O$ initiated by the 193 nm photolysis in a supersonic jet.

III-I-6 Development of Methodology to Detect Product in a Quantum State with Translational Energy Measurements

Suketu R. GANDHI and Ichiro HANAZAKI

In a course of a chemical reaction involving bond breaking (*i.e.*, ABC → AB + C) the products are characterized by their internal and translational energy. In many times, same products get formed from different channels. To study particular mechanism (or channel), it is necessary to get complete information on energetics on the product. Conventional method uses fluorescence detection with Doppler effect, where one needs to use a very narrow bandwidth tunable laser source. The available intensities by typical laser sources are weak, so it can be applied only to those systems that can undergo one photon process.

With the availability of intense UV laser source, it is possible to carry out detection of molecules down to 200 nm region with multi-photon ionization (MPI) detection scheme. When carrying out detection in a mass spectrometer, one can directly observe the products of interest. By detecting products in time-of-flight mass spectrometer (TOFMS) when operated in a low mass resolution mode, a possibility exists to measure translational energy of products in a particular quantum states (*i.e.*, rotational, vibrational or electronic). The resolution of the translational energy of photofragments depends on the ionization laser pulse duration and the E-field used to accelerate the ions. That is, one obtains better resolution by using a short laser pulse and small E-field as possible. However, by applying small E-field, one loses sensitivity due to not all ion trajectories can make it into a detector. For this reason, it is necessary to have short drift tube of a TOFMS.

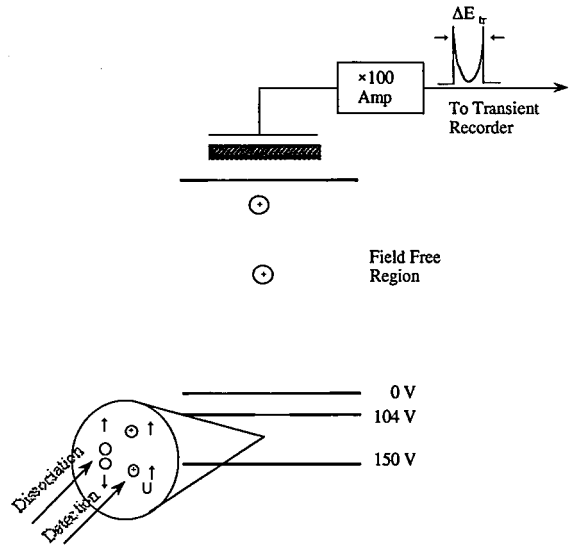

Figure 1. Sketch of a time of flight mass spectrometer used for making a translational energy measurements of photofragments. Here, molecules first get dissociated, that results in fragments having initial translational energy. Afterwards, the fragments are converted into their ions by MPI. Those ions initially moving upward get accelerated, while those ions having their velocity directed downwards first decelerate, and then accelerate upward before moving into the field free region. There, ions get detected by a pair of microchannel plates, and the resulting signal is amplified.

III-I-7 Translational Energy Measurements of CH_3 upon Dissociation of CH_3CHO after Irradiation the UV Photons

Suketu R. GANDHI and Ichiro HANAZAKI

When CH_3CHO gets irradiated with UV photons from 280-317 nm range, the molecule fragments into $\cdot CH_3$ and $\cdot CHO$. Furthermore, it is known that dissociation takes place on slow time scale (~10-100 ns). By detecting photofragments (*i.e.*, CH_3) by use of multi-photon ionization in a time-of-flight mass spectrometer (TOFMS), a possibility exists to measure translational energy. Here we operate the TOFMS in a low mass resolution mode (or high translational energy mode) to obtain translational energy of photofragment. From translational energy measurements of CH_3 in various ro-vibrational states, we ascertain the translational energy of the other fragment

(*i.e.*, HCO), hence the internal energy contents. This experimental approach for detecting fragments with translational energy measurements complements the previous studies on dissociation of CH_3CHO.

III-I-8 Dissociation Rate Measurements of CH_3CHO upon Irradiation of UV photons

Suketu R. GANDHI and Ichiro HANAZAKI

Upon irradiation of CH_3CHO with UV photons, the molecule dissociates into $\cdot CH_3$ and $\cdot CHO$. The dissociation time scales are on the order ~10-100 ns, which makes it possible to carry out the measurement of risetime of fragments with ns pulsed laser. To ensure that fragments-pair in particular products gets detected, it is necessary to detect the fragments having complete information (*i.e.*, rovibronic and translational energy). This is done by carrying out the MPI detection process in a time-of-flight mass spectrometer which is operated in a low mass resolution mode. By detecting products that arrive at a particular time, it is possible to determine the rise time of a fragment in a particular state.

III-I-9 Nascent State Distributions of OH Radicals Produced in the Reaction of $O(^1D)$ with H_2O

Nobuaki TANAKA, Masao TAKAYANAGI (*Tokyo Univ. of Agric. and Tech.*) **and Ichiro HANAZAKI**

The rotational and vibrational state distributions of OH radicals for the reaction $O(^1D) + H_2O \rightarrow 2OH$ using N_2O as a precursor of $O(^1D)$ have been measured by a laser-induced fluorescence technique. In order to distinguish two chemically identical OH products and determine their state distributions, isotopically labeled water $H_2{}^{18}O$ was used as a reactant. The rotational distributions of two OH products in the v"=0 level were characterized by Boltzmann statistics with temperatures of 6000 and 2600 K for ^{16}OH and ^{18}OH, respectively. ^{16}OH was formed with vibrational population in the ratio ~0.9 (v"=1/v"=0) while ^{18}OH was much colder. The observed differences between ^{18}OH and ^{16}OH were similar to those observed for the corresponding reaction where ^{16}O was formed by photolysis of O_3.[1] Both OH radicals produced in the bimolecular reaction were formed with more rotational energy than those (2000 K) obtained in the reactant-pair reaction $N_2O{\cdot}H_2O + h\nu \rightarrow 2OH + N_2$ where there was no difference in the rotational temperatures of two OH products.[2] These results seem to indicate the bimolecular reaction is explained in terms of the abstraction mechanism.

References

1) D. G. Sauder, J. C. Stephenson, D. S. King, and M. P. Casassa, *J. Chem. Phys.* **97**, 952 (1992).
2) H.-L. Kim, M. Takayanagi and I. Hanazaki, *Chem. Phys. Lett.* **218**, 151 (1994).

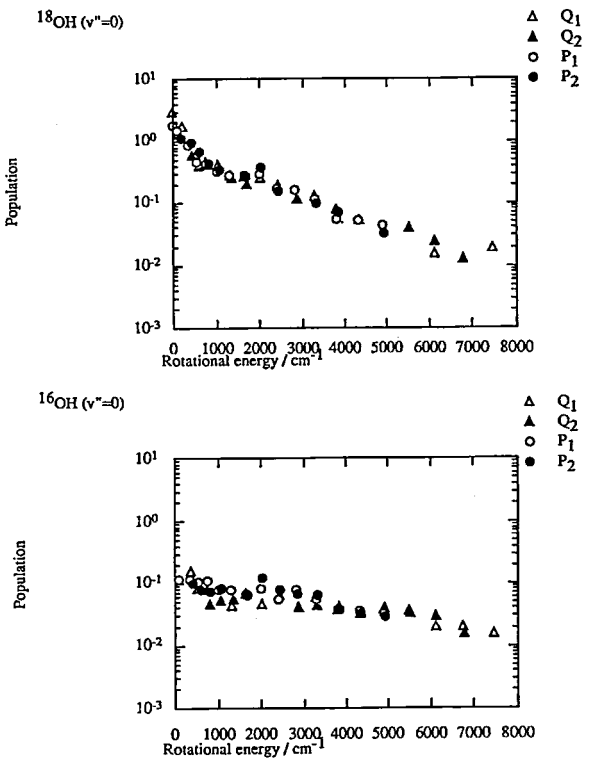

Figure 1. Boltzmann plots of relative populations for the v"=0 level of ^{18}OH and ^{16}OH.

III-J Self-Organization in Chemical Reactions

The self-organizing process in chemical systems is known to occur as a result of nonlinear chemical processes. This kind of chemical systems exhibit sustained temporal chemical oscillations and spatial pattern formation. Moreover, they sometimes exhibit more complicated nonlinear phenomena such as bistability, excitability, multi-frequency oscillations, and the chaotic behavior. They have received attention for their close relation to the activity of living systems in the spontaneously-organized dynamic behavior. Possible applications of such phenomena to the sensing- and image storage devices have also been interested in. We have paid a special attention to the response of chemical oscillator systems to photo-illumination, which is very important in view of the above-mentioned interests but have not been studied so far in any systematic manner. Here we present some results of the studies on bifurcation structures in the chemical oscillators under the stationary light illumination.

III-J-1 Photo-response of Chemical Oscillators

Ichiro HANAZAKI, Yoshihito MORI (*Nagoya Inst. Tech.*), **Tetsuo SEKIGUCHI** (*Graduate Univ. for Advanced Studies*) **and Gyula RÁBAI** (*Kossuth Rajos Univ., Hungary*)

[*Physica D* **84**, 228 (1995)]

The method proposed earlier by one of the authors to analyze quantitatively the wavelength- and intensity-dependence of the light irradiation effect on chemical oscillators is critically re-examined. By measuring the critical light power for the photo-induction or -inhibition of chemical oscillations, it is possible to determine the cross sections of photo-induction or -inhibition as a func-

tion of light wavelength. The action spectrum thus obtained shows clearly the wavelength-dependent photo-response of the chemical oscillator system. Some applications of this method to analyze the effect of stationary light illumination on the Belousov-Zhabotinsky and related minimal oscillator systems are discussed in detail to explore the primary process and subsequent reactions of the key intermediates responsible for the photo-response. Some hints are given for possible future developments for the photo-control of chemical oscillators together with a description of preliminary results of experiments being underway in our laboratory.

III-J-2 Oxidation of Thiocyanate by Bromate Is Not an Oscillatory Reaction in a Batch Reactor

Gyula RÁBAI (*Kossuth Rajos Univ., Hungary*) **and Ichiro HANAZAKI**

[*J. Phys. Chem.* **99**, 10061 (1995)]

Valent and Adamcikova's recent report on the strange dynamical behavior in the bromate-thiocyanate reaction in a batch reactor is re-examined and criticized. In our typical run, 9.25 mL of 0.10 M $HClO_4$ solution containing 0.081 M $NaBrO_3$ was prethermostated at 20 ± 0.1°C in a cylindrical-shaped glass vessel with a volume of 17 mL. N_2 was bubbled through the solution at 8 ± 1 mL s^{-1} flow rate. The reaction was initiated by injecting 0.75 mL of 0.10 M NaSCN dissolved in 0.10 M $HClO_4$. We have found that the redox potential suddenly drops to 565 mV upon addition of NaSCN and then rises in two well-separated stages. First, it reaches 875 mV with an increasing rate. At 875 mV, it slows suddenly and accelerates again and continues to rise to a final value. It is seen that only monotonous changes were observed and no oscillatory responses were found in contrast to Valent and Adamcikova's results. Based on this well-controlled experiments, we suggest that their irregular potentiometric traces are resulted from poorly controlled experimetal conditions rather than chemical reactions.

III-J-3 Photo-Induced Disproportionation of Iodomalonic Acid

Gyula RÁBAI (*Kossuth Rajos Univ., Hungary*) **and Ichiro HANAZAKI**

[*Intern. J. Chem. Kinetics* **27** 431 (1995)]

The stoichiometry, equilibrium, and kinetics of the photo-induced disproportionation of iodomalonic acid to I^-, I_2, and tartronic acid have been studied by means of spectrophotometry and iodide-selective electrode at 20.0 ± 0.2°C, pH 2.0 - 4.0. At pH > 2.9, only I^- and $HOCH(COOH)_2$ are detected as major products and the reaction reaches 100% conversion. At pH < 2.0, I_2 and malonic acid are also formed and the reaction stops at a conversion rate less than 100%. Both UV(band with a peak at 360 nm) and visible light (480 nm) have been found to be effective. Two primary photochemical processes are identified:

(M1) $ICH(COOH)_2 + h\nu \rightarrow I\cdot + \cdot CH(COOH)_2$

(M2) $I_2 + h\nu \rightarrow 2I\cdot$

While both reactions are sensitive to UV light, only (M2) can be affected by visible light. (M1) and (M2) are considered to initiate a chain sequence in which I· radicals oxidize iodomalonic acid.

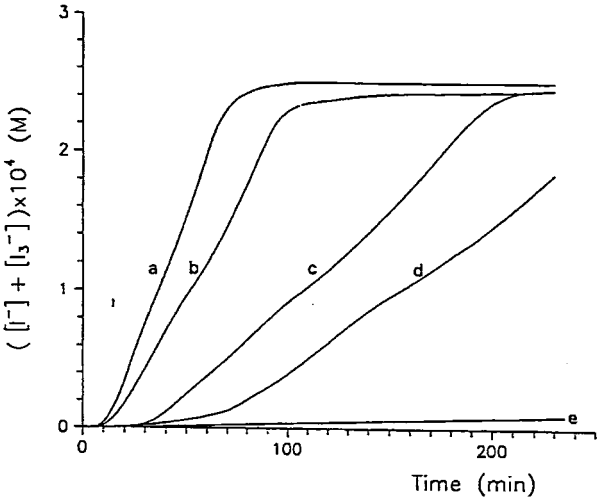

Figure 1. Typical ($[I^-] + [I_3^-]$) vs. time curves obtained in iodomalonic acid solution under illumination with 480 nm light. $[IMA]_0 = 1.0\times10^{-3}$ M, pH = 2.0. The integral light power was (a) 5.2, (b) 3.2, (c) 2.1 and (d) 1.4 μW/mL, T = 20°C.

III-J-4 The Role of the Dushman Reaction and the Ferricyanide Ion in the Oscillatory IO_3^- - SO_3^{2-} - $Fe(CN)_6^{4-}$ Reaction

Gyula RÁBAI (*Kossuth Rajos Univ., Hungary*), **Akiko KAMINAGA and Ichiro HANAZAKI**

[*J. Phys. Chem.* **99**, 9795 (1995)]

The effect of the iodide ions on the rate of the composite reactions of the oscillatory IO_3^- - SO_3^{2-} - $Fe(CN)_6^{4-}$ system suggests that the role of the iodate (Dushman) reaction is small in the composite reaction between IO_3^- and SO_3^{2-} (positive feedback pathway), while it appears to be the main route for the IO_3^- - $Fe(CN)_6^{4-}$ reaction (negative feedback). It is found that oscillations in a semibatch reactor are preceded by a long nonoscillatory period during which the pH is about 5. Oscillations start without a nonoscillatory period if iodide is added to the reaction mixture at the beginning. These experiments confirm the role of the Dushman reaction in the negative feedback loop. No preoscillatory period is observed in the analogous BrO_3^- - SO_3^{2-} - $Fe(CN)_6^{4-}$ oscillator in a semibatch reactor. It is also shown that ferricyanide is kinetically important as a consequence of its reaction with sulfite. Modeling of the behavior both in a semibatch configuration and in a CSTR with a set of composite reactions is carried out.

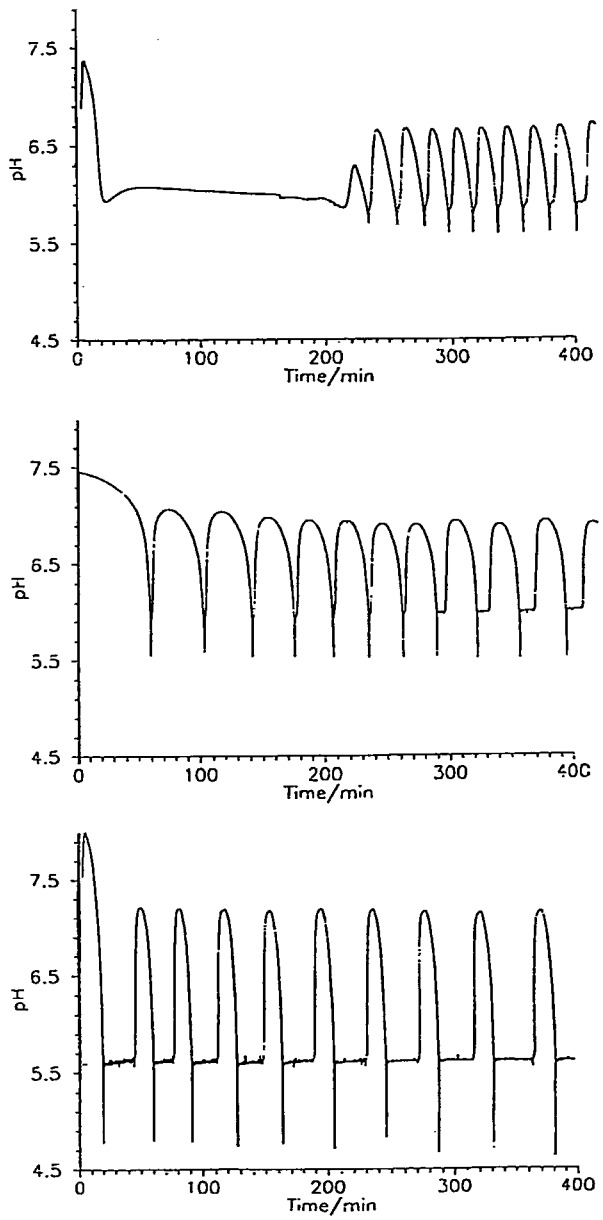

Figure 1. (**a**, top) Preoscillatory period and pH oscillations in a semibatch reactor. Solution of 0.2 M Na_2SO_3 containing 0.005 M H_2SO_4 is flowed, at 12 mL/h, into 200 mL of a solution containing 0.10 M $NaIO_3$ and 0.02 M $K_4Fe(CN)_6$. T = 40°C. (**b**, middle) The batch contains, besides iodate and ferrocyanide, 0.03 M KI. Other conditions are the same as in (a). Observe the lack of a preoscillatory period. (**c**, bottom) The batch contains, besides iodate and ferrocyanide, 0.03 M KI and 0.005 M $K_3Fe(CN)_6$. Other conditions are the same as in (a).

III-J-5 Frequency-Multiplying Bifurcation in the Oscillatory Belousov-Zhabotinsky Reaction Proceeding in Interacting Water Droplets of Reverse Microemulsion of Aerosol OT in Octane

Vladimir K. VANAG *(N. N. Semenov Institute of Chemical Physics, Russian Academy of Sciences)* **and Ichiro HANAZAKI**

[*J. Phys. Chem.* **99**, 6944 (1995)]

The ferroin-catalyzed Belousov-Zhabotinsky oscillatory reaction exhibits frequency-multiplying bifurcation including frequency-doubling, -tripling and -quadrupling when it proceeds in water-in-oil microemulsions of the anionic surfactant, Aerosol OT. This bifurcation occurs only when the water volume fraction ϕ_w is large enough (> 0.05) and the system is not flowed (batch conditions), or flowed at a very low rate. Bubbling gas through the reactor prohibits bifurcation. Clusters of microemulsion droplets (possibly in the percolation structure) appearing at relatively high ϕ_w are suggested to behave as mini-oscillators and their mutual coupling determines the mode of bifurcation. It is also suggested that bromine produced in oscillatory reactions is stored in the organic phase and governs the frequency-multiplying bifurcation by enhancing the coupling between clusters.

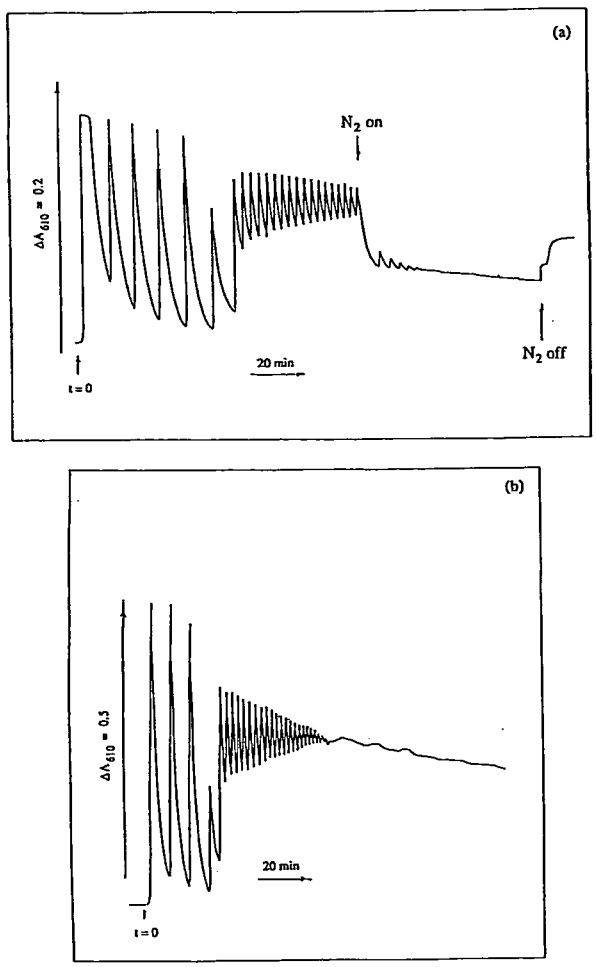

Figure 1. Kinetics of the ferroin-catalyzed BZ reaction in AOT reverse micelles in octane. (a) ω = 18, ϕ_w = 0.055, k_0 = 0 and stirring rate 720 rpm. $[H_2SO_4]_{0w}$ = 0.3 M, $[BrO_3^-)]_{0w}$ = 0.1 M, $[MA]_{0w}$ = 0.25 M and $[Ferroin]_{0w}$ = 2.24 M. Nitrogen bubbling was started at "N_2 on" and terminated at "N_2 off". (b) The experimental conditions are the same as those in (a) except for ω = 9.8 and ϕ_w = 0.11.

III-J-6 The pH Dependence of the Belousov-Zhabotinsky Reaction in Water-in-Oil Reverse Microemulsion of AOT in Octane

Vladimir K. VANAG *(N. N. Semenov Institute of Chemical Physics, Russian Academy of Sciences)* **and Ichiro HANAZAKI**

The ferroin-catalyzed Belousov-Zhabotinsky reaction in water-in-oil microemulsion with anionic surfactant Aerosol OT exhibits chemical oscillations in spite of the

extremely high pH in the aqueous pseudo-phase. We found that, unlike the reaction in homogeneous aqueous solution, the oscillation period is independent of the initial concentration of sulfuric acid for the range $[H_2SO_4]_0$ = 0.1 - 0.3 M. The exponent of the autocatalytic [ferriin] growth was found to depend on $[NaBrO_3]_0$ quadratically and on $[H_2SO_4]_0$ linearly. It is suggested that a possible increase in pKa of $HBrO_3$ in the reverse micelles requires a modified reaction scheme, which accounts for the observed dependency and explains why chemical oscillations can be observed in reverse micelles under unusually high pH conditions.

III-J-7 Molecular Dynamics Simulations of Non-equilibrium Spatial Correlations in a Reaction Diffusion System

Jerzy GORECKI *(Inst. Phys. Chem., Polish Acd. Sci., Poland)*, **Kazuo KITAHARA** *(Tokyo Inst. Tech.)*, **Kenichi YOSHIKAWA** *(Nagoya Univ.)* **and Ichiro HANAZAKI**

The mesoscopic description of a system with chemical reactions predicts that if the detailed balance condition is not satisfied, then nonequibrium spatial correlations between concentrations of reactions may appear. The present work is concerned with molecular dynamics simulations of such correlations in a model system of "reacting" hard spheres. The simulations have shown that if the detailed balance condition is satisfied, then the non-equilibrium spatial correlations are absent. In a steady state for which the detailed balance condition is not satisfied, the nonequilibrium correlations are present and their spatial exponential decay predicted by the theory based on a master equation, is confirmed in our simulations.

III-J-8 The Effect of the Light Irradiation for the Subsystem of the Ferrocyanide-Bromate-Sulfite System under the Batch Condition

Akiko KAMINAGA, Gyula RÁBAI *(Kossuth Lajos Univ., Hungary)* **and Ichiro HANAZAKI**

We have found that the ferrocyanide-bromate-sulfite system, one of the flow-controlled pH oscillators is sensitive to photoirradiation in the visible region. Photo-response of the two subsystems, the H^+-producing SO_3^{2-}-BrO_3^--H^+ system and the H^+-consuming $Fe(CN)_6^{4-}$-BrO_3^--H^+ system is studied in a batch configuration. No effect of light irradiation is observeed for the subsystem containing SO_3^{2-}, BrO_3^-, and sulfuric acid (Figure 1(A)). On the contrary, a remarkable effect of light irradiation has been found for the subsystem containing $Fe(CN)_6^{4-}$, BrO_3^-, and sulfuric acid (Figure 1(B)). As the irradiation light power increased, pH of the reaction mixture rise faster. It is postulated that the visible light causes photoaquation reaction of both $Fe(CN)_6^{4-}$ and $Fe(CN)_6^{3-}$.[2] Since the light with an strong line at λ = 436 nm, around which only $Fe(CN)_6^{3-}$ has large molar absorption coefficient can accelerate this process, the photoaquation of $Fe(CN)_6^{3-}$ must be mainly responsible to the observed photo-enhancement of the H^+-consuming process.

Reference

1) Gy. Rábai and I. R. Epstein, *Inorg. Chem.* **28**, 732 (1989).
2) A. W. Adamson, W. L. Waltz, E. Zintano, D. W. Watts, P. D. Fleischauer, and R. D. Lindholm, *Chem. Rev.* **68**, 541 (1968).

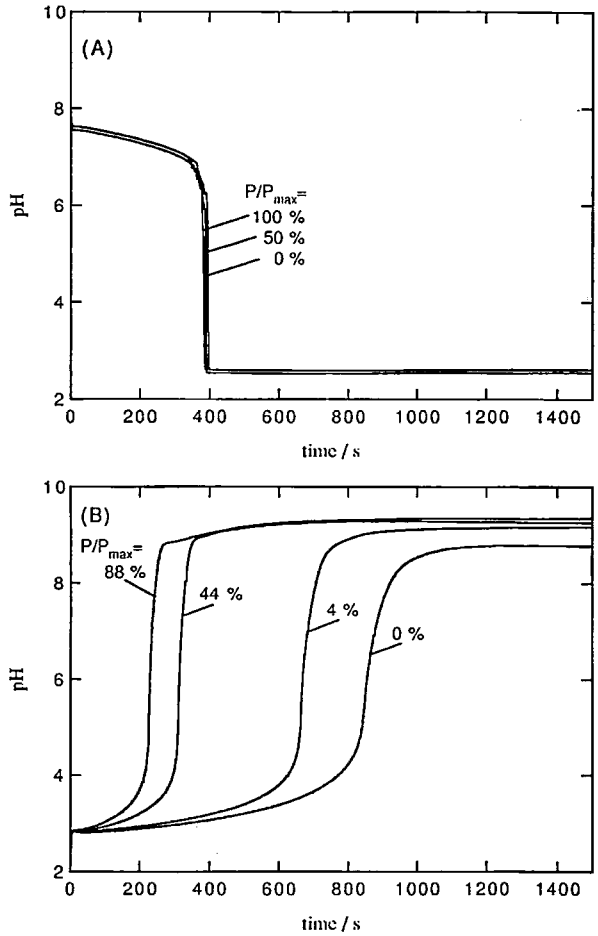

Figure 1. (A) Measured pH for the batch BrO_3^-- SO_3^{2-} reactions under the light irradiation with wavelengths λ > 375 nm by using a L40 filter. The initial concentrations are $[BrO_3^-]_0$ = 75 mM, $[SO_3^{2-}]_0$ = 90 mM, and $[H_2SO_4]_0$ = 7.5 mM. T = 35°C. (B) Measured pH for the batch BrO_3^--$Fe(CN)_6^{4-}$ reactions under the light irradiation with wavelengths λ > 405 nm by using a L42 filter. The initial concentrations are $[BrO_3^-]_0$ = 75 mM, $[Fe(CN)_6^{4-}]_0$ = 15 mM, and $[H_2SO_4]_0$ = 6.0 mM. T = 35°C.

III-J-9 Photo-Induced Bifurcation in the Ferrocyanide-Bromate-Sulfite System under the Flow Condition

Akiko KAMINAGA, Gyula RÁBAI *(Kossuth Lajos Univ., Hungary)* **and Ichiro HANAZAKI**

The ferrocyanide-bromate-sulfite system, which is flow-controlled pH oscillator, has been found to be photosensitive, exhibiting both photo-induction and -inhibition of oscillations. We have determined photo-response of this system for the visible light (λ > 375 nm) in the form of a state diagram spannded by the irradiation light intensity, P and the flow rate, k_0 (Figure 1). Hysterisis is observed for the bifurcation between Oscillatory (OSC) and high pH steady state (SSH) similarly to the dark case. The photo-response has been found to be due to the H^+-consuming ferrocyanide-bromate reaction (1).[1,2]

$$BrO_3^- + 2\,Fe(CN)_6^{4-} + 3H^+ \rightarrow HBrO_2 + 2Fe(CN)_6^{3-} + H_2O \quad (1)$$

If the system in the low pH steady state is irradiated, (1) is enhanced to become competable with the rate of H^+-production by the reaction between sulfite and bromate. Oscillations start at a lower k_0 than under the dark condition. Irradiation of the system oscillating in the dark results in over-enhancement of (1) bringing the system into SSH.

Reference

1) E. C. Edblom, Y. Luo, M. Orbán, K. Kustin and I. R. Epstein, *J. Phys. Chem.* **93**, 2722 (1989).
2) Gy. Rábai and I. R. Epstein, *Inorg. Chem.* **28**, 732 (1989).

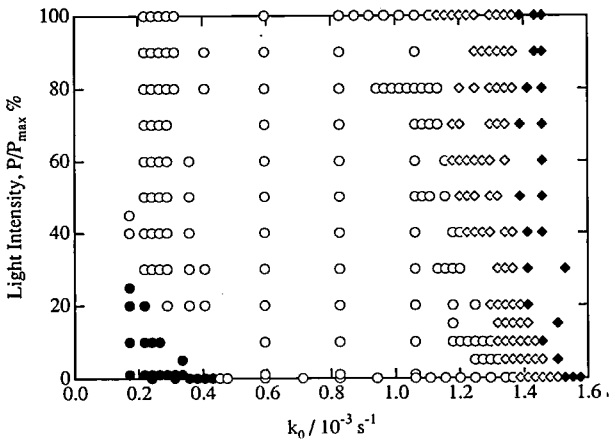

Figure 1. Phase diagram for the $Fe(CN)_6^{4-}$-BrO_3^--SO_3^{2-} oscillator in the k_0-P plane at T = 35°C. Symbols: (○) Oscillatory, (●) low pH steady, (◆) high pH steady, and (◇) bistable.

III-J-10 Photoinduced Bifurcation and Multistability in the Oscillatory Briggs-Rauscher Reaction

Noriaki OKAZAKI, Yoshihito MORI and Ichiro HANAZAKI

The effect of 460-nm monochromatic light irradiation in the Briggs-Rauscher system has been investigated by the continuous light-intensity scanning method, with a systematical variation of the initial concentration of I^- ($[I^-]_0$). A cross-shaped phase diagram has been established in the control-parameter plane spanned by $[I^-]_0$ and light power (P_0) as shown in Figure 1: increase of $[I^-]_0$ leads to the transition from the large-amplitude oscillatory state (OS) to the nonradical steady state (SSI), whereas increase of P_0 gives rise to the transition from OS to the radical steady state (SSII). Both the transitions are accompanied by hysteresis, resulting in the tristability among OS, SSI and SSII in the overlapped part of the two hysteresis regions. The critical value of $[I^-]_0$ for the SSI→OS transition tends to increase with P_0, making it possible to observe the photoinduction of oscillations in the restricted region of $[I^-]_0$. Within the low $[I^-]_0$ region, the existence of bistability between OS and another oscillatory state with small amplitude (OS') has been discovered. The transition between OS and SSI is simply interpreted as a result of the change in $[I^-]$ induced by the external supply of I^- and the photoirradiation. On the other hand, the transition between OS and SSII cannnot be explained satisfactorily only by these factors. A possible involvement of the photo-assisted positive feedback loop multiplying I_2 is suggested for the latter transition.

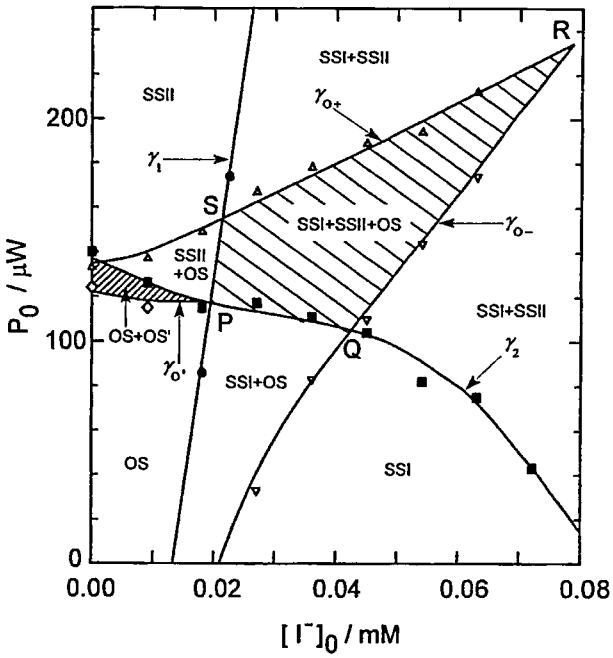

Figure 1. Two-dimensional state diagram spanned by the initial concentration of I^- ($[I^-]_0$) and the 460-nm monochromatic light intensity (P_0). Experimental conditions are: $[KIO_3]_0$ = 200 mM, $[MnSO_4]_0$ = 2.3 mM, $[HClO_4]_0$ = 25 mM, $[H_2O_2]$ = 200 mM, $[CH_2(COOH)_2]_0$ = 2.0 mM, temperature = 25.0°C and residence time = 3.6 min.

III-J-11 Photoinduced Bifurcation in the Starch-Added Briggs-Rauscher Reaction

Noriaki OKAZAKI, Yoshihito MORI and Ichiro HANAZAKI

The photoinduced bifurcations are studied for the starch-added Briggs-Rauscher system with varying the initial concentration of starch ($[starch]_0$) systematically. The results are summarized in the form of two-dimensional state diagram spanned by $[starch]_0$ and the 460-nm monochromatic light intensity (P_0) as shown in Figure 1. In the low $[starch]_0$ region, increase of P_0 makes the system bifurcate from large-amplitude oscillatory state (OS) to the radical steady state (SSII). As $[starch]_0$ is increased, a novel oscillatory state with small amplitude (OS") has been found to emerge in the higher light intensity region. The stable region of OS" broadens with increasing $[starch]_0$, untill finally it merges into the original large-amplitude oscillatory region. In the vicinity of the merging point, the bistability between OS and OS" has been discovered (the hatched region). Although the mechanism is still not clear at this stage, the nonlinearity associated with the screening effect of starch-iodine complex, which keeps I_2 from the photodissociation process, is considered to be one of the possible source leading to the complicated state diagram. A qualitative modeling is currently under way.

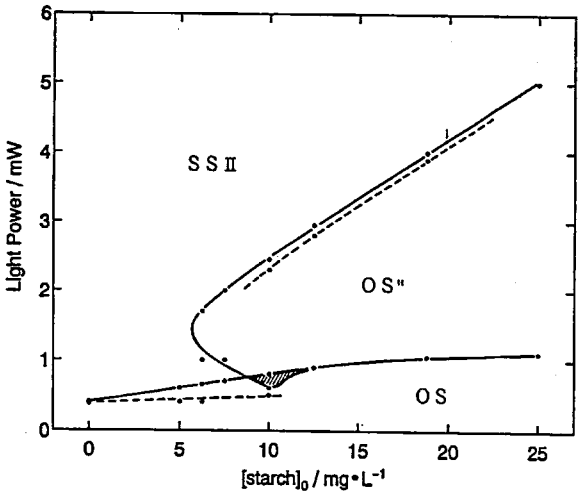

Figure 1. Two-dimensional state diagram spanned by the initial concentration of starch([starch]$_0$) and the 460-nm monochromatic light intensity (P_0). Experimental conditions are: $[KIO_3]_0$ = 50 mM, $[MnSO_4]_0$ = 50 mM, $[H_2SO_4]_0$ = 20 mM, $[H_2O_2]$ = 200 mM, $[CH_2(COOH)_2]_0$ = 5 mM, temperature = 24.5°C and residence time = 2.6 min.

III-K Laser Investigation of Molecular Photodissociation Dynamics

Detailed studies on photodissociation (half collision) dynamics provides the basis for understanding molecular photochemistry and also bimolecular reactions (full collisions). Experimental and theoretical studies must be extended beyond the well-studied triatomic systems (A+BC) in order to understand more complicated reactions encountered in upper atmosphere, interstellar space, and other environment (e.g. in flask). This project aims at, (1) the development of new experimental techniques to obtain complete information on quantum state distributions of reaction products, and (2) the elucidation of dissociation dynamics of polyatomic molecules. Lasers with high intensity, good monochromaticity, and well-defined polarization provide extremely sensitive detection methods of reaction products with the capability of examining their scalar (e.g. energy) and vector (e.g. linear and angular momenta) quantities. The extensive use of laser-based techniques is the key for the elucidation of complicated dynamics. In the past three years, our major effort have been directed to the development of two and three dimensional imaging techniques to visualize the scattering of atoms and molecules in reaction. By coupling the laser and imaging techniques, differential cross section (product velocity distribution) can be measured with complete internal state selection. In particular, we are interested in extracting stereochemical aspect of reactions by the analysis of the polarization dependence of 2D and 3D images. In our project, the imaging method has been applied to (direct) photodissociation that occurs faster than molecular rotation. On the other hand, slow predissociation processes have been studied by more conventional action spectroscopy, and the quantum state dependence of the reaction rate has been examined in detail.

III-K-1 UV Photodissociation of Dichloroethylenes: Cl Elimination Processes

Kenichi TONOKURA, Lizla S. BONTUYAN and Toshinori SUZUKI

Chlorine atomic elimination processes in ultraviolet photodissociation of *trans-*, *cis-*, and 1,1-dichloroethylene (DCE) have been studied by state-resolved 2D ion imaging technique. The speed and angular distributions of $Cl(^2P_{3/2})$ and $Cl^*(^2P_{1/2})$ have been measured for several excitation wavelengths (193, 210, 225, and 235 nm). Our preliminary analysis [1] has revealed that there exist rapid C-Cl bond rupture due to the surface crossing between the (π,π^*) and (n or π,σ^*) state and slow C-Cl bond rupture following the internal conversion to the ground electronic state. However, double C-Cl bond rupture is energetically possible in photodissociation with shorter wavelength used in our experiment. The speed and angular distributions, therefore, have been reanalyzed by considering momentum conservation in the sequential three body dissociation.

Reference

1) T. Suzuki et al., *J. Phys. Chem.* **98**, 13447 (1994).

III-K-2 Br Elimination by 193 nm Excitation of Vinylbromide

Lizla S. BONTUYAN, Nobuaki YONEKURA, Kenichi TONOKURA and Toshinori SUZUKI

In order to obtain more insight into the dissociation dynamics of halogenated ethylenes from the (π,π^*) state, we have extended our study to vinylbromide (VBr). This study was intended to clarify, (1) whether the low translational energy component observed by Wodtke et al.[1] for VBr is ascribed to the formation of the $\tilde{A}$ state of vinyl radical or to the internal conversion to the ground state of VBr followed by the formation of ground state vinyl radical as observed for chloroethylenes, and (2) whether the branching into two spin-orbit states occurs in the asymptotic region. For examining the latter point, the larger spin-orbit splitting in Br (10.5 kcal/mol) than in Cl (2.5 kcal/mol) is favorable for the experimental study. The

speed and angular distributions of Br ($^2P_{1/2}$ and $^2P_{3/2}$) atoms have been measured by 2D imaging. Two components have been observed for both of the states. The anisotropy parameters of the high energy components have been found to be the same (~1.6) for the two states, suggesting that both are produced by prompt dissociation from the (π,π^*) state. The peak (~ 40 kcal/mol) and the shape of the distribution of high components were almost identical for the two states despite of the large energy difference of the spin-orbit asymptotes (10.5 kcal/mol). This indicates that the branching into the two spin-orbit states occurs at small C-Br distance, possibly at the crossing from (π,π^*) to (n or π,σ^*) potential surfaces.

Reference

1) A. M. Wodtke et al., *Isr. J. Chem.* **29**, 383 (1989).

III-K-3 Semiclassical and Quantal Analyses on 2D Imaging of Photofragment Vector Correlation

Yuxiang MO and Toshinori SUZUKI

We have developed a theory to extract vector correlation (μ-v-J) in photodissociation from 2D and 3D imaging experiments. When the photofragments are detected by laser, the signal intensity depends on two factors; one is the multipolar moments of the fragments, and the other is the factor determined by detection scheme. The formulae for the latter factor have been obtained for atoms and for diatomic molecules in the intermediate coupling between Hund's cases (a) and (b). For large J, the formulae for multipolar moments have been obtained for the two limiting cases by semiclassical approximation. One is the case with a strong correlation between the transition dipole moment and angular momentum, and the other is the one with a strong correlation between the recoil velocity and angular momentum. The theory has been used to analyze the vector correlation in the photodissociation of N_2O, OCS, and NO_2.

III-K-4 Photodissociation Dynamics of N_2O at 193 nm: Analysis of Vector Correlation in $O(^1D)$ Fragment

Yuxiang MO, Hideki KATAYANAGI, Kenichi TONOKURA and Toshinori SUZUKI

The velocity distribution of $O(^1D)$ atoms produced by 205 nm photodissociation of N_2O has been measured by 2D ion imaging. Although photodissociation of N_2O in the ultraviolet region has been assigned to a single transition to $2^1A'$ state, this study has revealed that there are two components with different anisotropy parameters (β) in $O(^1D)$ velocity distribution. The major component has positive β value and is assigned to the parallel transition to $2^1A'$. The minor component, observed for the first time, has negligibly small β value. Figure 1 shows the angular distribution of $O(^1D)$ for the velocity range 3.3 - 3.6 km / sec. This distribution with a sharp spike in the center cannot be expressed by a standard equation for anisotropy, $I(\theta) \propto 1 + \beta P_2(\cos\theta)$, and needs higher order terms. The result clearly indicates the existence of vector correlation between the recoil velocity (v) and angular momentum (J) in $O(^1D)$ fragment.

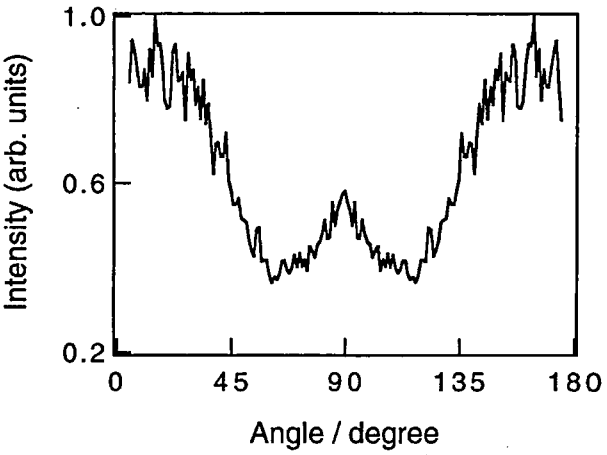

Figure 1. The angular distribution of the $O(^1D)$ atoms with the speed of v = 3.3 - 3.6 km/sec produced by 205 nm photodissociation of N_2O.

III-K-5 223 nm Photodissociation of OCS: Velocity Distribution of $S(^1D$ and $^3P)$ Atoms

Hideki KATAYANAGI, Yuxiang MO and Toshinori SUZUKI

[*Chem. Phys. Lett.*, in press]

The velocity distributions of S ($^1D_2$ and $^3P_2$ states) atoms produced by 223 nm photodissociation of OCS have been measured by 2D ion imaging. Figure 1 shows the inverse Abel transform of the 2D image of $S(^1D)$ atoms observed with the pump and probe laser polarization aligned vertical in the figure. Both of $S(^1D_2)$ and $S(^3P_2)$ have exhibited two velocity components. In the singlet channel, higher translational energy component is dominant, while in the triplet channel lower one has larger contribution. The effective anisotropy parameters (β_{eff}) of the high and low energy components are in agreement between the singlet and triplet channels, indicating that they have common origins. The image of $S(^1D_2)$ atoms have shown the dependence on probe laser polarization, which indicates the existence of v-J vector correlation in $S(^1D)$ fragment.

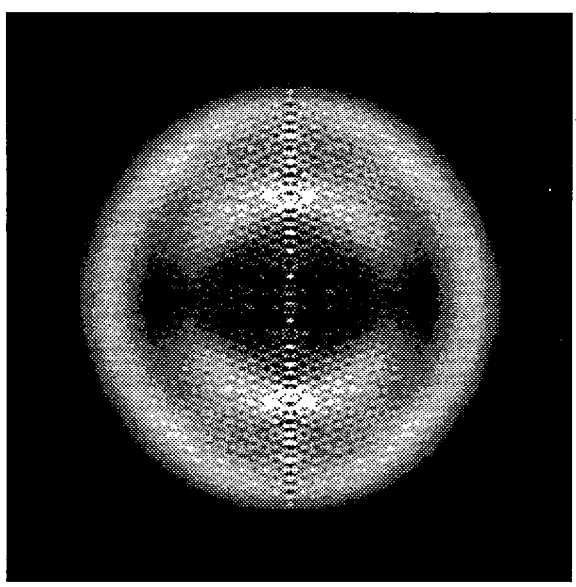

Figure 1. The inverse Abel transform of the 2D image of $S(^1D_2)$ produced by 223 nm photodissociation of OCS.

III-K-6 State-Dependence in the Predissociation of C_2H_2 in $\tilde{A}\ ^1A_u$ state Studied by H-Atom Action Spectroscopy

Nobuhisa HASHIMOTO *(Graduate Univ. for Advanced Studies)* **and Toshinori SUZUKI**

The energy threshold for and quantum state dependence of the predissociation of acetylene in $\tilde{A}\ ^1A_u$ state has been studied by H-atom action spectroscopy for the wavelength region of 201 - 224 nm. The shortest wavelength from 201 to 205 nm were generated by mixing the fundamental and the second harmonics of Nd^{3+}-YAG pumped dye laser. In order to have better spatial mode, a commercial dye laser has been modified to incorporate two stage Bethune cell amplifiers [1]. The typical output power was ~75 mJ/pulse for 0.07 cm^{-1} resolution in fundamental, from which the third harmonics of ~1 mJ/pulse has been obtained. An onset of the predissociation into $C_2H(\tilde{X}^1\Sigma)$ + $H(^2S)$ has been observed at V^4K^1 (46292 cm^{-1}) vibronic level that is 221cm^{-1} above the D_0 (HCC – H) = 46074 ± 8 cm^{-1} [2]. The relative yield of hydrogen atom (Φ_H) have increased with K quantum number, suggesting that the predissociation is accelerated by molecular rotation around the a-axis. On the other hand, the excitation of J unchanged or even suppressed (Φ_H), while fluorescence quantum yield (Φ_F) dropped dramatically with J. The result indicates that the quenching is enhanced by rotation around the b- and/or c-axis, while the predissociation is not. The result indicates that there are at least two deactivation pathways from optically prepared $\tilde{A}^1A_u$ state.

References

1) D. S. Bethune, *App. Opt.* **20** , 1897 (1981).

2) D. H. Mordaunt and M. N. R. Ashfold, *J. Chem. Phys.* **101** , 2630 (1994).

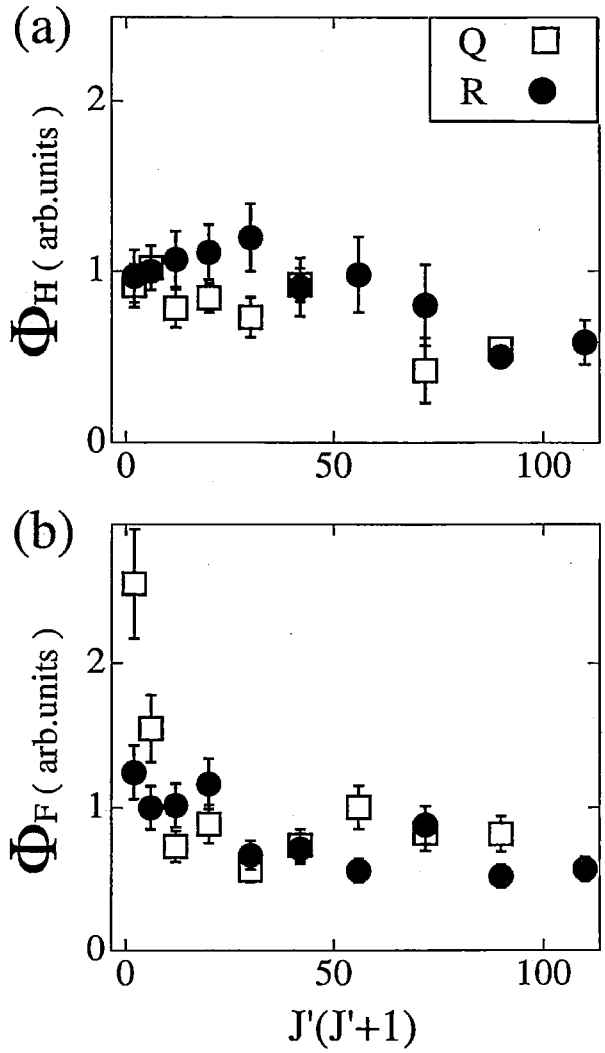

Figure 1. (a) The relative yield of hydrogen atoms (Φ_H) at each J level in V^4K^1 measured for jet-cooled sample. (b) The fluorescence quantum yield (Φ_F) measured for vapor. Each Φ(J) was normalized for the value at R(1) line to be unity. The symbols (● and □) are for Φ(J) for R (Π^e level) and Q (Π^f level) branches.

III-L Laser Investigation of Bimolecular Reactions

Based on the development and characterization of 2D imaging method in photodissociation experiments, we are planning to apply the method to inelastic and reactive scattering in crossed molecular beams. Because of the low signal level expected, preliminary experiments have been performed and the data obtained have been utilized for designing the apparatus.

III-L-1 Construction of Molecular Beam Diagnostics Chamber

Nobuaki YONEKURA, Hideki KATAYANAGI and Toshinori SUZUKI

A vacuum chamber has been constructed for the diagnostics of pulsed molecular beams. The chamber is pumped by 10" water-buffled oil diffusion pump (2000 l/s) backed by a mechanical booster pump (250 m^3/h). Piezo-electric valve have been constructed based on the design by Proch and Trickel,[1] and the time profile of the supersonic free jets generated have been measured with a fast ionization gauge. Typical pulse duration is 150-200 μs . An electroformed Ni skimmer has been placed at different distances from the nozzle, and the gas pulse-skimmer interaction have been examined for different configuration around the skimmer with the stagnation pressures up to 10 atm. The data have been used for designing intense pulsed molecular beam sources for crossed beam apparatus.

Reference

1) D. Proch and T. Trickl, *Rev. Sci. Instrum.* **60**, 713 (1989).

III-L-2 Construction and Characterization of Photolytic Hydrogen Beam

Kenichi TONOKURA and Toshinori SUZUKI

A pulsed hydrogen beam generated by photolytic source has been characterized by REMPI detection of H

atoms. A pulsed molecular beam of HI or H_2S has been generated by a pulsed valve and a skimmer, and these precursor molecules are photodissociated by 266 (HI) or 193 (H_2S) nm light at 79 mm downstream from the nozzle. The ejected H atoms that entered the interaction region through a collimater were detected by [2+1] REMPI at 243 nm or [1+1'] REMPI at Lyman-α. The Lyman-α radiation was obtained either by four wave mixing or direct tripling in Kr gas. The time duration of the H atom pulse has been found to be 35 ns. The propagation of the H pulse through the interaction region has been observed by 2D ion imaging method.

III-M Laser Ablation-Molecular Beam Method. Competitive Solvation of Monopositive Metal Ions in the Gas Phase

We have developed the laser ablation-molecular beam (LAMB) method, in which monopositive metal ions obtained by focusing pulsed laser light on a metal substrate in vacuum are allowed to react with molecules or clusters in a molecular beam injected near by. Product ions obtained on the ion-molecular reaction are probed by a quadrupole mass spectrometer. This method is a very simple and versatile diagnosis to study reactions of monopositive metal ions in the gas phase. Because any metal can be obtained as monopositive atomic ions, we can study novel chemistry of coordination (solvation) of monopositive metal ions in the gas phase. This year, competitive coordination (solvation) of monopositive metal ions has been studied by using binary clusters $(NH_3)_m(H_2O)_n$,$(NH_3)_m(CH_3OH)_m$ and $(CH_3OH)_m(H_2O)_n$.

III-M-1 Magic-Number-like Behavior of Ammonia Ligands in Mixed-Ligand Metal complexes $M^+(NH_3)_m(CH_3OH)_n$. Preferred Coordination of Ammonia Ligands in the First Coordination Sphere

Yasuhiro HORIKI, Satoru NISHIO, Hisanori SHINOHARA and Hiroyasu SATO* *(Mi'e Univ., Mi'e Univ. and IMS*)*

[*J. Phys. Chem.* **98**, 10436 (1994)]

Magic-number-like behavior in the ammonia constituents has been observed in mixed-ligand metal complexes $M^+(NH_3)_m(CH_3OH)_n$ prepared by reactions of several metal ions with ammonia-methanol binary clusters, using a laser ablation-molecular beam (LAMB) method. In typical cases it appears as the preponderance of ions with a certain number of ammonia constituents. It indicates preferred coordination and the metal specific coordination number of ammonia ligands in the first coordination sphere in these mixed-ligand metal complexes in the gas phase.

III-M-2 Highly Selective Solvation of Monopositive Metal Ions in the Gas Phase as Revealed by the Laser Ablation-Molecular Beam Method Using Ammonia-Water Binary Clusters

Osamu ITO, Yasuhiro HORIKI, Satoru NISHIO, Akiyoshi MATSUZAKI and Hiroyasu SATO* *(Mi'e Univ., Mi'e Univ and IMS*)*

[*Chem. Lett.* 9 (1995)]

Complex formation of metal ions Mg^+, Al^+, Mn^+, and Co^+ with ammonia-water binary clusters has been studied by the laser ablation-molecular beam method. While highly selective solvation favoring ammonia was observed for Mn^+ and Co^+, relatively nonselective solvation was realized for Mg^+ and Al^+.

III-M-3 Reactions of Monopositive Metal Ions (M^+) with Mixed Molecular Clusters like $(NH_3)_m(H_2O)_n$ As Studied by Laser Ablation-Molecular Beam (LAMB) Method. Preferred or Nonspecific Coordination

Hiroyasu SATO*, Akiyoshi MATSUZAKI, Satoru NISHIO, Yasuhiro HORIKI and Osamu ITO *(Mi'e Univ.and IMS*, Mi'e Univ.)*

[*Surf. Rev. Lett.*, in press]

Three distinct types of competitive solvation around monopositive metal ions in the gas phase have been revealed by the laser ablation-molecular beam method using binary clusters in the molecular beam: (1) preferred solvation of one of the two components, (2) essentially nonselective solvation, and (3) magic-number-like behavior of one component in the presence of the other component in the outer solvation sphere.

III-M-4 Laser Ablation-Molecular Beam (LAMB) Method. Coordination (Solvation) Chemistry of Monopositive Metal Ions in the Gas Phase

Hiroyasu SATO*, Yasuhiro HORIKI and Osamu ITO *(Mi'e Univ. and IMS*, Mi'e Univ.)*

[*J. Photochem. Photobiol. A Chem.*, in press]

Coordination (solvation) chemistry of monopositive metal ions in the gas phase has been studied with the laser ablation-molecular beam (LAMB) method developed by the authors' group. In this method, monopositive metal ions are prepared in the gas phase by laser ablation of metal substrates in vacuum, and allowed to react with molecules or clusters injected near by. From the distributions of complex ions obtained, one can deduce useful information on the coordination (solvation) number and/or preferential coordination (solvation) of monopositive metal ions in the gas phase. For reactions with ammonia clusters, intensity gaps are found in the distributions of complex ions obtained. They are intrinsic to each metal ion and indicate the coordination (solvation) number of ammonia ligands in the first coordination (solvation) sphere. For reactions with ammonia-water binary clusters, distributions of obtained mixed-ligand complex ions reveal another important aspect, the competitive coordination (solvation). While Mg^+ and Al^+ were relatively unselective, Mn^+ and Co^+ were highly selective

in the coordination (solvation) with ammonia and water molecules. The third type of competitive coordination (solvation), magic-number-like, is found for the reaction with ammonia-methanol and methanol-water clusters.

III-N Laser Chemistry of Polymers: Laser Ablation/Multiphoton-Mass Spectrometry Detection of Fragments, Reconstruction of Polymer Films from Laser-Ablated Fragments, Surface Treatment of Polymers with Pulsed Lasers, and CVD-like Preparation of Polymer Films fromMonomers

Laser chemistry of polymer materials are studied. Research directions are fourfold. (1) laser-ablated species are probed by multiphoton ionization (MPI)/time-of-flight (TOF) mass spectroscopic detection. Kinetic energy distributions of the neutral ablated species are determined by adjusting the time delay between the ablating laser and MPI laser. (2) Ablated fragments are deposited on a solid substrate, and reconstructed polymer films are prepared. Taking polyacrylonitrile (PAN) as an example, a remarkable wavelength dependence was observed for 308, 248 and 193 nm ablation. In addition, a very interesting intensity dependence was observed at 248 nm. (3) Surface treatment of polymer materials leads to semiconductive polymers, and (4) Chemical vapor deposition (CVD)-like treatment of monomers, like perylene derivatives and thiophene derivatives, are made to give conductive polymers.

III-N-1 Laser Ablation of Polymethylmethacrylate and Polystyrene at 308 nm: Demonstration of Thermal and Photothermal Mechanisms by a Time-of-Flight Mass Spectroscopic Study

Makoto TSUNEKAWA, Satoru NISHIO and Hiroyasu SATO* *(Mi'e Univ., Mi'e Univ. and IMS*)*

[*J. Appl. Phys.***76**, 5598 (1994)]

Laser ablation of polymethylmethacrylate and polystyrene films by an excimer laser at 308 nm was studied by detecting the fragments by time-of-flight mass spectroscopy after multiphoton ionization. Neutral fragments ablating from the polymer surface were predominantly monomer and dimer methylmethacrylate and monomer styrene, as deduced from the mass spectra. Thus, "unzipping" of these polymer occurs. The dependence of fragment yields on ablating laser fluence and kinetic energy distributions of ablating species demonstrates thermal and photothermal dissociation of these polymers under the experimental conditions.

III-N-2 Multiphoton Ionization-Mass Spectrometric Study on Laser Ablation of Polymethylmethacrylate and Polystyrene at 308 nm

Makoto TSUNEKAWA, Satoru NISHIO and Hiroyasu SATO* *(Mi'e Univ., Mi'e Univ. and IMS*)*

[*Jpn. J. Appl. Phys.* **34**, 218 (1995)]

A multiphoton ionization-mass spectrometric study has been made on laser ablation of polymethylmethacrylate (PMMA) and polystyrene (PS) films by an excimer laser at 308 nm. "Unzipping" reactions occurred, i.e., neutral fragments ablating from the polymer surface were predominantly monomer and dimer methylmethacrylate and monomer and dimer styrene. Exponential dependence of fragment yields on ablating laser fluence and the Maxwell-Boltzmann-type velocity distributions of ablating species were found. They are due to an essentially thermal or photothermal ablation mechanism of these polymers in the experimental conditions.

III-N-3 Preparation of Reorganized Films of Polyacrylonitrile by Ablation with an Excimer Laser

Satoru NISHIO, Tomonori CHIBA, Akiyoshi MATSUZAKI and Hiroyasu SATO* *(Mi'e Univ., Mi'e Univ. and IMS*)*

[*J. Appl. Phys.*, submitted]

Reorganized films of polyacrylonitrile (PAN) have been prepared on a quartz or KBr substrate by laser ablation of original PAN with 308 nm (XeCl), 248 nm (KrF) and 193 nm (ArF) excimer laser beams. Significant dependence of structures of reorganized films has been revealed by scanning electronic spectroscopy (SEM), infrared (IR) spectroscopy, X-ray photoelectron spectroscopy (XPS), electron spin resonance (ESR) and X-ray diffraction (XRD) measurements. Original structure of PAN is essentially preserved for the films deposited by ablation at 308 nm. Deformation and elimination of nitrile groups occur for the films prepared by ablation at 248 nm and 193nm, respectively. Furthermore, a remarkable power-dependent structural change has been observed at 248 nm. An increase in the laser power has led to the developent of π-conjugated systems by ring closure of nitrile groups. In addition, electronic conductivity in the order of 10^{-2} S cm^{-1} has been given to the films deposited by ablation at 248 nm and 193 nm on re-irradiation of the films with low-power excimer laser beams of 308 nm.

III-O Raman/IR Spectroscopy of Azacrown Ether Complexes

Stoichiometry of three sodium complexes (bromide, iodide and thiocyanate) of two azacrown ethers, 4,13-diaza-18-crown-6 and 4,13-diaza-15-crown-5, and the variation in the conformations of azacrown moiety on complex formation

have been studied by Raman/IR measurements and normal mode calculations.

III-O-1 Stoichiometry and Conformation of Azacrown Moiety in Sodium Complexes of Azacrown Ethers. A Raman/IR Spectroscopic Study. Part I. Complexes of 4,13-Diaza-18-Crown-6

Takayuki CHUJO, Isao SARAOKA, Shinobu KATO, Hiroyasu SATO*, Koichi FUKUHARA and Hiroatsu MATSUURA**** *(Mi'e Univ.,Mi'e Univ. and IMS*, Hiroshima Univ.**)*

[*J. Incl. Phenom.Mol. Recog. Chem.* **22**, 41 (1995)]

Three sodium complexes (bromide, iodide and thiocyanate) of 4, 13-diaza-18-crown-6 were studied using Raman and IR spectroscopy and normal coordinate calculations to probe the stoichiometry of the complexes and the variation in the conformation of azacrown moiety on complex formation. Complex formation is accompanied by characteristic shifts of the bands, especially of those in the 800-900 cm^{-1} region. Complexes of both 1:1 and 2:1 stoichiometry were observed. Normal coordinate calculations showed the reduction of symmetry of azacrown moiety to C_i , in contrast to the C_{2h} symmetry known for the parent azacrown and potassium thiocyanate complex.

III-O-2 Stoichiometry and Conformation of Azacrown Moiety in Sodium Complexes of Azacrown Ethers. A Raman/IR Spectroscopic Study. Part II. Complexes of 4,13-Diaza-15-Crown-5

Isao SARAOKA, Shinobu KATO, Takayuki CHUJO, Hiroyasu SATO*, Koichi FUKUHARA and Hiroatsu MATSUURA**** *(Mi'e Univ., Mi'e Univ. and IMS*, Hiroshima Univ.**)*

[*J. Incl. Phenom. Mol. Recog. Chem.* **22**, 59 (1995)]

4,13-Diaza-15-crown-5 and three of its sodium complexes (bromide, iodide and thiocyanate) were studied using Raman and IR spectroscopy and normal mode calculations, following the corresponding study on the sodium complexes of 4,13-diaza-18-crown-6 in the preceding paper. Complex formation was again accompanied by a characteristic shift of the bands, especially those in the 800-900 cm^{-1} region. The complexes of 4,13-diaza-15-crown-5 were distnct from those of 4,13-diaza-18-crown-6, in that both of the bands at 830 and 890 cm^{-1} of the parent azacrown were affected on complex formation and in that only 1:1 complex was formed. Normal mode calculations were made to predict conformations of azacron ring of the parent 4,13-diaza-15-crown-5 and its sodium complexes. Attention was paid to the different extent of mismatch in size of a sodium ion and azacrown cavities.

III-P External Magnetic Field Effects upon Chemical Reactions

Magnetic field effects upon chemical reactions provide us with useful methods for elucidating reaction mechanism and technique for controlling reaction rates, product yields, and concentration of a certain isotope. In the recent decade, the magnetic field effects upon photochemical reactions have been studied for a variety of organic molecules. Special attention has been paid to the hyperfine interaction between the electronic spin and nuclear magnetic moments within radical pair intermediates. In particular, intramolecular photoredox reactions in the solution phase have been extensively investigated for a series of aromatic carbonyl and nitro compounds. In most cases the photoreactions involving triplet biradicals have been elucidated in some detail. The formation yield for the cage product decreases in the presence of external magnetic fields, whereas that for the escape product correspondingly increases. Application of the magnetic field may cause an appreciable change in the relative yield of cage and escape products, *i.e.* the branching ratio of competitive processes. This means that the magnetic field effects have some potential for application, *e.g.* control of reaction yields or selection of reaction pathways. In addition, we have also studied the magnetic field effects on afterglow activated by a microwave discharge. One of the largest external magnetic field effects were observed for the β band of NO in the gaseous state. We have found that some halogen and interhalogen diatomic molecules exhibit magnetic quenching.

III-P-1 Magnetic Field and Magnetic Isotope Effects upon Biradical Photochemistry

Ryoichi NAKAGAKI *(Kanazawa Univ. and IMS)*, **Osamu TAKAHIRA** *(Kanazawa Univ.)* **and Ken-ichi HIRUTA** *(Kanazawa Univ.)*

[*Chem. Phys. Lett.* **233**, 41 (1995)]

We have studied magnetic field and magnetic isotope effects upon the lifetime of biradicals derived from methylene-linked bifunctional chain molecules consisting of benzophenone moiety and hydrogen donors. The photoinduced intramolecular hydrogen abstraction reaction takes place on excitation of the benzophenone chromophore. Since the benzophenone moiety in the excited triplet state abstracts a hydrogen from the donor, the resultant biradical intermediate is in the triplet manifold. The decay time of the triplet biradical was found to be lengthened in the presence of external magnetic field. The observed results are due to the change in the intersystem crossing rate induced by hyperfine interaction between the electronic spin and nuclear magnetic moment. On substituting the hydrogen or carbon nucleus at the particular site of the hydrogen donor with deuterium(isotopic purity of *ca.* 98%) or heavy carbon (C-13 purity of *ca.* 99%), the decay

profile of biradical intermediate produced by photoexcitation of the ketone chromophore is appreciably changed on application of the magnetic fields. The observed isotope effects are interpreted in terms of isotropic and anisotropic hyperfine interaction.

III-Q Magnetic Behavior of Stable Radical Crystals and ElectronicStructures of Organic High-Spin Molecules

New types of stable radicals crystals having thioaminyl groups have been investigated for promising candidates of molecular-based magnets. Some of them have shown ferromagnetic intermolecular interaction. The magnitude of their ferromagnetic interaction is fairly large compared than that of other radicals crystals, nitroxide and nitronyl nitroxide radicals. We continue to examine the low-temperature magnetic behavior and their magnetic phase transitions. Their spin relaxation and spin dynamics have been studied by a pulsed ESR technique. We are also studied the electronic structures of typical organic high-spin polycarbenes using ESR and ENDOR spectroscopies. Their spin density distributions have been determined by single-crystal ENDOR. The spin density distributions give the key information of the intramolecular spin alignment.

III-Q-1 Ferro- and Antiferromagnetic Behaviors of Stable Free Radical Crystals of *N*-(Arylthio)-2,4,6-triarylphenylaminyls

Yoshio TEKI *(IMS and Osaka City Univ.)*, **Yuko TAJIMA, Koichi ITOH, Sadaharu UENO, Yuichi KITAGISHI and Yozo MIURA** *(Osaka City Univ.)*

[*Mol. Cryst. Liq. Cryst.*, in press]

As promising candidates for organic molecule-based ferromagnets, we have investigated several stable thioaminyl radicals in the solid states. In addition to *N*-[(2,4-dichlorophenyl)thio]-2,4,6-tris(3-chlorophenyl)-phenylaminyl (**1**) which we have already reported (Mol. Cryst. Liq. Cryst., in press (1995)), other thioaminyl radical crystal showing ferromagnetic behaviors have been found. Thus, *N*-[(2,4-dichlorophenyl)thio]-2,4,6-tris(4-chlorophenyl)phenylaminyl (**2**) radical shows one-dimensional ferromagnetic behavior. The magnetic behavior has been well interpreted in terms of the one-dimensional Heisenberg model with ferromagnetic intermolecular interactions of J/k = 14.0 K. In contrast, *N*-[(2,4-dichlorophenyl)thio]-2,4,6-tris(4-chlorophenyl)-phenylaminyl (**3**) shows antiferromagnetic behavior described by an alternating linear chain model with J/k = -8.4 K and α=0.55.

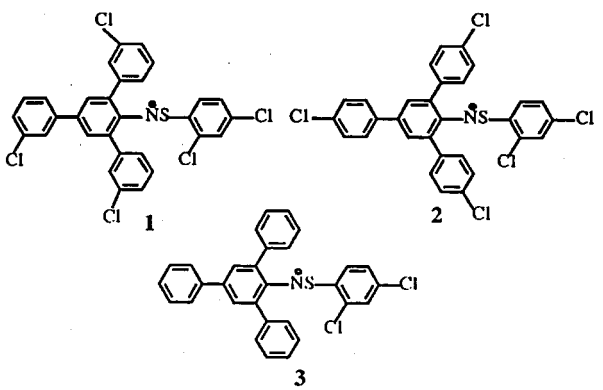

III-Q-2 Pulsed- and cw ESR Study of Exchange Interaction, Spin Relaxation and Spin Dynamics on Low-Dimensional Organic Magnetic Materials

Yoshio TEKI *(IMS and Osaka City Univ.)*, **Yuzo Miura, Takeji TAKUI and Koichi ITOH** *(Osaka City Univ.)*

In order to clarify the spin dynamics of the stable radical crystals, we have investigated their magnetic behavior and spin relaxation of low-dimensional ferro- and antiferromagnetic organic materials, *N*-(arylthio)-2,4,6-triphenylanilino radicals, by cw and pulsed ESR. With decreasing temperature from 298 to 20 K, the line width of the cw ESR spectrum increases in the case of *m*-NO_2 substituted radical. Upon further decreasing, exchange narrowing occurs below 10 K. The temperature dependence of the inverse of T_2 which has been determined by the analysis of FID, shows a peak at ca. 20 K. This temperature is consistent with the presence of an antiferromagnetic intermolecular interaction of J/k = -26 K in this radical crystal. The temperature behavior can be explained taking the spin pairing by the antiferromagnetic interaction and the one-dimensional spin diffusion into account.

III-Q-3 Spin Alignment and Spin Density Distributions of Organic High-Spin Molecules

Yoshio TEKI *(IMS and Osaka City Univ.)*, **Takamasa Kinoshita, Takeji TAKUI and Koichi ITOH** *(Osaka City Univ.)*

In order to clarify the mechanism and the physical picture of the intramolecular spin alignment, we have investigated the electronic structures of several organic high-spin molecules. Existence of a large negative spin polarization, which is induced by the spin density wave formed in the π electron network, can be predicted for organic high-spin molecules **1** and **2**. We have determined their spin density distributions by ENDOR (Electron-Nuclear DOuble Resonance) experiments. The ^{13}C labeled compounds have been used to determine the σ and π spin densities at the divalent carbon sites directly. The analysis of the anisotropic terms of ^{13}C hyperfine tensor gives a clear evidence of such large negative spin density. The spin alignment are also discussed in terms of VB picture based on a extended Hubbard model.

* : Site labeled by ^{13}C isotope

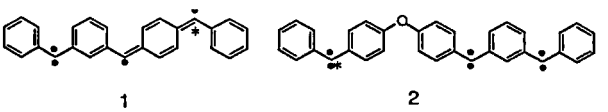

RESEARCH ACTIVITIES IV
Department of Molecular Assemblies

IV-A Solid State Properties of Phthalocyanine Salts and Related Compounds

Some phthalocyanine molecules contain unpaired d-electrons in the conjugated π-electron system. Owing to this special nature, the itinerant π-electrons and localized unpaired d-electrons coexist in solid phthalocyanine salts, in which a one-dimensional double-chain system is formed. The exchange interaction of itinerant π-electrons with localized magnetic moments is a new aspect in the field of organic metals. For the basic understanding of these materials and to search for a new phenomenon, where a magnetic interaction takes an important role, we prepare and characterize solid phthalocyanine salts and related compounds.

IV-A-1 Pressure-Induced Charge Transfer in One-Dimensional Phthalocyanine Conductor, NiPc $(AsF_6)_{0.5}$

Toshihiro HIEJIMA *(Grad. Univ. Adv. Studies)* **and Kyuya YAKUSHI**

[*Solid State Commun.*, **95**, 661 (1995)]

Pressure dependence of optical absorption spectra was measured for (phthalocyaninato)-nickel hexafluoroarsenate, $NiPc(AsF_6)_{0.5}$. Under high pressure we found an intramolecular charge transfer from the central metal ion to the macrocycle, that is, from the metal d-band to the macrocycle π-band. According to the electron-filling process into the π-band, a metal-insulator transition without accompanying a lattice distortion was observed.

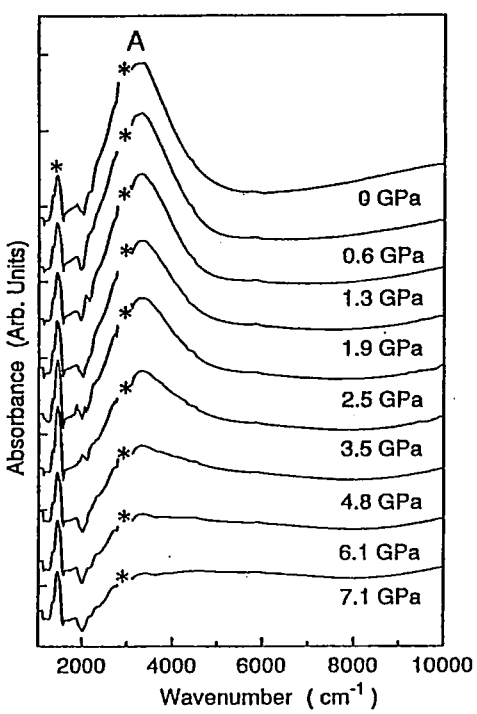

Figure 1. Pressure dependence of plasmon absorption spectrum of $NiPc(AsF_6)_{0.5}$. The dashed curve was calculated by the effective medium theory. The asterisks are the absorptoins by the pressure medium (liquid paraffin).

IV-A-2 Pressure-induced d-π charge transfer in one-dimensional phthalocyanine conductors, $NiPc(AsF_6)_{0.5}$ and $CoPc(AsF_6)_{0.5}$

Toshihiro HIEJIMA *(Grad. Univ. Adv. Studies)* **and Kyuya YAKUSHI**

[*J. Chem. Phys.*, **103**, 3950 (1995)]

Pressure dependence of optical absorption spectra were measured for (phthalocyaninato)-nickel hexafluoroarsenate, $NiPc(AsF_6)_{0.5}$ and (phthalocyaninato)-cobalt hexafluoroarsenate, $CoPc(AsF_6)_{0.5}$ We found and evidenced a pressure-induced charge transfer from the central metal ion to the macrocycle at 0.5 GPa in $NiPc(AsF_6)_{0.5}$ and 1.1 GPa in $CoPc(AsF_6)_{0.5}$. Above this pressure the charge transfer is continuously promoted up to 5 GPa. According to the electron-filling process in the π-conjugated band, a metal-insulator transition and an evolution of the energy gap was observed in $NiPc(AsF_6)_{0.5}$. On the other hand, nonmetallic $CoPc(AsF_6)_{0.5}$ showed a continuous change.

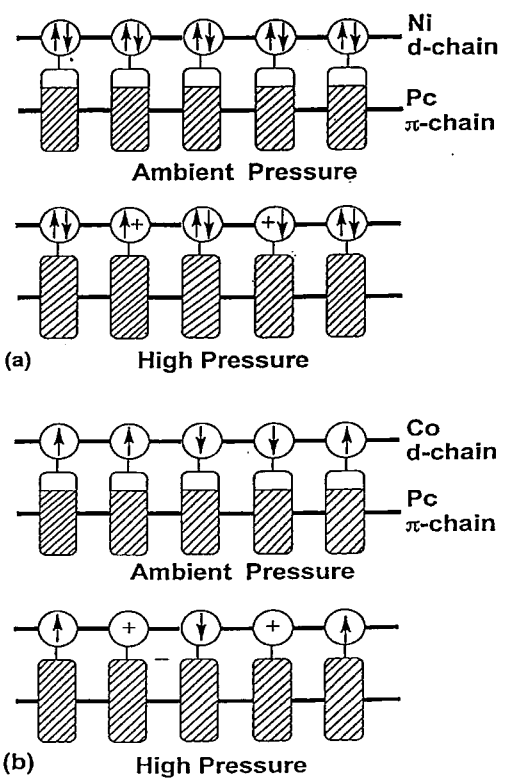

Figure 2. Schematic figure of the electronic structure of before and after the d-π charge transfer (a) $NiPc(AsF_6)_{0.5}$ and (b) $CoPc(AsF_6)_{0.5}$ The open area of the Pc π-chain in ambient pressure represents the incomplete band filling.

IV-A-3 The 130 K Transition in Bi Oxides Heavily Doped by Iron Phthalocyanine: Superconductivity versus Magnetism

L. Grigoryan, K. Yakushi and Chakravarty *(San Jose State Univ.)*

[*phys. stat. sol. (b)* **187**, 205 (1995)]

The observation and detailed investigation of the highly reproducible transition with onset at 130 K are reported in samples of Bi oxides (both 2212 and 2223 systems) doped with iron phthalocyanine, involving effects of temperature, magnetic field, and chemical composition on dc magnetization and microwave absorption spectra of the samples. The experimental magnetic data are suggestive of a superconducting nature of the transition; however, no reliable electrical resistivity drop is observed at 130 K to confirm the occurrence of superconductivity.

IV-B Structure and Properties of Organic Conductors

The study of organic metals rapidly developed when the dimensionality of an intermolecular charge-transfer interaction is expanded. This expansion of dimensionality has been brought about by the discovery of new molecules such as BEDT-TTF or C_{60}. In this project we treat one-, two-, and three-dimensional organic metals and superconductors to know what is most important for stabilizing a metallic state and for designing new superconducting materials. We are interested in new organic compounds which may expand the frontier of organic conductors.

IV-B-1 Spectroscopic Study of Solid BDNT and its Monocation and Dication Salts

Jian DONG *(Grad. Univ. for Adva. Studies)*, **Kyuya YAKUSHI and Yoshiro YAMASHITA**

[*J. Mater. Chem.*, **5**, 1735 (1995)]

The polarized reflection spectra of BDNT, BDNT-PF_6 and BDNT-$(PF_6)_2$ have been measured on several crystal faces of the single crystals and compared with the solution spectra of BDNT, $BDNT^+$ and $BDNT^{2+}$. The spectra of the BDNT crystals have been successfully interpreted in terms of the theory of directional dispersion. Based on this interpretation, the electronic spectra of BDNT, $BDNT^+$ and $BDNT^{2+}$ have been reasonably assigned to the electronic transitions expected from the molecular orbital calculations. We found a disproportionation reaction in the acetonitrile solution of *m*-BDNT-PF_6, which means that the dication state is close to the monocation state. This is in accord with the low excitation energy (3.5×10^3 cm^{-1}) of the charge-transfer band in m-BDNT-PF_6. The vibrational bands of BDNT, *m*-BDNT-PF_6 and BDNT-$(PF_6)_2$ are presented and discussed.

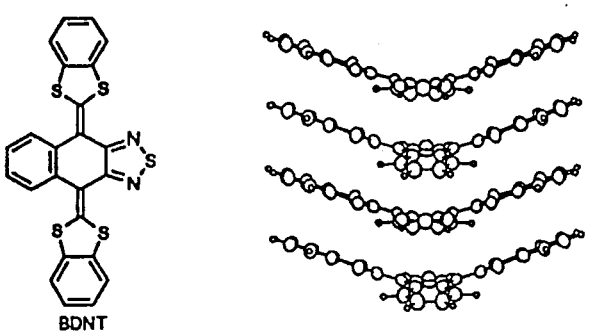

Figure 3. Structural formula of BDNT and the sideview of the molecular column of BDNT.

IV-B-2 Electronic and Vibronic Structure of Nonplanar Organic Charge-Transfer Salt, *m*-BDNT-PF_6

Jian DONG *(Grad. Univ. Adv. Studies)*, **Kyuya YAKUSHI, Yoshiro YAMASHITA, Kenichi IMAEDA and Hiroo INOKUCHI**

[*phys. stat. sol. (b)*, submitted]

The monoclinic form of BDNT-PF_6 (*m*-BDNT-PF_6) is characterized as the pseudo-one-dimensional half-filled Hubbard system from the electrical conductivity, magnetic susceptibility, and single crystal optical spectra. *m*-BDNT-PF_6 undergoes a spin-Peierls transition at about 150 K. The lattice dimerization was confirmed by the evolution of the vibronic modes at low temperature. The small polaron binding energy of this compound, which was estimated through the analysis of the vibronic modes, is smaller than those of TTF, TCNQ or CA. Hubbard parameters U and *t* were obtained to be 0.8 eV and 0.13 eV by analyzing the charge-transfer band. The optical and magnetic data are consistent with each other.

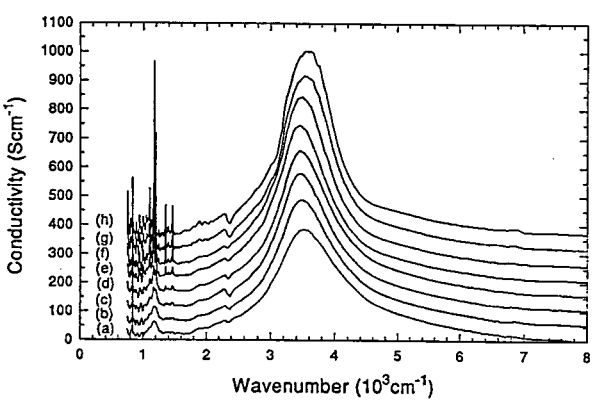

Figure 4. Temperature dependent conductivity spectrum of *m*-BDNT-PF_6, which was obtained from the *b*-polarized reflection spectrum of the single crystal. (a) 297 K, (b) 253 K, (c) 203 K, (d) 154 K, (e) 104 K, (f) 75 K, (g) 46 K, and (h) 15 K. The enhancement of the vibrational mode means the dimerization of BDNT along the *b*-axis.

IV-B-3 Resonant Raman Scattering in Single Crystals of BDNT, $BDNT^+$, and $BDNT^{2+}$

V. N. DENISOV*, A. N. IVLEV*, Boris N. MAVRIN* *(*Inst. Spectrosc.)*, **Kyuya YAKUSHI, Jian DONG and Yoshiro YAMASHITA**

[*Chem. Phys. Lett.*, **246**, 176 (1995)]

The polarized Raman spectra of the single crystals BDNT, BDNT-PF_6, BDNT-$(PF_6)_2$ and BDNT-$(ClO_4)_2$-CH_2Cl_2 are obtained in the region of 130-1700 cm^{-1}. It is shown that due to a resonant character of the Raman spectra only the Ag modes of intramolecular vibrations of the BDNT molecules were observed in the spectra of all crystals. A low-frequency shift of frequencies of the C=C bands with the increase of the oxidation degree is revealed that is due to a charge transfer from the BDNT molecules to the acceptors PF_6 or ClO_4. Moreover, this shift was larger for the band corresponding to the stretching vibration of the C=C bond which connected the dithiole and naphtho-thiadiazole rings. The Raman intensity of this band diminished strongly with the growth of oxidation due to likely a frustration of the bond conjugation. We have found that a molecular configuration in crystals depends on the oxidation degree, but it does not depend on the acceptor type.

IV-B-4 Crystal Structures of $BDNT^{2+}$ Salts, BDNT-$(ClO_4)_2$-CH_2Cl_2 and BDNT-$(SbF_6)_2$

Mikio URUICHI, Jian DONG, Kyuya YAKUSHI, Masaaki TOMURA and Yoshiro YAMASHITA

Crystal structures of $BDNT^{2+}$ salts, BDNT-$(ClO_4)_2$-CH_2Cl_2 and BDNT-$(SbF_6)_2$ were determined. Contrary to our expectation, $BDNT^{2+}$ has a different molecular geometry from $BDNT^0$ and $BDNT^{1+}$ which have butterfly- or V-shaped structure. In the crystal of BDNT-$(ClO_4)_2$-CH_2Cl_2, solvent molecule is involved in the crystal lattice and one of the benzodithiole rings are twisted by 46 degrees around the C-C bond connecting the naphthothiadiazole ring with benzodithiole ring. On the other hand both benzodithole rings are twisted by 59 degree in BDNT-$(SbF_6)_2$, and solvated molecules are not found. According to this remarkable geometrical change, C-C bond lengths are significantly elongated. This geometrical change seems to be related to the extreme closeness of the first and second oxidation potentials of BDNT.

IV-B-5 Superconductivity in Conducting Polymer-Fullerene Composite Doped by Alkali Metal

Hisashi ARAKI*, Anvar A. ZAKHIDOV, E. SAIKI*, Nobuo YAMASAKI*, Kyuya YAKUSHI and Katsumi YOSHINO* *(*Osaka Univ.)*

[*J. J. Appl. Phys.*, **34**, L1041 (1995]

Superconductivity in poly(3-alkylthiophene)-C_{60} composite (PAT-C_{60}) is found upon doping by potassium from vapor phase. The superconducting transition at T_c=17 K is detected by SQUID magnetometer, which showed 0.1 % of superconducting fraction for 5 mol % C_{60} content. Exceptionally strong low field microwave absorption (LFMA) implies the granular superconducting phase. Rather small hysteresis of LFMA indicates the important role of Josephson weak links net work, probably formed between superconducting K_xC_{60} clusters separated by conductive K_xPAT barriers. ESR of PAT$(C_{60})_yK_x$ composite shows two types of lines: one from negative polarons P^- in PAT chains, while other lines are assigned to K_xC_{60} clusters.

IV-B-6 Alkali-Metal Doping of Fullerene-Conducting Polymer Composite: Evolution of Conductivity and ESR

Hisashi ARAKI*, Anvar A. ZAKHIDOV, Kazuya TADA*, Kyuya YAKUSHI and Katsumi YOSHINO* *(*Osaka Univ.)*

[*Synthetic Metals*, **205**, 317 (1995)]

Doping effects of conducting polymer (CP)-C_{60} composites by n-type dopants, namely by alkali metals, is investigated, emphasizing the ESR spectroscopy together with conductivity changes upon K-doping of poly(3-alkylthiophene) PAT-$(C_{60})_y$ composites at various fullerene concentrations y. ESR showed two types of lines: one from polarons on PAT chains, and the other from K_3C_{60} clusters and monomolecular C_{60} radicals. The evolution of conductivity suggests that at comparatively large C_{60} content y=0.05, the composite can be viewed as a network of C_{60} clusters in the PAT host matrix at initial K-doping stage. K_3C_{60} metallic islands are formed, while the PAT matrix is still insulating so that increase of conductivity is slower than in pure PAT case. These results are consistent with granular nature of superconducting phases found by us in PAT$(C_{60})_yK_x$ at y>0.005 by LFMA (low field microwave absorption).

IV-B-7 Granular Superconductivity in "Conducting Polymer-Fullerene-Alkali Metal" Composite

Anvar A. ZAKHIDOV, Hisashi ARAKI*, Kazuya TADA*, Kyuya YAKUSHI and Katsumi YOSHINO* *(*Osaka Univ.)*

[*Physics Lett. A*, **205**, 317 (1995)]

Superconducting (SC) phase is found in poly(3-alkylthiophene) - $(C_{60})_y$-K_x composite by both low field microwave absorption (LFMA) and SQUID magnetometry. T_c varies from 12 to 17 K depending on y and x: so T_c (y=0.05) = 17 K, at optimal x. LFMA shows phase reversal just below Tc, in composites with y>0.025 indicating the granular SC phase of disordered K_3C_{60} clusters. The possibility of two-component SC phase in which electrons of conducting polymer chains are actively involved in SC pairing induced via hybridization with C_{60} molecules is discussed for small y<0.005case.

V-B-8 Photoconductivity of Poly(2,5-diheptyloxy -p-phenylenevinylene) in Air Atmosphere. Magnetic Field Effect and Mechanism of Generation and Recombination of Charge Carriers

Eugene FRANKEVICH, Anvar A. ZAKHIDOV, Katsumi YOSHINO *(Osaka Univ.)*, **Yusei MARUYAMA and Kyuya YAKUSHI**

[*Phys. Rev. B*, to be published]

Photoconductivity of poly (2,5-diheptyloxy-p-

phenylenevinylene) (HO-PPV) is found to be increased by external magnetic field. This magnetic field effect (MFE) is significantly enhanced in the presence of oxygen of air. Two types of MFE are revealed in samples of HO-PPV: Prompt one is connected with existence of coupled pairs of charge carriers, as precursors for photoconductivity: these pairs may dissociate thermally and under the assistant action of external electric field, producing mobile carriers. Delayed MFE is shown to be connected with the reaction of triplelt and singlet excitons with oxygen molecules. The reaction changes inertially the concentration of oxygen molecules dissolved in the bulk of the polymer, its rate being magnetic field dependent. MFE allowed to clarify mechanism of photogeneration in HO-PPV: Positive mobile charge carriers responsible for the photocurrent are produced in the reaction of dissociation of primary singlet species by oxygen, photooxidation products and other weak dopants like C_{60} molecules. The probability of charge carrier generation in the reaction with oxygen molecule is found to be higher than with C_{60} other molecules studied. An enhancement of the photoconductivity of samples in air is connected with that factor and also with great increase of the life time of charge carriers before recombination. Recombination of positive charge carriers with oxygen negative ions is very slow giving a quasi persistent photoconductivity of the polymer in air.

IV-B-9 Optical properties of high-pressure phases of C_{60} fullerene

Mikhail E. KOZLOV *(ETL and IMS)* **and Kyuya YAKUSHI**

[*J. Phys. Condens. Matter* 7, L209 (1995)]

High-pressure phases of C_{60} fullerene similar to those reported by Iwasa *et al.* were obtained at a non-hydrostatic pressure of 3 GPa and different temperatures in the 100-500 °C range. The substances were investigated by means of infrared, optical and micro-Raman spectroscopies. Compared with pristine C_{60}, the spectra of the transformed material reveal multiple changes which depend systematically on treatment conditions. They evidence a substantial modification of selection rules for allowed optical transition apparently due to formation of C_{60} molecules with deformed and/or partially destroyed cages.

IV-C NMR Study of Organic Conductors and Superconductors

The nuclear magnetic resonance (NMR) is a powerful method to examine electronic state of condensed matters. With this microscopic method, one can get further insight into nature of the metallic, superconducting and magnetic states than with other macroscopic measurements. This project aims at understanding the unsolved problems concerning the peculiar electronic structure in several organic materials.

IV-C-1 ^{13}C NMR Study of Layered Organic Superconductors Based on BEDT-TTF molecules

Atsushi KAWAMOTO *(Ochanomizu Univ.)*, **Kazuya MIYAGAWA, Yasuhiro NAKAZAWA and Kazushi KANODA**

[*Phys. Rev. Lett.* **74**, 3455 (1995)]

The normal state of the organic superconductors, κ-(BEDT-TTF)$_2$X [X=Cu(NCS)$_2$ and Cu[N(CN)$_2$]Br] where BEDT-TTF is bis(ethylenedithio)tetrathiafulvalene, has been investigated by ^{13}C-NMR on the selectively isotope-labelled samples for the first time. The nuclear spin lattice relaxation rate, T_1^{-1}, exhibits anomalous temperature dependence with a peak formation around 50 K for both compounds, as shown in Figure.1, while the Knight shift evaluated from the linewidth of powdered samples scale to the uniform spin susceptibility. The absolute value of T_1^{-1} is greatly enhanced above the value expected in the Korringa relation. These results show that there exists strong antiferromagnetic spin fluctuations with finite wave vector. The depression of the spin fluctuations below 50 K coincides with an appearance of Fermi liquid behavior in the the charge transport.

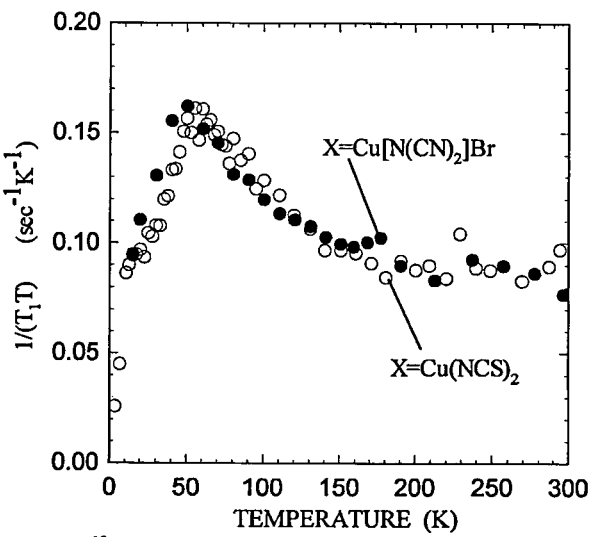

Figure.1 ^{13}C nuclear spin-lattice relaxation rate divided by temperature, $(T_1T)^{-1}$, as a function of temperature.

IV-C-2 Antiferromagnetic Ordering and Spin Structure in the Organic Conductor,κ-(BEDT-TTF)$_2$Cu[N(CN)$_2$]Cl

Kazuya MIYAGAWA, Atsushi KAWAMOTO *(Ochanomizu Univ.)*, **Yasuhiro NAKAZAWA and Kazushi KANODA**

[*Phys. Rev. Lett.* **75**, 1174 (1995)]

The metal-insulator (M-I) transition has been always

a center of interest in the physics of organic conductors since the discovery of the one-dimensional conductor, TTF-TCNQ. Quasi-two-dimensional electronic systems tend to be free from the nesting instability of Fermi surface and therefore are stabilized to be metallic or superconducting. Indeed, a family of layered systems, κ-(BEDT-TTF)$_2$X [X=Cu(NCS)$_2$ and Cu[N(CN)$_2$]Br], are superconductors with transition temperatures in excess of 10 K. In spite of structural similarity, however, the salt with X= Cu[N(CN)$_2$]Cl is an insulator. Considering two-dimensionality of the electronic state in the κ-phase family, one cannot take it for granted that the same scenario as in the above one-dimensional conductors will do as it is for the M-I transition in this case. In the present work, the magnetism of κ-(BEDT-TTF)$_2$Cu[N(CN)$_2$]Cl at ambient pressure has been investigated by NMR, for the first time, along with magnetization measurements. A divergent peak in $(T_1T)^{-1}$ at 26-27 K (Figure. 1) indicates a magnetic transition, where T_1 and T stand for ^1H nuclear spin-lattice relaxation rate and temperature, respectively. From analysis of the NMR spectra, the magnetic ordering was found to be antiferromagnetic and commensurate with a moment of 0.4-1.0 of μ_B/dimer. The features quite different from the conventional SDW suggest that the magnetic order is driven by strong electron correlation rather than nesting of the Fermi surface and that the present salt is a Mott insulator. Magnetization measurements show spin canting parallel to the conducting layer below 23 K at low fields. The M-I transition in the κ-type quasi-two-dimensional electronic systems has different aspects from that in the conventional quasi-one-dimensional systems.

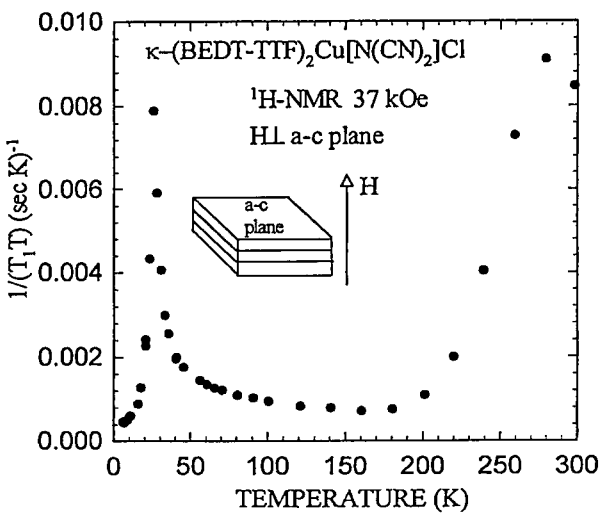

Figure.1 ^1H nuclear spin-lattice relaxation rate divided by temperature, $(T_1T)^{-1}$, as a function of temperature

IV-C-3 NMR Relaxation Rate in the Superconducting State of the Organic Conductor, κ-(BEDT-TTF)$_2$Cu[N(CN)$_2$]Br

Kazushi KANODA, Kazuya MIYAGAWA, Atsushi KAWAMOTO *(Ochanomizu Univ.)* **and Yasuhiro NAKAZAWA**

[*Phys. Rev.* **B** in press]

The mechanism of electron pairing in the organic superconductors is one of the fundamental but still open questions in condensed matter physics. Experimental research on symmetry of the pairing in κ-(BEDT-TTF)$_2$X (X=Cu(NCS)$_2$ and Cu[N(CN)$_2$]Br) has been done extensively through measurements of magnetic penetration depth with many kinds of experimental techniques. However, their results are quite controversial. NMR is another probe characterizing the nature of the electron pairing. In the present work, the ^{13}C nuclear spin-lattice relaxation rate, $^{13}T_1^{-1}$, has been measured in the superconducting state of κ-(BEDT-TTF)$_2$Cu[N(CN)$_2$]Br in a field parallel to the conducting layers. The $^{13}T_1^{-1}$ exhibits an abrupt decrease just below the transition temperature without any indication of the Hebel-Slichter coherence peak, as seen in Figure.1. By separation of the vortex-dynamics contribution to $^{13}T_1^{-1}$ with the use of ^{1}H-NMR, the quasi-particle contribution to $^{13}T_1^{-1}$ is found to follow a T^3-law (open circles in Figure.1), that is consistent with unconventional superconductivity with line nodes in gap parameter on the Fermi surface.

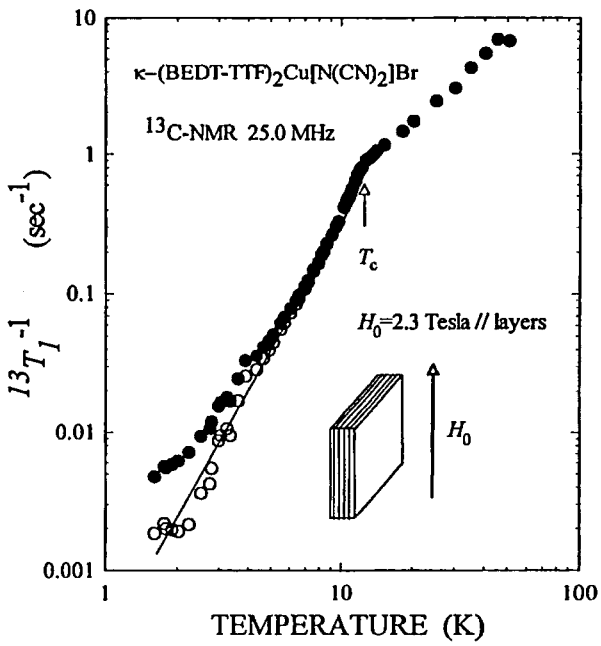

Figure.1 ^{13}C nuclear spin-lattice relaxation rate as a function of temperature. Closed circles; observed data of the relaxation rate. Open circles; quasi-particle contribution obtained by analysis with the use of the ^{1}H-NMR results (see text). The solid line represents a T^3 dependence.

IV-C-4 Electron Correlation in κ-Phase Family of BEDT-TTF Compounds Studied by ^{13}C-NMR, where BEDT-TTF is bis(ethylenedithio)-tetrathiafulvalene

Atsushi KAWAMOTO *(Ochanomizu Univ.)*, **Kazuya MIYAGAWA, Yasuhiro NAKAZAWA and Kazushi KANODA**

[*Phys. Rev.* **B** in press]

^{13}C NMR study on κ-(BEDT-TTF)$_2$X (X=Cu(NCS)$_2$, Cu[N(CN)$_2$]Br and Cu[N(CN)$_2$]Cl) is reported, where BEDT-TTF is bis(ethylenedithio)tetrathiafulvalene. The superconducting salts of X=Cu(NCS)$_2$ and Cu[N(CN)$_2$]Br show anomalous enhancement in nuclear spin-lattice relaxation rate, T_1^{-1}, around 50K, in spite of monotonic temperature dependence of anisotropic Knight shift, as seen in Fig.1. On the other hand, the insulating salt of

X=Cu[N(CN)$_2$]Cl exhibits a divergent peak in $(T_1T)^{-1}$ at 26-27K, as shown in Figure.1, which is confirmed as a manifestation of an antiferromagnetic transition by broadening of the NMR line. Above 27K, T_1^{-1} shows a temperature dependence typical of critical magnetic fluctuations. The $(T_1T)^{-1}$ and the line shape showed nearly the same profile for these three salts above 60K, that gives the first experimental evidence for a correspondence between the anomalous enhancement of $(T_1T)^{-1}$ in the superconducting salts and antiferromagnetic fluctuations established in the insulating salt of κ-type. The present results demonstrate the presence of strong electron correlation in both superconducting and insulating salts. Analytical expressions of T_1 and Knight shift of the ^{13}C NMR for κ-(BEDT-TTF)$_2$X are given, which are general formulae applicable to other pπ electronic systems.

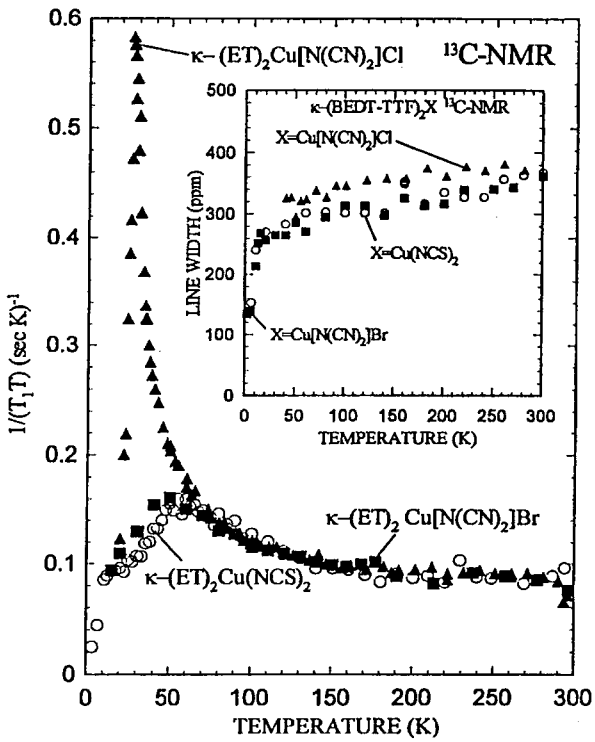

Figure.1 ^{13}C nuclear spin-lattice relaxation rate divided by temperature, $(T_1T)^{-1}$, as a function of temperature. Inset shows the linewidth of the NMR powder spectra, which characterizes temperature dependence of the anisotropic Knight shift.

IV-C-5 Systematic Study of the Electronic States Around the Metal-Insulator Transition of κ-(BEDT-TTF)$_2$X Salts by ^{13}C-NMR

Atsushi KAWAMOTO *(Ochanmizu Univ.)*, **Kazuya MIYAGAWA and Kazushi KANODA**

The κ-phase family of (BEDT-TTF)$_2$X system is interesting in that the well known10K class superconductor of κ-(BEDT-TTF)$_2$X (X=Cu(NCS)$_2$, Cu[N(CN)$_2$]Br) are situated very close to the isostructural insulater of κ-(BEDT-TTF)$_2$Cu[N(CN)$_2$]Cl. By applying pressure, this insulating property is known to change to metallic one with appearence of superconductivity at about 13K. On the othe hand, deutrated κ-(BEDT-TTF)$_2$Cu[N(CN)$_2$]Br is reported to be insulating, although some samples remains metallic. This suggest that the deutration of the Cu[N(CN)$_2$]Br salt tends to lead the metallic phase toward insulating phase. In this project, we plan to tune the system precisely around the metal-insulator transition at ambient pressure by alloying the deuterated and non-deuterated molecules in the Cu[N(CN)$_2$]Br salt and to characterize critical phenomena around the transition mainly through ^{13}C-NMR. By this experiment, we expect to vary *U/W*; a ratio of the on-site Coulomb energy to the band width, continuously from the insulating side to metallic region, without changing crystal structure or molecular arrangement. As a first step of this project, the ^{13}C-NMR study has been carried out for the fully deuterated Cu[N(CN)$_2$]Br where the double-bonded carbon sites in the center of BEDT-TTF are simultaneously enriched by ^{13}C isotope for NMR measurements. The nuclear spin-lattice relaxation rate, T_1^{-1}, is enhanced over that of the non-deuterated salt at low temperature and shows a sharp peak at ~15K, indicating a magnetic transition. Although the spectra at low temperature imply presence of both paramagnetic and antiferromagnetically ordered phase, it is clear that the deuteration leads to an enhancement of antiferromagnetic spin fluctuations or magnetic order.

IV-C-6 Strong Electron Correlation and Metal-Insulator Transition in (BEDT-TTF) (TCNQ)

Kazuya MIYAGAWA, Akiko SHIMIZU, Atsushi KAWAMOTO *(Ochanomizu Univ.)*, **Yasuhiro NAKAZAWA and Kazushi KANODA**

(BEDT-TTF)(TCNQ) has a layered structure composed of two-dimensional BEDT-TTF sheet and TCNQ sheet in which one-dimensional TCNQ chains are arranged side by side. Therefore, this compound is a hybrid system of two-dimensionality and one-dimensionality. With a view of investigating electronic states in BEDT-TTF layers and TCNQ chains separately, we synthesized BEDT-TTF molecules where the central double-bonded carbon sites and all hydrogen sites are simultaneously labelled by ^{13}C and deuterium, and performed ^{13}C-NMR measurements on BEDT-TTF sites and ^{1}H-NMR measurements on TCNQ sites. The temperature dependence of ^{13}C line-width, which characterizes anisotropic Knight shift, was found to be very weak between 60K and 380K, suggesting temperature-insensitivity of the spin susceptibility. In addition, we observed a linear temperature dependence of T_1^{-1} between 70K and 380K. However, the value of $(T_1T)^{-1}$ is one order of magnitude larger than that expected from usual Korringa relation. The T_1^{-1} starts to deviate up from the linearity below 70K and has a peak at 20K associated with an antiferromagnetic order of localized spins on each BEDT-TTF dimer. These results evidence that the paramagnetic state is dominated by strong electron correlation, which finally leads to an antiferromagnetic order. The T_1^{-1} of ^{1}H-NMR, on the other hand, shows a large ω-dependence characteristic of one-dimensional conductor.

IV-C-7 ^{13}C-NMR Study on the Organic Superconductor, β_L-(BEDT-TTF)$_2$I$_3$

Kazuya MIYAGAWA, Atsushi KAWAMOTO *(Ochanomizu Univ.)* **and Kazushi KANODA**

β-(BEDT-TTF)$_2$I$_3$ is an organic superconductor with

a superconducting transition temperature, T_c, of 1.0 ~ 1.5 K at ambient pressure (β_L-phase). An incommensurate superstructure is known to appear below 180 K, and the possibility of some phase transition around 20 K was pointed out by the Hall effect and specific heat measurements for β_L-phase. To get informations on the electronic state, magnetism were investigated by the ^{13}C-NMR and static susceptibility, χ_s, measurements. The NMR measurements were performed at a field of 80 kOe applied perpendicular to the conducting layers. At room temperature, the ^{13}C-NMR spectra consisted of four lines, which are explained by ^{13}C=^{13}C nuclear dipole splitting with inequivalent shift tensors in the two ^{13}C sites. Below 180 K, the spectra showed broadening, which grew progressively without structure at low temperatures. This is ascribed to an inhomogenious Knight shift caused by the incommensurate superstructure. The second moment showed a remarkable increase below 70 K rather than below 180 K. This indicates that inhomogenity of the Knight shift, namely disorder in the electronic state, develops even well below the superstructure transition. The temperature dependence of $1/(T_1T)$ was similar to that of χ_s^2 above 20 K, where T_1 is the spin - lattice relaxation time and T is temperature. There observed a slight kink in the temperature dependences of $1/(T_1T)$ and χ_s around 180 K. These are indications of influence of the superstructure on the electronic state. The χ_s showed a clear kink structure at ~23 K, giving another evidence of the anomaly observed in the Hall effect and specific heat. On the other hand, the $1/(T_1T)$ showed a similar kink at 15 K. The difference of the characteristic temperature may imply a field dependence of the anomaly; the susceptibility was measured at 10 kOe while the NMR measurements were at 80 kOe.

IV-C-8 Effect of Annealing on the Electronic State of β-(BEDT-TTF)$_2$I$_3$

Kazuya MIYAGAWA, Atsushi KAWAMOTO *(Ochanomizu Univ.)* **and Kazushi KANODA**

The T_c of the title compound is known to rise up to 8 K after annealing around 104 K (β_H-phase). The static susceptibility, χ_s, and ^{13}C-NMR measurements have been performed during and after the annealing in order to see the effect of the annealing on the electronic state. The sample was kept at 104 K for 190 hours and 140 hours in the ^{13}C-NMR and susceptibility measurements, respectively. During the annealing , T_1 , spectra and χ_s did not show appreciable change. The χ_s, T_1 and spectra after the annealing showed different profiles from those of β_L-phase well below 100 K. The kink structures in the temperature dependence of χ_s and $1/(T_1T)$ observed in β_L-phase disappeared. The spectra had a structure at low temperature, however the inhomogeneous broadening still remained. The T_1 seems to obey a Korringa's law, $T_1T\chi_s^2$ = constant. This behavior is in a strong contrast to that of the κ-phase family of BEDT-TTF salts, where the Korringa relation breaks down. This is attributed to a difference in the manifestation of the effect of the electron correlation.

IV-D Electron Transport and Magnetic Study of Anisotropic Superconductors

There are increasing interests in anisotropic transport and magnetic properties of layered superconductors, because their low-dimensional fluctuations around the transition temperature and dynamic properties of vortex motion are center of unsolved problems in physics of superconductors. In addition to this, such layered superconductors have some possibilities to be used as electronic devices. BEDT-TTF based organic charge transfer salts are typical examples for inquiry of such probems and possibilities, because of their structural peculiarity that the conducting donor layers are seperated by thick anion layers. In some BEDT-TTF salts extermely two-dimensional characters than that of Bi-based high-T_c oxide have so far been reported.

IV-D-1 Extremely Large Penetration Depth in α-(BEDT-TTF)$_2$NH$_4$Hg(SCN)$_4$

Hiromi TANIGUCHI, Hirohiko SATO *(Tokyo Institute of Technology)*, **Yasuhiro NAKAZAWA and Kazushi KANODA**

[*Phys. Rev.* **B** in press]

Because of a finite field penetration into a specimen, the diamagnetic signal of a superconductor in the Meissner state does not reach exactly to $-1/4\pi$. If the order of the penetration depth becomes the sample size, we can easily calculate the penetration depth from the value of ac susceptibility. We measured out-of-plane ac susceptibility, $\lambda_\perp$,(H_{ac} // conducting plane) for five different size of samples of α-(ET)$_2$NH$_4$Hg(SCN)$_4$ and plotted the diamagnetic signal at 0.4 K as a function of sample length L, shown in Figure.1. In this geometry the penetration depth can be represented by following formula .

$$-4\pi\chi' = 1 - (2\lambda_\perp / L) \tanh (L / 2\lambda_\perp)$$

The solid line is a fitted curve based on this formula and we can reproduce the data points by this formula fairly good. We, therefore, obtained the parallel penetration depth 1.65 mm at 0.4K. Extrapolation gives $\lambda_\perp$ of 1.4-1.5mm at zero Kelvin. Such a large values is never seen in any other quasi-two dimensional superconductor and indicate that the interplane coupling of this superconductor is extremely weak.

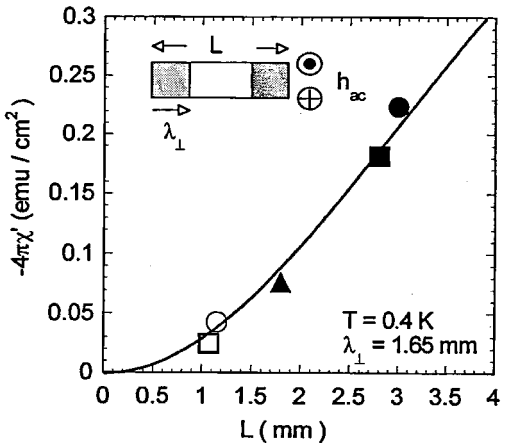

Figure 1. The diamagnetic signal at 0.4K of five different size of samples of α-(BEDT-TTF)$_2$NH$_4$Hg(SCN)$_4$.

IV-D-2 Construction of an AC Susceptibility Measurement System Combined with DC Magnetic Fields

Hiromi TANIGUCHI and Kazushi KANODA

In order to investigate the anisotropic properties of superconductors and magnetic materials, ac susceptibility measurements under dc magnetic field is important. Especially, in layered superconductors such as BEDT-TTF based organic superconductor, peculiar characters originating from weak Josephson coupling between layers and dynamics of vortex motion in the two-dimensional layer can be probed by measuring in-plane and out-of-plane susceptibility. By combining dc magnetic field in a direction perpendicular or parallel to the ac field, we can get information on the compressive mode and tilting mode of this vortex states. At present, our target is α-(BEDT-TTF)$_2$NH$_4$Hg(SCN)$_4$ which has been proved to have extremely anisotropic nature in its transport properties. The ^{3}He cryostat containing the ac susceptibility measurement system of mutual inductance method is inserted in an usual solenoid type superconducting magnet and split type of magnet. The minimum temperature obtained by this system is 0.4K and a maximum dc field reaches to about 2kOe in both configuration. In Figure 1, we show one example of data obtained in a configuration where the dc field is perpendicular to the conducting layers and the ac field.

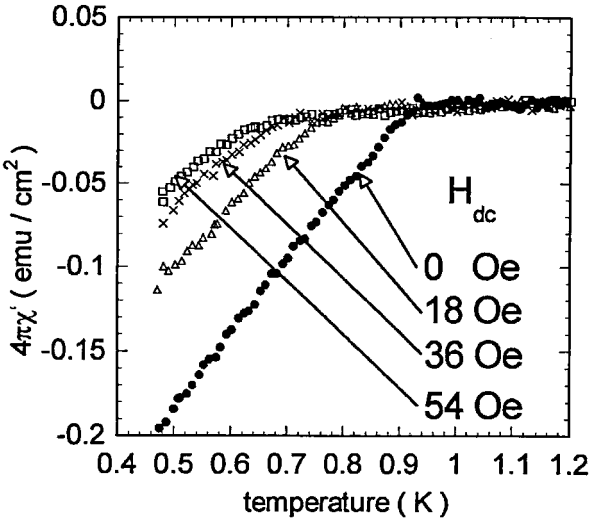

Figure 1. AC susceptibility data of α-(BEDT-TTF)$_2$NH$_4$Hg(SCN)$_4$ sample obtained in a configuration where the dc fields are applied perpendicular to the conducting layers and the ac field.

IV-D-3 Superconductivity of ZrRuSi Prepared at High Pressure

Ichimin SHIROTANI, Kenji TACHI, Keiki TAKEDA *(Muroran Institute of Technology)*, **Sakae TODO, Takehiko YAGI** *(Institute for Solid State Physics, The Univ. Tokyo)* **and Kazushi KANODA**

[*Phys. Rev.* **B 52** (1995) 6197]

Hexagonal ZrRuSi with Fe_2P-type structure (h-ZrRuSi) and orthorhombic ZrRuSi with Co_2P-type form (o-ZrRuSi) were prepared at high temperatures and high pressures. These metal silicides are interesting layered compounds. A resistivity of ZrRuSi was measured at low temperatures. The superconductivity was observed between 7-12K for h-ZrRuSi and between 3-5K for o-ZrRuSi. These silicides are new superconductors. The resistivity of h-ZrRuSi and h-ZrRuP was measured at various constant temperatures as a function of applied magnetic field. The upper critical field (H_{c2}) obtained from resistance vs. magnetic field curves was 1 tesla at 0K for h-ZrRuSi. This is a surprisingly small value. On the contrary, h-ZrRuP has a large H_{c2} of 17.5tesla at 0K.

IV-E Thermodynamic Study of Organic Conductors

In order to get reliable information on the absolute value of electron density of states and on the entropy distribution around the phase transition, the specific heat study is inevitable. In this project, we aim to construct several calorimeters available at low temperature region and also in magnetic fields and to perform a systematical investigation on BEDT-TTF based charge transfer salts from a thermodynamic viewpoints.

IV-E-1 Construction of Low-Temperature Specific Heat Apparatus of Themal Relaxation Method

Yasuhiro NAKAZAWA and Kazushi KANODA

In many cases, samples of organic charge transfer salts are usually harrested as small pieces of single crystals and it always become an obstacle to perform specific heat experiment by the most popular adiabatic heat-pulse technique, especially, at low temperatures where the thermal leak through wires is not negligibly small. Characterization of the ground state from a thermodynamic measurement gives insight into various unsolved problems related to the electronic states of organic conductors.

To estimate the electronic specific heat coefficint γ, accurate measurement of single piece of crystal below 2K is inevitable. For this purpose, the thermal relaxation method is best suited. The bolometer of our calorimeter is composed of thin sapphire plate, small chip thermometer and film heater, and is surrounded by a heat bath made of copper. The heat leak from the bath to the bolometer is now adjusted to the best condition of measuring heat capacity corresponding to about 1~5mg of BEDT-TTF salts in a temperature range of 0.8K~4.5K in ^{3}He refrigerator and 0.1~1.2K in dilution fridge (KELVINOX system at the low-temperature center of IMS). By adjusting the thermal leak, measurements of various kind of samples and in different temperature range is also possible. The themometer was calibrated also in typical magnetic field of 0T, 2T, 4T, and 8T so that magnetic field dependence of specific heat is also measureable.

IV-E-2 Characterization of Low-Temperature Electronic States of Organic Conductors, α-(BEDT-TTF)$_2$MHg(SCN)$_4$ [M=K, Rb, and NH$_4$], by Specific Heat Measurements

Yasuhiro NAKAZAWA, Atsushi KAWAMOTO *(Ochanomizu Univ.)* **and Kazushi KANODA**

[*Phys. Rev.* **B 52** (1995) 12890]

The mechanism of the electronic structure change around 10K in α-(BEDT-TTF)$_2$MHg (SCN)$_4$ (M=K,Rb, and Tl) salts is one of the open questions in physics of the organic conductors. This problem is widely discussed in terms of the structure of the Fermi surface and the magnetic properties of the groung state. Last year, we started a thermodynamic study to determine the exact electron density of states of this material by specific heat measurements as a characterization of the low-temperature anomalous electronic phase in these compounds. At first, we adopted adiabatic heat pulse method for about 3~7 pieces of crystals (total weight of 10mg~30mg) , however, the low-temperature data did not give enough resolution to determine γ value precisely. In order to get more reliable information in the low-temperature region, we performed specific heat measurements on single crystals of M =K, Rb and NH$_4$ salts by the thermal relaxation method. The γ values were determined to be about 7.0±0.6mJ.molK^2 for M=K, Rb salts, and 25~26mJ/molK^2 for M=NH$_4$ salt. The relatively large depression of γ in low-temperature phase of M=K, Rb, as compared with M=NH$_4$ case, implies that the electron density of states of low-temperature phase of the former two salts is depressed down to about 35% of that of high-temperature phase. This profile of specific heat keeps unchanged up to a field of 8T, which is consistent with magnetoresistance results.

IV-E-3 Specific Heat Around the Superconductive Transition of α- (BEDT-TTF)$_2$NH$_4$Hg (SCN)$_4$

Yasuhiro NAKAZAWA, Atsushi KAWAMOTO *(Ochanomizu Univ.)* **and Kazushi KANODA**

The superconductivity of α-(BEDT-TTF)$_2$NH$_4$Hg (SCN)$_4$ were studied by low-temperature specific heat measurements. The C_p/T gives a broad maximum around 0.9K. Figure 1 shows a temperature dependence of the difference between C_p/T in the superconducting and normal states defined by, $C_p(0T)/T$-$C_p(8T)/T$, around the transition temperature. The dashed line in the figure represents the mean-field profile given by the BCS theory with the specific-heat jump of $[(C(0T)-C(8T))/T]_{Tc}$ =1.43γ_{eff}. With the use of γ_{eff} =25mJ/molK^2 estimated from the data of H=8T and a bulk transition temperature, T_c, of 0.91K probed by ac susceptibility signal, the entropy associated with the peak is close to that estimated from the mean-field peak predicted by the BCS theory. This ensures that the superconducting transition is a bulk one. We analyzed the high-temperature tail of the peak in terms of the Gaussian fluctuation model, $C=C_0t^{-\alpha}(t=(T-T_c)/T_c>0)$ and $C=C_0'/t'^{\alpha'}(t<0)$ where $\alpha=\alpha'=2-d/2$ with d, dimensionality. The present data above 1K is well reproduced by the model with d=2 and T_c=0.91K. However, there remains serious discrepancy in the peak shape as is seen by dotted curve in the figure. The width of the peak for this salt, when normalized to the value of T_c, is 2~4 times larger than that for κ-(BEDT-TTF)$_2$Cu(NCS)$_2$ and κ-(BEDT-TTF)$_2$Cu[N(CN)$_2$]Br, which also have two-dimensional nature.

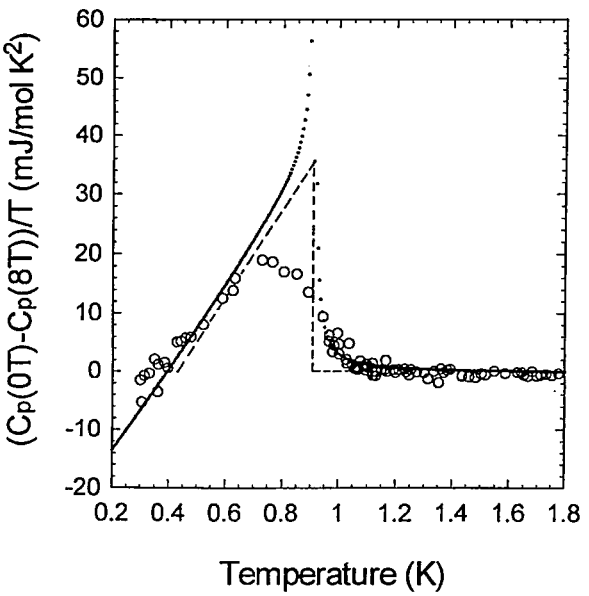

Figure 1. The difference of C_p/T in the superconducting states and normal states around the transition temperature. The dashed line is the peak predicted by BCS weak-coupling theory.

IV-E-4 Electronic Specific Heat Coefficient of κ-(BEDT-TTF)$_2$Cu[N(CN)$_2$]Cl

Yasuhiro NAKAZAWA and Kazushi KANODA

[*Phys. Rev.* **B** in press]

The electronic states of κ-(BEDT-TTF)$_2$Cu[N(CN)$_2$] Cl attracts much attention, because this material is insulating in transport properties and undergoes a magnetic transition at a low temperature, though the electronic-band calcuation predicts a metallic nature as in the isostructural superconductors. Recently, a picture of Mott insulator for this material is proposed. To clarify the nature of the magnetic and insulating state, we have started to study a family of the κ-phase compounds ranging from super-

conductors to insulators from a thermodynamic viewpoints. In Figure1, the low-temperature specific heat data obtained for a single piece of crystal of 4mg by thermal relaxation method is shown as a form of C_p/T *vs* T^2 plot. Because of the higher-order term in the lattice contribution at higher temperatures, the data gives the dependence of $C_p/T=\gamma+\beta T^2$ only below about 2K, that is a common feature found in various types of BEDT-TTF salts. The estimated γ value is 0mJ/molK^2 and is not affected by magnetic fields of up to 8T. This fact evidences that the increase of resistivity with decreasing temperature is not attributable to variable range hopping effects due to the disorder in the sample but originates from the opening of charge gap in the electronic structure.

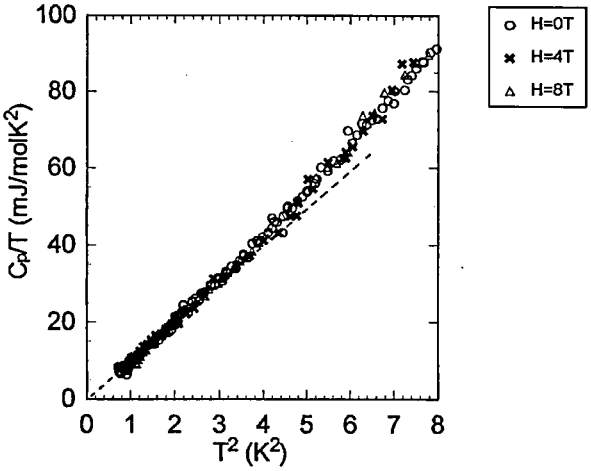

Figure 1. The low-temperature specific heat data of κ-(BEDT-TTF)$_2$Cu[N(CN)$_2$]Cl salt and their magnetic field dependences.

IV-F Novel Electronic States of d-π System of (DCNQI)$_2$*M*

The study on the electronic states of (DCNQI)$_2$*M* system contains many important unsolved problems on condensted matter physics. They show a very sharp metal-insulator transition accompanied with hysteresis and in the insulating state Spin-Peierls transition sometimes occurs. In addition to this, strong electron correlation is suggested in the metallic states. We are trying to clarify the mechanism of these interesting electronic phase transitions and ground state properties through several experimental probes and furthermore trying to control physical properties with an attempt of carrier doping in this system.

IV-F-1 ^{15}N and ^{13}C NMR Shift in (DMe-DCNQI)$_2$M [M=Li and Cu]

Kazuya MIYAGAWA, Atsushi KAWAMOTO *(Ochanomizu Univ.)* **and Kazushi KANODA**

The title two compounds have different electronic structures in spite of the same crystal structure. In the Li salt, the valence of Li is +1 and the p-π orbital of DMe-DCNQI molecule alone makes a conduction band. In the Cu salt, however, the Cu ion is reported to be of intermediate valence of ~+1.3 and therefore the Cu 3d orbital hybridized with the p-π orbital contributes to the conduction band. In this study, we aim at clarifying the effect of the π-d interaction on the electronic structure by comparison of ^{15}N and ^{13}C-NMR data for the two salts. For the purpose, the three sites in =N-CN of the DMe-DCNQI molecule are enriched by ^{15}N or ^{13}C isotopes selectively. The NMR measurements were performed for powder samples at fields of 8-9 Tesla. The ^{15}N-NMR spectra at the two sites have asymmetric lineshape typical of anisotropic Knight shift with uniaxial symmetry, implying that the hyperfine field is a dipole one coming from the 2p orbital of nitrogen. The ^{13}C-NMR spectra are nearly symmetric with isotropic shift, which is due to core-polarization. In the Li salt, the NMR shift at the three sites show the same temperature dependence, which scales to that of spin susceptibility. This is consistent with a picture of purely π band electronic system. In the Cu salt, however, shift at the three sites exhibit different temperature dependence, which does not scale to that of spin susceptibility. This fact is a direct evidence of multiband electronic structure originating from the π-d interaction for the Cu salt.

IV-F-2 Electronic States of (DI-DCNQI)$_2$*M* (*M*=Li, Cu, Ag)

Ko-ichi HIRAKI and Kazushi KANODA

The magnetism and conductivity of DI-DCNQI metal complexes have been investigated. Figure 1 shows the temperature dependence of spin susceptibilities of the isostructual organic compounds, (DI-DCNQI)$_2$*M* as well as (DMe-DCNQI)$_2$*M* (M=Li, Cu, Ag). We can summarize the results as follows.

(1) The DMe-, and DI-systems show characteristic behaviors independent of *M*=Li or Ag, as seen in the figure. The DMe-systems are known to be metallic in the high temperature region, and become a (Spin-) Peierls insulator at low temperatures. On the other hand, DI-system is paramagnetic insulator below the room temperature. Our preliminary NMR study suggests that the anomalies around 10K in the susceptibility are indication of magnetic transitions.

(2) The susceptibilities of DI-Li and DI-Ag salts form a Bonner-Fisher type peak around 40K. The Curie constant in the Curie-Weiss law fitted to at a high temperature region corresponds to *S*=1/2 spin per dimmer.

(3) The vallency of DI-DCNQI molecule in the Li- and Ag-salts should be -1/2. So, it has been expected that the filling of the one dimensional band is quarter. In spite of that, they are paramagnetic insulators unlike DMe-DCNQI systems. A formation of charge-density-wave state is ruled out by the paramagnetism. One possible explanation is a Mott insulator caused by half-filling of the 1D-π band due to possible dimerization of the DI-DCNQI molecule. Detailed *X*-ray structural study is required.

(4) The Cu-salts of both molecules are metallic while the Li- and Ag-salts are insulator. This implies that the 3d electrons of Cu in the DI-Cu salt hybridize with 1D-π-band like the DMe-Cu salt do.

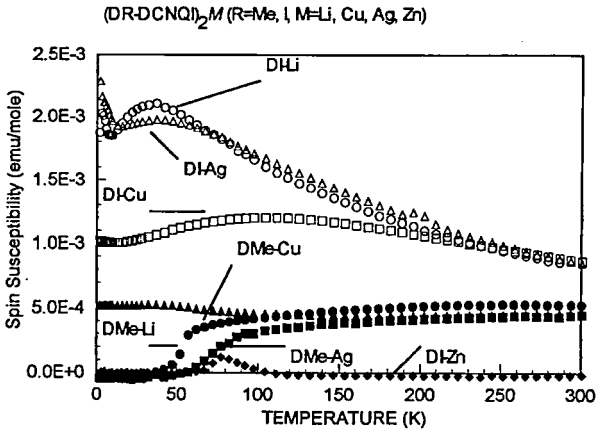

Figure 1. The temperature dependence of spin susceptibility of (DI-DCNQI)$_2M$ and (DMe-DCNQI)$_2M$ (M=Li,Cu,Ag).

IV-F-3 Carrier Doping to One-Dimensional Conductors, (DCNQI)$_2$Li

Ko-ichi HIRAKI and Kazushi KANODA

We are interested in the effect that the doping gives to the electronic state of the molecular conductors. In the case that M of the (DCNQI)$_2M$ is Li, the π-electrons in the DCNQI molecule form a conducting electronic system with one-dimensional (1D) band structure. Now, we consider alloy systems of Li and Cu (a) or Li and Zn (b) as M. The valence of each cation in the crystals is +1 for Li, close to +1.33 for Cu and +2 for Zn, respectively. The Cu-doping (a) can cause the hole-doping to the 1D π-band and increase of dimensionality in the electronic structure through the π-d hybridization. On the other hand, a dominant effect of the Zn-doping (b) is only the hole injection to the 1D-band. (DMe-DCNQI)$_2$Li (DMe-Li) and (DI-DCNQI)$_2$Li (DI-Li)were selected as the starting materials. The DMe-Li salt is known to show the (Spin-) Peierls transition. The DI-Li is a paramagnetic insulator below room temperature. It has been found that the conducting and magnetic properties changed systematically with increasing the doping content. In the (a) case, the (Spin-) Peierls transition was suppressed in DMe-system, and the susceptibility was reduced in DI-system. It has been found that the magnetic susceptibility of the system (b) to the DI-system increased with increasing the Zn doping content (up to 40%). This can not be explained by a simple mixing of each undoped salt (DI-Li and DI-Zn) but evidences an effect due to doping. We are now considering the mechanism of the crossover from the non-magnetic Peierls state or magnetic insulator to metallic in case (a), and possibility of 1D Luttinger liquid in case (b).

IV-G Ultra-Thin Organic Film Systems Prepared by Molecular Beam Epitaxy (MBE) Technique

As a strategy for a development of new molecular systems of organic materials, we have undertaken the fabrication of ultra-thin organic multi-layer systems with the use of an MBE technique. We are expecting the preparation of such novel 2-dimensional materials as molecutar superlattice systems or intercalation compounds in which special electronic states in the bulk and/or new charge-transfer states in the interfaces could be realized. We have prepared ultra-thin epitaxially grown phthalocyanine films on alkali halide single crystal substrates. On the basis of this single crystalline film, we are now fabricating double-layer systems of phthalocyanines. Nonlinear optical effects are found to be significantly correlated with the film structure. The spectral responses of the non-linear susceptibilities are now going to be studied for the phthalocyanine thin film systems.

IV-G-1 Spectral Dependence of the Anisotropy of $\chi^{(3)}$ of Epitaxially Grown Vanadyl Phthalocyanine Film

Shaoli FANG, Keiichi KOHAMA *(Toyota Motor Corp. and IMS)*, **Hajime Hoshi** *(Tokyo Institute of Technology)* **and Yusei MARUYAMA**

[*Chem. Phys. Lett.* **234**, 343 (1995)]

Spectral dependence of the anisotropy of $\chi^{(3)}$ of epitaxially grown vanadyl phthalocyanine has been studied through the technique of third harmonic generation. It is found that the variation of the anisotropy of $\chi^{(3)}$ is a result of the dispersion of the complex ratio $3\chi_{1221}/\chi_{1111}$. There is a sharp two-photon resonance in $\chi^{(3)}$ that may be attributed to the presence of the state 1.88eV above the ground state. Enhancement of $\chi^{(3)}$ is achieved in the unidirectionally oriented vanadyl phthalocyanine film by one order of magnitude.

IV-G-2 Nonliniar Optical Characteristics of MBE-Grown Phthalcyanine Thin Films

Yusei MARUYAMA, Hajime HOSHI *(Tokyo Institute of Technology)*, **Shaoli FANG and Keiichi KOHAMA** *(Toyota Motor Corp. and IMS)*

[*Synth. Met.* **71**, 1653 (1995)]

Vanadyl Phthalocyanine forms an epitaxially-ordered thin films on alkali halid single crystals. The square lattice symmetry (4mm) of the 2-dimensional film structure is confirmed by the anisotropic nature of nonlinear optical effects. A unique third-harmonic-generation peak appears in the spectrum of anisotropic response and it may originate in a two-photon resonance effect which might be correlated to exciton state.

IV-G-3 Nonlinear Optical Characteristics of Vanadyl Phthalocyanine Thin Film Grown by Molecular-Beam-Epitaxial Method

Shaoli FANG, Hajime HOSHI, *(Tokyo Institute of Technology)*, **Keiichi KOHAMA** *(Toyota Motor Corp. and IMS)* **and Yusei MARUYAMA**

[Submitted to *J. Phys. Chem.*]

We have studied several aspects of nonlinear optical behaviors of unidirectionally-oriented vanadyl phthalocyanine (VOPc) epitaxial film. The characteristic nature of the epitaxial film has been found to be the rotational anisotropy in third-harmonic intensity in the film surface plane and demonstrated to be associated with the symmetry elements of the film. The essential features are explained based on the symmetries of C_{4v} for VOPc/KBr epitaxial film and $C_{\infty v}$ for VOPc/silica polycrystalline film. The epitaxial film is distinguished from the polycrystalline one using in-plane angle-dependence THG measurement. It is found that the rotational anisotropy in the epitaxial film is strongly wavelength dependent. We attribute the spectral dependence to resonant coupling of the fundamental and harmonic fields with electronic states of the π-electron system of the epitaxial film. We have also discussed the orientation of VOPc molecules on KBr substrate and proposed an accommodation model of VOPc lattice on KBr (001) surface based on third-harmonic-generation measurement and computer simulation.

IV-H Novel Molecular System C_{60}: Fullerites and Fullerides

We have studied the charge-carrier transport properties in C_{60} and C_{70} vaper-grown single crystals, and also the magnetic properties of charge-transfer complexes of C_{60} such as C_{60} (TDAE).

IV-H-1 Laser Pulse Induced Transient Photoconductivity of C_{70} Single Crystal

Eugene FRANKEVICH *(The Institute for Energy Problems of Chemical Physics RAS and IMS)*, **Yusei MARUYAMA and Hironori OGATA**

[*J. Phys. Chem. Solids*, in press]

The transient photoconductivity of C_{70} single crystal excited by 800 ps N_2 laser pulse was studied. The mobility of positive and negative free charge carriers was determined (1 cm^2/Vs) which is found to be similar to that determined for C_{60} single crystal. Trapping of free carriers in C_{70} was revealed to be much faster than in C_{60} leaving for the lifetime of free carriers 16 ns only. Dark charge injection was shown to occur from gold or aluminum electrodes, and excitation in these condition resulted in delayed generation of the photocurrent within the time domain of microseconds. This phenomenon was shown to be connected with triplet excitons which detrap injected electrons or holes just producing photoenhanced current. Triplet exciton annihilation may be followed. Studying the decay of transient photocurrent within tens of microseconds time domain has permitted to characterize the trapping sites as being of 0.1 eV deep and having the size of about 25Å. The trapping sites are speculated to be caused by structural imperfections which cause the local increases of π-electron density and polarisability. A prominent electrical field effect (of Poole-Frenkel type) was revealed on the thermal detrapping rate that appears to be a rare example of the electrical field effect on the neutral trapping sites.

IV-H-2 Delayed Generation of Free Charge Carriers in C_{70} Single crystals

Eugene FRANKEVICH *(The Institute for Energy Problems of Chemical Physics RAS and IMS)*, **Yusei MARUYAMA and Hironori OGATA**

The transient photoconductivity of C_{70} single crystal excited by 800 ps N_2 laser pulse was studied. Trapping of free carriers in C_{70} was revealed to be much faster than in C_{60} leaving for the lifetime of free carriers only 16 ns. Dark charge injection into the crystal was shown to occur from gold or aluminum electrodes, and excitation in these conditions resulted in delayed genaration of the photocurrent within the time domain of tens microseconds. This phenomenon was shown to be connected with triplet excitons which detrap injected electrons or holes and produce a photoenhanced current which is a few orders of magnitude higher than in the absence of the injection. Triplet exciton annihitation may be followed up to 50 μs.

IV-H-3 Transport Property of C_{60} and C_{70} Single Crystals

Yuichi OCHIAI *(Dept. of Mater. Sci., Chiba Univ.)*, **K. YAMAMOTO** *(Dept. of Mater. Sci., Chiba Univ.)*, **H. YAMASAKI** *(Dept. of Mater. Sci., Chiba Univ.)*, **Y. SHIONOIRI** *(Dept. of Mater. Sci., Chiba Univ.)*, **Hironori OGATA and Yusei MARUYAMA**

[*Fullerenes Sci. & Tech.* **3**, 79 (1995)]

Temperature dependence of resistance was measured for the C_{60} and C_{70} single crystals prepared by a sublimation method. Transport property focusing on the activation energy and the phase transition was discussed.

IV-H-4 Magnetic and Electrical Behaviors of C_{60} (TDAE) Single Crystals

Atsushi SUZUKI, Toshiyasu SUZUKI and Yusei MARUYAMA

[*Solid State Commun.* **96**, 253 (1995)]

Significant size of single crystals of C_{60}(TDAE), where TDAE is tetrakis(dimethylamino)ethylene, have been prepared from a toluene solution for the first time by a deffusion method. The resulting conglomerate of black colored needles is found to consist of single crystals by X-ray diffraction analysis. A resistivity of $1.1 \times 10^5 \Omega$cm at room temperature and an activation energy of 0.4~0.8eV suggest that an obtained C_{60} (TDAE) crystal is not metallic but semiconducting. The crystals do not show a ferromagnetic behavior but Pauli- and Curie-Weiss paramagnetism with a negative Weiss constant, θ= -0.44K. It was found that the difference in the magnetic properties between crystal and powder samples may originate from the change of the lattice constants.

IV-I Development of New Organic Superconductors and Novel Molecular Metals

Since the first discovery of the organic superconductor $TMTSF_2PF_6$, about 60 organic superconductors have been reported including seven $M(dmit)_2$ compounds (M=Ni, Pd; dmit=1,3-dithiol-2-thione-4,5-dithiolate). The increasing number of the molecular superconductors shows that the molecular systems are surprisingly suited to the development of new superconducting materials. Among the various constituent molecules investigated, BEDT-TTF has produced the most organic superconductors. The discoveries of new BEDT-TTF superconductors are actively continued but the highest T_c-record of organic superconductors has been fixed since the report of κ-$(BEDT\text{-}TTF)_2Cu[N(CN)_2]Cl$ (T_c~13 K) by Williams et al. For the purpose of getting new attractive molecular conducting systems, the systematic examination of new constituent molecules will be required. In the development of new systems, the choice of donor molecule is of special importance, because the evasion from the insulating instability is still a bottle-neck for the design of molecular conducting systems. We selected BETS (bis(ethylenedithio)tetraselenafulvalene) molecule because it has a strong tendency to give stable two-dimensional metals.

IV-I-1 New Organic Superconductors, λ-$BETS_2GaX_{4-x}Y_x$ (BETS= bis(ethylenedithio)tetraselenafulvalene)

Hayao KOBAYASHI, Hisashi TANAKA*, Akiko KOBAYASHI* and Taro SAITO*(*Tokyo Univ.)

We have recently found a organic superconductor with new type of molecular arrangement, λ-$BETS_2GaCl_4$ (BETS =bis(ethylenedithio) tetraselenafulvalene) (T_c ~8 K). By using mixed-halogen gallium tetrahalides, we have obtained a series of new organic superconductors, λ-$BETS_2GaBrCl_3$ (T_c ~8 K), λ-$BETS_2GaBr_{0.5}Cl_{3.5}$ (T_c ~6.5 K) , λ-$BETS_2GaCl_3F$ (T_c ~3.5 K). Rougly speaking, the magnitude of T_c of isostructural organic superconductor is correlated with the size of the anion. Accordingly, T_c of λ-$BETS_2GaBr_4$ may be expected to become higher. But the crystal structure analysis of λ-$BETS_2GaBr_4$ showed that it has not λ-type structure but modified λ-type (λ'-type) one. In addition, the system is not a superconductor at least at ambient pressure. There must be a limit of Br-content (x) in λ-$BETS_2GaBr_xCl_{4-x}$. It is quite interesting that λ-$BETS_2GaBr_{1.5}Cl_{2.5}$ exhibits semiconducting behavior at ambient pressure. It is well-known that similar behavior is found in κ-$(BEDT\text{-}TTF)_2Cu[N(CN)_2]Cl$, which becomes a superconductor (T_c ~13 K) by applying "soft pressure". Although the molecular arrangement of λ-type superconductor is completely different from that of κ-type one, the close resemblance between the characteristic temperature dependences of the resistivities of these two types of salts strongly suggests the existence of the general phase diagram in organic superconductors.

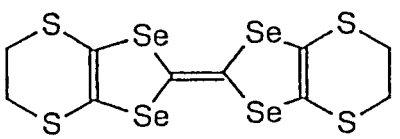

BETS

IV-I-2 New BETS Conductors with Magnetic Anions

Hayao KOBAYASHI, Toshio NAITO*, Akiko KOBAYASHI and Patrick CASSOUX***** *(*Toho Univ., **The Univ. of Tokyo, ***CNRS)*

Almost all the molecular metals ever reported are essentially π-electron systems. In order to make the solid state chemistry of conducting molecular solids more fertile, the entry of new types of "active electrons" is required. Since the functional electron orbits have open-shell structures, novel electronic properties will be expected in the system with two types of the open-shell electron orbits. It would be of interest to prepare π-metal systems with transition metal complex anions having localized magnetic moments, where both π and d electrons have incompletely filled orbits. Crystals of $BETS_2MCl_4$ (M=Mn, Fe, Co, Ni, Cu) were prepared electrochemically. Resistivities were measured down to 4 K. As was expected, new molecular metals where π metal electrons and localized magnetic moments coexist at liquid He temperature were obtained. The $FeCl_4^-$ anion gave two modifications (κ,λ). The salt with κ-type molecular arrangement, κ-$BETS_2FeCl_4$ is metallic down to at least 2 K. No sign of superconducting or magnetic transition was observed. In contrast to superconducting λ-$BETS_2GaCl_4$, λ-BETS2$FeCl_4$ exhibits a novel metal-insulator transition coupled with magnetic transition around 8 K. It is quite surprising that a superconducting transition was observed at 4.6 K in λ-$BETS_2(GaCl_4)_{0.5}(FeCl_4)_{0.5}$, where a half of the anion sites are occupied by magnetic ions. The $CoCl_4^{2-}$ salt has κ-type structure, which retains metallic state down to 4 K. The salts with $NiCl_4^{2-}$ and $MnCl_4^{2-}$ anions were semi-metallic down to about 100 K. The $Cu_2Cl_6^{2-}$ salt remains metallic down to 4 K.

IV-J Low-temperature Crystal Structures and Phase Transitions of Molecular Conducting Systems

The information about the crystal structure is of course very important for the studies on the crystalline solid. The recent development of the molecular design makes it possible to prepare molecular conducting systems with stable metallic

states, which enables the studies on the electric and magnetic properties of π metals at very low temperature. Molecular system has various structural freedom, which brings about the phase transition. Since the electronic structure of molecular metal is very sensitive to the structure change, the low-temperature structure determination is indispensable. However, the lack of the suitable X-ray systems prevented the structure analysis at low temperature (<80 K) until quite recently. Such a situation has been improved greately by the low-temperature X-ray IP system (IP=imaging plate) set up by us.

IV-J-1 Electronic Band Structure and Superconducting Transition of κ-(BEDT-TTF)$_2$I$_3$

Hayao KOBAYASHI, Koichi KAWANO*, Toshio NAITO* and Akiko KOBAYASHI** *(*Toho Univ., **The Univ. of Tokyo)*

[*J. Material Chem.*, **5**, 1681 (1995)]

Since the first synthesis of metallic compounds of BEDT-TTF by Mizuno et al., BEDT-TTF conductors have contributed greately to the production of various types of organic conductors. Among them, κ-(BEDT-TTF)$_2$I$_3$ is of special importance because it is the first example of κ-type organic superconductors, which have been leading materials since the end of 1980s. But the difficulty of preparing good single crystals prevented sufficient characterization of κ-(BEDT-TTF)$_2$I$_3$. Recently, we have tried to obtain good crystals and to reexamine the crystal and band structures and superconducting transition. A resistivity drop indicating a superconducting transition was observed at 4.2 K (mid-point), which is a little higher than the reported temperature (3.6 K). The T_c decreases with increasing pressure (dT_c/dP= -0.8 K kbar^{-1}). The resistivity exhibited an anomaly around 170 K, which was found to be coupled with the structural phase transition accompanied by the change of the space group ($P2_1/c \rightarrow P2_1$). The crystal structure was determined at 295, 150 and 10 K. The X-ray intensity distribution F(*h0l*) showed the absence of *c*-glide symmetry, which is related to the conformational change of ethylene groups. the low-temperature band structure calculated by the extended Huckel approximation gave Fermi surfaces consistent with the results of de Haas-van Alphen experiments.

IV-K Development of Pulsed Field Gradient NMR Spectroscopy

Pulsed field gradient (PFG) spin echo (SE) nuclear magnetic resonance (NMR) is a powerful method for the study of dynamics in condensed matter because it probes translational motion of molecules selectively, without being affected by vibrational or rotational motions. Due to this advantage it is now widely applied for liquids or for rapidly diffusing species in disordered solids. However, the application of this technique to strongly dipole-coupled spin systems with short T_2 or to the study of slow and anisotropic self-diffusion are still challenging problem because combined techniques of line-narrowing and sharp and intense field gradient pulses are absolutely necessary. In the present study we developed the PFG NMR spectroscopy to the study of slow and anisotropic self-diffusion dynamics in strongly dipole-coupled spin systems.

IV-K-1 New Pulsed Field Gradient NMR Spectrometer for Solids and Liquid Crystals

Osamu OISHI and Seiichi MIYAJIMA

We designed and constructed a new PFG NMR spectrometer for the study of slow and anisotropic self-diffusion in solids and liquid crystals. To overcome the strong dipolar coupling and the weak signal, the magic angle orientation technique was combined with ^{1}H NMR for smectic liquid crystals, and the broadband ^{1}H decoupling and cross polarization technique to ^{13}C NMR for nematic liquid crystals and plastic solids. To generate intense and sharp PFG, a rotatable quadrupole coil was used. Simulation (Figure 1) shows that our quadrupole coil generates intense and homogeneous field gradient in fairly large area. The PFG NMR experiment is done as follows: Within the pulse sequence of spin echo NMR, a number of controlled PFG are applied. The pulse current is fed from the bipolar capacitors as big as 0.125 F for each, through fast switching circuits consisting of twelve power MOSFETs in parallel for each polarity. The maximum FG of 7.8 T m^{-1} is achieved by applying currents as large as ±50 A. To avoid transient oscillations and voltage droop, the pulse shape is controlled by a negative feedback circuit made with high speed operational amplifiers. The total NMR system is constructed with a 1.4 T electromagnet, 300 W and 1 kW power amplifiers for dual channels, and laboratory made pulse programmer, modulator, and quadrature detectors. The pulse control and data taking is done by a 32 bit personal computer. FG was calibrated by taking NMR image of the cross section of water sample in a quartz cylinder. This method and a more classical method of fitting the free induction decay to the first Bessel function gave agreement with the calculated value. The self-diffusion coefficient of water was measured to check the total performance of the spectrometer, and the value of 1.9×10^{-9} m^2 s^{-1} was obtained at 23 °C in good agreement with the known data.

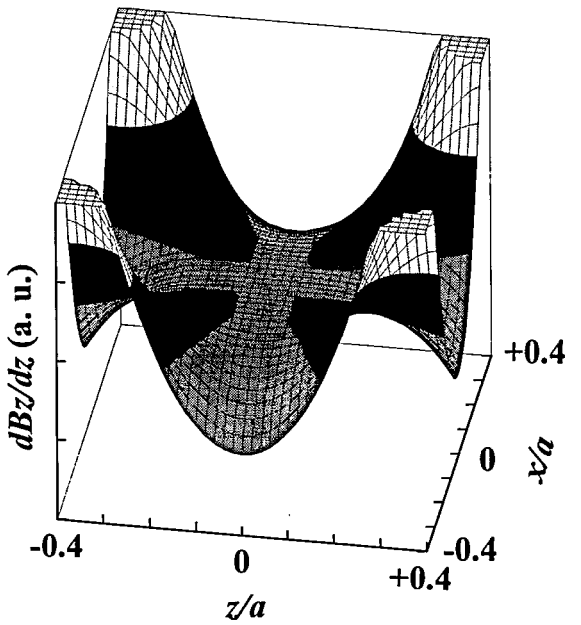

Figure 1. Two-dimensional distribution of the field gradient, $\partial B_Z / \partial Z$, generated by a quadrupole coil. The coil axis is tilted from the main external field (//z) by $\pi/4$.

IV-K-2 Measurement of Anisotropic Self-Diffusion Coefficient Tensor in Smectic Liquid Crystalline CBOOA

Osamu OISHI and Seiichi MIYAJIMA

PFG NMR method was applied to the study of slow and anisotropic self-diffusion. To test the ability of measuring slow dynamics, the temperature dependence of self-diffusion coefficient, D, of a viscous liquid, glycerol, was measured at temperatures including the supercooled region (Figure 1(a)). The result was in good agreement with the reported data,[1] verifying that the apparatus works well in this slow dynamics region. The D component of the anisotropic tensor can be measured by rotating the quadrupole coil in the external field. In the present case of smectic Ad liquid crystalline 4-Octyloxy-*N*-(4-cyanobenzylidene)aniline (CBOOA), D was measured as a function of the angle Φ between the coil axis and the main field, while the alignment axis of the sample (which is parallel to the director) was fixed at magic angle Θ_M from the main field to reduce the homonuclear magnetic dipole-dipole interaction. Considering the uniaxial symmetry of the smectic Ad liquid crystal, the observed component is expressed by

$$D(\phi) = D_{\perp}\sin^2(2\phi - \Theta_M) + D_{//}\cos^2(2\phi - \Theta_M)$$

where $D_{//}$ and $D_{\perp}$ represent the tensor components parallel and perpendicular to the director, respectively. Taking the layer structure in mind, they represent the diffusion across and within the layer, respectively. The experimental result in Figure 1(b) exhibits sinusoidal oscillation with the period of $\pi/2$, in good agreement with the above equation. Least squares fitting gave $D_{//}$ $=5.20\times10^{-11}$ m^2 s^{-1} and $D_{\perp}$ $=1.86\times10^{-11}$ m^2 s^{-1}. The present fact that diffusion across the layer ($D_{//}$) is faster than that within the layer ($D_{\perp}$) is related to the highly disordered one-dimensional lattice structure of this smectic Ad liquid crystal.

Reference

1) M. I. Hrovat and C. G. Wade, *J. Magn. Reson.* **44**, 62 (1981).

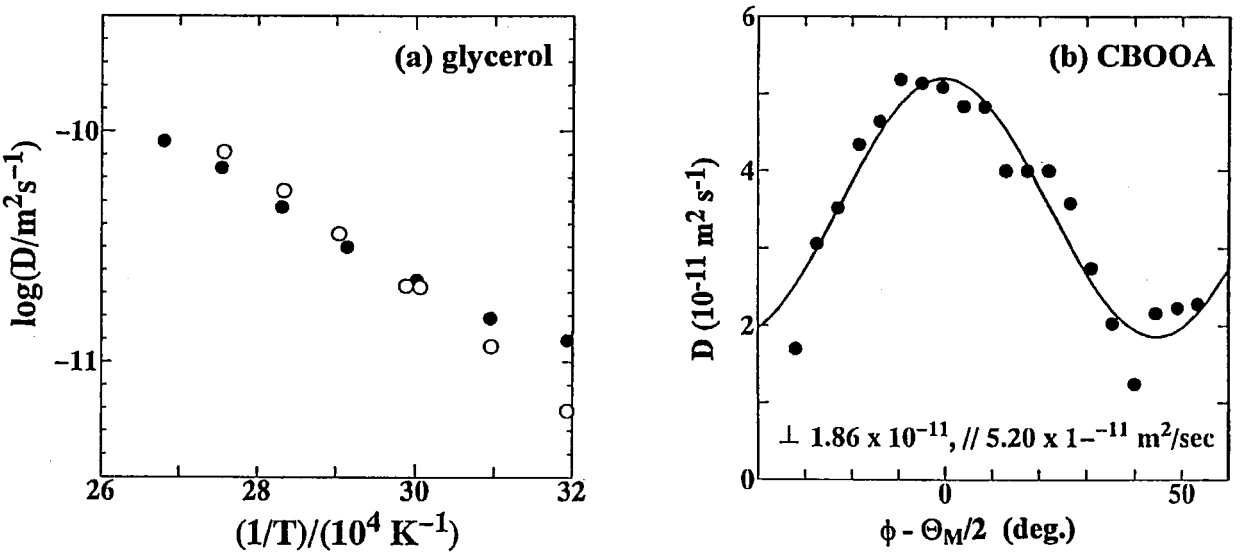

Figure 1.
(a). Temperature dependence of scalar self-diffusion coefficient of glycerol. ● for this work, and ○ for reference 1).
(b). Angular rotation pattern of the anisotropic self-diffusion components for CBOOA in its smectic Ad phase.

IV-L Phase Transitions and Dynamical Ordering in Liquid Crystals

In 1989 the research group in Tokyo Institute of Technology reported the first discovery of antiferroelectricity in liqid crystal. In an antiferroelectric chiral smectic C phase of this compound, (4-(1-methylheptyloxycarbonyl)phenyl 4'-octylbiphenyl-4-carboxylate), abbreviated as MHPOBC, the dielectric polarizations in the adjacent layers order in an anti-

parallel way. However, the microscopic origin for the coexistence of this dielectric order and dynamic disorder has not been resolved. Especially if the dielectric ordering is caused by direct interlayer interaction between the electric dipoles located at the carbonyl groups, the molecular structure of MHPOBC seems less suitable for this ordering because the bulky alkyl chain neighboring the carbonyl group hinders the electric dipoles belonging to the neighboring layers to approach each other. An idea to circumvent this difficulty is to assume the relevant alkyl chain (referred to as "chiral chain") to have bent-shaped conformation, but the idea has, thus far, not been proved experimentally. Using ^{13}C high-resolution NMR spectroscopy, we clarified the validity of this bent-chain model and also the relationship between the chain motion and the dielectric ordering.

IV-L-1 ^{13}C NMR Study on the Orientations and Motions of Alkyl Chains in Antiferroelectric Liquid Crystal MHPOBC

Toshihito NAKAI and Seiichi MIYAJIMA

The ^{13}C spectra of MHPOBC under magic-angle spinning at various temperatures showed that the conformation of the molecule is substantially invariable throughout the liquid crystalline phases. However, the time-scale of the chiral chain motion dramatically changes following the phase transition from the phase S_A, not showing the dielectric ordering, to the ferroelectric S_C^* phase or the antiferroelectric S_{CA}^* phase. In the high-temperature phase S_A, cross polarization was not effective, suggesting that the chiral chain is subject to a large-amplitude motion. From the measurements of ^{13}C T_1, this motion was found to be frozen in the dielectrically ordered phases, S_C^* and S_{CA}^*. The ^{13}C spectra for the field-oriented sample revealed difference in chemical shift behaviors between chiral and nonchiral chains. The smallness of the alignment-induced shift for the chiral chain imply that the chain is bent from the molecular-axis direction by as much as 50 degrees, while the nonchiral chain is almost parallel to the molecular long axis. Thus, we can draw a physical picture on the mechanism of the occurrence of the antiferroelectricity in MHPOBC. In all the phases, the molecule inherently has a bent-shaped chiral chain, which potentially allows the intermolecular electric dipoles to approach and interact. In the high-temperature phase, however, the fast precession of the chain around the molecular axis conceals the dipoles perpendicular to the axis. This motion, having large amplitudes and large steric hindrance, drastically slows down on cooling, and the dipoles interacting across the layers become ordered in an antiferroelectric manner.

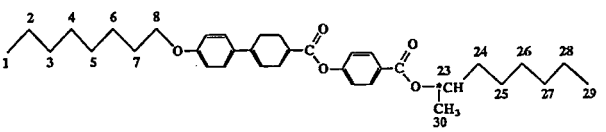

Figure 1. MHPOBC

IV-M Two-Dimensional Electronic Systems

Hydrogen or alkaline metal elements having one *s* electrons in their outermost orbital can, when intercalated into the planar galleries of graphite, possibly exhibit a variety of electronic states such as atomic, ionic, molecular, metallic, or even carbide states. The relative stability of the electronic ground states are controlled by charge transfer interaction with the host graphite, electron-electron, and electron-phonon interactions. Structural and electronic properties were studied for sodium-hydrogen-graphite intercalation compound by means of broadband and high resolution solid state NMR spectroscopies. Search for novel electronic properties in two-dimensional electronic systems was also extended to organic charge transfer complexes of BEDT-TTF with a number of TCNQ derivatives.

IV-M-1 NMR Study of Sodium-Hydrogen-Graphite Ternary Intercalation Compound

Hironori OGATA, Seiichi MIYAJIMA, Kazuto MATSUTSUJI* and Toshiaki ENOKI* *(*Tokyo Institute of Technology)*

[*J. Phys. Chem. Solids*, in press.]

Sodium-hydrogen-graphite intercalation compounds (NaH-GIC) with the stage structures of 2, 3, 4, and 5 were prepared by the reaction of HOPG (highly oriented pyrolytic graphite), sodium hydride, and the sodium metal. The stage 4 compound was found to be most stable, and was subjected to the ^{23}Na, ^{13}C, and ^{1}H NMR studies. ^{13}C NMR spectrum consisted of four lines attributable to the doublet coming from the bounding layers (layers 1) and the doublet due to the interior layers (layers 2). Figure 1 shows the angular rotation pattern of the ^{13}C NMR lines at room temperature. The magnetic shielding tensors were 85.9 and 139.5 ppm for the layers 1 and 2, respectively, showing that negative charge transferred from graphite is mainly distributed on layer 1. The rates of charge transfer were estimated to be 2.9% and 0.5%, for layers 1 and 2, respectively. ^{1}H NMR spectrum is consistent with the model of intercalate structure where the planar hydride lattice is placed between the sodium cationic layers. From the analysis of ^{1}H-^{1}H homonuclear and ^{1}H-^{23}Na heteronuclear dipole interactions, the layer structure and the in-plane concentration of hydride ions are similar to those of pottasium-hydrogen (KH)-GIC. However, the cation concentration is smaller than that in KH-GIC, and a more neutralized intercalate lattice thus formed explains the relatively localized electronic property of NaH-GIC. ^{1}H NMR also shows the existence of motionally-narrowed spectral component of 10-15 % in relative intensity at room temperature, attributable to hydrogen species related to cationic defects in the intercalate lattice.

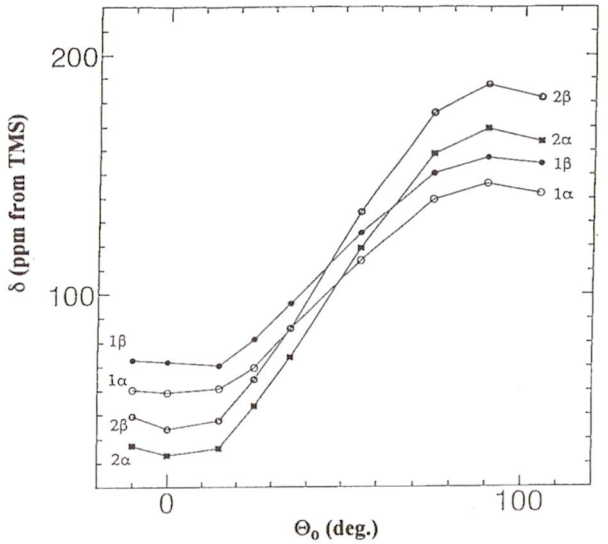

Figure 1. Rotation pattern of the ^{13}C NMR shielding constants in stage-4 NaH-GIC as a function of the angle (Θ_0) between the static external field and the c-axis. The lines 1α and 1β correspond to layer 1, and the lines 2α and 2β to layer 2. The shielding constants are measured relative to liquid TMS with positive value for the less shielded side.

IV-M-2 Preparation of Organic Charge Transfer Complexes with Two-Dimensional Conduction Layers and Their Electronic Properties

Tomoyuki MOCHIDA, Tatsuo HASEGAWA,* Seiichi KAGOSHIMA,* Sadaki SUGIURA and Yoshihiro IWASA**** *(*The University of Tokyo and **JAIST)*

To search for novel electronic phenomena through filling control of the two-dimensional conduction band of BEDT-TTF complexes, charge transfer complexes of BEDT-TTF with TCNQ derivatives of various electron affinities have been prepared. Despite the similarity in the size of the acceptors, isomorphous compounds were rarely obtained for the series of R_1R_2TCNQ (R_1, R_2=Cl, Br, CH_3). While BrMeTCNQ and Me_2TCNQ gave mixed stack complexes, the structures of Br_2TCNQ and BrMeTCNQ complexes were characterized by two-dimensional BEDT-TTF layers; the former undergoes a metal-insulator transition at around 200 K, being consistent with the rather one-dimensional character of the conduction band. The latter, being semiconductive, is considered to be a Mott insulator due to the strong dimerization of the donors. Thus, a strong correlation between the donor arrangement and the electronic properties is recognized.

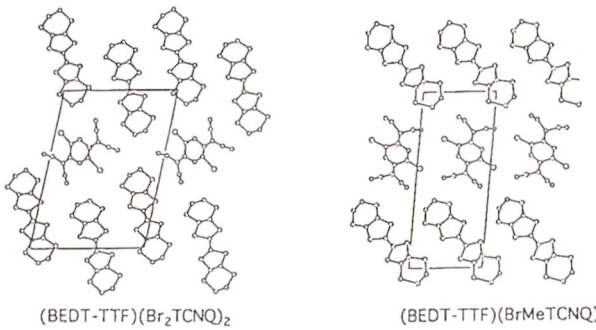

Figure 1. Crystal structures of $(BEDT\text{-}TTF)_2 \cdot Br_2TCNQ$ (left) and (BEDT-TTF)·BrMeTCNQ (right) viewed along the *c*-axis.

IV-N Synchrotron Radiation Excited Surface Reaction

SR excited-etching of covalent bonded materials of the group IV elements has been investigated. SiO_2 is more readily etched by SR excitation than Si surfaces. It seems that an insulator surface exhibits a higher reactivity than a conductive material when SR is shone on the surface in an etchant gas atmosphere. Last year chemically inert diamond surface can be successfully etched by irradiating synchrotron light in an etchant gas atmosphere even at low temperature (- 140°C). It is demonstrated that only the excited area by SR can be etched.

IV-N-1 Synchrotron Radiation Excited Etching of Diamond

Haruhiko OHASHI, Eiji ISHIGURO *(Univ. of the Ryukyus)*, **Tomohiko SASANO** *(Osaka City Univ.)* **and Kosuke SHOBATAKE** *(Nagoya Univ. and IMS)*

We have succeeded in synchrotron radiation (SR) excited etching of crystalline diamond. It proceeds even at low temperatures at which diamond is not thermally oxidized in the gaseous environment. It has been demonstrated that any of the three types of crystalline diamond, i.e., industrial diamond made at high pressures, thin films grown by chemical vapor deposition (CVD), and natural diamond, can be etched by irradiating SR in the O_2 atmosphere. A micrograph of a typical diamond surface etched by irradiating SR through the Ni mesh 5 mm above the surface is illustrated in Figure 1. The pressure of O_2 etchant gas was kept at 0.1 Torr. It is obvious that the shadow area due to 40 μm wide Ni wires is not etched and only the irradiated area is etched. The depth of the etched area was measured as 0.8μm. From the etched pattern it has been concluded that only the irradiated area is etched and thus surface excitation by SR is essential along with the supply of reactive radical species formed by photodissociation.

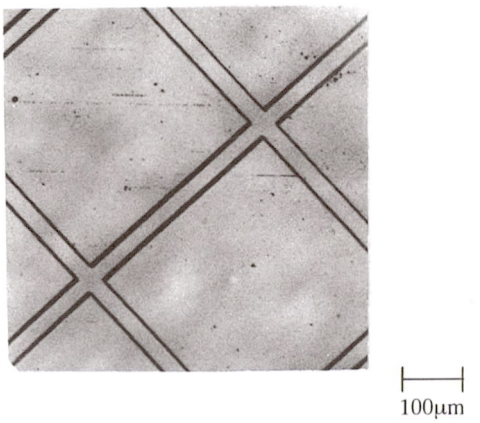

Figure 1.
A micrograph of a typical diamond surface etched by irradiating SR through a Ni mesh 5mm above the surface in O_2 gas envi-

ronment whose pressure was kept at 0.1 Torr. The temperature of the specimen was kept at -60°C.

IV-O New Physical Properties and Electronic Structures of Quasi-One-Dimensional Halogen-Bridged Mixed-Valence Metal Complexes (MX Chains)

Recently quasi-one-dimensional compounds have been attracting much attention since they show very interesting physical properties such as Peierls instability, spin-Peierls, charge density wave (CDW) state, spin density wave (SDW) state, superconductivity, etc.. Among these compounds, one-dimensional halogen-bridged mixed-valence metal compounds (MX chains) have been extensively investigated due to their interesting properties such as an intense intervalence charge transfer band, an overtone progression in resonance Raman, a luminescence with a large Stokes-shift, midgap absorptions attributable to a soliton or a polaron, large third-order nonlinear optical susceptibilities, one-dimensional model compounds of high T_c copperoxide superconductivities, etc.. Theoretrically these compounds are considered as Peierls-Hubbard system where the electron-phonon interaction (S), the electron transfer (T), the on-site and inter-site Coulomb interactions (U and V) are cooperated or competed with one another. Compared with other inorganic and organic semiconductors, these MX chains are characteristic as follows; (1)we can tune the magnitudes of their physical parameters (S, T, U, and V) and/or the energies of band gaps from IR to UV regions; (2)we can control the interchain interactions from one-dimensionally to two-dimensionally using the interchain hydrogen-bonds. Therefore, we can anticipate the interesting new physical properties and electronic states.

IV-O-1 Photogeneration of Solitons and Polalons in MX Chains

Hiroshi OKAMOTO, Yasuo OKA *(Tohoku Univ.)*, **Tadaoki MITANI** *(JAIST)*, **Koshiro TORIUMI** *(Himeji Institute of Tech.)* **and Masahiro YAMASHITA** *(Nagoya Univ. and IMS)*

[*Mol. Cryst. Liq. Cryst.*, **256**, 161(1994)

The photoinduced IR absorption spectra have been measured on single crystals with different dimensionalities of chain structures, $[Pt(en)_2][Pt(en)_2I_2](ClO_4)_4$ and $[Pt(chxn)_2][Pt(chxn)_2Br_2]Br_4$ where the former and the latter have one- and two-dimensional structures, respectively. A decrease of the interchain coupling via the hydrogen-bonds leads to the appearance of a new band which is attributable to photogeneration of solitons. The structures assigned to photogenerated polarons are rather insensitive to the interchain coupling. From the excitation spectra of the photoinduced absorption signals, it has been found that the excitonic effect completely quenches photogeneration of these gap states.

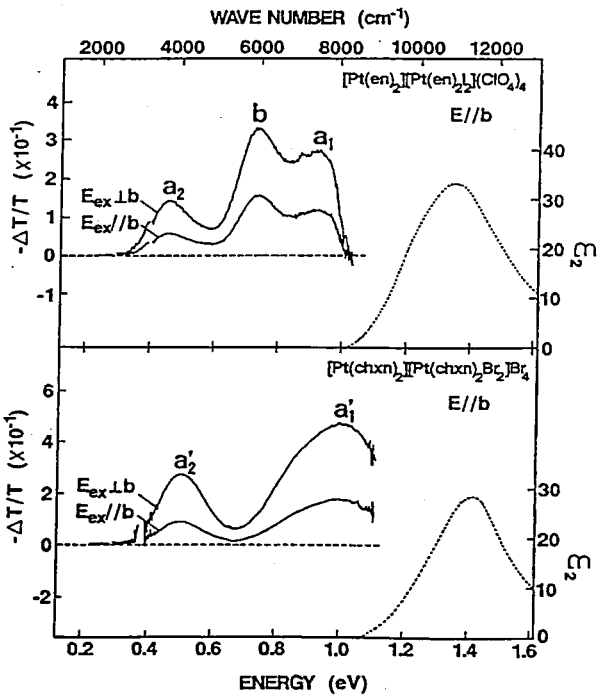

Figure 1. The photoinduced absorption spectra -ΔT/T (solid lines) at 77K, the absorption spectra (dotted lines) at 77K, and the imaginary parts of the dielectric constant ε_2 (broken lines) at room temperature are presented.

IV-O-2 d-π Interaction in MX Chains

Masahiro YAMASHITA *(Nagoya Univ. and IMS)* **and Yoshiki WADA** *(National Institute for Research in Inorganic Materials)*

[*Synth. Met.*, **71**, 1959(1995)]

The effects of the introduction of a π-donor molecule (pyridine) as an in-plane ligand have been investigated on $K_2[Pt(py)X_3][Pt(py)X_5].2H_2O$ by means of the single-crystals polarized reflectance spectra, and polarized excitation spectra of photocurrent and photo-induced absorption. The peak energies of the charge transfer excitons in these complexes are lower than those of compounds with

ligands of σ electrons. This is interpreted by the increase of the electron-electron repulsive energy on the Pt ions induced by the charge transfer from pyridine to Pt ions, which is observed in the electronic spectra polarized perpendicular to the chain axis. The excitation spectra of photocurrent and photo-induced absorption for the light polarized perpendicularly to the chain axis bigins from the energy region near the intervalence CT band, moreover, their efficiencies are higher than those polarized parallel to the chain, indicating that the charge carriers are efficiently generated from the charge transfer state between Pt and pyridine. Such results are in contrast to those of the compounds without π-donor ligands extensively investigated so far.

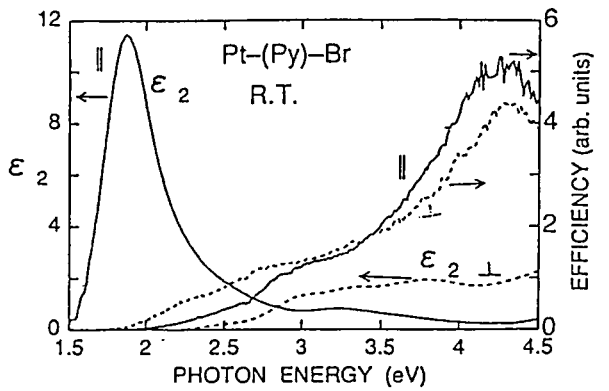

Figure 1. Polarized components of ε_2 and excitation spectra of photocurrent for the polarized excitation light parallel and perpendicular to the chain.

IV-O-3 Electronic Structure of Quasi-One-Dimensional Halogen-Bridged Nickel(III) Complexes: Model Compounds for High-T_c Superconductors ?

Masahiro YAMASHITA *(Nagoya Univ. and IMS)*, **Toshio MANABE** *(Nagoya Univ.)* **and Hiroshi OKAMOTO** *(Tohoku University)*

[*Phys. Rev. Lett.*, submitted]

The $[Ni(chxn)_2X]X_2$ (chxn=cyclohexanediamine: X=Cl and Br) have quasi-one-dimensional halogen-bridged structures where the bridging halogens are located at the midpoints between neighboring Ni atoms, whose oxidation states are +3. Each unpaired electron localized on dz^2 orbitals of each Ni^{3+} atoms are strongly coupled with one another antiferromagnetically. X-ray photoelectron spectra (XPS) and Auger electron spectra (AES) of these compounds have been measured in order to evaluate their electronic structure. The parameter U (on-site Coulomb repulsion energy) is estimated to be ~5 eV and parameter Δ (gap) is estimated to be ~1.5 eV for Cl-bridged compound and ~1.0 eV for the Br-bridged compound. From the results, these compounds are considered to be not Mott-Hubbard type insulators but charge-transfer type insulators. In the polarized single-crystal reflectance spectra with an electric vector parallel to the 1-D axis, the intensive bands are observed. These are attributable to the charge transfer from pz orbitals of the bridging halogens to the upper Hubbard bands composed of unoccupied dz^2 orbitals of Ni^{3+}. Their electronic structures are similar to those of copperoxide superconductors except for the difference of their dimensionality.

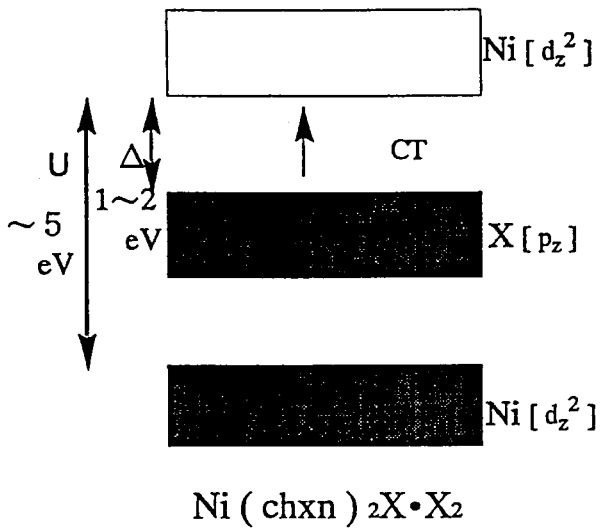

Figure 1. The electronic structure of the Ni^{3+} Compounds

IV-O-4 Electronic Structures and Physical Properties of Quasi-One-Dimensional Halogen-Bridged Binuclear Metal Compounds (MMX Chains)

Masahiro YAMASHITA *(Nagoya Univ. and IMS)*, **Tadaoki MITANI** *(JAIST)* **and Yoshiki WADA** *(National Institure for Researches in Inorganic Materials)*

[*Synth. Met.*, **71**, 1959(1995)]

As a development of MX chains, an MMX type of one-dimensional halogen-bridged binuclear metal compounds, $R_4[Pt_2(pop)_4X].nH_2O$ (R=K and NH_4: X=Cl, Br, and I: N=0, 2 and 3; pop=$P_2O_5H_2^{2-}$) and $M_2(dta)_4I$ (M=Pt and Ni: dta=CH_3CS^{2-}), were synthesized. The new MMX chains have some characteristics compared with the MX chains as follows: (i) the electronic structures of metal ions are strongly coupled with each other in the M-M dimer in the chain, (ii)the difference of the oxidation states of metal ions is smaller, (iii)three structures are possible as depicted in Figure 1. The optical, magnetical, and electronical conductivities of $R_4[Pt_2(pop)4_X].nH_2O$ showed that the compounds form a Peierls-type chain structure (b). On the other hand, the crystal structures of $M_2(dta)_4I$ show that the bridging iodines are located at the midpoints between two M-M dimers in the chains, indicating no Peierls distortion (c). The magnetic behavior of these compounds showed very strong antiferromagnetic coupling between spins localized on the M-M dimers. The Pt compound shows the metal-insulator transition around room temperature, while the Ni compound shows the semiconducting behavior.

(a) $\cdots M^{2+}—M^{2+}\cdots X—M^{3+}—M^{3+}—X\cdots$

(b) $\cdots M^{2+}—M^{3+}—X\cdots M^{2+}—M^{3+}—X\cdots$

(c) $—M^{2.5+}–M^{2.5+}–X–M^{2.5+}–M^{2.5+}–X—$

Figure 1. Electronic structures of the MMX chains

IV-P Low-Dimensional Charge Transfer Metal Complexes Connected with Hydrogen-Bonds

So far low-dimensional charge transfer organic compounds have been extensively investigated to create interesting physical properties such as superconductivity, CDW, SDW, etc.. However only a few charge transfer compounds composed of both donor metal complexes and acceptor metal complexes have been synthesized. Since the electronic states and structures can be tuned more widely by combining metal ions and organic ligands compared with those of inorganic and organic materials, the metal complexes are more promissing to create the interesting physical properties. Moreover, in this system we introduce the hydrogen-bonds between donor metal complexes and acceptor metal complexes. In this strategy, we can anticipated more interesting physical properties by the cooperative interaction between H-bonds and electron transfer.

IV-P-1 Synthesis and Physical Properties of Charge Transfer Metal Complexes Connected with Hydrogen-Bonds, [Pt(H_2dag)(Hdag)][Ni(dmit)$_2$].solvent

Masahiro YAMASHITA *(Nagoya Univ. and IMS)*, **Akimasa ICHIKAWA** *(Nagoya Univ.)*, **Hiroshi MIYAMAE** *(Jyosai Univ.)*, **Hiroshi KITAGAWA** *(JAIST)* **and Tadaoki MITANI** *(JAIST)*

We have synthesized low-dimensional charge transfer metal complex, [Pt(H_2dag)(Hdag)][Ni(dmit)$_2$]. 1/2H_2O.CH_3CN.CH_3OH (H_2dag=diaminoglyoxime ; dmit=1,3-dithiol-2-thione-4,5-dithiolate) by mixing of Pt(Hdag)$_2$.2$H_2$0 and (n-Bu_4N)[Ni(dmit)$_2$] in the methanol and acetonitrile. In the crystal, [Pt(H_2dag)(Hdag)] molecules and [Ni(dmit)$_2$] molecules are dimerized, respectively, and the dimerized molecules are stacked alternatively, forming a linear chain structure. Intermolecular S···S interactions between [Ni(dmit)$_2$] molecules perpendicular to linear chains are observed. Intermolecular hydrogen-bonds between S of dmit and H of dag are also observed. Sigle-crystal electrical conductivity measurement shows semimetallic behavior down to 200K and semiconducting behavior below 200K. Such behavior may be due to the intermolecular hydrogen-bonds.

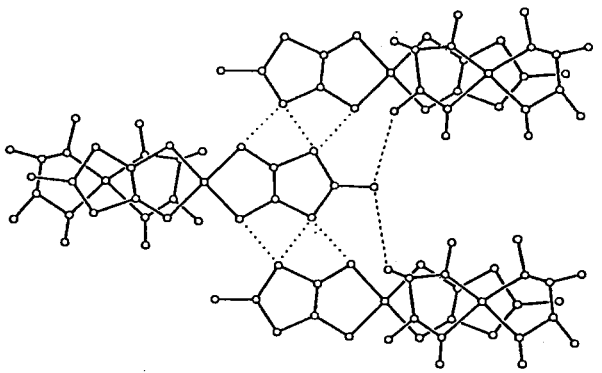

Figure 1. Intermolecular S..S interaction (.....) and hydrogen-bonds (-------)

IV-Q Low-Dimensional Magnetic Systems with S=1/2, 1, 3/2 , 2

Low-dimensional megnetic systems are of current interest because they show peculiar quantum effects. A striking phenomenon is the strong spin-dependent behavior at T=0, of the one-dimensional Heisenberg antiferromagnet (1D-HAF). Haldane predicted that for the integer spin values S the 1D-HAF exhibits a singlet ground states separated from the first triplet excited state by an energy gap Eg (Haldane Gap), while for the half-integer spin values S the 1D-HAF has a gapless spectrum of the excitation. More recently, Guo et al. have theoretically studied the low-dimensional magnetic systems with the integer and half-integer spins. That is, their results indicate the absence of spin-Peierls transitons in systems with integer spins and suggest transitions in systems with half-integer spins. Although there have been many theoretical works on low-dimensional magnetic systems, only a few systematic works on syntheses and magnetic measurements have been carried out so far.

IV-Q-1 New Haldane gap system with S=1: Syntheses, Crystal structures, and Magnetic Properties of Linear-Chain Azido-Bridged Nickel(II) complexes

Masahiro YAMASHITA *(Nagoya Univ. and IMS)*, **Tachi OHISHI** *(Nagoya Univ.)*, **Tetsuya TAKEUCHI** *(Osaka Univ.)*, **Taturu YOSHIDA** *(Nakanihon Automotive College)* **and Koichi KATSUMATA** (RIKEN)

[*Mol. Cryst. Lig. Cryst.*, in press]

We have synthesized new Haldane gap compounds with S=1, [Ni(AA)$_2N_3$]Y (AA=dimethyl-propylenediamine (dmpn), 1,4,8,11-tetraazacyclotetradecane ([14]aneN$_4$), 1,4,8,12-tetraazacyclopentadecane ([15]aneN$_4$), and 5,5,7,12,12,14-hexamethyl-1,4,8,11-tetraazacyclotetradecane (Me$_6$[14]aneN$_4$); Y=ClO_4, BF_4, PF_6). These compounds have linear-chain azido bridged structures where each chain is separated to each other by counterions. We have obtained the values of Haldane gaps of these compounds by measuring temperature-dependent magnetic susceptibilities and high field magnetizations. The magnitudes of Haldane gaps of the N_3^--bridged compounds are larger than those of NO_2^--bridged compounds so far reported. In the same N_3^--bridged compounds, the magnitudes of Haldane gaps as for in-plane ligands are in the order of tn> dmpn> [14]aneN$_4$~ Me$_6$[14]aneN$_4$~ [15]aneN$_4$. From these results, it has been found that the magnitudes of Haldane gap can be controlled by substituting the bridging groups and in-plane

ligands.

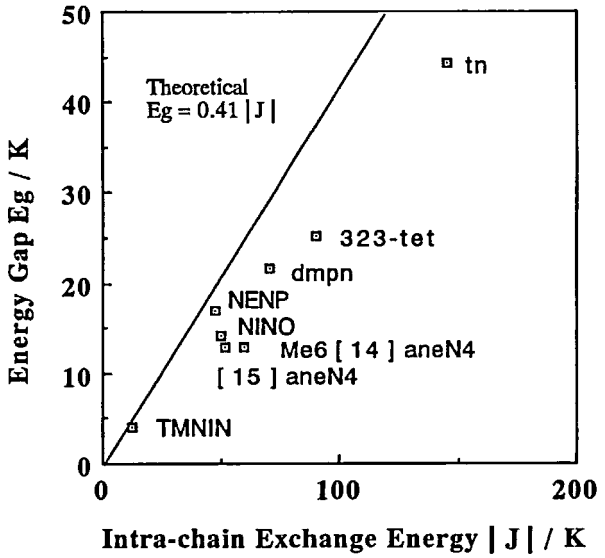

Figure 1. Relationship between energy gaps and intra-chain exchange energies

IV-R Ultraviolet Photoelectron Spectroscopy and X-rayAbsorption Near Edge Structure Spectroscopy of Organic Solids

IV-R-1 Angle-resolved photoemission from oriented thin films of naphthacene:comparison with theoretical spectra

Shinji HASEGAWA, Hiroo INOKUCHI, Kazuhiko SEKI* and Nobuo UENO**(**Nagoya Univ., **Chiba Univ.)*

[*J. Electron Spectrosc. Relat. Phenom.*, in press]

The comparison was made between the measured and calculated take-off angle dependencies of the valence-band photoelectron spectra for the thin films of naphthacene on HOPG graphite. A good agreement was obtained between them (see **Figure 1**), and the molecular orientation in the thin films was estimated. In the present calculation, the single-scattering of the outgoing photoelectrons was taken into account. The calculation of the full valence-band spectra is the first example to the organic thin films.

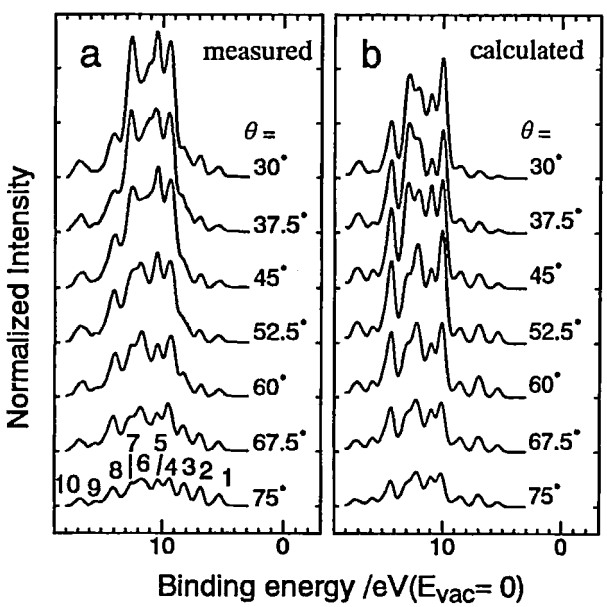

Figure 1. The comparison between the measured and calculated θ dependencies of the valence-band spectra for the naphthacene thin films. **a:** the measured spectra after a background subtraction. **b:** the calculated spectra by considering the single-scattering in the similar orientation to that in the single crystal. The mean free path of the photoelectrons λ_e = 5.0Å was used in the calculation.

IV-R-2 UPS Study of $NiPS_3$ and $FePS_3$ Crystals Using Synchrotron Radiation

Takafumi MIYAZAKI, Hitoshi FUJIMOTO*, Kenji ICHIMURA*, Kwang Pill LEE, Shinji HASEGAWA and Hiroo INOKUCHI** *(*Kumamoto Univ., **Kyungpook National Univ.)*

Ultraviolet photoemission spectroscopy (UPS) has been applied to the investigation of the valence band

structures of nickel and iron trisulfo-phosphates ($NiPS_3$ and $FePS_3$) using synchrotron radiation. The electronic structures of $NiPS_3$ and $FePS_3$ are carefully examined by the combined approach of UPS and constant initial state spectroscopy (CIS), in conjunction with the photon energy dependence of the UPS spectra. The UPS spectra of $NiPS_3$ and $FePS_3$ show several structures, and every feature can be assigned to the metal and P_2S_6 bands through the $h\nu$ dependence of UPS spectra and CIS spectra. The yield spectra of these compounds show three features. One of them is assigned to the metal 3*p* absorption, and other two structures are explained by the atomic subshell photoionization cross sections for the orbitals of P and S atoms. From the UPS and CIS spectral analysis, some remarkable results are obtained as follows: (1)the values of the band gap in $NiPS_3$ and $FePS_3$ are estimated to be 1.6 and 1.0~eV, respectively, (2)the top of the valence bands of $FePS_3$ has some contribution from orbitals of both Fe atoms and P_2S_6 clusters, while that of $NiPS_3$ is assigned to the P_2S_6 cluster state, (3)the UPS spectral structures derived from metal 3*d* orbitals are explained using the multiplet terms split by the crystal field and the final state effect, and (4)there exists the possibility of mixing between orbitals of metal atoms and of P_2S_6 clusters in $FePS_3$ but no such evidence is observed in $NiPS_3$. These results may be used to explain the difference in the electric properties of $NiPS_3$ and $FePS_3$. The orbital mixing between Fe atoms and P_2S_6 clusters makes the *d* states delocalized, and causes the top of the valence band to move upwards toward E_f. This results in a small band gap and the high conductivity.

IV-R-3 Photoelectron Angular Distribution of Thin Films of Copper Phthalocyanine on MoS_2 Surfaces: Quantitative Determination of Molecular Orientation

Koji KAMIYA*, Masahiro MOMOSE*, Yoshiya HARADA*, Nobuo UENO*, Takafumi MIYAZAKI, Shinji HASEGAWA, Hiroo INOKUCHI and Kazuhiko SEKI** *(*Chiba University, **Nagoya University)*

[*Mol. Cryst. Liq. Cryst.*, **267**, 211 (1995)]

The angle-resolved ultraviolet photoelectron spectra (ARUPS) of ultrathin films of copper phthalocyanine film on the MoS_2 substrate were measured using synchrotron radiation. We analyzed azimuthal angle (ϕ) dependence of the photoelectron intensity using IAC/MNDO calculation, and determined the relation between the direction of the molecular orientation in CuPc ultrathin films and the crystal axes at the surface of MoS_2 substrate.

IV-R-4 Ultraviolet Photoelectron Spectroscopy of Poly(pyridine-2,5-diyl), Poly(2,2'-bipyridine-5,5'-diyl), and their K-doped States

Takayuki MIYAMAE, Daisuke YOSHIMURA*, Hisao ISHII*, Yukio OUCHI*, Kazuhiko SEKI*, Takafumi MIYAZAKI, Tsuneaki KOIKE and Takakazu YAMAMOTO***** *(*Nagoya Univ., **Mitsui Petrochemical Industries, LTD., ***Tokyo Institute of Technology)*

[*J. Chem. Phys.* in press]

Ultraviolet photoelectron spectra were measured using synchrotron radiation for two kinds of p-conjugated polymers, poly(pyridine-2,5-diyl) (PPy) and poly(2,2'-bipyridine-5,5'-diyl) (PBPy) which exhibit n-type electrically conducting properties. The two compounds show similar spectra and they were analyzed with MO calculations and the comparison with the data of related molecules. The ionization threshold energies of PPy and PBPy were found to be 6.3 and 6.35 eV, respectively. These values are higher than those of π-conjugated conducting polymers capable of p-doping. Upon potassium doping of PBPy, two new states appeared in the originally empty energy gap and the intensity of the state at 0.65 eV from E_F grows as the doping proceeds. This finding and the change of optical absorption spectra upon doping indicate that bipolaron bands are formed in K-doped PBPy. While K-doped PPy also shows similar gap states, it requires higher dopant concentration to create bipolaron bands than in the case of K-doped PBPy. The difference of the dependence on dopant concentration between K-doped PPy and K-doped PBPy is discussed based on the conformational difference between these polymers.

IV-R-5 Ultraviolet Photoelectron Spectroscopy of Alkaline-metal Doped Polyacetylene

Takayuki MIYAMAE, Koji KAMIYA*, Shinji HASEGAWA, Kazuhiko SEKI, Chizuko TANAKA*** and Jiro TANAKA***** *(*Chiba Univ., **Nagoya Univ., ***Kanagawa Univ.)*

[*Bull. Chem. Soc. Jpn.*, **68**, 1897 (1995)]

Sodium- and potassium-doped highly conducting polyacetylenes were studied by ultraviolet photoelectron spectroscopy (UPS) using synchrotron radiation. Upon doping, the UPS spectra immediately show a large shift toward the higher binding energy side relative to E_F. At intermediate doping level, a new state is created in the empty energy gap region. The gap state in the UPS spectra is assigned to the charged soliton band. This is the first direct observation of emission from the charged soliton state in doped polyacetylene. At heavily doped level, quasi-metallic density of states are found just below the Fermi level and the broadening of the UPS spectra occurs at the regions of C 2p and C 2s levels. However, no finite density of states were observed at the Fermi level in the case of unoriented polyacetylene. This result is incontrast to the case of oriented polyacetylene doped with perchlorate, where the existence of a finite density of states at E_F is reported. The spectral shape of UPS near the Fermi level is accordance with Tomonaga-Luttinger liquid model of strong electron correlated system. Ab initio molecular orbital calculations taking account of nearest-neighbor chain effect gives a good description of the UPS for all the C 2s, C 2pπ, and C 2pσ bands.

IV-R-6 UV Photoemission Study of Amorphous n-$C_{36}H_{74}$ Films and Their Annealing Process

Kazuhiko SEKI*, Nobuo UENO and Hiroo INOKUCHI** *(*Nagoya Univ., **Chiba Univ.)*

[*Chem. Phys.* **182**, 353 (1994)]

Amorphous films of hexatriacontane n-$C_{36}H_{74}$ were prepared by vacuum evaporation on low-temperature substrates (*ca.* 80 K), and their electronic structure including the change at annealing was studied by UV photoemission spectroscopy. The spectra of as deposited films (Figure 1(a)) were similar to those of molten state of n-$C_{44}H_{90}$ (Figure 1(c)), but indicate a smaller degree of disorder. Upon annealing, the spectra changed drastically, reflecting the change of unoccupied states, with a sharp change at *ca.* 268 K corresponding to crystallization. The resultant spectra agree well with the spectra (Figure 1(b)) of crystalline n-$C_{36}H_{74}$ film prepared by evaporation onto room temperature substrate. The change was discussed with reference to structural studies by vibrational spectroscopies. The results show that the appearance of fine structures in unoccupied states requires not only extended (all-*trans*) chains but also regular intermolecular arrangements.

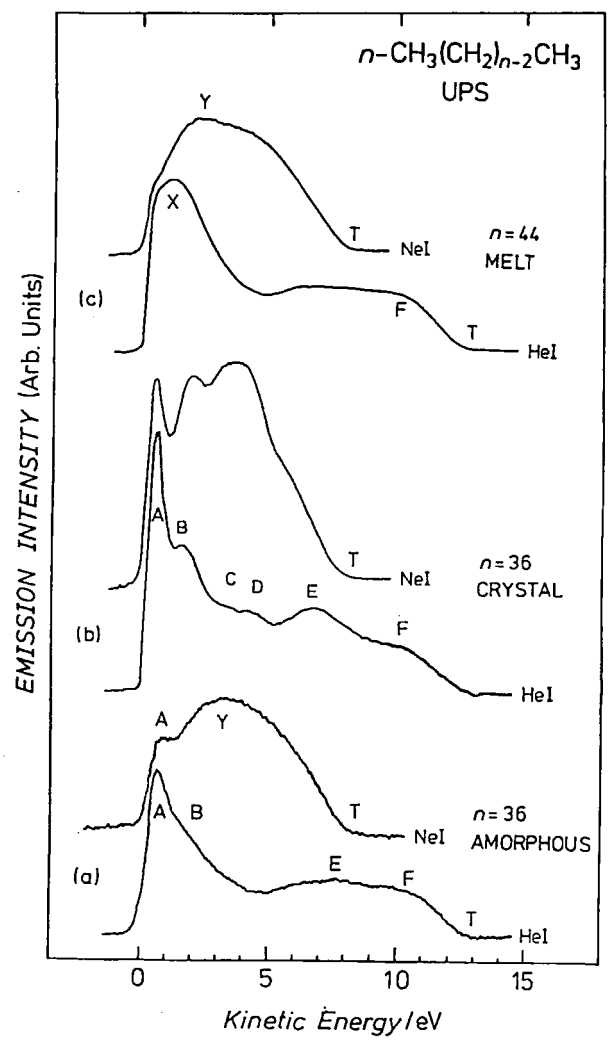

Figure 1. HeI and NeI photoelectron spectra of alkanes in (a) amorphous solid of n-$C_{36}H_{74}$, (b) crystalline solid of n-$C_{36}H_{74}$, and (c) molten (liquid) state of n-$C_{44}H_{90}$.

IV-R-7 Ultraviolet Photoelectron Spectra of C_{78} and C_{96}

Shojun HINO*, Hiroaki TAKAHASHI* Kentaro IWASAKI*, Takafumi MIYAZAKI, Ko-ichi KIKUCHI and Yohji ACHIBA**** *(*Chiba University, **Tokyo Metropolitan University)*

[*Chem. Phys. Letts.* **230** (1994) 165-170.]

Ultraviolet photoelectron spectra of higher fullerenes C_{78} and C_{96} are measured with a synchrotron radiation light source. The spectral intensity oscillates and the peak positions shift, when the incident photon energy is changes. The $h\nu$ = 20 eV spectrum of C_{78} resembles that of C_{76}, which suggests their analogous electronic structures. Comparison of the results with theoretical calculations is in favor of a C_{2v}' geometry for the main isomer and C_1 geometry for C_{96}. Upon potassium dosing onto C_{96}, a new peak emerges just above the first (HOMO) band of C_{96}. The spectra are deformed at high dosage.

IV-R-8 Molecular Orientation and Electronic Structure of Evaporated Porphyrin Films

Satoru NARIOKA,* Masaki SEI,* Hisao ISHII,* Shinji HASEGAWA, Yukio OUCHI,* Toshiaki OHTA and Kazuhiko SEKI*** *(*Nagoya Univ., **Univ. of Tokyo)*

[*Trans. Mat. Res. Soc. Jpn.*, **15A**, 631 (1994)]

The molecular orientation in evaporated 5,1015,20-zinctetraphenylporphyrin (ZnTPP) and 5,10,15,20-tetraphenylporphyrin (H_2TPP) films was studied by X-ray-Absorption Near Edge Structure (XANES) spectroscopy. For ZnTPP, the film deposited on Ag/Cu substrate at 367 K had highly oriented structure with the central molecular plane inclining at 25° ± 10° relative to the substrate surface. While ZnTPP film evaporated on the substrate at room temperature and H_2TPP films showed little indication of regular orientation. Electronic structures of ZnTPP, H2TPP and porphine were studied by ultraviolet photoelectron spectroscopy. Reliable spectrum of sold porphine was obtained. The spectra of ZnTPP and H_2TPP can be explained as the superposition of those of porphine and its substituents.

IV-S Electrical Conductions and its Related Properties of Organic Solids

IV-S-1 New Low-Dimensional Organic Metals of $(BEDT\text{-}ATD)_2X(THF)$ (X=PF_6, AsF_6), Stable at Low Temperature

Kenichi IMAEDA, Yoshiro YAMASHITA, Shoji TANAKA and Hiroo INOKUCHI

[*Synth. Met.* **73**, 107 (1995)]

The cation radical salts with a new electron donor 4,11-bis(4',5'-ethylenedithio-1',3'-dithiol-2'-ylidene)-4,11-dihydroanthre [2,3-c][1,2,5]thiadiazole (BEDT-ATD)

have been prepared by an electrochemical oxidation in a tetrahydrofuran (THF). The salts with $PF6^-$ and AsF_6^- anions were obtained as $(BEDT\text{-}ATD)_2X(THF)$ (X=PF_6, AsF_6). The electrical resistivity at room temperature was 0.04 Ωcm and 0.02 Ωcm for the PF_6 salt and the AsF_6 salt, respectively. Both salts showed a metal-like behavior in the electrical conduction. Figure 1 shows the temperature dependent-spin susceptibility of the PF_6 salt. It revealed a Pauli paramagnetism down to 3 K, indicating a metallic state. A semiconducting phase appeared by applying pressure above 2.5 kbar.

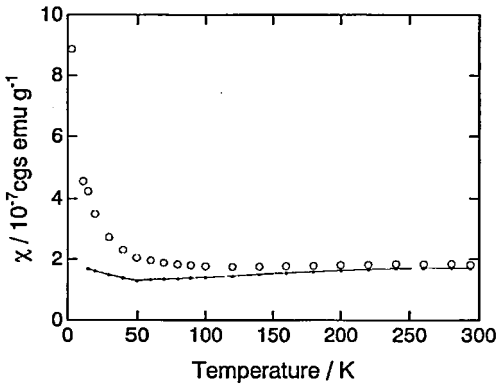

Figure 1. Temperature dependence of the spin susceptibility of $(BEDT\text{-}ATD)_2PF_6(THF)$. The solid line denotes the spin susceptibility obtained by the Curie-component subtraction.

IV-S-2 Preparation and Properties of Lithium-Doped C_{60} by Lithium Azide

Kenichi IMAEDA, Kyuya YAKUSHI and Hiroo INOKUCHI

[*Fullerene Sci. Technol.* in press]

Lithium-doped C_{60} was prepared by the thermal decomposition of lithium azide (LiN_3). The samples of the nominal composition Li_4C_{60} and Li_8C_{60} showed a Curie-like behavior of ESR intensity, indicating an insulating state. Inevitably, they were not superconducting (SC) without a low-field signal (LFS).Table 1 summarizes the SC properties of alkali metal-doped C_{60} prepared by use of alkali metal azides MN_3 (M=Li, Na, K, Rb and Cs). Only NaN_3 among alkali metal azides gave nitrogen-alkali metal-C_{60} ternary compound. The SC transition temperature (T_c) of 20 K and 30 K in K_3C_{60} and Rb_3C_{60} prepared by KN_3 and RbN_3 is almost the same as 18 K of K_3C_{60} and 28 K of Rb_3C_{60} prepared by a metal-vapor doping. It seems that K_3C_{60} and Rb_3C_{60} prepared by azides do not include any nitrogen. We consider the following two reasons: (1) There will be not enough space for accepting nitrogen molecule at a vacancy of the octahedral site, due to the large ionic radii of K^+, Rb^+ and Cs^+. (2) The decomposition temperature (T_d) of MN_3 (M=K, Rb and Cs) is so high that N_2 will escape from the C_{60} lattice. On the contrary, T_d of LiN_3 is so low that lithium is not doped to C_{60} at the moment of the decomposition. This means no possibility of an intercalation of N_2. We can conclude that the SC $Na_xN_yC_{60}$ phase has appeared under peculiar circumstances that NaN_3 has T_d suitable for Na doping and simultaneous intercalation of N_2.

Table 1. T_d of alkali matal azides and the detected SC phase and T_c alkali matal - doped C_{60} prepared by the thermal decomposition of alkali matal azides

MN_3	T_d (°C)	SC phase	T_c (K)
LiN_3	180-230	-----	-----
NaN_3	340-370	$Na_xN_yC_{60}$	12-15
KN_3	480	K_3C_{60}	20
RbN_3	510	Rb_3C_{60}	30
CsN_3	520	-----	-----

IV-S-3 X-ray Photoelectron Spectroscopy Characteristics of a Novel Organic Semiconductor BTQBT amd Its Derivatives

Shuqin ZHOU, Kenji ICHIMURA* and Hiroo INOKUCHI *(* Kumamoto Univ.)*

[*J. Mater. Chem.* **5** (1995) in press]

X-ray photoelectron spectra of bis[1,2,5]thiadiazole-p-quinobis(1,3-dithiole)(BTQBT) reveal that the sulfur and carbon atoms in the molecules show four- and two-peak profiles, respectively, and are in mixed-valence states. Substitution of the sulfur atoms linked to nitrogen atoms by selenium atoms removes the mixed valency of sulfur. In systems with asymmetrical molecular skeltons, such as TMBTQBT, TMTBTQBT and DBBTQBT, sulfur and carbon atoms are also in mixed-valence states. TMBTQBT shows tha largest energy difference between the C 1s and S 2p peaks, indicating the largest charge distribution. Each of the S 2p and C 1s peaks is accompanied by shake-up satellites located to higher energy at ca. 2.7 eV from the corresponding photoelectron main peak.

IV-S-4 Electronic Structure of the Quasi One-Dimensional Organic Conductors DCNQI (N, Ndicyanoquinonediimine)-Cu Salts

Akinori TANAKA*, Ashish CHAINANI*, Takayoshi YOKOYA, Takashi TAKAHASHI*, Takafumi MIYAZAKI, Shinji HASEGAWA and Takehiko MORI** *(*Tohoku Univ., **Tokyo Institute of Technology)*

[*Solid State Commun.* **93**, 1 (1995) and *Phys. Rev.* B, in press]

A comparative study of the electronic structure of *in-situ* synthesized quasi one-dimensional organic conductor $(DMe\text{-}DCNQI)_2Cu$ and $(MeBr\text{-}DCNQI)_2Cu$ has been carried out using various techniques of electron spectroscopy, where DMe-DCNQI and MeBr-DCNQI are 2,5-dimethyl-*N,N'*-dicyanoquinonediimine a nd 2,5-methyl, bromine-*N,N'*-dicyanoquinonediimine, respectively. From the photon energy dependence of the valence band photoemission spectra obtained using synchrotron radiation, the origins of each observed feature are unambiguously characterized. While the feature at the Fermi level is primarily derived from π-bonded C and N 2*p* states, the contribution of Cu 3*d* states at the Fermi level is larger in the $(MeBr\text{-}DCNQI)_2Cu$ compound to the $(DMe\text{-}DCNQI)_2Cu$. X-ray photoemission spectrum of the valence band implies extensive hybridization of the Cu 3*d* states with C and N 2*p* states near the Fermi level. Line

shape analysis of the Cu 2*p* core level spectra show that the ratio of Cu^{2+} to Cu^{1+} is higher in (MeBr-DCNQI)$_2$Cu compound to (DMe-DCNQI)$_2$Cu, with the ratio being closer to 1:2 for (MeBr-DCNQI)$_2$Cu. From a comparison of C *KVV* and Cu *LVV* Auger spectra with the self-convolution of the valence band spectra, it is found that the effective on-site Coulomb correlation energies between the valence electrons are high on C sites as well as Cu sites in both salts, with *U(pp)*=6.5 eV and *U(dd)*=8.0 eV, respectively. In conjunction with core level spectra, the spectra indicate that the on-site Coulomb correlation, the hybridization strength and the charge-transfer energy between the Cu 3*d* and N 2*p* ligands are very similar in the two salts. The metal-insulator transition in (MeBr-DCNQI)$_2$Cu at 160K is then facilitated by the proximity of the Cu^{2+} to Cu^{1+} ratio to 1:2, supporting charge disproportion, while deviation from it stabilizes the metallic phase in (DMe-DCNQI)$_2$Cu down to very low temperatures.

IV-S-5 Thermal Expansion of Tetrakis (alkylthio) tetrathiafulvalenes

Zurong SHI , Kenichi IMAEDA, Chikako NAKANO, Toshiaki ENOKI*, Gunzi SAITO and Hiroo INOKUCHI** *(*Tokyo Institute of Technology, **Kyoto University)*

[*Mol. Cryst. Liq. Cryst.* **268**, 161 (1995)]

The thermal expansion of tetrakis (alkylthio) tetrathiafulvalenes (abbreviated to TTC_n-TTFs (n=l*11)) having alkyl chains with n carbon atoms has been investigated from room temperature down to about 100 K by means of the four-circle X-ray diffraction technique. A linear thermal expansion parameter dl(=Dl/DT) is suggested for correlating intermolecular interaction of TTC_n-TTF crystals. For the compounds with larger n, n*8, the linear thermal expansion along the c-axis, dc, is smallest, while db is largest and da intermediate. This is consistent with the intermolecular interaction analyses for the crystal structure of TTC_n-TTF compounds. The molecular fastener effect is also found in the thermal expansion measurements. The contributions of the molecular fastener effect and the packing effect of the end C-atoms in the alkyl chains of TTC_n-TTF (n=8-11) to the thermal expansion are discussed.

RESEARCH ACTIVITIES V
Department of Applied Molecular Science

V-A Highly Oxidized Iron Porphyrin Complexes

As models for monooxygenases and peroxidases such as cytochromes P-450, horseradish peroxidase (HR.) and cytochrome c peroxidase (CcP), a series of reactive iron porphyrin complexes, which are capable to oxidize olefins and many other organic compounds, have been prepared and characterized. These studies are quite important to understand biological strategy to activate molecular oxygen and its two electron reduced form.

V-A-1 Acylperoxo-Iron(III) Porphyrin Complexes: A New Entry of Potent Oxidants for the Alkene Epoxidation

Kenji MACHII *(Kyoto Univ.)*, **Yoshihito WATANABE and Isao MORISHIMA** *(Kyoto Univ. and IMS)*

[*J. Am. Chem. Soc.* **117**, 6691 (1995)]

Competitive epoxidation of norbornylene and α-methylstyrene by peracids in the presence of iron porphyrins has been carried out in methylene chloride and toluene at -78°C. When (TMP)$Fe^{III}(RCO_2)$ (TMP = 5,10,15,20-tetramesitylporphyrin) is used as a catalyst *in methylene chloride,* selectivity of norbornylene oxide over α-methylstyrene oxide is almost identical even though a variety of peracids are used, since O=Fe^{IV}TMP π-cation radical **2a** is the common oxidant in the reactions. On the other hand, the selectivity in the epoxidations catalyzed by (TDCPP)Fe^{III}(X) (TDCPP: 5,10,15,20-tetrakis(2,6-dichlorophenyl)porphyrin) is found to be dependent on the structure of peracids. The latter type of the results is also obtained for the reactions catalyzed both by (TMP)Fe^{III}(X) and by (TDCPP)Fe^{III}(X) *in toluene.* The dependence of the selectivity in the epoxidation on the structure of peracids is attributed to the alteration of the oxidant from **2** to peracid-Fe(III) complexes **1.** The direct involvement of **1** in the epoxidation has been further confirmed by spectroscopic studies of the reactions. Under the catalytic epoxidation conditions at low temperature, the participation of **1** and **2** as the active species is controlled either by electronic structure of iron porphyrin complexes (push pull effect) or by alteration of the solvent.

V-A-2 High Valent Fe Porphyrin Complexes. O=Fe^{IV} Porphyrin π-Cation Radical vs. O=Fe^{V} Porphyrins

Tatsuya MURAKAMI *(Kyoto Univ.)*, **Yoshihito WATANABE and Isao MORISHIMA** *(Kyoto Univ. and IMS)*

Oxoiron(V) porphyrin complexes (**2**), which had been only prepared under acidic conditions, were successfully synthesized under neutral condition by using pentafluoroiodosylbenzene (F_5PhIO). The UV-vis spectrum of **3a,** the oxidized product of FeTDCPP [TDCPP: 5,10,15,20-tetrakis(2,6-dichlorophenyl)porphyrin] by PFIB, showed the λ_{max} at 418 and 532 nm, similar to those of oxoiron(IV) porphyrin complexes (λ_{max} 419 and 543 nm). According to the titration of **3a** by iodide ion, however, **3a** was found to be in a higher oxidation state than the ferric state by 2-oxidizing equivalents. ^{2}H-NMR spectrum of **3a** showed deuterium resonances at -22.9 ppm for β-pyrrole D and 8.8 ppm for phenyl *meta*-D, ruling out the formulation of **3a** as a π-cation radical complex. These results indicate 3a being oxoiron(V) porphyrin complex. Furthermore, we have shown that the electronic structure of the active species, O=Fe^{IV}porphyrin π-cation radical (**1**) vs. O=Fe^{V}porphyrin (**2**), are controlled by the alteration of the π energy level of the porphyrin ring. In the case of FeTCMPP [TCMPP: 5,10,15,20-tetrakis(2-chloro-6-methylphenyl)-porphyrin], a mixture of **1** and **2** was obtained since the HOMO of the porphyrin ring is close to that of O=Fe.

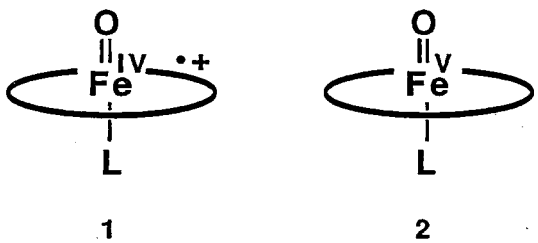

1 **2**

V-A-3 Preparation and Characterization of Oxoiron(IV) Chlorin Complexes as the First Models for a Reaction Intermediate in the Catalytic Cycle of Cytochrome *d*

Shinji OZAWA *(Kyoto Univ.)*, **Yoshihito WATANABE, Satoru NAKASHIMA, Teizo KITAGAWA and Isao MORISHIMA** *(Kyoto Univ. and IMS)*

[*J. Am. Chem. Soc.* **116**, 634 (1994)]

As models for a reaction intermediate in the catalytic cycle of cytochrome *d,* two types of oxoferryl chlorin complexes, (TPC)Fe^{IV}O(*N*-MeIm) and (TPC)Fe^{IV}O (TPC = tetraphenylchlorin, *N*-MeIm = *N*-methylimidazole), have been prepared for the first time by an autoxidation reaction of (TPC)Fe^{II} with O_2. Oxyiron(II)(TPC) and μ-peroxo-bridged iron(III) dimmer, (TPC)Fe^{III}OOFe^{III}(TPC), are also detected in the course of the reaction. The six-coordinated (TPC)Fe^{IV}O(*N*-MeIm) complex is produced by adding *N*-methylimidazole to the μ-peroxo-bridged iron(III) chlorin dimmer at -80 °C. The μ-peroxo-bridged iron(III) dimmer, the formation of which has been confirmed by paramagnetic NMR, undergoes homolytic cleavage of the O-O bond upon laser illumination to yield the five-coordinated (TPC)Fe^{IV}O complex. The absorption spectrum of (TPC)Fe^{IV}O(*N*-MeIm) shows a characteristic red-shifted band at 630 nm as observed in the case

of the oxoferryl intermediate of cytochrome *d*. Proton NMR spectra of (TPC)$Fe^{IV}O$(*N*-MeIm) exhibit a small hyperfine shift of the pyrrole protons, consistent with the oxoferryl formulation. However, the paramagnetic NMR resonances of the saturated pyrrole (pyrroline) ring protons show unusual splitting into upfield and downfield region, suggesting deformation of the pyrroline ring of the chlorin complex. While the unusually high frequency of $\nu(Fe^{IV}=O)$ (815 cm^{-1}) and large isotopic shift ($\Delta\nu$ = 46 cm^{-1}) observed for the oxoferryl intermediate of cytochrome *d* have been attributed to the chlorin macrocycle (heme *d*), the five- and six-coordinated oxoferryl chlorin complexes reported here exhibit $\nu(Fe^{IV}=O)$ frequencies and isotopic ($^{16}O/^{18}O$) frequency shifts nearly identical to those of the corresponding porphyrin complexes, respectively.

V-A-4 Resonance Raman Characterization of Iron(III) Porphyrin *N*-Oxide: Evidence for an Fe-O-N Bridged Structure

Yasuhisa MIZUTANI *(Grad. Univ. Adv. Studies)*, **Yoshihito WATANABE and Teizo KITAGAWA**

[*J. Am. Chem. Soc.* **116**, 3439 (1994)]

Resonance Raman (RR) spectra are reported for iron(III) tetramesityl porphyrin (TMP) *N*-oxide and its ^{18}O and ^{15}N derivatives. The RR bands assignable to the Fe-O stretching, O-N stretching and Fe-O-N bending vibrations were observed at 506, 1123 and 743 and 708 cm^{-1}, respectively. This confirms that the complex has the Fe-O-N bridged structure. The RR bands of the macrocycle such as the $C_\beta C_\beta$ and $C_\alpha N$ stretching modes were split into doublets due to lowering of symmetry. The RR band arising from the C_m-phenyl stretching band exhibited a downshift by 4 cm^{-1} upon formation of the *N*-oxide, suggesting considerable distortion of the macrocyle.

V-B Model Studies on Nitrite Reductase

In spite of intensive spectroscopic and kinetic studies, several major problems are still unsolved in *cd*1-type nitrite reductases. For instance, the mechanism of the reaction with nitrite and the nature of the reaction product (NO or N_2O or both) are still obscure. Further, relevance of the utilization of the dioxoisobacteriochlorin macrocycle on the enzymic reaction has been unclear at all. Thus, model complexes for the reaction intermediate have been studied.

V-B-1 Model Studies of Nitrosyl Intermediates in the Catalytic Cycle of Dissimilatory Nitrite Reductases

Shinji OZAWA*, Eigo SAKAMOTO*, Taroh ICHIKAWA*, Yoshihito WATANABE and Isao MORISHIMA* *(*Kyoto Univ.)*

[*Inorg. Chem.* **34**, 6362 (1995)]

As models for a reaction intermediate in the catalytic cycle of dissimilatory nitrite reductases, we have examined one-electron oxidation of nitrosyl-iron(II) complexes of octaethylporphyrin (OEP, **1a**), oxo-octaethylchlorin (oxo-OEC, **1b**) and dioxo-octaethylisobacteriochlorin (dioxo-OEiBC, **1c**). While (OEP)Fe^{III}(NO) **2a** is obtained in the oxidation of **1a**, the oxidation products of **1b** and **1c** afford absorption spectra characteristic of chlorin and isobacteriochlorin π-cation radicals. The formation of the π-cation radical complexes (**2b** and **2c**) is confirmed by a variety of methods including electronic absorption, ESR, NMR and IR spectroscopies. Presence of NO in **2b** and **2c** as the 5th ligands is evidenced by the observation of ν_{15NO} bands at 1686 and 1700 cm^{-1}, respectively. These results are rationalized by the stabilization of the iron d orbital levels in **2b** and **2c**. Sixth ligand effect on the electronic structures of the oxidation products (**2a-c**) have also been investigated. Ligation of *N*-methylimidazole (*N*-MeIm) to **2b** and **2c** causes valence isomerization to give $Fe^{II}(NO^+)$(*N*-MeIm) complexes (**3b** and **3c**) as well as (OEP)$Fe^{II}(NO^+)$(*N*-MeIm) **3a**. Although the six-coordinated imidazole adducts (**3a-c**) are formulated as $Fe^{II}(NO^+)$(*N*-MeIm), the oxo derivatives (**3b** and **3c**) readily release the NO ligand in the presence of an additional one equiv mole of *N*-MeIm, **3a** is relatively stable under the same condition.

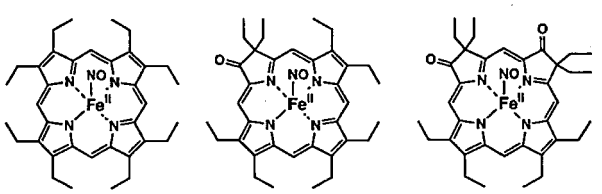

1a **1b** **1c**

V-C Alteration of Biological Functions of Heme Enzymes by Site-Directed Mutagenesis

In order to understand roles of amino acid residues around heme vicinity and design artificial heme enzymes, we have prepared a series of heme enzymes in which several amino acid residues in peroxidases and myoglobin are replaced by site-directed mutagenesis.

V-C-1 Putative Hydrogen Bond Network in Distal Site of Horseradish Peroxidase

Shingo NAGANO*, Motomasa TANAKA*, Yoshihito WATANABE and Isao MORISHIMA* *(*Kyoto Univ.)*

[*Biochem. Biophys. Res. Commun.* **207**, 417 (1995)]

The $N_{\delta1}$ atom of the distal His of several peroxidases are known to make a hydrogen bond with the side chain

oxygen of Asn. Thus, a mutant horseradish peroxidase, in which Asn70 is replaced by Val, has been expressed in *Escherichia coli* to disrupt the putative hydrogen bond. Substitution of Asn70 to Val reduces the rate constant for the compound I formation from 1.6 x 10^7 $M^{-1}s^{-1}$ (native) to 6 x 10^5 $M^{-1}s^{-1}$. The rate constant for reduction of compound I of N70V by guaiacol has been also reduced to 1.2 x 10^5 $M^{-1}s^{-1}$. While compound I of N70V is stable and reduced to the resting state of the mutant without apparent formation of compound II at neutral pH, compound II of N70V is obtained as a stable intermediate at alkaline pH. Similar alteration of the reactivity has been observed in the reaction with guaiacol.

V-C-2 Rolls of Amino Acid Residues in Heme Vicinity on the Oxygen Activation

Toshitaka MATSUI *(*Grad. Univ. Adv. Studies)*, **Shingo NAGANO** *(Kyoto Univ.)*, **Koichiro ISHIMORI** *(Kyoto Univ.)*, **Yoshihito WATANABE and Isao MORISHIMA** *(Kyoto Univ. and IMS)*

[*Biochemistry* in submission]

We have reported that H93C human myoglobin (Mb), in which proximal His (His93, F8) was replaced to Cys, gave nearly identical spectroscopic features with P450 and its oxygenase activities were increased as compared with wild-type Mb.[1] However, it was suggested that H93C Mb catalyzed styrene epoxidation not through P450-type ferryl oxygen transfer due to its small distal cavity. To provide a substrate binding pocket in the active site, distal His (His64, E7) of H93C Mb is replaced by site-directed mutagenesis to Gly (H64G/H93C Mb) and Val (H64V/H93C Mb). Various spectroscopic studies on these double-mutated Mbs reveal Cys ligation to ferric heme as a thiolate form. Anionic nature of proximal Cys in the mutants exclusively facilitates heterolytic O-O bond cleavage and the oxidation products by ferryl oxygen transfer are increased in H64V/H93C and H64G/H93C Mbs. On the other hand, oxygenation activities of H64G/H93C and H64V/H93C Mbs are decreased when H_2O_2 is employed as the oxidant and these low activities are due to large K_m values for H_2O_2 in these mutants.

Reference

1) S. Adachi, S. Nagano, K. Ishimori, Y. Watanabe, I. Morishima, T. Egawa, T. Kitagawa and R. Makino, *Biochemistry* **32**, 241 (1993).

V-D Transition Metal Sulfide Clusters

M-S bond functionality in high nuclearity compounds plays an important role in redox reactions as seen in biological and industry processes due to its covalency in bonding. We have continued to develop the methodology for the rational synthesis of sulfide clusters by using WS_4^{2-} and RhCp* as key groups. We are also using fast atom bombardment mass spectrometry (FAB-MS) which gives important information on higher-nuclearity clusters that might be synthesized.

V-D-1 A Unique Three-Step Cyclic Reaction Sequence of Heterotrimetallic Sulfide Clusters. Structures and Properties of [{Cp*RhP(OEt)$_3$(μ-WS$_4$)(CuCl)Cu}$_2$(μ-Cl)$_2$] (Cp* = η^5-C$_5$Me$_5$) with a Branched Structure and [{Cp*RhP(OEt)$_3$(μ-WOS$_3$)(CuCl)Cu}$_2$(μ-Cl)$_2$] with a Linked Incomplete Cubane-Type Structure

Seiji OGO *(Grad. Univ. for Adv. Studies and IMS)*, **Takayoshi SUZUKI and Kiyoshi ISOBE** *(Osaka City Univ.)*

[*Inorg. Chem.* **34**, 1304 (1995)]

The trinuclear cluster, [Cp*RhP(OEt)$_3$(μ-WS$_4$)CuCl] (**1**), shows a unique three-step recycle reaction with significant structural changes involving a regiospecific CuCl-addition of **1** to form [{Cp*RhP(OEt)$_3$(μ-WS$_4$)(CuCl)Cu}$_2$(μ-Cl)$_2$] (**2**), substitution of one bridging S atom in the WS_4 group in **2** for an O atom of H_2O to convert to [{Cp*RhP(OEt)$_3$(μ-WOS$_3$)(CuCl)Cu}$_2$(μ-Cl)$_2$] (**3**) and recovery of **1** from **3** based on a specific reactivity of the CuCl group(s) in **1** and **3** towards excess H_2S. The structures of **2** and **3** were determined by a single crystal X-ray diffraction method. Cluster **2** has an octanuclear structure in the crystal. The Rh···W···Cu1 is almost linear (172.43°) and the Rh···W···Cu2 is an approximately right angle (90.73°) and hence the eight metals are arranged in a branched configuration. Crystal data for **2**: *FW* = 1828.81; monoclinic, space group *P*21/*n* (No. 14), *a* = 10.170(3), *b* = 14.495(3), *c* = 19.411(3) Å, β = 104.42(1)°, *V* = 2771.5(8) Å^3, *Dc* = 2.19 g cm^{-3}, *Z* = 2, μ(Mo Kα) = 67.5 cm^{-1} and *R*(*Rw*) = 0.043(0.043) for 5504 independent unique reflections ($|Fo| > 3\sigma(|Fo|)$). Cluster **3** has a linked incomplete cubane-type octanuclear structure. The replacement of one bridging S atom in **2** with an O atom causes a significant alteration in the cluster framework. Crystal data for **3**·2DMF: *FW* = 1942.86; monoclinic, space group *P*21/*c* (No. 14), *a* = 10.011(3), *b* = 17.115(3), *c* = 18.678(3) Å, β = 95.10(2)°, *V* = 3188(1) Å$_3$, *Dc* = 2.02 g cm^{-3}, *Z* = 2, μ(Mo Kα) = 58.5 cm^{-1} and *R*(*Rw*) = 0.047(0.051) for 5670 independent unique reflections ($|Fo| > 3\sigma(|Fo|)$). In dichloromethane **2** and **3** exist as a tetranuclear complex as a result of a chloride-bridge cleavage.

V-D-2 Synthesis and Property of Pentanuclear (Cu^{I}-Rh$^{III}_2$-W$^{VI}_2$) Heterometallic Sulfide Cluster Ion Predicted by Fast Atom Bombardment Mass Spectrometry

Seiji OGO *(Grad. Univ. for Adv. Studies and IMS)*, **Takayoshi SUZUKI, Sachiyo NOMURA, Kiyotaka ASAKURA** *(Univ. of Tokyo)* **and Kiyoshi ISOBE** *(Osaka City Univ.)*

[*J. Cluster Sci.* **6**, 421 (1995)]

The positive ion FAB mass spectrum of a linear

trinuclear sulfide cluster, $[RhCp^*P(OEt)_3(\mu\text{-}WS_4)CuCl]$ ($Cp^* = \eta^5\text{-}C_5Me_5$), shows many ions heavier than the molecular ion. One of the envelopes corresponds to a pentanuclear cationic cluster of $[\{RhCp^*P(OEt)_3(WS_4)\}_2Cu]^+$. It has been synthesized by a reaction between $[RhCp^*P(OEt)_3(WS_4)]$ and Cu^+ in a 2:1 molar ratio as the PF_6 salt $[\{RhCp^*P(OEt)_3(WS_4)\}_2Cu][PF_6]$, which is characterized by a single-crystal X-ray diffraction, EXAFS and IR measurements.

V-E Helical Arrays

Helical metal complexes termed by "helicates" are the compounds of current interest in coordination chemistry. Since the helicate has an optical activity, the left-handed and its right-handed helicate are helical enantiomers. Recent studies of this field are directed toward the enantioselective synthesis of the helicate using an optically active bridging ligand and diastereoisomerism. For this purpose, we have continued to prepare a unique helicate with optically active bridging ligands, 1,3-dioxolane derivatives.

V-E-1 Drastic Structural Change in Silver(I) Complexes with Alteration of the Optical Activity of a Pyridine Derivative Ligand: Helical Arrays with Extended Structure and an Optically Inactive Dinuclear Complex

Takayoshi SUZUKI, Hiyoshizo KOTUKI *(Kochi Univ.)*, **Kiyoshi ISOBE** *(Osaka City Univ.)*, **Narimasa MORIYA** *(Kochi Univ.)*, **Yuichi NAKAGAWA** *(Kochi Univ.)* **and Masamitu OCHI** *(Kochi Univ.)*

[*Inorg. Chem.* **34**, 530 (1995)]

Treatment of the optically pure 1,3-dioxolane derivatives with silver(I) trifluoromethanesulfonate (AgOTf) in methanol gave colorless prismatic crystals in nearly quantitative yield. The X-ray diffraction analyses of these complexes revealed that they are crystallized in the orthorhombic space group $P2_12_12_1$ with the same lattice constants (within the standard deviations) and are completely enantiotopic with each other. Each complex cation has an extended structure consisting of Ag^+ with a slightly distorted linear geometry and the bridging ligands. The Ag^+ cation has a weak interaction with the O atom in OTf^- (the shortest distance between them is 2.893 (8) Å). The array with extended structure runs toward a crystallographic 2-fold screw axis, but the Ag^+ ion is not sited on the axis and the extended array has a "helical" structure.

V-E-2 A Novel Synthesis of Optically Active *C2*-Symmetric Pyridine Derivatives. Efficient Reaction of Chiral Triflates with 2-Picolyllithium Reagents

Hiyoshizo KOTUKI *(Kochi Univ.)*, **Yuichi NAKAGAWA** *(Kochi Univ.)*, **Narimasa MORIYA** *(Kochi Univ.)*, **Hirotaka TATEISHI** *(Kochi Univ.)*, **Masamitu OCHI** *(Kochi Univ.)*, **Takayoshi SUZUKI and Kiyoshi ISOBE** *(Osaka City Univ.)*

[*Tetrahedron: Asymmetry* **6**, 1165 (1995)]

A variety of optically active *C2*-symmetric pyridine derivatives have been prepared from L- or D-tartaric acid as a chiral source via efficient coupling reactions of triflates with 2-picolyllithium reagents and the utility of the pyridine derivatives as chiral ligands in the catalytic enantioselective addition of diethylzinc to benzaldehyde has been demonstrated (up to 41% ee). The synthetic procedure for the corresponding *meso*-isomer was also described.

V-F Strong Correlation Effects in Organic Conductors

A variety of electronic states in organic conductors results from the competition between mutual Coulomb interactions among electrons and electron-lattice coupling. Such a unique feature of organic conductors is enhanced by the existence of larger degrees of freedom in a unit cell than in inorganic crystals in general, i.e. many molecules in a unit cell. This fact has been elucidated by considering the case of $(ET)_2X$ salts. Even though the number of electrons are the same in this family, the electronic states vary in an essential way. It turns out that α-$(ET)_2I_3$ can be basically considered as a band insulator, while κ-$(ET)_2$ is the Mott insulator. Moreover important parameters have been identified which bridge between these two apparently very different states.

V-F-1 On the Phase Transition of α-$(ET)_2I_3$

Hiori KINO and Hidetoshi FUKUYAMA *(University of Tokyo)*

[*J. Phys. Soc. Jpn.*, **64**, 1877, (1995)]

The nature of the metal-insulator (MI) trnsition of α-$(ET)_2I_3$ has been studied theoretically. The effect of the on-site Coulomb interaction has been investigated at absolute zero within the Hartree-Fock approximation. If the Coulomb interaction exceeds some critical value, charge transfer occurs between different stacks and antiferromagnetic spin ordering is stabilized one-dimensionally along one stack, which results in the MI transition. It is also argued that this MI transition will lead to spin-Peierls-like distortion making the ground state nonmagnetic. Hence the present theoretical results offer a possible explanation for the intriguing feature of the MI transition of the title material.

V-F-2 Electronic States of Conducting Organic κ-$(BEDT\text{-}TTF)_2X$

Hiori KINO and Hidetoshi FUKUYAMA *(University of Tokyo)*

[*J. Phys. Soc. Jpn.*, **64**, 2726 (1995)]

1-W : Electronic states of κ-(BEDT-TTF)$_2$X are studied theoretically. The effects of the one-site Coulomb interaction and dimer structure have been explored at absolute zero within the Hartree-Fock approximation. If Coulomb interaction exceeds some critical value, localized spins which are antiferromagnetically ordered within a unit cell emerge resulting in the reduction of the band overlap and eventually leading to the insulating state.

V-F-3 Intereationship of Electronic States among α-(ET)$_2$I$_3$, (ET)$_2$MHg (SCN)$_4$ and κ-(ET)$_2$X

Hiori KINO and Hidetoshi FUKUYAMA *(University of Tokyo)*

[*J. Phys. Soc. Jpn.*, **64**, 4523, (1995)]

Interrelationship of electronic structures among α-(ET)$_2$I$_3$, (ET)$_2$MHg (SCN)$_4$ and α-(ET)$_2$X are studied theoretically. The effects of on-site Coulomb energy are investigated at absolute zero within the Hartree-Fock approximation. If coulomb interaction exceeds some critical value, various kinds of antiferromagnetic states emerge, which depend crucially on the transfer in tegrals between ET molecules in the unit cell. Above 3 types of materials are classified on the axies of two transfer integrals leading to a unified view of the compounds.

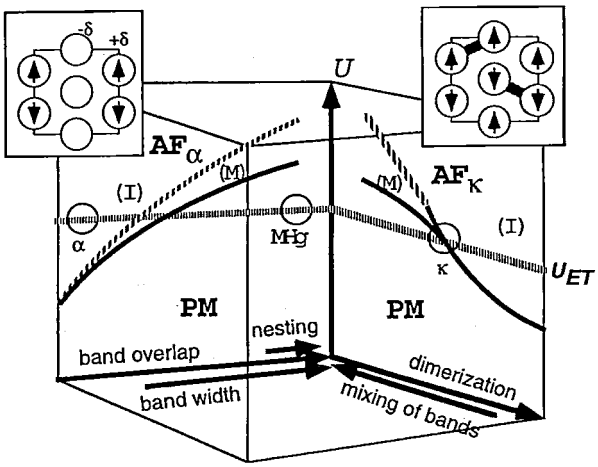

Figure 1.
A schematic phase diagram of (EX)$_2$X interpolating between α- andκ- polytypes.

V-G Syntheses, Crystal Structures and Solid State Properties of Halogen-Bridged Metal Complexes with Linear Chain Structures

Halogen-bridged mixed-valence complexes, which have a linear chain structure with a repeating unit of ···M^{II}···X–M^{IV}–X··· (M=Pt or Pd), have been extensively studied as a typical one-dimensional system having strong electron-phonon interaction. In addition, we succeeded in preparing novel Ni^{III}–X–Ni^{III} compounds which have a one-dimensional chain structure with no Peierls distortion. From a series of structural and optical studies for the M–X–M compounds, it has been elucidated that the amplitudes of the Peierls distortion can be controlled by modifying the chemical parameters, such as changing central metal (M), bridging halogen (X), organic ligand and counter anions. By applying the electrochemical oxidation technique which enables various combinations of bridging ion and counteranion in crystals, novel Ni^{III}–X–Ni^{III} compounds were obtained and their crystal structure analyses and magnetic susceptibility measurements were made to reveal the anomalous magnetic behavior.

V-G-1 Electrochemical Synthesis and Crystal Structure of a Novel One-Dimensional Halogen-Bridged Nickel(III) Complex

Yoshiki OZAWA *(Himeji Inst. Tech.)* **and Koshiro TORIUMI** *(Himeji Inst. Tech. and IMS)*

[*Chem. Letters*, 257 (1995)]

A novel Halogen-bridged one-dimensional Ni^{III}–X–Ni^{III} compound, {[Ni^{III}(en)$_2$Cl]Cl$_2$}$_\infty$ (en=C$_2$H$_8$N$_2$) has been synthesized by electrochemical oxidation (Figure 1). Single crystal X-ray crystallography revealed that a bridging halogen ion is located on the midpoint between two Ni(III) atoms with Ni–Cl 2.438(1) Å. This is the first example for electrocrystallization of halogen-bridged one-dimensional complexes.

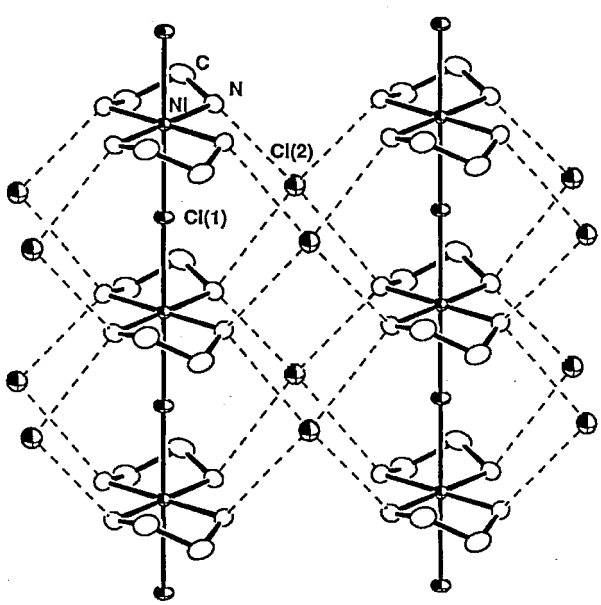

Figure 1. ORTEP drawing of the infinite linear chains of {[Ni^{III}(en)$_2$Cl]Cl$_2$}$_\infty$. Dashed lines indicate hydrogen bonds between Cl$^-$ and amino-groups of ethylenediamine ligands.

V-G-2 Electrocrystallization, Crystal Structure and Solid State Properties of Halogen-Bridged One-Dimensional Compound, $\{[Ni(en)_2Br](ClO_4)_2\}_\infty$, Having an Elongated Ni···Ni Distance

Yoshiki OZAWA,* Takayuki IKUNO,* Shin-ichi AMANO,* Takashi IDA,* Akito IBARAKI,* Keisaku KIMURA* and Koshiro TORIUMI** *(*Himeji Inst. Tech., **Himeji Inst. Tech. and IMS)*

[*Mol. Cryst. Liq. Cryst.*, in press]

Two crystal forms (α and β) of a novel halogen bridged one-dimensional Ni^{III}–Br–Ni^{III} compound, $\{[Ni(en)_2Br](ClO_4)_2\}_\infty$(en=$C_2H_8N_2$) have been prepared by electrochemical oxidation. X-ray crystal structure analysis of the α form revealed that a bridging Br ion is located on the midpoint between two Ni atoms and the Ni–Br distance of 2.640(1) Å is significantly elongated by introducing a bulky ClO_4^- ion as a counter anion (Figure 1). An average Ni–Br distance of 2.693(2) Å for the β form can be estimated from the lattice parameter along the chain. X-ray photoelectron spectra indicate that both forms have the Ni^{III}–X–Ni^{III} structure. Magnetic susceptibility data for both forms show strong antiferromagnetic coupling (J=-1700K) between electronic spins (S=1/2) localized on the Ni^{III} on the linear chain.

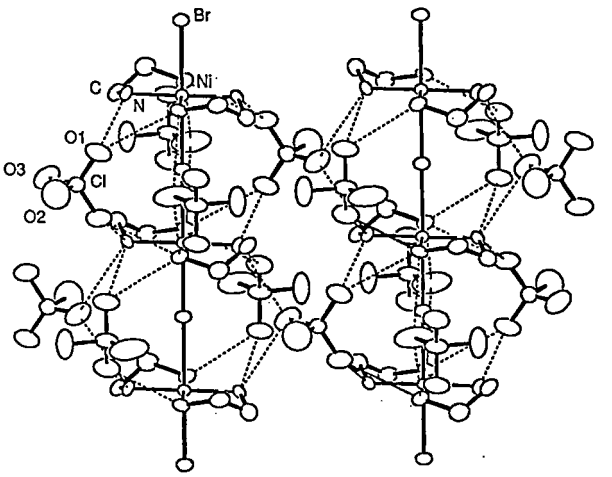

Figure 1. ORTEP drawing of the infinite linear chains of $\{[Ni(en)_2Br](ClO_4)_2\}_\infty$(α-form). Dashed lines indicate hydrogen bonds between ClO_4^- and amino-groups of ethylenediamine ligands.

V-H Modeling Reaction of Metalloenzyme Active Center

Metalloenzymes play key roles in various chemical conversions in biological systems. Most of them have not been well characterized structurally and/or mechanistically due to their instability and structural complexity. To build new reaction systems and to obtain further insight into the natural systems, artificial models of several important metalloenzyme active centers were prepared and were used to simulate the natural enzymatic reactions. In this research project, four metalloenzymes were studied by means of the construction of the corresponding artificial models. (1) In the functional modeling of water oxidation enzymes, we found manganese porphyrin dimers with a suitable Mn-Mn separation could oxidize water and evolve oxygen. (2) The relating manganese porphyrin dimers can mediate disproportionation of hydrogen peroxide and they are a new model of Mn catalases. We determined the reaction mechanism of by kinetic study with use of the high valent manganese complex. (3) Tripyrazolylporphyrin complex was prepared as a model complex of Fe-Cu center in cytochrome *c* oxidase and its stability of evaluated its structure and stability. (4) Oligomeric porphyrin arrays and Fe catecholate-quinone complexes were prepared as functional models in photosynthetic reaction center.

V-H-1 Oxygen Evolution by Water Oxidation with Manganese Porphyrin Dimers

Yoshinori NARUTA, Masa-aki SASAYAMA[a] and Takao SASAKI[a] *([a] Kyoto University)*

[*Angew. Chem.*, **106**, 1964-1965 (1994); *Angew. Chem. Int. Ed. Engl.*, **33**, 1839-1842 (1994)]

Photosystem II in plant RC contains a tetranuclear manganese complex, which catalyzes evolution of oxygen by oxidation of water. Manganese porphyrin dimers linked by an *o*-phenylene bridge were good functional model compounds and evolved oxygen in an aqueous media by means of anodic oxidation. It is established that evolved oxygen came from water through four electron oxidation process by use of $H_2{}^{18}O$ and a rotating electrode method.

V-H-2 Importance of Mn-Mn Separation and Their Relative Arrangement on the Development of High Catalase Activity in Manganese Porphyrin Dimer Catalysts

Yoshinori NARUTA and Masa-aki SASAYAMA[a] *([a] Kyoto University)*

[*J. Chem. Soc., Chem. Commun.*, 2667-2668 (1994)]

Manganese porphyrin dimers having appropriate metal-metal separations showed high catalase activity. The intensive correlation between the Mn-Mn separation of the catalyst and their catalytic activity was found. To find the optimum separation, ten kinds of dimers, whose metal separation are ranging from 3.5 to 13 Å, were prepared and measured its catalytic activity. When the Mn-Mn separation is ≈ 4 Å, the dimer showed the highest catalase activity among the dimers examined.

V-H-3 How Do Nitrogen Bases Accelerate Decomposition of H_2O_2 in a Manganese Porphyrin Dimer ? Quantitative Evaluation of the Effect by Its Axial Ligation *vs.* General-base Catalysis

Yoshinori NARUTA and Masa-aki SASAYAMA[a] *([a] Kyoto University)*

[*Chem Lett.*, 2411-2414 (1994)]

Catalytic disproportioation of H_2O_2 with a Mn porphyrin dimers requires the presence of an appropriate base in the solution. A nitrogen base is supposed to function in the following two modes: (1) as a general base catalyst, deprotonation of hydrogen peroxide to facilitate its coordination with the manganese ion and (2) as an axial ligand, acceleration of the O-O bond cleavage of the coordinated HOO^- to the Mn ion by its electron-pushing effect. In their modeling reaction, these two roles have never been separately and quantitatively evaluated in spite of their importance, presumably because the H_2O_2 disproportionation with the applied manganese porphyrin *monomer* is rather slow process. Cofacial manganese porphyrin dimers have following advantages over the reported ones on the evaluation of these base effects (Figure 1): (1) a relatively bulky nitrogen base cannot enter the molecular cleft of the dimer and does not form the corresponding inactive six-coordinated species on account of the steric hindrance of the porphyrin peripherals, as long as one uses the dimers with a short Mn-Mn separation. (2) The rate determining step of the H_2O_2 disproportionation with the manganese porphyrin dimers is the stage of the reaction of the initial H_2O_2 molecule with the $Mn(III)_2$ complex to form the corresponding $Mn(IV)_2$,

$$\frac{d[O_2]}{dt} = k_1[H_2O_2][Mn/Mn] + k_2[H_2O_2][Mn/Mn{:}B]$$

where **[Mn/Mn]** and **[Mn/Mn:B]** are the concentration of the base-uncoordinated and coordinated manganese porphyrin dimers, respectively. The first term expresses the rate simply accelerated by the general-base catalysis of the added nitrogen base. The second one shows the rate which affected by the axial coordination of the base coupled with the general base effect. By the application of 2,6-disubstituted pyridines, the unknown k_1 of the reaction containing a coordinative base can be evaluated according to the linear relationship between pKa of the base and log k_1 (Figure 2). Rate constant k_2 can be determined for each coordinative nitrogen base by use of the formation constant of the five-coordinated species. Thus, the O-O bond cleavage rate was accerarated in 6.5 times higher by the coordination of a nitrogen base.

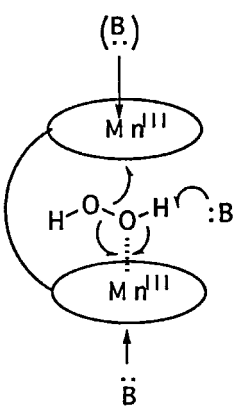

Figure 1. Schematic drawing of H_2O_2 reaction and effect of a nitrogen base in a manganese porphyrin dimer.

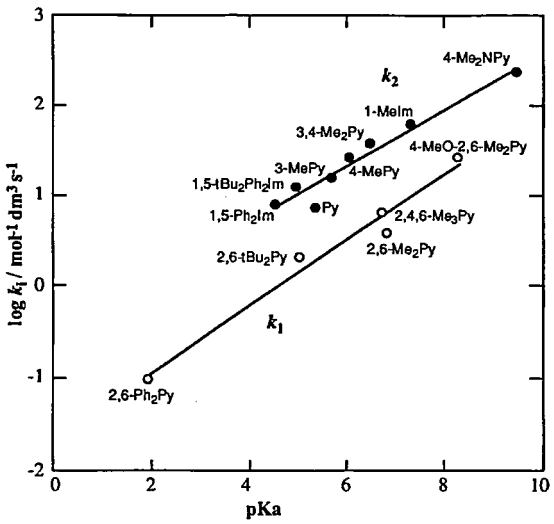

Figure 2. Effect of base pKa to rate constants $k1$ and $k2$.

V-H-4 Preparation of a 1,8-Anthracene-linked Manganese(IV) Porphyrin dimer and Its Reduction with H_2O_2. The O_2 Evolution Stage by the Reduction of the $Mn(IV)_2$ Complex Is Not a Rate-determining Step in the Catalytic Disproportionation of H_2O_2

Masa-aki SASAYAMA[a] and Yoshinori NARUTA
([a] Kyoto University)

[*Chem. Lett.*, 63-64 (1995)]

In the previous study, we demonstrated that Mn(III) porphyrin dimers having a short Mn-Mn separation excellently catalyzed the disproportionation of H_2O_2 in the presence of an appropriate nitrogen base. In this model study, the formation of the corresponding $Mn(IV)_2$ complex as an intermediate by the homolytic O-O bond cleavage of the Mn-O-O-H. To confirm this catalytic cycle, we separately prepared a Mn(IV) porphyrin dimer and compared its reduction rate by H_2O_2 with the O_2-evolution rate in the Mn(III) dimer-H_2O_2 system. By hypochlorite oxidation at -10°C,. dimanganese(III) complex (**1**) of 1,8-bis[5-(10,15,20-trimesityl)porphrinyl]anthracene was converted to the corresponding $Mn(IV)_2$ **2**, which was characterized by electronic absorption (λ_{max} = 423 nm), ESR (g = 4.4), and IR spectra (υ (Mn-O) = 558 cm^{-1}). The reduction rate of the $Mn(IV)_2$ complex **2** with H_2O_2 was determined from the time-course of its UV-vis spectral change in CH_3CN at the temperature range from -40 to -20 °C. Absorption at 422 nm that corresponds to the Soret band of the Mn(IV) complex was decreased according to the increase of the absorption at 468 nm (the Mn(III) complex). From kinetic analysis, the rate constant $k3$ was determined by the time-course of the absorption change at 468 nm to be 2.61 × 10^5 mol^{-2} dm^6 s^{-1} at -40°C. Arrhenius plot of this reaction (T = -20 to -40°C) gave the activation parameters, E_a = 8.9 kcal mol^{-1} and A = 4.3 × 10^{13} mol^{-2} dm^6 s^{-1}. Under a certain reaction conditions ([Mn^{III}$_2$P] = 1.25 × 10^{-4} mol dm^{-3}, [H_2O_2] = 6.4 × 10^{-2} mol dm^{-3}, T = 10°C), the estimated reduction rate of the $Mn(IV)_2$ by H_2O_2 is 1.3 × 10^{-2} mol dm^{-3} s^{-1}. The O_2 evolution rate of the catalytic H_2O_2 disproportionation with **1** was 2.0 × 10^{-3} mol dm^{-3} s^{-1} under the same conditions in the presence of 4-dimethylaminopyridine. Thus, the re-

duction rate of the $Mn(IV)_2$ complex was 6.5 times higher than the overall disproportionation reaction of H_2O_2 with the corresponding $Mn(III)_2$ catalyst. These results support that the rate-determining step in the catalase reaction is the formation of Mn(IV) dimer as expected in our previous work.

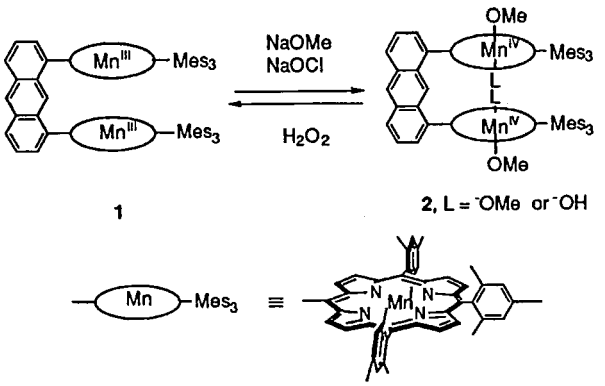

V-H-5 Siteselective Oxidation of Olefins by Menas of Lipophilic Metalloporphyrin Catalysts in Liposome Membranes

Yoshinori NARUTA and Masa-oki GOTO[a] *([a] Kyoto University)*

Siteselective reaction of substrates bearing similar functional groups in one molecule is a difficult problem in organic synthesis. Terminal hydroxylation of a straight-chain aliphatic carboxylic acid is one of typical reactions demonstrating by cytochrome P-450 monooxygenase. To realize such high selectivity in an artificial catalytic system, lipophilic iron porphyrins, **1** and **2**, are prepared and selective epoxidation of ubiquinone-3 and linolenic acid was examined in liposome membrane systems. In the catalytic epoxidation of ubiquinone-3 with **1** and dimyristoyl phosphatidylcholine, gave the 10,11-epoxide in 90% selectivity over the corresponding 6,7-epoxide (10% selectivity). The oxidation of linolenic acid was run under liposome conditions consisted by dihexadecyldimethylammonium bromide with catalyst **2** preferentially to give the terminal epoxide (15,16-epoxide) in 81% selectivity over 9,10- (7%) and 12,13-epoxide (11%). In consideration with the statistical distribution of the epoxides in a homogenious conditions, the marked high selectivity of the terminal epoxide is attributed to the arrangement of the substrate and catalyst in the liposome membrane.

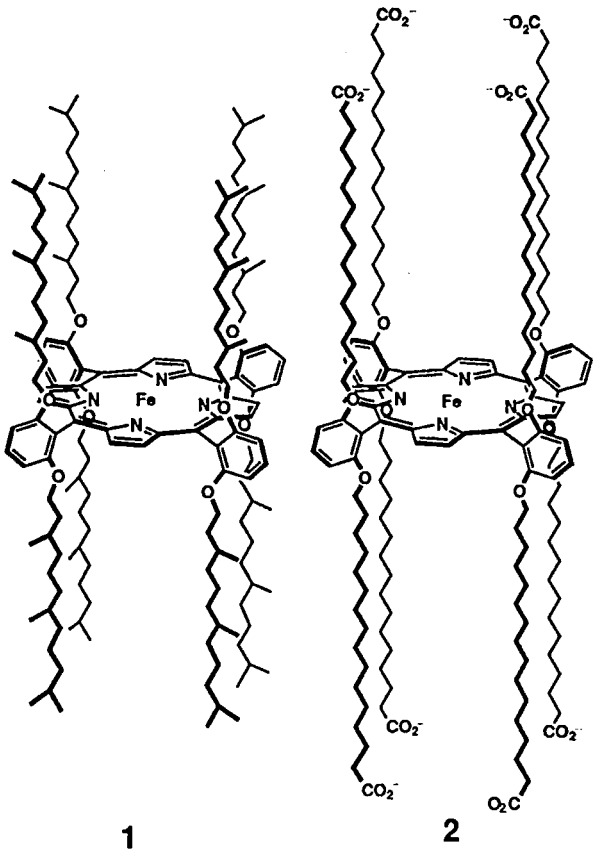

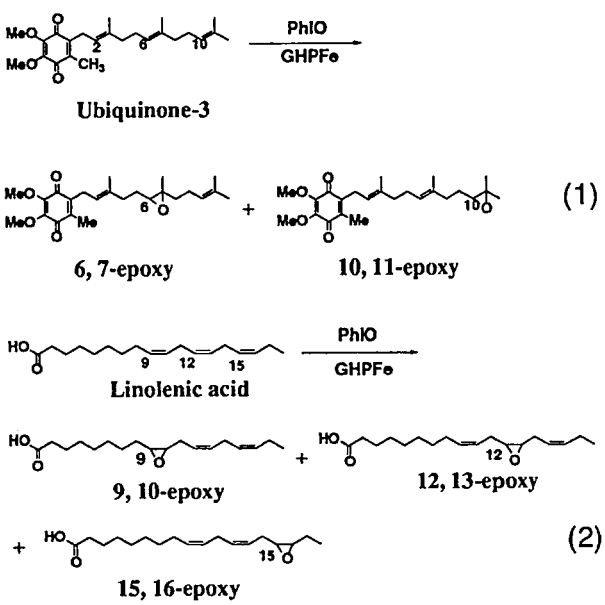

V-H-6 New and Efficient Synthesis of Oligomeric Porphyrins *via* Stepwise Nucleophilic Substitution of Aminoporphyrins to Cyanuric Chloride

Kanako ICHIHARA[a] **and Yoshiori NARUTA** *(a Kyoto University)*

[*Chem. Lett.*, 631-632 (1995)]

In biological systems, aggregation of several prosthetic groups and their coupled activity are ubiquitous strategy to construct catalytic reaction centers. A number of tetrapyrrole dimers and oligomers have been synthesized to construct artificial models for understanding these

catalytic reactions. A new strategy to synthesize porphyrin oligomers was developed by use of 1,3,5-triazine as a linker molecule (Figure. 1). Selective substitution of cyanuric chloride by monoaminoporphyrin gave dimeric porphyrin **P2** at 0°C. By applying elevated temperature, porphyrin dimer **P2** was prepared in quantitative yield. In this way, up to pentamer **P5** was prepared in the range of yields, 45-100%. Each 1,3,5-triazine ring in these oligomeric porphyrins has a remaining chloride, which also can be substituted by various nucleophiles at higher temperature to introduce functional groups to the porphyrin oligomers. Using NH_4OH or aminotriethylsilane, amino groups were smoothly introduced at 110°C in a good yield (ca. 90% for **P4**). Resultant 1,3,5-triaminotriazine (melamine) derivative is known as a good device for hydrogen-bonded molecular assemblies.

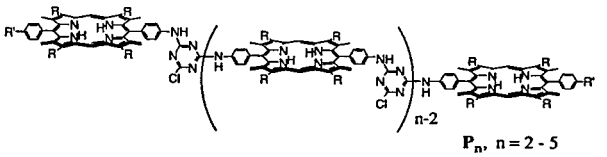

Figure 1. 1,3,5-Triazine-linked porphyrin oligomers.

V-H-7 Formation and Characterization of $Pz_3Cu(II)$-Fe(III) Porphyrin Complex as Structural Model of Cytochrome *c* Oxidase

Takao SASAKI[a] and Yoshinori NARUTA *([a] Kyoto University)*

[*Chem. Lett.*, 663-664 (1995)]

Cytochrome *c* oxidase is the terminal oxidase at the aerobic respiratory chain and catalyzes the four-electron reduction of dioxygen to water. The active site of this enzyme contains a dinuclear Fe/Cu site (heme a_3 - CuB) and these transition metal ions couple with the reduction process of O_2. Very recently, its detailed structure was revealed by high resolution X-ray crystallographic analysis. We synthesized the porphyrins bearing tripyrazolyl ligand, which can form heteronuclear complexes to take advantage of the difference of the coordination strength between two ligands (Figure 1). By spectrophotometric titration, Formation constants of the copper(II) complexes of $\mathbf{C_n}$(Fe)-non in CH_2Cl_2 at 25 °C were determined to be $K_1 = 1.04 \times 10^6$ M and 1.37×10^5 M for $\mathbf{C_1}$ and $\mathbf{C_2}$, respectively. Mass spectra of the resultant $[\mathbf{C_1}\text{ (Fe)-Cu}]^{3+}$ complexes showed a peak at m/z = 1194, which was assigned to be $[\mathbf{C_1}\text{(Fe)-CuCl}]^{2+}$. This showed the incorporation of a Cl^- ion as a bridging ligand between two metal ions. However, $\mathbf{C_1}$ (Fe)-non did not give the corresponding Cl^- bridged peak. Only $\mathbf{C_1}$ (Fe)-Cu showed the ESR signals at $g\perp$ = 6.2 and $g//$ = 2.0 attributed to high spin porphyrin Fe(III) complex and g = 2.2 assigned to typical S = 1/2 copper(II) in the tetragonal field with three nitrogen and one Cl^- ligands. The $\mathbf{C_2}$ (Fe) derivative did not showed any Cu signal, presumably because of the instability of the Cu complex in the applied media and conditions. From MM+ calculation, the Fe-Cu separation in $\mathbf{C_1}$ (Fe)-Cu was estimated to be around 4.88 Å and is likely to be more stable than the $\mathbf{C_2}$ complex 5.02 Å.

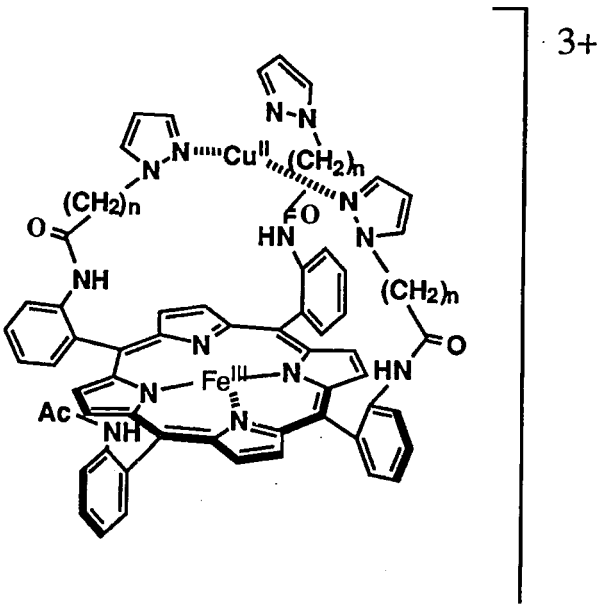

Figure 1. Tripyrazoryl Cu-Fe porphyrin complex $[\mathbf{C_n}\text{(Fe)-Cu}]^{3+}$, n = 1, 2 as activesite models of cytochrome *c* oxidase.

V-H-8 Preparation of Tricatecole Fe-Quinone Complexes and its Electrochemical Study

Yoshinori NARUTA and Hideki TANAKA[a] *([a]Kyoto University)*

In an electron acceptor site of photosynthetic reaction center, low-spin Fe(II)-quinone complex is considered to facilitate electron transfer from quinone A (Q_A) to remote Q_B. However, the role of Fe between two quinones are not clear. To make a mimic system (**1**), which contains tricatecholate ion(III) complex (M = Fe) and a quninone residue (R = anthraquinone) (Figure 1). When the separation between the quinone and the iron is appropriate, large positive shift (+180 mV) of the reduction potential of the quinone was observed. This indicates the stabilization of the quinone cation radical by the interaction with the proximal Fe(III). The structure of the corresponding Cr complex with alanine linkers (R'=Me) was clarified by CD spectra.

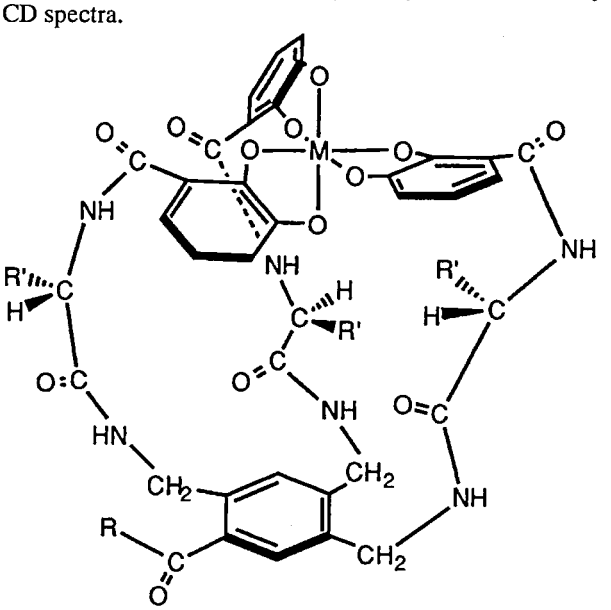

Figure 1. Tricatecholate metal complexes as a quninone-Fe complex in a photosynthetic electron acceptor site.

V-I Design, Properties and Reactivity of New Organometallic Compounds

A variety of carbon-metal bonds can produce unconventional reactivities and properties of the organometallic compounds. At present, development of new organometallic reagents for organic chemical transformations especially asymmetric reactions is one of our important projects. The other is synthesis of new organometallic compounds, especially organoboron compounds having strong affinity to cancer cells for Neutron Capture Therapy.

V-I-1 Synthesis of Boron Carriers for Neutron Capture Therapy and the Studies of Activated Imines

Hisao NEMOTO

[*J. Syn. Org. Chem. Jpn.*, **52**, 1044 (1994)]

Boron Neutron Capture Therapy has promising therapeutic principles of cancers. Synthesis of several new boron carriers having more appropriate biological activities than clinically used boron compounds has been accomplished. New methods for the synthesis of boron carriers are also described. In addition, studies of activated imines like an acyliminium ion or an imine attached with electron withdrawing group on nitrogen, are presented. New synthetic methods and reagents for the reaction of activated imines are also described.

V-I-2 Synthesis and Biological Properties of Water-soluble *p*-Boronophenylalanine Derivatives. Relationship between Water Solubility, Cytotoxicity and Cellar Uptake

Hisao NEMOTO, Jianping CAI, Naoki ASAO, Satoshi IWAMOTO[a] and Yoshinori YAMAMOTO[a] *([a]Tohoku Univ.)*

[*J. Med. Chem.*, **38**, 1673 (1995)]

Synthesis and examination of the biological evaluation toward B16 Melanoma cells of three new water-soluble p-boronophenylalanine derivatives were carried out. The more number of hydroxy groups the derivative has, the higher selective incorporation toward B16-Melanoma cells *vs.* TIG-1-20 hybrobrast cells was observed.

V-I-3 Synthesis of Netropsin and Destamycin Analogues Bearing ortho-Carborane and their DNA Recognition

Yoshinori YAMAMOTO[a], Jianping CAI, Hiroyuki NAKAMURA[a], Naoki SADAYORI[a], Naoki ASAO and Hisao NEMOTO *([a]Tohoku Univ.)*

[*J. Org. Chem.*, **60**, 3352 (1995)]

Netropsin and distamycin A analogues containing o-carborane framework were synthesized to investigate DNA binding sequence of these molecules. Cascade type polyols, diol or tetraol, were attached to the carboranes in certain cases. MPE-Fe(II) footprinting on the 216 base pair Pvu I/Bam HI restriction fragment from pBLUESCRIPT KS(+1-) (bp2958) indicated that the compounds without cascade type polyols bound only slightly to the DNA fragment, whereas the diol derivatives bound to the A,T-rich base pairs. The compounds containing tetraol unit bound most selectively to the DNA fragments. In general, the compound containing three pyrrole rings in their molecules bound to the DNA more selectively than the corresponding two pyrrole ring-bearing compounds.

V-I-4 Synthesis of All Carboxylate-free DTPA Derivatives via Palladium Catalyzed Carbon-carbon Bond Formation Reaction

Hisao NEMOTO, Jianping CAI and Yoshinori YAMAMOTO[a] *([a]Tohoku Univ.)*

[*J. Org. Chem.*, in press]

Diethylenetriaminepentaacetic acid (DTPA) is one of the well-known chelating reagents to form a stable complex with heavy metal ions, which could be used for MRI, Radioactive Labeling of Antibody and Neutron Capture Therapy. We report the preparation of a new DTPA derivative having malonic moiety (**1**) and its palladium catalyzed carbon-carbon bond formation reaction for synthesis of DTPA derivatives in all carboxylate-free form (**2**).

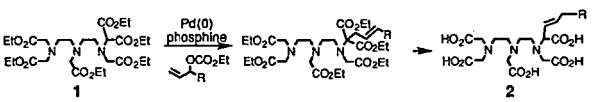

V-I-5 Highly Stereocontrolled and Concise Asymmetric Synthesis of the β-Lactam Framework via a TCC Method

Naoki ASAO, Takashi SHIMADA[a], Naofumi TSUKADA[a] and Yoshinori YAMAMOTO[a] *([a]Tohoku Univ.)*

[*Tetrahedron Lett.*, **35**, 8425 (1994)]

The conjugate addition of LSA **1** to t-butyl (4S)-4-(trityl)oxy-2-pentenoate **2** followed by aldol condensation with acetaldehyde produces a key intermediate **3** to β-lactam derivatives as a single diastereoisomer in 77% yield.

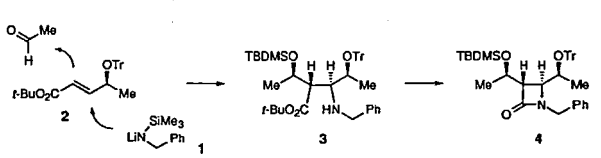

RESEARCH ACTIVITIES VI
Department of Vacuum UV Photoscience

VI-A Electronic Structure and Decay Mechanism of Inner-Shell Excited Molecules

This project is being carried out in collaboration with Photon Factory (KEK-PF), Tohoku University, McMaster University and Université Paris-Sud. We have interest in ultrafast fragmentation in the molecular inner-shell decay process, where the ionic fragmentation following the Auger decay takes place in much shorter time than the period of the molecular rotation. Last year we investigated vibronic states in the inner-shell excitation of linear triatomic molecules and found that the fragmentation takes place on the way of bending vibrations [See, J. Adachi, N. Kosugi, E. Shigemasa, A. Yagishita, *J. Chem. Phys.* **102**, 7369 (1995)]. This year we have extended our approaches to some polyatomic molecules.

VI-A-1 Angular Distribution of Fragment Ions Following the C 1s Photoexcitation of C_2H_2

Jun-ichi ADACHI, Nobuhiro KOSUGI, Eiji SHIGEMASA* and Akira YAGISHITA* *(*KEK-PF)*

We have measured angle-resolved ion-yield spectra for the C 1s excited C_2H_2 using linearly polarized synchrotron radiation. The fragment ions following the C 1s $\rightarrow \pi^*$ excitation are detected not only in the 90° direction to the electric vector of the incident light but also in the 0° direction. The relative intensity of the peak observed in the 0° is enhanced on the lower energy side of the peak maximum. These results indicate that the π^* excited state is strongly affected by the Renner-Teller effect to remove the two fold degeneracy and the equilibrium geometry in the lower π^* state is bent. The $3s\sigma_g$, $3p\sigma_u$, $3p\pi_u$ and the higher Rydberg peaks are observed. The $3s\sigma_g$ and $3p\sigma_u$, Rydberg excited states may be influenced by the $4\sigma_g$ and $3\sigma_u$ valence excited ones, respectively.

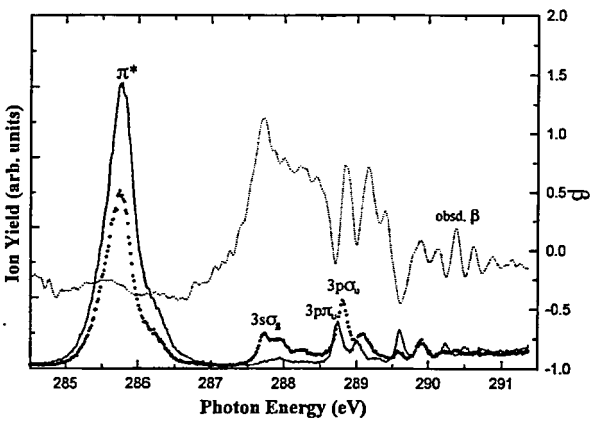

Figure 1. C K-edge angle-resolved ion-yield spectra of C_2H_2. The solid line shows the ion-yield in the 90° direction to the electric vector of the incident light and the dotted line shows one in the 0° direction.

VI-A-2 Molecular Symmetries and Angular Distribution of Fragment Ions Following the S 1s Excited SO_2

Jun-ichi ADACHI, Atsunari HIRAYA, Yasutaka TAKATA, Nobuhiro KOSUGI, Eiji SHIGEMASA*, Akira YAGISHITA* and Yoshinori KITAJIMA* *(*KEK-PF)*

We have measured angle-resolved ion-yield spectra for the S 1s excited SO_2 using linearly polarized synchrotron radiation. Assuming that the stable bond angle in the exicted state is nearly equal to that in the ground state, anisotropic parameters (β) for the ejected fragment ions following the lowest three excitations, S 1s $\rightarrow 3b_1$, $9a_1$ and $6b_2$, are -1, -0.24 and +1.24. The observed β values for the three lowest peaks are -0.86, +0.32 and +0.16; these peaks are tentatively assigned to $3b_1$, $6b_2$ and $9a_1$, respectively. Large differences in β for the $6b_2$ and $9a_1$ excited states indicate that the angular distributions of the fragment ions would be affected by the molecular bending motion.

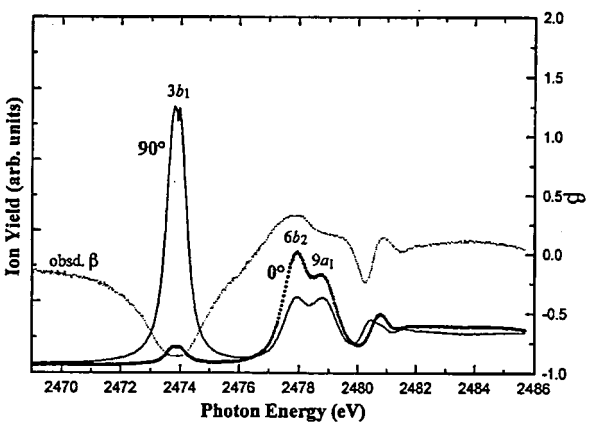

Figure 1. S K-edge angle-resolved ion-yield spectra of SO_2. The solid line shows the ion-yield in the 90° direction to the electric vector of the incident light and the dotted line shows one in the 0° direction.

VI-A-3 Electronic States of Gaseous and Adsorbed Thiophene C_4H_4S Studied by the S 1s Photoabsorption Spectra

Jun-ichi ADACHI, Yasutaka TAKATA, Atsunari HIRAYA, Nobuhiro KOSUGI, Eiji SHIGEMASA*, Akira YAGISHITA* and Yoshinori KITAJIMA* *(*KEK-PF)*

We have measured angle-resolved ion-yield spectra for the S 1s excited thiophene (C_4H_4S) in gas phase using linearly polarized synchrotron radiation. The lowest two excited states S 1s $\rightarrow 4b_1(\pi^*)$ and $8b_2(\sigma^*)$ of the gaseous C_4H_4S are located at 2473.25 and 2473.72 eV and are differenciated at the first time. The $4b_1$ peak for the adsorbted molecule C_4H_4S / Ni(100) is shifted to about 1.2 eV lower energy side than that for the gaseous molecule. This implies that interaction of the $4b_1$ orbital with Ni

metal is large. The present result supports the previous conclusion that the C_4H_4S molecules are orientated in parallel to the surface.

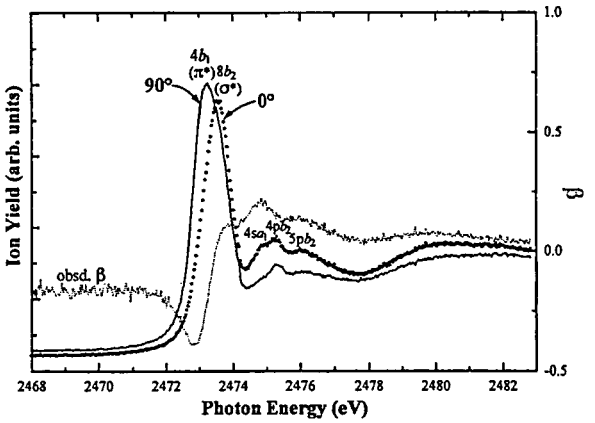

Figure 1. S K-edge angle-resolved ion-yield spectra of thiophene. The solid line shows the ion-yield in the 90° direction to the electric vector of the incident light and the dotted line shows one in the 0° direction.

VI-A-4 Angular Distribution of 1sσ Photoelectrons from Fixed-in-Space N_2 Molecules

Eiji SHIGEMASA*, Jun-ichi ADACHI, Masaki OURA and Akira YAGISHITA*** *(*KEK-PF, **RIKEN)*

[Phys. Rev. Lett. 74, 359 (1995)]

The angular distribution of 1sσ photoelectrons from N_2 molecules held fixed in space has been measured around the σ* shape resonance for the first time. The angular distributions have been very rich in structure, which are completely different from ususal photoelectron angular distributions from randomly oriented molecules. The orbital angular momentum properties of the 1sσ photoelectrons around the σ* shape resonanace have been made clear from the angular distribution patterns.

VI-A-5 Angular Distribution of 1s Photoelectrons from Spatially Aligned CO Using Angle-Resolved PEPICO

Paul A. HATHERLY*, Jun-ichi ADACHI, Eiji SHIGEMASA and Akira YAGISHITA**** *(*Univ. of Reading, **KEK-PF)*

[*J. Phys.* **B 28**, 2643 (1995)]

Results are presented for the angular distributions of electrons from spatially aligned core excited CO using an angle-resolved photoelectron-photoion coincidence technique in the regions of the C and O 1s edges and σ* resonance. Coincidence measurements were recorded between ions ejected at 0° and 90° with respect to the electric field of the linearly polarized radiation and for photoelectrons ranging from 0° and 90° with respect to the molecular axis. The results show a strong departure from angular distribution measurements made more conventionally; in particular multiple outgoing partial waves of high angular momentum are seen to make a significant contribution.

VI-A-6 Electron Impact Core Excitation of SF_6: S 2p, S 2s and F 1s Spectroscopy

James T. FRANCIS*, Cassia C. TURCI*, Tolek TYLISZCZAK*, G. Gerson B. de SOUZA*, Nobuhiro KOSUGI and Adam P. HITCHCOCK* *(*McMaster Univ.)*

[*Phys. Rev. A,* in press]

Electron energy-loss spectra of SF_6 have been recorded in the region of S 2p, S 2s and F 1s excitation, using both dipole and non-dipole electron scattering conditions. Impact energies between 700 and 3200 eV and scattering angles between 0° and 30° were used. Relative to dipole-EELS or photoabsorption, there are large intensity redistributions in both the S 2p and S 2s spectra under non-dipole conditions. In contrast, the F 1s spectrum is essentially the same in near-dipole and non-dipole scattering regimes. A novel, higher order electric multipole S 2p spectral feature is observed at 181 eV. It has an unusual multipeaked line shape, whose components are more closely spaced than the typical 1.15 eV S 2p spin-orbit splitting. It is attributed to the overlap of several quadrupole-coupled states, which are likely associated with the S 2p $t_{1u} \rightarrow t_{1u}^*$ configuration.

VI-A-7 Dissociation Dynamics of Core-Excited BF_3 Probed by the Photoelectron-Photoion-Photoion Coincidence

Mark SIMON*, Paul MORIN*, Pascal LABLANQUIE*, Michel LAVOLLÉE*, Kiyoshi UEDA and Nobuhiro KOSUGI** *(*Université Paris-Sud, **Tohoku Univ.)*

[*Chem. Phys. Lett.* **238**, 42 (1995)]

The photoelectron-photoion-photoion coincidence (PEPIPICO) has been measured to study the decay dynamics of the B 1s excited states of BF_3. The results of PEPIPICO indicate that the dynamics of ion-pair production, B^+-F^+ and B^{++}-F^+, following the discrete resonance excitation B 1s→$2a_2''$ (π*) is completely different from that following the continuum shape resonance excitation B 1s→$4e'$ (σ*); the momentum of the boron ion is larger than that of the fluorine ion in the B 1s→ π* excited state. The difference is caused by a distortion from the D_{3h} planar geometry to the C_{3v} pyramidal geometry in the B 1s→ π* excited state.

VI-A-8 Rydberg-Valence Mixing in the C 1s Excited States of CH_4 Probed by Electron Spectroscopy

Kiyoshi UEDA*, Misaki OKUNISHI*, Hiroshi CHIBA*, Yuichiro SHIMIZU*, Kenji OHMORI*, Yukinori SATO*, Eiji SHIGEMASA and Nobuhiro KOSUGI** *(*Tohoku Univ., **KEK-PF)*

[*Chem. Phys. Lett.* **236**, 311 (1995)]

In the C 1s threshold region of CH_4 the electron-yield spectrum has been measured at the photon energy resolu-

tion of ~ 60 meV. The C 1s→n$d t_2$ Rydberg series and the v=1 vibrational levels of the symmetric mode (ν_1) in the dominant C 1s→n$p t_2$ series are clearly identified. The resonance Auger electron spectra have been also measured by the C 1s→Rydberg excitations. The participant Auger decay rate following the C 1s→3$s a_1$, 3$p t_2$ and 3$d t_2$ excitations are 5.5%, 2.5% and 3.7% of the total Auger decays, respectively, indicating that these Rydberg states do not have so strongly mixed valence character. The ordering of the valence contribution as $3s a_1 > 3d t_2 > 3p t_2$ is consistent with the theoretical prediction. The calculation shows that the repulsive valence states are significantly destabilized through large avoided curve crossings with the Rydberg states and should be alive as continuum resonances.

VI-B Soft X-ray Photoelectron-Photoabsorption Spectroscopy and Electronic Structure of Transition Metal Compounds

Last year we constructed a new UHV apparatus for photoelectron-photoabsorption spectroscopy using a high-performance electron energy analyzer connected to the soft X-ray double crystal monochromator of the beamline BL1A at the UVSOR facility. This year we have investigated electronic structures of some Ni compounds by combining Ni 2p photoabsorption and Ni 3p and Ni 3s resonant photoemission.

VI-B-1 Resonant Ni 3p and 3s Photoelectron Spectra Following the Ni 2p Excitation in NiO

Motohiko NAKAMURA, Yasutaka TAKATA and Nobuhiro KOSUGI

[*UVSOR Activ. Rep.*, **26** (1994)]

We have measured Ni 3p and 3s photoelectron spectra following the Ni 2p photoabsorption in NiO which is known to be a Mott insulator with large electron correlation. Figure 1 shows photoelectron spectra measured at the photon energies marked in the absorption spectrum. At the Ni $2p_{3/2}$→3d (1, 2) and $2p_{1/2}$→3d (3) resonances, strong resonance enhancements are observed for the Ni 3p and 3s photoelectron region. The energy positions of all the observed peaks except (c) are equal to those of the peaks of the off-resonant spectrum (0) and are not dependent on the photon energies. This means that the peaks arise from the same single ionic states. The binding energy of the peak (c) shifts with increase of the photon energy with the ratio of about 0.65. This result indicates that the peak (c) does not originate from usual resonant photoemission. On the other hand, for the 3p main peak (a), no resonance enhancement is observed.

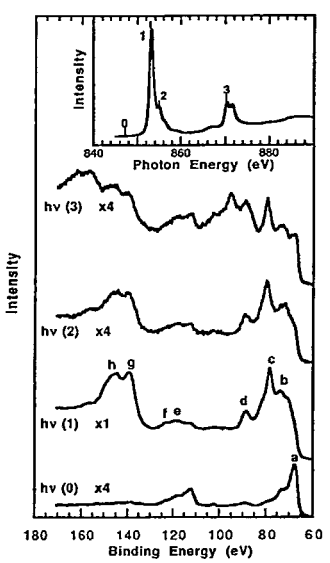

Figure 1. Ni 3p and 3s photoelectron spectra of NiO. The inset shows the Ni 2p absorption spectrum.

VI-B-2 Ni $L_{2,3}$MM Resonant Auger Spectra of $K_2Ni(CN)_4$ Following the Ni 2p Excitation

Yasutaka TAKATA, Motohiko NAKAMURA and Nobuhiro KOSUGI

We have measured Ni $L_{2,3}$MM resonant Auger spectra of $K_2Ni(CN)_4$ following Ni 2p photoabsorption. Figure 1 shows the Auger spectra measured at the photon energy marked in the photoabsorption spectra. The Ni 3p and 3s photoelectron peaks, whose kinetic energies shift in proportion to the photon energy and binding energies are constant, show no resonance enhancement. On the other hand, all the peaks (a-e) enhanced by resonant photoabsorption are shifted as converging to the L_3MM normal Auger transitions; the energy dependence (kinetic energy vs. photon energy) is about -0.5. These shifts can be explained if we assume that the photoexcited spectator electron behaves hydrogenic. This is the first observation of the energy shifts of several spectator Auger decays of the tightly bound states in solid.

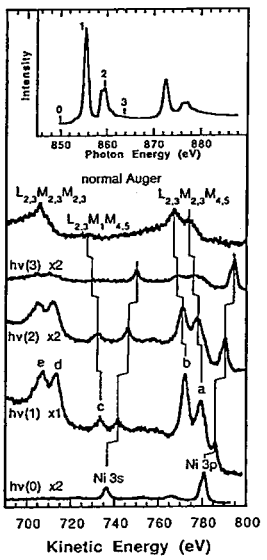

Figure 1. Ni $L_{2,3}$MM resonant Auger spectra of $K_2Ni(CN)_4$. The inset shows the Ni 2p absorption spectrum.

VI-C Studies of Photochemical Reactions using Ultrafast Laser and Synchrotron Radiation

Ultrafast lasers have been playing essential roles in the physicochemical studies of photochemical reactions. Thanks to recent advances of the laser technology, we are now able to examine not only primary reaction processes of the solute molecules but also dynamics of the surrounding solvent molecules with pico/femtosecond time resolution. Synchrotron radiation, on the other hand, affords photons in a very wide energy range from X-ray to far-infrared, which is not accessible by the present lasers. It can also open up new possibility of time-resolved spectroscopy since the radiation is intrinsically given in the form of a picosecond pulse train. In this project, we investigate photochemical reactions, mainly in condensed phase, taking advantage of these two light sources which are complementary to each other. This new project just started in January 1995, when Prof. Tahara joined IMS. Dr. Takeuchi, Dr. Matsuo and Ms. Kayama joined his group recently.

VI-C-1 Time-Domain Approach to the Solute-Solvent Interactions in Photochemical Reactions

Satoshi TAKEUCHI and Tahei TAHARA

The solvation dynamics of molecular liquids has been attracting much interest because it plays important roles in solution-phase chemical reactions. With a benefit of ultrashort optical pulses available from recently-developed solid-state lasers, the solvent response can be directly investigated by time-domain spectroscopies such as impulsive Raman scattering. They offer a unique chance to reveal low-frequency Rayleigh-wing spectra which contain much information about the intermolecular dynamical properties of liquids. We have just installed a Kerr-lens mode-locked Ti:sapphire laser which generates femtosecond coherent pulses around λ = 800 nm. Figure 1 shows an observed fringe-resolved autocorrelation trace which indicates a chirp-free pulse with a typical duration of 45 ± 5 fs. The time-domain measurements using the ultrashort pulses with a spectral coverage of ca. 300cm^{-1} as well as a detection of time-dependent fluorescence Stokes-shift of photoexcited solute molecules are now in progress to elucidate the dynamical solute-solvent interactions. In addition, we are interested in vibrational coherence during photochemical reactions. A further amplification of the ultrashort pulses is also planned.

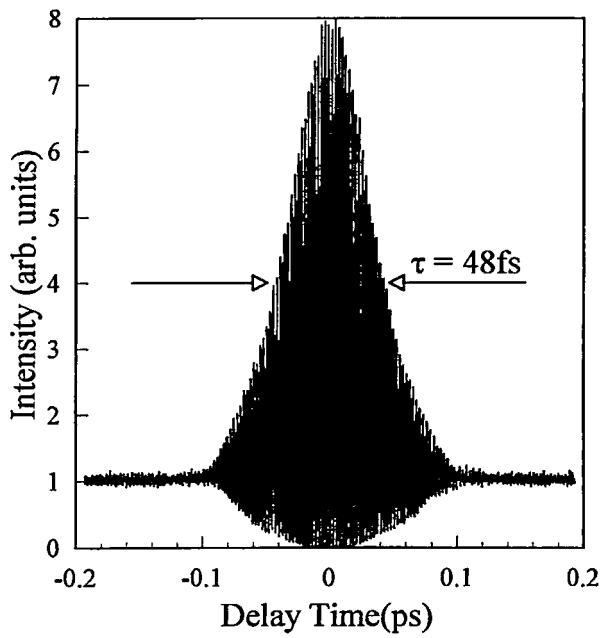

Figure 1. Fringe-resolved autocorrelation trace of the output pulse.

VI-C-2 Application of Broadband Incoherent Light to Femtosecond Time-Resolved Spectroscopy

Shigeki MATSUO and Tahei TAHARA

Femtosecond time-resolved spectroscopy is a powerful tool to investigate the dynamics of liquid-phase molecules. It has been known that femtosecond time resolution is attainable not only by femtosecond pulses but also by making use of the short correlation time of broadband incoherent light.[1] We are now constructing an experimental setup for femtosecond spectroscopy with incoherent light, using a nanosecond Ti:sapphire laser pumped by a Q-switched Nd:YAG laser. At the present, broadband lasing with band width of about 160 cm^{-1} is obtained around λ= 760 nm. A typical autocorrelation trace is shown in Figure 1, which was measured by the second harmonic generation with a background-free configuration. A correlation time of 150 fs with a contrast ratio of ca 2:1 was obtained.

Reference

1) Norio Morita and Tatsuo Yajima, *Phys.Rev.* A30, **2525** (1984).

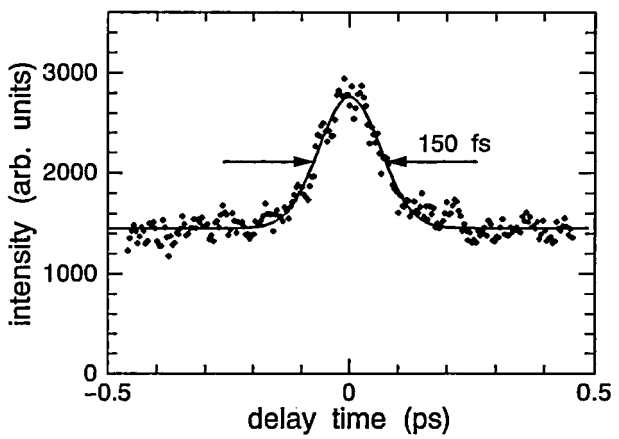

Figure 1. A typical autocorrelation trace of the broadband radiation from a nanosecond Ti:sapphire laser (Solid circles: obtained data; solid curve: Gaussian fit).

VI-C-3 Construction of an Optical Cell for Spectroscopic Studies on Supercritical Fluids

Misa KAYAMA and Tahei TAHARA

Supercritical fluids exhibit intriguing features due to their hybrid nature of gases and liquids. Physical properties of supercritical fluids (e.g., density, viscosity, dielec-

tric constant) can be largely changed by controlling temperature and pressure. The supercritical fluids are, therefore, unique solvents which allow intensive investigation on solvent effects in chemical reactions. An optical cell was designed for spectroscopic studies on supercritical fluids (Figure 1). We employed a synthetic diamond (type IIa) as a window material because of (1) the high transparency in a wide range from UV to far-infrared and (2) its hardness. This cell can confine high pressure fluids up to 500 kg/cm^2 with thin diamond windows of 0.5 mm thickness. The temperature of the sample fluids is controlled by circulating water inside the cell-wall and is monitored bya thermocouple. The optical path length can be varied in the range of 0 - 2 mm by adjusting the screw plugs. Firstly, we are planning to measure far-infrared absorption spectra of several supercritical fluids with / without solute molecules by using synchrotron radiation.

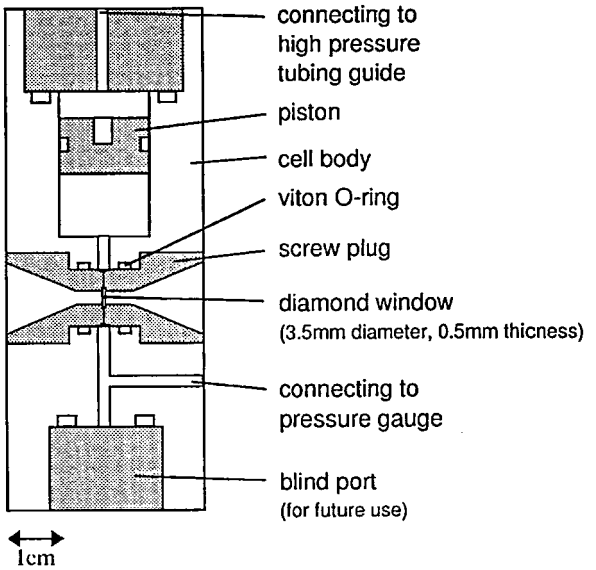

Figure 1 Cross section of the optical cell for supercritical fluids.

VI-D Synchrotron Radiation Stimulated Surface Reactions

Study of synchrotron radiation (SR) stimulated surface reaction is a promising topic in fundamental science, because dynamical processes induced by the photostimulated core-electron excitations on surfaces are scarcely explored so far. This field is important also in applied science, since the fundamental study is expected to develop the new techniques for semiconductor processing such as SR stimulated etching and SR stimulated epitaxial growth.

VI-D-1 *In Situ* Detection of Surface SiH_n in Synchrotron-Radiation-Induced Chemical Vapor Deposition of a-Si on a SiO_2 Substrate

A. YOSHIGOE, M. NAGASONO, K. MASE, S. SEKI* *(*Takushoku Univ.)*, Y. NAKAGAWA** *(**Toray Research Center, Inc.)* and Tsuneo URISU

[*J. Synchrotron Rad.*, 2, 196 (1995)]

The sensitivity and linearity of infrared reflection absorption spectroscopy (IRAS) has been significantly improved by using a buried-metal-layer (BML) substrate having a SiO_2 (15nm)/Al(200 nm)/Si(100) structure, instead of a plain Si(100) substrate. By applying this BML-IRAS technique to the *in situ* observation of synchrotron-radiation-induced a-Si chemical vapor deposition on a SiO_2 surface using Si_2H_6 gas, the vibrational spectra of surface SiH_n species in this reaction system have been observed for the first time with sufficient sensitivity for a submonolayer coverage (Figure 1). The main silicon hydride species after deposition at 423 K are surface SiH_2 and SiH. Surface SiH_3 and SiH_2 are observed to be easily decomposed by synchrotron radiation irradiation. The decomposition rate of SiH by synchrotron radiation irradiation is much slower than those of SiH_2 and SiH_3.

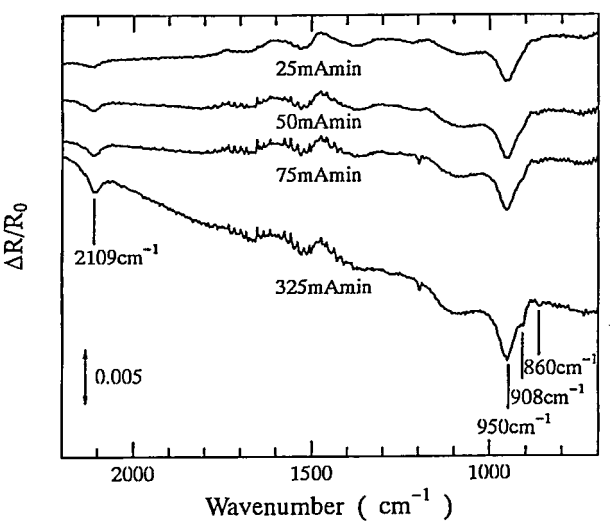

Figure 1. The IRAS spectra of the *in situ* observation with the a-Si deposited on the SiO_2 BML substrate by synchrotron radiation-CVD. The dose (synchrotron radiation beam current × irradiation time) dependence is shown. The substrate temperature was 423 K. The Si_2H_6 gas pressure was 1.0×10^{-3} Torr.

VI-D-2 Infrared Reflection Absorption Spectra for Trimethyl Aluminum and Dimethyl Aluminum Hydride Condensed Layer on SiO_2 Surface with Buried Metal Layer

Yoshiaki IMAIZUMI, Yoshiyuki TSUSAKA and Tsuneo URISU

[*Journal of Molecular Structure*, 352/353, 447 (1995)]

The infrared reflection absorption spectra (IRAS) of trimethyl aluminum (TMA) and dimethyl aluminum hy-

dride (DMAH) layer condensed on an SiO_2 surface were measured by using a buried metal layer (BML) substrate. TMA was a dimer at the experimental temperature range of 110 K < T < 160 K. The molecular orientation varied depending on the deposition temperature. The condensed layer of DMAH as-deposited at the temperature ranging from 110 to 130 K was a mixture of trimers and dimers (Figure 1(a)). A dimer changed to a trimer as the temperature increased, practically disappearing above 130 K (Figure 1(c)). This temperature dependence was not reversible. The trimer did not change to a dimer below 130 K (Figure 1(d)). The ordered orientation of the trimer molecules was a stable DMAH condensed layer structure on the SiO_2 surface. The usefulness of BML-IRAS for a study of the structure and molecular orientation of the adsorbed layers on the semiconductor materials is discussed.

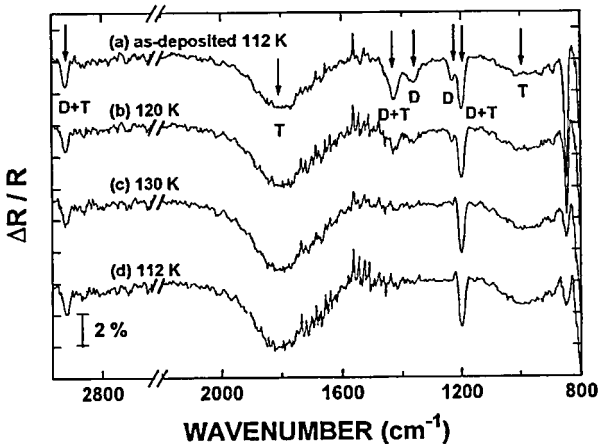

Figure 1. Observed IRAS spectra of DMAH : (a) as-deposited at the substrate temperature of 112 K and 30 L dose, (b) the temperature was then increased to 120 K, (c) then to 130 K and (d) then cooled to 112 K. The assignments of the observed vibrational peaks are; Al-H asymmetric stretching of trimer at 1800 cm^{-1}, Al-H symmetric bending of trimer at 979 cm^{-1}, CH_3 asymmetric bending of dimer and trimer at 1435 cm^{-1}, Al-H asymmetric stretching of dimer at 1362 cm^{-1}, Al-H symmetric stretching of dimer at 1224 cm^{-1}, CH_3 symmetric bending of trimer and dimer bands at 1200 cm^{-1} and CH_3 asymmetric stretching of trimer and dimer bands at 2946 cm^{-1}.

VI-D-3 Design of Double Multilayer Monochromator for Surface Photochemical Reactions Induced by Synchrotron Radiation

Yoshiyuki TSUSAKA, Yoshiaki IMAIZUMU, Tsuneo URISU, Atsunari HIRAYA, Masao KAMADA, Toyohiko KINOSHITA and Eiken NAKAMURA

Double multilayer monochromator have been designed at BL4A of the UVSOR, where a strong photon flux is to be delivered to experiments of photo-chemical reactions. The experimental station on the BL4A is schematically shown in figure 1. The SR beam with a divergence angle of 16 mrad in the horizontal direction is focused to STM chamber by elliptically bent cylindrical mirror. Mo/Si, Mo/C, Ni/Ti and W/Si multilayers with d spacing between 40-125 Å cover the photon energy range of 50-100, 80-200, 180-400 and 350-800 eV, respectively, with high reflectivity and the energy resolution of about 10. In order to obtain monochromatic X-rays, the low and high energy contaminated X-rays, which are caused by total reflection and second harmonic, suppressed by carbon and metal filters of 500-2000 Å thickness. With above design parameters, intensity of 5 x 10^{14} photons/sec at 80 eV is estimated.

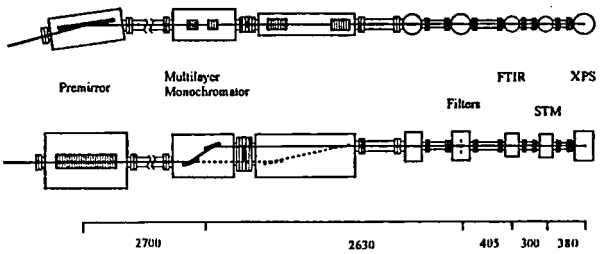

Figure 1. Schematic view of new BL4A.

VI-D-4 Development of Electron-Ion Coincidence Spectroscopy for Study of Surface Dynamics

Kazuhiko MASE, Mitsuru NAGASONO and Tsuneo URISU

[*Bull. Chem. Soc. Jpn.*, submitted]

Electron-ion coincidence spectroscopy for surface dynamics study is developed (Figure 1). The equipment consists of an electron gun, a cylindrical mirror analyzer (CMA) and a time-of-flight ion mass analyzer (TOF-MS). A sample surface is excited with electron beam and energy of emitted electrons is analyzed by CMA. TOF spectra of desorbed ions are measured with a multichannel scaler taking the energy-analyzed electron signal as the starting trigger. Ions coincidentally desorbed with the electron give a characteristic peak in the TOF spectrum. The apparatus is evaluated on the basis of Auger electron-ion coincidence measurements for $F/SrTiO_3(100)$ and $H_2O/SiO_2/Si(111)$ surfaces.

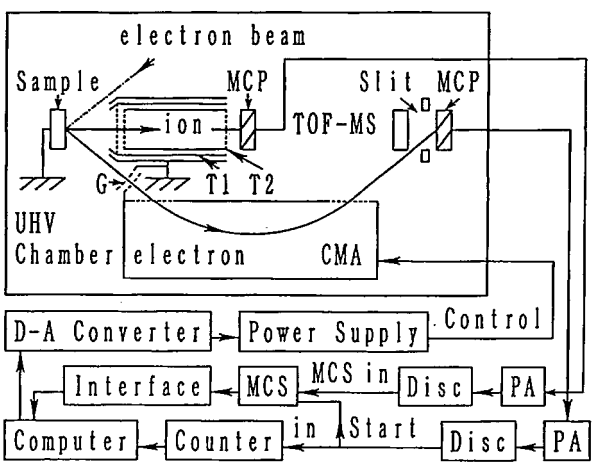

Figure 1. Schematic diagram of the apparatus for electron-ion coincidence spectroscopy. The abbreviations used are as follows: PA, preamplifier; Disc, discriminator; T1, drift tube with an extraction grid; T2, 35-mm-drift tube; G, retarding grids.

VI-D-5 Auger Electron-Ion Coincidence Study for H_2O Condenced on $SiO_2/Si(111)$

Mitsuru NAGASONO, Kazuhiko MASE and Tsuneo URISU

[*Surf. Sci.*, in *press*]

Electron stimulated ion desorption induced by core level excitations is studied for H_2O condensed on a SiO_2/Si(111) surface at 80 K (H_2O/ SiO_2/Si(111)) by using Auger electron-ion coincidence spectroscopy. The coincidence H^+ yield from the $H_2O/SiO_2/Si(111)$ is found to be enhanced at the electron kinetic energies corresponding to O(KVV) Auger transitions (Figure 1). This result presents a direct and clear evidence of Auger stimulated ion desorption mechanism accompanied by the cleavage of a covalent bond. A $KV_{NB}V_{NB}$ Auger process is concluded to lead to ion desorption less efficiently than KV_BV_{NB} and KV_BV_B processes (V_{NB} and V_B represent the non-bonding and bonding valence orbitals, respectively).

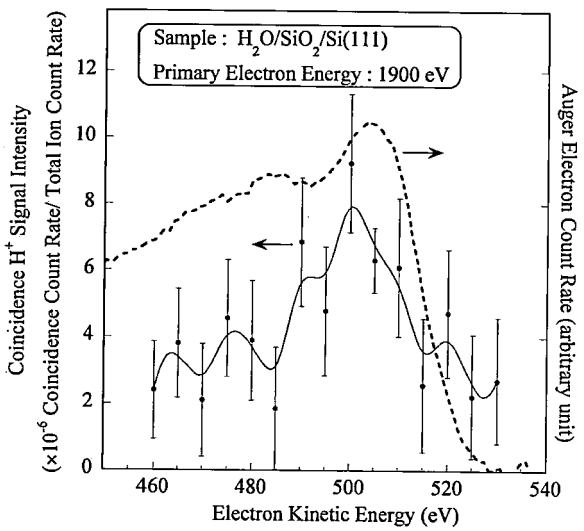

Figure 1. Auger electron-ion coincidence signals (closed circles) and the smoothed spectrum (solid line). The coincidence H^+ signals are the raw coincidence count rate normalized to the total ion count rate. Typical fluctuation of the coincidence intensities is 1.9×10^{-6} at 1 s error level. For a comparison the O(KVV) Auger electron spectrum (broken line) under the same extraction voltage is shown, where the background due to the energy loss of the primary electron is subtracted. Each channel is measured for 3 seconds at the step of 0.5 eV.

VI-D-6 Synchrotron Radiation Assisted Surface Processes of Diethylzinc on GaAs(100)

Syed Irfan GHEYAS*, Toshihiro OGATA*, Mitsuhiro NISHIO*, Tsuneo URISU and Hiroshi OGAWA* *(*Saga Univ.)*

The effect of sapphire window transmitted synchrotron radiation (longer than 150 nm photons) and white light synchrotron radiation (SR) on diethylzinc (DEZn), adsorbed on GaAs(100) at various temperatures, was investigated *in situ* using x-ray photoelectron spectroscopy. Light longer than 150 nm seems to have little impact on the adsorbed state whereas white light SR decomposes DEZn effectively, with the quantum yield for dissociation for adlayer thickness of around 3 nm to be roughly about 8.5×10^{-3} per shorter than 150 nm photon. Dissociation of DEZn seems to trigger formation of clusters or islands of metallic zinc. At 115 K, we have found that carbons and/or hydrocarbons desorb during white light SR assisted dissociation and the desorption stops once dissociation gets completed. In the process carbon decreases by approximately 40% and not more than that no matter how much excess photons are used on top of what is necessary for the scission of all the Zn-C bonds. The surface becomes carbon free once it is heated up to about 560 K. White light SR irradiation of DEZn at 300 K, on the other hand, helps in to desorb all carbon species leaving a clean Zn coverage over the GaAs(100) surface.

VI-D-7 Adsorption and Thermal Decomposition of Diethyltellurium on GaAs(100)

Syed Irfan GHEYAS*, Mitsuhiro NISHIO*, Tsuneo URISU and Hiroshi OGAWA* *(*Saga Univ.)*

Adsorption and thermal decomposition of diethyltellurium (DETe) on GaAs(100) have been studied using *in situ* x-ray photoelectron spectroscopy (XPS) and temperature programmed desorption (TPD) techniques. Multilayer adsorption of DETe is achievable at 130 K but adlayer thickness saturates at a little over one monolayer at 310 K. DETe is primarily found to adsorb molecularly at 130 K for multilayer coverage. By 150 K the physisorbed layers of DETe desorb leaving only the chemisorbed metalalkyl on the surface. This metalalkyl dissociates before 200 K producing adsorbed tellurium (Te) atoms which in turn interact rather heavily with the surface gallium atoms. Carbons/hydrocarbons resulting from DETe dissociation desorb from the surface by 300 K. Te atoms, on the other hand, remain firmly attached to the surface well after 600 K.

VI-E Photoionization Dynamics Studied by Electron Spectroscopy Combined with a Continuous Synchrotron Radiation Source

Molecular photoionization is a major phenomenon in vacuum UV excitation and provides a large amount of information on fundamental electron-core interactions in molecules. Especially, autoionizing and shape resonances become of main interest, since they often dominate photoabsorption cross sections and lead to various vibronic states which are inaccessible in direct ionization. In order to elucidate dynamical aspects of photoionization, we have developed a versatile machine for photoelectron spectroscopy. This year, introduction of a new methodology, two-dimensional photoelectron spectroscopy, allows us to investigate autoionization and predissociation of superexcited states of acetylene and nitric oxide. In this method, the photoelectron yield is measured as a function of both photon energy and electron kinetic energy (binding energy). The spectrum, usually represented as a contour plot, contains rich information on photoionization dynamics.

VI-E-1 Autoionizing Resonance in Photoionization from the $1\pi_u$ Level of Acetylene

Koichiro MITSUKE and Hideo HATTORI

[*J.Chem.Phys.* **102**, 5288 (1995)]

Autoionizing resonance of acetylene is studied by photoelectron spectroscopy using synchrotron radiation. Pronounced vibrational excitation in the C-H stretching mode ν_1 is observed in the $(1\pi_u)^{-1}X\,^2\Pi_u$ band of $C_2H_2^+$ at a restricted photon energy range from 12.8 to 14.1eV. It is concluded that the $3\sigma_g \rightarrow 3\sigma_u$ autoionizing transition at ~13.3eV gives rise to an anomalously broad maximum in the $(1\pi_u)^{-1}$ photoionization cross section curve. The strong ν_1 excitation is explained as that the equilibrium C-H bond length differs from the neutral and ionic ground states to the $(3\sigma_g)^{-1}(3\sigma_u)^1$ resonance state. Constant ionic state spectra for the ν_1=3 and 4 levels of the $X\,^2\Pi_u$ state measured over the same energy region show fine structures with regular spacings which correspond to the vibrational levels of the $(3\sigma_g)^{-1}(3\sigma_u)^1$ state.

VI-E-2 Autoionization of Acetylene Studied by Two-Dimensional Photoelectron Spectroscopy

Hideo HATTORI and Koichiro MITSUKE

[*J. Electron Spectrosc. Relat. Phenom.,* in press]

A two-dimensional photoelectron spectrum of acetylene is measured by using monochromatized synchrotron radiation as shown in Figure 1. Extensive vibrational excitation in the C-H stretching mode ν_1 of $C_2H_2^+$ ($X\,^2\Pi_u$) is observed over a photon energy region from 13.0 to 14.1eV, which is due to autoionization of a valence state $(3\sigma_g)^{-1}$ $(3\sigma_u)^1$. Constant ionic state spectra for the (ν_1',ν_2')=(3,0), (3,1), (4,0) and (4,1) vibrational levels of $C_2H_2^+(X\,^2\Pi_u)$ show two progressions originating from the ν_1 motion in the $(3\sigma_g)^{-1}(3\sigma_u)^1$ state. It is likely that an autoionization lifetime of the valence state is comparable to vibrational periods of the ν_1 and ν_2 modes.

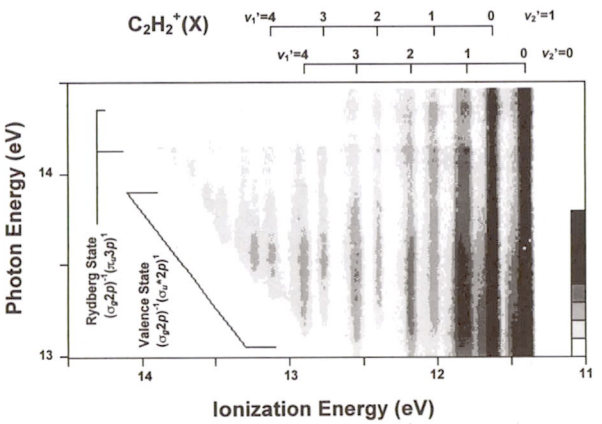

Figure 1. Two-dimensional photoelectron spectrum of C_2H_2 taken at the photon energy range from 13.0 to 14.45 eV. Electron yields are presented by the plots with eight tones from light to dark on a logarithmic scale.

VI-E-3 Autoionization of NO in an Excited Valence State Affected by Perturbations of Valence-Rydberg Mixing

Yasumasa HIKOSAKA*, Hideo HATTORI, Takumi HIKIDA* and Koichiro MITSUKE *(*Tokyo Inst. of Tech.)*

[*J. Electron Spectrosc. Relat. Phenom.*, in press]

A superexcited state of nitric oxide lying in the 11-13 eV excitation energy range is studied by photoelectron and photoionization spectroscopy. The photoelectron spectra from 11.4-13 eV show several minima in their vibrational distribution. The number of the minimum positions increases monotonically with the photon energy. This trend is simulated by Franck-Condon analysis assuming the presence of a superexcited state NO*. The photoionization efficiency curve contains a number of irregularly spaced peaks resulting from autoionization of NO*. The complexity of the spectrum is understood as that vibrational levels of NO* are substantially perturbed by the Rydberg states converging to $NO^+(X\,^1\Sigma^+)$. Each zero-order vibrational level of NO* is placed at the center of a group of peaks which arise from interaction between the level of NO* and several levels of perturbing Rydberg states. This assumption permits us to determine a functional shape of the potential energy curve of NO*. The transition frequency from $NO(X\,^2\Pi, v_g=0)$ to $NO^*(v_d=0)$ is estimated to be ν_{00}=88410cm^{-1} and the vibrational coefficients to ω_e =2060cm^{-1} and x_e=0.0094. The equilibrium bond length r_e is then determined by simulating the photoelectron spectra through the Franck-Condon analysis, using the above values of ω_e and x_e. The simulation at r_e=1.29Å is in the best agreement with the experimental spectra. The potential energy curve of NO* thus obtained is found to undergo pseudocrossing on its attractive branch with curves of several Rydberg states converging to $NO^+(X\,^1\Sigma^+)$. These potential relations are consistent well with the strong valence-Rydberg mixing.

VI-E-4 Autoionization of Nitrogen Atoms Produced by Dissociation of Superexcited NO Moleules

Yasumasa HIKOSAKA*, Hideo HATTORI, Takumi HIKIDA* and Koichiro MITSUKE *(*Tokyo Inst. of Tech.)*

Photodissociation of nitric oxide followed by autoionization of an atomic fragment is studied by two-dimensional photoelectron spectroscopy using synchrotron radiation. Figure 1 shows a spectrum in the energy range from 20 to 27.4 eV. The ordinate is the photon energy and the abscissa the kinetic energy of the ejected electron. Diagonal stripes varying in width from several tens to a few hundreds millielectron volts on this spectrum correspond to direct ionization continua of vibronic states of NO^+. If an autoionizing transition of atomic fragments takes place between two particular states, one may expect that emission of electrons with a constant kinetic energy results in a pattern running parallel to the photon energy axis. Actually, five or more patterns due to this mechanism are observed at photon energies around 22.5-26 eV. They are assigned to resulting from autoionization of the Rydberg states converging to $N^+(^1D)$ into the ground state $N^+(^3P)$. The solid lines in Figure 1 represent the dissociation limits of NO for the formation of $N^+(^3P)$+$O(^3P)$ or $N^+(^3P)$+$O(^1D)$ as a function of the energy of the ejected electron. The above patterns show apparent steplike structure in their intensity near the limit for $N^+(^3P)$+$O(^1D)$ and seem to persist throughout the region between the two dissociation limits. The following mechanism can there-

fore be proposed: (1) dissociation of Rydberg states converging to an NO^+ state which correlates to $N^+(^1D)+O(^3P)$ or $N^+(^1D)+O(^1D)$ and (2) subsequent autoionization of the formed atomic Rydberg states into $N^+(^3P)$.

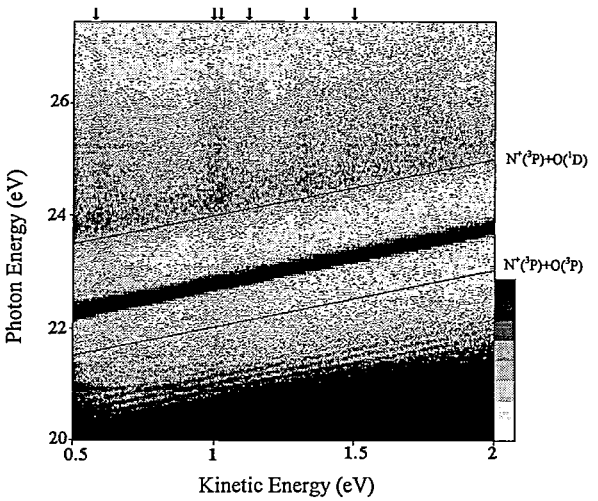

Figure 1. Two-dimensional photoelectron spectrum of NO. The Electron intensity is shown increasing from light to dark on a linear scale. The solid lines represent the dissociation limits of O for $N^+(^3P)+O(^3P)$ or $N^+(^3P)+O(^1D)$ channels and the arrows indicate the bands resulting from autoionization of atomic Rydberg states converging to $N^+(^1D)$.

VI-F Rebuilding the Monochromator on the Beam Line BL2B2 in UVSOR

On the beam line BL2B2, we are planning to construct a grazing incidence monochromator which supplies photons in the energy region from 20 to 200eV. This monochromator will bridge the energy gap between the beam lines BL3A2 and BL8B1, thus providing for an accelerating demand for the high-resolution and high-flux photon beam from the research field of photoexcitation of inner-valence electrons or *L*-shell electrons in the second-row atom.

VI-F-1 Tentative Design of an 18m Spherical Grating Monochromator

Hiroaki YOSHIDA and Koichiro MITSUKE

An 18m spherical grating monochromator (SGM) with high resolution and high photon flux has been designed at the bending-magnet beam line BL2B2 in UVSOR for the study of ionization satellites and multiply-excited neutral states of molecules. A schematic layout of the monochromator is shown in Figure 1. The optical system consists of two prefocussing mirrors, a spherical grating monochromator with a movable exit slit and a refocussing mirror. The monochromator is designed to cover the energy range of 20-200 eV with three gratings: *G1* (2400 lines/mm, *R*=18m) at 80-200 eV, *G2* (1200 lines/mm, *R*=18m) at 40-100 eV and *G3* (2400 lines/mm, *R*=9.3m) at 20-50 eV. A wavelength scanning mechanism is very simple because movement of the gratings is confined only to mechanical rotation. The directions of incident and exit photon beams are fixed. To suppress the high-order light in the low energy range, we adopt (a) *G3* with a small including angle of 140° and (b) two Al-coated plane mirrors *M2* and *M3* as optical filters which are located between *G3* and the exit slit.

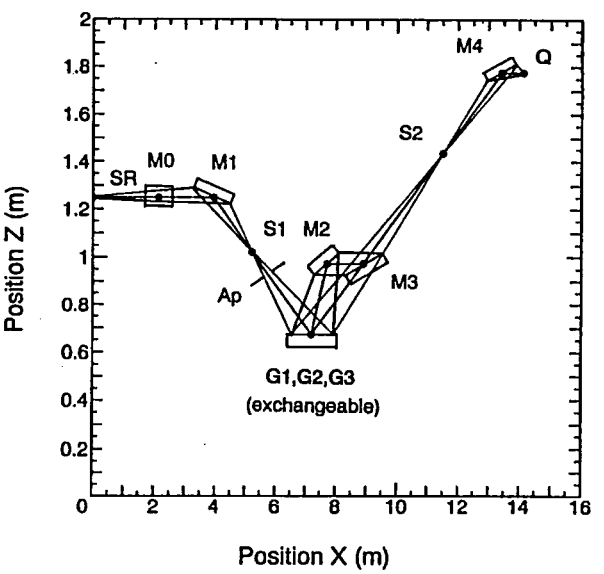

Figure 1. Schematic layout of the monochromator. Horizontal and vertical axes denote the distance from the synchrotron radiation source and the height from the floor, respectively. Two optical paths with including angles of 160° for *G1* and *G2* and 140° for *G3* are indicated. *SR*, synchrotron radiation source; *M0*, cylindrical mirror; *M1*, spherical mirror; *S1*, entrance slit; *Ap*, aperture; *G1-G3*, spherical gratings; *M2* and *M3*, plane mirrors; *S2*, exit slit; *M4*, toroidal mirror; *Q*, sample position.

VI-F-2 Evaluation of the Resolving Power and Photon Flux of the 18m SGM by Ray Tracing

Hiroaki YOSHIDA and Koichiro MITSUKE

A spherical grating monochromator (SGM) with a large radius of curvature is well known to have a resolving power higher than 10^4. However, it is difficult to achieve such a high resolving power because of a relatively large size of an electron beam (0.27 mmϕ) and a moderate emittance (1.15×10^{-8} πmrad) in the storage ring of UVSOR. We, therefore, plan to set a resolving power of 5×10^3 in a standard operation. This performance requires the following conditions: a movable exit slit can be made to set at the focal distance of the dispersed light; the widths of entrance and exit slits are adjustable to decrease the aberration; and coma aberration at the exit slit can be reduced by shutting off a diverged light using an aperture. Figure 1 shows image patterns at the exit slit obtained by ray tracing with photon wavelengths of (a) 60 and 60±0.012 Å for *G1*, (b) 180 and 180±0.036 Å for *G2* and (c) 600 and 600±0.12 Å for *G3*. The exit slit is placed at the focal distances for the respective gratings. The widths of the exit slit corresponding to an expected resolving power of 5×10^3 are also indicated with pairs of horizontal lines. In every case, the central wavelength is well resolved from two neighboring wavelengths. Hence, we conclude that this monochromator provides the expected resolving power as far as other factors, such as a shape error of a grating, are ignored. The photon flux with this resolving power is evaluated to be about 1×10^{11} photons/s/100mA/0.1%BW.

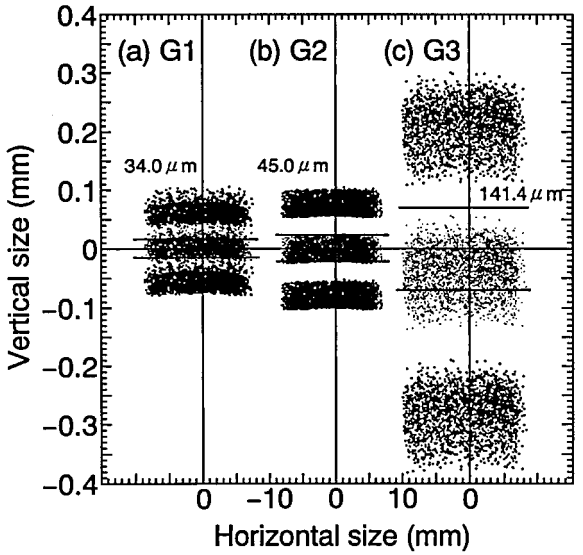

Figure 1. Image patterns at the exit slit obtained by ray tracing with photon wavelengths of (a) 60 and 60±0.012 Å for *G1*, (b) 180 and 180±0.036 Å for *G2* and (c) 600 and 600±0.12 Å for *G3*. Pairs of horizontal lines indicate the widths of the exit slit corresponding to a resolving power of 5×10^3.

VI-G Desorption Induced by Electronic Transitions on the Solid Surface of Condensed Gases

Photon-stimulated desorption (PSD) of molecules or ions from condensed gases is a direct probe of surface reactions induced by electronic excitation of absorbed molecules and diverse relaxation processes which subsequently occur. It is proposed by several authors that surface and bulk excitons play important roles in PSD of rare gas solids. We have measured angular and kinetic energy distributions of desorbed Ne metastable atoms from a Ne surface. We also obtain direct evidence on PSD of O^- ions from O_2 condensed on an Ar multilayer film. Using monochromatized synchrotron radiation enables us to discuss the detailed mechanism of excitation and decay of excitons.

VI-G-1 Angular and Kinetic Energy Distributions of the Desorption of Ne Metastable Induced by Excitons at the Surface of Solid Ne

Ichiro ARAKAWA*, Daniel E. WEIBEL*, Toshiki NAGAI*, Munehide ABO*, Takato HIRAYAMA*, Minoru KANNO, Koichiro MITSUKE and Makoto SAKURAI** *(*Gakushuin Univ., **Kobe Univ.)*

[*Nucl. Instrum. Meth. Phys. Res.* **B101**, 195 (1995)]

The origin of the Ne metastables desorbed by excitonic excitations was investigated. The measurement of the angular and kinetic energy distributions of Ne metastables and their excitation energy dependence revealed that there are, at least, five components desorbed through different desorption kinetics: excimer dissociation species from the higher-order exciton, cavity ejection from three kind of surface excitons and ejection of metastables from a bulk exciton in an underlying layer. The metastable desorbed through the cavity-ejection mechanism by the excitation of the first-order surface exciton showed a narrow angular distribution along the surface normal with an FWHM between 30° and 90°, which depends on the velocity of a desorbed Ne metastable.

VI-G-2 Photon Stimulated Desorption of O^- from O_2 Condensed on an Ar Film

Koichiro MITSUKE, Takato HIRAYAMA*, Toshiki NAGAI*, Munehide ABO*, Ichiro ARAKAWA* and Makoto SAKURAI** *(*Gakushuin Univ., **Kobe Univ.)*

We install a negative-ion detection system in an ultraviolet vacuum apparatus developed for studies on photon-stimulated desorption of metastable atoms. A sample is prepared by gas deposition of O_2 onto a thin Ar multilayer film which covers a Pt(111) substrate at a temperature of 6K. The Ar film is 30 atomic layers, while a coverage of O_2 is varied from 0.5 to 30 monolayers (ML). The monochromatized synchrotron radiation impinges onto the surface and desorbed O^- ions are detected by a microchannel plate detector placed on the axis of the surface normal. Mass separation is performed by using a conventional time-of-flight technique. The photon-wavelength dependence of the efficiency of O^- is measured as a function of the thickness of the O_2 layer. A broad peak with a maximum at about 21eV on the efficiency curve at 0.5ML is considered to originate from

dissociative attachment of photoelectrons emitted from the solid Ar through an $O_2^-(^2\Pi_u)$ resonance state. The peak position is shifted to higher photon energies with increasing coverage of O_2. This tendency can be accounted for by participation of another resonance state of $O_2^-(^2\Sigma_g^+)$ in dissociative electron attachment.

VI-H Elucidation of Ion-Solid Chemistry in Ion-Implanted Amorphous SiO_2 and Creation of Novel Materials by Implantation

A variety of structural defects are produced in amorphous SiO_2 and related materials by ion implantation. Characterization of structures, concentrations and depth profiles may provide valuable information on interactions of implanted ions with substrate structure. We consider that some defects may be the origin of new photonic functions such as refractive index gratings and second harmonic generations. In this sense, "defects" may be regarded as "active species" for optoelectronic applications. The purpose of this project is to elucidate chemical interactions of implanted ions with amorphous SiO_2 through structural defects and to create novel photonic materials utilizing activities to photons.

VI-H-1 Optical and Electrical Properties of Proton-Implanted Amorphous SiO_2, GeO_2-SiO_2, MgO-P_2O_5 and Nanocrystalline $MgIn_2O_4$: Novel Materials by Proton Implantation

Hideo HOSONO*, Naoyuki UEDA Hiroshi KAWAZOE and Noriaki MATSUNAMI** *(*Tokyo Inst. Tech., **Nagoya Univ.)*

[*J. Non-Cryst. Solids* **182**, 109 (1995)]

The optical and electrical properties of proton-implanted SiO_2, GeO_2-SiO_2, MgO-P_2O_5 glasses and nanocrystalline $MgIn_2O_4$(spinel-type structure) films were examined and several drastic changes in them were observed. The results obtained are summarized as follows. (1) Fast proton conduction(conductivity at 300 K = ~10^{-5} S cm^{-1}) was obtained in $Mg(PO_3)_2$ glasses implanted with H^+ ions to a fluence of 10^{18} cm^{-2}. (2) Nanocrystalline Ge colloid particles were created by implantation of H^+ ions into $1GeO_2$-$9SiO_2$ glasses without post heat treatment. (3) Electronic conductivities in $MgIn_2O_4$ sputter-deposited films at 300 K increased from 10^{-7} S cm^{-1} to 1.5×10^1 S cm^{-1} on implantation of H^+ to a fluence of 2×10^{16} cm^{-2}. (4) Peroxy radicals in SiO_2 glasses were created primarily by electronic excitation with 1.5 MeV H^+ ions.

VI-H-2 Chemical Interaction in Ion-Implanted Amorphous SiO_2 and Application to Formation and Modification of Nanosize Colloid Particles

Hideo HOSONO

[*J. Non-Cryst. Solids* **187**, 457 (1995)]

Ion-Solid Chemistry approached from structural defects produced by implantation is summarized for implanted amorphous SiO_2(a-SiO_2). The primary factor controlling the chemical interaction of implanted ions with substrate structure is the electronegative nature of implants. Implants with electropositive nature (M) pull oxygens out from the silica network structure to form M-O bonds, leaving Si-Si bonds at concentrations comparable to those of the implant,whereas implants (A) with electronegative nature react chemically with Si atoms to form Si-A bonds, forming O_2 molecules and peroxy radicals. Implants with weak chemical reactivity occur in a neutral state such as diatomic molecules and elementary colloids. The importance of Si-Si bonds as an active intermediate in dual implantation is stressed illustrating the formation of Si-N bonds. The effectiveness of ion implantation as a tool to fabricate nanosize colloids embedded in glass is demonstrated and a criterion of colloid formation in a-SiO_2 by implantation established. The morphology and optical absorptions of Cu colloid particles have been found to be modified by subsequent implantation of F ions and the mechanism is considered on the basis of ion-solid chemistry. Formation of and nature of nanosize colloids of a-phosphorus and a novel approach to synthesize Ge nanocrystals are briefly described.

VI-I Electronic Structure Design of Wide Gap Conductors and Control of Their Conduction Behavior

Electronic structure of highly oxidized p-block metal oxides is of interest from the view point of their variety of the optical and electrical properties. The oxides with band gaps near 3 eV are attractive because they have the specific properties of metallic conduction keeping the transparency to the visible light and have various application such as a transparent electrode of a liquid crystal display, a heat reflector glass, solar cell and so on. In this project, it is aimed to establish a basis of the material design of wide gap semiconductors and to create nobel materials. Ongoing study is characterization of the electronic structure of these materials by using synchrotron radiation, control of conduction behavior by ion-implantation and construction of the apparatus of inverse photoemission spectroscopy.

VI-I-1 Generation of Electron Carriers in Insulating Thin Film of $MgIn_2O_4$ Spinel by Li^+ Implantation

Hiroshi KAWAZOE, Naoyuki UEDA, H. UNNO*, Takahisa OMATA*, Hideo HOSONO* and H. TANOUE** *(*Tokyo Inst. Tech., **Electrotech. Lab.)*

[*J. Appl. Phys.* **76**, L7935 (1994)]

Li^+ implantation at room temperature of insulating thin films of polycrystalline $MgIn_2O_4$ spinel(~1.3 μm thick) was found to generate electron carriers efficiently. Li^+ ions were implanted at 80 keV to a fluence of 1×10^{16} cm^{-2} and subsequently at 160 keV to the same fluence. Some implanted films were subjected to a post-annealing at 300 °C. Depth profiles of implanted Li^+ ions measured with secondary-ion-mass spectroscopy agreed with that calculated with the TRIM code. Conductivity at room temperature increased from $\sigma<10^{-7}$ to ~10^1 S cm^{-1} upon the Li^+ implantation. The generation yield of electron carriers in the as-implanted film was 20% and increased up to ~40% upon post-annealing. Two optical-absorption bands were induced upon the implantation, one at about ~500 nm and another above ~1000 nm extending to the IR region, which was attributed to plasma oscillation of electron carriers. The former band faded and the latter absorption increased its intensity upon post-annealing. He^+ implantation, which was done for comparison, induced no change in electrical conductivity and no absorption band above ~1000 nm.

VI-I-2 Preparation of Electroconductive and Transparent Thin Films of $AgSbO_3$

Masahiro YASUKAWA*, Hideo HOSONO, Naoyuki UEDA and Hiroshi KAWAZOE* *(*Tokyo Inst. Tech.)*

[*J. Ceram.Soc. Jpn.* **103,** 455 (1995)]

Sintered ceramics and RF-sputter deposited thin films of $AgSbO_3$ with defect pyrochlore structure were prepared and their electrical conductivities and optical properties were measured. Sintered ceramics of $AgSbO_3$ showed n-type electric conduction with a conductivity of ~2×10^{-1} $\Omega^{-1}\cdot cm^{-1}$ and the cut off wavelength of ~400 nm for optical transmittance at room temperature. Polycrystalline thin films obtained by post-annealing at 675°C in O_2 gas flow also showed n-type conduction with a conductivity of ~10^0 $\Omega^{-1}\cdot cm^{-1}$ at room temperature. The optical transmission spectrum of the film with the thickness of ~200 nm showed the optical transmittance of ~80% at a wavelength of 400 nm. The carrier concentration and the Hall mobility of the polycrystalline film were ~3×10^{18} cm^{-3} and ~8 $cm^2\cdot V^{-1}\cdot s^{-1}$, respectively.

VI-I-3 Novel Transparent and Electroconductive Amorphous Semiconductor: Amorphous $AgSbO_3$ Film

Masahiro YASUKAWA*, Hideo HOSONO*, Naoyuki UEDA and Hiroshi KAWAZOE *(*Tokyo Inst. Tech.)*

[*Jpn. J. Appl. Phys.* **34,** L281 (1995)]

Amorphous $AgSbO_3$ films prepared by RF sputtering under O_2 gas Plasma and by subsequent post annealing at 500°C in O_2 gas flow were found to be novel transparent and electroconductive amorphous semiconductors. The optical band gap of the films was ~2.3 eV. The electrical conductivity was ~10^{-1} $\Omega^{-1}\cdot cm^{-1}$ at room temperature and its temperature dependence showed thermal activation-type behavior with an activation energy of ~0.23 eV. Hall measurements indicated n-type conduction. Concentration of carrier electrons and the Hall mobility at room temperature of the sample were ~3×10^{17} cm^{-3} and ~7 $cm^2\cdot V^{-1}\cdot s^{-1}$, respectively. The value of the mobility was close to that of the polycrystalline films(~$8cm^2\cdot V^{-1}\cdot s^{-1}$).

VI-I-4 Photoemission Studies on Valence Band Structure of $AgSbO_3$

Masahiro YASUKAWA*, Hideo HOSONO*, Naoyuki UEDA and Hiroshi KAWAZOE *(*Tokyo Inst. Tech.)*

[*Solid State Commun.* **95,** 399 (1995)]

Valence band structure of sintered $AgSbO_3$ with defect pyrochlore structure was examined using ultraviolet photoemission spectroscopy(UPS). The upper valence band has a structure with peaks at the binding energies of 2.5eV, 3.5eV, 5.5eV and 7.5eV. Constant initial state(CIS) spectra measured on these peaks demonstrated that the upper valence bands are mainly composed of the mixture of occupied O 2p and Ag 4d orbitals. Even the top of Valence band with the peak at 2.5eV includes a signiifficant amount of Ag 4d component. The present result suggests that this material is a good candidate as a novel wide gap and p-type conductive oxide.

VI-J Absolute Photoabsorption Cross Section and Breakdown Pathways of Molecules Containing *d*-Electrons

This project has been carried out in collaboration with The University of British Columbia (UBC) in Canada. Total photoabsorption cross sections of molecules in the wide energy range of 5-450 eV have been measured by using dipole (e, e) spectroscopy at UBC. Breakdown pathways of the multiply charged ion have been measured at the beamline BL3A2 of the UVSOR facility. We have investigated BrCN molecule and the next target is ICN.

VI-J-1 Absolute Photoabsorption of BrCN in the Valence Shell and the Bromine M, Carbon K and Nitrogen K Shell Regions (5-450 eV)

Terry N. OLNEY,* C. E. BRION* and Toshio IBUKI *(*Univ. British Columbia)*

Absolute oscillator strengths (cross sections) for photoabsorption by BrCN have been measured throughout the VUV and soft X-ray regions (5-450 eV) using dipole (e, e) spectroscopy at both high (0.05-0.10 eV fwhm) and low (1 eV fwhm) resolution. Measurement of the valence shell oscillator strengths are compared with the very limited direct optical data in the literature. For the sharper (Rydberg) bands the presently determined dipole (e, e) oscillator strengths are considerably larger indicating that significant line saturation (bandwidth) errors are occurring in the previously published direct optical (Beer-

Lambert law) measurements. The first absolute measurements and inner shell photoabsorption spectra are reported in the carbon K (1s), nitrogen K (1s) and bromine M (3d, 3p and 3s) regions of BrCN. The carbon and nitrogen 1s spectra show vibrational resolution in the respective, strongly resonance enhanced, $3\pi(\pi^*)\leftarrow 1s$ bands. The Br 3d spectra of BrCN show clear evidence of ligand field splitting in the $3d_{5/2}$(δ, π and σ) and $3d_{3/2}$(δ and π) excitations to the 5p Rydberg states. The first estimates of the inner shell ionization potentials for the C 1s and N 1s core orbitals of BrCN are obtained from density functional theory calculations. The Br $3d_{5/2,3/2}$ ligand field split inner shell ionization energies are estimated using the 5$p\leftarrow$Br 3d excitation energies and considerations of the (transferable) 5p Rydberg term values from the C 1s, N 1s and valence shell spectra.

VI-J-2 Ionic Photofragmentation (11.5-100 eV) and PIPICO Spectroscopy (40-130 eV) of BrCN in the Valence Shell and Bromine 3d Regions

Toshio IBUKI, Atsunari HIRAYA, Terry N. OLNEY* and C. E. BRION* *(* Univ. British Columbia)*

Molecular and dissociative photoionization branching ratios and photofragment appearance potentials of BrCN have been determined using dipole (e, e+ion) spectroscopy at equivalent photon energies from the first ionization threshold up to 100 eV. Absolute partial photoionization oscillator strengths (cross sections) for the molecular and dissociative photoions have been obtained from the triplet product of the photofragment branching ratio, the photoionization efficiency and previously reported absolute photoabsorption oscillator strengths. Information on the Coulomb explosion decay channels of doubly and triply charged molecular ions has been obtained from photoion-photoion coincidence (PIPICO) spectroscopy using synchrotron radiation as a light source in the 40-130 eV photon energy range. While stable doubly charged ions are observed in both the valence and the Br 3d regions no stable triply charged ions are observed. However, the PIPICO measurements detect time correlated singly and doubly charged fragment species resulting from Coulomb explosion of triply charged ions which are first formed at the Br 3d excitation threshold and throughout the ionization continuum by triple autoionization and double Auger type processes. The experimental results provide information on the dipole induced breakdown pathways resulting from valence shell and Br 3d ionization processes in BrCN.

VI-K Electronic States and Dissociative Channels of Valence Shell Excited Molecules

The greater part of photoabsorption cross section of molecule is distributed above 10 eV, in which the Rydberg, superexcited and ionized states lie. Photoabsorption cross section and radiative dissociation processes of electronically excited molecule have been measured in the 6-30 eV region using synchrotron radiation as a light source.

VI-K-1 Radiative Dissociation of C_2H_2, C_2HD and C_2D_2 Superexcited at 50-90 nm Region

Toshio IBUKI, Yasuhiko HORIE,[a] Akira KAMIUCHI,[a] Yoshikazu MORIMOTO,[b] Marcia C. K. TINNONE,[c] Kenichiro TANAKA[d] and Kenji HONMA[e] *([a]Kyoto Univ. Educ., [b]Univ. Tokyo, [c]The Graduate Univ. Adv. Studies, [d]Hiroshima Univ., [e]Himeji Inst. Tech.)*

[*J. Chem. Phys.* **102**, 5301 (1995)]

Radiative dissociation of superexcited acetylene was studied at $h\nu$=13.8-24.8 eV (90-50 nm) by using C_2H_2, C_2HD and C_2D_2. The observed emission bands were $d\ ^3\Pi_g \rightarrow a\ ^3\Pi_u$, $e\ ^3\Pi_g \rightarrow a\ ^3\Pi_u$, $C\ ^1\Pi_g \rightarrow A\ ^1\Pi_u$ and $D\ ^1\Sigma_u^+ \rightarrow X\ ^1\Sigma_g^-$ of C_2 radical and $A\ ^2\Delta \rightarrow X\ ^2\Pi_r$, $B\ ^2\Sigma^- \rightarrow X\ ^2\Pi_r$ and $C\ ^2\Sigma^+ \rightarrow X\ ^2\Pi_r$ of CH and CD radicals. The fluorescence cross sections of the electronically excited C2* radicals showed a hydrogen isotope effect, i.e., the cross sections were in order of $\sigma_f[C_2(C_2H_2)] > \sigma_f[C_2(C_2HD)] > \sigma_f[C_2(C_2D_2)]$. Reverse is true for the fluorescence cross sections of CH* and CD*, i.e., $\sigma_f(C_2H_2) < \sigma_f(C_2HD) < \sigma_f(C_2D_2)$. These isotope effects were interpreted by the competition of some decay processes from the superexcited states. Hydrogen isotope effect in simple C-H and C-D bond dissociation important for the C_2* formation. As a result of the competition with this C_2* formation, the "reverse" isotope effect emerges in the CH* and CD* formation. Another important competing process is the isomerization followed by formation of nonradiative fragments. Since H atom migrates more easily than D atom through a cyclic activated complex and the nonradiative fragmentation competes with the CH* and CD* formation, the radiative intensities of the CH* and CD* radicals inevitably show the apparent inverse hydrogen isotope effect. The isomerization seems specially important in the wavelength region λ>80 nm, where a *trans*-bent superexcited state is formed.

VI-K-2 Photoabsorption and Fluorescence Cross Sections of $SiCl_4$ in the Region of 6.2-31 eV

Toshio IBUKI, Atsunari HIRAYA, Mitsuhiko KONO and Kosuke SHOBATAKE[a] *([a] Nagoya Univ. and IMS)*

Photoabsorption cross section of gaseous $SiCl_4$ has been measured in the energy region of 6.2-31 eV using synchrotron radiation as a light source. The higher order light from a 1-m Seya monochormator has been filtered by use of an argon gas in the region 11.3-15.5 eV (110-80 nm) an a LiF window at $h\nu$<11.8 eV (105 nm). Radiative processes have been observed for the $\tilde{C}^2T_2 \rightarrow \tilde{A}^2T_2$ and $\tilde{C}^2T_2 \rightarrow \tilde{X}^2T_1$ transitions of $SiCl_4^+$ molecular ion and $\tilde{A}^1B_1 \rightarrow \tilde{X}^1A_1$ and $\tilde{a}^3B_1 \rightarrow \tilde{X}^1A_1$ of $SiCl_2$ radical. Total emission cross section has been determined to be 2.4± 1.0 Mb at 21.22 eV. By comparing with the partial formation cross section of the $\tilde{C}^2T_2$ ionic state [Carlson et al, *J. Chem. Phys.* **84**, 641 (1986)], it has been concluded that

formed $SiCl_4^+(\tilde{C})$ decays through radiative processes with the quantum yield ϕ=1. The bands observed in photoabsorption and fluorescence excitation spectra have been assigned as the Rydberg transitions. The series converging to 14.70±0.03 eV has been first observed and assigned as the excitation to the nd(n>4)←$2t_2$ Rydberg levels. The Rydberg series of (4*s* and n*p*)←$3t_2$, (4*s* and n*p*)←1*e* *and* (n*p* and n*d*)←$2a_1$ have also been assigned.

VI-L Growth and Characterization of II-VI Compound Semiconductor Thin Film Using Metalorganic Sources

Epitaxial growth at low temperature is essential to control the electrical and optical properties of the layer in the fields of II-VI materials. We believe that photon-assisted growth using metalorganic sources is useful as a low temperature growth technique of these materials. Especially, we consider that a use of synchrotron radiation as a light source for the growth is valuable for the low temperature growth. We have investigated the growth characteristics and the characterization of the grown layer in order to clarify the growth process in the photon-assisted growth.

VI-L-1 Phown by Photo-Assisted Metalorganic Vapor Phase Epitaxy

Syed Irfan GHEYAS*, Makoto IKEJIRI*, Toshihiro OGATA*, Hiroshi OGAWA* and Mitsuhiro NISHIO *(*Saga Univ.)*

[*J. Crystal Growth* **145**, 576 (1994)]

Effects of light illumination on the photoluminescence properties of ZnTe has been investigated by using epitaxial layers grown with different carrier gases, transport rate of source materials and light sources or by introducing triethylaluminum as a dopant. Free exciton emission can be observed in only the epitaxial layers grown with illumination under H_2 atmosphere, implying that the illumination is effective for the growth of good quality ZnTe layers. The illumination strengthens the transition due to excitons bound to donor impurities, namely Cl which is substituted into Te lattice site, at low substrate temperature. These effects are closely related to the use of photons having an energy higher than the bandgap of ZnTe. It seems that the photo-assisted metalorganic vapor phase epitaxy technique also brings about the effective formation of Al donor by suppressing the generation of the complex of Al and Zn-vacancy in the ZnTe epitaxial layer.

VI-L-2 Synchrotron Radiation Excited Growth of ZnTe Using Metalorganic Sources

Toshihiro OGATA*, Syed Irfan GHEYAS*, Makoto IKEJIRI*, Hiroshi OGAWA* and Mitsuhiro NISHIO *(*Saga Univ.)*

[*J. Crystal Growth* **146**, 587 (1995)]

The photon-excited growth of ZnTe on the (100) GaAs substrate has been studied at a very low pressure of 10^{-5}Torr using synchrotron radiation as a light source. Diethylzinc and diethyltelluride were used as source materials, while hydrogen was employed as a carrier gas. The epitaxial layer of ZnTe can be obtained even at room temperature. It is expected that the surface excitation plays an important role in the growth, whereas thermal or gas phase excitation does not contribute. The quantum yield for forming ZnTe molecules by photons is estimated to be higher than 0.7%.

VI-L-3 Construction of a System for Novel Low-Temperature Growth of II-VI Compound Semiconductors Using Synchrotron Radiation

Toshihiro OGATA*, Makoto IKEJIRI*, Syed Irfan GHEYAS*, Hiroshi OGAWA* and Mitsuhiro NISHIO *(*Saga Univ.)*

[*Rev. Sci. Instrum.* **66**, 1086 (1995)]

As a novel application of synchrotron radiation, we describe a growth technique for the II-VI compound semiconductors. A growth system suitable for synchrotron-radiation excited deposition has been designed and constructed in the beam line BL4A at the UVSOR facility. Characteristics of this growth system and experimental results with respect to ZnTe as an example are described. It has been confirmed by using the system constructed that this method is useful as a low-temperature growth technique of II-VI compounds.

VI-L-4 Synchrotron-Radiation-Excited Growth of ZnTe by Alternating Gas Supply Using Metalorganic Sources

Toshihiro OGATA*, Syed Irfan GHEYAS*, Hiroshi OGAWA* and Mitsuhiro NISHIO *(*Saga Univ.)*

[*Jpn. J. Appl. Phys.* **34**, L841 (1995)]

Crystal growth of ZnTe has studied using synchrotron radiation as a light source, by the atomic layer epitaxial technique, *i.e.*, by supplying diethylzinc and diethyltelluride alternately. It has been confirmed by X-ray photoelectron spectroscopy that no carbon is included in the ZnTe film. The growth rate becomes almost saturated at one monolayer per cycle.

VI-L-5 Low Temperature Deposition of II-VI Compound Semiconductors by Synchrotron Radiation Using Metalorganic Sources

Toshihiro OGATA*, Syed Irfan GHEYAS*, Hiroshi OGAWA* and Mitsuhiro NISHIO *(*Saga Univ.)*

[*Thin Solid Films,* in press]

Photon-assisted deposition of compound semiconductors using metalorganic sources is attracting much atten-

tion for the purpose of low-temperature growth. So far many experiments on photo-assisted growth of II-VI or III-V compound semiconductors have been performed using ultraviolet or visible light sources. In order to decompose the metalorganic reagents efficiently and so achieve much lower temperature deposition, however, a use of vacuum ultraviolet light might be useful since even the electron in the orbital of the inner shell can be excited by absorbing the photon energy. Synchrotron radiation (SR) has a high photon flux density in the vacuum ultraviolet region. Thus, virtually any metalorganic sources are expected to decompose efficiently with the help of SR irradiation. However, there have only a few researches on the SR excited deposition of compounds using metalorganic sources. We describe the first successful ZnSe deposition on the GaAs substrate at room temperature using SR as a light source. The deposition of ZnSe has been investigated at very low pressure of 10^{-5} Torr using diethylzinc and diethylselenide as the precursor sources and hydrogen as carrier gas. X-ray photoelectron spectroscopy shows that no carbon is included in the ZnSe film, similar to the case of ZnTe deposition[1]. The deposition rate is governed by the supply of diethylselenide as a VI-group source. Similar tendency is also observed in the synchrotron radiation excited deposition of ZnTe using diethylzinc and diethyltelluride.

Reference
1) M.Ikejiri, T.Ogata, H.Ogawa, M.Nishio and A.Yoshida, *J. Vac. Sci. & Technol.* **A12**, 278 (1994).

VI-L-6 Growth of High-Quality ZnTe Layers by MOVPE

Syed Irfan GHEYAS*, Shinya HIRANO*, Mitsuhiro NISHIO and Hiroshi OGAWA* *(*Saga Univ.)*

[*Appl. Surf. Sci.*, in press]

ZnTe is a wide band-gap II-VI compound semiconductor with great potential in optoelectronic devices. So far, several workers have studied growth of ZnTe by metalorganic vapor phase epitaxy (MOVPE) and examined photoluminescence (PL) properties of the films. In order to obtain high-quality ZnTe films, growth conditions for the film should be optimized through the understanding of growth process related to actual growth. However, the effects of growth conditions upon layer quality of ZnTe are not yet clear. Low substrate temperature and low pressure are known to lead to the deterioration of crystalline quality as well as to the reduction of growth rate. This may be closely related to the actual partial pressures of source materials in the vicinity of the growing surface which gets high under low substrate temperature and low pressure. Photo-assisted MOVPE growth of ZnTe using Ar^+ laser enhances surface reaction and thus reduces the actual concentration of precursors at the interface. As a result of this approach, free exciton emission can be observed predominantly in the PL spectrum of ZnTe films. However, illumination looks to be effective in enhancing the decomposition of impurity molecules of source materials too, since the donor related exciton emission and donor-acceptor pair emission regarding Cl impurity are found in the PL spectrum of ZnTe film. Another approach to a reduced actual concentration of precursors in the vicinity of the growing surface is to lower the transport rates of both dimethylzinc (DMZn) and diethyltelluride (DETe) at a suitable substrate temperature. Thus, we have investigated the effects of substrate temperature and transport rate of source materials (DMZn and DETe) upon the growth rate and PL property of ZnTe layers grown on the (100) ZnTe substrate by atmospheric-pressure MOVPE. Strong free exciton emission and Y bands appear predominantly in films grown under low transport rate (e.g., 10-15 μmol/min) and moderate temperature (*e.g.*, 380°C). It has been shown that growth in the mass-transport-limited region yields high quality ZnTe films.

VI-L-7 Aluminum Doping of ZnTe Grown by MOVPE

Syed Irfan GHEYAS*, Shinya HIRANO*, Mitsuhiro NISHIO and Hiroshi OGAWA* *(*Saga Univ.)*

[*Appl. Surf. Sci.*, in press]

ZnTe is a II-VI compound semiconductor with a direct bandgap of 2.26 eV at room temperature. Hence, this material has potential applications for purely green light emitting diode. ZnTe usually shows p-type conductivity due to the generation of Zn vacancy or Zn vacancy-impurity complex and the incorporation of residual acceptor impurities into the crystal. Recently we have found that growth in the mass transport limited region under moderate temperature by metalorganic vapor phase epitaxy (MOVPE) gives the best of films. So we have now reached an exciting stage from where n-type doping of ZnTe will have a real chance of succeeding. Triethylaluminum (TEAl) is a promising dopant source for MOVPE growth, since low-resistivity n-type ZnTe layers can be obtained[1]. But even with TEAl, it is still somehow difficult to control the conductivity of the grown layers. We believe that investigation leading to the clarification of the relationship between the photoluminescence properties of n-type impurity doped ZnTe layers and growth conditions, would be a vital step towards achieving reproducible low resistivity n-type films. Thus, we have investigated aluminum as a n-type dopant for ZnTe layer grown by atmospheric pressure MOVPE using TEAl as the dopant source. The effects of substrate temperature and transport rate ratio of diethyltelluride to diethylzinc upon the photoluminescence property of ZnTe layer have been clarified. The substrate temperature considerably influences the photoluminescence property of the layer. With decreasing substrate temperature, the emissions associated with an acceptor-type complex of Al donor and Zn vacancy become remarkably weak in the spectrum, implying that self-compensation gets eliminated. We have also discovered that Al incorporation is facilitated when Te rich growth condition is adopted. Also very high quality doped films can be obtained under this condition.

Reference
1) H. Ogawa, S. I. Gheyas, H. Nakayama, M. Nishio and A. Yoshida, *Jpn. J. Appl. Phys.* **33**, L980 (1994).

VI-M Electronic Structures of Organic/Inorganic Interfaces Studied by UV Photoemission

Recently, electronically functional organic materials attracted much attention in relation to their possible applications such as molecular devices, photography, electrophotography, organic electroluminescint devices and organic solar cells. Often these functions appear at the interfaces of the organic material with inorganic materials, such as metals, semiconductors and ionic crystals. Thus the elucidation of the electronic structures of these interfaces is of crucial importance in understanding and improving the devices. As a first step we focus on the electronic structure of organic/metal interface, especially on the mechanism of energy level alignment at the interface.

VI-M-1 The Electronic Structure and Energy Level Alignment of Porphyrin/Metal Interfaces Studied by Ultraviolet Photoelectron Spectroscopy

Hisao ISHII, Daisuke YOSHIMURA*, Satoru NARIOKA*, Masaki SEI*, Takafumi MIYAZAKI*, Yukio OUCHI*, Shinji HASEGAWA, Yutaka HARIMA, Kazuo YAMASHITA** and Kazuhiko SEKI*** *(*Nagoya Univ., **Hiroshima Univ.)*

[*Appl. Phys. Lett.*, **67**, 1899 (1995).]

Recently the applications of various organic semiconductors to electric devices have been extensively studied. The electronic structure of organic compound/metal interface is indispensable for understanding and refining the performance of organic devices. However there have been few studies even about the details of band lineup at organic / metal interface and this basic problem for organic devices is not yet well understood. In this study, we investigated the electronic structure of interfaces between 5,10,15,20-tetraphenylporphynatozinc (ZnTPP) and four metals (Mg, Al, Ag and Au) by ultraviolet photoelectron spectroscopy (UPS). The energy levels of ZnTPP relative to the Fermi level of substrate metals could be expressed as linear functions of the work function of metals with the shift of the vacuum level at interface (Δ). The slope of the linear functions was about unity. This indicates that the energy levels of ZnTPP are fixed to the vacuum level of substrate metal with constant interfacial dipole. 5,10,15,20-Tetra(4-pyridyl)porphyrin ($H_2T(4\text{-}Py)P$)/metal and 5,10,15,20-tetra-phenylporphyrin (H_2TPP)/metal interfaces were also investigated and similar linearity was observed between the energy levels of porphyrin and the work function of metal with the slope of much smaller than unity. This deviation of the slope from unity might be explained by the existence of interface state.

VI-M-2 The Electronic Structure of 8-Hydroxyquinoline Aluminum/Metal Interfaces Studied by Ultraviolet Photoelectron Spectroscopy

Hisao ISHII, Daisuke YOSHIMURA*, Satoru NARIOKA*, Yukiko HAMATANI*, Ikuko KAWAMOTO*, Takafumi MIYAZAKI*, Yukio OUCHI* and Kazuhiko SEKI* *(*Nagoya Univ.)*

Recently the studies of organic electroluminescent (EL) devices have been extensively performed in relation to display applications. Elucidation of the mechanism of carrier injection from metal electrode to organic thin film is indispensable for understanding and improving the performance of EL devices. In order to examine the carrier injection mechanism, we investigated the electronic structure of 8-hydroxyquinoline aluminum (Alq_3)/metal interfaces by ultraviolet photoelectron spectroscopy (UPS). Alq_3 has been widely used for light emitting layer compound in which both electron and hole should be injected. We found the abrupt shift of the vacuum level (Δ) at the interface in contrast to the traditional model of energy level alignment in which common vacuum level is assumed at interface. Such a shift was also observed at porphyrin/metal interface as reported previously[1]. In the case of porphyrin, Δ could be expressed as a linear function of work function of metal substrate (Φ_m)[1]. In this case, the extent of Δ depends on not only Φ_m but also the species of metals. At Alq_3/Al interface, large Δ of about -1.5 eV caused the lowest unoccupied molecular orbital (LUMO) to shift downwards close to the Fermi level of the substrate metal. Thus electron injection can be expected at the interface. On the other hand, at Alq3 / Au interface, smaller Δ of about -1 eV and the increase of Φ_m relative to Al surface make the LUMO allocated far from the Fermi level of the substrate, suggesting less electron injection character. Such trends are consistent with the electric characteristics of EL devices fabricated from Alq_3. These results suggest that carrier injection is responsible for tunneling process at the interface of EL devices.

Reference

1) S. Narioka, H. Ishii, D. Yoshimura, M. Sei, Y. Ouchi, S. Hasegawa, T. Miyazaki, Y. Harima, K. Yamashita and K. Seki, *Appl. Phys. Lett.*, Vol.**67**, 1899 (1995).

RESEARCH ACTIVITIES VII
Coordination Chemistry Laboratories

Prof. Akira Nakamura retired from the position of the Director in March, 1995 and moved to Osaka University as Prof. of Macromolecular Science. We sincerely thank his effort and the progress made during his period here. His contribution to the Coordination Chemistry Laboratories (CCL) is immense and highly acknowledged. Prof. Koji Tanaka took the position of the Director of the CCL. Prof. Mitsuhiko Shionoya joined to CCL from Hiroshima University as Prof. of Complex Catalysis in June, 1995. Prof. Yuzo Yoshikawa, Assoc. Prof. Hiroshi Nakazawa, Dr. Yasushige Kuroda, and Dr. Tsumotsu Mizuta continued their positions at the laboratory of Synthetic Coordination Chemistry. Dr. Thomas Daniel and Dr. Hirotaka Nagao moved to Wurzburg University and Sophia University, respectively. Dr. Kiyoshi Tsuge took the position of Assist. Prof. of Functional Coordination Chemistry. Prof. Kazuko Matsumoto (Waseda University) and Assoc. Prof. Akira Nagasawa (Saitama University) as Adjunct Prof. finished their term in March 1995 in the Laboratory of Complex Catalysis. Their effort during their term is gratefully appreciated. Prof. Megumu Munakata (Kinki University) and Assoc. Prof. Naohide Matsumoto (Kyushu University) are newly appointed as Adjunct Prof. of the laboratory of Coordination Bond.

VII-A Stereochemistry of Coordination Compounds and Adsorption Phenomena of Various Gases on Inorganic Solids

Several metal coordination compounds including higher-coordinate silicon(IV) complexes are going to be synthesized and some of them are studied stereochemically. Dielectric properties of inorganic solids adsorbed H_2O, on which the two-dimensional condensation of water occurs, were investigated as a function of surface coverage. Adsorption properties of copper-ion-exchanged mordenite were also investigated.

VII-A-1 Stereochemistry of Six-Coordinated Silicon(IV) Complexes

Yasuharu OHMORI, Masaaki KOJIMA,* Hong Ling LIU,* Motoyuki TASAKA,* Shunji UTSUNO and Yuzo YOSHIKAWA** *(*Okayama Univ., **Shizuoka Univ.)*

[*J. Coord. Chem.*, in press]

Higher(than four)-coordinated complexes of silicon(IV) are not very familiar as compared to four-coordinated tetrahedral compounds. We already reported the complete optical resolution and the properties of $[Si(phen)_3]^{4+}$. Successively the ion-association constants between the optically-active complex cations(Λ- or Δ-$[Si(phen)_3]^{4+}$) and the resolving agent anions($[Sb_2\{(+)\text{-tart}\}_2]^{2-}$, tart = tartrate(4-) ion) were determined spectrophotometrically. The ion association between the complex cation and the resolving agent anions occurred in two steps and the stereoselective interaction was observed in the second step. The second-step association constant for the Λ-enantiomer(K_2 =1.41 ×10^3) is larger than that for the Δ-one(K_2 =1.07 ×10^3). The second-step association plays a dominant role in determining the elution order in column-chromatographic resolution. The molecular mechanics calculations for the ion-associated species were performed to obtain the information about the microscopic interaction between the ions. The total strain energy for the species containing the Λ-enantiomer is smaller than that containing the Δ-one and this result can explain the experimental finding that the Λ-enantiomer is eluted faster than the Δ-one. The *ab initio* MO calculation for $[Si(phen)_3]^{4+}$ is currently in progress in order to obtain the partial charges on the atoms and some of the force constants. In the present section, the optical resolution of $[Si(bpy)_3]^{4+}$ was also attempted by a chromatographic method using an SP-Sephadex C-25 column and various resolving-agent solutions, sodium (+)-bitartrate (NaHtart), sodium (+)-tartrate(Na_2tart), potassium bis((+)-tartrato) diantimonate (III) ($K_2[Sb_2\{(+)\text{-tart}\}_2]$), and sodium (2*R*,3*R*)-*O*,*O*'-dibenzoyltartrate($Na_2(benz)_2$tart) as eluents. The faster-moving enantiomer was Λ except the Δ moved faster for $K_2[Sb_2\{(+)\text{-tart}\}_2]$. However, the complete resolution(i.e. the complete separation of the elution band) was attained only by the use of an aqueous solution(0.16 M) of sodium (2*R*,3*R*)-*O*,*O*'-dibenzoyltartrate as the eluent. Now we are carrying out the force-field calculations of the above ion-pair systems in order to elucidate the chromatographic elution mechanism. This section was developed to syntheses and stereochemistry of five-coordinated silicon(IV) compounds. At present the stereoselective formation is being investigated about the silatrane derivatives having L-alaninol and L-valinol skeletons.

VII-A-2 Photochemistry of Cobalt(III) Complexes Containing a Sulfinate-*S* Ligand. Linkage and Geometrical Isomerization

Farooque MD. AKHTER,* Masakazu HIROTSU,* Isamu SUGIMOTO,* Masaaki KOJIMA,* Setsuo KASHINO* and Yuzo YOSHIKAWA *(*Okayama Univ.)*

[*Chem. Lett.*, 2393(1994)]

On photolysis of *trans*(*t*-N,S)-$[Co\{S(O)_2CH_2COO\text{-}S,O\}(tren)]^+$(**1**, *t*-N = tertiary amine nitrogen; tren = tris(2-aminoethyl)amine) with visible light, two complexes(orange and red) were obtained. The molecular structure of the orange complex perchlorate was determined by the X-ray method to be *cis*(*t*-N,O(S))-$[Co\{OS(O)CH_2COO\text{-}O,O\}(tren)]ClO_4\cdot H_2O$(**2**, O(S) = oxygen of sulfinate group); geometrical isomerization as well as linkage isomerization took place upon photolysis.

The crystal data and final R value are : monoclinic, $C2/c$, a = 23.316(4) Å, b = 8.005(1) Å, c = 18.631(4) Å, β = 108.03(1)°, V =3307(2)Å^3, Z = 8, and R = 0.035 for 2503 unique reflections. The mechanism for geometrical isomerization was proposed. The red complex, which was assigned as *trans*(*t*-N,O(S))-[Co{OS(O)CH_2COO-*O,O*}(tren)]$^+$ (**3**) was thermally unstable and reverts to the starting complex. This observation is in accord with molecular mechanics calculations, which estimate the starting complex to be more stable. The kinetics was studied by the HPLC method in the temperature range 28-70 °C, giving $\Delta H^{\ddagger}$= 100 kJ mol^{-1} and $\Delta S^{\ddagger}$= -23 J K^{-1} mol^{-1}. Photolysis of a cobalt(III) complex containing the L-cysteinesulfinate-*S,N* ligand, *cis*(*t*-N,S)-[Co{$S(O)_2CH_2$ $CH(COOH)NH_2$-*S,N*}(tren)]$^{2+}$ (**4**) with visible light provided two types of linkage isomers, *cis*(*t*-N,O(C))-[Co{$NH_2CH(CH_2SO_2)$COO-*N,O*}(tren)]$^+$(**4b**, O(C) = oxygen of carboxylate group) with an uncoordinated sulfinate group, and a pair of diastereomers of *cis*(*t*-N,O(S))-[Co{OS(O)$CH_2CH(COOH)NH_2$-*O,N*}(tren)]$^+$ (**4a**). The molecular structures of the perchlorate of **4b** and the bromide of **4a** with the (*S*)-sulfur atom have been determined by X-ray diffraction. Crystal data and final R values: for **4b**, triclinic, $P1$, a = 8.801(3) Å, b = 8.894(7) Å, c = 6.781(2) Å, α = 92.26(4)°, β = 91.30(3)°, γ = 70.50(4)°, V = 500.0(8) Å^3, Z = 1, and R = 0.020 for 2199 unique reflections; for **4a-*S***, orthorhombic, $P2_12_12_1$, a = 11.386(8) Å, b = 16.81(1) Å, c = 9.189(7) Å, V= 1759(2) Å^3, Z = 4, and R = 0.027 for 2200 unique reflections. Isomerization (epimerization) from **4a-R** to **4a-*S*** was studied in the temperature range 55-75 °C, giving $\Delta H^{\ddagger}$=105 kJ mol^{-1} and $\Delta S^{\ddagger}$= -20 J K^{-1} mol^{-1}. Photolysis of *trans*(*t*-N,S)-[Co{$S(O)_2CH_2CH(COOH)NH_2$-*S,N*}(tren)]$^{2+}$ (**5**) yielded six products, and three of them were the same as those obtained by photolysis of **4**, indicating that geometrical isomerization took place.

VII-A-3 Force Field Calculation of Metal Complex Systems Including Antitumor Platinum(II) Complexes

Toshihito YOSHII,* Farooque MD. AKHTER,* Masaaki KOJIMA,* Koji YUTO, Yuri MIZUNO and Yuzo YOSHIKAWA *(*Okayama Univ.)*

[*J. Coord. Chem.*, in press]

Strain-energy minimization of adducts of the cisplatin-type platinum(II) complexes with the sequence d(pCpGpAp)·d(pGpCpTp) of a synthetic B-DNA was carried out and the results were already reported. This research is being developed to the syntheses of new triamine-type platinum(II) complexes which monofunctionally react with N7 of guanosine bases in DNA differing from cisplatin and where DNA-aromatic ring interactions such as intercalation or stacking are expected. This strain-energy minimization technique was developed to photochemical products of tris(L-cysteinesulfinato)cobaltate(III) ion, *trans*(*t*-N,S)-[Co{$S(O)_2CH_2$COO-*S,O*}(tren)]$^+$ (*t*-N = tertiary amine nitrogen; tren = tris(2-aminoethyl)amine), and *cis*(*t*-N,S)-[Co{$S(O)_2CH_2CH(COOH)NH_2$-*S,N*} (tren)]$^{2+}$. On photolysis of *trans*(*t*-N,S)-[Co{$S(O)_2CH_2$ COO-*S,O*}(tren)]$^+$ with visible light(See section 2), two products were obtained, the orange (assigned to *cis*(*t*-N,O(S)) and the red(assigned to *trans*(*t*-N,O(S)) complexes. The orange complex is thermally stable, and no detectable change is observed in the absorption spectrum and in the chromatogram for at least 360 h at 25°C. The difference in stability to a thermal linkage isomerization between the orange and red complexes can be explained by considering the difference in the intramolecular strain between the respective *S*-bonded isomers which the *O*-bonded ones should change into. While the strain energies of both *O*-bonded isomers are very similar, *S*-bonded *cis*(*t*-N,S) is much more unstable than the *S*-bonded *trans*(*t*-N,S) ones. Thus, though the *O*-bonded red complex easily changes to the more stable *S*-bonded one, the *O*-bonded orange complex does not change to the corresponding unstable *S*-bonded one. Photolysis of *cis*(*t*-N,S)-[Co{$S(O)_2CH_2CH(COOH)NH_2$-*S,N*}(tren)]$^{2+}$ with visible light(See section 2) yielded three products, the yellow-1(assigned to *cis*-(*t*-N,O(C))), red-1(assigned to (*R*)-*cis*(*t*-N,O(S))), and red-2(assigned to (*S*)-*cis*(*t*-N,O(S))) complexes. Both red-1 and red-2 complexes(a pair of diastereomers) are stable toward a thermal back-reaction. However, the red-1 complex changes to the red-2 one; inversion at the chiral sulfur center occurs. Molecular mechanics calculations on the two diastereomers, the red-1 and red-2 isomers, were carried out in the hope of getting support that the red-2 isomer is more stable than the red-1 isomer. However, the result was not in accord with our observation; the red-1 isomer was calculated to be a little more stable than the red-2 isomer(by ca. 0.2 kcal/mol). This inconsistency may be accounted for as follows. In the structure of the red-2 isomer, we can see the non-bonded distance of ca. 2.5 Å between the uncoordinated oxygen bonded to the sulfur and one of hydrogens attached to the nearest nitrogen of tren. There is no such distance in the red-1 isomer. Thus, the red-2 isomer can be much more stabilized with the intramolecular hydrogen bonding and/or electrostatic interaction than the red-1. The molecular mechanics calculations mentioned in section 1 are contained in the present section. This technique is also being developed to ion-pair systems containing tris (cyclohexanediamine) cobalt(III).

VII-A-4 Manganese(III) Complexes Containing Optically-Active Tetradentate Schiff-Base Ligands. The Effect of Phenyl Substituents

Masakazu HIROTSU,* Kiyohiko NAKAJIMA, Masaaki KOJIMA* and Yuzo YOSHIKAWA** *(*Okayama Univ., **Aichi Univ. of Educ.)*

[*Inorg. Chem.*, in press]

Manganese(III) complexes containing optically-active tetradentate Schiff-base ligands have been prepared. The crystal structure of the complex, [Mn{7-Phsal-(*SS*)-stien}Cl]·CH_2Cl_2, where 7-Phsal-(*SS*)-stien is the dianion of the product formed from the condensation of two moles of 2-hydroxybenzophenone and one mole of (*S,S*)-1,2-diphenylethylenediamine, has been established by the X-ray method. Crystal data: monoclinic, $P2_1$, a = 16.796(2) Å, b = 14.366(2) Å, c = 15.266(2) Å, β = 101.84(1)°, V = 3605.2(9) Å^3, Z = 4. The structure has been refined to R = 0.058 and R_w = 0.063. The coordination polyhedron is a distorted square pyramid, the Schiff-base ligand oc-

cupying the basal sites while the chloride ion the apical site. The two phenyl groups of the diamine moiety are in the axial positions and the central chelate ring of the Schiff-base ligand takes a λ gauche conformation. On the basis of the circular dichroism spectral data for [Mn{7-Phsal-(*SS*)-stien}Cl] and related complexes, the preferred conformation of the central chelate ring in solution has been assigned. The effects of phenyl substituents on the redox potentials, Mn(III)/Mn(II) and Mn(IV)/Mn(III), have been discussed in terms of the conformational behavior of the Schiff-base ligands. The manganese(III) complexes with axial phenyl groups offer great opposition to oxidation. We have already reported that the corresponding cobalt(II) complex, [Co{7-Phsal-(*rac*)-stien}] is also very difficult to oxidize

[*Chem. Lett.*, 2183(1994)].

VII-A-5 Dielectric Behaviors in the Inorganic Solid-H_2O Systems

Yasushige KURODA, Daisuke KATAOKA, Toshinori MORI, Yuzo YOSHIKAWA, Tetsuo MORIMOTO, Hideaki HAMANO* and Mahiko NAGAO*** *(*Okayama Univ., **Okayama Univ. Science)*

(a) The SrF_2-H_2O System. Part 2. Measurement at Low Temperature

[*Langmuir,* **11,** 2173(1995)]

Dielectric properties of water adsorbed on the SrF_2 surface have been investigated under the various conditions: the frequency region of 0.1 Hz to 5 MHz, the temperature range from 77 to 298 K, and the surface coverage of 0 to 1.26 monolayers. A small relaxation was found at 33 kHz and at 159 K in the coverage of 0.74, besides a large relaxation observed at 298 K which has been described in Part 1[*Langmuir,* **11,** 259(1995)]. This small relaxation is observed only when the physisorbed water molecules are present. Furthermore, the chord length of Cole-Cole plots for this relaxation is found to be a function of the coverage. These findings are interpreted in terms of the Debye-type rotational polarization of the adsorbed water, and therefore confirm that the relaxation observed at 298 K is ascribed to the Maxwell-Wagner type relaxation. An activation energy for the dipole rotation is also calculated from the variation of frequency corresponding to a maximum in the dielectric loss curve with temperature. This finding suggests that the rotation of the water molecule condensed two-dimensionally is expected to be more hindered than that of bulk liquid water, though not so much as in ice. The state of two-dimensionally condensed water on SrF_2 is discussed on the basis of the concept of the lateral interaction.

(b) Desorption Phenomenon of Adsorbed Water on Homogeneous SrF_2 Surface at Lower Temperatures

[*Langmuir,* in press]

The adsorbed state of water on SrF_2 has been studied through the dielectric measurement in the temperature range from 298 to 77 K and in the coverage range up to 4. The relaxation attributable to the orientational polarization of adsorbed water was found at 415 kHz and at 159 K near the monolayer coverage. It was also found that the chord length of the Cole-Cole plots for this relaxation varies linearly with coverage until a complete monolayer is formed, and that it suppresses and ultimately stops to increase in magnitude beyond the surface coverage of ca. 1. These findings are interpreted in terms of the desorption of adsorbed water from the second or more higher layers on the SrF_2 surface at lower temperatures, resulting from a weaker interaction between adsorbed water molecules and/or between adsorbed water and the solid surface, as compared to the mutual interaction of water molecules in the bulk phase.

(c) The Y_2O_3-H_2O System at Lower Temperatures: In Comparison with Desorption Phenomenon of Adsorbed H_2O in the SrF_2-H_2O System

[*Langmuir,* submitted]

In the present study we aimed to examine the desorption behavior of adsorbed water on Y_2O_3, on which water molecules are expected to interact strongly with the hydroxylated surface, through the dielectric measurement at lower temperatures. It may also give us an evidence for our interpretation of desorption behavior in the SrF_2-H_2O system. The relaxation observed at lower temperatures is due to the orientational polarization of adsorbed water molecules, in accordance with the relationship derived by Onsager. Another feature that the Cole-Cole arc length increases with coverage, even beyond the coverage of ca. 1, is quite different from the tendency observed in the SrF_2-H_2O system. This finding suggests that water molecules adsorbed on Y_2O_3 even in exceeding the coverage of about 1 cannot be detached from the surface even below 159 K. At the initial stage of adsorption, water molecules interact strongly with the surface hydroxyl groups on Y_2O_3 through the formation of hydrogen bonding . The adsorption heats fall with increasing coverage owing to a geometrical and energetic heterogeneity of the adsorption sites. In the system of Y_2O_3-H_2O, the straight line of the Clausius-Clapeyron plots for the coverage greater than unity does not intersect the line for water or ice even at lower temperatures, which is distinct from the observation in the SrF_2-H_2O system. The adsorption heats are larger than the heat of liquefaction or solidification of water vapor even after the attainment of physisorbed layers to 2.5, suggesting that the adsorbed water remains on the Y_2O_3 surface at lower temperatures. This is a piece of evidence in support of our preceding report that the adsorbed water in more than the first layer can be removed from the SrF_2 surface at lower temperatures. Such dielectric behavior is also being searched for the Cu_2O-H_2O and Ag_2O-H_2O systems.

VII-A-6 Stabilization of Copper Metal Clusters in Mordenite Nanopores: Water Treatment of Evacuated Copper-Ion-Exchanged Mordenite at 300 K

Yasushige KURODA, Yuzo YOSHIKAWA, Shin-ichi KONNO,* Hironobu MAEDA,* Yoshihiro KUBOZONO,* Hideaki HAMANO,* Ryotaro KUMASHIRO* and Mahiko NAGAO* *(*Okayama*

Univ.)

[*J. Phys. Chem.*, submitted]

The change of the state of copper ion in mordenite due to the heat treatment and subsequent rehydration at 300 K were investigated using electron spin resonance(ESR), X-ray absorption fine structure(XAFS) – both in the extended region(EXAFS) and in the near-edge region(XANES) – , and infrared(IR) spectroscopic techniques. The ESR intensity attributed to Cu(II) species exchanged in mordenite decreased with increasing temperature of the pretreatment in vacuo. The XANES spectra gave the band at 8.976 keV for copper-ion-exchanged mordenite evacuated at 300 K and the bands at 8.981 and 8.992 keV for the sample evacuated at 873 K. These findings are interpreted in terms of the reduction of Cu(II) to Cu(I) species in the mordenite nanopores by evacuation at higher temperatures. An increase in the intensity of ESR spectra and a decrease in intensity of the 1s-4p band(8.981 keV) in XANES spectra proved that treating the 873 K-evacuated sample with H_2O vapor at 300 K brings about a reoxidation of Cu(I) to Cu(II). There is also a direct evidence for an existence of the cluster of metal copper with low crystallinity in the cavity of mordenite nanopores, which is formed by ion-exchange, followed by heat treatment at 873 K and subsequent treatment with H_2O vapor at 300 K; the Fourier-transform of EXAFS gives the band at 2.16 Å(without phase-shift correction) which is attributable to the scattering from Cu-Cu pair in metal. These results can be interpreted by assuming a disproportionation reaction of cuprous ions(to Cu(II) and Cu(0)) which are formed by heat treatment in mordenite with H_2O vapor at 300 K. On the ground of the coordination number calculated from EXAFS data, the average size of the metal clusters is estimated to be 10-15 Å. The formation of such small metal clusters may be due to the stabilization of small clusters in the zeolite nanopores. The driving force for the disproportionation reaction, which was examined by IR spectroscopy, seems to come from the formation of the Brønsted acid sites on the mordenite lattice through the H_2O treatment. Such an easy conversion of valence state for copper ions may be due to the spatial distribution of ion-exchanged sites in mordenite. In high-silica zeolites, the distance between Al ions is large, and hence the two separated single charges in the mordenite lattice are compensated by two Cu(I) species in the 873 K-treated sample and by $CuOH^+$, H^+, and Cu(0) species upon treating the 873 K-treated sample with H_2O vapor.

VII-A-7 Solid-State Circular Dichroism Spectra of *trans*-Diamminetetranitrocobalt(III) Salts and *mer*-Triamminetrinitrocobalt(III)

Shunji UTSUNO,* Akiomi SUGANUMA* and Yuzo YOSHIKAWA *(*Shizuoka Univ.)*

[*Inorg. Chim. Acta*, in press]

Circular dichroism(CD) spectra of solid complexes(mentioned in the title) have been observed and attributed to the propeller arrangements of the nitro-groups. Potassium *trans*-diamminetetranitrocobalt (III), $K[Co(NO_2)_4(NH_3)_2]$ crystallizes as a spontaneously resolved form with space group of $P2_12_12_1$. Its ammonium salt("Erdmann's salt") is isomorphous with the potassium one. The situation is the same as in *mer*-triamminetrinitrocobalt(III), which also forms a single crystal of $P2_12_12_1$. Their absolute conformations are possible to be related to the signs of the CD spectra in terms of the hexadecadal regional rule. The CD band of $K[Co(NO_2)_4(NH_3)_2]$ at 21,300 cm^{-1} corresponds to a transition $^1E_g \leftarrow {}^1A_{1g}$ under D_{4h} symmetry. Actually, the complex anion in this salt does not form a four-bladed propeller. Crystal structure analysis showed that only a half of the nitro-groups seems to be responsible for the chirality of the whole complex. In order to examine the relation between the sign of the CD band and the conformation of the complex anion, the diastereisomer Δ-$\{-\}_{300}$-*cis*-$[Rh(NO_2)_2(en)_2]$-*trans*-$[Co(NO_2)_4(NH_3)_2]$[†] was prepared. The complex anion is expected to take a *P* conformation in the diastereoisomer of Λ-*cis*-$[Co(NO_2)_2(en)_2]$-*trans*-$[Co(NO_2)_4(NH_3)_2]$. The sign of the CD spectrum of the diastereoisomer was well in accord with the one deduced from the regional rule. On the other hand, *mer*-triamminetrinitrocobalt(III) exhibits a CD spectrum with twice as much intensity as those of $K[Co(NO_2)_4(NH_3)_2]$ and Erdmann's salt. The rotational strengths of these propeller complexes seem to be affected mainly by the inclination of the nitro-groups(the blade parts of propeller). In order to explain well the abnormally-intense rotational strengths of *mer*-triamminetrinitrocobalt(III), it is desirable to accumulate CD spectra of other samples of atropisomers together with their accurate structural data.

[†] $\{-\}_{300}$ represents that the sign of the CD spectrum at 300 nm is negative.

VII-A-8 Polymeric and Monomeric Structures of a Schiff-Base Oxovanadium(IV) Complex: Orange and Green Forms of [VO{sal-(*RR*)-stien}] and Interconversion between these Species

Kiyohiko NAKAJIMA,* Masaaki KOJIMA,[†] Masanobu TSUCHIMOTO,[‡] Setsuo KASHINO,[†] Shigeru OHBA,[‡] Paul M. TREICHEL,[#] Yuzo YOSHIKAWA and Junnosuke FUJITA *(† Okayama Univ., * Aichi Univ. of Educ., ‡ Keio Univ., # Univ. of Wisconsin-Madison, ¶ International Christian Univ.)*

[*Proc. Japan Acad.*, **71B**, 175(1995)]

The orange and green forms of the Schiff-base oxovanadium(IV) complex, [VO{sal-(*RR*)-stien}]·CH_3OH(**1**, green), [VO{sal-(*RR*)-stien}]·$2CHCl_3$ (**2**, green), and $[VO\{sal\text{-}(RR)\text{-}stien\}]_n \cdot nCH_3CN$(**3**, orange)($H_2${sal-(*RR*)-stien} = *N,N'*-disalicylidene-(*RR*)-1,2-diphenyl-1,2-ethanediamine) have been prepared, and their crystal structures were determined by the X-ray method. The green forms consist of mononuclear units, while the orange form polymeric linear chains of the complexes. Both green complexes have a five-coordinate square-pyramidal structure and the orange complex has a six-coordinate distorted-octahedral structure where the vanadyl oxygen bridges the neighboring vanadium. **1**, which crystallizes as monoclinic in space group $P2_1$, with $Z = 4$, has the cell parameters a = 16.684(2) Å, b = 16.923(4) Å, c = 9.249(3) Å, β = 105.76(2)°; and V = 2513(1) $Å^3$. **2**, which crystallizes as triclinic in space

group $P1$ with Z = 2, has the cell parameters a = 13.187(3) Å, b = 13.469(3) Å, c = 10.450(3) Å, α = 103.72(2)°, β = 103.20(3)°, γ = 63.03(3)°, and V = 1591.2(7) Å^3. **3** crystallizes as triclinic in space group $P1$ with Z = 2. The cell parameters are a = 13.300(3) Å, b = 13.667(4) Å, c = 7.551(1) Å, α = 90.44(2)°, β = 94.51(2)°, γ = 97.36(2)°, and V = 1357(1) Å^3. The final R indices are R = 0.056 and R_w = 0.057 for **1**, R = 0.098 and R_w = 0.090 for **2**, and R = 0.053 and R_w = 0.042 for **3**. The structural characteristics of these complexes were compared and discussed. These complexes showed piezochroism(mechanochroism); it exhibited color change from orange to green on grinding and from green to orange on exposure to acetonitrile vapor. The color remained unchanged even after **3**(orange form) was heated at 150 °C for two hours. On the other hand, **1** and **2**(green forms) changed their colors to orange on heating. All of the complexes were very resistant to pressure; the complexes were pressed at 10^4 kg cm^{-2} for a few minutes, but their color did not change.

VII-B Creation of Complexes Containing New Types of Bonds between a Transition Metal and a Phosphorus

The most typical bond fashion between a transition metal and a phosphorus is a dative bond, where the lone-pair electrons on a phosphorus atom are donated to a vacant d orbital of a transition metal. We focus on rather new types of bond fashion between a transition metal and a phosphorus, such as a covalent bond, a multiple bond, and a hypervalent bond. New preparative methods of complexes containing such bonds have been developed and the reactivities of these complexes have been examined.

VII-B-1 Cationic Phosphenium Complexes of Group 6 Transition Metals: Reactivity, Isomerization, and X-ray Structures

Hiroshi NAKAZAWA, Yoshitaka YAMAGUCHI, Tsutomu MIZUTA and Katsuhiko MIYOSHI* *(*Hiroshima University)*

[*Organometallics*, in press]

The reaction of cationic diamino-substituted phosphenium complexes of group 6 transition metals *mer*-$[(bpy)(CO)_3M\{PN(Me)CH_2CH_2X\}]^+$ (X = NMe, O) with a phosphite derivative (L) proceeds with substitution of L for CO to produce $[(bpy)(CO)_2LM\{PN(Me)CH_2CH_2X\}]^+$. During the reaction, the phosphenium ligand remains intact. The product consists of trans and cis isomers, and they equilibrate. The cis form is electronically and the trans form is sterically favored. Two of them have been characterized by X-ray diffraction. The bond distance of Mo-P(phosphenium) is significantly shorter than that of Mo-P(phosphite) for both complexes, indicating a significant double bond character between Mo and P(phosphenium). For both complexes, the P-N bond distances in phosphenium and in phosphite ligands are almost equal, indicating that there is no significant N to P(phosphenium) π donation. The role of the amino groups on the phosphenium phosphorus is probably to protect the approach of a nucleophile to phosphenium phosphorus by high pπ lone pair density flanking the phosphenium center.

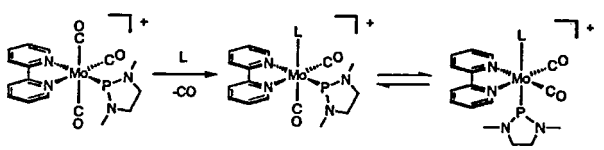

VII-B-2 Migratory Insertion of a Phosphorus Ligand into a Transition Metal-Alkyl Bond

Hiroshi NAKAZAWA, Yoshitaka YAMAGUCHI, Tsutomu MIZUTA, Satoshi ICHIMURA* and Katsuhiko MIYOSHI* *(*Hiroshima University)*

[*Organometallics*, in press]

Treatment of $[Cp(CO)(R^1)Fe\{PN(Me)CH_2CH_2NMe(OR^2)\}]$ (R^1 = Me, CH_2Ph; R^2 = Me, Et) with $BF_3{\cdot}OEt_2$ and then with PPh_3 yields $[Cp(CO)(PPh_3)Fe\{PN(Me)CH_2CH_2NMe(R^1)\}]^+$. The reaction proceeds via the formation of a cationic phosphenium complex $[Cp(CO)(R^1)Fe\{PN(Me)CH_2CH_2NMe\}]^+$, by the abstraction of an OR group as an anion from a phosphorus atom, and then a migratory insertion of the phosphenium ligand into the iron-alkyl bond takes place to give $[Cp(CO)(BR_2OR^2)Fe\{PN(Me)CH_2CH_2NMe(R^1)\}]^+$, which is characterized by spectroscopic data. The cationic complex readily reacts with PPh_3 to give the final product. The reaction of silyl complexes $[Cp(CO)(SiMe_3)Fe\{PN(Me)CH_2CH_2NMe(OR)\}]$ with $BE_3{\cdot}OEt_2$ affords a phoephenium complex, which does not show the migratory insertion into an iron-silyl bond. Iron complexes $[Cp(CO)(CH_2OMe)Fe\{PN(Me)CH_2CH_2N\ Me(OR)\}]$ (R = Me, Et) having an alkoxy group both on a carbon and on a phosphorus react with $BF_3{\cdot}OEt_2$ and then PPh_3 to give $[Cp(CO)(CH_2PPh_3)Fe\{PN(Me)CH_2CH_2N\ Me(OR)\}]^+$. The results prove that the OMe in the CH_2OMe lignad is selectively abstracted to give the methylidene complex which is trapped with PPh_3 to give a phosphine ylide complex.

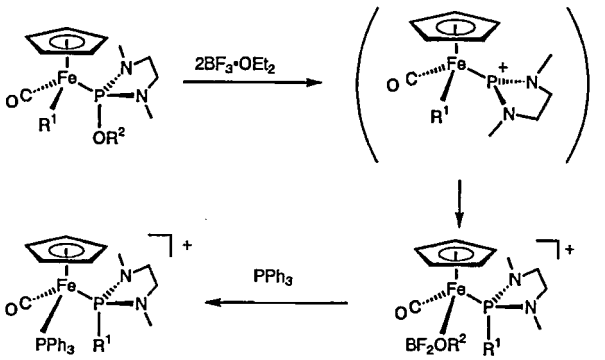

VII-B-3 Reactivity of Cationic Transition-Metal Phosphenium Complexes

Hiroshi NAKAZAWA, Yoshitaka YAMAGUCHI and Katsuhiko MIYOSHI* *(*Hiroshima University)*

[*Phosphorus, Sulfur and Silicon,* in press]

Reactivity of cationic transition metal phosphenium complexes has been investigated. Reaction of *mer*-$[(bpy)(CO)_3M\{PN(Me)CH_2CH_2NMe\}]^+$ (M = Cr, Mo, W) with X^- (X = Me, OEt) exhibits a nucleophilic attack at the phosphenium phosphorus, whereas that with L (L = phosphine, phosphite) shows CO/L substitution. Iron phosphenium complexes, $[Cp(CO)RFe\{PN(Me)CH_2CH_2NMe\}]^+$ undergoes a migratory insertion of the phosphenium ligand into the Fe-alkyl bond.

VII-B-4 Conversion of Transition-Metal Complexes with Stannyl and Phosphenium Ligands into those with Stannylene and Phosphine Ligands by Alkyl Migration from Sn to P

Hiroshi NAKAZAWA, Yoshitaka YAMAGUCHI and Katsuhiko MIYOSHI* *(*Hiroshima University)*

Treatment of [Cp(CO) ($SnMe_3$)Fe {$PN(Me)CH_2CH_2$ NMe(OR)}] (R = Me, Et) with $Me_3SiOSO_2CF_3$ (TMSOTf) at -78 °C yields a reaction mixture from which yellow crystals can be isolated. Elemental analysis, and IR, ^1H, ^{13}C, and ^{31}P, and ^{119}Sn NMR spectra established the formation of a stannylene complex formulated as $[Cp(CO)(SnMe_2)FePN(Me)CH_2CH_2NMe(Me)\}]OTf$, showing that P-OR bond cleavage and Me migration from Sn to P take place. The X-ray analysis of the product reveals that this is a stannylene complex of iron stabilized by both an OTf^- and N atom in the phosphorus ligand. In solution, there may be an equilibrium between a base-stabilized stannylene form as shown in a solid state and a base-free one, but the equilibrium seems to be shifted toward the base-free form. The molar conductivity in nitromethane showed 76.1 ohm^{-1} cm^2 mol^{-1} which is a reasonable value for a 1:1 electrolyte. The ^1H and ^{13}C NMR spectra in CD_2Cl_2 at room temperature show that the two Me groups are magnetically equivalent, indicating that an OTf anion and an amino group in the phosphorus ligand dissociate from the Sn resulting in the rotation of the $SnMe_2$ group along the Fe-Sn bond.

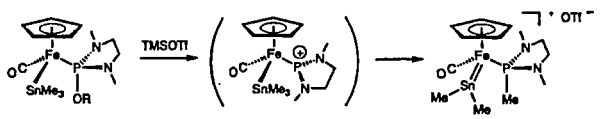

VII-B-5 P-C Bond Cleavage of Phosphorus Bridged [1]Ferrocenophane Coordinating to $[Cp(CO)_2Fe]^+$ Fragment

Tsutomu MIZUTA, Tomoaki YAMASAKI, Hiroshi NAKAZAWA and Katsuhiko MIYOSHI* *(*Hiroshima University)*

An Iron complex, $[Cp(CO)_2Fe(FCPP)]PF_6$ (**1**), with (1,1'-ferrocenyl)phenylphosphine (FCPP) as a ligand, was prepared from $[Cp(CO)_2Fe(THF)]PF_6$ and FCPP, and its X-ray crystal structure was determined. Photo irradiation of **1** resulted in the Cp ring migration from a P to an Fe atom. Addition of H_2O or $(n\text{-}Bu)_4NF$ to the reaction mixture gave an isolable complex formulated as $[Cp(CO)Fe(C_5H_4FeC_5H_4PFPh)]$. The structure for one of the racemic isomers was determined with X-ray analysis. The isomer was a kinetic product, and isomerized to its thermodynamically stable isomer in the presence of an F^- anion.

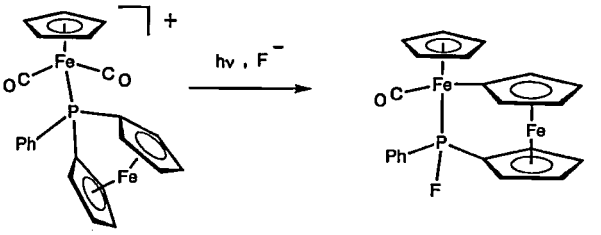

VII-B-6 Synthesis and Stereochemistry of Transition-Metal Complexes with Tetraphosphamaclocycle

Tsutomu MIZUTA, Akihiro OKANO*, Katsuya YAMAMOTO, Hiroshi NAKAZAWA and Katsuhiko MIYOSHI* *(*Hiroshima University)*

The trans isomer of $[Pd(Me_4\text{-}14aneP_4)]Br_2$ was isolated, and its X-ray crystal structure was determined as shown in Figure 1. A coordination geometry around the Pd is exactly square-planner. Thus, the macrocyclic ligand affords an enough hole size for Pd^{2+} with a Pd-P distance of 2.262(4) Å. Two Br^- counter anions are located out of the coordination sphere with the distance of 3.462(3) Å from the Pd. The phosphorus analog of a cyclam was synthesized as a phosphamaclocycle ligand having no substituent on the ring. An Arbuzov reaction of $(i\text{-}PrO)_2PCH_2CH_2P(Oi\text{-}Pr)_2$ with 1,3-dibromopropane gives a macrocyclic framework in a good yield. Reduction of the product with an appropriate hydride reagent affords 1,5,8,12-tetraphosphacyclotetradecane.

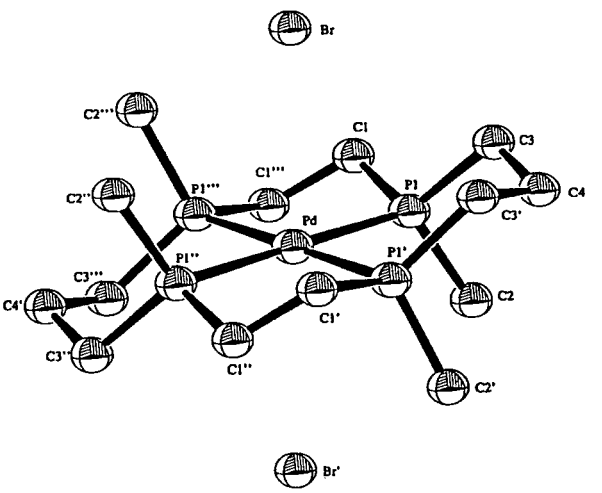

Figure 1.ORTEP drawing of trans-$[Pd(Me_4\text{-}14aneP_4)]Br_2$.

VII-B-7 Synthesis and Structure of Poly (pyrazolyl)borate Complexes of Zirconium (IV)

Hiroshi NAKAZAWA, Kouichirou TOYOTA, Tsutomu MIZUTA and Katsuhiko MIYOSHI* *(*Hiroshima University)*

Although transition metal complexes having poly(pyrazolyl)borate as a ligand have been widely investigated because poly(pyrazolyl)borate is isoelectronic to a cyclopentadienido anion, the chemistry of early transition metal complexes with poly(pyrazolyl)borate still remains to be exploited. We examined the reaction of Tp^*ZrCl_3 (Tp^* = hydrotris(3,5-dimethylpyrazolyl)borate) with some phenols in CH_2Cl_2 at room temperature in the presence of amine. The product in the reaction with HOAr was $Tp^*Zr(OAr)_3$, whereas the product in the reaction with catechol was $Tp^*Zr(cat)_3ZrTp^*$ where two Tp^*Zr fragments were bridged by three $O_2C_6H_4$ units. The structure was determined by ^1H and ^{13}C NMR measurements and X-ray diffraction. This type structure is unprecedented.

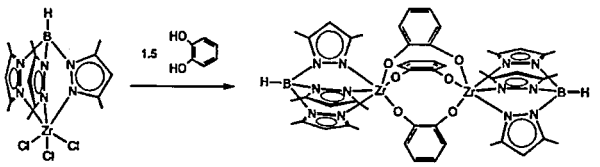

VII-C Metal Complexes as Targeting Agents for Nucleic Acids

Molecular recognition of DNA, RNA, and related biomolecules is responsible for a wide range of biochemical processes such as complementary base pairings in genetic information storage and transfer, or oligonucleotide recognition by ribozymes and restriction enzymes, etc. Metal coordination can serve as an effective binding element for host-guest interactions in aqueous solution. Therefore, metal complexes with well-designed ligands have a bright prospect of developing new targeting agents for biomolecules such as nucleic acids.

VII-C-1 Three-point Recognition of Thymine Base by a Zn^{II}-Cyclen Complex

Mitsuhiko SHIONOYA, Eiichi KIMURA* and Motoo SHIRO** *(*Hiroshima Univ., **Rigaku Corp.)*

The fundamental knowledge derived from the model study of zinc enzymes using Zn^{II}-macrocyclic polyamine complexes has been successfully developed to a new aspect of the molecular recognition of nucleobases containing an "imide" functionality. Strong association was found in a 1 : 1 ternary complex between Zn^{II}-cyclen complex **1** and AZT (azidothymidine), which was isolated from an aqueous solution at pH ~ 8.5. The X-ray crystal analysis of the ternary complex revealed a distorted square-pyramidal N_5-coordinate structure with a strong interaction between Zn^{II} and the N(3)-deprotonated "imide" anion and the two complementary hydrogen bonds between cyclen NH groups and the "imide" carbonyls. Potentiometric and spectroscopic titrations of deoxyribonucleosides, dA, dG, dC, and dT, and related compounds in the presence of **1** disclosed highly selective 1:1 binding of this complex to dT (log K = 5.6, K = [ZnL-S]/([ZnL][S]) M^{-1} at 25°C) and its derivatives, AZT (log K = 5.6), uridine (5.2), and ftorafur (4.6). The present Zn^{II} complex **1** has thus set a new prototype of host molecules for DNA/RNA nucleobase recognition in hydrophilic environment.

Reference

1) M. Shionoya, E. Kimura, and M. Shiro, *J. Am. Chem. Soc.*, **1993**, *115*, 6730.

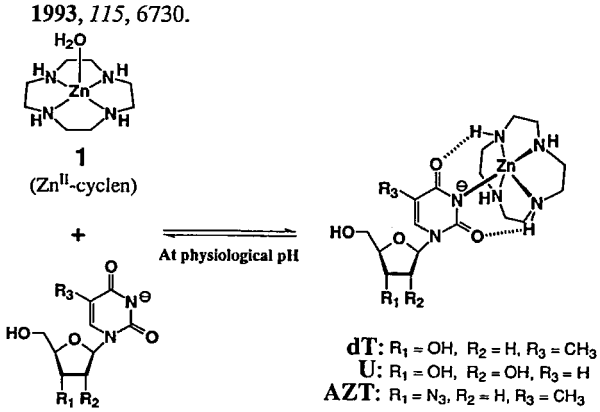

VII-C-2 Multipoint Recognition of Nucleobases by a Zn^{II} Complex of Acridine-Pendant Cyclen

Mitsuhiko SHIONOYA, Takuya IKEDA*, Eiichi KIMURA* and Motoo SHIRO** *(*Hiroshima Univ., **Rigaku Corp.)*

Zn^{II}-cyclen complex is a highly selective host for thymine or uracil base in aqueous media. In anticipation of a more efficient "multipoint" recognition, an acridine pendant has been introduced onto the cyclen ring (see, **1**). Potentiometric pH titrations of **1** were conducted in the presence of dT or its homologues. The complex formation constants were all found to be greater than those with the original Zn^{II}-cyclen complex to support our prediction of an additional binding force from a π-π stacking interaction. The order of the affinities, dT (log K = 7.2), AZT (7.2) > bromouridine (7.0) > uridine (6.9) > ftorafur (6.6) > azauridine (6.3), is consistent with that of the basicities of the conjugate base $N(3)^-$. ^1H NMR spectra of dT in the presence of **1** in aqueous media exhibit upfield shifts for a set of thymine and anomeric sugar protons as well as for the acridine protons which points to an appreciable π-π stacking interaction accompanying the coordination of thymine to Zn^{II}. In addition, the very slow deuterium exchange of the two NH groups of cyclen supports the notion of strong hydrogen bonding between the two NH groups in **1** and the two "imide" carbonyl oxygens of dT. The X-ray structure of the 1:1 ternary complex of **1** with N(3)-deprotonated 1-methylthymine is consistent with the structure concluded from the above solution behavior. It is evident that 1-methylthymine firmly binds to Zn^{II} in **1**. This complex assumes a distorted square-pyramidal structure with coordination from four nitrogens of the cyclen moiety and an N(3")-deprotonated "imide" anion of 1-methylthymine with a short Zn-N(3") bond distance of 1.987(4) Å. The carbonyl oxygen O(2") of the pyrimidine ring forms a hydrogen bond directly with a cyclen NH group, while the other carbonyl oxygen O(4") binds indirectly via a water molecule to a diagonal NH group. The acridine lies face-to-face with the plane of the thymine substrate with the inter-plane separation ranging from 3.285 to 3.419 Å, showing a well arranged inter-facial

stacking between them.

Reference

1) M. Shionoya, T. Ikeda, E. Kimura, and M. Shiro, *J. Am. Chem. Soc.*, **1994**, *116*, 3848.

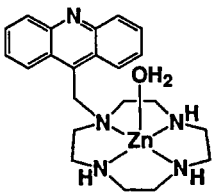

1

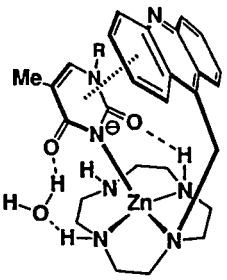

1-methylthymine complex

VII-C-3 Inhibition of Polynucleotide Hybridization and *in vitro* Poly(Phe) Synthesis by a Zn^{II}-Cyclen Complex

Mitsuhiko SHIONOYA, Masanori SUGIYAMA* and Eiichi KIMURA* *(*Hiroshima Univ.)*

Zn^{II}-cyclen complex **1** is a highly selective host in aqueous solution at physiological pH for thymine and uracil among the DNA and RNA nucleobases, respectively. Such a selective nucleobase receptor should inhibit or control some key genetic processes that involve molecular recognition via base pairing. In accordance with this notion, we have examined the biochemical ability of **1** to regulate genetic processes which involve poly (U). The effect of Zn^{II}-cyclen complex **1** on the hybridization of poly (A) and poly (U) to poly (A+U) was checked by the time-course of A_{260}. As the concentration of **1** increased ($r = [\mathbf{1}]_{added}/[uracil]_{poly(U)} = 0 \sim 2$), the rate at which the absorbance lowered decreased. At $r > 1$, practically no hybridization occurred at all. Subsequent melting experiments were performed to examine the degree of hybridization. Without **1** the hybridized strand showed a single break in the A_{260} with T_m 42 °C and hyperchromicity 31%. On the other hand, with increasing amounts of **1** ($r < 2$), the break in the absorbance plot shifted to lower temperatures with smaller hyperchromicities, until at $r = 2$ there was no break at all, which implies that the hybridization was completely inhibited at this ratio. A UV titration study showed that 48% of the total uracil bases in poly (U) formed a ternary complex with **1** at $r = 2$. A ^{31}P NMR study provided additional evidence for the inhibition of poly (A)-poly (U) hybridization by **1**. The biochemical inhibitory effect of **1** on *in vitro* polyphenylalanine synthesis in cell-free extracts was studies. Poly (U) was used as a messenger RNA (where a UUU sequence is a codon for phenylalanine). In the presence of 0.558 mM ($r = 1$) and 5.58 mM of **1** ($r = 10$), the poly(Phe) synthesis underwent 15% and 26% inhibition, respectively. This inhibition reaction may possibly involve the formation of the ternary complex of **1** with uracil bases in poly (U).

Reference

1) M. Shionoya, M. Sugiyama, and E. Kimura, *J. Chem. Soc., Chem. Commun.*, **1994**, 1747.

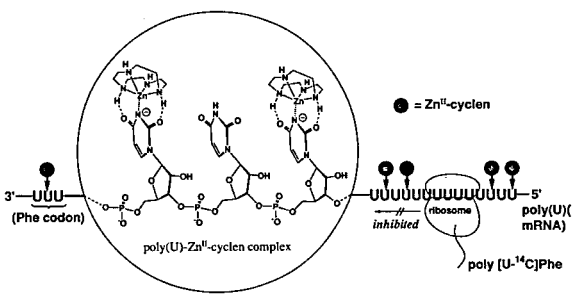

VII-D Organometallic Chemistry of Early Transition Metals

VII-D-1 Polyethylene with Extremely Narrow Polydispersity Obtained from the New Catalyst Systems $Nb(C_5Me_5)(diene)Cl_2$-MAO and $Nb(C_5Me_5)(diene)_2$-MAO

K. MASHIMA, S. FUJIKAWA, H. URATA, E. TANAKA and A. NAKAMURA

[*J. Chem. Soc., Chem. Comm.*, 1623 (1994)]

The catalyst systems described in the title were found to be active for polymerization of ethylene(1 atm) at -20° – +20°C in toluene. The activity varied with the identity of the coordinated diene in an order, butadiene > 2,3-dimethylbutadiene > isoprene. The polydispercities, *M*w/*M*n, of the polymer was found to be 1.05 for the polymer obtained at - 20°C. This low value and the time-conversion curves indicate that the polymerization proceeds in living fashion. The structure of the active species is suggested as a 14-electron cationic alkylniobium species containing cyclopentadienyl and 1,3-diene ligands. This unique combination of organic ligands with niobium is thus found to be the key for production of polyethylene with extremely narrow molecular weight distribution.

VII-D-2 Diene Complex of Lanthanum: The Crystal Structure of a Diene-bridged Dilanthanum Complex, $[LaI_2(thf)_3(\mu\text{-}\eta^4 : \eta^4\text{-}PhCH{=}CH\text{-}CH{=}CH\text{-}Ph)LaI_2(thf)_3]$

K. MASHIMA, H. SUGIYAMA and A. NAKAMURA

[*J. Chem. Soc., Chem. Comm.*, 1581 (1994)]

The direct reaction (50°C, 2 days) of metallic lanthanum with 1,4-diphenylbutadiene and iodine in THF gave the titled complex as red crystals highly sensitive to air and moisture. This is the first well-defined diene-lanthanoid complex and the structure determined by X-ray analysis indicated the presence of interesting diene-bridged dimetal structure as shown in the Figure.

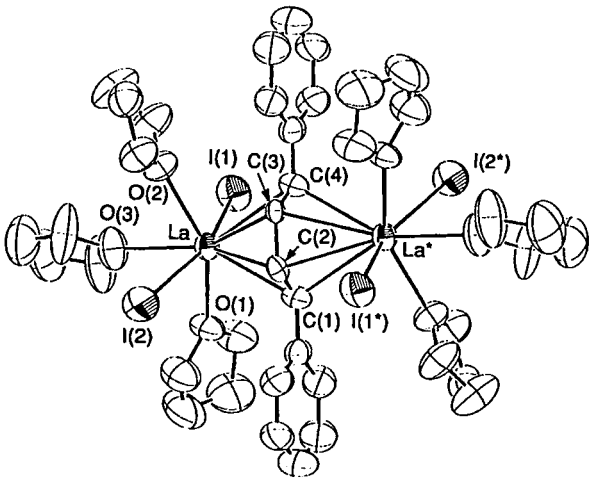

VII-E Studies on Mixed Ligand Complexes

Mixed ligand complexes which contain different kinds of ligands around the central metal ion show interesting properties such as chromotropic phenomena(solvatochromism, thermochromism etc.), plasticity, and intramolecular interligand chargetransfer. We could also obtain a tetranuclear mixed metal complex containing Fe(II) and Yb(III) which are d and f metal ions, respectively.

VII-E-1 4- and 5-Coordinate Dinuclear Copper(II) Complexes with the Tetraacetylethanediide and an N-Alkylated Diamine or a Triamine

Hide KAMBAYASHI, Junko YUZURIHARA *(Ochanomizu Univ.)*, **Yuichi MASUDA***(Ochanomizu Univ.)*, **Hiroko NAKAGAWA***(Josai Univ.)*, **Wolfgang LINERT***(Technical Univ. Vienna)* **and Yutaka FUKUDA**

[*Z. Naturforsch.*, **50b**, 536(1995)]

We have synthesized several Cu(II) dinuclear complexes with tetraketonate bridging ligand (teke=tetraacetylethanediide) and a diamine or a triamine, $[(amine)Cu(teke)Cu(amine)]X_2$. The structures of these complexes are determined by X-ray crystal structural analysis; 4-coordinate-4-coordinate, 5-coordinate-5-coordinate depending upon the polyamine used(tmen= N,N,N',N'-tetramethylethylenediamine as diamine, pmdt= N,N,N',N'',N''-pentamethyldiethylenetriamine as triamine). In organic solvents, the structure of the former complexes changes from 4-coordinate to 6-coordinate due to the donor properties of the solvents used, but the latter ones show no such behavior due to the large steric hindrance.

VII-E-2 Thermo-analytical and X-Ray Diffractometoric Observations of a Plastically Crystalline Phase in Molecular Mixed Ligand Complex

Tomoko YOSHIDA*(Tokyo Institute of Technology)*, **Masaharu OGUNI***(Tokyo Institute of Technology)*, **Yukie MORI***(Ochanomizu Univ.)* **and Yutaka FUKUDA**

[*Solid State Commun.*, **93**, 159(1995)]

We have synthesized $[M(hfac)_2(tmen)]$ where M=Ni, Cu, hfac=1,1,1,5,5,5-hexafluoroacetylacetonate, tmen= N,N,N',N'-tetramethylethylenediamine, which are non-charged complexes, are very soluble in non-polar organic solvents and show very low melting point(less than 100°C). From the DSC and X-ray diffractometry of the Ni(II) complex, there were two phase transitions I-II and II-L(liquid), among which the phase II of the Ni(II) complex was concluded to be in the plastically crystalline phese and in the face-centered cubic system.

VII-E-3 Copper(II) Mixed Ligand Complex with an N-alkylated Diamine and a New β-Diketonate

Farideh JALILEHVAND*(Ochanomizu Univ.)*, **Youichi ISHII***(Tokyo Univ.)*, **Masanobu HIDAI***(Tokyo Univ.)* **and Yutaka FUKUDA**

[*Chem. Lett.*, **1995**, 743(1995)]

Along with the line VII-E-1 we have tried to get other types of tetraketonate ligand by the reaction between two acetylacetonate and aldehydes acoording to the reported method. We could obtain a new ↓-diketonate(L) due to the aldol-condensation which can form a mixed ligand complex with copper(II) ion, [Cu(L)(tmen)Cl]. Structure of the complex is 5-coordinate square-pyramidal one. The complex shows solvatochromism(blue to green) due to the coordinated chloride dissociation which depends upon the acceptor properties of the solvents used.

VII-E-4 Electronic Structure and Electronic Transitions of (Catecholate)(1,10-phenanthroline) copper (II): Intramolecular Interligand Electronic Interaction

Yasunori YAMADA*(Aoyamagakuin Univ.)*, **Toshihiko HOSHI***(Aoyamagakuin Univ.)* **and Yutaka FUKUDA**

[*J.Coord. Chem.*, in press, 1995]

So far, there is no report concerned with the intra-

molecular interligand charge transfer in the mixed ligand complexes. In the mixed complex, [Cu(cat)(phen)], they say that the stability constant of the system(Cu + cat + phen = [Cu(cat)(phen)]) is tremendously higher than the corresponding bis-chelates ($[Cu(cat)2]^{2-}$ or $[Cu(phen)2]^{2+}$) and that the meaning of this high stability is due to an interligand interaction in the system, i.e., π-acid(phen) and p-base(cat) suitable combination. But, unfortunately, there is no good evidence about that except one report(Inorg. Chim. Acta, 1993) which was not correct. In this study, we could calculate the MO of the system and measured polarization spectra using streched PVA films, from which the observed bands were assigned and the interligand CT-transfer was discussed.

VII-E-5 d-f Matal Ion Interaction through Fe-CN-Ln Bridge between Dicyanobis (1,10-phenanthroline) iron (II) Complex and $LnCl_3$

Kazumasa HARADA(*Rikkyo Univ.*) **Junko YUZURIHARA**(*Ochanomizu Univ.*), **Youichi ISHII**(*Tokyo Univ.*), **Noriko SATO**(*ToshibaCorp.*), **Hide KAMBAYASHI**(*Ochanomizu Univ.*) **and Yutaka FUKUDA**

[*Chem. Lett.*, 1995, 887]

We have studied chromotropic phenomena of the metal complexes, among which $[Fe(CN)_2(phen)_2]$ is a typical color indicator for the accepter strength of solvents. On the other hand, a series of lanthanide ions shows a lanthanide contraction, which means that a heavier lanthanide ion is stronger acid than the lighter one. Then, in an appropriate solvent such as alcohol, the color of the iron-complex changes with the acidity of Ln^{3+} ion, i.e., with decreading ionic size of the lathanide ions used. On the other hand, in the solvent with very strong donor properties such as DMSO, we could not observe any noticeable color change of the iron-complex with different Ln^{3+} ions. We could obtain a good single crystal of $[Fe(phen)_2(CN)_2]_2[Yb(H_2O)Cl_3]_2$, which is a tetranuclear complex with CN bridge.

VII-F Activation of Carbon Dioxide by Metal Complexes

Reduction of carbon dioxide has been extensively studied. A variety of metal complexes have been shown to be active for electro- and photochemical CO_2 reductions. Most of the products in those reductions, however, are limited to formic acid and carbon monoxide. Development of multi-electron reduction of CO_2 accompanied by carbon-carbon bond formation by homogeneous catalysts is expected to contribute for the utilization of CO_2 as possible C1 resources for preparations of various chemicals. An electron density of CO_2 ligated on reduced metal complexes is highly enhanced due to π-back donation from d-orbital of the complexes. The reactivity of the CO_2 molecule bonded to metal complexes, therefore, is controlled by the selection of metals and ligands. Not only metals but also sulfur ligands are possible reaction sites for reduction of CO_2 accompanied by C-O bond cleavage and fixation of CO_2 to organic molecules with maintaining CO_2 moiety.

VII-F-1 Ruthenium Formyl Complexes as the Branch Point in Two- and Multi-Electron Reduction of CO_2

Kiyotuna TOYOHARA, Hirotaka NAGAO, Tetsunori MIZUKAWA and Koji TANAKA

[*Inorg. Chem.*, in press]

We have found that $[Ru(bpy)(trpy)(CHO)]^+$ (bpy=2,2'-bipyridine; trpy= terpyridine) formed in electrochemical reduction of $[Ru(bpy)(trpy)(CO)]^{2+}$ in $EtOH/H_2O$ at -20°C plays the key roles in not only the multi-electron reduction of CO_2 affording HCHO, CH_3OH, HOOCCHO, and $HOOCCH_2OH$ but also two-electron reduction producing $HCOO^-$ and CO. Both CO evolution and formyl complexes generation take place competitively by a two electron reduction of metal-CO complexes resulting from acid-base equilibrium between CO_2 and CO on metal. Further reduction the formyl produces affording hydroxymethyl species as a precursor to CH_3OH and the reaction with CO_2 producing $HCOO^-$ with regeneration of metal carbonyl complexes as the precursor of CO evolution occur also competitively. Formyl intermediates (Scheme 1), therefore, are the branch point for two- and multi-electron reduction of CO_2, which well explains why most of the reduction products have been limited to CO and/or HCOOH in electro- and photochemical CO_2 reduction catalyzed by metal complexes reported so far.

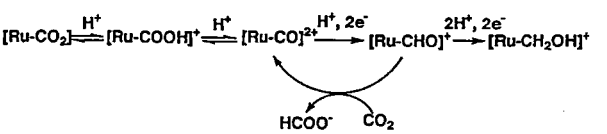

Scheme 1. Formyl intermediate as the branch point in two-and multi-electron reduction of CO_2

VII-F-2 Multi-Step CO_2 Reduction Catalyzed by $[Ru(bpy)_2(CO)]^{2+}$ (bpy = 2,2'-bipyridine, qu = quinoline). Double Methylation of Carbonyl Moiety Resulting from Reductive Disproportionation of CO_2

Hiroshi NAKAJIMA, Yoshinori KUSHI, Hirotaka NAGAO and Koji TANAKA

[*Organometallics* in press]

From the viewpoint of CO_2 as potential C1 sources for organic compounds, multi-electron reduction of CO_2 using organic electrophiles in place of proton may provide more versatile routes for catalytic carbon-carbon bond formation. Oxide transfer from $[M\text{-}\eta^1\text{-}CO_2]^{n+}$ to CO_2 affording $[M\text{-}CO]^{2+}$ and CO_3^{2-} in aprotic media, therefore, is expected to serve the multi-electron reduction of CO_2 in the presence of organic nucleophiles. Although well characterized $[Ru(bpy)_2(CO)(\eta^1\text{-}CO_2)]$ shows no reactivity toward CO_2, replacement of the CO ligand of the η^1-CO_2 complex with an electron donating group would greatly

enhance the basicity of the η^1-CO_2 moiety. Conversion from CO_2 to CO in aprotic media would serve for multi-electron reduction of CO_2 in the presence of organic electrophiles. Indeed, $[Ru(bpy)_2(qu)(CO)]^{2+}$ and CO_3^{2-} are smoothly produced in the reaction of $[Ru(bpy)_2(qu)(\eta^1\text{-}CO_2)]$ (qu = quinoline) with CO_2, and effectively catalyzes reductive disproportionation of CO_2 forming CO and CO_3^{2-} in the electrochemical CO_2 reduction in the presence of $LiBF_4$. The same reduction using $(CH_3)_4NBF_4$ in place of $LiBF_4$ in DMSO/CH_3CN produced CO, $CH_3C(O)CH_3$, $CH_3C(O)CH_2COO^-$, and $HCOO^-$ where $[Ru(bpy)_2(qu)\{C(O)CH_3\}]^+$ functions as precursor to $CH_3C(O)CH_3$. Furthermore, $CH_3C(O)CH_3$ undergoes carboxylation by $[Ru(bpy)_2(qu)(\eta^1\text{-}CO_2)]$ to give $CH_3C(O)CH_2COO^-$ and $HCOO^-$. The first catalytic formation of ketones by double methylation of metal-carbonyl resulting from reductive disproportionation of CO_2 is explained by Sheme 1.

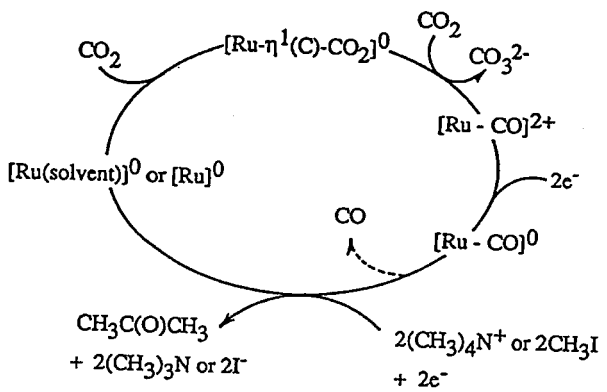

[Ru] = $[Ru(bpy)_2(qu)]$

Schrme 1. Catalytic formation of $CH_3C(O)CH_3$ in electrochemical CO_2 reduction

VII-F-3 Catalytic Formation Ketones by Double Alkylation of CO Formed by Reductive Disproportionation of CO_2 on a Ruthenium Complex

Hiroshi NAKAJIMA, Hirotaka NAGAO, Tetsunori MIZUKAWA and Koji TANAKA

[*Chem. Lett.*, **251** (1995)]

Electrochemical CO_2 reduction by $[Ru(bpy)_2(L)(CO)]^{2+}$ (L = quinoline derivatives) produces CO and HCOOH in protic conditions. On the other hand, reductive disproportionation reaction of CO_2 affording CO and CO_3^{2-} smoothly takes place in the absence of proton source under the similar electrochemical CO_2 reduction. (eq 1). Furthermore, the similar electrolysis in the presence of CH_3I gives rise to

$$2CO_2 + 2e^- \longrightarrow CO + CO_3^{2-} \quad (1)$$

the formation of ketones and β-keto acids together with concomitant evolution of ethane. The formation of ketones results from double alkylation of CO formed in the reductive disproportionation of CO_2 (eq 1). The reaction (2) is explained by an acyl intermediate in the catalytic cycle of the CO_2 reduction.

$$2CO_2 + 2CH_3I + 4e^- \longrightarrow CH_3C(O)CH_3 + CO_3^{2-} + 2I^- \quad (2)$$

VII-F-4 Comparison of Ru-C Bond Characters Involved in Successive Reduction of Ru-CO_2 to Ru-CO_2OH

Kiyotuna TOYOHARA, Kiyoshi TSUGE and Koji TANAKA

[Organometallics, in press]

Smooth conversion of CO_2 to highly reduced organic compounds under mild conditions is highly desired from the viewpoint of utilization of CO_2 as C1 resources. Electrochemical CO_2 reduction by $[Ru(bpy)(trpy)(CO)]^{2+}$ in EtOH/H_2O at -20°C proceeeds via Ru-CO_2, Ru-C(O)OH, Ru-CO, Ru-CHO, and Ru-CH_2OH species to produce HCOOH, CO, HCHO, CH_2OH, HOOCCHO, and $HOOCCH_2OH$. Such multi-step conversion of CO_2 on Ru is accomplished by variation in the carbon orbital of the Ru-C bonds (sp^2, sp, and sp^3). Taking into account that multi-electron reduction of CO_2 is more favorable than two-electron reduction in a thermodynamic sense, the changes in the bond character involved in multi-electron reduction of CO_2 by metal complexes would give crucial influence on the formation energy of HCOOH, CO, HCHO, CH_3OH, and CH_4. Comparisons of raman spectra of a series of $[Ru(bpy)_2(CO)X]^{n+}$ (X = CO, C(O)OH, $C(O)OCH_3$, CO_2, CHO, and CO_2OH; n = 0, 1, 2) and their ^{18}O or deuterium isotope analogs permit reasonable assignments of ν(Ru-X) and ν(Ru-CO) bands around 520 and 470 cm^{-1}, respectively. The ν(Ru-X) bands shift to higher wavenumbers with lengthening the Ru-X bond distances (d(Ru-X)) (Figure 1). Such unusual dependence of ν(Ru-X) upon d(Ru-X) may be associated with multi-bond characters of the C≡O, C=O, and C-O bonds in the Ru-X moieties.

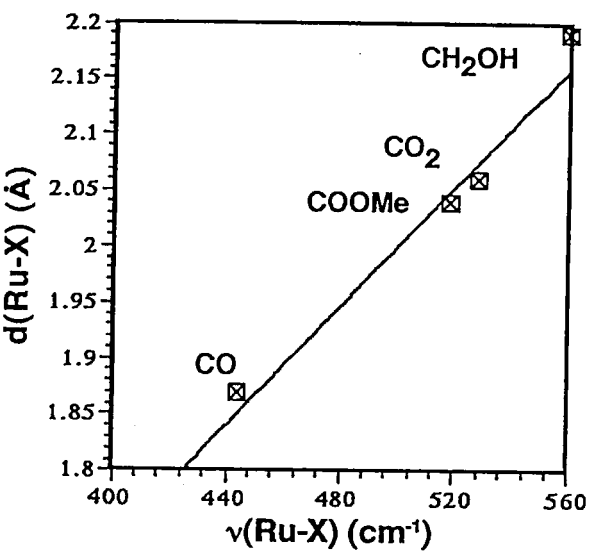

Figure 1. Relationship between Ru-X bond length (d(Ru-X)) and ν(Ru-X)) band of $[Ru(bpy)_2(CO)X]^{n+}$ (X = CO, C(O)OMe, CO_2 and CH_2OH; n = 0, 1, 2).

VII-F-5 Crystal Structure of $[Ru(bpy)_2(CO)(\eta^1\text{-}C(O)OH)]^+$ as a Key Intermediate in CO_2/CO Conversion

Kiyotuna TOYOHARA, Hirotaka NAGAO and Koji TANAKA

[*Chem. Lett.*, 2175 (1994)]

Activation of CO_2 on metal complexes is a subject of continuing importance in utilization of CO_2 as C1 resources. The CO_2/CO conversion under protic conditions is generally explained by an acid-base equilibrium among η^1-CO_2, -COOH and -CO metal complexes (eq 1), and amphoteric reactivity of metal-C(O)OH complexes plays the key

$$[M\text{-}CO_2]^{n+} \underset{OH^-}{\overset{H^+}{\rightleftharpoons}} [M\text{-}C(O)OH]^{(n+1)+} \underset{OH^-}{\overset{H^+}{\rightleftharpoons}} [M\text{-}CO]^{(n+2)+} \quad (1)$$

role in the smooth conversion from CO_2 to CO. The comparison of molecular structures of η^1-COOH and -CO_2 metal complexes would serve to understand an enormous wide range of pK_a values of metal-COOH complexes (from 2.5 to over 14) compared with those of organic carboxylic acids. The molecular structure of $[Ru(bpy)_2(CO)(C(O)OH)]^+$ (pK_a 9.5) which exists as equilibrium mixtures with $[Ru(bpy)_2(CO)(CO_2)]$ and $[Ru(bpy)_2(CO)_2]^{2+}$ in H_2O is expected to afford fundamental knowledge with respect to the amphoteric reactivity of metal-COOH species. X-ray analysis of $[Ru(bpy)_2(CO)(C(O)OH)](PF_6)$ (Figure 1) revealed that the Ru-COOH bond distance of $[Ru(bpy)_2(CO)(C(O)OH)]^+$ (2.003 Å) is much shorter than the Ru-CO_2 one of $[Ru(bpy)_2(CO)(CO_2)]$ (2.064 Å). The shortening of the former is ascribed to an increase in a π-acceptor ability of the COOH moiety, which also reflects a blue shift of the ν(CO) band at 1952 of $[Ru(bpy)_2(CO)(CO_2)]$ to 1911 cm^{-1} upon the protonation of the CO_2 moiety. The smooth conversion of eq. 1 in H_2O is found to be assited by synergic σ-donor and π-acceptor chracteristics of not only COOH but also CO and bpy ligands.

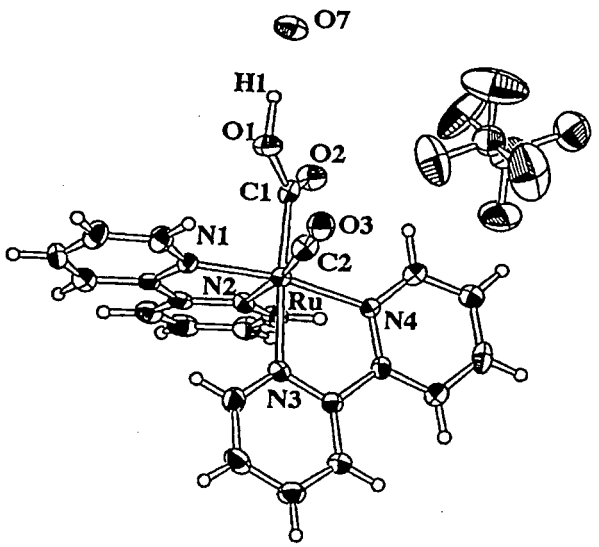

Figure 1. Crystal structure of $[Ru(bpy)_2(CO)(C(O)OH)](PF_6)\cdot H_2O$.

VII-F-6 Oxalate Formation in Electrochemical CO_2 Reduction Catalyzed by a Rhodium-Sulfur Cluster

Yoshinori KUSHI, Hirotaka NAGAO, Takanori NISHIOKA, Kiyoshi ISOBE and Koji TANAKA

A variety of transition metal complexes have been shown to catalyze electrochemical CO_2 reduction affording CO and/or HCOOH, where metal-η^1-CO_2 intermediates are generally believed as the precursors for those products. On the other hand, smooth conversion from metal-η^1-CO_2 to -C(O)OH and -CO complexes strongly interfares oxalate formation in electrochemical CO_2 reduction by homogeneous catalysts. Activation of CO_2 on a $M_3(\mu_3\text{-}S)$ framework was conducted to avoid the C-O bond cleavage via metal-η^1-CO_2 complexes. Electrochemical CO_2 reduction catalyzed by $[(Cp^*Rh)_3(\mu_3\text{-}S)_2](BPh_4)_2$ selectively produced oxalate without accompanying CO and HCOOH generation. A solution IR spectrum evidenced formation of a 1: 2 adduct of $[(RhCp^*)_2(\mu_3\text{-}S)_2]^0$ with CO_2. The first successful oxalate generation by $[(RhCp^*)_2(\mu_3\text{-}S)_2]^0$ is explained by a coupling reaction of two CO_2 molecules activated on the cluster.

VII-F-7 Remarkable Decrease in Overpotential of Oxalate Formation in Electrochemical CO_2 Reduction by a Metal- Sulfide Cluster

Yoshinori KUSHI, Hirotaka NAGAO Takanori NISHIOKA, Kiyoshi ISOBE and Koji TANAKA

[*J. Chem. Soc., Chem. Commun.*, 1231 (1995)]

Metal sulfur clusters with a M_3S framework may become feasible catalysts for CO_2 activation as a result of our finding of oxalate generation in CO_2 reduction by $[(RhCp^*)_3(\mu_3\text{-}S)_2](B(C_6H_5)_4)_2$. A blue CH_3CN solution of $[(IrCp^*)_3(\mu_3\text{-}S)_2]$ ($[Ir_3S_2]$) rapidly turned to an orange one upon exposure to CO_2 in the presence of $(CH_3)_4NBF_4$, and $C_2O_4^{2-}$ and $[(Ir\text{-}\eta^5\text{-}Cp^*)_2(Ir\text{-}\eta^4\text{-}Cp^*CH_2CN)(\mu_3\text{-}S)_2]^+$ ($[Ir_3S_2(CH_2CN)]^+$) (Figure 1) were obtained. Furthermore, the controlled potential electrolysis of a CO_2-saturated CH_3CN solution containing a BPh_4 salt of $[Ir_3S_2]^{2+}$ or $[Ir_3S_2(CH_2CN)]^+$ and $LiBF_4$ at -1.30 V catalytically produced $Li_2(C_2O_4)$ with a current efficiency of 60% without accompanying CO and CO_3^{2-} formation. Similarly, the electrolysis of $[(CoCp')_3(\mu_3\text{-}S)_2](BPh_4)_2$ ($[Co_3S_2]^{2+}$) at -0.70 V in CH_3CN in the presence of $LiBF_4$ under CO_2 atmosphere also afforded $C_2O_4^{2-}$ in an 80% current efficiency. Although the metals in the $[M_3S_2]^{2+}$ framework appear to be no vacant site to interact with CO_2, $[Ir_3S_2(CH_2CN)]^+$ having a coordinatively unsaturated Ir atom slowly reacted with CO_2 in CD_3CN to exhibit a strong $\nu(CO_2)$ band at 1682 cm^{-1} in the solution IR spectra. Electrolysis of $[Ir_3S_2(CH_2CN)]^+$ in CD_3CN under CO_2 showed another $\nu(CO_2)$ band in addition to the 1682 cm^{-1}. Thus, two CO_2 molecules are activated on $[Ir_3S_2CH_2CN]^0$, on which $C_2O_4^{2-}$ is produced by the coupling reaction. The oxalate formation by the $[Co_3S_2]^{2+}$ at -0.70 V is particularly noteworthy in the viewpoint of the standard redox potential of $H_2C_2O_4$ (-0.475 V *vs.* NHE) in H_2O (pH = 0) at 25°C.

VII-F-8 Control of Coordination Mode of η^{1-} and η^{2-} 1,8-Naphthyridine Ligated to Ru(II)-bis(bipyridine) Complexes

Hiroshi NAKAJIMA, Hirotaka NAGAO and Koji TANAKA

Control of site-opening and -closing woud be preferable to construct efficeint homogeneous catalysts because of stabilization of the catalysts, inihibition of side reactions, and promotion of eliminating the products from the reaction center. Along this line, $[Ru(bpy)_2(\eta^1\text{-napy})(CH_3CN)](PF_6)_2$ and $[Ru(bpy)_2(\eta^2\text{-napy})](PF_6)_2$ were prepared to compare the relative stability in solutions and their crystal structures were determined by X-ray analysis (Figure 1). An equilibrium between the η^1- and η^2-napy complexes in solutions shifts to the former. The euilibrium mixture undergoes an irreversible reduction at -0.98 V (vs. Ag/AgCl) in DMF. The process gradually becomes a reversible redox reaction on raising temperature, suggesting that one electron reduction of the η^1- and η^2-napy complexes at higher temperature gives rise to shift of the equilibrium to the latter. EPR study of one electron reduced forms of these complexes at 0°C revealed that odd electron is accomodated into a localized orbital of napy without an appreciable increase in the electron density on one of the nitrogen atom of the ligand. An inclinatrion of the charge density between two nitrogen atoms of singly reduced napy results in stabilization of the η^1-napy mode rather than η^2-napy one. Thus, the coordination mode of η^1- and η^2-napy is controlled by both the redox reaction and temperatures.

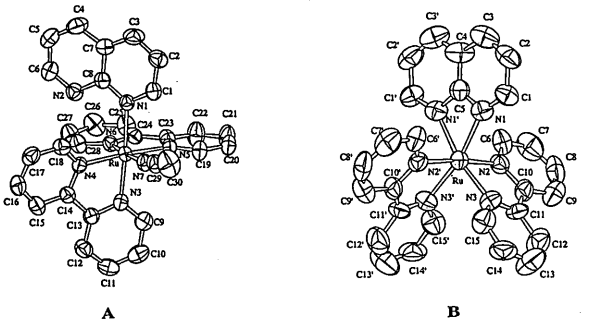

A B

Figure 1. Crystal structures of $[Ru(bpy)_2(\eta^1\text{-napy})(CH3CN)]^{2+}$ (A) and $[Ru(bpy)_2(\eta^2\text{-napy})]^{2+}$ (B).

VII-G Development of Highly Selective Reactions Using Early Transition Metal Complexes

Highly Selective bond formation reactions have been investigated using early transition metal complexes, especially zirconium complexes, Zirconium alkene or alkyne complexes, zirconacyclopentene, zirconacyclopentadienes could be used for selective C-C bond formation or selective functionalization.

VII-G-1 Intramolecular Coupling of Alkynyl Groups of Bis(alkynyl)silane Mediated by Zirconocene Compounds: Formation of Silacyclobutene Derivatives

Tamotsu TAKAHASHI, Zhenfeng XI, Yasushi OBORA and Noriyuki SUZUKI

[*J. Am. Chem. Soc.*, 117, 2665 (1995)]

Carbon-carbon bond forming reaction from diorganometal compounds has been well known for transition metals (eq 1). However, this type of reaction has been very rare for diorganosilicon compounds.

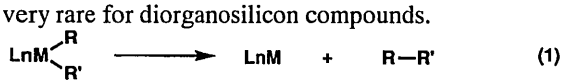

Treatment of bis(alkynyl)silane 2 (R = Ph, R' = Me : 2a, Et : 2b, Ph : 2c) with Cp_2ZrEt_2 and iodine in this order gave diphenyldiyne 3 in high yields (eq 2).

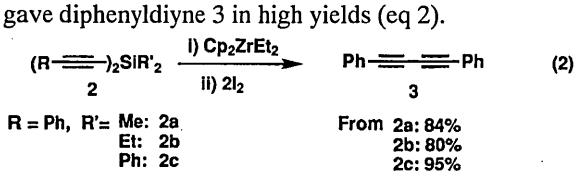

In order to understand the mechanism, we investigated the reaction mixture of **2a-c** with Cp_2ZrEt_2. Very interestingly, silacyclobutene derivatives **7** were formed in high yields after hydrolysis. A plausible mechanism is shown in the following Scheme 2 which involves (i)a replacement of an ethylene ligand of **1** by an alkynyl group of **2a-c** to form a zirconacyclopropene compound, (ii) an insertion of the second alkynyl group of **2a-c** into a Zr-C bond of the zirconacyclopropene to form **11**, and (iii)1,2-migration of a silyl group from **12** to **13** leading to **9**. (iv) Iodination of **9** affords a diiodide species as an intermediate followed by an elimination of silyl and iodine groups which gives diphenyldiyne **3**.

Scheme 1

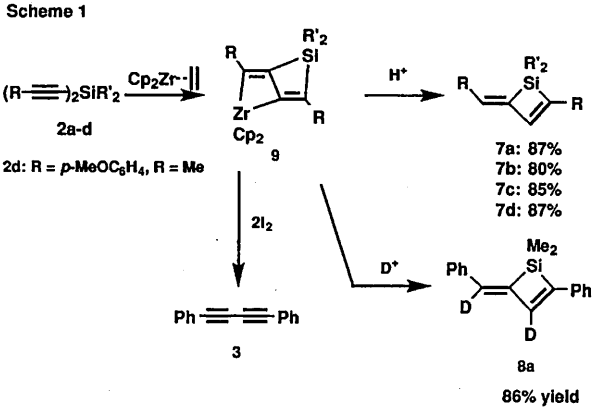

Scheme 2

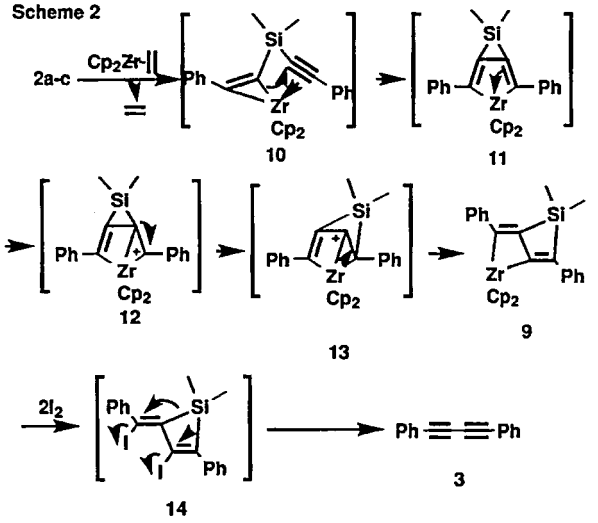

VII-G-2 A Vinylzirconation Reaction of Alkynes

Tamotsu TAKAHASHI, Denis Y. KONDAKOV, Zhenfeng XI and Noriyuki SUZUKI

[*J. Am. Chem. Soc.*, 117, 5871 (1995)]

Carbometalation is a very attractive method to prepare directly organometallic compounds. However, some carbometalation products such as alkenylmetalation products of alkynes have a similar reactivity to the starting organometallic compounds. This type of carbometalation results in oligomerization or polymerization reactions. This is one of the major reasons to limit the scope of alkenylmetalation of alkynes.

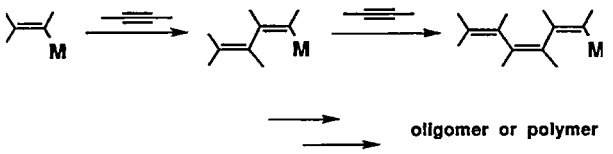

A vinylzirconation reaction of unactivated alkynes proceeded when alkynes were treated with diethylzirconocene followed by vinyl ethers. Hydrolysis, iodinolysis and deuterolysis of the reaction mixtures gave the corresponding dienes, dienyl iodides and deuterated dienes, respectively, in good yields. A proposed mechanism of the vinylzirconation involves the formation of a zirconacyclopentene, replacement of ethylene moiety of zirconacyclopentene by a vinyl ether, and β-abstaction of OR group. A reaction of zirconacyclopentene prepared from diphenylacetylene and diethylzirconocene with vinyl ethyl ether gave the vinylzirconation product of diphenylacetylene in 85% yield.

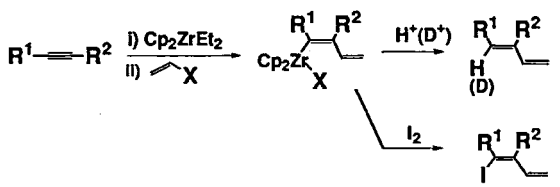

VII-G-3 Oxidative Addition of 2-Haloalkene to Zirconocene

Tamotsu TAKAHASHI, Martin KOTORA, Reinald FISCHER, Yasushi NISHIHARA and Kiyohiko NAKAJIMA* *(*Aichi Univ of Education)*

[*J. Am. Chem. Soc.*, in press]

Alkenylzirconocene compounds, which are easily prepared by the hydrozirconation of alkynes, have been very useful intermediates in organic synthesis. Hydrozirconation of terminal alkynes regio- and stereo-selectively affords alkenylzirconocene compounds of type I. Even though compound II is formed *in situ*, it immediately isomerizes to I in the presence of Cp_2ZrHCl. Consequently an alkenylzirconocene of type II can not be obtained by this method.

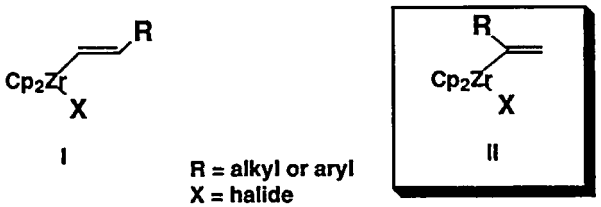

In order to prepare a type II compound, we have investigated novel oxidative addition reactions of 2-haloalkenes to Zr(II). Compared with late transition metal chemistry, only a few examples of intermolecular oxidative addition reactions are known for zirconocene using alkyl halides, arenes, phosphorus compounds, silanes and allyl ethers. In some cases, further useful synthetic applications were reported but the oxidative addition intermediates have not been structurally characterized. In addition, there is no report of oxidative addition for alkenyl halides to zirconocene, to the best of our knowledge.

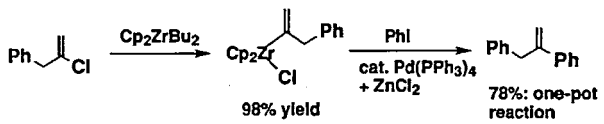

VII-G-4 Highly Selective and Practical Alkyne-Alkyne Cross Coupling Reaction Using Cp_2ZrBu_2 and Ethylene

Zhenfeng XI, Ryuichiro HARA and Tamotsu TAKAHASHI

[*J. Org. Chem.*, **60**, 4444 (1995)]

Highly selective alkyne-alkyne cross coupling reactions were achieved using Cp_2ZrBu_2 and ethylene gas. First alkynes were treated with 1.2 equiv of Cp_2ZrBu_2 under ethylene gas to give zirconacyclopentenes with high selectivities. Subsequent addition of second alkynes to the solution of zirconacyclopentenes at 50°C gave unsymmetrical zirconacyclopentadienes selectively. After hydrolysis unsymmetrical dienes were obtained in high yields.

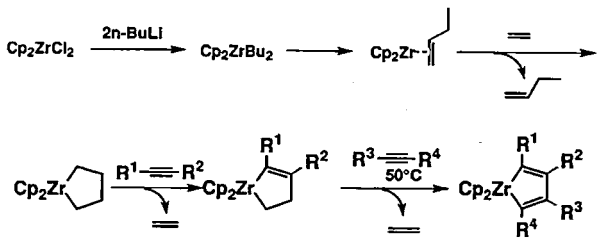

VII-G-5 Reaction of Zirconocene Ethylene Complex with Diynes: Formation of Bridged Zirconacyclopentenes

Tamotsu TAKAHASHI, Kayoko KASAI, Zhenfeng XI and Victor DENISOV

[*Chem. Lett.*, **347** (1995)]

Reactions of diynes RCC-X-CCR with zirconocene ethylene complex $Cp_2Zr(CH_2{=}CH_2)$ were investigated. When X was C_6H_4 or C_4H_2S, bridged zirconacyclopentenes were selectively formed. They were easily converted into bridged cyclopentenone derivatives. In the case of $(CH_2)n$ groups as X, the reaction products were strongly dependent on the R group.

VII-G-6 Cycloaddition of Zirconacyclopentadienes to Alkynes Using Copper Salts: Formation of Benzene Derivatives

Tamotsu TAKAHASHI, Martin KOTORA and Zhenfeng XI

[*J. Chem. Soc., Chem. Commun.*, **361** (1995)]

Reaction of zirconacyclopentadienes with alkynes such as dimethyl acetylenedicarboxylate gave benzene derivatives in the presence of CuCl/LiCl. Metallacyclopentadienes containing transition metals such as cobalt, rhodium and titanium have been known to react with one equiv of alkynes to give benzene derivatives (eq 1). This type of reaction is very attractive and very useful, since metallacyclopentadienes can be easily prepared from two equiv of alkynes.

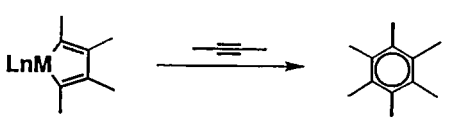

(1)

One of the major problem of this reaction concerns the control of combination of alkynes. It has been difficult to prepare cleanly the unsymmetrical metallacyclopentadienes using these metals by the intermolecular coupling of two different alkynes. This is the reason why there is no report for the selective formation of benzene derivatives from three different alkynes. Recently a variety of unsymmetrical zirconacyclopentadienes have been prepared by several methods. However, unfortunately, there is no precedent of the cycloaddition reaction of these zirconacyclopentadienes to third alkynes. We found the novel cycloaddition reaction of zirconacyclopentadienes to the third alkynes in the presence of a stoichiometric amount of CuCl/LiCl.

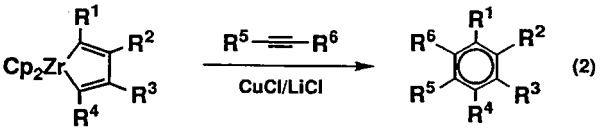

(2)

VII-G-7 Practical and Selective Method for Preparation and Reactions of Cp_2HfRCl and Cp_2HfRR'

Tamotsu TAKAHASHI, Toyohisa ISHIDA and Yasushi NISHIHARA

[*Chem. Lett.*, 159 (1955)]

Practical method for preparation of Cp_2HfRCl and Cp_2HfRR' has been investigated. Mono(alkyl)hafnocene chloride complexes were selectively prepared by three methods; (i) a reaction of $Cp_2HfR(OMe)$ with MeCOCl, (ii) a reaction of Cp_2HfCl_2 with an excess of R_3Al and (iii) a reaction of one equiv of n-RLi. Treatment of Cp_2HfRCl with R'_3Al led to an alkyl exchange reaction to form $Cp_2HfR'Cl$. Mono(alkyl)hafnocene complexes in situ prepared by (iii) reacted with one equiv of R'Li to give Cp_2HfRR' ($R \neq R'$) with a high selectivity.

VII-G-8 Formation of a Five-Membered Carbocyclic Ring by Reaction of Zirconacyclopentane with RCOCl

Tamotsu TAKAHASHI, Martin KOTORA and Zhenfeng XI

[*J. Chem. Soc., Chem. Commun.*, 1503 (1995)]

Zirconacyclopentane is a very attractive compound since it is easily prepared from alkenes or dienes. In order to produce a five-membered carbocyclic ring from a zirconacyclopentane, one carbon unit is required to react with it. Only carbon monoxide or isonitrile has been used so far as the one carbon unit for zirconacycles such as zirconacyclopentanes.

(1)

Here we found that zirconacyclopentane reacted with RCOCl in the presence of a catalytic amount of CuCl/LiCl to give a five-membered carbocyclic ring.

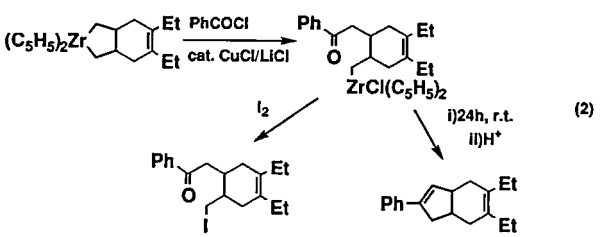

(2)

VII-G-9 Zirconium Mediated or Catalyzed Highly Stereoselective Cyclization of 1,4,7-Trienes

Tamotsu TAKAHASHI, Martin KOTORA and Kayoko KASAI

[*J. Chem. Soc., Chem. Comm.*, 2693 (1994)]

Cyclization reaction of 1,4,7-trienes, which are easily prepared by double allylation reaction of alkynes, proceeded in the presence of stoichiometric or catalytic amount of zirconocene compounds to give only cis isomer (>98% stereoselectivity).

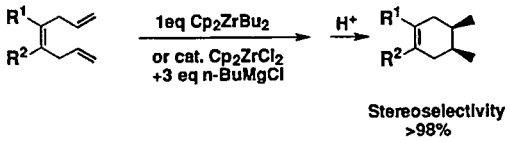

VII-G-10 Chemoselective Carbon-Carbon Bond Formation Reaction of Zirconacyclopentenes with Allylic Compounds

Kayoko KASAI, Martin KOTORA, Noriyuki SUZUKI and Tamotsu TAKAHASHI

[*J. Chem.Soc. Chem. Commun.*, **109** (1995)]

The reaction of zirconacyclopentenes with allyl chloride in the presence of cuprous salt and lithium salt proceeded at the alkenyl carbon on zirconium with high selectivity to give allylation products; allylation at alkyl carbon was also achieved by treatment of zirconacyclopentenes with cuprous salt, methanol and allyl chloride in this order.

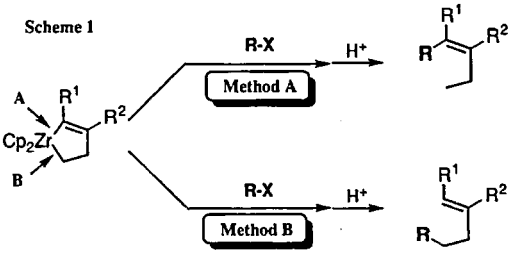

VII-H Building of Two and Three-Dimensional Coordination Polymers Possessing Potential High Electrical Conductivity, Novel Host Metal Complexes and Polynuclear Complexes

A global persistent searching for new materials with improved properties has led to an extensive investigation into inorganic and organic polymers. The reasoning behind this strategy is that if these new materials possess some properties unique to either organic polymers or inorganic polymers, they may produce revolutionary development in fundamental science and technology. Thus, attention is being focused increasingly on polymeric metal complexes which possess both properties of inorganic and organic compounds. We have synthesized a number of one-, two- and three-dimensional metal complexes with donor organic compounds, which have been found to give high electrical conductivity. Novel host metal complexes, polynuclear nickel(0), copper(I and II) and silver(I) complexes were also synthesized.

VII-H-1 Building of 2D Sheet of Tetrakis (methylthio)tetrathiafulvalenes Coordinating to Copper(I) Halides with Zigzag and Helical Frames and the 3D Network through the S···S Contacts.

Megumu MUNAKATA (*[a]Kinki Univ. and IMS*), **Takayoshi KURODA-SOWA,[a] Masahiko MAEKAWA,[a] Akihiro HIROTA[a] and Susumu KITAGAWA** (*Tokyo Metropol. Univ.*)

[*Inorg. Chem.*, **34**, 2705-2710 (1995)]

Three copper (I) complexes with tetrakis(methylthio) tetrathiafulvalene (TMT-TTF), $[(Cu_2(\mu\text{-}X)_2(\mu\text{-TMT-TTF})]_\infty$ (X=Cl, **1**; X=Br, **2** and X=I, **3**) were synthesized. **1** is 2D sheet composed of TMT-TTF molecules arranged between new zigzag frames of CuCl and 3D structure is formed through S····S contacts of 3.53 Å and 3.63 Å between the 2D sheets. **2** has 2D structure in which TMT-TTF molecules are connected between novel helical frames of CuBr and the S····S contacts of 3.68 Å exist between the neighboring molecules. The methyl thioether groups of TMT-TTF in **3** are coordinated to the coppers of rhomboid Cu_2I_2 to give linear chains. The black I_2-doped **1-3** show a new broad band at ca 880 nm indicative of the oxidation of TMT-TTF molecules and give electrical conductivity.

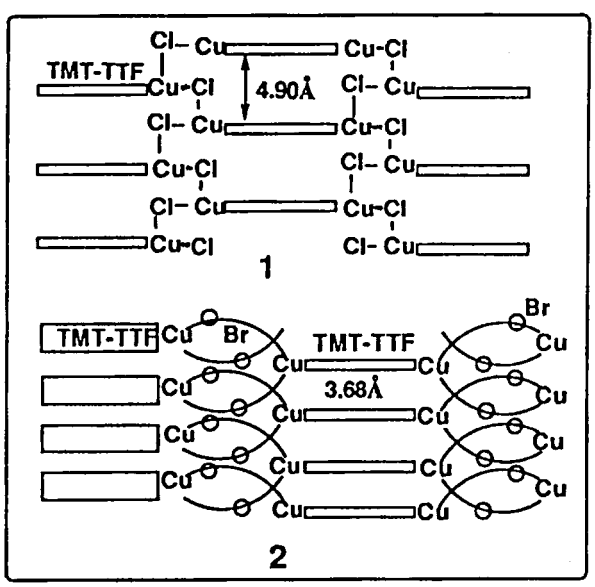

VII-H-2 Syntheses, Structures and Properties of Copper(I) Coordination Polymers with Bridging Phenazine: Construction of One- and Two-dimensional Structures with π-π Stacking of Phenazine.

Takayoshi KURODA-SOWA,[a] Megumu MUNAKATA (*[a]Kinki Univ. and IMS*), **Hajime MATSUDA,[a] Shin-ichi AKIYAMA[a] and Masahiko**

MAEKAWA[a]

[*J. Chem. Soc. Dalton Trans.*, 2201-2208 (1995)]

Four novel copper(I) phenazine (phz) compounds, $[Cu(phz)(NO_3)]_\infty$ (**1**), $\{[Cu(acr)_2(NO_3)]_2(phz)(H_2O)\}_\infty$ (**2**) (acr=acridine), $[Cu_2(phz)(PFO_3)]_\infty$ (**3**), $\{[Cu(phz)(MeCN)]_2(C_{16}H_{10})(PF_6)_2\}_\infty$ (**4**) have been synthesized which have one- or two-dimensional polymeric structures with π-π stacking of phz. Electrical conductivity of these polymer compounds were studied.

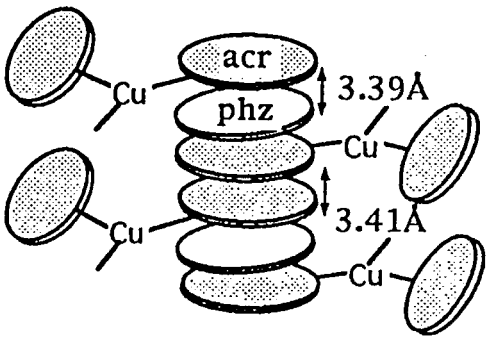

$[Cu(acr)_2(NO_3)]_2(phz)(H_2O)$ (2)

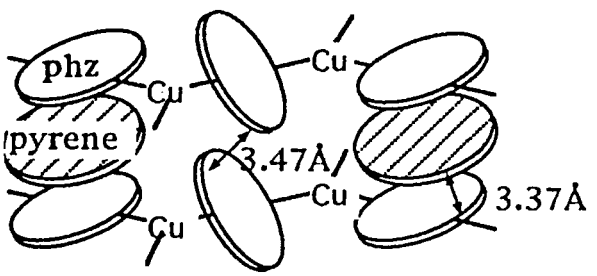

$\{[Cu(phz)(CH_3CN)]_2(pyrene)(PF_6)_2\}_\infty$ (4)

VII-H-3 Synthesis and Structures of Tetranuclear and Hexanuclear Copper(I) Complexes with Iminomethanethiolate Bridges Derived from Isothiocyanate

Takayoshi KURODA-SOWA,[a] Megumu MUNAKATA (*[a]Kinki Univ. and IMS*), **Makoto MIYAZAKI[a] and Masahiko MAEKAWA[a]**

[*Polyhedron*,**14**, 1003-1009 (1995)]

Methylisothiocyanate (MeNCS) in ethanol and allylisothiocyanate (C_3H_5NCS) in methanol reacted with Cu(I) giving a tetranuclear complex $[Cu_4\{\mu_3\text{-}SC(NME)(OEt)\}_4]$ and a hexanuclear complex $[Cu_6\{\mu_3\text{-}SC(NC_3H_5)(OMe)\}_6]$, respectively. The reaction mechanism of isothiocyanate with alcohol and the molecular structures were clarified.

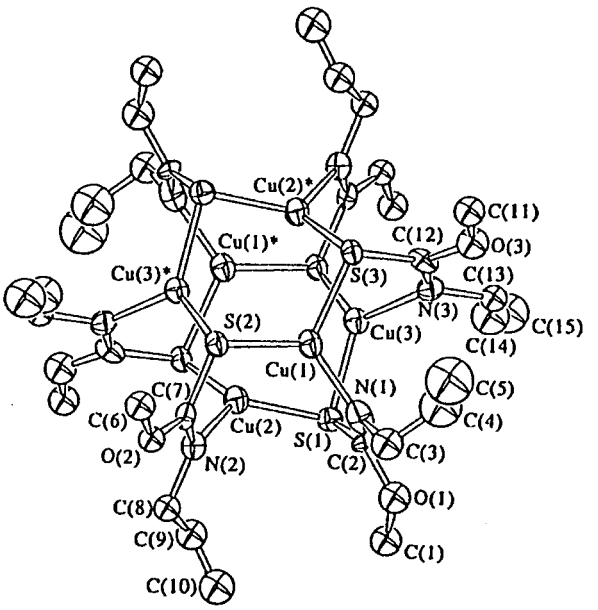

$[Cu_6\{\mu_3\text{-}SC(NC_3H_5)(OMe)\}_6]$

VII-H-4 Syntheses and Characterization of One- and Two-dimensional Copper(I) Coordination Polymers with Tetrakis (ethylthio)tetrathiafulvalene and the Properties of their Iodine-doped Compounds

Xinmin GAN,[a] Megumu MUNAKATA (*[a]Kinki Univ. and IMS*), **Takayoshi KURODA-SOWA,[a] Masahiko MEKAWA[a] and Yoshiharu MISAKI[a]**

[*Polyhedron*, **14**, 1343-1350 (1995)]

Two copper (I) complexes with tetrakis(ethylthio) tetrathiafulvalene (TTC_2-TTF), $[(CuCl)_2TTC_2\text{-}TTF]$ (**1**) and $[(CuBr)_2TTC_2\text{-}TTF]$ (**2**) have been synthesized and characterized by spectroscopic and X-ray crystallographic methods. The crystal of **1** has 2D structure in which TTC_2-TTF molecules are connected between novel helical CuCl frames. While the crystal of **2** has 1D polymeric chain structure. **1** and **2** were doped with iodine to afford $[(CuCl)_2TTC_2\text{-}TTF]I$ (**3**) and $[(CuBr)_2TTC_2\text{-}TTF]I$ (**4**) which exhibit electrical conductivities, respectively.

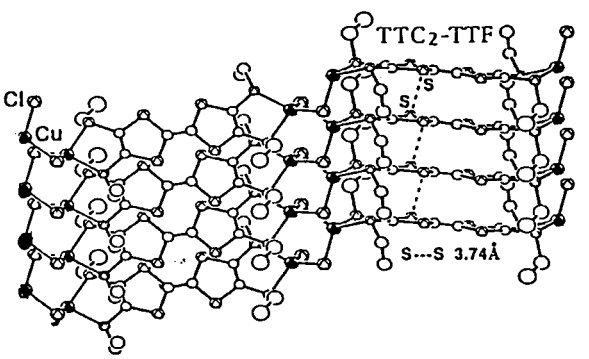

$[(CuCl)_2(TTC_2\text{-}TTF)]$ (1)

VII-H-5 Syntheses, Structures and Properties of a Linear Copper(I) Coordination Polymers with Tetrakis(ethylthio)tetrathiafulvalene

Xinmin GAN,[a] Megumu MUNAKATA *([a]Kinki Univ. and IMS)*, **Takayoshi KURODA-SOWA,[a] Masahiko MAEKAWA[a] and Mikiko YAMAMOTO[a]**

[*Polyhedron*, **14**,1647-1651 (1995)]

The sulfur-rich tetrakis(ethylthio)tetrathiafulvalene (TTC_2-TTF) reacted with copper(I) perchlorate to form a 1:1 (metal/ligand) complex $[Cu(TTC_2\text{-}TTF)]ClO_4$. All the copper atoms in the complex are coordinated to the sulfur atoms from the bridging organic ligand to form coordination linear chains. The iodine-doped product behaves as a semiconductor.

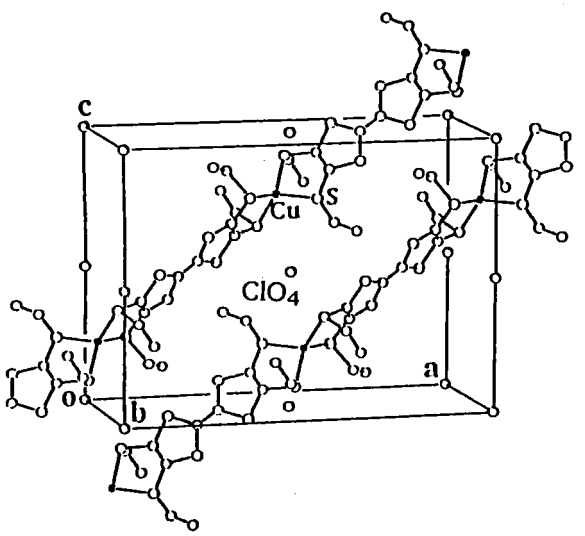

$[Cu(TTC_2\text{-}TTF)]ClO_4$

VII-H-6 Synthesis and Crystal Structure of Three-dimensional Lanthanum(III) Coordination Polymer with Mellitate, $\{La_2[C_6(COO)_6](H_2O)_9\}\cdot 2H_2O$

Liang Ping WU,[a] Megumu MUNAKATA *([a]Kinki Univ. and IMS)*, **Mikiko YAMAMOTO,[a] Takayoshi KURODA-SOWA[a] and Masahiko MAEKAWA[a]**

[*J. Coord. Chem.*, in press]

The crystal and molecular structure of lanthanum(III) mellitate, $La_2C_{12}H_{22}O_{23}$, has been determined by X-ray structure analysis. The crystal structure consists of layers perpendicular to the *a*-axis. Each layer is formed by an extended network of lanthanum ions coordinated with mellitate anions and water molecules, and linked through a complex three-dimensional hydrogen-bonding network. The two independent lanthanum ions are both nine-coordinate and the configuration around lanthanum is tricapped trigonal prism with the La-O bond distances ranging from 2.457 Å to 2.704 Å.

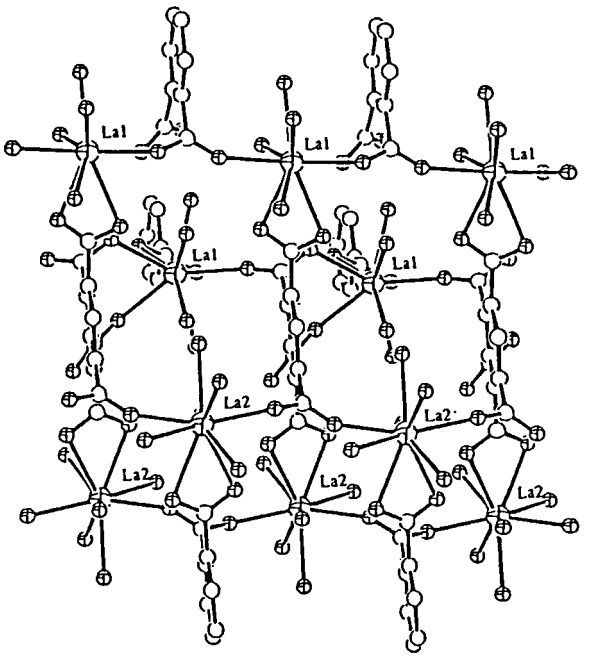

$\{La_2[C_6(COO)_6](H_2O)_9\}\bullet 2H_2O$

VII-H-7 Crystal Structure and Magnetic Properties of Manganese(II) Mellitate, $[Mn_2\{C_6(COO)_6\}(H_2O)_6][Mn(H_2O)_6]\cdot 2H_2O$ with Two-Dimensional Layer Structure and Three-Dimensional Hydrogen Bonding Networks

Liang Ping WU,[a] Mikiko YAMAMOTO,[a] Takayoshi KURODA-SOWA,[a] Masahiko MAEKAWA,[a] Jun-ichi FUKUI[a] and Megumu MUNAKATA *([a]Kinki Univ. and IMS)*

[*Inorg. Chim. Acta*, **239**, 163-167 (1995)]

There are two types of manganese ions in the structure. Mn(1) is situated on a crystallographic center of symmetry and bound to six water molecules while Mn(2) is coordinated octahedrally by three water molecules and three carboxylate oxygen atoms. The major structure feature is that the polyanion formed by Mn(2) ions and the mellitate hexanions with composition of $[Mn_2\{C_6(COO)_6\}(H_2O)_6]_n^{2n-}$ possesses a two-dimensional layer structure which is linked through a complex three-dimensional hydrogen-bonding associated with the Mn(1) cation $[Mn(H_2O)_6]^{2+}$ and the water of crystallization. Analysis of variable-temperature magnetic susceptibility data (5.0-300 K) shows that the complex displays antiferromagnetic exchange.

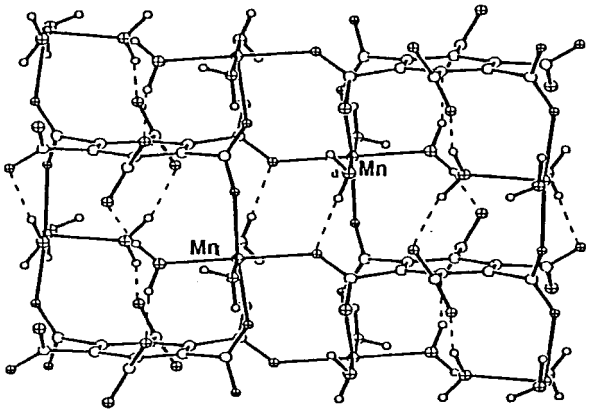

$[Mn_2\{C_6(COO)_6\}(H_2O)_6]_n^{2n-}$

VII-H-8 Synthesis and Structural Characterization of Crown Thioether Complexes of Silver(I) and Copper(II)

Megumu MUNAKATA (*[a]Kinki Univ. and IMS*), **Liang Ping WU,[a] Mikiko YAMAMOTO,[a] Takayoshi KURODA-SOWA[a] and Masahiko MAEKAWA[a]**

[*J. Chem. Soc. Dalton Trans.*, 3215-3220 (1995)]

Crown thioether Ag(I) complexes, $\{[Ag([16]aneS_4(OH)_2)](NO_3)\}_\infty$ (**1**) and $\{[Ag([16]aneS_4(OH)_2)](CH_3COO)\}_\infty$ (**2**), and Cu(II) complex $[Cu([16]aneS_4(OH)_2)](ClO_4)_2$ (**3**), where $[16]aneS_4(OH)_2$ = 1,5,9,13-tetrathiacyclohexadecane-3,11-diol, have been prepared and structures determined. In both **1** and **2** each ligand molecule $[16]aneS_4(OH)_2$ coordinates to four separate Ag(I) ions in a *exo*dentate fashion to yield a tetrahedral connected polymeric network, while in **3** Cu(II) ion forms a monomeric complex with the tetradentate macrocycle in the *endo*dentate conformation. Control of structures and dimensionalities for this type complexes by counter anion as well as metal ion is discussed.

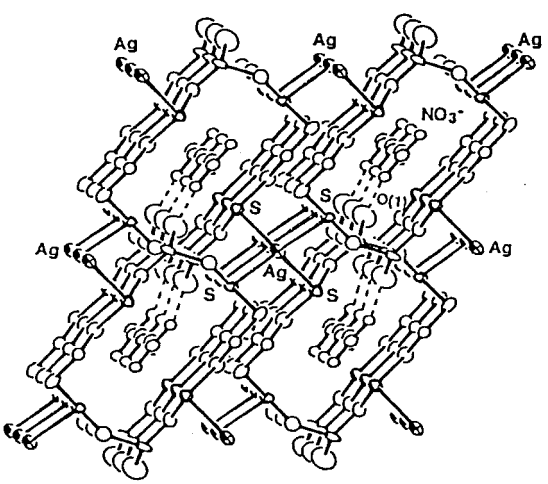

$\{[Ag([16]aneS_4(OH)_2)](NO_3)\}_\infty$ (**1**)

VII-H-9 A Molecular Cavity for Tetrahedral and Y-Shaped Anions. Synthetic and Structural Studies of Macrocyclic Dicopper(I) and Disilver(I) Compounds of 1,6-Bis(diphenylphosphino)hexane.

Susumu KITAGAWA,[a] Mitsuru KONDO,[a] Satoshi KAWADA (*[a]Tokyo Metropol. Univ.*), **Shigetoshi WADA,[b] Masahiko MAEKAWA[b] and Megumu MUNAKATA** (*[b]Kinki Univ. and IMS*)

[*Inorg. Chem.*, **34**, 1455-1465 (1995)]

New binuclear macrocyclic systems of 1,6-Bis(diphenylphosphino)hexane (dpph) $[(Cu_2(dpph)_2(\mu\text{-}X)_2]$ (X=ClO_4, **1**; X=NO_3, **2** and X=PF_2O_2, **3**; CH_3CO_2, **4**; $C_2H_5CO_2$, **5**) have been synthesized and structurally characterized. For complexes of **1-3** each copper atom shares a tetrahedral geometry with P_2O_2 donor set, giving a molecular structure having two rings: the common outer large ring is composed of copper atoms and bridging dpphs while the inner rings is composed of copper atoms and anions.

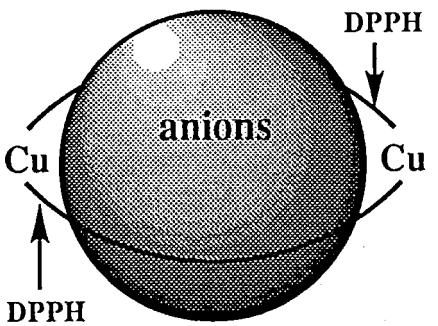

Dinuclear compound having two rings

VII-H-10 Cooperative Metal Ions Binding by Metal-Organized Crown Ether

Yoshiaki KOBUKE,[a] Katuaki KOKUBO (*[a]Shizuoka Univ.*) **and Megumu MUNAKATA** (*Kinki Univ. and IMS*)

[*J. Am. Chem. Soc.*, in press]

The compound of copper(II)-organized host with K^+ picrate $[\{K(picrate)\}_2\{(1,2\text{-benzene-bis}(1,4\text{-dioxanonyl-}6,8\text{-dionate})Cu\}_2]$ was synthesized and structurally characterized. The intermolecular coordination of β-ketoenolate oxygens to the copper furnished an organized cavity into which potassium cation was entrapped. The copper-organized crown showed a good size-fit selectivity, characteristic of macrocycles and a superior extraction efficiency.

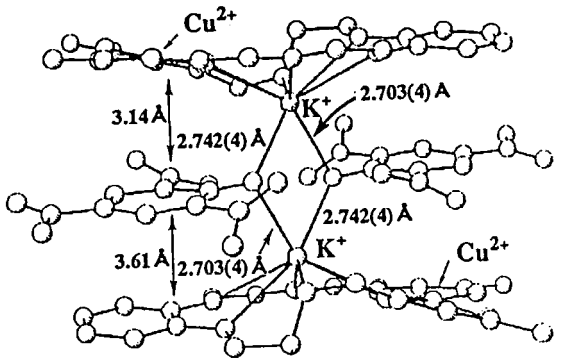

Copper(II)-organized host compound with K+ picrate

VII-H-11 Formation of a Metallocycle by Dimerization of Acrylonitrile. Crystal Structure of the Hexakis{(1,4-dicyanobutene-1,4-diyl)-nickel(II)} complex

Masahiko MAEKAWA,[a] Megumu MUNAKATA (*[a]Kinki Univ. and IMS*), **Takayoshi KURODA-SOWA[a] and Koji HACHIYA[a]**

[*Inorg. Chim. Acta*, **230**, 249-252 (1995)]

A novel hexanickel(II) complex $[Ni_6(NCCHCH_2CH_2CHCN)_6]$ with 1,4-dicyanobutene-1,4-diyl ($NCCHCH_2CH_2CHCN$) which was produced by the metal-induced dimerization of acrylonitrile has been isolated and structurally characterized.

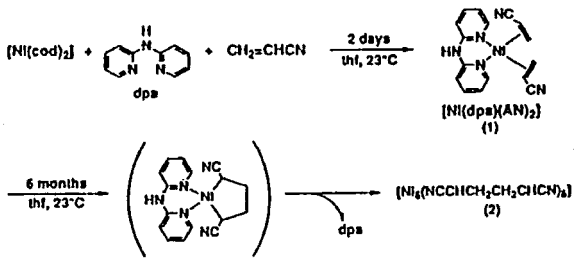

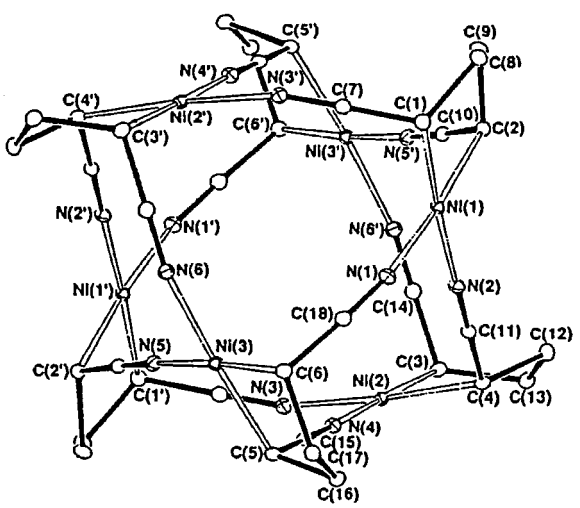

$[Ni_6(NCCHCH_2CH_2CHCN)_6]$

VII-H-12 Synthesis and Crystal Structure of a Mono- and Dinuclear Nickel(0) Ethylene Complex with 4,4'-Bipyridine (bpy); $\{[Ni(bpy)(C_2H_4)]_2[Ni_2(bpy)(C_2H_4)_4]\}$

Masahiko MAEKAWA,[a] Megumu MUNAKATA (*[a]Kinki Univ. and IMS*), **Takayoshi KURODA-SOWA[a] and Koji HACHIYA[a]**

[*Inorg. Chim. Acta*, **232**, 231-234 (1995)]

A nickel(0) ethylene complex $\{[Ni(bpy)(C_2H_4)]_2[Ni_2(bpy)(C_2H_4)_4]\}$ with 1,4-dicyanobutene-1,4-diyl ($NCCHCH_2CH_2CHCN$) which includes two species of mono- and dinuclear nickel (0) ethylene complex in a unite cell was been prepared and the nickel(0)-ethylene bond was elucidated

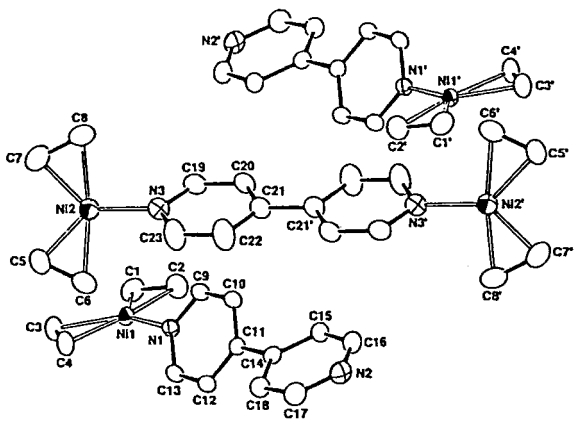

$[Ni(bpy)(C_2H_4)]_2[Ni_2(bpy)(C_2H_4)_4]$

VII-H-13 Co-ordinative Versatility of Pyrazole Derivative Ligand 3,5-Bis(2-Pyridyl)Pyrazole (Hbpypz) in Silver and Copper Compounds. Synthesis, Characterization and Crystal Structures of $[Ag_2(Hbpypz)_4](ClO_4)_2$- $2(CH_3)_2CO$, $\{[Ag(Hbpypz)](ClO_4)\}_\infty$ and $[Cu_4(bpypz)_4(ClO_4)_4]$-$2H_2O$

Megumu MUNAKATA (*[a]Kinki Univ. and IMS*), **Liang Ping WU,[a] Mikiko YAMAMOTO,[a] Takayoshi KURODA-SOWA,[a] Masahiko MAEKAWA,[a] Satoshi KAWATA[b] and Susumu KITAGAWA** (*[b]Tokyo Metropol. Univ.*)

[*J. Chem. Soc. Dalton Trans.*, in press]

In the dinuclear complex $[Ag_2(Hbpypz)_4](ClO_4)_2{\cdot}2(CH_3)_2CO$ there are two crystallographically independent monomeric units linked by intramolecular hydrogen bonds. In the polymeric complex $\{[Ag(Hbpypz)](ClO_4)\}_\infty$ each Ag(I) ion is coordinated with three nitrogen atoms of two different Hbpypz ligands forming an infinite-chain structure. The tetranuclear complex $[Cu_4(bpypz)_4(ClO_4)_4]{\cdot}2H_2O$ consists of two weakly associated dimeric units coupled via intramolecular stacking interaction. The temperature dependence of magnetic susceptibility indicates presence of antiferromagnetic interaction in the system.

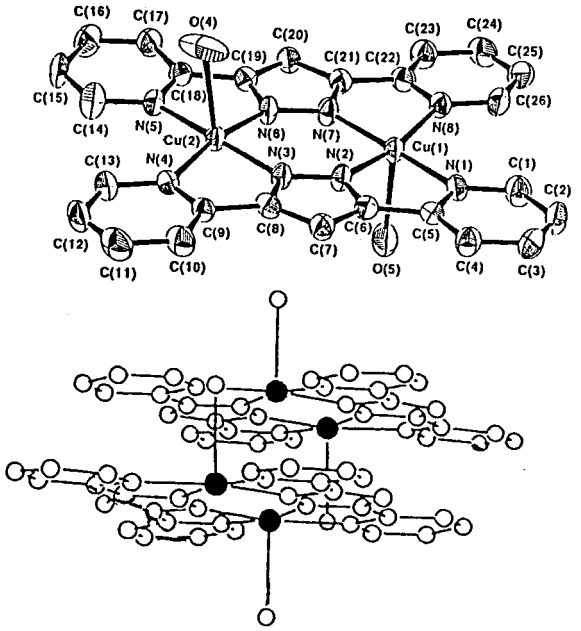

$[Cu_4(bpypz)_4(ClO_4)_4]\bullet 2H_2O$

VII-I Design, Synthesis, and Property of Metal-Complex Based Magnetic Materials

The field of molecular magnetism has shown quite spectacular advances in the last decade and several different approaches are currently used. The molecular engineering and the crystal engineering are necessary to design the magnetic material. The approach based on metal-complex is a promising method to align the magnetic centers ferromagnetically in three-dimensional crystal lattice. Our synthetic design of magnetic materials is based on the assembly reaction of the two building components which have donor and acceptor character in coordination mode, respectively. For example, $[Fe^{III}(CN)_6]^{3-}$ ion assumes donor coordination ability and acts as a multidentate "ligand-complex" and the manganese(III) complex with the quadridentate salen analog $[Mn(L)(H_2O)]^+$ assumes acceptor coordination ability at two apical substitutable coordination sites. The reaction of two building components, $[MnL(H_2O)]ClO_4$ and $K_3[Fe(CN)_6]$, produces the hetero-metal assembly exhibiting extended structure and various magnetic properties.

VII-I-1 Complexes Derived from the Reaction of Manganese(III) Schiff Base Complexes and Hexacyanoferrate(III): Syntheses, Multi-Dimensional Network Structures, and Magnetic Properties

Hitoshi MIYASAKA, Naohide MATSUMOTO* *(*Kyushu Univ. and IMS)*, **Hisashi OKAWA***(Kyushu Univ.)*, **Nazzareno RE, Emma GALLO and Carlo FLORIANI** *(Lausanne Univ.)*

The reaction between the $[Mn(BS)(H_2O)]$ monomeric and $[Mn_2(\mu\text{-}BS)_2(H_2O)_2]^{2+}$ dimeric cations with $[Fe(CN)_6]^{3-}$gave rise to cation-anion interaction via the formation of [Fe-C≡N-Mn] bridges. Depending on the nature of the Schiff base and regardless of the stoichiometry used, two building blocks are formed, either the trimeric anion $[\{Mn(BS)\}_2\{Fe(CN)_6\}]$- (BS = 3-MeOsalen, **6**; 5-Clsalen, **7**; 5-Brsalen, **8**; salcy, **10**) or the pentameric cation $[\{Mn(BS)\}_4\{Fe(CN)_6\}]^+$ (BS = saltmen, **9**). The X-ray analysis of $[K\{Mn(3\text{-}MeOsalen)\}_2\{Fe(CN)_6\}]_n$, **6**, revealed a two-dimensional network layer structure consisting of a cyclic octamer (-Mn-NC-Fe-CN-)$_4$ involving K^+ ion at the center as a net unit. The two-dimensional layers stack along the *a* axis due to van der Waals contacts and the DMF molecules of crystallization fill the interlayer space. The magnetic measurements (μ_{eff} vs. T, *M* vs. H under various temperatures, field cooled magnetization under various weak magnetic fields(FCM), and hysteresis loops) showed its metamagnetic behavior, where the ferromagnetic interaction operates within each layer and the antiferromagnetic interaction operates between the layers. The Neel temperature, T_N, is 9.2 K and the critical field at 2 K is 300 Oe. The structure of $[\{Mn(saltmen)\}_4\{Fe(CN)_6\}]ClO_4.H_2O$, **9**, is a two-dimensional layer consisting of a cyclic dodecamer (-NC-Fe-CN-Mn··Mn)$_4$. as repeating unit. The layers stack along the *c* axis and ClO_4^- anions are positioned between the layers. The magnetic measurements showed this compound's ferromagnetic behavior. There are, in fact, two kinds of intralayer magnetic interactions, the interaction between the Fe(III) and Mn(III) ions bridged by CN groups and the interaction between two Mn(III) ion in the dimer $[Mn_2(saltmen)_2]$, both being ferromagnetic. The interlayer magnetic interaction is ferromagnetic, all of which render to **9** an overall ferromagnetic behavior. The Curie temperature Tc is 4.5K.

[*Angew. Chem.* 1995, **107**, 1565.]

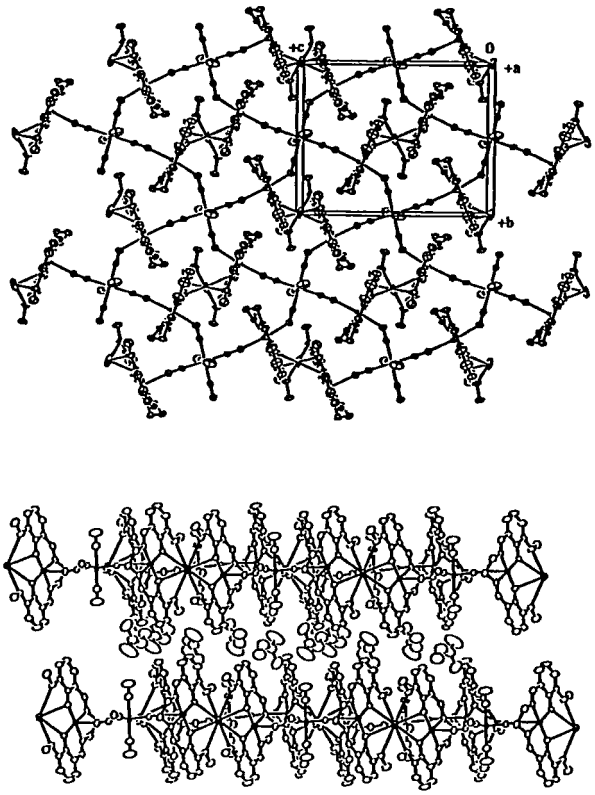

Figure 1. (a) Projection along the *a*-axis for **6**, showing a two-dimensional network structure, in which a net unit is composed of a cyclic octamer structure (-Mn-NC-Fe-CN-)$_4$ and involves a sandwich structure. (b) Projection perpendicular to the *a*-axis, showing a stacking of the layers by Van der Waals contact, where DMF molecules of crystallization fill the interlayer space.

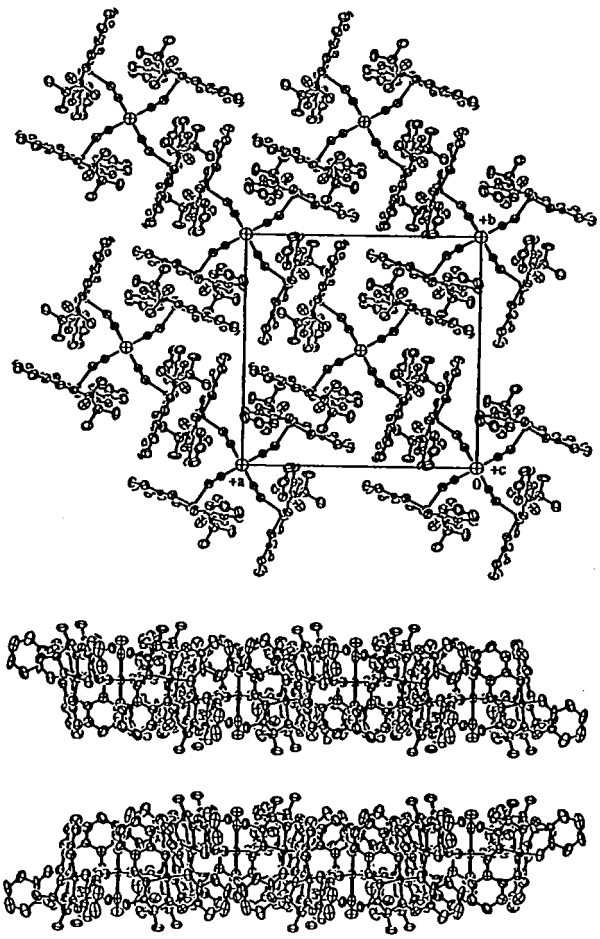

Figure 2. (a) Projection along the *c*-axis of **9**, showing a two-dimensional network structure, in which out-of-plane structure between [Mn(saltmen)]$^+$ is composed and a net unit is composed of a cyclic dodecamer structure (···Mn-NC-Fe-CN-Mn···)$_4$. (b) Projection perpendicular to the *c*-axis, showing a stacking of the layers by Van der Waals contact.

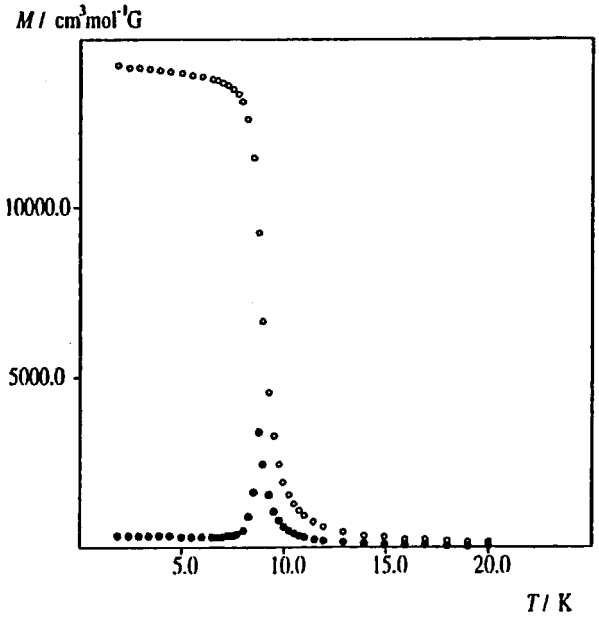

Figure 3. FCM (field-cooled magnetization vs. T) curves under magnetic fields 100 and 300 Oe for **6c**.

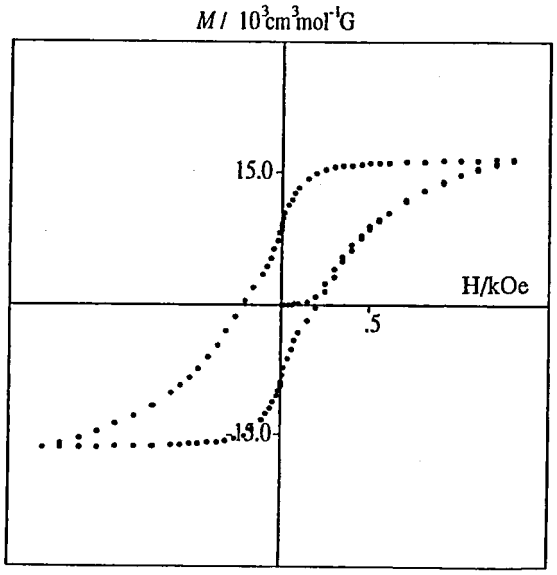

Figure 4. Hysteresis loop ($M/N\mu_B$ vs. H) at 4.5 K for **6c**.

VII-I-2 Metamagnetic Property of Cyano(N,N-ethylenebis(salicylideneamino))manganese(III)

Hitoshi MIYASAKA, Naohide MATSUMOTO*(Kyushu Univ. and IMS)*, **Hisashi OKAWA, Yuzo HASHIMOTO, Nazzareno RE, Emma GALLO and Carlo FLORIANI***(Lausanne Univ.)*

Six Mn(III) complexes with cyano ion and salen analogs [MnCNL^n] (n=1-6) were prepared and characterized. These complexes are classified into three groups (A), (B), and (C) by their magnetic properties. The complexes of (A) are discrete monomeric high-spin(S=2) Mn(III) complexes. The effective magnetic moments per Mn of (B) and (C) at 300 K (ca. 4.09 μ_B) do not agree with the spin-only value of high-spin(S=2, 4.89 μ_B) and low-spin(S=1, 2.83 μ_B)). The $1/\chi A$ vs. T plot obeys the Curie-Weiss law with the positive Weiss constant of θ=5.6 K for (B) and the negative Weiss constant for (C). As the temperature is lowered, the μ_B of (B) increases gradually, reaches to the maximum value 9.02 μ_B at 6 K, and then abruptly decreases to 4.93 μ_B at 4.2 K. The magnetic property of (B) showed a metamagnetism.

VII-J Interconversion between Monomeric and its Self-assembled Oligomeric Metal Complexes

The self-assembly metal complex that interconverts between monomer and self-assembled oligomer by inputting external information would be one of the latest targets, because such a metal complex is not only a new self-assembly molecule but can reveal also the chemistry of functional materials exhibiting a switching ability. The metal complex with the multidentate ligand involving an imidazole moiety could be potentially useful for this purpose. Our concept to develop such a compound can be summarized as follows. Such a self-assembly metal complex should behave like a simple building block that exhibits the following characteristics; (1) The complex has potential donor coordination ability at the imidazolate nitrogen atom; (2) At the same time, the complex has potential acceptor coordination ability at the vacant or substitutable coordination site; (3) When the imidazole proton is associated at a lower pH, either or both of the donor and acceptor abilities is/are absent and the complex exists as a monomer. Under higher pH conditions, donor and acceptor coordination ability appear and the self-assembly process is promoted. In this system, the construction processes from isolated molecules to an assembled molecule and the reverse deconstruction processes are both available by utilizing pH as external information; and (4) The resulting assembled molecular structure would be cooperatively determined by the ligand framework and metal ion, because the ligand framework can provide steric restriction and the metal ion then assumes its preferable coordination geometry.

VII-J-1 Proton Promoted Interconversion between Monomer and Self-Assembled Cyclic Oligomer of Cu(II) and Pd(II) Complexes with 2-(4-imidazolyl)-ethylimino-6-methylpyridine

Naohide MATSUMOTO*(Kyshu Univ. and IMS)*, **Genjin MAGO, Takeshi NOZAKI, Shingo EGUCHI, Hitoshi MIYASAKA, Hisashi OKAWA***(Kyushu Univ.)* **and Toshio NAKASHIMA***(Ohita Univ.)*

Proton promoted interconversion between monomer and self-assembled cyclic oligomer of Cu(II) and Pd(II) complexes with 2-(4-imidazolyl)-ethylimino-6-methylpyridine (HL) has been realized. The interconversion of Cu(II) complex occurs reversibly between the protonated monomer and the deprotonated cyclic hexamer. The protonated complex **1** is a monomer and the coordination geometry is a penta-coordinated trigonal bipyramid with the N_3 donor atoms of the tridentate ligand and two Cl^- ions, where the trigonal basal plane is composed of a central imine nitrogen atom of the tridentate ligand and two Cl^- ions. On the other hand, the deprotonated complex **2** is an imidazolate-bridged cyclic hexamer having the inversion center at the center of a cyclic hexamer. The interconversion between the monomer **1** and the hexamer **2** can be confirmed by the potentiometric pH titration and the pH dependence of the electronic spectra. When the Pd(II) ion is used instead of Cu(II) ion, the structures of both the protonated and the deprotonated Pd(II) complexes are different from the corresponding Cu(II) complexes, demonstrating the structural tuning by the metal ion. The structures of the protonated Pd(II) complex **3** is a

monomer and the coordination geometry is a tetracoordinated square planar with the N_3 donor atom of the tridentate ligand and a Cl^- ion. The deprotonated self-assembled species **4** is a cyclic tetramer, which differs from the cyclic hexamer of the corresponding Cu(II) complex **2**. The pH titration of Pd(II) complex showed a different behavior from that of Cu(II). The cyclic tetramer is rather stable and in the reverse titration proton does not bind to the imidazole group easily, indicating that the interconversion is irreversible.

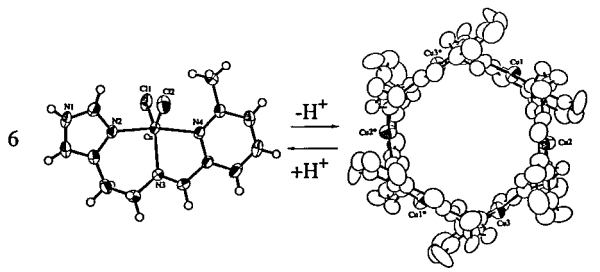

Figure 1. Interconversion between Monomer and Hexamer for Cu(II) Complex

VII-J-2 B-N Bond Formation by the Reaction of (N-3-Methoxysalicylidene-N'-(imidazol-4-ylmethylene)-1,3-propanediamino)copper(II) Perchlorate and Sodium Tetraphenylborate

Takeshi NOZAKI, Naohide MATSUMOTO* *(*Kyushu Univ. and IMS)*, **Hisashi OKAWA, Hitoshi MIYASAKA and Genjin MAGO** *(Kyushu Univ.)*

We have previously reported that a series of copper(II) complexes of quadridentate Schiff base ligands involving an imidazole moiety exhibits a self-assembly process, where the copper(II) complexes have potentially both donor and acceptor abilities in the coordination mode. When the complexes were conditioned in the high pH region, the imidazole proton deprotonates and then a self-assembly reaction is motivated. In the processes, monomer species with the general formula of $[Cu(HL)]ClO_4$ converts to a self-assembly polymer species exhibiting an infinite helical or zigzag chain structure $[Cu(L)]_n$, where the reverse conversion from $[Cu(L)]_n$ to $[Cu(HL)]^+$ is also available by protonation. During the course of our study, it was noticed that a compound obtained by mixing of the perchlorate salt and sodium tetraphenylborate ($NaBPh_4$) in *N,N*-dimethylformamide (DMF) does not show the same self-assembly process. It was found that the compound had a unique structure with a B-N bond $[Cu(LBPh_3)]$ (**2**). The copper(II) complex (*N*-3-methoxysalicylidene-*N'*-(imidazol-4-ylmethylene)-1,3-propanediamino)copper(II) perchlorate $[Cu(HL)]ClO_4$ (**1**) reacts with sodium tetraphenylborate ($NaBPh_4$) in *N,N*-dimethylformamide to give an electrically neutral complex exhibiting a B-N bond $[Cu(LBPh_3)]$.DMF (**2**).

[*Inorg. Chem.* **34**, 2108-2112, (1995)]

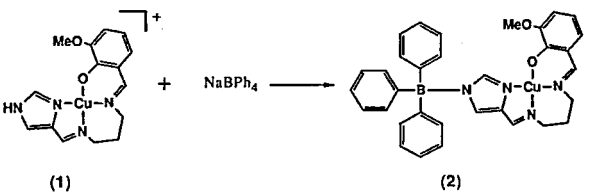

(1) (2)

VII-K Study of Metallomesogens

Liquid crystalline materials containing metal ions(metallomesogens) have attracted much attention, because the combination of properties of organic liquid crystals with those of transition metals can produce the new liquid crystalline materials containing unique molecular structures, and optical, magnetic, and electronic properties. Metal complexes show a remarkable variety of coordination geometries, so that the coordination of liquid crystalline ligands to metal ion can give a wide choice of the geometrical shapes. In addition to the coordination geometry of the mononuclear metal complex, the arrangements of the ligands of polynuclear metal complex can be useful to produce the variety of shapes for liquid crystalline phase.

VII-K-1 Synthesis and Characterization of Alkoxo-oxygen Bridged Copper(II) Complexes exhibiting Disk-Like and Rod-Like Shapes

Shingo EGUCHI Takeshi NOZAKI, Hitoshi MIYASAKA, Naohide MATSUMOTO, Hisashi OKAWA, Susumu KOHATA *(Kyushu Univ.)* **and Naomi MIYAJIMA*** *(*Hokkaido Univ.)*

A series of the copper(II) complexes with the tridentate Schiff base ligands derived from the 1:1 condensation of salicylaldehyde derivative and aminoalcohol have been prepared and characterized, where the salicylaldehyde derivative is 4-(p-n-alkoxybenzoyloxy)salicylaldehyde with n-alkoxy groups=n-propyloxy, n-butyloxy, n-hexyloxy, n-octyloxy, n-hexadecyloxy, and n-octadecyloxy and aminoalcohol is either of 2-aminoethanol, 3-aminopropanol, (S)-, and (R)-leucinol. These eighteen complexes can be classified into two groups A and B, in which group A contains 3-aminopropanol and group B contains either of 2-aminoethanol, (R)- or (S)-leucinol. Group A shows reddish violet color, almost diamagnetic, and rod-like shape due to binuclear structure with Cu_2O_2 core, while group B shows blue color, paramagnetic, and disk-like shape due to tetranuclear structure with Cu_4O_4 core. The thermotropic liquid crystalline behaviors have been investigated by the polarized microscopic observation and the differential scanning calorimetry.

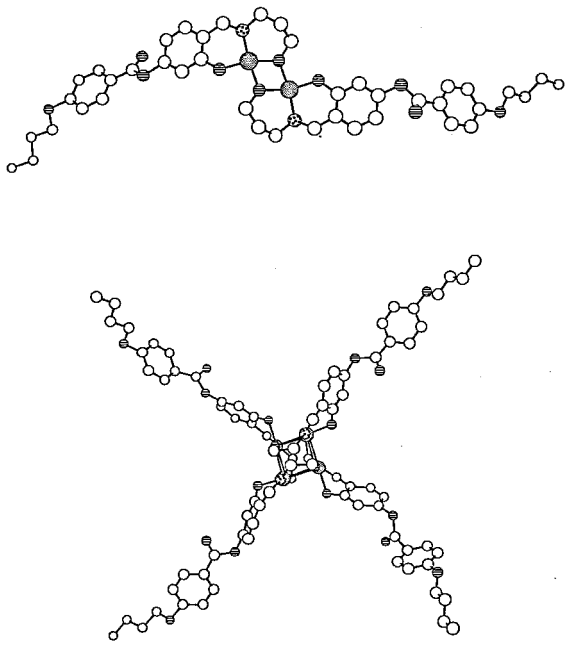

Figure 1. Possible structures for these species darwn on the basis of the X-ray analyses of the analogus compounds without p-n-alkoxybenzoyloxy groups. Proposed structures for cubane tetranuclear molecule and dinuclear molecule, showing a disk-like and rod-like structures, respectively

RESEARCH ACTIVITIES VIII
Computer Center

VIII-A Theoretical Studies of Highly Excited Vibrational States in Polyatomic Molecules

Research activities of this year include : (a) semiclassical study of avoided crossing for nonintegrable systems, (b) electronic structure and dynamics of small polyatomic molecules, and (c) development of parallel computational environment for large scale electronic structure calculations.

VIII-A-1 Semiclassical Study of Avoided Crossings

Toshiya TAKAMI

[*Phys. Rev.* E, **52**, 2434(1995)]

The origin of avoided crossings in nonintegrable systems is investigated in detail by semiclassical methods. It is well known that avoided crossings in nearly integrable systems occur around resonances between tori, i.e., the origin of them is the tunneling trajectory with imaginary action. In the nonintegrable systems like highly excited molecules, however, the origin will be due to real trajectories rather than imaginary ones because the existence of the real one is always guaranteed by the ergodicity. In order to study the relation between avoided crossings and real trajectories in nonintegrable systems, the trace formula for the stadium billiard system is analyzed quantitatively through Fourier analysis. We introduce a diabatic transformation around avoided crossings and show that the spectral density after the transformation become higher for several short periodic orbits. Further, we carry out the periodic-orbit quantization to study semiclassical reproduction of avoided crossings. From these analysis, we conclude that the origin of avoided crossings in nonintegrable systems is the long and complicated periodic orbits around short and simple ones.

VIII-A-2 Rotation Induced Vibrational Mixing in Highly Excited Vibrational States of Formaldehyde II

Mutsumi AOYAGI

The effects of both anharmonic and Coriolis interactions on the intramolecular dynamics in Formaldehyde are investigated quantum mechanically. Variational calculations including all of the vibrational modes, and the rotational modes are performed using the ab initio SDCI potential energy surface. Both time-dependent and time-independent analyses are made on the calculated eigenstates (up to 12000 cm^{-1}) to elucidate the role of Coriolis interaction in highly excited vibrational states. We also carried out the analyses of curvature distribution with respect to Hamiltonian parameters both on H_2CO and model Hamiltonian systems; the stadium billiard and the kicked rotator systems. We found that the anharmonic couplings assisted by b- and c-type Coriolis interactions and extensive K-mixings play a crucial role in the intramolecular dynamics at high energy region(E>7500 cm^{-1}). We also found that curvature distribution obtained from the H_2CO results shows similar characteristics with one from the stadium billiard system. Based on these results, we developed effective Hamiltonian of H_2CO system with a reduced dimensionality approximation.

VIII-A-3 Wave packet dynamics of CaNC/CaCN

Shinkoh NANBU, Satoshi MINAMINO and Mutsumi AOYAGI

Multireference configuration-interaction (MR-CI) calculation for numerous geometrical configurations of CaNC and CaCN are carried out to obtain the global potential energy surfaces for the electronic ground state. By the vibrational analysis for the obtained potential surfaces, three local minima were found: those are two linear conformations (CaNC and CaCN) and a trianglar conformation. The relative energy dfference among these minima is less than 1625 cm^{-1}. Unharmonicity of the potential surface along the large amplitude Ca-NC bending motion is quite strong. Calculations of wavepacket dynamics using the two dimensional model, where CN distance was fixed at 1.2Å, were performed to elucidate the role of the large amplitude bending motion in the procceses of intramolecular vibrational energy redistribution. It is found that there are many bending vibrational levels which should be assigned as hindered rotational states.

Chemical Materials Center

VIII-B Preparation and Properties of Novel Heterocyclic Compounds

Heterocycles containing chalcogen atoms are useful as components of organic conductors since heteroatoms in their rings are helpful to stabilize ions or ion-radical species, and extended π-conjugation decreases Coulombic repulsion. In addition intermolecular interactions caused by heteroatom contacts can be expected to form unique molecular assemblies. In this project novel electron acceptors and donors based on heterocycles such as 1,2,5-thiadiazole and 1,3-dithiole were synthesized and their properties including those of the charge-transfer complexes or ion-radical salts were investigated. Thiophene derivatives were also prepared and led to new types of polythiophenes having narrow bandgaps by electrochemical oxidation.

VIII-B-1 Benzobis(thiadiazole)s Containing Hypervalent Sulfur Atoms: Novel Heterocycles with High Electron Affinity and Short Intermolecular Contacts between Heteroatoms

Katsuhiko ONO, Shoji TANAKA and Yoshiro YAMASHITA

[*Angew. Chem., Int. Ed. Engl.*, **33**, 1977 (1994)]

Novel non-classical heterocycles **1** containing a tetravalent sulfur atom were synthesized from 4,7-dibromo-5,6-dinitrobenzo[c][1,2,5]thiadiazole, where the second thiadiazole ring was formed by reaction of the corresponding diamines with thionyl chloride or thionylaniline in pyridine. The absorption maxima of **1a,b** were observed at 524 and 558 nm, respectively. They showed strong fluorescence emission at 557 and 642 nm, respectively. The first reduction potentials of these heterocycles are comparable to that of p-benzoquinone, indicating that they have high electron affinity although they have no electron-withdrawing groups. The crystal structure of **1a** is constructed by ribbon columns including intermolecular interactions by short S---N contacts and these ribbon columns interact with each other to form a unique network through short Br···N contacts.

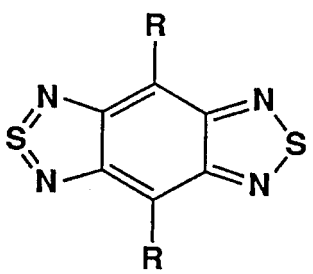

1a; R = Br
1b; R = Ph

VIII-B-2 Synthesis and Properties of Tetrathiafulvalene Derivatives Containing Quinoid Structures: Novel Electron Donors of Organic Conductors

Katsuhiro SAITO*, Chikayuki SUGIURA*, Emi TANIMOTO*, Katsushi SAITO* and Yoshiro YAMASHITA(**Nagoya Institute of Technology*)

[*Heterocycles*, **38**, 2153 (1994)]

Wittig-Horner reactions of 2-dimethoxyphosphinyl-1,3-dithiole derivatives with a benzoquinone-cyclopentadiene adduct followed by a retro-Diels-Alder reaction afforded a new type of electron donors **1** with a quinoid structure. Chloro and methylthio substituents are useful to increase both the solubility and stability. The cyclic voltammograms showed reversible two-stage one-electron oxidation waves whose potentials are lower than TTF. The differences between the first and second oxidation potentials are small, indicating decreased on-site Coulombic repulsion. The new donor molecules formed conductive charge-transfer complexes with TCNQ and DDQ.

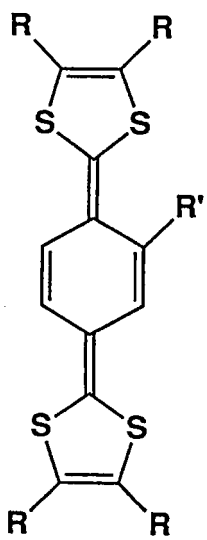

R = benzo, SMe
R' = Cl, SMe

1

VIII-B-3 Preparation and Properties of Tris(1,3-dithiole) Donors Containing Thiophene Spacer Units

Akira OHTA (*Graduate Univ. for Advanced Studies*) **and Yoshiro YAMASHITA**

[*Heterocycles*, **40**, 123 (1995)]

Novel tris(1,3-dithiole) donors **1** containing thiophene spacer units have been prepared using a Wittig-Horner reaction of the corresponding aldehyde or ketones with phosphonate esters. The cyclic voltammograms indicate that the donors **1** are oxidized to trication radicals or tetracations and on-site Coulombic repulsion in the dication state is reduced. The donors afforded charge-transfer

complexes with iodine. The electrical conductivities of these complexes measured on compressed pellets were 10^{-2} to 10^{-5} S cm^{-1}. An electroactive polymer was formed from **1** (R = SCH_2CH_2S, R' = H) by electrochemical oxidation.

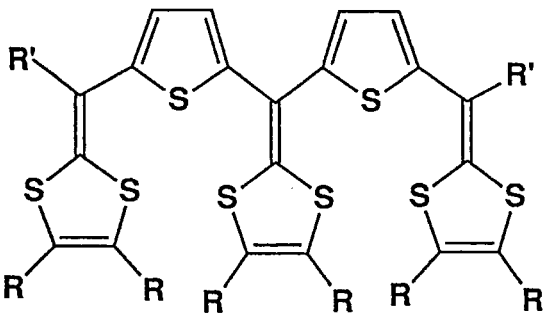

1

R = H, SMe, SCH_2CH_2S, benzo
R' = H, Me

VIII-B-4 Organic Metals Based on Butterfly-Shaped Donor Molecules

Yoshiro YAMASHITA, Shoji TANAKA and Kenichi IMAEDA

[*Synth. Metals*, **71**, 1965 (1995)]

Usual electron donors and acceptors giving organic conductors are planar molecules. In contrast, bis(1,3-dithiole) donors **1** containing a fused naphthalene and a 1,2,5-thiadiazole ring are a nonplanar molecule owing to the steric interactions caused by the peri-hydrogens. The donors were prepared by using a Wittig-Horner reaction from the corresponding dione. The oxidation potentials of the donors are a little higher than that of TTF due to the electron withdrawing property of the thiadiazole ring. The donors **1a,b,d** show reversible one-stage two-electron oxidation, while the ethylenedithio derivative **1c** undergoes stepwise oxidation with a small difference between the first and second oxidation potentials. The donor **1c** gave cation radical salts with inorganic anions as single crystals by electrochemical oxidation in THF. The composition was 2:1:1 (donor:anion:solvent) and they showed metallic temperature dependence of conductivity. The X-ray analysis of the PF_6 salt revealed that the butterfly-shaped donor molecules are uniformly stacked and intermolecular S···S contacts exist.

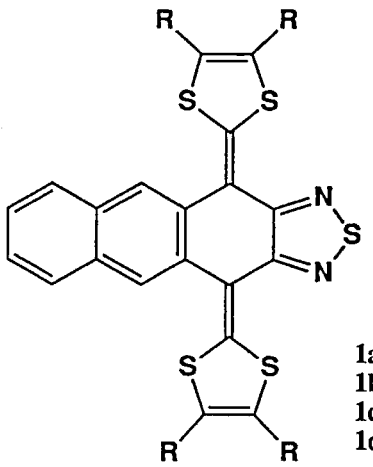

1a; R = H
1b; R = Me
1c; R, R= SCH_2CH_2S
1d; R,R = benzo

VIII-B-5 Preparation and Properties of Bis[5-(6-methyl-1,4-dithiafulven-6-yl)-2-thienyl]methanes Affording Near-Infrared Absorbing Cations by Oxidation

Akira OHTA *(Graduate Univ. for Advanced Studies)* **and Yoshiro YAMASHITA**

[*J. Chem. Soc., Chem. Commun.*, 557 (1995)]

Title bis(1,3-dithiole) compounds **1** were prepared using a Wittig-Horner reaction. The X-ray structure analysis of the ethylenedithio derivative shows that the two thiophene rings are orthogonal, while the thienyldithiafulvenyl subunits are nearly planar. The cyclic voltammograms of **1** showed irreversible oxidation waves, but in the reverse scan new reduction peaks due to the oxidation products were observed at lower potentials. This fact suggests that oxidation of **1** gives cations **2** by deprotonation. The cations **2** were actually obtained by chemical oxidation of **1** with nitrosyl tetrafluoroborate. The cations show intense absorptions in the NIR region (900-980 nm in acetonitrile) due to their polymethinecyanine type structure. The absorptions are blue-shifted in thin films and methylthio derivative exhibited a maximum at 824 nm as a thin film.

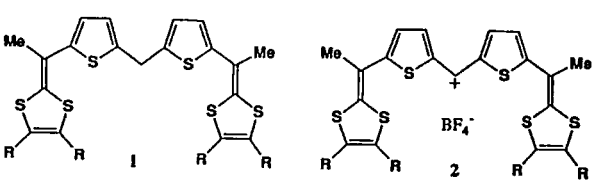

R = H, SMe, SCH_2CH_2S, benzo

VIII-B-6 New Narrow-Bandgap Polymer Composed of Benzobis(1,2,5-thiadiazole) and Thiophenes

Michinori KARIKOMI *(Utsunomiya Univ.)*, **Chitoshi KITAMURA** *(Graduate Univ. for Advanced Studies)*, **Shoji TANAKA and Yoshiro YAMASHITA**

[*J. Am. Chem. Soc.*, **117**, 6791 (1995)]

4,8-Di(2-thienyl)benzo[1,2-c:4,5-c']bis[1,2,5] thiadiazole (**1**) was prepared from benzo[c][1,2,5] thiadiazole

by several steps, where the thieny groups were introduced by coupling reaction of a dibromide with tributyl(2-thienyl)tin in the presence of $Pd(PPh_3)_2Cl_2$. The absorption maximum was observed at 702 nm, indicating that **1** has a small HOMO-LUMO separation. The cyclic voltammogram showed both an irreversible oxidation wave and a reversible reduction wave. The reduction potential is as high as that of p-benzoquinone, indicating its high electron affinity. X- ray structure analysis reveals the planar molecule structure containing nonclassical thiadiazole rings. Electrochemical oxidation of **1** afforded an electroactive polymer whose cyclic voltammogram shows both oxidation and reduction waves. The difference in the threshold potentials is very small and indicative of a very narrow bandgap. The optical bandgap could be estimated from the absorption edge of the dedoped film to be below 0.5 eV.

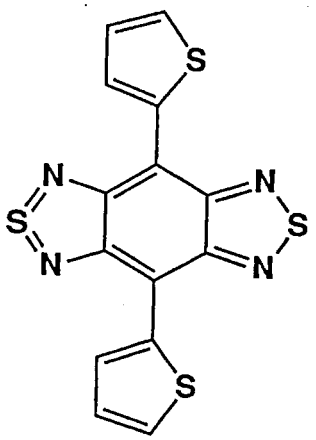

1

VIII-B-7 Synthesis and Properties of 5,7-Di(2-pyrrolyl)[1,2,5]thiadiazolo[3,4-b]thieno[3,4-e]pyrazine: A New Monomer Candidate for Intrinsically Conducting Polymer

Shoji TANAKA, Masaaki TOMURA and Yoshiro YAMASHITA

One of the fundamental challenges in the field of polymer science is the design of intrinsically conducting π-conjugated polymer (**ICP**) possessing a vanishingly small band gap (*Eg* ~0 eV) in the undoped state. As a promising monomer candidate for **ICP**, we have designed and synthesized a mixed trimer **1** consisting of tricyclic nonclassical thiophene unit and pyrrole units. The compound **1** was prepared from 2,5-dibromo-3,4-dinitrothiophene by six steps. The electronic spectrum of **1** showed a 1000 nm red shift of the long wavelength absorption band compared to terthiophene; the lowest - energy absorption maximum of **1** and the absorption edge were observed at 1345 nm (0.92 eV) and 2100 nm (~0.6 eV), respectively. According to the MO calculations, this can be attributed to the efficient inter-unit CT interaction between the high-lying HOMO of pyrrole units and the low- lying LUMO of the nonclassical thiophene unit. It should be noted that the "monomer" **1** has a lower optical energy gap value compared with almost all the low band gap "polymers" reported up till now. The cyclic voltammograms revealed that **1** has a highly amphoteric redox property ($E_{p,a}$ of +0.42 V and an $E_{p,c}$ of -0.22 V *vs.* SCE). The anodic oxidation of **1** gave the electroactive polymer. The observed electrochemical band gap was vanishingly small. The detailed characterization of this polymer is now in progress.

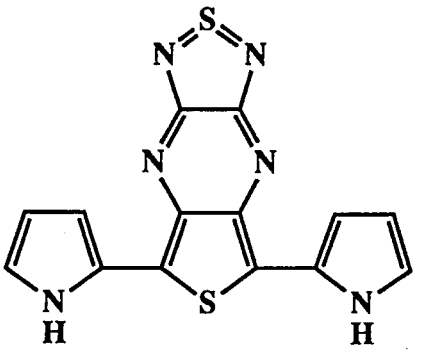

1

VIII-B-8 Syntheses and Properties of Novel Conducting Dithiolato-Metal Complexes Having Peripheral Heteroatoms and Extended π-Conjugated Systems

Masaaki TOMURA and Yoshiro YAMASHITA

[*J. Mater. Chem.*, **5**, 1753 (1995)]

In order to enhance intermolecular interactions in conducting dithiolato-metal complex by S···N and S···S heteroatom contacts, we have prepared novel dithiolato-nickel complexes derived from 2-dicyanomethylene-4,5-dimercapto-1,3-dithiole (H_2dcndmdt), 2,3-dimercapto [1,2,5]thiadiazolo[3,4-*b*]pyrazine (H_2dmtdap), and 2-(2-propylidene)-4,5-dimercapto-1,3-dithiole (H_2pdmdt) ligands. The cyclic voltammograms of the nickel complexes, $(Bu^n_4N)_2[Ni(dcndmdt)_2]$ and $(Bu^n_4N)_2[Ni(dmtdap)_2]$ (*vs.* SCE, in benzonitrile) showed a reversible oxidation peak at $E_{1/2}^{ox1}$ = +0.02 and an irreversible peak at E_p^{ox2} = +0.54 V, and a single reversible peak at $E_{1/2}^{ox1}$ = +0.57 V, respectively. The nickel complex, $(Bu^n_4N)_2[Ni(dcndmdt)_2]_3$, however, was unstable under the atmosphere. The room temperature electrical conductivities of the $Ni(dcndmdt)_2$ salts, which are prepared by electrochemical oxidation, were found to lie between 10^{-5} and 10^{-2} S cm^{-1}.

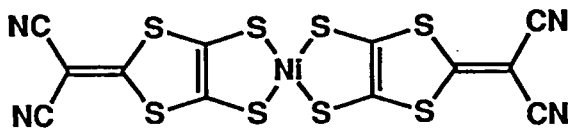

Ni(dcndmdt)$_2$

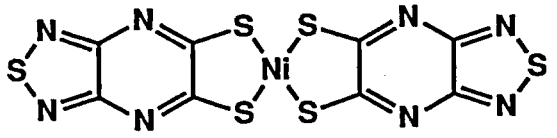

Ni(dmtdap)$_2$

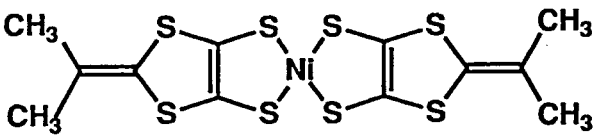

Ni(pdmdt)$_2$

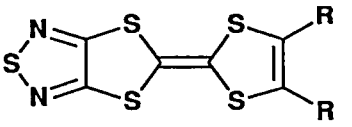

EDTTDA-TTF: R = SCH_2CH_2S
DMTTDA-TTF: R = SCH_3

VIII-B-9 Structures and Physical Properties of Cation-Radical Salts of Unsymmetrical Tetrathiafulvalene Derivatives Fused with a 1,2,5-Thiadiazole Ring

Masaaki TOMURA, Shoji TANAKA and Yoshiro YAMASHITA

Several cation-radical salts of unsymmetrical tetrathiafulvalene (TTF) derivatives fused with a 1,2,5-thiadiazole ring were prepared by electrochemical oxidation. The electrical conductivities of (EDTTDA-TTF)ClO_4 and (EDTTDA-TTF)$Au(CN)_2$ were 1.6×10^{-3} and 1.4×10^{-3} S cm^{-1} at room temperature, respectively. Temperature dependence of the conductivity indicates that these salts are semiconductors (E_a = 0.14 and 0.12 eV). The X-ray crystallographic analysis of (EDTTDA-TTF)ClO_4 shows that a coplanar two-dimensional network by short intermolecular S···S and S···N contacts and a column structure formed by the dimer of EDTTDA-TTF molecule exist in the crystal, as shown in Figure 1. Crystal data for (EDTTDA-TTF)ClO_4 are: monoclinic, *C2/m*, a = 16.194(3) Å, b = 9.908(3) Å, c = 9.167(3) Å, β = 97.52(2)°, V = 1958.2(7) Å^3, and Z = 4. On the other hand, a mixed stack column structure with DMTTDA-TTF molecule and $Au(CN)_2$ anion was found in the crystal of (DMTTDA-TTF)$Au(CN)_2$. Crystal data for (DMTTDA-TTF)$Au(CN)_2$ are: triclinic, *P*1 , a = 12.547(5) Å, b = 12.969(4) Å, c = 5.955(2) Å, α = 91.49(3)°; β = 102.80(3)°; γ = 114.13(2)°; V = 855.0(5) Å^3, and Z = 2.

(a)

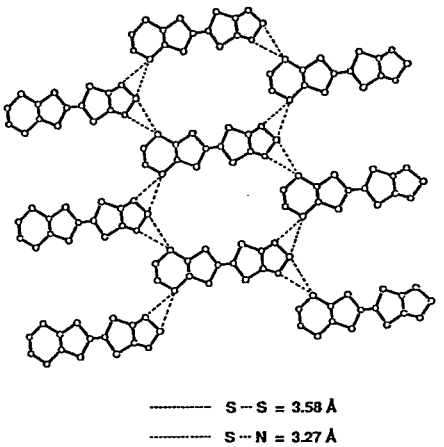

(b)

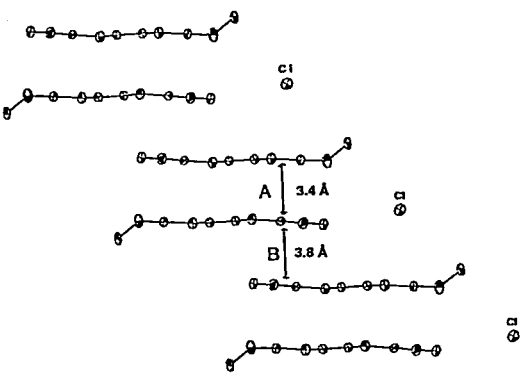

Figure 1. (a) The two-dimensional network in the crystal of (EDTTDA-TTF) ClO_4. The dotted lines show intermolecular S···S and S···N contacts. (b) The column structure of EDTTDA-TTF dimer in the crystal of (EDTTDA-TTF) ClO_4.

Instrument Center

VIII-C Studies of Solvated Metal Clusters

Solvated metal ions/cluster ions afford a particularly interesting collection of systems for study because they bridge the gap between bare, isolated ions and ionic solids and electrolyte solutions. From the point of view of cluster chemistry, the question of charge delocalization, the formation of solvation shells, microscopic solvation dynamics, and the interaction of solvent with metal surfaces appear especially attractive. In order to obtain information on the electron localization mode in clusters, we have been studied the photoionization process of alkali metal atom such as Cs embedded in polar solvent molecules. We have also been studied the photodissociation spectra and the intracluster reactions for the clusters containing Mg^+, which is isoelectronic with alkali metal atom. In this project we investigate further on the photodissociation and photoelectron spectroscopies of various kinds of solvated metal atom (ion) clusters to unveil the microscopic aspect of solvation dynamics.

VIII-C-1 Photodissociation Spectra of $Ca^+(H_2O)_n$ (n=1-9)

Masaomi SANEKATA, Fuminori MISAIZU and Kiyokazu FUKE

[*J. Chem. Phys.*, in press]

Photodissociation spectra of size-selected $Ca^+(H_2O)_n$ (n= 1-9) were studied in the wavelength region from 335 nm to 1440 nm using a reflectron mass spectrometer coupled with laser spectroscopy. Figure 1 shows the spectra of $Ca^+(H_2O)_n$ (n= 1-6). The spectra for n=1 and 2 were found to agree reasonably well with the calculated spectra by Bauchlicher, et al.[1] and were assigned mainly to the transitions having a character of the ^2P–^2S excitation for the free Ca^+ ion. We also found some evidences of the theoretically predicted p–d mixing in the spectrum for n=2, however, the degree of mixing was expected to be small. The spectra for this entire series of clusters exhibit large redshifts as large as ~16000 cm^{-1} with respect to the Ca^+ ^2P–^2S resonance line and show the converging trend in spectral shift at $n \sim 6$. As for n=7-9, no absorption was observed in the energy region below 7000 cm^{-1}, and also, the band positions were found to be almost the same as that for n=6, except for a weak shoulder at 8000cm^{-1} for n=9. The spectra for $Mg^+(H_2O)_n$, reported previously[2] show the solvation shell closing at n=3, while the absorption bands for $Ca^+(H_2O)_n$ shift monotonically to the red with increasing n and exhibit the converging trend at $n \sim 6$ as seen in Figure 1. This discrepancy was attributed to the difference in the number of solvent molecules filling the first shell for these metal ions: Ca^+ undergoes $sd\sigma$ hybridization and its first shell may be filled with ~6 water molecules, while that of Mg^+ is closed at n=3 because of sp hybridization. These arguments seem to be consistent with the calculated structures for these clusters.[3] We also discussed on the possible involvement of charge-transfer character in the ground and excited states of the Ca^+ systems on the basis of the results for the photoelectron spectroscopy (see VIII-C- 2).

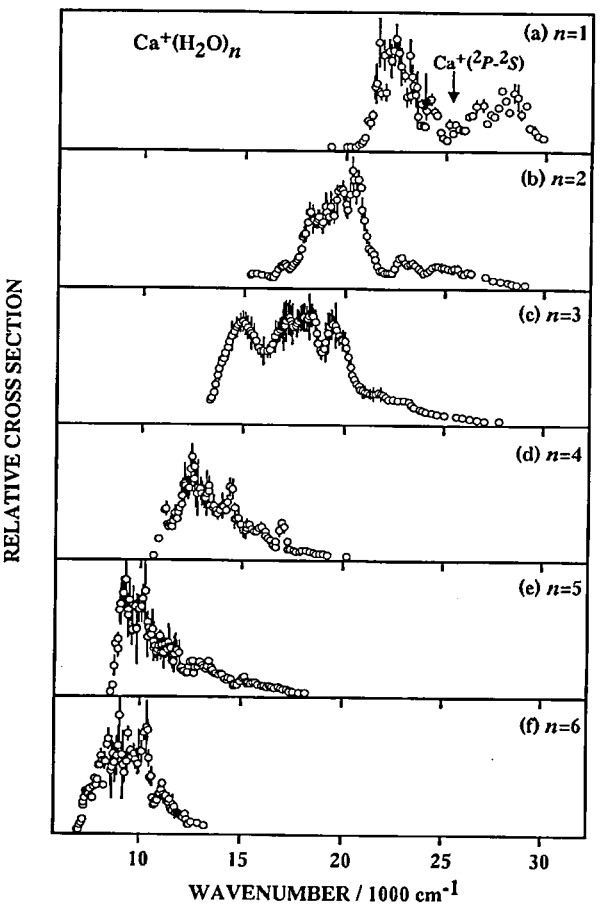

Figure 1. Photodissociation spectra of $Ca^+(H_2O)n$ with n=1 (a) to n=6 (f). Thesespectra were obtained by plotting the total yield of fragment ions as a function of photon energy. The intensities of the spectra were normalized at the peak positions.

VIII-C-2 Photoelectron Spectroscopy of Mass-Selected $Na^-(NH_3)_n$ Ions

Fuminori MISAIZU, Ryozo TAKASU and Kiyokazu FUKE

[submitted to *Chem. Phys. Lett*]

Recently, we measured the ionization potentials of solvated clusters containing alkali atom and obtained the results indicating that the ion-pair state, which is a counterpart to the bulk solvated electrons, may be stabilized at fairly small number of solvent molecules.[1] In order to

References

1) C. W. Bauschlicher, Jr., M. Sodupe, and H. Partridge, *J. Chem. Phys.* 96, **4453** (1992).
2) F. Misaizu, M. Sanekata, K. Fuke, and S. Iwata, *J. Chem. Phys.* **100**, 1161 (1994).
3) H. Watanabe and S. Iwata, to be submitted.

obtain further information on the electronic structure of these clusters, we investigated the photoelectron spectra of the $Na^-(NH_3)_n$ ions produced by a laser vaporization technique coupled with supersonic expansion method. Figure 1 shows the photoelectron spectra of $Na^-(NH_3)_n$ ($n \leq 14$) cluster ions recorded at the detachment wavelength of 355 nm using a magnetic-bottle type spectrometer. The spectrum of Na^- (Figure 1a) consists of two bands peaked at the vertical detachment energy (VDE) of 0.55 and 2.65 eV, which correspond to the Na (^2S) ← Na^- (^1S) and Na (^2P) ← Na^- (^1S) transitions, respectively. As for n=1 (Figure 1b), three peaks at 0.37, 0.58, and 0.81 eV were observed, but the band at 0.81 eV was ascribed to the signals from $Na^-(H_2O)$, which coexists as an impurity. Based on the theoretical calculations,[2] the first and second bands of n=1 were assigned to the transitions to the Na(^2S)-like states for two conformational isomers; NH_3 is bonded to Na^- from the nitrogen and hydrogen sides, respectively. The weak bands at ca. 2.4 eV were ascribed to the transitions to the Na(^2P)-like states for these isomers. As seen in Figures 1c-1j, this transition is largely shifted to the lower VDE with increasing n. Interestingly, VDEs of the Na(^2S)-like states at ca. 0.5 eV also show a decreasing trend: The results indicate that the solvation energies of the neutral forms are equal to or larger than those for anions. Recently, Hashimoto and Morokuma reported the theoretical study on the electronic structures of $Na(NH_3)_n$ and found that SOMO is spread out widely all over or even beyond the cluster for $n \leq 4$;[2] the diffusification of the s orbital occurs for larger clusters. These theoretical predictions seem to be consistent with the above experimental findings.

References

1) F. Misaizu, K. Tsukamoto, M. Sanekata and K. Fuke. *Chem. Phys. Lett.*, **188**, 241 (1992).
2) K. Hashimoto and K. Morokuma, *J. Am. Chem. Soc.* **117**, 4151 (1995).

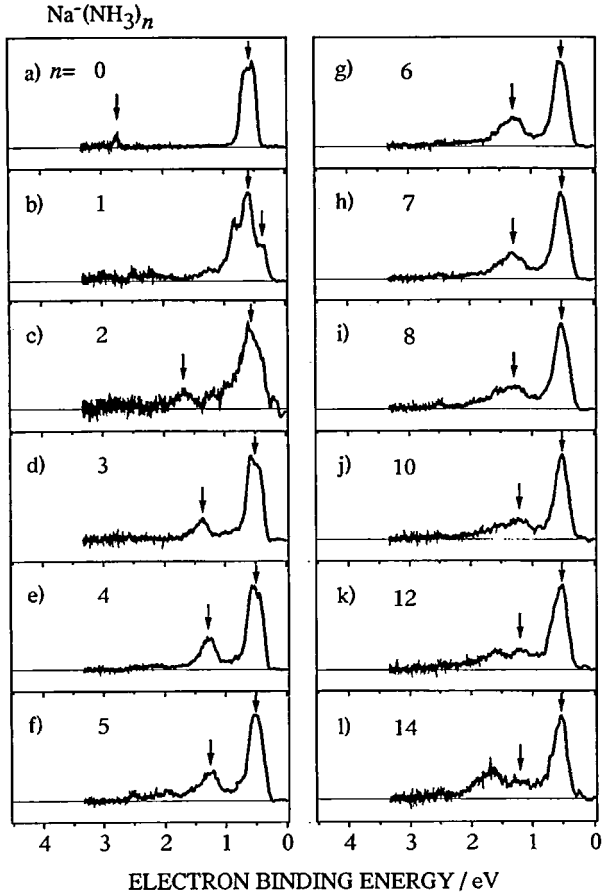

Figure. 1. Photoelectron Spectra of Na^- bound to n ammonia molecules for $n \leq 14$. The spectra were obtained with detachment wavelength at 355 nm (3.49 eV).

VIII-C-3 Photoelectron Spectroscopy of Mass-Selected $Li^-(NH_3)_n$ Ions

Ryozo TAKASU and Kiyokazu FUKE

In the present study, we report on further studies of alkali metal anion solvated by a finite number of polar solvent molecules using a photoelectron spectroscopy. This work follows up on our earlier reports to confirm the involvement of ion-pair character in the neural ground state of these clusters.

Figure 1 shows the photoelectron spectra of mass-selected $Li^-(NH3)_n$. The spectrum of Li^- (Figure 1a) exhibits two bands at the VDE of 0.6 and 2.75 eV, which correspond to the Li (^2S) ← Li^- (^1S) and Li (^2P) ← Li^- (^1S) transitions, respectively. As for n=1 and 3 (Figures 1b and 1c), the bands at ca. 0.5 eV, which correspond to the transitions to the Li (^2S) states, exhibit weak shoulders indicating the presence of conformational isomers as in the case of the Na^- systems (VIII-C-2). The figure also shows that the band at ca. 2.7 eV for n=1, derived from the Li (^2P) ← Li^- (^1S) transition, rapidly shifts to the lower VDE and becomes very diffuse with increasing n. Moreover, VDEs of the states derived from the Li (^2S) were found to decrease gradually with increasing n. These trends were also observed for the Na- systems (VIII-C-2). The latter results clearly indicate that the solvation energy of the neutral ground state is larger than that of the cluster anions in this size region. Recently, these systems were also examined theoretically by Hashimoto and coworkers

and their calculations reproduced the spectra for small clusters with reasonable accuracy.[1] The large solvation energy in the neutral ground state seems to imply that *ns*-valence electron on alkali-metal atom partially moves away to the solvent molecules with increasing *n* and the binding character in neutral forms is as ionic as that in anions. The above findings may be the first evidence to show that an alkali atom spontaneously ionizes and dissolves in finite clusters.

Reference

1) K. Hashimoto and T. Kamimoto, to be published.

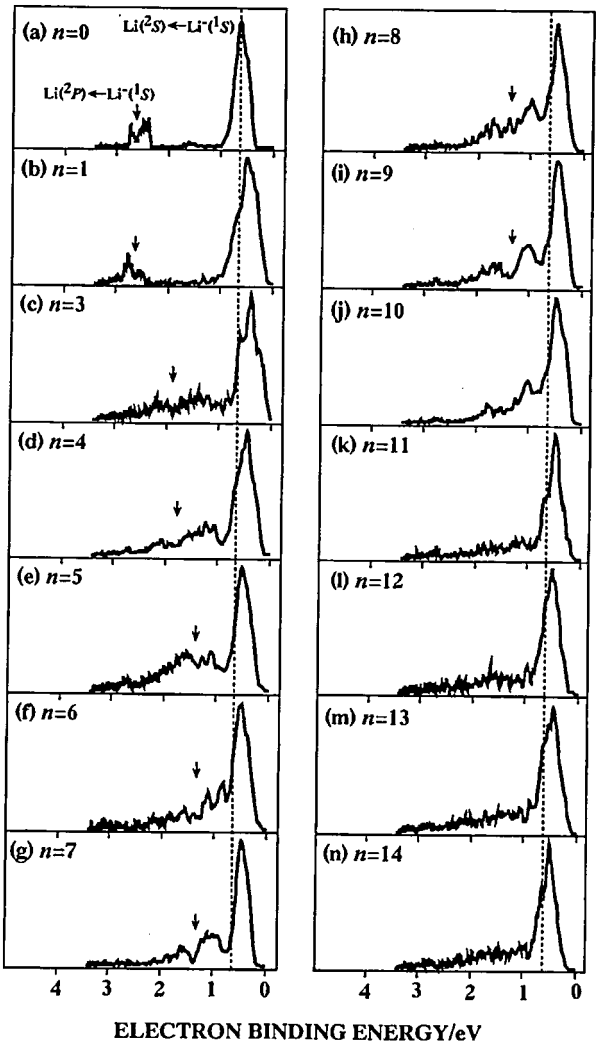

Figure. 1. Photoelectron Spectra of $La^-(NH_3)_n$ obtained with detachment wavelength at 355 nm (3.49 eV) for . $n \leq 14$

VIII-D Studies on Hypervalent Molecular Clusters

Electron delocalization mode in finite clusters has been the subject of intensive studies. Various clusters such as negatively-charged cluster ions, clusters containing neutral alkali atoms, etc., have been investigated in relation to this topic. Recently, we extended these studies to the clusters containing a Rydberg radical such as NH_4, which are readily formed through the photochemical reaction of ammonia clusters in the first excited state. This radical is isoelectronic with an alkali atom, and thus its solvated clusters may serve as a new model to get further information regarding the fundamental interaction of electrons with polar solvent molecules. NH_4 has also been considered to be an important intermediate in solution chemistry and its possible existence in the reaction of the solvated electron and in electrochemistry has been speculated on for many years. The study on the stability of $NH_4(NH_3)_n$ as a function of n may provide a clue regarding the long-standing problems in bulk solution. Moreover, these clusters have been known to be the key species in the resonance-enhanced two-photon ionization (RE2PI) of ammonia clusters *via* the A state. The RE2PI process including the predissociation of the A-state ammonia has been studied extensively, however, our understanding for the photochemistry of $(NH_3)_n$ still seems to be incomplete; only the process to produce $NH_4(NH_3)_m$, involving a concomitant NH_2 loss, has been determined. These results raise an interesting question as to whether a cluster containing the NH_2 radical is formed or not in the molecular beam after photolysis. This issue seems to be quite important in order to fully understand the photochemistry of $(NH_3)_n$ on the A-state surface as well as the mechanism of the RE2PI process. In order to clarify these problems, we studied the formation and decomposition processes of $NH_4(NH_3)_n$ using pump-probe techniques with femtosecond and nanosecond lasers.

VIII-D-1 Ultrafast Photochemistry of Ammonia Clusters: Formation of Hypervalent Molecular Clusters Containing the NH_4 Radical

Kiyokazu Fuke and Ryozo Takasu

[*Bull. Chem. Soc. Jpn*, **68**, 3295 (1995)]

The formation process of $NH_4(NH_3)_n$ through the photodissociation of the A-state ammonia clusters was investigated by a femtosecond pump-probe technique and a time-of-flight mass spectroscopy. Femtosecond pulses generated by a Ti-sapphire laser were amplified by a regenerative amplifier pumped by a 10 Hz Nd:YAG laser. The output wavelength, pulse width, and energy were ca. 789 nm, 120 fs and 6 mJ/pulse, respectively. The pump pulses at 197 nm were generated by phase-matched sequential conversion of the 789 nm pulses in three BBO crystals arranged in a nonlinear sum-frequency mixing scheme. The energy of the pump pulses was typically 2 μJ/pulse (290 fs). While the third harmonic at 263 nm (ca. 200 fs, 20 μJ/pulse) was used as the probe pulses. Figure 1 shows the pump-probe curves of small ammonia cluster ions with a time step of 83 fs. NH_3^+ is formed within a time-response function of the experimental system by one-photon ionization of NH_3 [A (v'=5)] with the probe pulses. NH_4^+ exhibits fast and slow decay components corresponding to the predissociation of the A-state dimer and the decomposition of NH_4 ($NH_4 \rightarrow NH_3 + H$), respectively; NH_4 is formed within 0.5 ps and decomposes with a lifetime of 13 ps. The curve for $NH_4^+(NH_3)$ (Figure 1c) also shows fast and slow decay components, however, the decay of the latter component is seen to be faster than that for NH_4^+. $NH_4^+(NH_3)_n$ (n=2-4) were also found to exhibit two decay components with slower time constants. From the comparison of these results with those for NH_4^+, the fast decay signals for $NH_4^+(NH_3)_n$ (n=1-4) were attributed to the predissociation of the A-state ammonia clusters, while the slow ones were ascribed to the solvation process of NH_4 in $(NH_3)_n$. As seen in Figure 1d, $(NH_3)_2^+$ shows a rising curve. This result, as well as those for the nanosecond pump-probe experiments, indicates that $(NH_3)_2^+$ is formed mainly through the one-photon ionization of a new photolysis product such as an excited-state NH_4*-NH_2. This intermediate corresponds to a cage product in the dissociation process of larger ammonia clusters and its formation and decay times are ca. 1 ps and < 1 ns, respectively. These findings give new insight into the photochemical reaction dynamics of ammonia clusters in the A state and the mechanism of RE2PI as well.

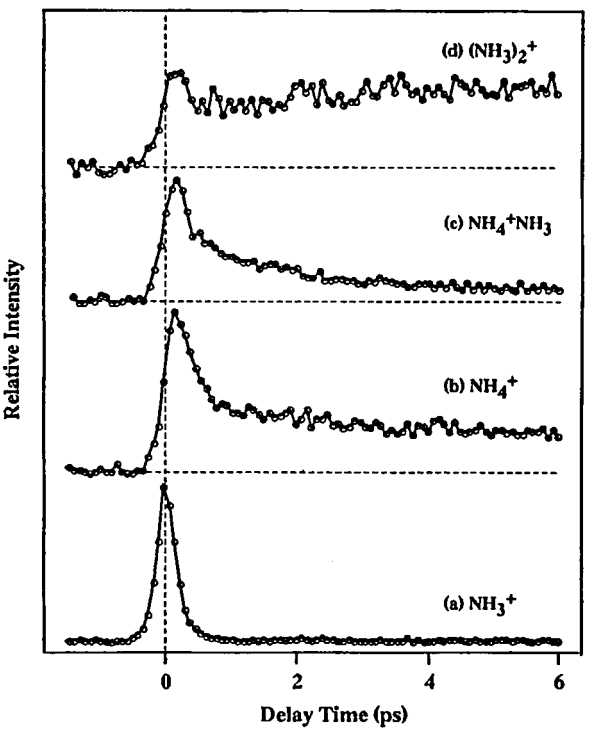

Figure. 1. Pump-probe curves of NH_3^+, NH_4^+, $NH_4^+NH_3$, and $(NH_3)_2^+$ with a scan step of 83 fs; pump pulses at 197 nm, $A(v_2'=5)$, and probe pulses at 263 nm. The signals, at the time when the probe is ahead of the pump, are the background ion signals from one color ionization by the pump laser alone. The signals of $NH_4^+(NH_3)$ do not fall back to the background level. The intracluster reaction, which form the long-lived $NH_4(NH_3)$, is responsible for these signals.

VIII-D-2. Stability of Hypervalent Molecular Clusters Containing the NH_4 Radical

Kiyokazu FUKE and Ryozo TAKASU

NH_4 is metastable and dissociates into (NH_3+H) (the lifetime is 13 ps), however, the radical has found to be stabilized extensively in ammonia clusters.[1] In order to get further information regarding the mechanism of stabilization of NH_4 and the localization mode of excess H-atom in clusters, we examined the lifetime of $NH_4(NH_3)_n$ using the pump-probe technique with nanosecond lasers. We used a far-field beam of XeCl excimer laser (308 nm) with a top-flat beam as the probe pulses to suppress the loss of clusters in the ionization region; the width and height of the beam were ca. 15 and 5 mm, respectively, and the uniformity of the laser fluence was estimated to be less than ± 5%. An ArF excimer laser used as the pump laser (1 mm diameter) was introduced colinearly at 5 mm upstream with regard to the probe beam. Figure 1 shows the pump-probe curves for $NH_4^+(NH_3)_n$ (n=1-3, 5). As for n=1 and 2, the decomposition lifetimes were determined to be 3 ± 1 and 7 ± 2 μs, respectively. Although the lifetime of larger clusters are longer than 10 μs, that for n=5 is finite. Thus the lifetime of NH_4 is elongated more than 10^6 times in clusters. The huge stabilization was ascribed to the semi-ionic character of the NH_4 radical.[1] Since $NH_4(NH_3)_n$ is expected to be rather hot and an energy barrier of H-atom migration in clusters is substantially low, the excess H atom may be to some extent delocalized over the cluster. The fact, that the lifetime of n > 4 is finite, seems to support this possibility.

Reference

1) K. Fuke, R. Takasu, and F. Misaizu, *Chem. Phys. Lett.* **229**, 597 (1994).

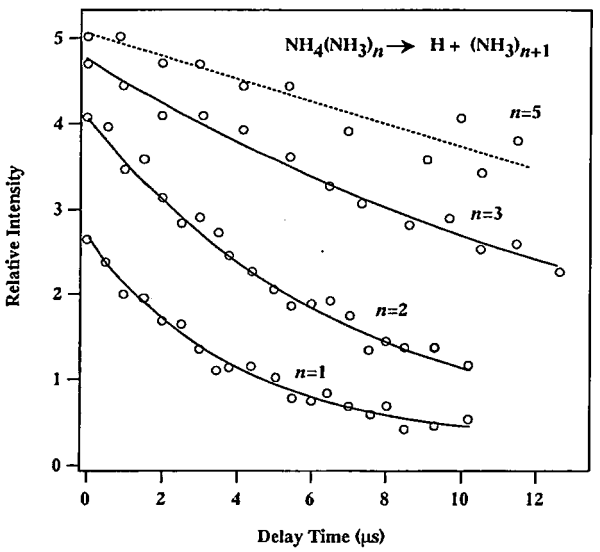

Figure 1. Pump-probe curves of $NH_4^+(NH_3)_n$, n=1-3 and 5; pump pulses at 193 nm and probe pulses at 308 nm. Clusters with n≥3 have a lifetime of longer than 10 μs and drift out from the time window.

VIII-D-3 Construction of a New Reaction Cell for the Study of Metastable Dissociation Dynamics

Ryozo TAKASU and Kiyokazu FUKE

Metastable dissociation is a familiar phenomenon in clusters: The process is induced by photoexcitation, photoionization, intracluster reaction, collision, and so on. In most of the cluster researches, clusters are produced by expansion of the gases into vacuum. In this case, the clusters undergo a directed translational motion along the streamline; clusters drift downstream with time. Thus it is usually difficult to study the dissociation process of clusters having a decay time of longer than microseconds, because of the loss of clusters in the probing region. To overcome this experimental difficulty, we designed and constructed a new reaction cell as depicted in Figure 1. The apparatus consists of an octopole ion guide (OIG), einzel lens, bending quadrupole, and quadrupole mass spectrometer: These are placed in differentially evacuated chambers. The ions introduced through an entrance of OIG or generated in the OIG are guided without loss to the mass spectrometer through the bending quadrupole, and then mass-analyzed. The bending quadrupole allows to introduce a probe laser beam colinearly to the cluster beam and to maximize the interaction of two beams. We plan to use this reaction cell to study the metastable dissociation dynamics of clusters containing NH_4 produced by photolysis of $(NH_3)_n$ (see VIII-D-2). Since the length of OIG designed is 1086 mm and the velocity of the clusters in molecular beam is expected to be typically 10^3 m/s, an upper limit of the lifetime we can measure may be ca. 1 ms. We also plan to apply this apparatus to investigate the infrared photodissociation spectrum of solvated metal ions such as those in VIII-C-1.

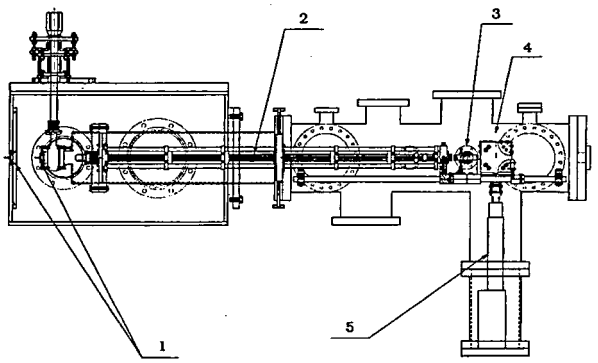

Figure 1. Side view of a newly constructed reaction cell for study of metastable dissociation dynamics. 1: skimmer, 2: octopole ion guide, 3: einzel lens, 4: bending quadrupole, 5: quadrupole mass spectrometer.

VIII-E Studies of Ultrafine Particles

To study the size effect of small binary or ternary metal compounds, new preparation technique to synthesis ultrafine carbides, nitrides and sulfides particles has been considered.

VIII-E-1 New Preparation Technique to Synthesis Metal Carbide System

Shunji BANDOW

To date, the gas evaporation has been used to prepare the ultrafine particles. This method is based on the thermal vaporization of metals or metal compounds in a depressurized gas condition. Hence, the decomposition is often occurred when we try to make ultrafine metal compounds particles. Laser pyrolysis (LP) is one of the candidate to prepare ultrafine metal compounds particles and we succeeded to prepare the finite particles of carbides, nitrides and sulfides. Although LP is one of the useful method to prepare the finite particles, it is easy to mix the other phase of compounds due to the smallness of the reaction area. Here we apply a glow discharge to make wide homogenous reaction area. The new apparatus to prepare ultrafine metal compounds particles is now designing.

VIII-E-2 Isolation and Agglomeration of Zinc Nanocolloids Observed by ESR Spectroscopy

Keisaku KIMURA *(Himeji Inst. Tech.)* **and Shunji BANDOW**

[*J. Colloid Interface Sci.* **171**, 356 (1995)]

Electron spin resonance (ESR) spectroscopy is applied to colloidal Zn nanocolloids in both isolated and agglomerated states. ESR lineshape is dependent on the extent of particle contact from isolated to agglomerated states and the relevant ESR lineshape parameters, electron spin life times, and *g*-values, are determined. It is deduced from both ESR and static magnetic susceptibility measurements the electronic state of the assembly of ultrafine particles is different from that of the bulk and is peculiar for colloidal states as it is for isolated and agglomerated states. The properties of particle assembly approaches that of a bulk sample only when the colloidal solution is dried.

VIII-F Studies of Nanoscale Carbons

The carbon nanotube is an interesting material in the electronic and vibrational properties. Electronically, it will be either semiconducting or metallic depending on its chirality and tube diameter. Vibrationally, the cyclic boundary conditions around a tube wall activate new first-order Raman and IR-active modes, *so called,* zone folded modes. The vibrational and magnetic properties of arc-derived single- and multi-wall carbon nanotubes are studied by Raman, IR, ESR and magnetic susceptibility measurements. The carbon nanotubes are purified /or concentrated by the centrifugation technique.

VIII-F-1 Concentration of Single Wall Carbon Nanotubes

Shunji BANDOW

The raw soot synthesized *via* Fe/Ni catalyzed carbon plasma was dispersed into distilled water with a 0.1 wt % of cationic surfactant (benzalkonium chloride) using the ultrasonic irradiation. The suspension was first centrifuged at 8000 rpm and separated into the precipitation and suspension. The latter component was again centrifuged at 15000 rpm and separated into the precipitation and suspension. After drove off water, each centrifuged sample was washed by methanol to remove excess surfactant and heat treated in dry air (315 C, 2000 min) to remove surfactant completely and other contaminants. These sample purification process was summarized in Fig. 1 with each sample identification code (sample ID). The percentage indicated under the sample ID is the single wall carbon nanotube content determined by the scanning electron microscopy. It should be noted here that 35, 55, 45 and 15% of weight loss were observed at the heat treatment process for **RS-H, P-1, P-2** and **S-2**, respectively.

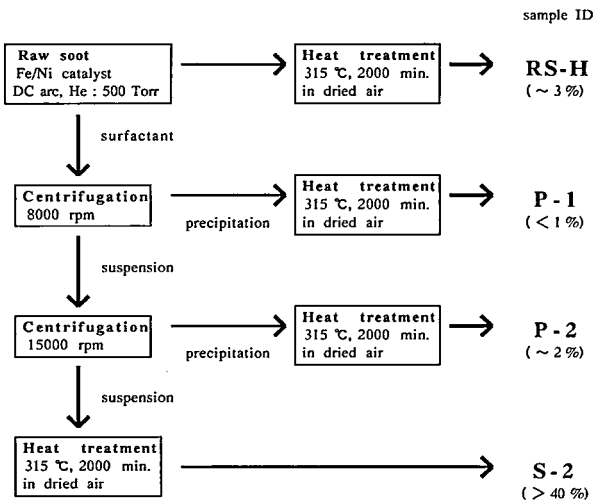

Figure. 1. Flow chart of purification process. The percentages under sample ID are the concentration of the single wall nanotubes.

VIII-F-2 Raman Scattering from Single Wall Carbon Nanotubes Concentrated by Centrifugation

Shunji BANDOW, Apparao M. RAO*, K. Williams*, J.M. HOLDEN* and Peter C. EKLUND*
*(*Department of Physics and Astronomy and Center for Applied Energy Research, University of Kentucky)*

[*to be submitted to Chem. Phys. Lett.*]

The single wall carbon nanotubes (1.0 nm in tube diameter with a distribution width of ~0.6 nm) synthesized from Fe/Ni catalyzed carbon plasma were highly concentrated (> 40%) by the centrifugation using a cationic surfactant; benzalkonium chloride, from the original raw soot containing ~3% of single wall carbon nanotubes. The Raman spectrum of the single wall carbon nanotubes was obtained by subtracting the background spectrum associating with sp^2 carbon nanospheres from the spectrum of the concentrated tubule sample (Fig. 1). The first-order "difference" Raman spectrum thus obtained revealed a broad doublet feature for $E_{2g}^{(2)}$, (ω = 1566 cm^{-1}, FWHM = 72 cm^{-1}) and (1605 cm^{-1}, 42 cm^{-1}), which are inconsistent with the previous results[1,2]), and also broad D-band, (1343 cm^{-1}, 69 cm^{-1}). These broad features for $E_{2g}^{(2)}$ were explained by the zone-folded mode incorporating with the tube diameter distribution and the tube chirality: A broad feature at 1605 cm^{-1} stemmed from the chirality of the tubules and that at 1566 cm^{-1} was mainly due to the tube diameter distribution. The D-band spectrum might be induced by the curved nature of carbon nanotube.

References

1) J.M. Holden, P. Zhou, X.-X. Bi, P.C. Eklund, S. Bandow, R.A. Jishi, K.D. Chowdhury, G. Dresselhaus and M.S. Dresselhaus, *Chem. Phys. Lett.* **220**, 186 (1994).

2) J.M. Holden, R.A. Loufty and P.C. Eklund, (unpublished)

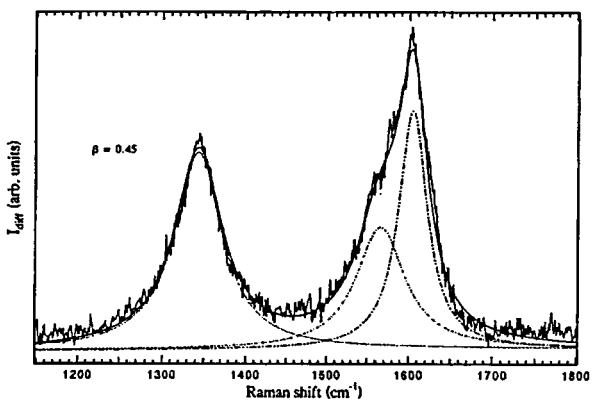

Figure. 1. Difference Raman spectrum. b = 0.45 means that 45% of background spectrum associating with sp^2 carbon nanospheres has been subtracted from the original spectrum. The peak position and FWHM (full width at half maximum) of the Lorentzian components determined by the peak separation are (ω = 1343 cm^{-1},FW HM = 69 cm^{-1}), (1566, 72 cm^{-1}) and (1605, 42 cm^{-1}) for b = 0.45.

VIII-F-3 Magnetic Properties of Carbon Nanostructures Studied by ESR and Magnetic Susceptibility

Shunji BANDOW

[*submitted to J. Appl. Phys.*]

Arc derived carbon nanostructures (nanotubes and nanoballs) are purified by the centrifugation and low temperature heat treatment. The purification process is monitored by electron spin resonance (ESR). The carbon nanostructures thus purified are studied by ESR and magnetic susceptibility measurements. The temperature dependence of the conduction-ESR (CESR) intensity for the carbon nanostructures behaves as that of graphite, while the g-value is almost independent on temperature, giving g = 2.0096 0.0004 at room temperature, in contrast to that of graphite. The CESR line width decreases with decreasing temperature, following Elliott mechanism. The differential magnetic susceptibility at low magnetic field (H < ~2 kG) reveals the abrupt increase and reaches to the positive value with decreasing magnetic field. This fact is explained by the magnetic properties of metallic carbon nanotube enunciated by Ajiki and Ando[1]).

Reference

1) H. Ajiki and T. Ando, *J. Phys. Soc. Jpn.* **62**, 2470 (1993) and **63**, 4267 (1994).

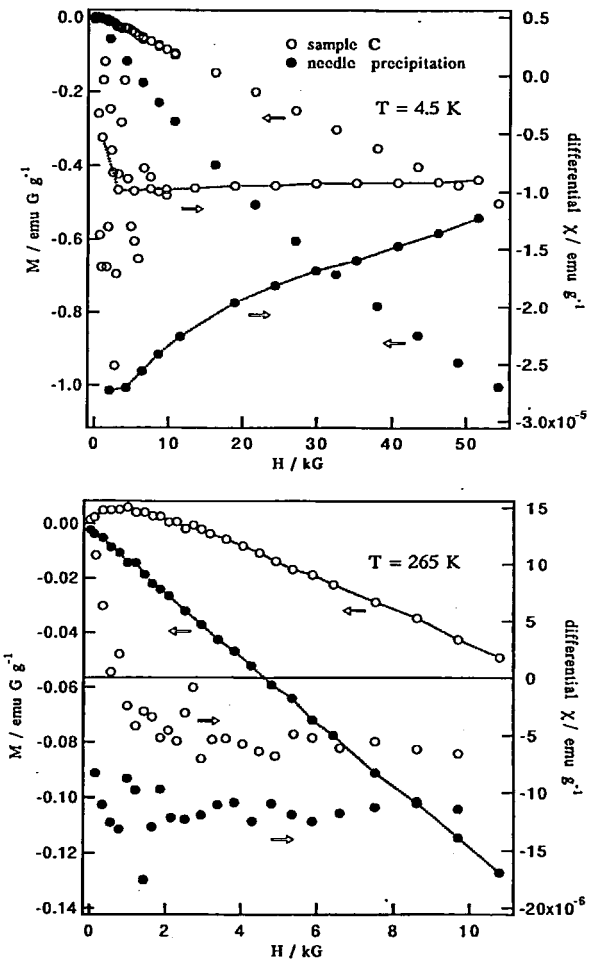

Figuer. 1. Magnetization curves and differential magnetic susceptibilities. Closed and open circles are for needle precipitation (needle shaped deposit; without carbon nanotubes) and sample **C** (purified carbon nanostructures; nanotubes and nanoballs), respectively. Top; data taken at 4.5 K with the magnetic field up to 55 kG, and bottom; at 265 K with the magnetic field up to 11 kG. The differential magnetic susceptibilities were calculated by averaging over 3 points of the magnetization data at H < 11 kG. Dotted lines are for the eye guide.

VIII-F-4 Structural Characterization of Multiwall Carbon Nanotubes by Electron Diffraction

Harutaka MEKARU *(Japan Adv. Inst. of Sci. and Tech.)*, **Kazuya SUZUKI** *(Yokohama Nat. Univ.)* **and Shunji BANDOW**

The carbon nanotubes were prepared by using DC arc burning of composite rod (anode) made by stuffing a mixture of La : B : C = 1 : 2 : 2 into a 6 mm in diameter hole bored in the center of a 10 mm in diameter carbon rod. The inner part of carbonaceous deposit grown on a negative end of the carbon rod was carefully scraped and dispersed in ethanol by ultrasonic irradiation. The suspension thus prepared was dropped onto the carbon microgrid for the TEM (transmission electron microscopy) observation. Figure 1 shows bright image of TEM. Inserted figure shows electron diffraction pattern. The lattice constants *a* and *c* are, respectively, 0.239 0.002 nm (from 100 diffraction spot) and 0.705 0.002 nm (from 002 and 004 ones). These values are inconsistent with the lattice constants of the multiwall carbon nanotubes, a = 0.2468 nm and c = 0.6884 nm:[1]) a = 0.239 0.002 nm is 3.2 % shorter and c = 0.705 0.002 nm is 2.4 % longer than those of the multiwall carbon nanotubes. Large change of lattice constants from the multiwall carbon nanotubes is probably due to the effect of B-doping to the honeycomb lattice.

Reference

1) Y. Saito, T. Yoshikawa, S. Bandow, M. Tomita and T. Hayashi, *Phys. Rev.* **B48**, 1907 (1993).

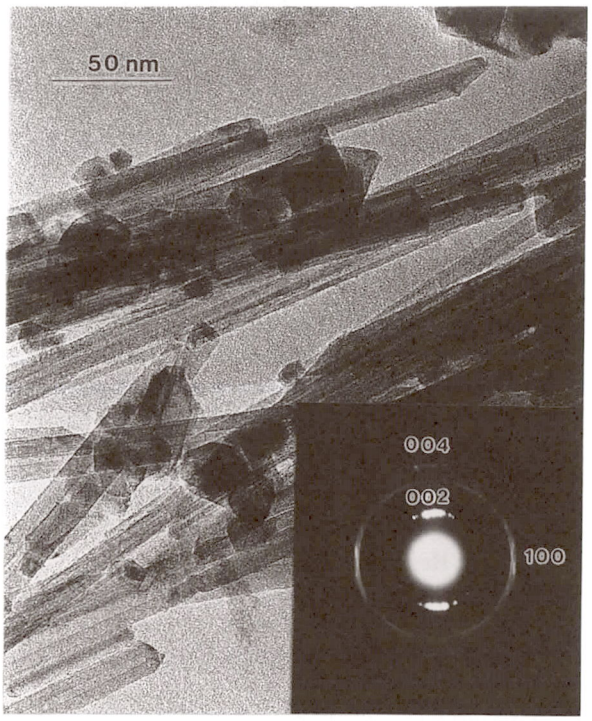

Figuer. 1. Transmission electron micrograph and electron diffraction pattern of multiwall carbon nanotubes *via* La/B/C composite.

VIII-G Solid State NMR

VIII-G-1 Simulation of Homonuclear Two Spin-1/2 Systems under Sample Spinning. Effects of Jump Motions on NMR Line Shapes

Daisuke KUWAHARA

[*Chem. Phys. Lett.* **231**, 414 (1994)]

During the last 20 years, magic angle sample spinning(MASS) has become widely used to obtain high resolution NMR spectra of dilute spin-1/2 systems and homonuclear spin-1/2 systems in solids. Many groups have completed line shape simulation methods for homonuclear spin-1/2 systems under sample spinning conditions. However, these studies did not deal with motional effects on NMR line shapes for the spin systems. Recently, Schmidt et al. and Luz et al. extended Floquet formalism to MASS line shape calculations for the spin systems jumping among a finite number of sites. The spin Hamiltonians treated by them were all "inhomogeneous" interactions in the terminology of Maricq and Waugh. Concerning the spin systems which have "homogeneous" interactions like solid state homonuclear two spin-1/2 systems, no treatment has yet been given. In the present paper, the author discusses an NMR line shape simulation method for the homonuclear two spin-1/2 systems which perform jump motions among a finite number of sites under MASS or OMAS(off magic angle spinning) conditions. Although the method is based on the work of Suwelack et al., it utilizes a numerical integration instead of analytical expressions in calculating the propagation operators describing time evolutions of the spin systems. The propagation operators produce an average relaxation superoperator, and Master Equation can be approximately solved by substituting the relaxation superoprator for its average.

VIII-G-2 Spinning Sideband Superposition for Quadrupole MAS NMR Spectra Using a Magic-Angle-Turning Technique

Toshihito NAKAI and Daisuke KUWAHARA

A two-dimensional (2D) magic-angle-spinning (MAS) NMR measure-ments for unraveling the overlapping spinning sidebands (SSBs) for quadrupolar nuclei having half-integer spins were reported; the method utilizes a magic-angle-turning technique recently exploited for chemical-shift spectra. The projection of the resultant 2D spectrum reconstructs the inherent MAS lineshapes without SSBs, which can be straightforwardly analyzed to yield quadrupolar parameters. SSB-free 23Na MAS spectra for Na_2SO_4 and Na2MoO4, which would otherwise be observed under an infinite spinning speed, were obtained.

Equipment Development Center

VIII-H Activities of Division of "IMS Machines"

Equipment Development Center has the division of constructing "IMS Machines", which are experimental apparatuses designed and constructed based on novel ideas proposed by researchers and technical staff of the Institute. New technologies necessary for their construction are developed or introduced by the staff of this division. Design and construction of the machines are performed principally in collaboration with researchers of the Institute, as well as staffs of other institutes, universities and facilities of industries if necessary. The primary purpose of this system is to keep technical ability and activity of this Center so that it can continuously meet the needs to support the molecular science now and in the future. In this fiscal year, 1994, the project themes listed below were adopted as IMS Machines. Their construction is now under way.

1. High Precision Slit Driver for Ultra-High-Vacuum Monochromator
(Proposed by Masao KAMADA)
2. Electron-Stimulated-Desorption-Ion-Angular-Distribution Detector with Time-of-Flight Type Mass separator
(Proposed by Kyoichi SAWABE)
3. Light Beam Path Stabilizer
(Proposed by Shuji ASAKA)
4. ESR Resonator for High-Pressure and Low-Temperature Sample (survey project)
(Proposed by Kyuya YAKUSHI)

Two machines for fiscal year of 1993 have been completed after six months of extension period. Their results were demonstrated at a meeting on May 1995.
1. Broad-Band Infra-Red Window for Ultra-High-Vacuum Apparatus
(Tsuneo URISU and Norio OKADA, Shuji ASAKA, and Toshio HORIGOME, cooperated by Takao NAMBA (Kobe University) and Sumitomo Electron Industry)
2. Time-of-Flight Type Mass-Spectrometer for High-Mass Materials
(Mitsukazu SUZUI, Hisashi YOSHIDA, Harutaka MEKARU*, Sachiyo NOMURA, Tadaoki MITANI*(*Japan Advanced Institute of Science and Technology), and Shimadzu Corporation).

Application of patents is promoted in this division. For fiscal year of 1994, the following patent was applied.
1. Optical Window and its Fabrication Method (applied in collaboration with Sumitomo Electron Industry)

VIII-H-1 Broad-Band Infra-Red Window for Ultra-High-Vacuum Apparatus

Norio OKADA, Tsuneo URISU, Shuji ASAKA and Toshio HORIGOME

The purpose of this project is to develop an infra-red optical window applicable to ultra-high-vacuum apparatus by using a CVD diamond plate. High purity diamond has several advantages as an optical window material: a wide optical transmission range extending from ultra-violet to sub-millimeter region except the intrinsic absorption around 2000 cm^{-1}, no deliquescence, and a high mechanical strength. The recently developed diamonds synthesized with a vapor phase deposition (chemical vapor deposition, CVD) method enabled us to obtain diamond plates with very high purity and large areas at reasonable price. We have successfully produced view ports with diamond plates by using our own technique of connecting a single crystal window material to a UHV flange. The present diamonds supplied by Sumitomo Electron Industries and manufactured with a microwave plasma CVD method have a polycrystalline structure, and are classified to type IIa. Their optical transmission property was reported in Annual Review 1994. The plates we obtained have thickness 0.2 ~ 0.5 mm, diameter 20 mm, and are optically polished on both sides. We have used two kinds of plates: one with parallel surfaces and the other with wedged surfaces. The latter is for avoiding the interference effect between the reflections on the two faces. Owing to the effort of Sumitomo, we could obtain plates with wedge angles of about 0.25 degrees. Here we describe the outline of the present connecting method. First, we formed a gold film along the edge of the diamond plate by coating "aqueous gold" liquid there. At the center of the stainless vacuum flange, we welded a silver joint frame with electron beam welding. By pouring melted AgCl between the gold film and the silver frame, the two parts were firmly connected after cooling. Finally to protect AgCl from UV illumination we coated the connection area with vacuum evaporated gold. The finished window had a clear aperture of 18 mm (Figure 1). Vacuum test with a helium leak detector showed no detectable leak at sensitivity of $3x10^{-11}$ Torr Litter/sec. The authors acknowledge Naoji FUJIMORI and Keiichiro TANABE of Sumitomo Electron Industry for developing CVD diamond plates, and Prof. Takao NAMBA of Kobe University for measuring optical transmission spectrum.

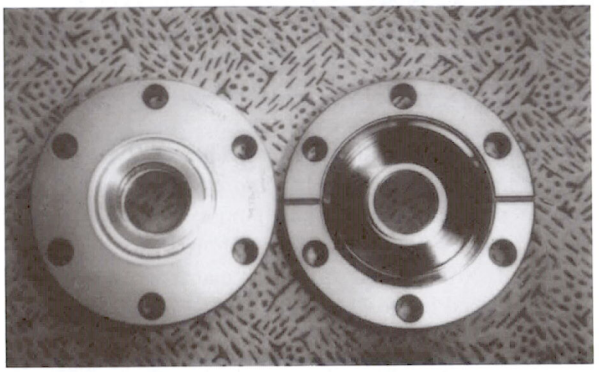

Figure 1. Diamond window for ultra-high vacuum

VIII-H-2 Time-of-Flight-Type Mass-Spectrometer for High-Mass Materials

Mitsukazu SUZUI, Hisashi YOSHIDA, Harutaka MEKARU*, Sachiyo NOMURA, Tadaoki MITANI*
*(*JAIST and Shimadzu Corporation)*

This project is aimed at developing a mass spectrometer for analyzing fullerenes with carbon atoms over 100. This machine designed in collaboration with Shimadzu Co. is a time-of-flight type mass- analyzer with an ion stream chopper (outline design is shown in Annual Review 94). Its goal includes a resolution of 200 and applicability of EI, CI, and LI ionization methods. The constructed apparatus consists mainly of an ionization chamber into which CI gas can be introduced and can be heated up to 250°C, a DI probe that can be heated up to 600°C, a drift tube of about 1.4 m in length, ion lenses, an ion beam chopper with voltage inverting time of 20 ns, micro-channel-plate ion detector, and their voltage supplies (Figure 1). The angle and longitudinal position of the ion detector can be adjusted from outside. Inside of the apparatus is evacuated and kept at 10^{-6} to 10^{-7} Torr. Ion signals from the MCP are data-processed on a digital oscilloscope. The main feature of the designed spectrometer is that ion beams converge longitudinally at a specific distance from the ion chopper, so that the mass resolution can become high in a simple structure (patent applied). In the constructed machine, however, this convergence effect has not been observed clearly due to the shortage of the movable length of the detector. A measurement of detector angle dependencies to the mass resolution has shown its maximum value at the designed angle. The design goal of the resolution 200 has been reached in the constructed machine, but high carbon fullerene ions have not yet detected. Through designing and constructing the present machine, the staff of the equipment development center had experiences of an integrated technology. It ranged from mechanical, electronic, and magnetic elements to the simulation of ion trajectory and high speed digital data processing. We hope these experiences may do much in future works of this Center.

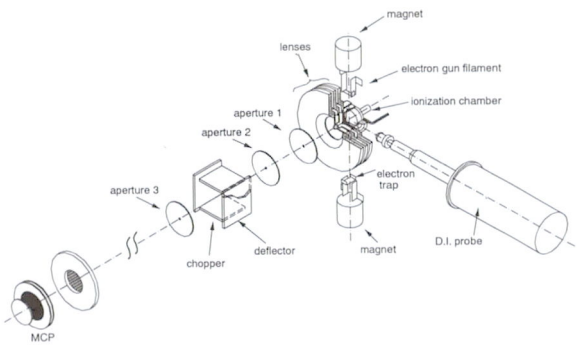

Figure 1. Outline design of time-of-flight-type mass-spectrometer for high-mass materials.

VIII-I Development of Experimental Devices

VIII-I-1 16-Channel Programmable Pulse Generator for NMR

Tomonori TOYODA

Multi-channel pulse sequences of respective different settings are frequently needed in controlling NMR devices. An apparatus necessary to this purpose must have the ability that a user can set the pulse sequences at his will, can store them (programmable), and can retrieve these pulse sequences simultaneously (multi-channel). A block diagram of the newly constructed multi-channel programmable pulse generator is shown in Figure 1. The pulse generator has 16 output channels of TTL level. Programming data for the pulses are built up with a developed software on a computer (PC-9801), which is then transferred into an S-RAM in the box through the printer interface. Once the box starts its output, it continues to generate pulse sequences according to the data stored in the S-RAM until a stop signal is sensed. An external clock to synchronize to other instruments can be accepted, and an external reset input is prepared to continually repeat specific pulse sequence. Pulse widths can be set between 100 nsec and 2^{32}x100 nsec (about 7 min and 9 sec) when the internal clock of 10 MHz is used. The reliability and the precision of this type of pulse generator depend on the dead times of the down-counters inside. In the present machine many efforts have been made to reduce dead times by adopting high speed F-type TTL chips and using signal synthesis technique utilizing gate delay times. Use of surface mounting chips and print circuit board milling machine was effective for down-sizing the machine itself as well as the construction period.

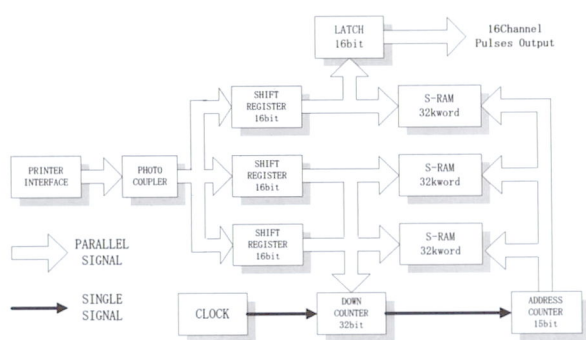

Figure 1. Newly developed multi-channel programmable pulse generator

Ultraviolet Synchrotron Orbital Radiation Facility

VIII-J Development of the UVSOR Light Source

VIII-J-1 Study of Radiation Properties from a Helical Optical Klystron for the UV Free Electron Laser on the UVSOR

Hiroyuki HAMA, Kazuhiko KIMURA, Jun-ichiro YAMAZAKI, Toshio KINOSHITA and Shin-ichi KIMURA

An optical klystron with helical undulators for the UV free electron laser has been designed for the UVSOR storage ring. The helical optical klystron (HOK) is favorable not only to obtain higher gain but also to avoid mirror degradation because of more fundamental and less higher harmonic radiation on the axis. Target wavelength of the FEL has been chosen to be around 240 nm that can excite molecular states of aromatic compounds. It may hopefully bring wide applications for study of molecular chemistry by employing two-color experiments with synchrotron radiation (SR). The new helical undulator looks like a transverse undulator but each magnet array consists with three lanes. Center lane and side lanes provide vertical and horizontal magnetic fields, respectively. Phase between the horizontal and the vertical fields can be changed by shifting the side lanes, so that direction and degree of circular polarization are able to be varied. Magnets of three periods at the center part of the helical undulator is able to be replaced with another set of magnets to make a dispersive section for the HOK mode. The current UVSOR FEL has been carried out with the electron energy of 500 MeV to obtain higher gain, while the nominal energy for the user experiments is 750 MeV. Considering pump-probe experiments via combined use of FEL and SR, a higher beam energy is preferred to obtain sufficient energy and intensity of SR, then the energy of 600 MeV is employed for the HOK in this study. Characteristics of the radiation and the FEL gain for the helical optical klystron has been investigated by a calculation based on Fourier transform of Lienard-Wiechert potentials. Integrated spatial power distributions of the HOK radiation at the position of the cavity mirror for the low energy region (e_{photon} < 10 eV) and the high energy region (10 < e_{photon} < 200 eV) are shown in Figure. 1. For the front mirror aperture, radiation power of higher energy photons emitted from the HOK is significantly reduced. Then the heating of the mirror may be considerably suppressed. Particularly the photon number onto the small on-axis area of 1 cm2, which covers most of the laser spot area, is reduced to be less than 20% of that from the planar optical klystron currently used in the FEL experiments in spite of increasing the electron energy from 500 to 600 MeV. These results of calculation are quite favorable to make less degradation rate for the mirrors. The FEL gain is also evaluated from the calculated frequency spectrum of spontaneous radiation. Estimated effective gain at the laser wavelength of 235 nm is 2 times higher than that at the visible laser in the present FEL. We can conclude that the new designed HOK has enough performance not only to obtain a UV lasing but also to utilize the SRFEL in actual synchrotron radiation experiments.

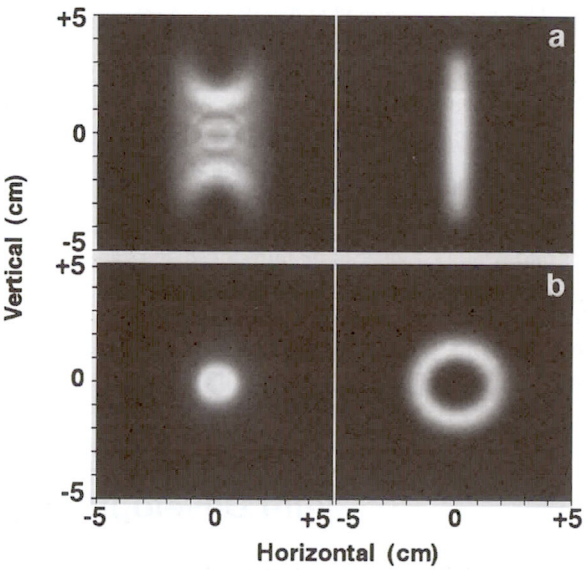

Figure 1. Calculated spatial distribution of radiation from the POK (a) and the HOK (b) at the location of front mirror. Left hands of the both figures show integration of the low energy photons (<10 eV), and right hands are that of the high energy photons (10 < e_{photon} < 200 eV).

VIII-K Development of Beam Lines and Equipment for UVSOR

VIII-K-1 Construction of a Photoelectron Spectroscopy and Microscopy System

Toyohiko KINOSHITA, Shinya YAGI and Shin-ichi KIMURA

In order to investigate the surfaces and interfaces of solids, we are constructing an experimental system for photoelectron spectroscopy and photoelectron microscopy. Two types of photoelectron microscopy have been developed so far to achieve micro-analysis. One combines a micro-photon beam with a conventional photoelectron analyzer. The other uses a special electron energy analyzer and an electrostatic lens element to obtain magnified image of the photoelectrons, in which light with normal beam size (several mm ϕ) can be used. Since it is rather difficult to obtain micro- photon beam with enough intensity at UVSOR, we have chosen the latter system. It is expected that spatial resolution of 2μm for the imaging mode and 20μm for the spectroscopic mode respectively, can be achieved. The picture of the apparatus is shown in Figure 1. It consists a hemispherical electron analyzer with 150 mm radius, an electrostatic lens system, a magneto lens system for further magnification of the photoelectron image, a X-ray tube (Mg Kα, Al Kα) for photoexcitation, a sputtering gun, and so on. Ultra high vacuum of

less than $2x10^{-10}$ mbar can be achieved. In conjunction with monochromatized synchrotron radiation light from UVSOR storage ring, we plan to undertake the following studies with this apparatus.

(1) Observation of magnetic domains of ferro- and antiferromagnetic urfaces by means of magnetic dichroism effects.
(2) Observation of adosorbates on metal and semiconductor surfaces.
(3) Photoelectron spectroscopy studies of very small crystals.
(4) In situ observation of photochemical reaction on surfaces.

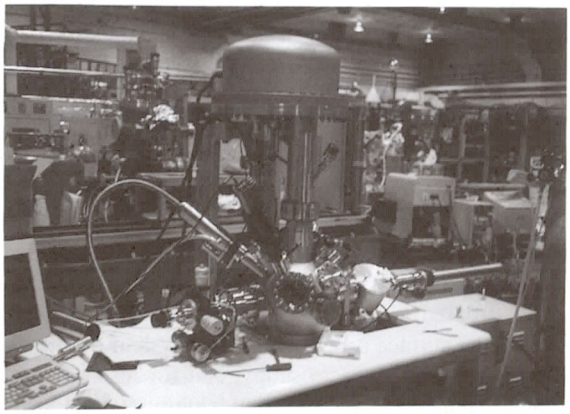

Figure 1. Photoelectron spectro-microscopy equipment.

VIII-L Researches by the Use of UVSOR

VIII-L-1 Dynamics of Photon-Stimulated Desorption of Excited-State Alkali Atoms from Alkali Halides

Sayumi HIROSE and Masao KAMADA

[*J. Phys. Soc. Jpn.* **64** (1995), *in Press*]

The time response of photon-stimulated desorption (PSD) of excited-state alkali atoms from alkali halides has been investigated with synchrotron radiation pulses. It was found that the substance having a larger Rabin-Klick parameter shows a larger efficiency of the fast desorption. It was also found that there is a delay for the fast PSD, indicating the existence of the precursor state. It is proposed that the fast desorption may be produced by electronic transition in the surface layer, while the slow desorption may be due to the thermal instability of surface defects.

VIII-L-2 Effect of Quenching Process on the Decay of the Fast Luminescence from Barium Fluoride Excited by VUV Synchrotron Radiation

M. A. TELEKHIN*, A. N. VASIL'EV*, Masao KAMADA, Eiken NAKAMURA and Sinzo KUBOTA** *(*Krachatov Inst. Russia, **Rikkyo Univ.)*

[*Phys. Rev.* **B 52**, 3117 (1995)]

The problem of quenching the luminescence associated with interatomic radiative transitions from the valence band to the deeper lying core level is studied for BaF_2, which is known to be the fastest inorganic scintillator. The measurements of excitation spectra and time decay kinetics of the fast fluorescence component (220 nm) for BaF_2 crystal excited by photons in the VUV spectral region from 16 to 100 eV are discussed. The quenching process is exhibited in the shortening of this decay and in the decrease of the quantum efficiency. The kinetics is nonexponential for all energies. These effects depend on the excitation photon energy and the angle of light incidence. This behavior is explained by the surface quenching (as has been supposed earlier) and the energy transfer to the excitations produced by the same photon. The relative effect of these processes depends on the excitation energy. For energies below 30 eV the surface quenching dominates, whereas, for higher energies the main quenching process is caused by the energy transfer from the core hole to other electronic excitations. The same effect can be observed in other ionic crystals in which the Auger decay of core hole is energetically forbidden.

VIII-L-3 Optical and Photoelectrical Studies of Electronic Structure of $R_3Au_3Sb_4$ (R=La, Ce and Pr)

Shin-ichi KIMURA, Yasuhiko SATO*, Fumitaka ARAI*, Mikihiko IKEZAWA*, Masao KAMADA, Kenichi KATOH* and Mitsuo KASAYA* *(*Tohoku Univ.)*

[*J. Phys. Soc. Jpn.* **64** (1995), *in press*]

The electronic structures of a magnetic semiconductor $Ce_3Au_3Sb_4$ and the related materials, $La_3Au_3Sb_4$ and $Pr_3Au_3Sb_4$, have been investigated by reflectivity and resonant photoemission spectra. From the resonant photoemission spectra of $Ce_3Au_3Sb_4$, the hybridization between the Ce 4f state and the Sb 5p valence band was found to be weak. This result is consistent with the electronic structure which is derived from the analysis of the optical data about the energy gap. The experimentally determined electronic structure is compared with a band calculation of $La_3Au_3Sb_4$. The unoccupied 4f state is concluded to be about 3 eV above the Fermi level, which is higher by 2 eV than the result of the band calculation. The exciton like absorption due to the transition from 4f to 5d states was observed. The intra-atomic Coulomb interaction between 4f and 5d states is thought to play an important role.

VIII-L-4 The Investigation of Well-Defined NaCl Surface

Shin-ichiro TANAKA and Masao KAMADA

Alkali halide is a typical ionic crystal, and has been extensively studied experimentally and theoretically for many years. However, its surface properties are not well known, mainly because it is an insulator and then cannot

be investigated due to the charging effect using usual techniques in surface analysis for conducting materials. We have produced the thin crystalline films of NaCl on the well-ordered Si(100)(2x1) and Ge(100)(2x1) surfaces in UHV, and investigated their surface properties. The charging effect can be avoided because the film is thin enough. Figure 1 shows the LEED (Low Energy Electron Diffraction) image of NaCl film deposited on Ge(100)(2x1) surface at 105K and subsequently annealed. Clear (1x1) pattern is observed, and it is considered that the well ordered NaCl(100) surface has been produced. We study the surface properties of this system by the use of the photoelectron spectroscopy, and for instance, a) it was shown that the change in Maudelung potential at the surface causes the surface shift of the excitation energies for the core excitons at Cl-$L_{2,3}$ edge, b) it was shown that the adsorbed K and Cs atoms on the NaCl surface are metallic at low temparature.

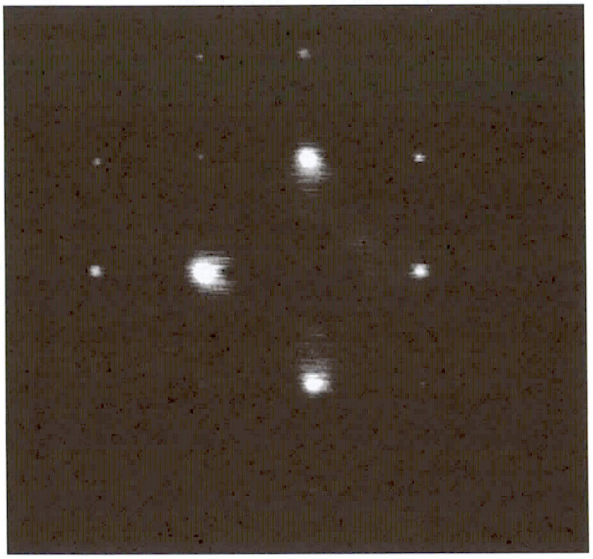

Figure 1. The LEED image of NaCl(100) surface on the Ge(100)(2x1) surface. The thickness of the film is estimated to be 30 ML.

RESEARCH FACILITIES

For the sake of brevity the present issue includes only the newly installed facilities and the activities since September 1994. Concerning the activities and facilities before September 1994, please refer to older IMS Annual Review issues(1978~1994).

Computer Center

The main computers at the center are a supercomputer NEC SX-3/34R, a parallel computer IBM SP2(48 cpu nodes), and a unix based main-frame NEC HSP. Total CPU performance of these system is about 24 G FLOPS. These CPU servers are linked to international networks through Science Information Network(SINET). About 30% of the computer time is used by the research staff at IMS, and the remaining 70% is given out as research grants to scientists outside the institute in molecular science and related field. As of March 1995, the number of project group was 222, consisting of 740 users. The library programs of the Center amount to 203. Among them, about 40 programs can be executed immediately. Recent additions include Gaussian 94 and parallel version HONDO8. The Quantum Chemistry Literature Database (QCLDB) has been developed by the Center in collaboration with the QCLDB group. The Force Constant Database (FCDB) are also available at the center.

Chemical Materials Center

The Chemical Materials Center plays an important role in the synthesis and purification of chemical substances in IMS. The scientists and technical associates of this facility support other people in IMS to carry out the above works. Upon request, technicians carry out elemental and mass spectrometric analyses of new compounds prepared at IMS. They also carry out their own researches on synthesis of new interesting compounds, developments of new selective chemical transformations, elucidation of reaction mechanism, and application of new methodologies developed in IMS to the analysis of chemical substances and reactions.

Instrument Center

For the efficient use of instruments, the Center is equipped with various types of instruments for general use[1]).One instrument has been newly installed in 1995. High Resolution Fourier Transform NMR spectrometer system(JEOL LNM-LA500). The system consists of a superconducting magnet (proton resonance frequency of 500MHz), four kinds of NMR probeheads for solutions, a spectrometer unit, a computer system for data analysis(DEC-3000), and a field gradient unit. Liquid nitorgen is automatically supplyed from Nitrogen Supplier NS-50 which produces liquid nitrogen by cooling air. It is possible to observe ^{1}H, ^{19}F, and nuclues from ^{103}Rh to ^{31}P in a temperature range of -100 to 150°C. The field gradient unit reduces the experimental period of a two dimensional NMR spectroscopy remarkably.

Reference

1)*List of Instruments*, No.9, IMS Instrument Center(1994)

Low-Temperature Center

The main task of Low-Temperature Center is a steady supply of liquid helium and liquid nitrogen to the users in the Institute. The total amounts of liquid helium and liquid nitrogen supplied in 1994 were 40,736*l* and 71,972*l*, respectively. A dilution refrigerator (KELVINOX 36115, Oxford Instruments) and a SQUID magnetometer (MPMS 2, Quantum Design) are now available for general users. A high-resolution solid state NMR spectrometer (DSX-400, Bruker Analytical Instrument) was newly equipped in 1995.

Equipment Development Center

A number of research instruments have been designed and constructed by making use of the mechanical, electronic and glass-blowing technologies at this Facility. Representative instruments developed during this fiscal year of 1994 are listed below.

Support of A_xC_{60} furnace
Radome-membrane holder for evaluating an ice-coating
Low temperature sample holder for SR etching
Molecular beam diagnostic apparatus
Cylindrical cell and cell spinner for experiments using high repetition laser
Frequency Multiplier for 600 GHz band
Image Detector for Diffracting Metastable Atoms
High pressure cell
Laser-Beam Focusing Instrument with Focus-Position Adjustment
Gas cell for LIF

Division of IMS Machines

Equipment Development Center has the division of IMS Machines. Activitiy of this division is described in detail in section "RESEARCH ACTIVITIES".

Ultraviolet Synchrotron Orbital Radiation Facility

The UVSOR light source is usually operated at an electron energy of 750 MeV with an initial current of 200 mA. A higher harmonic RF system has been installed in order to suppress longitudinal coupled bunch instabillity with a double RF system. The instability was successfully suppressed in machine study and the system is routinely used for user experiments in multi-bunch operation. Another advantage of the double RF system is that the beam lifetime increases from 200 to 350 min. in multi-bunch operation at 200 mA because the bunch length becomes 2-3 times longer. The superconducting Wiggler with a magnetic field of 4 T is operated to provide soft x-rays up to 1.5 A (8.3 keV).The gate valves have been installed into the storage ring to separate the beam pipe into four sections. At BL8B1, a 15-m Constant-Deviation-Grazing-Incidence monochromator has been constructed for soft x-ray spectroscopy and a high resolving power of 4,000 is achieved at 400 eV. A new monochromator named SGM-TRAIN, which covers the photon energy range of 5-250 eV, is under construction. This monochromator will be used for experiments using circularly polarized radiation with a spin resolved photoelectron spectrometer. The circularly polarized light will be produced by a helical undulator which is also under construction.

SPECIAL RESEARCH PROJECTS

IMS has special research projects supported by national funds. Two projects carried out until March 1995 are:
(1) Development and evaluation of molecular synergistic systems and their application to chemical energy conversion (1990-1995).
(2) Materials science on molecular devices (1990-1995).
And three projects in progress are:
(3) Material control in multi-reaction centers (1993-).
(4) Development of microscopic environments with functionality and quantum steering for reactions (1995-).
(5) Study of molecular solid toward molecular electronics (1995-).
These three projects are being carried out with close collaboration between research divisions and facilities. Collaborations from outside also make important contributions. Research fellows join these projects. The results in 1994 are also reviewed in this report(1995-).

(1) Development and Evaluation of Molecular Synergistic Systems and their Application to Chemical Energy Conversion

Development of High-Sensitivity Submillimeter-Wave to Far Infrared Spectroscopic System for the Study of Transient Molecules

Hiroyuki OZEKI and Shuji SAITO

Spectroscopy in the submillimeter-wave to far infrared region has been less exploited when compared with that in other regions, because high-spectral purity and tunable radiation sources have not been available. We develop a frequency-tunable far-infrared sideband spectrometer suitable for the study of transient molecules. We installed a stable high-power CO_2 laser and an optically pumped far-infrared laser which generates several fixed frequency radiation between 600 to 300 GHz. We designed and constructed a mixer mounting with a nonlinear element of GaAs Schottky diode, which is mounted in a Martin-Puplett diplexer separating a tunable sideband radiation from the fundamental laser beam. Currently we obtained a small output power of the sideband component in the frequency range of 2522±26 GHz, with which we plan to carry out spectroscopy by installing an absorption cell for transient species. We are also constructing a frequency standard which determines the oscillating frequency of free-running far infrared laser with an accuracy less than 100 kHz.

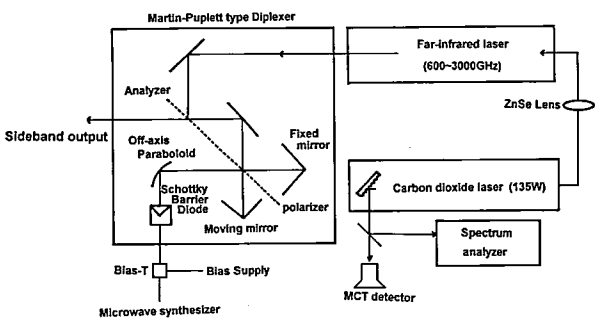

Block diagram of tunable far-infrared sideband spectrometer

Studies on Laser Cooling and Trapping of Neutral Atoms

Norio MORITA, Mitsutaka KUMAKURA and Yoshiki MORIWAKI

Using the highly efficient discharge source of metastable atoms and gas-circulation-purification system, which were developed last year, we laser-trapped metastable ^{4}He and ^{3}He atoms and measured Penning ionization rates in He*-He* ultracold collision processes. The Penning ionization is known to be the main loss mechanism in laser traps of rare gas atoms, and should be overcome to increase the trap density. We performed two kinds of experiments to measure the ionization rates in the He trap at a temperature of about 600μK; one was simply to observe the time evolution of fluorescence intensity from the trap after atomic feeding was shut off with the trapping laser kept on. In this case, we found that the decay rate was linearly dependent on the trap density, and the rate coefficient was determined to be 3.2×10^{-9} cm^3s^{-1} for the ^{4}He trap and 6.3×10^{9} cm^3s^{-1} for the ^{3}He trap. Since the typical trap density was 4×10^{10} cm^{-3}, the ionization rates at this density were estimated to be 1.3×10^{2} s^{-1} and 2.5×10^{2} s^{-1} for the ^{4}He and ^{3}He traps, respectively. Although these values represent the collisional ionization rates in the real trap, which is always irradiated by the trapping laser, those rates are due to a mixture of 2*s*-2*s*, 2*p*-2*p* and 2*s*-2*p* collisions. We then performed another measurement to obtain the ionization rate only due to the 2*s*-2*s* collision; after atomic feeding was shut off, the trapping laser was alternately on and off with a repetition rate of 10 kHz and a duty ratio of 10%. In this case, since the fluorescence lifetime of the upper level (2*p*) is 97 ns, the trapped atoms spend 90 % of the time in the lower level (2*s*). Therefore, the decay rate of the envelope of successive fluorescence peaks at the laser-on periods approximately represents the ionization rate only due to the 2*s*-2*s* collision. However, the rates thus obtained for the ^{4}He and ^{3}He traps, 1.1 s^{-1} and 1.5 s^{-1}, respectively, were both independent of the trap density, This means that the ionization rates due to the 2*s*-2*s* collision were much smaller than those caused by collisions with residual gases in the vacuum chamber used. From these results, we see that, for both ^{4}He and ^{3}He, the ionization rates due to the 2*s*-2*s* collision are more than two orders of magnitude smaller than those due

to the mixed collisional processes under the normal trap condition. This fact means that, if we can somehow trap only the 2*s* atoms, it is possible to increase the trap density by more than an order of magnitude (see II-D-1).

Mechanism of Oxygen Activation by Heme-Copper Terminal Oxidase Superfamily

Teizo KITAGAWA, Takashi OGURA, Shun Hirota, Denis A. PROSHLYAKOV, Shinya YOSHIKAWA *(Himeji Inst. Tech.)*, **Tatsushi MOGI** *(Univ. of Tokyo)*, **Nobuhito SONE** *(Kyushu Inst. Tech.)* **and Evan H. APPELMAN** *(Argonne Natl. Lab.)*

The terminal oxidase in respiratory chains is cytochrome *c* oxidase for aerobic organisms and quinol oxidase for *E. coli*. Both have two heme groups; one works for electron transfers and the other provides the catalytic site for dioxygen reduction. The heme iron at the catalytic site is antiferromagnetically coupled with a copper ion in the oxidized state. The dioxygen reduction is coupled with proton translocation through membrane, generating electrochemical potential which could be used for ATP synthesis. The final goal of this study is to elucidate the coupling mechanism between the electron- and proton transfers, but currently a mechanism of dioxygen reduction at the catalytic site is of spectroscopic concern. This year we treated *bd*-type cytochrome oxidase and assigned the axial ligand-related Raman bands. For bovine cytochrome *c* oxidase, we investigated reaction intermediates present in the time range between 0.1 and 11 ms following initiation of the reaction by using time-resolved resonance Raman spectroscopy combined with our original "artificial cardiovascular system for pursuit of enzymic reaction". The first intermediate gave the oxygen-isotope-sensitive band at 571 cm^{-1} for $^{16}O_2$. Since the corresponding band for $^{16}O^{18}O$ split into two bands, it became confident that the binding of O_2 is of an end-on type. In subsequent steps, we observed three oxygen-isotope-sensitive bands at 804/769, 785/750 and 355/340 cm^{-1} for $^{16}O_2/^{18}O_2$ derivatives. Experiments at lower temperatures clarified that the 804 cm^{-1} species appears prior to the 785 cm^{-1} species, while the 355 cm^{-1} band was seen together with the 804 cm^{-1} band. Although the 804 cm^{-1} band appeared with a similar rate in H_2O and D_2O, the appearance of the 788 cm^{-1} band was significantly delayed in D_2O, suggesting that the generation of 788 cm^{-1} species from the 804 cm^{-1} species is coupled with the proton translocation. The experiments with $^{16}O^{18}O$ demonstrated that both bands should arise from the Fe^{IV}=O stretching but not from the O-O stretching. The reaction of oxidized enzyme with hydrogen peroxide also gave the three sets of the oxygen-isotope-sensitive bands at the same frequencies as those of dioxygen reduction. It is likely that the 804 and 788 cm^{-1} bands arise from the Fe^{V}=O and Fe^{IV}=O stretching modes, respectively, while the 355 cm^{-1} band is associated with the His-Fe=O bending mode.

Laser Raman Beat Detection of Magnetic Resonance

Tatsuhisa KATO and Michio MATSUSHITA

Laser Raman beat detection is a coherent optical- RF double resonance technique where the optical and RF field induce coherence within a three level system and a resultant Raman beat signal is detected using heterodyne detection. This technique can be applied to the study of electron paramagnetic resonance and nuclear magnetic resonance not only in the ground state of a molecule but also in the electronic excited state. There are some causes to hide the Raman beat signal, that is, the inhomogeneity of the circumstance of the molecule, the fluctuation of the applied field, and the interference by the crystal phonon. It is the key to success in the Raman beat detection to eliminate these cause of the incoherence. Then it is needed to prepare the sophisticated single crystal sample, the highly stabilized magnetic field, and a cryostat of liquid helium. It has been completed to set up the apparatus, and the Raman beat detection was applied to the study on the zero-field NMR transitions of Pr^{3+} in LaF_3 crystal, as reported in Section II-H-1.

Liquid Dynamics Studied by New Ultrafast Nonlinear Spectroscopies

Keitaro YOSHIHARA, Keisuke TOMINAGA, Yukito NAITOH, Tai Jong KANG *(Taegu Univ. and IMS)* **and Gary P. KEOGH** *(Imperial College and IMS)*

Understanding of microscopic dynamics and structures of liquids is quite important in chemistry because many chemical reactions and various relaxation phenomena in condensed phases such as vibrational dephasing or energy relaxation are strongly affected by microscopic details of liquid molecules. In this research we have developed ultrafast spectroscopic techniques based on nonlinearity of liquids, especially higher order (higher than fifth order) nonlinearity. Followings are the experiments we are performing.

1) Raman echo experiments for vibrational dephasing of high-frequency intramolecular modes.

2) Five-pulse correlation experiments for vibrational dephasing of low-frequency intermolecular modes.

Studies of Laser-Induced Photochemistry on Solid Surfaces

Yoshiyasu MATSUMOTO, Kyoichi SAWABE, Kazuo WATANABE, Hiroyuki KATO *(Graduate Univ. for Advanced Studies)*, **Yuri A. GRUZDKOV and M.C. Lin**

Light sources such as lasers and synchrotron radiation can be very useful for the various processes in the fabrication of microelectronics, including etching, chemical vapor deposition, atomic layer epitaxy. On the other hand, it has also been well recognized that there is an important class of catalytic reactions with the aid of photon irradiation. Although those applications of light are practically useful and important, fundamental understandings of these processes are still lacking. Therefore, this project is mainly aimed for investigating how the interaction of light and adsorbates and /or substrates promotes chemical reactions from the fundamental point of view. We have developed a UHV apparatus equipped with a retractable LEED/Auger electron spectrometer, a differentially pumped quadrupole mass spectrometer, a X-ray source, a photoelectron analyzer, an ion gun, a high precision sample manipulator, a closed cycle He refrigerator, and a gas doser. The main chamber was evacuated to a base pres-

sure of 1×10^{-10} Torr by cascaded turbo-molecular pumps. With this apparatus, we can perform not only conventional analytical measurements in surface science including LEED, AES, temperature-programmed desorption, XPS, and work function measurements, but also measurements providing information on nuclei dynamics including angular-resolved time-of-flight spectroscopy of neutral species desorbed from the surface with submonolayer coverage. We have investigated photodissociation dynamics of nitrous oxide adsorbed on semiconductor surfaces and found that photodissociation dynamics depends significantly on the adsorbed state of N_2O and a peculiar photofragment angular distribution. In addition, we have uncovered that methane physisorbed on Pt(111) can be effectively dissociated with the irradiation of 193 nm-photons, yielding a chemisorbed CH_3 radical and an adsorbed H atom as products. Furthermore, we have started to develop a new technique, i.e. two-photon photoemission spectroscopy, which provides important information of electronically excited state of adsorbates.

Light Sesitivity of the Self-Organizing Chemical Systems

Ichiro HANAZAKI, Akiko KAMINAGA, Yoshihito MORI*, Noriaki OKAZAKI, Vladimir K. VANAG*** and Gyula RÁBAI****** *(*Nagoya Inst. Tech., **JSPS fellow, ***N.N.Semenov Inst. Chem. Phys. Russ. Acad. Sciences, Moscow, Russia, ***Inst. Phys. Chem., Kossuth Lajos Univ., Debrecen, Hungary)*

The self-organizing process in chemical systems is known to occur as a result of nonlinear chemical events. The temporal (oscillatory) behavior and the possibility of spatial pattern formation in such systems have been interested in relation to the understanding of living systems and also to their possible application to sensing and memory-storage devices. The response of such systems to light illumination has been studied many times but not in a systematic manner. We have established the method by which the response of these systems to light illumination and applied it to determine the state diagram and photo-induced bifurcation structure for the Belousov-Zhabotinsky system, the minimal bromate oscillator, the $Fe(CN)_6^{4-}/ H_2O_2$ system, and the Briggs-Rauscher system. Very recently we have applied this method to the study of photoresponse of the BrO_3^--SO_3^{2-}-ferrocyanide system, which is one of the pH-oscillators and seems to be unique in its origin of nonlinearity leading to chemical oscillations. This system can be divided into two subsystems, namely, the BrO_3^--SO_3^{2-}-H^+ system and the BrO_3^--ferrocyanide-H^+ system. We have found that the former is insensitive at all to the illumination at $\lambda > 400$ nm, while the latter process is enhanced by illumination. This system is interesting in exploiring the chemical reaction mechanism as well as its close relation to the iodate-sulfite system which has recently benn reported to exhibit spatial pattern formation.

Spectroscopy of Polyatomic Molecules with a Combination of Ultraviolet Laser and Synchrotron Radiation

Masakazu MIZUTANI, Shuji ASAKA, Atsunari HIRAYA and Koichiro MITSUKE

We are planning to develop new spectroscopy of polyatomic molecules based on synchronization of photon pulses between an undulator light and a mode-locked ultraviolet laser. Our primary goal is to investigate the photodissociation and photoionization dynamics of molecules in a particular vibronic state. The experimental setup is as follows. A mode-locked Ti:sapphire laser is made to operate synchronously with the master oscillator (90.115 MHz) for a harmonic RF cavity on the UVSOR ring. Then the second and third harmonics are generated by using an LBO and BBO crystals, respectively. The output power of the third harmonics is found to be about 80 mW at 260 nm. The ultraviolet laser light is introduced into a photoionization chamber. The undulator light from the beam line BL3A2 passes coaxially with the laser light. The molecular beam intersects at 90° with the two photon beams. Photoions are analyzed by a quadrupole mass filter placed perpendicularly to the photon beams. The high photon flux of the second or third harmonics permits a valence electron to be excited to a Rydberg or antibonding orbital. If temporal overlap between the laser and undulator photon pulses is sufficient, it can be expected that the excited molecule is further dissociated or ionized by an undulator photon. We will make a preliminary experiment on photodissociation of NO_2 to examine the efficiency of the two-color excitation. The second harmonics (370 nm) of the laser leads to dissociation of NO_2 into NO + O. Subsequently, an NO fragment is ionized by a ~9.6 eV undulator photon. Since parent NO_2 molecules cannot be ionized at this photon energy, any ion signal proves that two different photons are successively absorbed.

Electronic Structure and Reaction Dynamics of Solvated Metal Ions

Kiyokazu FUKE and Fuminori MISAIZU

Metal ions are intimately involved in chemistry and biochemistry and play a crucial role in many reactions. Although there has been extensive progress in the thermodynamic and kinetic studies of solvated metal ions, the study on microscopic aspect of solvation dynamics has been rather limited. Spectroscopic studies of the solvated metal ion clusters as a function of cluster size can provide detailed information on energetic and dynamics of solvation. The advent of mass spectrometry and metal cluster beam techniques in conjunction with laser probes now allow an attack on the problems for the solvation of metal ions and metal cluster ions through studies probing energy levels and dynamical processes occurring in solvated metal clusters.

In the present research project, we have investigated the photodissociation spectra of mass-selected $Ca^+(H_2O)_n$, (n=1-9) in the wavelength region of 330-1440 nm using a reflectron-type TOF mass spectrometer (see VIII-C-1). Using the recently developed magnetic-bottle type photoelectron spectrometer, we have investigated the photoelectron spectra of $Na^-(NH_3)_n$ and $Li^-(NH_3)_n$. From these studies, we could obtain the first direct evidence to show that single alkali-metal atom spontaneously ionizes and dissolves in small clusters (see VIII-C-2, 3). We have also studied the formation and decay processes of solvated

Rydberg radical such as $NH_4(NH_3)_n$, to get further insight into the mechanism of stabilization of NH_4 in clusters and the photochemistry of ammonia clusters in the first excited state as well (see VIII-D-1,2). Moreover, we constructed a new reaction cell consisting of an octopole ion guide and a quadrupole mass spectrometer in order to investigate the dissociation dynamics of $NH_4(NH_3)_n$, (see VIII-D-3).

Organic Conductors Based on Novel Heterocyclic Compounds

Yoshiro YAMASHITA, Shoji TANAKA and Masaaki TOMURA

We have succeeded in preparing new electron donors giving organic conductors. For example, π-extended tetrathiafulvalene analogs containing quinoid structures were prepared. They are strong electron donors and afforded highly conducting charge-transfer complexes. Novel tris(1,3-dithiole) donors containing thiophene spacer units were also prepared. They are oxidized to trication or tetracations. Although planar molecules are usually used for organic conductors, we have found that butterfly-shaped bis(1,3-dithiole) donors containing a fused naphthalene and a thiadiazole ring gave metallic cation radical salts. The metallic property of one salt maintains down to low temperature. The donor molecule has small on-site Coulombic repulsion. In the crystal structure of a metallic salt, deformed donor molecules are uniformly stacked. A novel type of donor-π-acceptor system was also prepared. A benzobis(thiadiazole) moiety was found to have a high electron affinity and to be used as an acceptor unit. The dithienyl derivative gave a narrow bandgap polymer (*Eg* ~ 0.5 eV) by electrochemical oxidation. Other heterocyclic donor-acceptor systems were used to construct narrow bandgap polymers. Details of those works are described in VIII-B section.

(2) Materials Science on Molecular Devices

π-d Interaction in Molecular Metals

Kyuya YAKUSHI and Toshihiro HIEJIMA

We have undertaken a systematic study on the solid molecular systems in which transition metals are embedded in a π-conjugated system from the viewpoint of the future design of the superconducting material. The highly conductive phthalocyanine salts such as $CoPc(AsF_6)_{0.5}$ and $NiPc(AsF_6)_{0.5}$ are the prototype of the one-dimensional conductors in which the d- and π-orbitals form a double-chain (two-bands) system. Subsequently to the finding of the pressure-induced charge transfer in the last year, we analyzed thoroughly the pressure dependence of the absorption spectra of visible, near-infrared and infrared regions in these conductive phthalocyanine salts, and evidenced the pressure-induced charge transfer from the d-band to π-band. *(see IV-A-1 and 2)* This phenomenon is quite unique and implies that the pressure can control the carrier concentration of these two bands, which is usually very difficult in a organic conductor. However, it was found from our analysis that a metal-insulator transition occured at 0.5 GPa in$NiPc(AsF_6)_{0.5}$ and 1.1 GPa in $CoPc(AsF_6)_{0.5}$. This conclusion was confirmed by the pressure dependent electrical conductivity measurement.

Fabrication of Novel Organic Molecular Assemblies with the Use of the Molecular Beam Epitaxy Technique

Yusei MARUYAMA, Hajime HOSHI *(Tokyo Institute of Technology)*, **Keiichi KOHAMA** *(Toyota Motor Corp. and IMS)* **and Shaoli FANG**

In order to prepare new materials which could be useful for molecular devices elements, we have started to design and fabricate ultra-thin organic multi-layered systems. In the first place, we have prepared ultra-thin single component phthalocyanine thin films to investigate epitaxial growth conditions on alkali halide single crystals. Fairly well oriented, uni-or bi-directionally, crystalline films are obtainable on the alkali halide substrates. Based on this kind of mono-film, we are going to fabricate a multi-layered system. The SHG and/or THG of the films are investigated from the view point of the molecular structure and the epitaxy or orientation of the films.

Study on the Solid State Properties of Fullerenes

Yusei MARUYAMA, Hironori OGATA, Roger WHITEHEAD *(Durham Univ. and IMS)*, **Toshiyasu SUZUKI, Takeshi ARAI and Atsushi SUZUKI**

In order to clarify the nature of novel molecular systems, fullerenes, we have started to measure the electronic properties of fullerene solids, mainly concerning on the transport properties of pure and/or alkali metal-doped fullerene crystals. Charge-carrier drift mobilities of pure C_{60} single crystals were measured with the use of time-of-flight technique and the temperature dependence of the mobilities was also investigated. As for the alkali metal (K or Rb) doped C_{60} crystals, the temperature dependences of the electrical conductivities and the thermoelectric power were observed, and the "metallic" nature of these substances was revealed. Through these measurements we are going to understand the electronic nature of this novel molecular system.

NMR Studies on the Dynamical Properties of Condensed Matter Systems

Seiichi MIYAJIMA, Hironori OGATA, Tomoyuki MOCHIDA, Osamu OISHI and Toshihito NAKAI

We are studying the dynamics-related properties of condensed matter systems by means of nuclear magnetic resonance (NMR) spectroscopy. The following three subprojects are reported.

(1) Development of pulsed field gradient (PFG) NMR spectroscopy to the strongly dipole-coupled spin systems

To this goal we designed and constructed a new PFG-NMR spectrometer. Combining the line-narrowing technique with sharp, intense, and rotatable PFG, we obtained anisotropic diffusion coefficient tensors in smectic Ad liquid crystal. This method is being applied to study the molecular dynamics related to dielectric order/disorder phenomena in liquid crystals, and the ionic transport in solids.

(2) Microscopic origin of antiferroelectricity in liquid crystals

How the antiferroelectricity and dynamic disorder can coexist in chiral smectic liquid crystals is an interesting problem. To reveal the key to interlayer correlation of electric dipoles, we performed high resolution ^{13}C NMR study for MHPOBC, and clarified the validity of bent-chain model, and also the relationship between the chain motion and the dielectric ordering.

(3) Electronic states of alkali-hydrogen-graphite intercalation compounds

Hydrogen or alkaline metal elements can, when intercalated into the graphite layers, exhibit various electronic states depending on charge transfer, electron-electron, and electron-phonon interactions. ^{13}C, ^{1}H, and ^{23}Na NMR studies revealed a rather localized electronic property for Na-H-GIC compared to KH-GIC. Highly mobile hydrogen species were found, which is related to cationic defects in the planar intercalate lattice.

(3) Material Control in Multi-Reaction Centers

Chemical Modification of Home Enzymes

Yoshihito WATANABE, Shin-ichi OZAKI, Senji WADA, Toshitaka MATSUI and Yoshio GOTO

Among the most of heme enzymes, a super family of cytochromes P-450 is a quite unique, since P-450 catalyzes a wide variety of chemical reactions including hydroxylation of unactivated hydrocarbons, oxidative degradation of steroids, and preparation of NO through the oxidation of arginine. Possibly because of its high reactivity, the active species responsible for those oxidations has never been characterized, while there have been several model complexes which mimic P-450 type oxidations. Though the active species is expected to be observable at low temperature, one can not run enzymic reaction at low temperature. Therefore, in this project we have planned to prepare hybrid P-450 by employing chemical modification of enzymes to allow enzymes soluble in organic solvents such as toluene, chloroform, and so on. For example, activated polyethylene glycol can be used to modify lysine residues exposed on the surface of the enzymes. Currently, we have succeeded to prepare cytochrome P-450cam modified with cationic micelle and activated polyethylene glycol and their enzymic activities are under investigation. Further, we have been examining possible alteration of myoglobin to a peroxidase by replacing a few amino acids around heme vicinity. These tudies are believed to serve for the full understanding of roles of reaction environment of enzymes and their catalytic activities and allow to design artificial heme enzymes.

Specific Feature of Copper-Ion-Exchanged Mordenite for Dinitrogen Adsorption at Room Temperature

Yasushige KURODA, Yuzo YOSHIKAWA, Shin-ichi KONNO,* Hideaki HAMANO,* Hironobu MAEDA,* Ryotaro KUMASHIRO* and Mahiko NAGAO* *(*Okayama Univ.)*

[*J. Phys. Chem.*, 99 , 10621(1995)]

The synthetic zeolite are extensively used as catalysts or adsorbents in a variety of chemical reactions and separation processes. In particular, a great deal of attention was given to the zeolite molecular sieves containing transition metal ions. Notably, copper-ion-exchanged zeolite has been reported to be active in the catalytic decomposition of the nitrogen oxides that are considered as one of the causes of air pollution. Especially, zeolite containing copper ions in greater amount than that expected from a stoichiometric considerstion, which is referred to as the nonstoichiometrically copper-ion-exchanged one, is supposed to be appreciably effective for the decomposition of nitrogen oxides. We have been investigating the state of copper ions exchanged in mordenite and the adsorption properties of zeolites, and found a new feature that the mordenite-type zeolite can strongly adsorb dinitrogen molecules at room temperature(298 K). Few works examined a strong adsorption N_2 on oxide samples at room temperature. The interaction of such molecules with the solid surface is particularly interesting in the field of catalysis, *e.g.*, N_2 fixation. The purpuse of the present study is to elucidate the exchanged state of copper ion on mordenite and to obtain information on the strongly-N_2-adsorbed sites. Unusual properties of copper-ion-exchanged mordenite for N_2 adsorption at room temperature are discussed on the basis of the data of adsorption calorimetry, IR, XAFS, ESR, and emission spectroscopy. Adsorption properties of copper-ion-exchanged mordenite (CuM) for dinitrogen molecules (N_2) were examined at 298 K. The intensive IR absorption band observed at 2299 cm^{-1} was attributed to the N_2 species strongly adsorbed on CuM. The interaction of N_2 with CuM is explored using adsorption calorimetry, X-ray absorption fine structure (XAFS), and photoemission spectroscopy. Furthermore, it is proved from the emission data that the adsorption site including Cu(I) species easily formed by heat treatment at 873 K in vacuo is effective for N_2 adsorption. Such easy conversion of Cu(II) to Cu(I) may be due to the spatial distribution of ion-exchanged sites on mordenite. Although a rather high value of heat of adsorption might suggest a chemisorption, it is made plausible that this type of N_2 adsorption is physisorption.

Migration Reactions of a Transition-Metal Fragment to the Cyclopentadienyl Ring with Bond Cleavage between Transition Metals

Hiroshi NAKAZAWA, Michiyo KOKKA, Tsutomu MIZUTA and Katsuhiko MIYOSHI *(Hiroshima Univ.)*

It has been reported for transition-metal complexes containing an η^5-cyclopentadienyl (Cp) ligand that one electron-donor ligand migrates from a transition metal to the Cp ring in the reaction with a strong Lewis base such as n-BuLi or $LiN(i\text{-}Pr)_2$ (LDA). The migration is considered to proceed by the nucleophilic attack of the Cp anion produced by the Lewis base toward the vacant orbital(s) on the coordination atom such as a π^* orbital or a vacant d orbital. If the reaction mechanism can be applied to dinuclear transition-metal complexes, a transition-metal fragment would migrate from a transition metal to a Cp ring because a transition-metal fragment has a vacant d orbital. Based on the way of thinking, we started to examine the reaction of a variety of dinuclear transition-metal complexes having a single M-M bond and at least one Cp ligand. The reaction of $Cp_2M_2(CO)_{2n}$ (M = Fe, Ru ; n = 2: M = Mo, W; n = 3) with LDA and then MeI yielded (η^5-$C_5H_4\{CpM(CO)_n\}$)$M(CO)_2Me$ indicating the migration of a $CpM(CO)_2$ fragment from M to a Cp ring. Heterodinuclear complexes also exhibit the migration reaction. Although no selective migration was observed in the reaction of $Cp(CO)Fe(CO)_2Ru(CO)Cp$, the selective migration of a $Cp(CO)_3Mo$ fragment was observed in the reaction of $Cp(CO)_2FeMo(CO)_3Cp$. The selectivity is suggested to be related to the reduction potential of a transition-metal fragment.

Metal Complexes as Targeting Agents for Nucleic Acids

Mitsuhiko SHIONOYA

Molecular recognition of DNA, RNA, and related biomolecules is responsible for a wide range of biochemical processes such as complementary base pairings in genetic information storage and transfer, or oligonucleotide recognition by ribozymes and restriction enzymes, etc. Simple compounds that recognize and strongly bind to a specific nucleobase or sequence to compete with natural gene control elements might make new prototypes for biochemical as well as chemical probes for nucleic acids. For this purpose, transition metal complexes are quite advantageous and are currently attracting great interest. We demonstrated that Zn^{II}-cyclen complex and its functionalized derivatives are a new type of ideal receptor molecules that in neutral aqueous solution recognize and bind selectively and reversibly to thymine base and its homologues. Recently, we also discovered that the same Zn^{II}-cyclen complex induces a dramatic transition from right-handed B form to putative left-handed Z form of poly(dG-dC).poly(dG-dC) at very low concentration. These findings suggest that Zn^{II} as macrocyclic polyamine complexes may become a new tool to control some gene expressions involving base pairing processes with single-stranded nucleic acids as well as chemical probes of unusual DNA structures. Further investigation to develop new dynamic functions of metal species such as unwinding or melting of double-stranded DNA is now in progress.

Activation of Carbon Dioxide by Metal Complexes Directed Toward Carbon-Carbon Bond Formation

Koji TANAKA, Kiyoshi TSUGE, Masato KURIHARA and Tetsunori MIZUKAWA

Carbon dioxide behaves as an electrophile under mild conditions, but direct electrochemical CO_2 reduction is a thermodynamically unfavorable process due to the large negative redox potential of $E°(CO_2/CO_2^-)$ at -2.21 V (*vs.* SCE). On the other hand, the electron density of CO_2 ligated on low valent metal complexes is highly enhanced by π-back donation from occupied d orbital to empty π^* orbital of CO_2. Metal complexes, therefore, effectively reduces the high overpotential energy for the CO_2 reduction. Although a variety of metal complexes have proven to be active CO_2 reduction, most of the products are limited to CO and HCOOH so far. We have elucidated that CO dissociation from metal-CO complexes is effectively depressed by accommodation of additional two electrons into π^*-orbital of polypyridyl ligands, and succeeded the first multi-electron reduction of CO_2 accompanied by carbon-carbon bond formation affording HCHO, CH_2OH, HOOCCHO, and $HOOCCH_2OH$. From the viewpoint of CO_2 as potential C1 sources for organic compounds, multi-electron reduction of CO_2 using organic electrophiles in place of proton may provide more versatile routes for catalytic carbon-carbon bond formation. The purpose of this project is to develop new catalytic systems capable of carbon-carbon bond formation in the reduction of CO_2. Along this line, metals and sulfur ligands are expected to provide suitable reaction sites for both reduction of CO_2 accompanied by C-O bond cleavage and fixation of CO_2 to organic molecules with maintaining the CO_2 moiety.

Novel Type of Carbozirconation Reaction of Alkynes

Noriyuki SUZUKI, Denis Y. KONDAKOV, Motohiro KAGEYAMA, Martin KOTORA, Ryuichiro HARA and Tamotsu TAKAHASHI

Carbometalation of unsaturated hydrocarbons is an attractive reaction from the viewpoint of synthetic application of organometallic chemistry. Although allylmetalation of alkynes is a valuable reaction among them, only allylmetals containing Li, Mg, B, Zn or Al have been used. In addition, the allylmetalation with such allylmetals always involves a problem of regioselectivity. The formation of a new C-C bond can take place at the α- or γ-carbon of an allylic moiety. This regioselectivity depends on its mechanism, and the reactions often give a mixture of two isomers. On the other hand, zirconium mediated or catalyzed organic reactions have been extensively explored for the last two decades. Particularly, the reductive coupling of alkynes with other unsaturated compounds on zirconocene species has been intensively investigated. We have reported previously the zirconium mediated functionalization of unactivated alkynes via the formation of zirconacyclopentenes. This reaction could afford alcohols, ketones or halides as organic products involving the formation of new C-C bonds. In concern with the allylmetalation, zirconium mediated allylzincation of alkynes or zirconium catalyzed allylalumination has been reported. However, allylzirconocene compounds, which are easily prepared by the reaction of Cp_2ZrCl_2 with allyl Grignard or by the oxidative addition of allylic ethers to a 'zircono-

cene equivalent', are inert for the allylzirconation of alkynes. Recently we found that the zirconium-ethylene complex reacted with an allylic ether to afford the allylzirconation product of ethylene. Furthermore, this reaction could be catalytic as an allylation reaction in the presence of EtMgBr. The reaction proceeded via a five membered zirconacyclopentane intermediate, and elimination of the β-alkoxy group was the key step.

(4)Development of Microscopic Environments with Functionality and Quantum Steering for Reactions

Structures, Reactions and Spectroscopy of Molecules and Molecular Clusters

Suehiro IWATA, Seiichiro TEN-NO and Tsutomu IKEGAMI

To develop the new program systems for the study of structures, reactions and spectroscopy of molecules and molecular clusters, a local area network of workstations was constructed. The ne twork consists of four YHP 735, two SONY NEWS5100 and one IBM 6000. Using our own programs as well as the public domain and commercially available programs, we have studied a number of molecules and clusters. The complexes of water clusters with a metal ion and with a phenol are systematically studied. We have examined the similarity and difference of $[M(H_2O)_n]^+$, M = Mg and Ca and $[M(H_2O)_n]^+$, M = B and Al. For $[M(H_2O)_n]^+$, M = Mg and Ca, the theoretical results for the intra-cluster reactions are compared with the recent experimental works by Fuke's group(IMS), and the first product switch found in the experiments is quantitatively explained. For $[M(H_2O)_n]^+$, M = B and Al, a novel intra-cluster reaction is predicted. An apparent insertion reaction to a OH bond as well as a proton transfer takes place without a barrier for boron ion - water clusters. To analyze the photoelectron spectra of binary element cluster anions reported by Kaya's group in Keio University, a series of calculations are carried out for $Al_nS_m^-$, $Si_nC_m^-$, Si_nNa_m and C_nN^-. The geometric structures and their relative energies of possible isomers are carefully examined, and the vertical electron detachment energies are compared with the experimental ones. For small clusters, the photoelectron spectra are more thoroughly analyzed. A method to calculate the photoabsorption cross section from the classical trajectory is developed and applied to the visible bands of Ar_m^+ ions under finite temperature. The cluster size dependence of the red shift of the bands is influenced by the thermal motion within clusters.

Prediction of Protein Tertiary Structures by Multicanonical Algorithms

Yuko OKAMOTO, Ulrich H.E. HANSMANN *(IPS, ETH Zürich, Switzerland)*, **Takashi NAKAZAWA** *(Nara Women's Univ.)* **and Ayori MITSUTAKE** *(Nara Women's Univ.)*

Proteins are the most complicated molecules that exist in nature. Since protein structures are closely related to their biological functions, the prediction of their three-dimensional stuructures from the first principles (by minimizing their energy functions) is not only very challenging but also very important a problem in theoretical molecular science. To be more specific, it is widely believed that three-dimensional structures of proteins are determined by their amino-acid sequences. However, nobody has succeeded in predicting it solely from the amino-acid-sequence information (prediction from the first principles). This is because there exist huge number of local minima in the energy function, and conventional simulation techniques will necessarily get trapped in one of the local minima without ever finding the energy global minimum. Multicanonical algorithms are new Monte Carlo algorithms that are known in other research fields (such as a spinglass problem in condensed matter physics) to alleviate this difficulty. We proposed to apply this method to the protein folding problem (U.H.E. Hansmann and Y. Okamoto, *J. Comp. Chem.* **14**, 1333 (1993)). The goal of the present project is to further test the effectiveness of the multicanonical algorithms in the protein folding problem and to succeed eventually in the prediction of tertiary structures of proteins from the first principles.

Quantum Mechanical and Semiclassical Studies of Chemical Reaction Dynamics

Kengo MORIBAYASHI, Miyabi HIYAMA *(Graduate Univ. for Advanced Studies)*, **Chaoyuan ZHU and Hiroki NAKAMURA**

A computer code for accurate evaluations of triatomic chemical reactions has been completed based on the hyperspherical coordinate approach. The code has been successfully applied to the O (^{3}P) + HCl → OH + Cl reaction; and we could evaluate the cross sections and the rate constants accurately. In addition to that we could clarify the reaction mechanisms and effects of potential energy surface topography. A general procedure has been developed to investigate characteristics and dynamics of superexcited states of diatomic molecules. This includes a restriced CI calculation of the first kind of superexcited states, an SCF calculation of the second kind of superexcited states, evaluation of electronic coupling matrix element as a function of the internuclear distance and electron energy, and a nonperturbative solution of the K-matrix integral equation. The procedure is now applied to CO. A symmetrical two-dimensional conical intersection problem has been analyzed semiclassical theoretically as well as numerically. Mechanisms of the nonadiabatic transition by conical intersection has been clarified.

Multi-State Quantum Fokker-Planck Approach to Nonlinear Optical Spectroscopy of Displaced Morse Oscillators System

Yoshitaka TANIMURA

A rigorous procedure for calculating the dynamics of optical transitions in condensed phases and their monitor-

ing by femtosecond pump-probe spectroscopy is developed using Multi-state quantum Fokker-Planck equation proposed by Tanimura and Mukamel. Calculations for displaced Morse potential system with various damping rates are presented. Nuclear wavepackets in phase space related to electronic coherence are shown to provide an insight into the mechanism of nonadiabatic transitions. This method can be used to study effects of laser interactions on chemical reactions in the condensed phase.

Dynamics and Design of Chemical Reactions in Liquid Water

Masaki SASAI *(Nagoya Univ. and IMS)*

A new lattice model of liquid water and water solutions is developed. The hydrogen bond network is represented by the Ising variables with the method similar to the one used in combinatorial problems in random graph. Dynamical peoperties of the network are investigated by using the coupled-map-dynamics method. Solvation and its dynamical effects to chemical reactions are studied with this new lattice model.

Ultrafast Chemical Reactions in Condensed Phase

Keitaro YOSHIHARA, Keisuke TOMINAGA, Shigeichi KUMAZAKI, Yukito NAITOH, Valey F. KAMALOV, Isamu IKEGAMI *(Teikyo Univ.)*, **Shigeru ITOH** *(NIBB)*, **Masayo IWAKI** *(NIBB)*, **Hisanobu OGOSHI** *(Kyoto Univ.)*, **Takashi HAYASHI** *(Kyoto Univ.)* **and Steve R. MEECH** *(Univ. of East Anglia and IMS)*

Recent developments of ultrafast solid state laser, especially Ti:sapphire laser and its amplifier, have enabled us to get stable pulses with high energy and short durations (< 100 fs) at high repetition rates (1 - 5 kHz) in the broad wavelength region (200 - 1000 nm). With these new light sources, chemical reactions in condensed phases of a broad range, for example from photodissociation of small molecules to energy transfer in proteins, are now subjects of research. Followings are the experiments we are performing.

1) Development of UV-pump and UV-probe transient absorption spectrometer and its application to the photodissociation of small molecules such as CH_2I_2 or CHBrI in condensed phase.
2) Energy and electron transfers in photosynthetic reaction center.
3) Photoinduced electron transfer in the intermolecular hydrogen-bonded porphyrine-Zn complexes.
4) Exciton dynamics of J-aggregates.

Laser Investigation of Photodissociation and Bimolecular Reactions

Toshinori SUZUKI, Kenichi TONOKURA, Nobuaki YONEKURA, Yuxiang MO, Lizla S. BONTUYAN, Hideki KATAYANAGI, Nobuhisa HASHIMOTO *(Graduate Univ. for Advanced Studies)* **and Takeshi SHIBATA** *(Graduate Univ. for Advanced Studies)*

Lasers provide the most sensitive detection methods of atoms and molecules with the capability of examing their scaler (e.g. energy) and vector (e.g. linear and angular momenta) quantities. By coupling laser spectroscopy and two/three dimensional imaging methods, multiply differential cross sections of photodissociation and of inelastic and reactive scattering can be measured. Our effort has been directed to construct an imaging apparatus and to develop theoretical method to extract stereochemical aspect of reactions from 2D and 3D data. The experimental and theoretical methods have been tested in studies on photodissociation, and their application to crossed molecular beams is in preparation. Another extention of our study is the experiment using femto second laser. The preliminary experiment has been performed with a femto second Ti:Spphire laser with regenerative amplifier system at the instrument center of IMS.

In Situ Observation of Silicon Hydrides on Si(100) Surfaces during Synchrotron-Radiation-Stimulated Si_2H_6 Gas Source Molecular Beam Epitaxy

A. YOSHIGOE, K. MASE, Y. TSUSAKA, Y. KOBAYASHI*, T. OGINO* *(*NTT Basic Research Laboratories)* **and T. URISU**

Silicon hydrides (SiH_n) on the Si(100) surface during synchrotron-radiation (SR)- stimulated Si_2H_6 gas source molecular beam epitaxy has been observed *in situ* at low temperatures (≤ 400°C), by means of infrared reflection absorption spectroscopy using $CoSi_2$ buried metal layer substrates. At high temperatures (400°C and 370°C), SiH is a dominant surface species, while with temperature decrease from 275°C to 50°C, the number of SiH decreases, on the other hand, SiH_2 and SiH_3 appear and increase. This result explains the change of RHEED pattern from 2×1 to 1×1. The SiH in the bulk network has not been observed. SR irradiation on the film at 140 °C after deposition shows that SiH_2 and SiH_3 are easily decomposed to SiH, and that SiH decomposes much more slowly than SiH_2 and SiH_3 (Figure 1).

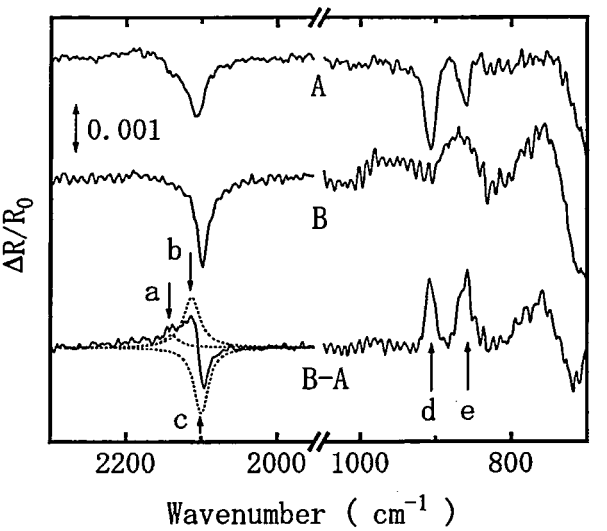

Figure 1. Changes of the IRAS spectra due to SR irradiation at 140°C. A) The spectrum just after the deposition at 140°C under 1.0×10^{-3} Torr of Si_2H_6 gas and by a deposition dose of 3115 mA·min. B) After SR irradiation of 11090 mA·min without

Si_2H_6 on the sample A. B-A) The difference spectrum between B and A. Results of the curve resolution analysis assuming three peaks with Lorentzian form for SiH_3, SiH_2,and SiH stretching vibrations are shown by broken lines. The peaks indicated by arrows are assigned as (a) SiH_3, 2140 cm^{-1}, (b) SiH_2, 2113 cm^{-1}, (c) SiH, 2100 cm^{-1}, (d) SiH_2, 908 cm^{-1} and (e) SiH_3, 860 cm^{-1}.

New Apparatus for Studying Reaction Dynamics of Inner Core Excited Molecules

Toshio IBUKI, Atsunari HIRAYA, Jun-ichi ADACHI and Eiji ISHIGURO *(Ryukyu Univ.)*

A constant-deviation constant-length spherical grating monochormator (CDCL-SGM) has been newly constructed on the BL8B1 beamline of the UVSOR facility. The available photon energy is 200-800 eV, in which the core 1s photoabsorption of C, N, O, and F atoms lie. The resolution of the CDCL-SGM is $E/\Delta E$ = 4000 at 400 eV, which enables us to resolve the vibrational structures of the core excitation. Apparatus for studying reaction dynamics of the inner core excited organic molecules is under construction for the BL8B1 beamline. This apparatus has the following characteristics: In order to get the angle-resolved data of the fragment ion produced, the reaction chamber is designed to be rotatable at the angles from -10 to 100° with respect to the direction of the linear polarization of synchrotron radiation. A reflectron type time-of-flight (TOF) mass analyzer is installed. In general, the photofragment ions produced after inner core excitation have a considerable kinetic energy distribution which makes the mass resolution poor in the linear TOF mass spectrometer. Mass resolution of the present reflectron TOF spectrometer is estimated to be $M/\Delta M \geq 100$. From the standpoint of chemical reaction dynamics the fragment ions such as CO^+ and CHO^+ have different dynamical information and hence the ions with the difference $\Delta M/e$=1 should be separated. Study of reaction dynamics depending on the vibrational levels in the core excitation may be available. The reaction chamber has the extra ports to install analyzers such as electron analyzer and a quadruple mass spectrometer in the near future.

Multi-Purpose Testing Equipment in Ultra-High-Vacuum

Toshio HORIGOME, Shuji ASAKA and Michio WATANABE

Actuators that can operate in ultra-high-vacuum are useful for experimental apparatus in many fields of molecular science such as surface analysis or VUV spectroscopy. In order to evaluate and to develop various types of such actuators, we have newly designed a testing equipment in ultra-high-vacuum. The present equipment will be able to test not only actuators but also general mechanical parts with sizes up to tens of centimeters.

The design of the testing equipment is shown in Figure 1, and its construction is now under way.

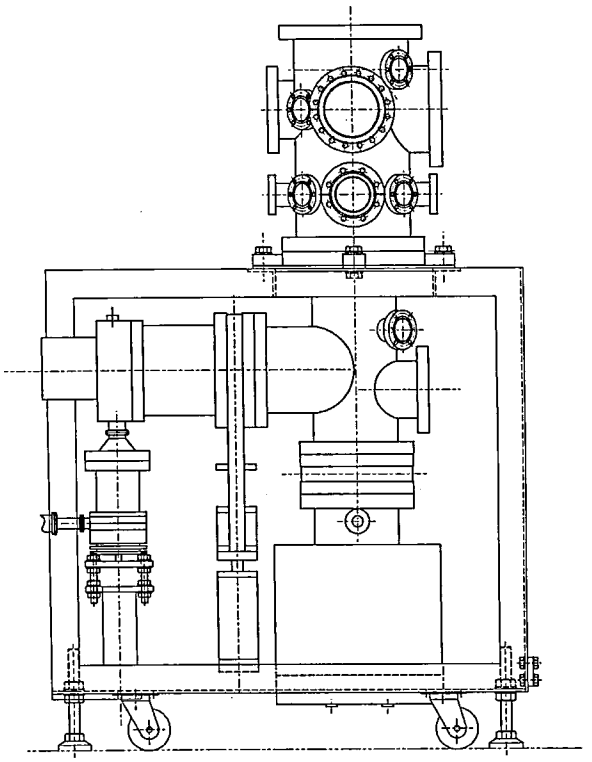

Figure 1. Outline design of the multi-purpose testing equipment in ultra-high-vacuum

Study for High Brilliant Radiation Using the UVSOR Electron Storage Ring

Hiroyuki HAMA, Shiro TAKANO *(SPring-8)*, **Jun-ichiro YAMAZAKI and Toshio KINOSHITA**

Cross section size of the electron beam on the storage ring expresses important features of the radiation source such as the beam emittance and the energy spread. The beam emittance, which is an important factor for the brilliance of radiation, has never been measured on the UVSOR storage ring so far. To progress performance of the light source, the measurement system for the electron beam size at one of the bending magnets of the UVSOR storage ring has been developed by using optical transform elements and a digital camera. Variation of the cross section profile of the beam induced by momentum coupling rate due to the excitation of the skew quadrupoles has been clearly observed by the system.

Our current goal of the beam size measurement is determination of the beam emittance. Calibration of magnification for the profile image and measurements of the lattice function of the ring to deduce absolute value of the emittance are also under way.

(5)Study of Molecular Solid Toward Molecular Electronics

Search for Negative-*U* Materials in Molecular Solid

Kyuya YAKUSHI, Jian DONG, Mikio URUICHI and Yoshiro YAMASHITA

The negative-U material comprises the molecule which has a negative on-site Coulomb energy or, in other words, an attractive force between two electrons within the molecule. A strong electron-phonon interaction is the characteristics of organic conductors, so in some molecules, a strong interaction may overcome the repulsive force within the molecule and stabilize a on-site bipolaron state. The similar state has been found in the insulating compound, Cs_2SbCl_6, superconducting compound, $BaPb_{1-x}Bi_xO_3$, and conducting polymer, polypyrrole, but never been in a organic charge-transfer compound. To look for such molecules, multi-step-oxidation properties of electron donors are one of the key parameters. Generally, the difference (ΔE) between the first and second oxidation potentials is thought to be a measure of the on-site Coulomb energy in the organic conductor. BDNT shows an unusual property that the first and second oxidation potentials are not resolved. From the analysis of the width of the oxidation wave, ΔE is estimated to be 0.024 eV. Due to the extreme closeness of the first and second oxidation potentials, a stable monocationic salt (BDNT-PF_6) and dicationic (BDNT-$(PF_6)_2$) salt are isolated. However, the monoclinic form of BDNT-PF_6 was characterized that this charge-transfer salt was not the negative-U compound but an conventional charge-transfer salt. (*See IV-B-1, 2, 3, and 4*) We are still looking for negative-U compounds by applying high pressure, changing counter anions, or changing donor molecules.

Toward Comprehensive Understanding of Various Electronic Phases in Molecular Conductors; Control of Metal-Insulator Transition

Kazushi KANODA, Yasuhiro NAKAZAWA, Kazuya MIYAGAWA, Ko-ichi HIRAKI, Hiromi TANIGUCHI and Atsushi KAWAMOTO *(Ochanomizu Univ.)*

Various kinds of electronic phases have been uncovered in several types of organic conductors. In the κ-phase family of BEDT-TTF charge transfer complexes, insulating, superconducting and metallic phases appear, depending on anion. The DCNQI metal complexes, $(DCNQI)_2M$ [M=Cu, Li, Ag etc.], also show a variety of conducting and magnetic properties. Among them, metal-insulator transition is in the center of the problems. We have so far investigated the electronic states for several key materials in these two families. As for the κ-phase family of BEDT-TTF compounds, the salts taken for investigation were κ-$(BEDT\text{-}TTF)_2X$ [X=$Cu(NCS)_2$ and $Cu[N(CN)_2]Br$] as metals (or superconductors) and κ-$(BEDT\text{-}TTF)_2Cu[N(CN)_2]Cl$ as an insulator. The ^{13}C and ^1H NMR study suggests that the metal-insulator transition in the κ-phase family can be viewed as the Mott transition. On the other hand, $(DMe\text{-}DCNQI)_2M$ [M=Li or Ag] are known to be quasi-one-dimensional non-magnetic Peierls insulators. Our recent study revealed that $(DI\text{-}DCNQI)_2M$ [M=Li and Ag] are antiferromagnetic insulators, very probably one-dimensional Mott insulator. As is well known, the isostructural Cu salts are metals for both molecules. In order to get a comprehensive understanding of these metal-insulator transitions, it is a promising way to introduce a parameter to control the system between the two extreme phases. In this project, we try to find such a parameter and then examine the electronic states as a function of the parameter for the two family of compounds. For κ-$(BEDT\text{-}TTF)_2X$ system, we found that the deuterated $Cu[N(CN)_2]Br$ salt (d_8-Br salt) is situated on the border of the metal-insulator transition. Now, we have the h_8-Br salt for a metallic phase, the d_8-Br salt for the "border" and the Cl salt for an insulating phase. Therefore, alloying of the (d_8, h_8)-Br salts can control the system in the metallic side precisely, while the alloying of h_8-(Br,Cl) salts may be a method to control the system across the border of the metal-insulator transition. What is going on by the alloying is considered to be a slight variation in the electronic bandwidth and on-dimer Coulomb energy while the band filling remains unchanged (half-filling). The susceptibility measurements of a series of compounds suggest that the content of the alloy can be a good parameter although inhomogeneity is introduced in the system. For $(DCNQI)_2M$ system, we consider (Li, Zn) alloy system and (Li, Cu) alloy system. The starting materials for both cases are Li salts, namely Peierls or Mott insulators. In the former case, carrier concentration or band filling can be varied in the one-dimensional electronic system, while in the latter case the dimensionality of the electronic structure as well as the band filling can be controlled through hybridization of the DCNQI π-orbital and the Cu 3d orbital. The conductivity and magnetic susceptibility were found to vary systematically against the Zn or Cu concentration. The NMR examination of the homogeneity, which is crucial in this kind of research, is underway.

The Electronic Structure and Energy Level Alignment of Porphyrin/Metal Interfaces Studied by Ultraviolet Photoelectron Spectroscopy

Hisao ISHII, Daisuke YOSHIMURA*, Satoru NARIOKA*, Masaki SEI*, Takafumi MIYAZAKI*, Yukio OUCHI*, Shinji HASEGAWA, Yutaka HARIMA, Kazuo YAMASHITA** and Kazuhiko SEKI*** *(*Nagoya Univ., **Hiroshima Univ.)*

[*Appl. Phys. Lett.*, **67**, 1899 (1995)]

Recently the applications of various organic semiconductors to electric devices have been extensively studied. The electronic structure of organic compound/metal interface is indispensable for understanding and refining the performance of organic devices. However there have been few studies even about the details of band lineup at organic / metal interface and this basic problem for organic devices is not yet well understood. In this study, we investigated the electronic structure of interfaces between 5,10,15,20-tetraphenylporphynatozinc (ZnTPP) and four metals (Mg, Al, Ag, and Au) by ultraviolet photoelectron spectroscopy (UPS). The energy levels of ZnTPP relative to the Fermi level of substrate metals could be expressed as linear functions of the work function of metals with the shift of the vacuum level at interface (Δ). The slope of the linear functions was about unity. This indicates that the energy levels of ZnTPP are fixed to the vacuum level of substrate metal with constant interfacial dipole. 5,10,15,20-Tetra(4-pyridyl)porphyrin ($H_2T(4\text{-}Py)P$)/metal and 5,10,15,20-tetra-phenylporphyrin (H_2TPP)/metal interfaces were also investigated, and similar linearity was observed between the energy levels of porphyrin and the

work function of metal with the slope of much smaller than unity. This deviation of the slope from unity might be explained by the existence of interface state. For a deeper insight into the mechanism of energy level alignment, it is important to clarify the origin of the interfacial dipole based on the interaction between metal and the porphyrin layer. Investigation of monolayer porphyrins / Cu(001) systems using UPS and X-ray photoelectron spectroscopy to clarify this point is now underway.

OKAZAKI CONFERENCES

The Fiftieth Okazaki Conference

Functions of Electron Deficient Transition Metal Complexes
(August 1-3)

Organizers: K.TATSUMI *(Nagoya Univ.)* **and T.TAKAHASHI** *(IMS)*
Invited Overseas Speakers: S.GAMBAROTTA *(Univ. of Ottawa, Canada)*, **W. J. EVANS** *(Univ. of California, Irvine, U.S.A.)*, **E. NEGISHI** *(Purdue Univ., U.S.A.)* **G. ERKER** *(Wilhelm Univ., Germany)*, **T. D. TILLEY** *(Univ. of California, San Diego, U.S.A.)* **and R. F. JORDAN**, *(Iowa Univ., U.S.A.)*

Electron deficient transition metal complexes are metal complexes containing early transition metals, lanthanide and metal cation species. Recently these complexes are very attractive, since they have quite different reactivities and functions from those of late transition metal complexes.

The conference was organized to discuss on the following subjects (1) Kaminsky catalysis (2) Metathesis reaction (3) Catalytic asymmetric induction (4) Relation between reactivity and structure (5) Metal complexes with unusual electron state (6) Selective carbon-carbon bond formation.

The conference consisted of 21 overseas speakers and 13 Japanese speakers and was attended by 82 scientists including 19 scientists of IMS. Noteworthy was that about 30 foreign scientists attended this conference. Panel discussion and Poster session were organized in the evening and until 9 o'clock after dinner, respectively. The outside temperature in Okazaki was more than 40°C in the afternoon during the conference.

The Fifty-First Okazaki Conference

Dynamics of Photo-Induced Processes at Surfaces
(October 5-7, 1994)

Organizers: Y. MURATA *(Univ. of Tokyo)* **and Y. YAMAMURA** *(IMS)*
Invited Overseas Speakers: E. Hasselbrink *(Fritz-Harber-Institute der Max-Planck Gesellschaft, Germany)*, **H. -J. Freund** *(Ruhr-Universität Bochum Germany)*, **J. W. Gadzuk** *(National Institute of Standards and Technology, U.S.A.)*, **R. R. Cavanagh** *(National Institute of Standards and Technology, U.S.A.)* **and D. R. Jennison** *(Sandia National Laboratories, U.S.A.)*

Although photo-induced processes at solid surfaces play important roles in the application are still lacking. There are variety of photo-induced processes: photo-stimulates desorption, photodissociation, photoreactions, rearrangements, etching, etc. The aim of the Conference is to share most recent result on the photo-induced processes at well-defined surfaces and to discuss fundamental issues in this new field.

A unique feature of the Conference is that the scientific fields of the participants were quite diverse. There include theoretical and experimental solid state physics, quantum chemistry, laser spectroscopy, surface science, catalysis, and microelectronics. This is primarily due to the fact that the field of photo-induced processes is really interdisciplinary and there are mutual interests between theories and experiments, and between fundamental science and applied science.

One of the most important issues in the Conference was to clarify excitation mechanisms in the photo-induced processes. Two different excitation mechanisms were discussed: direct electronic excitation of adsorbate-substrate complexes and indirect excitation via substrate photon absorption. Some mechanistic models were proposed from the experimental side and the models were discussed in terms of extensive first principle calculations of electronic states of adsorbates. It was remarkable to see that various experimental techniques have been applied to elucidate nuclei dynamics following the electronic excitation. Energetics of desorbed species has been probed by time-of-flight measurements and resonance-enhanced multiphoton ionization even with spatial resolution. Some of nonlinear spectroscopy in the ultrafast time domain has been also proven to be very useful to probe dynamics of adsorbates. These new techniques will enhance our fundamental understandings of photo-induced processes and dynamics.

The Fifty-Second Okazaki Conference

Laboratory and Astronomical Submillimeter-Wave Spectroscopy: Present Status and Future Trends
(March 14-16,1995)

Organizers: S. Saito *(IMS)* **and S. Yamamoto** *(Univ. of Tokyo)*
Invited Overseas Speakers: J. M. Brown *(Oxford Univ., U. K.)*, **K. M. Evenson** *(National Institute of Standards and Technology, U.S.A.)* **M. Guelin** *(Istitut de Radio Astronomie Millimetrique, France)*, **P. T. Ho** *(Harvard-Smithonian Center for Astrophysics, U.S.A.)*, **T. G. Phillips** *(California Institute for Technology, U.S.A.)*, **G. J. White** *(Univ., of London, U.K.)* **and G. Winnewisser** *(Univ., zu Koln, Germany)*

Spectroscopy in the submillimeter-wave to far infrared region has been relatively slowly developed, because radiation sources of high quality for spectroscopy have not been available until recent years. Now in the laboratory the microwave spectroscopic method has been developed into the submillimeter-wave region, and new and pioneering laser-spectroscopic methods have been introduced in the far infrared region, and in the field of astronomy several submillimeter-wave to far infrared telescopes have been developed to study astrophysics and astrochemistry of warm regions of interstellar molecular clouds through atomic and molecular lines. The conference was organized for discussions of new techniques of laboratory and astronomical spectroscopy in the boundary region between radio wave and infrared. Seven invited scientists and sixteen domestic researchers gave stimulating lectures on their recent activities for laboratory spectroscopy of astronomical atomic and molecular species, new techniques of laboratory far-infrared spectroscopy, astronomical observations with submillimeter-wave telescopes and their physical and chemical significances, and several new projects for submillimeter-wave telescopes and arrays. The discussions during sessions and between sessions were very fruitful in exchange of various new information on related boundary fields.

JOINT STUDIES PROGRAMS

As one of the important functions of an inter-university research institution, IMS undertakes joint studies programs for which funds are available to cover research expenses as well as travel and living expenses of individuals. The proposals from domestic scientists are reviewed and controlled by inter-university commitee. The programs are carried out under one of five categories:

1) Joint Studies on special projects (a special project of significant relevance to the advancement of molecular science can be carried out by a team of several groups of scientists).
2) Research Symposia (on timely topics in collaboration with both outside and IMS scientists).
3) Cooperative Research (carried out in collaboration with both outside and IMS scientists).
4) Use of Facility (the Computer Center, Instrument Center and other research facilities at IMS are open to all researchers throughout the country).
5) Joint studies programs using UVSOR facilities.
   a) Special Project, b) Cooperative Research, c) Use of UVSOR Facility.
   In the fiscal year 1994, numbers of joint studies programs accepted amounted to 2,8,128 and 269 for categories 1) - 4), respectively 2, 23 and 136 for 5a) - 5c), respectively.

1) Special Projects

Synthesis and Catalysis of Oxide Clusters

Contributors: **Koji TANAKA, Kiyoshi ISOBE**(*Osaka City Univ.*), **Masaaki ABE, Masaru ICHIKAWA** (*Hokkaido Univ.*), **Takafumi SIDO** (*Hokkaido Univ.*) **and Yusuke IZUMI** (*Nagoya Univ.*)

This research project aims at synthesis of new types of oxide clusters that have active sites for chemical reactions, and at development of unique catalytic reactions for hydrocarbon transformation by using newly prepared oxide clusters

(1) Synthesis and Reactivity of Organometallic Oxide Clusters: Dynamic Behavior of a Newly Prepared Organometallic Vanadium Oxide Cluster

Polyoxoanion-supported organometallic compounds are of particular interest in view of novel and versatile solid state structures and reactivities as well as of structural relevance to metal oxide surfaces which function as catalysts. Dynamic behavior of organometallic groups has been clarified to play a vital role on surface reactions. However, detailed mechanistic and kinetic studies have been limited to date. We have found that a series of vanadium oxide-supported organometallic compounds are fluxional in solution, and thus they may serve molecular models to elucidate dynamics of organometallic fragments on surfaces. In this project, we have found dynamic properties of a new family of vanadium oxide-supported cyclooctadienerhodium(I) complexes, $[(RhCOD)_2(V_4O_{12})]^{2-}$ (**1**) and $[(RhCOD)(V_4O_{12})]^{3-}$ (**2**) (COD = η^4-1,5-cyclooctadiene), by using variable-temperature NMR methods. Temperature-dependence of ^{17}O NMR as well as ^{51}V and ^{103}Rh NMR spectra have led us to propose that a fluxional process observed in **1** and **2** is due to intramolecular rearrangements of RhCOD fragment(s) on the vanadium oxide surface (Scheme 1).

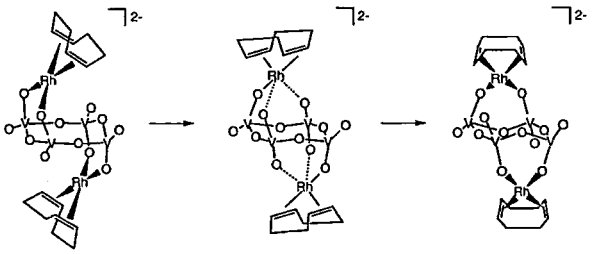

Scheme 1

(2) Molecular Modeling of Suppoted Metal Catalysts; SiO_2-Grafted $[\{\eta^3\text{-}C_4H_7)_2Rh\}_2V_4O_{12}]$ Catalytically Active in Selective Olefin Hydroformylation and Propene Oxidation Towards Acetone

A novel organometallic oxide cluster of $[\{\eta^3\text{-}C_4H_7)_2Rh\}_2V_4O_{12}]$ was grafted on SiO_2 as molecular modeling of supported metal catalysts. The attached multi-centered metal oxide cluster was well-characterized by EXAFS, FTIR, Raman and TPD studies, showing the "vanadate tetramer" oxide cluster framework capped by the Rh group, keeping remained under the surface grafting with silanol-Rh interaction. The $Rh_2V_4O_{12}/SiO_2$ exhibited higher activities and selectivities in ethene hydroformylation to C_2H_5CHO and propene oxidation towards acetone at 300-423 K. By contrast, a negligible and small activity was observed on non-Rh capped vanadate dodecamer and conventional V_2O_5/SiO_2, suggesting the coordinatively unsaturated Rh sites capped with vanadate oxide cluster frameworks are associated with the selective catalysis for olefin hydroformylation via the intermediate formation $Rh(CO)_2V_4O_{12}/SiO_2$. Propene oxidation to give acetone is catalyzed by the Rh site. The vanadate cluster moiety interacts with olefins to promote O_2 oxidation in high selectivities (Scheme 2).

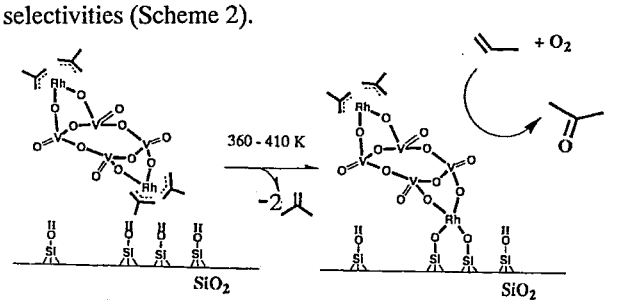

Scheme 2

Advanced Research of Carbon Clusters

Contributors: **Yusei MARUYAMA** *(Housei Univ.)*, **Kyuya YAKUSHI, Tadaoki MITANI** *(JAIST)*, **Yoshihiro IWASA** *(JAIST)*, **Hirotsugu ACHIBA** *(Tokyo Metropolitan Univ.)*, **Tatsuhisa KATO, Hidetoshi FUKUYAMA** *(Univ. of Tokyo)*, **Hirohito SUEMATSU** *(Univ. of Tokyo)*, **Toshiyasu SUZUKI** *(NEC)*, **Seiichi MIYAJIMA and Keiichirou NASU** *(KEK)*

The aim of this research project is to built a new aspect of research of carbon clusters so called a family of fullarene.

(1) Cage size dependence of electronic parameters in higher fullerenes

Systematic study on electronic structures of higher fullerenes C_N (N =60, 70, 76, 78, 82, 84, 86)were made by means of cyclic voltammetry, optical absorption, and photo-ionization. The ionization potential decreases as the cage size (number of carbon atoms, N) increases. This trend is in accord with a simple expectation that the higher fullerenes are extrapolated to graphite. The effective Coulomb interaction between two electrons on molecules also decreases with N indicating that electrons are delocalized on molecules with increase of N. The gap between the highest occupied molecular orbital (HOMO) and the lowest unoccupied molecular orbital (LUMO) rapidly decreases with increasing N . Small deviations from the above mentioned general trend are observed for specific fullerenes, indicating that the electronic structures are affected not only by the cage size but also by the cage shape, reflecting the individuality of each molecule.

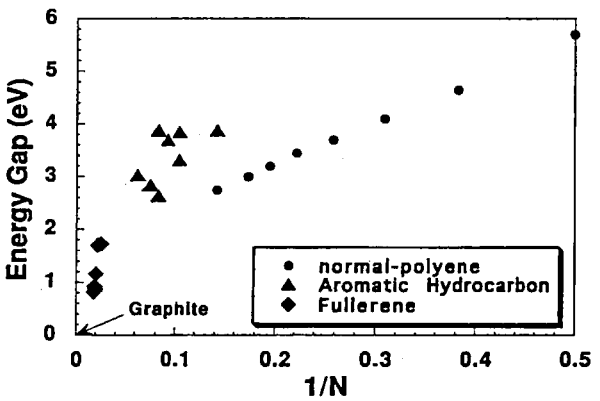

Figure 1. Plot of the HOMO-LUMO gap in normal polyenes, aromatics hydrocarbons and fullerenes versus the reciprocal of the number of carbon atoms, 1/N. Each group shows characteristic behaviour against 1/N.

(2) Magnetic and Electrical Behaviors of C60(TDAE) Single Crystal

Significant size of single crystals of C_{60}(TDAE), where TDAE is tetrakis(Dimethylamino)ethylene, have been prepared from a toluene solution for the first time by a diffusion method. The resulting conglomerate of black colored needles is found to consist of single crystals by X-ray diffraction analysis. A resistivity of 1.1 x10^5 Ωcm at room temperature and an activation energy of 0.4~ 0.8 eV suggest that an obtained C_{60}(TDAE) crystal is not metallic but semiconducting. The crystal do not show a ferromagnetic behavior but Pauli and Curie-Weiss paramagnetism with a negative Weiss constant, θ =-0.44 K. It was found that the difference in the magnetic properties between crystal and powder samples may originate from the change of the lattice constants.

(3) Metal-insulator transition in ammoniated K_3C_{60}

Ammoniated K_3C_{60}, $NH_3K_3C_{60}$, does not superconduct against the empirical rule that T_c of fullerene superconductors is controlled by the lattice dimensions. We found that the superconductivity of this compound is suppressed by the metal-insulator transition at 40K. This transition was confirmed by ESR, magnetic susceptibility and NMR measurements. This transition suppresses the superconductivity that is expected to occur at around 30K according to the simple empirical relation between T_c and the cell volume in alkali doped C_{60} superconductors. The present finding indicates that an insulating state exists in the phase diagram at the large cell parameter side possibly due to too much band narrowing. This situation is very similar to that for the organic superconductors.

2) Research Symposia

1. Molecular Science by Using linear and circular polarization of synchrotron radiation
   (November 2nd-3rd, 1994)
   Organizer: T. Ohta
2. Toward New Developments of Fine Structure-Function Studies of Oxygen-Binding Proteins
   (December 5th-6th, 1994)
   Organizer: K. Imai
3. Recent Topics of Chemical Physics
   (December 8th-10th, 1994)
   Organizer: Y. Tanimura
4. Dynamics of Molecular Processes at Surfaces
   (February 23th-25th, 1995)
   Organizer: T. Matsushima
5. Symposium on Physical Chemistry for Young Researchers of Molecular Science
   (May 18th, 1995)
   Organizer: Y. Aoki
6. π-d Hybrid Systems in Organic Solids and Their Novel Properties
   (June 9th-11th, 1995)
   Organizer: M. Yamashita
7. Vacuum Ultra Violet Photon Processing
   (August 2nd-3rd, 1995)
   Organizer: M. Azusa
8. Theoretical Molecular Science for Experimentalists and Experimental Molecular Science for Theorists
   (September 26th, 1995)
   Organizer: Y. Tanimura

3) Cooperative Research

This is the most important programs IMS undertakes for conducting its own research of the common interest to both outside and IMS scientists by using the facilities at IMS. During the first half of fiscal year of 1994 ending on September 30, 63 outside scientists; and during the second half of the fiscal year, 65 outside scientists, the names and affiliations of those collaborators are found in the

Research Activities.

4) Use of Facilities

The numbers of projects accepted for the Use of Facility Program of the Computer Center during the fiscal year of 1994 amounted to 222 (740 users) and the computer time spent for these projects is 19393 hours (converted to the HITAC M-680H time), and amounted to 70% of the total annual CPU time used. Projects (92 users)were accepted for the Use of Facility Program of the Instrument Center during the fiscal year of 1994.

5) UVSOR

In the UVSOR Facility with the 750 MeV electron storage ring, there are nineteen beam lines available for synchrotron radiation research (see "UVSOR ACTIVITY REPORT 1995"). The Experimental Facility of each beam line is discribed in the introductory pamphlet "OUTLINE OF UVSOR". The Japanese and English versions are available through the UVSOR Facility. Under the following programs, a number of SR studies have been carried out by many users outside and inside IMS: a) the UVSOR Special Projects, b) the UVSOR Cooperative Research Projects, c) the UVSOR Invited Research Projects, and d) the Use-of-UVSOR Projects.

5-a) UVSOR Special Project

Development of the Spin-Resolved Photoelectron Spectrometer System

Masao KAMADA, Kusuo SAKAI, Shin-ichi KIMURA, Kazutoshi FUKUI, Nobuo MIZUTANI, Toshio HORIGOME, Masami HASUMOTO, Sayumi HIROSE, Naoshi TAKAHASHI, Shin-ichiro TANAKA, Hiroyuki HAMA, Yasuo FUJII,* Eiji ISHIGURO, Kouichi ICHIKAWA,*** Kazuo SODA****, Kazumichi NAKAGAWA,*****Shigeo OHARA****** and Hideo KITAMURA********* *(*Osaka City Univ., **Ryukyus Univ., ***Univ. of Osaka Pref., ****Nagoya Univ., *****Kobe Univ., ******Nagoya Institute Tech., *******Riken)*

The "complete" experiment, where the energy, the momentum, and the spin polarization of photoelectrons can be observed, has been a long desire for scientists in the world. The purpose of the present project is to construct the spin-resolved photoelectron spectrometer system, which consists of a helical undulator, a monochromator, and a spin-resolved spectrometer. And thus this project needs lots of efforts to be completed. The spin detector has been installed on the back of the angle-resolved electron energy analyser last year. The parameters of electron lens system were carefully determined by using photoelectrons excited with a He-lamp. The new monochromator, which is called as SGM-TRAIN, is just under construction this summer. High precise machining was required to achieve the high-resolution. It is not so easy to allign the optical elements and the mechanical components within inaccuracy of micro-meter range. The design of helical undulator has been finished and now the detailed discussion on the drive mechanics and the controll system is in progress. The UVSOR will have a 9-weeks shut-down next spring to install the helical undulator into the storage ring.

Extension of Spectroscopic System at the Beam Line 6A1 to a Wide Wavelength Region

Takao NANBA*, Makoto SAKURAI*, Kazuhide OKAMURA*, Michihiro KOBAYASHI, Yasuhiko KONDOH***, Masao KAMADA, Kyuya YAKUSHI and Tsuneo URISU** *(*Kobe Univ., **Osaka Univ., ***Tohoku Univ.)*

In order to improve the spectroscopic system at the BL6A1, so as to cover a very wide energy region from a millimeter wave (3mm) to a near infrared region (1μm), a second interferometer, Bruker IFS66v, was successfully installed in addition to a Martin Puplett interferometer in the far-infrared region. A part of the available spectral distribution curve measured by the second interferometer with the UVSOR is shown in the figure in comparison with that by a globar lamp. With a beam aperture of a diameter of 0.5 mm, UVSOR gives a comparible intensity with a globar lamp even in the middle infrared region.

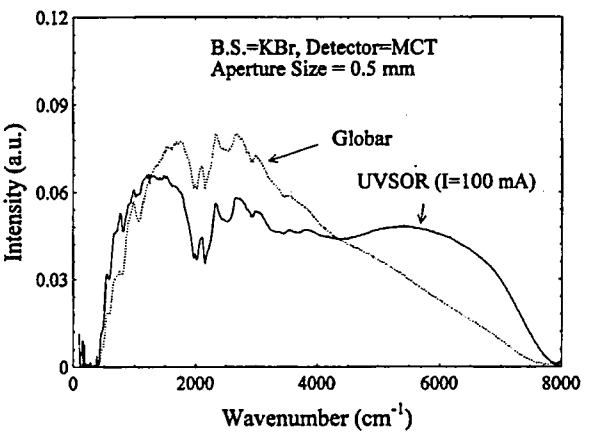

Figure 1. Spectral distribution curve of UVSOR which was measured by a middle infrared interferometer. Spectrum which passes through an aperture with 0.5 mm diameter at the focal position in the sample chamber was measured by an MCT detector. Dashed curve was obtained by a globar lamp in the same condition with that by UVSOR.

5-b) UVSOR Cooperative Research Projects

Under this joint-study program, many synchrotron radiation experiments have been carried out with the beam lines of in-house staff in cooperation with scientists who were invited from other institutions. The total number of the projects in this category was 23 in the fiscal year of 1994.

5-c) The UVSOR Invited Research Projects

Under this joint-study program, several scientists were invited from other institutions of help for construction of new beam lines and improvement of the UVSOR storage ring and others. The total number of the projects in this category was 4 in the fiscal year of 1994.

5-d) The Use-of-UVSOR Projects

Ten out of the total of nineteen UVSOR beam lines

are available for general users outside and inside IMS for their synchrotron radiation studies in the field of molecular science. The total number of the projects in this category was 132 in the fiscal year of 1994.

FOREIGN SCHOLARS

Visitors from abroad play an important role in research activities and always welcome at IMS. The following is the list of foreign scientist who visited IMS in the past year (Aug. 1994 - Jul. 1995). The sign *[1] indicates an attendant to an Okazaki Conference, *[2] an IMS or Japan Society for the Promotion of Science Invited Foreign Scholar, *[3] an IMS councillor, *[4] an IMS visiting scientst, and *[5] an IMS adjunct professor or associate professor from abroad (period of stay from 9 to 12 months). Scientists who wish to visit IMS under program *[2] and *[5] are invited to make contact with an IMS faculty in a related field.

Dr. A. Lesar	Jozef Stefan Inst., Univ.of Ljubljana	(Slovenia)	Aug. 1994
Dr. B. Vallone	Univ. of Rome "La Spienza"	(Italy)	Aug. 1994
Dr. J. Mc Combie	Univ. of Nottingham	(U.K.)	Aug. 1994
Prof. R. Naaman	Weitzman Inst. of Sci.	(Israel)	Aug.-Sep. 1994 Mar. 1995
Prof. E. E. Nikitin*[2]	Technion Israel Inst. of Tech.	(Israel)	Aug.-Oct. 1994
Ms. T. I. Igumenova*[4]	Inst. of Catalysis	(Russia)	Aug. 1994- Feb. 1995
Dr. S. R. Gandhi*[2]	Max-Planck-Inst.	(Germany)	Aug. 1994 - May 1995
Ms. M. Joseph	Imperial Coll.	(U.K.)	Sep.-Dec. 1994
Dr. G. Roberts	Univ. of Cambridge	(U.K.)	Sep. 1994
Dr. A. Hodgson	Univ. of Liverpool	(U.K.)	Sep. 1994
Prof. D. Phillips	Imperial Coll.	(U.K.)	Sep. 1994
Dr. C. Whitehead	Univ. of Manchester	(U.K.)	Sep. 1994
Prof. R. Donovan	Univ. of Edinburgh	(U.K.)	Sep. 1994
Prof. Yuan Ji Pei	NSRL USTC	(China)	Sep. 1994
Mr. Shouming Hu	NSRL USTC	(China)	Sep. 1994
Mr. Guirong Huang	NSRL USTC	(China)	Sep. 1994
Dr. Dong-Eon Kim	POSTEC	(Korea)	Sep. 1994
Mr. Dongho Cha	POSTEC	(Korea)	Sep. 1994
Dr. T. Moller	BESSY	(Germany)	Sep. 1994
Dr. Wang Ping *[2]	Univ. of Alabama	(China)	Sep. 1994 - Feb. 1995
Dr. M. E. Kozlov	Inst. of Semiconductor	(Ukraine)	Sep. - Dec. 1994
Dr. J. V. Kröber*[2]	Paris XI Univ.	(Germany)	Sep. 1994-
Prof. J. Elguero*[4]	Inst. de Quimica Medica	(Spain)	Oct. 1994
Prof. G. A. Mourou	Director of the NSF Center on Ultrafast Optical Sci., Univ. of Michigan	(France)	Oct., Dec. 1994
Dr. D. R. Jennison*[1]	Sandia Natl. Lab.	(U.S.A.)	Oct. 1994
Dr. R. R. Cavangh*[1]	Natl. Inst. of Standards & Tech.	(U.S.A.)	Oct. 1994
Dr. E. Hasselbrink*[1]	Fritz-Harber-Inst. der Max-Planck-Gesellshaft	(Germany)	Oct. 1994
Prof. H.- J. Freund*[1]	Ruhr-Univ. Bochum	(Germany)	Oct. 1994
Dr. J. W. Gadzuk*[1]	Natl. Inst. of Standards & Tech.	(U.S.A.)	Oct. 1994
Prof. E. B. Yagubskii	Inst. Chem. Phys.	(Russia)	Oct. 1994
Dr. M.-E. Couprie	LURE	(France)	Oct. 1994
Dr. Chanyong Hwang	Korean Res. Inst.	(Korea)	Oct. - Nov. 1994
Mr. Jong Wan Lee	Korean Res. Inst.	(Korea)	Oct. - Nov. 1994
Mr. Yong Joo Lee	Korean Res. Inst.	(Korea)	Oct. - Nov. 1994
Dr. Zhang Bin *[2]	Inst. of Chem., Acad. Sinica	(China)	Oct. 1994 - Jan. 1995
Dr. Mo Yuxiang*[4]	Wuhan Inst. of Phys.	(China)	Oct. 1994 - Mar. 1995
Dr. A. A. Zakhidov*[2]	Uzbek Acad. Sci.	(Uzbekistan)	Oct. 1994 - Mar. 1995
Dr. Yasng Cao	Univ. of California Santa Babara	(U.S.A.)	Nov. 1994
Mr. Koo Ja Yong	Korean Res. Inst.	(Korea)	Nov. 1994
Mr. Choi Yi Sang	Korean Res. Inst.	(Korea)	Nov. 1994
Mr. Han Gil Lee	Korean Res. Inst.	(Korea)	Nov. 1994
Dr. V. G. Stankevitch	Kurchatov Inst.	(Russia)	Nov. - Dec. 1994
Dr. A. A. Kolmakov	Kurchatov Inst.	(Russia)	Nov. - Dec. 1994
Dr. Åke Andersson	MAX-Lab. Univ. of Lunf	(Sweden)	Nov. - Dec. 1994
Dr. Jangseok Ma*[4]	Univ. of Texas	(Korea)	Nov. 1994 -
Prof. F. O. Goodman*[5]	Univ. of Waterloo	(Canada)	Nov. 1994 -
Dr. B. Singaram*[2]	Univ. of Calofornia, Santa Cruz	(India)	Dec. 1994 - Mar. 1995
Prof.Hee Kwon Chae*[2]	Hankuk Univ. of Foreign Studies	(Korea)	Dec. 1994 - Feb. 1995
Prof. M. Maroncelli	Pennsylvania State Univ.	(U.S.A.)	Dec. 1994
Dr. R. Zadoyan	Univ. of California, Irvine	(U.S.A.)	Dec. 1994
Prof. V. Agranovich	Inst. of Spectroscopy	(Russia)	Dec. 1994

Prof. R. Fischer*[5]	Friedrich-Schiller Univ. Jena	(Germany)	Dec. 1994 -
Prof. P. Day*[3]	Royal Inst.	(U.K.)	Jan., Jul. 1995
Prof. Bongsoo Kim	Kyungpook Natl. Univ.	(Korea)	Jan. - Feb. 1995
Ms. Hyun Suk Jeong	Kyungpook Natl. Univ.	(Korea)	Jan. - Feb. 1995
Dr. Hong Lae Kim	Kangweon Natl. Univ.	(Korea)	Jan. - Feb. 1995
Dr. Jae M. Seo	Jeonbuk Univ.	(Korea)	Jan. - Feb. 1995
Dr. Sehun Kim	KAIST	(Korea)	Jan. - Feb. 1995
Mr. Young Su Chung	KAIST	(Korea)	Jan. - Feb. 1995
Mr. Yukwon Kim	KAIST	(Korea)	Jan. - Feb. 1995
Mr. Han Gil Lee	KAIST	(Korea)	Jan. - Feb. 1995
Dr. Kwang-Pill Lee	Kyngpook Natl. Univ.	(Korea)	Jan. - Mar. 1995
Prof. Ming Chang Lin*[5]	Emory Univ.	(Taiwan)	Jan.1995 -
Dr. Yong Qiang Cai*[4]	The Flinders Univ. of South Australia	(Australia)	Jan. 1995 -
Prof. R. R. Aliev	Inst. of Tech. & Experimental Biophys. of Russian Acad. of Sci.	(Russia)	Feb. 1995
Ms. L. S. Smoliar	Univ. of California, Berkeley	(U.S.A.)	Feb. 1995
Prof. Fanao Kong	Inst. of Chem., Acad. Sinica	(China)	Feb. 1995
Prof. S. H. Lin	Inst. of Acad. & Mol. Sci., Acad. Sinica Taiwan	(Taiwan)	Feb. 1995
Prof. G. Kulipanov	Novosibirsk Inst. of Nucl. Phys.	(Russia)	Feb. 1995
Dr. D. Craig	Imperial Coll.	(U.K.)	Feb. - Mar. 1995
Prof. E. Frankevich*[2]	Russian Acad. of Sci.	(Russia)	Feb. - Mar. 1995
Prof. V. Ivanov*[5] *[2]	Russian Acad. of Sci., Kurnakov Inst.	(Russia)	- Mar. 1995
Prof. J. Dyke	Univ. of Southampton	(U.K.)	Mar. 1995
Prof. H. Frei	Univ. of California, Berkely	(U.S.A.)	Mar. 1995
Prof. J. M. Brown*[1]	Oxford Univ.	(U.K.)	Mar. 1995
Dr. K. M. Evenson*[1]	NIST	(U.S.A.)	Mar. 1995
Dr. M. Guélin*[1]	IRAM	(France)	Mar. 1995
Dr. P.T.P. Ho*[1]	Harvard-Smithsonian Center for Astrophys.	(U.S.A.)	Mar. 1995
Prof. T. G. Phillips*[1]	Cal. Inst. Tech.	(U.S.A.)	Mar. 1995
Prof. G. J. White*[1]	Univ. of London	(U.K.)	Mar. 1995
Prof. G. Winnewissen*[1]	Univ. of Cologne	(Germany)	Mar. 1995
Prof. T. Luty	Tech. Univ. of Wroclaw	(Poland)	Mar. 1995
Prof. J. C. Polanyi	Univ. of Toronto	(Canada)	Mar. - Apr. 1995
Prof. Seung C. Park*[2]	Sung Kyun Kwan Univ.	(Korea)	Mar. - Apr. 1995
Dr. P. D. Landrè*[2]	Inst. for Res. on Catalysis, CNRS	(France)	Mar. 1995 -
Dr. E. Slobodchikov	Chem. Phys. Inst.	(Russia)	Apr. - Jul. 1995
Prof. V. Zadkov	Inst. Laser Center, Moscow State Univ.	(Russia)	Apr. 1995
Dr. L. S. Bontuyan*[2]	Cornell Univ.	(U.S.A.)	- May 1995
Prof. R. Coalson	Univ. of Pittsburg	(U.S.A.)	May 1995
Prof. A. W. Kleyn	FOM-Inst. for Atom. & Mol. Phys.	(Netherlands)	May 1995
Prof. Chang-guo Zhan	Central China Normal Univ.	(China)	May 1995 -
Dr. Jong Keun Park*[4]	Pohang Univ. of Sci. & Tech.	(Korea)	May 1995 -
Dr. Li Yumin*[2]	Shanghai Inst. of Materia Medica Acad. Sinica	(China)	May 1995 -
Dr. T. Radnai*[4]	CRIC, Hung. Acad. of Sci.	(Hungary)	May. 1995 -
Dr. Huo Shou-Quan*[4]	Shanghai Inst. of Org. Chem.	(China)	May 1995 -
Mr. S. H. S. Wilson	Univ. of Bristol	(U.K.)	Jun. 1995
Dr. J. Frey	Univ. of Southampton	(U.K.)	Jun. 1995
Prof. F. F. Crim	Univ. of Wisconsin	(U.S.A.)	Jun. 1995
Dr. A. Rizzo	CNR, Risa	(Italy)	Jun. 1995
Dr. M. Eichholtz	Univ. of Gottingen	(Germany)	Jun. 1995
Dr. D. V. Stucken	Univ. of Gottingen	(Germany)	Jun. 1995
Dr. Jinwook Chung	Pohang Inst. of Sci. & Tech.	(Korea)	Jun. 1995
Prof. T. C. Steimle	Arizona State Univ.	(U.S.A.)	Jun. 1995
Prof. Duck Hwan Lee*[2]	Songang Univ.	(Korea)	Jun. 1995 -
Dr. A. H. Saleck*[2]	Univ. of Cologne	(Germany)	- Jun. 1995
Prof. Dae Young Kim*[4]	Hallym Univ., Coll. of Natural Sci.	(Korea)	Jul. 1995
Dr. A. Kung	Inst. of Atom. & Mol. Sci., Acad. Sinica	(U.S.A.)	Jul. 1995
Prof. K. A. Nelson	Massachusetts Inst. of Tech.	(U.S.A.)	Jul. 1995

Prof. B. Schrader	Univ. of Essen	(Germany)	Jul. 1995
Prof. T. Yonetani	Univ. of Pennsylvania	(U.S.A.)	Jul. 1995
Dr. A. K. Mishra	Indian Inst. of Tech.	(India)	Jul. 1995
Prof. Xu Xin	Xiamen Univ.	(China)	Jul. 1995
Prof. M. Okamura	Univ. of California, San Diego	(U.S.A.)	Jul. 1995
Prof. N. Schwentner	Freie Univ. Berlin	(Germany)	Jul. 1995
Dr. M. Kurmoo	Oxford Univ.	(U.K.)	Jul. 1995
Dr. A. K. Bakshi	Panjab Univ.	(India)	Jul. 1995
Dr. I. Ahmad*[2]	Univ. of London	(U.K.)	Jul. 1995 -
Mr. M. P. Leese	Univ. of Nottingham	(U.K.)	Jul. 1995 -
Prof. Yong Kwang	Kangwon Natl. Univ.	(Korea)	Jul. 1995 -

AWARDS

The Cultural Achievements of Professor Inokuchi

Professor Hiroo Inokuchi, the former Director-General of IMS (1987-1993), was honored as a Person of Cultural Merit by the Government for his contributions to culture through his achievements in molecular science. Person of Cultural Merit is the most distinguished title that can be awarded to scientists and artists in Japan. Among his important research achievements, the followings are the most widely recognized: the creation of the field of organic semiconductor that was expanded to the discovery of organic metal and organic superconductor, and the studies of organic molecules by the photoelectron spectroscopy that gave a guiding principle for the design of organic semiconductor device.

Associate Professor Hosono's Scientific Achievements

Associate Professor Hideo Hosono of the department of vacuum UV photoscience received the 1994 W.H.Zachariasen Award (sponsored by the Journal of Non-Crystalline Solids) for his contribution to "Elucidation of Ion-implantation Effects in Amorphous SiO_2 and Creation of Nanometer-sized Colloid Particles Embedded in Glass by Implantation". This international award is made every 2 years for a scientist younger than forty-one years old, who made an outstanding contribution in the field of amorphous materials. He approached the chemical interaction of implanted ions with substrate structure of amorphous SiO_2 through elucidation of structural defects created during implantation and established a criterion to predict the nanosized colloid formation implanted SiO_2, illustrating novel materials with a large third-order nonlinear optical susceptibility.

Mr. Sakai's Technical Achievements

Mr. Kusuo Sakai, the technical section chief, received the Chemical Society of Japan Award for Technical Achievements in 1994 for his contribution to "Design and Fabrication of Spectrometer for Molecular Science Utilizing Synchrotron Radiation" . The synchrotron radiation facility of IMS (UVSOR) has been operational as a chemical machine since 1983. Mr. Sakai contributed to the construction and the design of many instruments including the beam pipes of the storage ring from the beginning stage. Especially, his contribution to the design and fabrication of monochromators was excellent and is still now great. The details are as follows.

1. He designed the unique exchange mechanism of the gratings for Seya-Namioka type monochromators which were installed on beam line 1B and 7B. His precise mechanism provided the reliable wavelength and stable intensities in the vacuum ultraviolet region.
2. The glancing-incident monochromators which were installed on beam lines 3A2 and 8B1 were well designed by him. Many scientists and engineers have been attempting to make various kinds of glancing-incident monochromators in the extreme ultraviolet region, but few success. This means that the design and fabrication of the monochromators in this energy region are so difficult and need lots of efforts. The monochromator designed by Mr. Sakai is a so-called constant-length and constant-deviation monochromator, and it is now recognized as one of the best monochromators in the world.
3. He also designed the simple and precise mechanism for double-crystal monochromator on beam lines 1A and 7A. His mechanism made it possible to rotate and translate the monochromator crystals in the vacuum, providing high-quality photons in soft x-ray region. The performance of the double-crystal monochromator is well known worldwide and thus he was invited to Hefei synchrotron radiation facility in China two years ago.

Dr. Mizutani's Scientific Achievements

Inoue Research Award for Young Scientists in 1995 was given to Dr. Yasuhisa Mizutani, who is a research associate in the Molecular Dynamics Laboratory. This award is given to young scientists (under 35 years old) who obtained remarkable results during their Ph. D. work in the fields of basic science, engineering, medicine, pharmacy and agriculture. Dr. Mizutani was awarded this prize for his Ph. D. thesis, "Resonance Raman Studies on Chromoproteins and Their Model Compounds".

LIST OF PUBLICATIONS

Y. SONODA and S. IWATA, "Theoretical Studies of the Internal Rotation of the Methyl Group in o-, m- and p-Fluorotoluenes and their Cation", *Chem. Phys. Letters* **243**, 176 (1995).

M. KAWATA, S. TEN-NO, S. KATO and F. HIRATA, "Irregular Order in Basicities of Methylamines in Aqueous Solution: A RISM-SCF Study", *J. Am. Chem. Soc.* **117**, 1638 (1995).

M. KAWATA, S. TEN-NO, S. KATO and F. HIRATA, "The Solvent Effect on the Acidities of Haloacetic Acids in Aqueous Solution. A RISM-SCF Study", *Chem. Phys. Letters* **240**, 199 (1995).

A. NAKAJIMA, K. NAKAO, M. GOMEI, R. KISHI, S. IWATA and K. KAYA, "Electronic Properties of Silicon - M Binary Clusters (M = C and Na)", *Mat. Res. Soc. Sym. Proc.* **358**, 61 (1995).

S. TEN-NO and S. IWATA, "Three-center Expansion of Electronic Repulsion Integrals with Linear Combination of Atomic Electron Distribution", *Chem. Phys. Letters* **240**, 578 (1995).

H. WATANABE, S. IWATA, K. HASHIMOTO, F. MISAIZU and K. FUKE, "Molecular Orbital Studies of the Structures and Reactions of Singly Charged Magnesium Ion with Water Clusters, $Mg^+(H_2O)_n$", *J. Am. Chem. Soc.* **117**, 755 (1995).

M. SANEKATA, F. MISAIZU, K. FUKE, S. IWATA and K. HASHIMOTO, "Reactions of Singly Charged Alkaline-Earth Metal Ions with Water Clusters: Characteristic Size Distribution of Product Ions", *J. Am. Chem. Soc.* **117**, 747 (1995).

A. NAKAJIMA, T. TAGUWA, K. NAKAO, K. HOSHINO, S. IWATA and K. KAYA, "Photoelectron Spectroscopy of Al_nS^- Clusters (n=1 - 9)", *J. Chem. Phys.* **102**, 660 (1995).

C.-G. ZHAN and S. IWATA, "Ab Initio Studies on the Structures and Vertical Electron Detachment Energies of Copper-Water Negative Ion Clusters $Cu^-(H_2O)_n$ and $CuOH^-(H_2O)_{n-1}$", *Chem. Phys. Letts.* **232**, 72 (1995).

T. IKEGAMI and S. IWATA, "Theoretical Studies on the Non-adiabatic Photodissociation Process of Argon Cluster Ions Ar_7^+", *Int. J. Quantum. Chem. Symp.* **28**, 529(1994).

T. KOBAYASHI, H. MATSUZAWA and S. IWATA, "Theoretical Studies of Ammonia-halogen and Methylamine-halogen Complexes: Geometries, Harmonic Vibrational Frequencies and their Infra-red Intensities and Excited States of Ammonia-Chlorine Monofluoride Complex", *Bull. Chem. Soc. Jpn.* **67**, 3172 (1994).

S. NANBU, M. GOMYO and S. IWATA, "Potential Energy Surfaces of Some Low-Lying States of Fluoroformyl Radical FCO", *Chem. Phys.* **184**, 97 (1994).

Y. OKAMOTO and U. H. E. HANSMANN, " Thermodynamics of Helix-Coil Transitions Studied by Multicanonical Algorithms ", *J. Phys. Chem.* **99**, 11276 (1995).

Y. SHIMIZU and A. SHUDO, "Polygonal Billiards: Correspondence between Classical and Trajectories and Quantum Eigenstates", *Chaos, Solitons and Fractals* **5**, 1337 (1995).

A. SHUDO and K. S. IKEDA, "Complex Classical Trajectories and Chaotic Tunneling", *Phys. Rev. Lett.* **74**, 682 (1995).

T. HARAYAMA, A. SHUDO and Y. SHIMIZU, "Semiclassical Quantization and Periodic Orbits of Dispersing Billiards", *Prog. Theor. Phys. Suppl.* **116**, 259 (1994).

Y. SHIMIZU and A. SHUDO, "Statistical Properties of Eigenfunctions for Quantum Billiards with and without Positive Lyapunov Exponent", *Prog. Theor. Phys. Suppl.* **116**, 267 (1994).

A. SHUDO and K. IKEDA, "Toward the Classical Understandings of Quantum Chaological Phenomena: Dynamical Localization and Chaotic Tunneling", *Prog. Theor. Phys. Suppl.* **116**, 283(1994).

A. SHUDO, Y. SHIMIZU, P. ŠEBA, J. STEIN, H.-J. STÖCKMANN and K. ZYKZKOWSKI, "Statistical Properties of Spectra of Pseudointegrable System", *Phys. Rev. E***49** , 3748 (1994).

A. SHUDO, "Level Statistics and Semiclassical Periodic-orbit expansion for Polygonal Billiards", *Adv. of Dynamical Systems* **14**, 71 (1994).

S. TAKADA and H. NAKAMURA, "WKB Theory of Tunneling between Tori", *Prog. Theor. Phys. Suppl.* **116**, 295 (1994).

K. SOMEDA, H. NAKAMURA and F. H. MIES, "Overlapping-Resonance Scattering and Statistical Theory of Unimolecular Decomposition", *Prog. Theor. Phys. Suppl.* **116**, 443 (1994).

K. SOMEDA, H. NAKAMURA and F. H. MIES, "Systematics of the Average Resonance Widths in Overlapping Resonance-scattering and Its Connection with the RRKM Theory", *Chem. Phys.* **187**, 195 (1994).

C. ZHU and H. NAKAMURA, "The Two-State Linear Curve Crossing Problems Revisited:IV. The Best Analytical Formulas for Scattering Matrices", *J. Chem. Phys.* **101**, 4855 (1994).

K. SOMEDA and H. NAKAMURA, "Decoupling Surface Analysis of $Cl+Cl_2$ Reaction Embedded in Al_{52} Cluster", *Bull. Chem. Soc. Japan.* **67**, 2659 (1994).

C. ZHU and H. NAKAMURA, "Theory of Nonadiabatic Transition for General Two-State Curve Crossing Problems. I. Nonadiabatic Tunneling Case", *J. Chem. Phys.* **101**, 10630 (1994).

K. TSUDA, K. MORIBAYASHI and H. NAKAMURA, "Quantum Dynamics of the $Mu+H_2$ and $Mu + D_2$ Reactions", *Chem. Phys. Lett.* **231**, 439 (1994).

K. SOMEDA, H. NAKAMURA and F. H. MIES, "Competition between Intermolecular Vibrational Energy Redistribution and Unimolecular Dissociation: A Scattering Theoretical Point of View", *Laser Chemistry* **15**, 145 (1995).

S. TAKADA and H. NAKAMURA, "Effects of Vibrational Excitation on Multidimensional Tunneling: General Study and Proton Tunneling in Tropolone", *J. Chem. Phys.* **102**, 3977 (1995).

C. ZHU and H. NAKAMURA, "Theory of Nonadiabatic Transition for General Two-State Curve Crossing Problems. II. Landau-Zener Case", *J. Chem. Phys.* **102**, 7448 (1995).
Y. TANIMURA and S. MUKAMEL, "Femtosecond Pump-Probe Spectroscopy of Intermolecular Vibrations in Molecular Dimers," *J. Chem. Phys. (communications)* **103**, 1981 (1995).
K. OKUMURA, "A Systematic Analysis of the Ferromagnetism in the Itinerant Electron Model", *J. Magn. Magn. Mater.* **140-141**, 191 (1995).
N. TOMITA, A. IKAWA and H. FUKUTOME, "The SDW-CDW Phase Transition in the One Dimensional Extended Hubbard Model", *Synth. Met.* **69**, 679 (1995).
M. GOTO, S. TAKANO, S. YAMAMOTO, H. ITO and S. SAITO, "Microwave Spectra of the AlO($X\ ^2\Sigma^+$) Radical in the v=1 and 2 States", *Chem. Phys. Lett.* **227**, 287 (1994).
M. IZUHA, S. YAMAMOTO and S. SAITO, "Microwave Spectrum and Molecular Structure of Silacyclopropenylidene c-C_2H_2Si", *Can. J. Phys.* **72**, 1206 (1994).
S. K. LEE, H. OZEKI and S. SAITO, "Microwave Spectrum of the NS Radical in the $^2\Pi_r$ Ground Electronic State", *Astrophys. J. Suppl.* **98**, 351 (1995).
J. TANG and S. SAITO, "Microwave Spectrum of the C_3S Molecule in the Vibrationally Excited States of Bending Modes, ν_4 and ν_5", *J. Mol. Spectrosc.* **169**, 92 (1995).
R. S. HAYANO, F. E. MAAS, H. A. TORII, N. MORITA, M. KUMAKURA, T. YAMAZAKI, H. MASUDA, I. SUGAI, F. J. HARTMANN, H. DANIEL, T. von EGIDY, B. KETZER, W. MÜLER, W. SCHUMID, D. HORVATH, J. EADES and E. WIDMANN, "Laser Studies of the Decay Chain of Metastable Antiprotonic Helium Atoms", *Phys. Rev. Lett.* **73**, 1485 (1994).
E. WIDMANN, I. SUGAI, T. YAMAZAKI, R. S. HAYANO, M. IWASAKI, S. N. NAKAMURA, H. TAMURA, T. M. ITO, A. KAWACHI, N. NISHIDA, W. HIGEMOTO, Y. ITO, N. MORITA, F. J. HARTMANN, H. DANIEL, T. von EGIDY, W. SCHMID, J. HOFFMANN and J. EADES, "Phase and Density Dependence of the Delayed Annihilation of Metastable Antiprotonic Helium Atoms in Gas, Liquid and Solid Helium", *Phys. Rev. A* **51**, 2870 (1995).
F. E. MAAS, R. S. HAYANO, T. ISHIKAWA, H. TAMURA, H. A. TORII, N. MORITA, T. YAMAZAKI, I. SUGAI, K. NAKAYOSHI, F. J. HARTMANN, H. DANIEL, T. von EGIDY, B. KETZER, A. NIESTROJ, S. SCHMID, W. SCHMID, D. HORVATH, J. EADES and E. WIDMANN, "A New Laser Induced Resonant Transition at 470.724 nm in the $v = n - l - 1 = 2$ Cascade of Metastable Antiprotonic Helium Atoms", *Phys. Rev. A* **52**, 1287 (1995).
A. FUJII and N. MORITA, "Three-Color Triple Resonance Spectroscopy of Highly Excited *ng* Rydberg States of NO: Decay Dynamics of High-*l* Rydberg States", *J. Chem. Phys.* **88**, 2158 (1995).
N. KITAJIMA, N. TAMURA, H. AMAGAI, H. FUKUI, Y. MORO-OKA, Y. MIZUTANI, T. KITAGAWA, R. METHUR, K. HEERWEGH, C. A. REED, C. R. RANDALL, J. L. QUE and K. TATSUMI, "Monomeric Carboxylate Ferrous Complexes as Models for the Dioxygen Binding Sites in Non-Heme Iron Proteins. The Reversible Formation and Characterization of μ-peroxo Diferric Complexes", *J. Am. Chem. Soc.* **116**, 9071 (1994).
S. NAKASHIMA and T. KITAGAWA, "Recombination Intermediates of Photodissociated CO Myoglobin at Ambient Temperatures Detected by Time-resolved Resonance Raman Spectroscopy", *J. Am. Chem. Soc.* **116**, 10318 (1994).
D. A. PROSHLYAKOV, T. OGURA, K. SHINZAWA-ITOH, S. YOSHIKAWA, E. H. APPELMAN and T. KITAGAWA, "Selective Resonance Raman Observation of the "607 nm" form Generated in the Reaction of Oxidized Cytochrome *c* Oxidase with Hydrogen Peroxide", *J. Biol. Chem.* **269**, 29385 (1994).
S. HIROTA, T. OGURA, E. H. APPELMAN, K. SHINZAWA-ITOH, S. YOSHIKAWA and T. KITAGAWA, "Observation of a New Oxygen-Isotope-Sensitive Raman Band for Oxyhemoproteins and its Implications in Heme Pocket Structures", *J. Am. Chem. Soc.* **116**, 10564 (1994).
P. JEWSBURY and T. KITAGAWA, "The Distal Redidue-CO Interaction in Carbonmonoxy Myoglobins: a Molecular Dynamics Study of Two Distal Histidine Tautomers", *Biophys. J.* **67**, 2236 (1994).
M. SATO-WATANABE, T. MOGI, T. OGURA, T. KITAGAWA, H. MIYOSHI, H. IWAMURA and Y. ANRAKU, "Indentification of Novel Quinone-Binding Site in the Cytochrome *bo* Complex from *Escherichia Coli*", *J. Biol. Chem.* **269**, 28908 (1994).
K. ISOBE, Y. OZAWA, A. VAZQUEZ DE MIGUEL, T.-W. ZHU, K.-M. ZHAO, T. NISHIOKA, T. OGURA and T. KITAGAWA, "$[\{Rh_2Cp^*(\mu\text{-}Ch_2)_2\}_2(m\text{-}S_4)]^{2+}$: A Novel Tetranuclear Cationic Complex with a Rectangular S_4 Unit", *Angew. Chem. Int. Ed. Engl.* **33**, 1882 (1994).
M. TSUBAKI, T. MOGI, H. HORI, S. HIROTA, T. OGURA, T. KITAGAWA and Y. ANRAKU, "Molecular Structure of Redox Metal Centers of the Cytochrome *bo* Complex from *Escherichia coli* : Spectroscopic Characterizations of the Subunit I Histidine Mutant Oxidases", *J. Biol. Chem.* **269**, 30861 (1994).
P. JEWSBURY, S. YAMAMOTO, T. MINATO, M. SAITO and T. KITAGAWA, "The Proximal Residue Largely Determines the CO Orientation in Carbonmonoxy Globin Proteins. An *ab initio* Study of a Haem Prosthetic Unit", *J. Am. Chem. Soc.* **116**, 11586 (1994).
Y. SHIRO, T. IIZUKA, K. MARUBAYASHI, T. OGURA, T. KITAGAWA, S. BALASUBRAMANIAN and S. G. BOXER, "Spectroscopic Study of Ser92 Mutants of Human Myoglobin: Hydrogen Bonding Effect of Ser92 to Proximal His93 on Structure and Property of Myoglobin", *Biochemistry* **33**, 14986 (1994).
S. HIROTA, T. OGURA and T. KITAGAWA, "Observation of Nonfundamental Fe=O_2 and Fe-CO Vibrations and Potential Anharmonicities for Oxy- and Carbonmonoxy-Hemoglobin; Evidence Supporting a New Assignment of the Fe-C-O Bending Fundamental", *J. Am. Chem. Soc.* **117**, 821 (1995).
M. NAGAI, S. KAMINAKA, Y. OHBA, Y. NAGAI, Y. MIZUTANI and T. KITAGAWA, "Ultraviolet resonance Raman Studies of Quaternary Structure of Hemoglobin Using a Tryptophan β37 Mutant", *J. Biol. Chem.* **270**, 1636

(1995).
S. KAMINAKA and T. KITAGAWA, "A Novel Spinning Cell System for UVRR Measurements of Powder- and Small Volume Solution Samples in Back-Scattering Geometry: Application to Solid Tryptophan and Mutant Hemoglobin Solution", *Appl. Spectrosc.* **49**, 685 (1995).
S. SATO, K. AOYAGI, T. HAYA and T. KITAGAWA, "Time-Resolved Resonance Raman Study of Free-Base Octaethyl Porphyrins in the S_0, S_1 and T_1 states", *J. Phys. Chem.* **99**, 7766 (1995).
T. KODAMA, T. KATO, T. MORIWAKI, H. SHIROMARU and Y. ACHIBA,"Laser Study on the Resonance-Enhanced Multiphoton Electron Detachment (REMPED) Processes for C_{60}^- and C_{70}^-", *J. Phys. Chem.* **98**, 10671 (1994).
T. KATO, S. BANDOW, M. INAKUMA and H. SHINOHARA, "ESR Study on Structures and Dynamics of $Sc_3@C_{82}$", *J. Phys. Chem.* **99**, 856 (1995).
T. AKASAKA, T. KATO, K. KOBAYASHI, S. NAGASE, K. YAMAMOTO, H. FUNASAKA and T. TAKAHASHI, "Exohedral Derivatives of $La@C_{82}$", *Nature*, **374**, 600 (1995).
T. AKASAKA, S. NAGASE, K. KOBAYASHI, T. SUZUKI, T. KATO, K. YAMAMOTO, H. FUNASAKA and T. TAKAHASHI, "Exohedral Derivatization of an Endohedral Metallofullerene $Gd@C_{82}$", *J. Chem. Soc., Chem. Commun.* 1343 (1995).
V. F. KAMALOV, I. A. STRUGANOVA, Y. KOYAMA and K. YOSHIHARA, "Two-Exciton Emission of BIC J-Aggregates", *Chem. Phys. Lett.* **226**, 132 (1994).
R. HOWELL, D. PHILLIPS, H. PETEK and K. YOSHIHARA, "Fluorescence of Jet-Cooled Dimethylamino Benzonitrile, Its Aggregates and Solvated Complexes", *Chem. Phys.* **188**, 303 (1994).
Y. NAGASAWA, A. P. YARTSEV, K. TOMINAGA, A. E. JOHNSON and K. YOSHIHARA, "Temperature Dependence of Ultrafast Intermolecular Electron Transfer Faster than Solvation Process", *J. Chem. Phys.* **101**, 5717 (1994).
S. KUMAZAKI, H. KANDORI, H. PETEK, K. YOSHIHARA and I. IKEGAMI, "Primary Photochemical Processes in P700-Enriched Photosystem I Particles: Trap-Limited Excitation Decay and Primary Charge Separation", *J. Phys. Chem.* **98**, 10335 (1994).
S. KUMAZAKI, M. IWAKI, I. IKEGAMI, H. KANDORI, K. YOSHIHARA and S. ITOH, "Rates of Primary Electron Transfer Reactions in the Photosystem I Reaction Reconstructed with Different Quinones as the Secondary Acceptor", *J. Phys. Chem.* **98**, 11220 (1994).
Y. NAGASAWA, A. P. YARTSEV, K. TOMINAGA, P. B. BISHT, A. E. JOHNSON and K. YOSHIHARA, "Dynamical Aspects of Ultrafast Intermolecular Electron Transfer Faster than Solvation Process: Substitutent Effects and Energy Gap Law", *J. Phys. Chem.* **99**, 653 (1995).
K. TOMINAGA and K. YOSHIHARA, "Fifth Order Optical Response of Liquid CS_2 Observed by Ultrafast Non-Resonant Six-Wave Mixing", *Phys. Rev. Lett.* **74**, 3061 (1995).
H. PETEK, A. J. BELL, Y. S. CHOI, K. YOSHIHARA, B. A. TOUNGE and R. L. CHRISTENSEN, "One- and Two-Photon Fluorescence Excitation Spectra of the 2^1Ag States of Linear Tetraene in Free Jet Expansions", *J. Chem. Phys.* **102**, 4726 (1995).
H. PAL, Y. NAGASAWA, K. TOMINAGA, S. KUMAZAKI and K. YOSHIHARA, "Deuterium Isotope Effect on the Solvation Dynamics", *J. Chem. Phys.* **102**, 7758 (1995).
Y. NAGASAWA, A. P. YARTSEV, K. TOMINAGA and K. YOSHIHARA, "Chemical-Substitution and Deuterium Isotope Effects on Ultrafast Intermolecular Electron Transfer: Possible Role of Molecular Vibrations", in *"Ultrafast Phenomena IX"*, P. F. Barbara, W. H. Knox, G. A. Mourou and A. H. Zewail Eds. Springer, p.84 (1994).
K. TOMINAGA, Y. NAITOH, T. J. KANG and K. YOSHIHARA, "Observation of Fifth-Order Optical Response of Liquid CS_2 by Non-Resonant Six-Wave Mixing", in *"Ultrafast Phenomena IX"*, P.F. Barbara, W. H. Knox, G. A. Mourou and A. H. Zewail Eds. Springer, p.143 (1994).
S. KUMAZAKI, M. IWAKI, I. IKEGAMI, H. KANDORI, S. ITO and K. YOSHIHARA, "Primary Electron-Transfer Steps in Photosystem I Reaction Center with Reduced Number of Antenna Chlorophylls (12-30 Chls/P700)", in *"Ultrafast Phenomena IX"*, P. F. Barbara, W. H. Knox, G. A. Mourou and A. H. Zewail Eds. Springer, p.466 (1994).
K. TOMINAGA, R. INABA, T. J. KANG, Y. NAITOH, K. A. NELSON, M. TASUMI and K. YOSHIHARA, "Liquid Dynamics Studied by Ultrafast Raman Echo Technique", in *"XIV International Conference on Raman Spectroscopy"*, N.-T. Yu and X.-Y. Li Eds. John Wiley & Sons, p.444 (1994).
B. KIM and K. YOSHIHARA, "Molecular Resonances Observed in the Predissociation of CS_2 ", *Laser Chem.* **16**, 19 (1995).
K. TOMINAGA, G. P. KEOGH, Y. NAITOH and K. YOSHIHARA, "Temporally Two-Dimensional Raman Spectroscopy of Liquids by Six-Wave Mixing with Ultrashort Pulses", *J. Raman Spect.* **26**, 495 (1995).
P. B. BISHT, H. PETEK, K. YOSHIHARA and U. NAGASHIMA, "Excited State Enol-Keto Tautomerization in Salicylic Acid: A Supersonic Free Jet Study", *J. Chem. Phys.* **103**, 5290 (1995).
J. LEE, H. KATO, K. SAWABE and Y. MATSUMOTO, "Angular Distributions of N_2 in Photodissociation of N_2O Adsorbed on a Partially Oxidized Si(100) Surface at 95K", *Chem. Phys. Lett.* **240**, 417(1995).
K. SAWABE, Y. MATSUMOTO, J. YOSHINOBU and M. KAWAI, "The Reactivity of Molecular and Atomic Oxygen in Oxygen-Exchange Reaction between NO and O_2 Coadsorbed on a Pt(111) Surface", *J. Chem. Phys.* **103**, 4757 (1995).
M. TAKAYANAGI and I. HANAZAKI, "Geometry and Torsional Potential of *2,2'*-Bithiophene in a Supersonic Jet", *J. Phys. Chem.* **98**, 12893 (1994).
G. RÁBAI and I. HANAZAKI, "Light-Induced State Transitions in the Oscillatory ClO_2^--Cl^-- Iodomalonic Acid System in a Semibatch Reactor", *J. Phys. Chem.* **98**, 10550 (1994).

V. K. VANAG, Y. MORI and I. HANAZAKI, "Photoinduced pH Oscillations in the Hydrogen Peroxide-Sulfite-Ferrocyanide System in the Presence of Bromocresol Purple in a Continuous-Flow Stirred Tank Reactor", *J. Phys. Chem.* **98**, 8392 (1994).

J. GORECKI, K. KITAHARA, K. YOSHIKAWA and I. HANAZAKI, "Molecular Dynamics Simulations of Non-equilibrium Spatial Correlations in a Reaction Diffusion System", *Physica A* **211**, 327 (1994).

I. HANAZAKI, H. L. KIM and M. TAKAYANAGI, "Photochemistry of N_2O•H_2O Complexes Produced in Supersonic Jets", *Laser Techniques for State-Selected and State-to-State Chemistry II, SPIE Proceedings* **2124**, 10 (1994).

Y. MORI, G. RÁBAI and I. HANAZAKI, "Photoinduced Bifurcation between Steady and Oscillatory States in the $Fe(CN)_6^{4-}$-H_2O_2 Reaction in a Flow Reactor", *J. Phys. Chem.* **98**, 12968 (1994).

G. RÁBAI and I. HANAZAKI, "Photo-Induced Disproportionation of Iodomalonic Acid", *Intern. J. Chem. Kinetics* **27**, 431 (1995).

I. HANAZAKI, Y. MORI, T. SEKIGUCHI and G. RÁBAI, "Photo-response of Chemical Oscillators", *Physica D* **84**, 228 (1995).

T. KONO, M. TAKAYANAGI and I. HANAZAKI, "The C=O Stretching Frequency in the $S_1(\pi^*$-n) State of Acetaldehyde and its Deuterated Derivatives Ddetermined with the Photofragment Excitation Spectroscopy", *Laser Chem.* **15**, 249 (1995).

G. RÁBAI and I. HANAZAKI, "Oxidation of Thiocyanate by Bromate is not an Oscillatory Rreaction in a Batch Reactor", *J. Phys. Chem.* **99**, 10061 (1995).

V. K. VANAG and I. HANAZAKI, "Frequency Multipying Bifurcations in the Oscillatory Belousov-Zhabotinskii Reaction in Interacting Water Droplets of Reverse Microemulsions of Aerozol OT in Octane", *J. Phys. Chem.* **99**, 6944 (1995).

G. RÁBAI, A. KAMINAGA and I. HANAZAKI, "The Role of the Dushman Reaction and the Ferricyanide Ion in the Oscillatory IO_3^--SO_3^{2-}-$Fe(CN)_6^{4-}$ Reaction", *J. Phys. Chem.* **99**, 9795 (1995).

T. SUZUKI, K. TONOKURA, L. S. BONTUYAN and N. HASHIMOTO, "Photodissociation of *trans*-Dichloroethylene: State-Resolved Speed and Angular Distributions of Cl Atoms", *J. Phys. Chem.* **98**, 13447 (1994).

Y. HORIKI, S. NISHIO, H. SHINOHARA and H. SATO, "Magic-Number-like Behavior of Ammonia Ligands in Mixed-Ligand Metal Complexes $M^+(NH_3)_m(CH_3OH)_n$. Preferred Coodination of Ammonia Ligands in the First Coordination Sphere", *J. Phys. Chem.* **98**, 10436 (1994).

M. TSUNEKAWA, S. NISHIO and H. SATO, "Laser Ablation of Polymethylmethacrylate and Polystyrene at 308 nm: Demonstration of Thermal and Photothermal Mechanisms by a Time-of-Flight Mass Spectroscopic Study", *J. Appl.Phys.* **76**, 5598 (1994).

O. ITO, Y. HORIKI, S. NISHIO, A. MATSUZAKI and H. SATO, "Highly Selective Solvation of Monopositive Metal Ions in the Gas Phase as Revealed by the Laser Ablation-Molecular Beam Method Using Ammonia-Water Binary Clusters", *Chem. Lett.* 9 (1995).

M. TSUNEKAWA, S. NISHIO and H. SATO, "Multiphoton Ionization-Mass Spectrometric Study on Laser Ablation of Polymethylmethacrylate and Polystyrene at 308 nm", *Jpn. J. Appl. Phys.* **34**, 218 (1995).

T. CHUJO, I. SARAOKA, S. KATO, H. SATO, K. FUKUHARA and H. MATSUURA, "Stoichiometry and Conformation of the Azacrown Moiety in Sodium Complexes of Azacrown Ethers. A Raman/IR Spectroscopic Study. Part I: Complexes of 4,13-Diaza-18-Crown-6", *J. Incl. Phenomen. Mol. Recog. Chem.* **20**, 173 (1995).

I. SARAOKA, S. KATO, T. CHUJO, H. SATO, K. FUKUHARA and H. MATSUURA, "Stoichiometry and Conformation of the Azacrown Moiety in Sodium Complexes of Azacrown Ethers. A Raman/IR Spectroscopic Study. Part II: Complexes of 4,13-Diaza-15-Crown-5", *J. Incl. Phenomen. Mol. Recog. Chem.* **20**, 191 (1995).

R. NAKAGAKI, "Comment on Photochemical Reaction of 4-Methyl-2-quinolinecarbonitrile with Optically Active (*S*)- or (*R*)-2-Phenylpropionic Acid. The Magnetic Field and Solvent Effects and Chiral-symmetry Breaking", *Chem. Phys.* **67**, 86 (1994).

R. NAKAGAKI and K. MUTAI, "Magnetic Field Effects on Reaction Yields for Photochemistry Involving Biradical Intermediates", *Magnetic Resonance in Medicine,* ed. H. Kamada, H. Ohya-Nishiguchi and T. Yoshikawa, **6**, 404 (1995).

R. NAKAGAKI, O. TAKAHIRA and K. HIRUTA, "External Magnetic Field and Magnetic Isotope Effects upon Lifetimes of Biradicals Derived from Benzophenone Derivatives", *Chem. Phys. Lett.* **233**, 41 (1995).

K. TSUKAHARA, N. SAWAI, S. HAMADA, T. NAKAZAWA and R. NAKAGAKI, "Kinetics and Mechanisms of Photoinduced Reduction of Methylviologen by N-Alkyltetraphenylporphinatozinc (II) in Methanol", *Bull. Chem. Soc. Jpn.* **68**, 1947 (1995).

I. I. KHAIRULLIN, K. IMAEDA, K. YAKUSHI and H. INOKUCHI, "Superconducting Properties of Na-doped C_{60} Prepared from Sodium Azide", *Physica C* **231**, 26 (1994).

T. ENOKI, K. TSUJIKAWA, K. SUZUKI, A. UCHIDA, Y. OHASHI, H. YAMAKADO, K. YAKUSHI and G. SAITO, "Metal-Semiconductor Transition and Structural Change in $(BEDT\text{-}TTF)_3(ClO_4)_2$", *Phys. Rev. B* **50**, 16287 (1994).

T. ISHII, Y. KOMATSU, K. SUZUKI, T. ENOKI, A. UGAWA, K. YAKUSHI and S. BANDOW, "Electronic Structure and Transport Properties of $AuCl_3$-GIC", *Mol. Cryst. Liq. Cryst.* **245**, 1 (1994).

J. G. LIN, C. Y. HUANG, Y. Y. XUE, C. W. CHU, L. GRIGORYAN and K. YAKUSHI, "High Pressure Study on High-T_c (ZnPc)Bi-2223 Oxides", *Physica C* **231**, 177 (1994).

K. YAKUSHI, I. SHROTANI, I. I. KHAIRULLIN, Y. NAKAZAWA, K. KANODA, N. KOSUGI and S. TAKEDA, "Characterization of Poly-CuPc Sheet Polymers Synthesized under High Pressure", *Synthetic Metals* **71**, 2289 (1995).

T. HIEJIMA and K. YAKUSHI, "Pressure Dependence of the Infrared and Visible Spectra of Metallophthalocyanine

Salts", *Synthetic Metals* **71**, 2305 (1995).

T. HIEJIMA and K. YAKUSHI, "Pressure-Iduced Charge-Transfer in One-Dimensional Phthalocyanine Conductor, $NiPc(AsF_6)_{0.5}$", *Solid State Commun.* **95**, 661 (1995).

A. UGAWA, D. B. TANNER and K. YAKUSHI, "Far-Infrared Reflectance of β"-$(BEDT\text{-}TTF)_2AuBr_2$: Co-Existence of Free Carriers and a Single-Particle Gap at $2\Delta=130\ cm^{-1}$", *Synthetic Metals* **70**, 979 (1995).

K. IMAEDA, I. I. KHAIRULLIN, K. YAKUSHI and H. INOKUCHI, "Magnetic and Structure Characterization of Superconducting Sodium-Doped C_{60} Parepared with the Thermal Decomiposition of Sodium Azide", *Synthetic Metals* **70**, 1375 (1995).

I. I. KHAIRULLIN, K. IMAEDA, K. YAKUSHI and H. INOKUCHI, "Superconducting Properties of Na-doped C_{60} Prepared from Sodium Azide", *Synthetic Metals* **70**, 1369 (1995).

L. GRIGORYAN, K. YAKUSHI and N. CHAKRAVATY, "The 130 K Transition in Bi-Oxides Heavily Doped by Iron Phthalocyanine: Superconductivitiy vs Magnetism", *phys. stat. sol. (b)* **187**, 205 (1995).

Z. J. HUAN, J. G. LIN, J. J. LIN, C. Y. HUANG, L. GRIGORYAN and K. YAKUSHI, "Thermoelectric Power Study on High-T_c Bi-2212 and 2223 Oxides Intercalated with Organic Molecules Zincphthalocyanine", *Physica C* **244**, 305 (1995).

M. E. KOZLOV and K. YAKUSHI, "Optical Properties of High-Pressure Phases of C_{60} Fullerene", *J. Phys.: Condens. Matter* **7**, L209 (1995).

Y. KOBAYASHI, T. NAKAMURA, T. TAKAHASHI, K. KANODA, B.HILTI and J.S.ZAMBOUNIS, "Observation of the Coherence Peak of ^{1}H-NMR Relaxation Rate in the Superconducting State of $(MDT\text{-}TTF)_2AuI_2$", *Synth. Met.* **70**, 871 (1995).

K. MIYAGAWA, H. SATO, A. KAWAMOTO, K. KANODA and T. MORI, "Electronic State of κ-$(BMDT\text{-}TTF)_2Au(CN)_2$ Studied by NMR and Thermoelectric Measurements", *Synth. Met.* **70**, 879 (1995).

H. SATO, H. TANIGUCHI, Y. NAKAZAWA, A. KAWAMOTO, K. KATO and K. KANODA, "Resistive Transition in an Extremely Two-Dimensional Superconductor, α-$(BEDT\text{-}TTF)_2NH_4Hg(SCN)_4$", *Synth. Met.* **70**, 915 (1995).

Y. NAKAZAWA, H. SATO, A. KAWAMOTO, K. KATO and K. KANODA, "Complex Susceptibility and Penetration Depth of BEDT-TTF based Layered Superconductors", *Synth. Met.* **70**, 919 (1995).

Y. NAKAZAWA, H. SATO, A. KAWAMOTO and K. KANODA, "Specific Heat Study of α-$(BEDT\text{-}TTF)_2MHg(SCN)_4$", *Synth. Met.* **70**, 943 (1995).

K. MIYAGAWA, A. KAWAMOTO, Y. NAKAZAWA and K. KANODA, "^{13}C-NMR Study on κ-$(BEDT\text{-}TTF)_2X$", *Synth. Met.* **70**, 969 (1995).

K. KANODA, A. KAWAMOTO, K. MIYAGAWA and Y. NAKAZAWA, "^{13}C-NMR Study on α-$(BEDT\text{-}TTF)_2MHg(SCN)_4$", *Synth. Met.* **70**, 973(1995).

A. KAWAMOTO, K. MIYAGAWA, Y. NAKAZAWA and K. KANODA, "Systematic Study of DCNQI-Cu Salts by NMR at Selective Nuclear Sites", *Synth. Met.* **70**, 1079(1995).

A. KAWAMOTO, K. MIYAGAWA, Y. NAKAZAWA and K. KANODA, "^{13}C NMR Study of Layered Organic Superconductors Based on BEDT-TTF Molecules", *Phys. Rev. Lett.* **74**, 3455(1995).

K. MIYAGAWA, A. KAWAMOTO, Y. NAKAZAWA and K. KANODA, "Antiferromagnetic Ordering and Spin Structure in the Organic Conductor, κ-$(BEDT\text{-}TTF)_2Cu[N(CN)_2]Cl$", *Phys. Rev. Lett.* **75**, 1174(1995).

S. L. FANG, K. KOHAMA, H. HOSHI and Y. MARUYAMA, "Spectral Dependence of the Anisotropy of $\chi^{(3)}$ of Epitaxially Grown Vanadyl Phthalocyanine Film", *Chem. Phys. Lett.* **234**, 343 (1995).

Y. MARUYAMA, H. HOSHI, S. L. FANG and K. KOHAMA, "Nonlinear Optical Characteristics of MBE-Grown Phthalocyanine Thin Films", *Synth. Met.* **71**, 1653 (1995).

Y. OUCHI, K. YAMAMOTO, H. YAMASAKI, Y. SHIONOIRI, H. OGATA and Y. MARUYAMA, "Transport Properties of C_{60} and C_{70} Single Crystals", *Fullerene Sci. & Tech.* **3**, 79 (1995).

A. SUZUKI, T. SUZUKI and Y. MARUYAMA, "Magnetic and Electrical Behaviors of C_{60}(TDAE) Single Crystal", *Solid State Commun.* **96**, 253 (1995).

K. AWAGA, T. OKUNO, A. YAMAGUCHI, M. HASEGAWA, T. INABE, Y. MARUYAMA and N. WADA, "Crystal Structures and Magnetic Properties of (m-pyridinium mitronyl nitrozide)$^+X^-$: Possible Spin-1 Kagome Antiferromagnet", *Synth. Met.* **71**, 1807 (1995).

H. MORI, I. HIRABAYASHI, S. TANAKA, T. MORI and Y. MARUYAMA, "Organic Conductors with Three-Component System Containing Co, Zn and Cd Based upon BEDT-TTF", *Synth. Met.* **70**, 789 (1995).

H. MORI, I. HIRABAYASHI, S. TANAKA, T. MORI and Y. MARUYAMA, "Physical and Chemical Properties of MDS-TTF and EDSe-TTF Solids", *Synth. Met.* **70**, 877 (1995).

H. MORI, I. HIRABAYASHI, S. TANAKA, T. MORI and Y. MARUYAMA, "Preparation, Properties and Structures of Planar Anion Complexes", *Synth. Met.* **70**, 1177 (1995).

H. MORI, S. TANAKA, T. MORI and Y. MARUYAMA, "Crystal Structures and Electrical Resistivities of Three-Component Organic Conductors : $(BEDT\text{-}TTF)_2MM'(SCN)_4$ [M = K, Rb, Cs ; M' = Co, Zn, Cd]", *Bull. Chem. Soc. Jpn.* **68**, 1136 (1995).

H. HOSHI, K. HAMAMOTO, T. YAMADA, K. ISHIKAWA, H. TAKEZOE, A. FUKUDA, S. L. FANG, K. KOHAMA and Y. MARUYAMA, "Thickness Dependence of the Epitaxial Structure of Vanadyl Phthalocyanine Film", *Jpn. J. Appl. Phys.* **33**, L1555 (1994).

S. MIYAJIMA, T. CHIBA, G. SAITO and H. INOKUCHI, "Solid-State High-Resolution ^{13}C NMR Study of the Intermolecular Interaction in Organic Semiconductors $TTC_n\text{-}TTF$", *J. Phys. Chem.* **99**, 1582 (1995).

S. MIYAJIMA, A. NAKAZATO, N. SAKODA and T. CHIBA, "Liquid Crystals of 4-Octyloxy-*N*-

(benzylidene)aniline Derivatives Bearing Trifluoromethyl or Trifluoromethoxy End Groups", *Liq. Cryst.* **18**, 651 (1995).
S. MIYAJIMA and T. HOSOKAWA, "^{1}H and ^{2}H NMR Studies of Dynamic Orientational, Translational and Dipolar Orders in the Doubly Reentrant Liquid Crystal 4-Cyanobenzoyloxy-[4-octylbenzoyloxy]-*p*-phenylene and its Deuterated Analogue", *Phys. Rev. B* **52**, 4060 (1995).
H. GOTO, H. ASAHI, T. INABE, H. OGATA, S. MIYAJIMA and Y. MARUYAMA, "High-Resistance Phase and Low-Resistance Phase in 1,6-Diaminopyrene-*p*-Chloranil (DAP-CHL)", *Synth. Metals* **70**, 1237 (1995).
Y. OCHIAI, K. YAMAMOTO, H. YAMASAKI, Y. SHIONOIRI, H. OGATA and Y. MARUYAMA, "Transport Property of C_{60} and C_{70} Single Crystals", *Fullerene Sci. & Tech.* **3**, 79 (1995).
M. KONO and K. SHOBATAKE, "Photodissociative Excitation Processes of XeF_2 in the Vacuum Ultraviolet Region 105-108nm", *J. Chem. Phys.* **102**, 5966 (1995).
K. KAMIYA, M. MOMOSE, Y. HARADA, N. UENO, T. MIYAZAKI, S. HASEGAWA, H. INOKUCHI and K. SEKI, "Photoelectron Angular Distribution of Thin Films of Copper Phthalocyanine on MoS_2 Surfaces: Quantitative Determination of Molecular Orientation", *Mol. Cryst. Liq. Cryst.* **267**, 211(1995).
K. SEKI, N. UENO and H. INOKUCHI, "UV Photoemission Study of Amorphous *n*-$C_{36}H_{74}$ Films and their Annealing Process", *Chem. Phys.* **182**, 353 (1994).
S. NARIOKA, M. SEI, H. ISHII, S. HASEGAWA, Y. OUCHI, T. OHTA and K. SEKI, "Molecular Orientation and Electronic Structure of Evaporated Porphyrin Films", *Trans. Mat. Res. Soc. Jpn.* **15A**, 631 (1994).
J. TANAKA, C. TANAKA, T. MIYAMAE, M. SHIMIZU, S. HASEGAWA, K. KAMIYA and K. SEKI, "Experimental and Theoretical Basis for Polson Model of Doped Polyacetylene", *Syn. Metals* **65**, 173 (1994).
T. MIYAMAE, T. MORI, K. SEKI and J. TANAKA, "Electrical Transport Properties of Perchlorate-Doped Oriented Polyacetylene", *Bull. Chem. Soc. Jpn.* **68**, 803 (1995).
T. MIYAMAE, T. MORI, K. SEKI and J. TANAKA, "Electrical Conductivity of Perchlorate Doped Polyacetylene", *Syn. Metals* **69**, 59 (1995).
T. MIYAMAE, K. KAMIYA, S. HASEGAWA, K. SEKI, C. TANAKA and J. TANAKA, "Ultraviolet Photoelectron Spectroscopy of Alkaline-Metal Doped Polyacetylene", *Bull. Chem. Soc. Jpn.* **68**, 1897 (1995).
S. HINO, H. TAKAHASHI, K. IWASAKI, T. MIYAZAKI, K. KIKUCHI and Y. ACHIBA, "Ultraviolet Photoelectron Spectra of C_{78} and C_{96}", *Chem. Phys. Letts.* **230**, 165 (1994).
S. HINO, K. KIKUCHI and Y. ACHIBA, "Photoelectron Spectra of Higher Fullerenes and their Potassium Complexes", *Synthetic Metals* **70**, 1337 (1995).
K. IMAEDA, I. I. KHAIRULLIN, K. YAKUSHI and H. INOKUCHI, "Magnetic and Structural Characterization of Superconducting Sodium-Doped C_{60} Prepared with the Thermal Decomposition of Sodium Azide", *Synth. Met.* **70**, 1375 (1995).
K. IMAEDA, Y. LI, Y. YAMASHITA, H. INOKUCHI and M. SANO, "Temperature Dependence of Hall Mobility in a Single Crystal of the Organic Semiconductor BTQBT", *J. Mater. Chem.* **5**, 861 (1995).
K. IMAEDA, Y. YAMASHITA, S. TANAKA and H. INOKUCHI, "New Low-Dimensional Organic Metals of $(BEDT\text{-}ATD)_2X(THF)$ ($X=PF_6$, AsF_6), Stable at Low Temperature", *Synth. Met.* **73**, 107 (1995).
Z. SHI, K. IMAEDA, C. NAKANO, H. INOKUCHI, T. ENOKI and G. SAITO, "Thermal Expansion of Tetrakis (alkylthio) tetrathiafulvalenes", *Mol. Cryst. Liq. Cryst.* **268**, 161 (1995).
A. TANAKA, A. CHAINANI, T. YOKOYA, T. TAKAHASHI, T. MIYAZAKI, S. HASEGAWA and T. MORI, "Synchrotron-radiation Photoemission Study of in-situ Synthesized DCNQI (*N, N'*-dicyanoquinonediimine)-Cu salts", *Solid State Commun.* **93**, 1 (1995).
K. MACHII, Y. WATANABE and I. MORISHIMA, "Acylperoxo-Iron(III) Porphyrin Complexes: A New Entry of Potent Oxidants for the Alkene Epoxidation", *J. Am. Chem. Soc.* **117**, 6691 (1995).
S. OZAWA, Y. WATANABE, S. NAKASHIMA, T. KITAGAWA and I. MORISHIMA, "Preparation and Characterization of Oxoiron(IV) Chlorin Complexes as the First Models for a Reaction Intermediate in the Catalytic Cycle of Cytochrome *d*", *J. Am. Chem. Soc.* **116**, 634 (1994).
Y. MIZUTANI, Y. WATANABE and T. KITAGAWA, "Resonance Raman Characterization of Iron(III) Porphyrin *N*-Oxide: Evidence for an Fe-O-N Bridged Structure", *J. Am. Chem. Soc.* **116**, 3439 (1994).
S. NAGANO, M. TANAKA, Y. WATANABE and I. MORISHIMA, "Putative Hydrogen Bond Network in Distal Site of Horseradish Peroxidase", *Biochem. Biophys. Res. Commun.* **207**, 417 (1995).
K. ISOBE, Y. OZAWA, A. VÁZQUEZ DE MIGUEL, T. -W. ZHU, K.-M. ZHAO, T. NISHIOKA, T. OGURA and T. KITAGAWA, "$[\{Rh_2Cp^*_2(\mu\text{-}CH_2)_2\}_2(\mu\text{-}S_4)]^{2+}$: A Novel Tetranuclear Cationic Complex with a Rectangular S_4 Unit", *Angew. Chem. Int. Ed. Engl.* **33**, 1882 (1994).
M. ABE, K. ISOBE, K. KIDA, A. NAGASAWA and A. YAGASAKI, "Intramolecular Rearrangements of Cyclooctadienerhodium(I) Fragments Supported on a Vanadium Oxide Cluster as Evidenced by Dynamic ^{17}O NMR Spectroscopy", *J. Cluster Sci.* **5**, 565 (1994).
T. SUZUKI, H. KOTSUKI, K. ISOBE, N. MORIYA, Y. NAKAGAWA and M. OCHI, "Drastic Structural Change in Silver(I) Complexes with Alteration of the Optical Activity of a Pyridine Derivative Ligand: Helical Arrays with Extended Structure and an Optically Inactive Dinuclear Complex", *Inorg. Chem.* **34**, 530 (1995).
S. OGO, T. SUZUKI and K. ISOBE, "A Unique Three-Step Cyclic Reaction Sequence of Heterotrimetallic Sulfide Clusters. Structures and Properties of $[\{Cp^*RhP(OEt)_3(m\text{-}WS_4)(CuCl)Cu\}_2(m\text{-}Cl)_2]$ ($Cp^* = h^5\text{-}C_5Me_5$) with a Branched Structure and $[\{Cp^*RhP(OEt)_3(m\text{-}WOS_3)(CuCl)Cu\}_2(m\text{-}Cl)_2]$ with a Linked Incomplete Cubane-Type Structure", *Inorg. Chem.* **34**, 1304 (1995).
S. OKEYA, H. KAMEDA, H. KAWASHIMA, H. SHIMOMURA, T. NISHIOKA and K. ISOBE, "C=S Bond Fis-

sion in Coordinated Thioureas and Formation of a Sulfide-bridged Dinuclear Pd(II) Complex", *Chem. Lett.* 501 (1995).

H. KOTSUKI, Y. NAKAGAWA, N. MORIYA, H. TATEISHI, M. OCHI, T. SUZUKI and K. ISOBE, "A Novel Synthesis of Optically Active C_2-Symmetric Pyridine Derivatives. Efficient Reaction of Chiral Triflates with 2-Picolyllithium Reagents", *Tetrahedron: Asymmetry* **6**, 1165 (1995).

S. OGO, T. SUZUKI, S. NOMURA, K. ASAKURA and K. ISOBE, "Synthesis of a Linear-Type Pentanuclear (Rh^{III}-W^{VI}-Cu^{I}-W^{VI}-Rh^{III}) Sulfide Cluster Predicted by Fast Atom Bombardment Mass Spectrometry", *J. Cluster Sci.* **6**, 421 (1995).

Y. OZAWA and K. TORIUMI, "Electrochemical Synthesis and Crystal Structure of a Novel One-Dimensional Halogen-Bridged Nickel(III) Complex", *Chem. Lett.* 257 (1995).

Y. NARUTA, N. SAWADA and M. TADOKORO, "Imidazole-Mediated Antiferromagnetic Coupling between Fe(III) Ions in Rigidly-Linked Porphyrin Dimers and Trimers", *Chem. Lett.* 1713 (1994).

Y. NARUTA, M. SASAYAMA and T. SASAKI, "Oxygen Evolution by Water Oxidation with Manganese Porphyrin Dimers", *Angew. Chem. Int. Ed. Engl.* **33**, 1839 (1994); *Angew. Chem.* **106**, 1964 (1994).

Y. NARUTA and M. SASAYAMA, "Importance of Mn-Mn Separation and their Relative Arrangement on the Development of High Catalase Activity in Manganese Porphyrin Dimer Catalysts", *J. Chem. Soc., Chem. Commun.* 2667 (1994).

Y. NARUTA and M. SASAYAMA, "How Do Nitrogen Bases Accerarate Decomposition of H_2O_2 in a Manganese Porphyrin Dimer ? Quantitative Evaluation of the Effect by its Axial Ligation *vs.* General-Base Catalysis", *Chem Lett.* 2411 (1994).

M. SASAYAMA and Y. NARUTA , "Preparation of a 1,8-Anthracene-Linked Manganese(IV) Porphyrin Dimer and its Reduction with H_2O_2. The O_2 Evolution Stage by the Reduction of the $Mn(IV)_2$ Complex is Not a Rate-determining Step in the Catalytic Disproportionation of H_2O_2", *Chem. Lett.* 63 (1995).

K. ICHIHARA and Y. NARUTA, "New and Efficient Synthesis of Oligomeric Porphyrins *via* Stepwise Nucleophilic Substitution of Aminoporphyrins to Cyanuric Chloride", *Chem. Lett.* 631 (1995).

T. SASAKI and Y. NARUTA, "Formation and Characterization of $Pz_3Cu(II)$-Fe(III) Porphyrin Complex as Structural Model of Cytochrome *c* Oxidase", *Chem. Lett.* 663 (1995).

H. NEMOTO, "Synthesis of Boron Carriers for Neutron Capture Therapy and the Studies of Activated Imines", *J. Syn. Org. Chem. Jpn.* **52**, 1044 (1994).

H. NEMOTO, "Synthesis and Biological Properties of Water-Soluble p-Boronophenylalanine Derivatives. Relationship between Water Solubility, Cytotoxicity and Cellar Uptake", *J. Med. Chem.* **38**, 1673 (1995).

Y. YAMAMOTO, J. CAI, H. NAKAMURA, N. SADAYORI, N. ASAO and H. NEMOTO, "Synthesis of Netropsin and Destamycin Analogues Bearing ortho-Carborane and their DNA Recognition", *J. Org. Chem.* **60**, 3352 (1995).

N. ASAO, T. SHIMADA, N. TSUKADA and Y. YAMAMOTO, "Highly Stereocontrolled and Concise Asymmetric Synthesis of the β-Lactam Framework via a TCC Method", *Tetrahedron Lett.* **35**, 8425 (1994).

J. T. FRANCIS, N. KOSUGI and A. P. HITCHCOCK, "Experimental and Theoretical Studies of the ($C\ 1s^{-1}$, π^*) $^3\Pi$ State of CO : Momentum Transfer Dependence and Vibrational Structure", *J. Chem. Phys.* **101**, 10429 (1994).

K. YAKUSHI, I. SHIROTANI, I. I. KHAIRULLIN, Y. NAKAZAWA, K. KANODA, N. KOSUGI and S. TAKEDA, "Characterization of poly-CuPc Sheet Polymers Synthesized under High Pressure", *Synthetic Metals* **71**, 2287 (1995).

K. UEDA, M. OKUNISHI, H. CHIBA, Y. SHIMIZU, K. OHMORI, Y. SATO, E. SHIGEMASA and N. KOSUGI, "Rydberg-Valence Mixing in the C 1s Excited States of CH_4 Probed by Electron Spectroscopy", *Chem. Phys. Lett.* **236**, 311 (1995).

M. SIMON, P. MORIN, P. LABLANQUIE, M. LAVOLLOÉE, K. UEDA and N. KOSUGI, "Dissociation Dynamics of Core-Excited BF_3 Probed by the Photoelectron-Photoion-Photoion Coincidence", *Chem. Phys. Lett.* **238**, 42 (1995).

J. ADACHI, N. KOSUGI, E. SHIGEMASA and A. YAGISHITA, "Renner-Teller Effect and Rydberg-Valence Mixing in the N and O K-edge Photoabsorption Spectra of N_2O", *J. Chem. Phys.* **102**, 7369 (1995).

E. SHIGEMASA, J. ADACHI, M. OURA and A. YAGISHITA, "Angular Distributions of 1sσ Photoelectrons from Fixed-in-Space N_2 Molecules", *Phys. Rev. Lett.* **74**, 359 (1995).

P. A. HATHERLY, J. ADACHI, E. SHIGEMASA and A. YAGISHITA, "The Angular Distributions of 1s Photoelctrons from Spatially Aligned CO using Angle-Resolved PEPICO", *J. Phys. B* **28**, 2643 (1995).

T. URISU, J. TAKAHASHI, Y. UTSUMI, T. AKUTSU and K. KUCHITSU, "Synchrotron Radiation Assisted Si Epitaxial Growth Using Si_2H_6 and SiH_2Cl_2 Gases -Properties in the Low Temperature Region-", *J. Electrochem. Soc.* **141**, 1562 (1994).

T. URISU, Y. ZHANG, M. NAGASONO, A. YOSHIGOE, Y. IMAIZUMI, H. OHSHIMA, T. HATTORI and S. SATO, "Molecular Orientation and Photochemical Reaction of Organoaluminum Compounds Investigated by Buried Metal Layer Infrared Reflection Absorption Spectroscopy", *Jpn. J. Appl. Phys.* **33**, 7123 (1994).

H. OHSHIMA, T. URISU, Y. YAMADA and T. HATTORI, "High Sensitivity FT-IR-RAS for Silicon Surface Study", *Mat. Res. Soc. Symp. Proc.* **318**, 413 (1994).

Y. IMAIZUMI, Y. ZHANG, Y. TSUSAKA, T. URISU and S. SATO, "Structure of the Organoaluminum Compounds Condensed Layer Investigated by Buried Metal Layer Reflection Absorption Spectroscopy", *J. Mole. Structure* **352/353** 447 (1995).

Y. YAMADA, T. HATTORI, T. URISU and H. OHSHIMA, "Measurement of Adsorbed F Atoms on a HF Treated Si Surface Using Infrared Reflection Absorption Spectroscopy", *Appl. Phys. Lett.* **66**, 496 (1995).

A. YOSHIGOE, M. NAGASONO, K. MASE, T. URISU, S. SEKI and Y. NAKAGAWA, "*In Situ* Detection of Sur-

face SiH_n in Synchrotron-Radiation-Induced Chemical Vapor Deposition of a-Si on an SiO_2 Substrate", *J. Synchrotron Rad.* **2**, 196 (1995).

Y. B. PARK, S. W. RHEE, Y. IMAIZUMI and T. URISU, "Effect of SR Irradiation on SiO_2 Thin Film", *J. Korean Vac. Soci.* **4**, 156 (1995).

K. MITSUKE and H. HATTORI, "Autoionizing Resonance in Photoionization from the $1\pi_u$ Level of Acetylene", *J. Chem. Phys.* **102**, 5288 (1995).

I. ARAKAWA, D. E. WEIBEL, T. NAGAI, M. ABO, T. HIRAYAMA, M. KANNO, K. MITSUKE and M. SAKURAI, "Angular and Kinetic Energy Distributions of the Desorption of Ne Metastable Induced by Excitons at the Surface of Solid Ne", *Nuclear Instrum. Meth. Phys. Res. B* **101**, 195 (1995).

H. HOSONO, N. UEDA, H. KAWAZOE and N. MATSUNAMI, "Optical and Electrical Properties of Proton-Implanted Amorphous SiO_2, GeO_2-SiO_2, MgO-P_2O_5 and Nanocrystalline $MgIn_2O_4$: Novel Materials by Proton Implantation", *J. Non-Cryst. Solids* **182**, 109 (1995).

H. HOSONO,"Chemical Interaction in Ion-Implanted Amorphous SiO_2 and Application to Formation and Modification of Nanosize Colloid Particles", *J. Non-Cryst. Solids* **187**, 457 (1995).

H. KAWAZOE, N. UEDA, H. UNNO, T. OMATA, H. HOSONO and H. TANOUE,"Generation of Electron Carriers in Insulating Thin Film of $MgIn_2O_4$ Spinel by Li^+ Implantation", *J. Appl. Phys.* **76**, L7935 (1994) .

M. YASUKAWA, H. HOSONO, N. UEDA and H. KAWAZOE, "Preparation of Electroconductive and Transparent Thin Films of $AgSbO_3$", *J. Ceram. Soc. Jpn.* **103**, 455 (1995).

M. YASUKAWA, H. HOSONO, N. UEDA and H. KAWAZOE, "Novel Transparent and Electroconductive Amorphous Semiconductor: Amorphous $AgSbO_3$ Film", *Jpn. J. Appl. Phys.* **34**, L281 (1995).

M. YASUKAWA, H. HOSONO, N. UEDA and H. KAWAZOE, "Photoemission Studies on Valence Band Structure of $AgSbO_3$", *Solid State Commun.* **95**, 399 (1995).

T. IBUKI, Y. HORIE, A. KAMIUCHI, Y. MORIMOTO, M. C. K. TINONE, K. TANAKA and K. HONMA, "Radiative Dissociation of C_2H_2, C_2HD and C_2D_2 Superexcited at 50-90 nm Region", *J. Chem. Phys.* **102**, 5301 (1995).

S. I. GHEYAS, M. IKEJIRI, T. OGATA, H. OGAWA and M. NISHIO, "Photoluminescence Properties of ZnTe Layers Grown by Photo-Assisted Metalorganic Vapor Phase Epitaxy", *J. Crystal Growth* **145**, 576 (1994).

T. OGATA, S. I. GHEYAS, M. IKEJIRI, H. OGAWA and M. NISHIO, "Synchrotron Radiation Excited Growth of ZnTe Using Metalorganic Sources", *J. Crystal Growth* **146**, 587 (1995).

T. OGATA, M. IKEJIRI, S. I. GHEYAS, H. OGAWA and M. NISHIO, "Construction of a System for Novel Low-Temperature Growth of II-VI Compound Semiconductors Using Synchrotron Radiation", *Rev. Sci. Instrum.* **66**, 1086 (1995).

T. OGATA, M. IKEJIRI, S. I. GHEYAS, H. OGAWA and M. NISHIO, "Synchrotron-Radiation-Excited Growth of ZnTe by Alternating Gas Supply Using Metalorganic Sources", *Jpn. J. Appl. Phys.* **34**, L841 (1995).

H. ISHII, A. YUYAMA, S. NARIOKA, K. SEKI, S. HASEGAWA, M. FUJINO, H. ISAKA, M. FUJIKI and N. MATSUMOTO, "Photoelectron Spectroscopy of Polysilanes, Polygermanes and Related Compounds", *Synthetic Metals* **69**, 595 (1995).

M. KOJIMA, I. SUGIMOTO, Y. SHIMIZU and Y. YOSHIKAWA, "Photochemistry of Tris(L-cysteinesulfinato-*N,S*)cobalt(III). Linkage Isomerization from Sulfinato-*S* to sulfinato-*O*", *Proc. Japan Acad.* **70B**, 101 (1994).

M. HIROTSU, M. KOJIMA, K. NAKAJIMA, S. KASHINO and Y. YOSHIKAWA, "Steric Control of Redox Potentials of Cobalt(III) Schiff Base Complexes with Phenyl Substituents", *Chem. Lett.* 2183 (1994).

F. MD. AKHTER, M. KOJIMA, M. HIROTSU, S. KASHINO and Y. YOSHIKAWA, "Photochemical Reaction of (L-cysteinesulfinato-*N,S*){tris(2-aminoethyl)-amine}cobalt(III). Formation of a Cobalt(III) Complex with an Uncoordinated Sulfinate Group", *Chem. Lett.* 2393 (1994).

Y. KURODA, Y. YOSHIKAWA, T. MORIMOTO and M. NAGAO, "Dielectric Behavior in the SrF_2-H_2O System. 1. Measurement at Room Temperature", *Langmuir* **11**, 259 (1995).

Y. KURODA, Y. YOSHIKAWA, T. MORIMOTO and M. NAGAO, "Dielectric Behavior in the SrF_2-H_2O System. 2. Measurement at Low Temperatures", *Langmuir* **11**, 2173 (1995).

Y. KURODA, Y. YOSHIKAWA, S. KONNO, H. HAMANO, H. MAEDA, R. KUMASHIRO and M. NAGAO, "Specific Feature of Copper-Ion-Exchanged Mordenite for Dinitrigen Adsorption at Room Temperature", *J. Phys. Chem.* **99**, 10621 (1995).

M. KOJIMA, K. NAKAJIMA, M. TSUCHIMOTO, P. M. TREICHEL, S. KASHINO and Y. YOSHIKAWA, "Characterization of Monomeric Green and Polymeric Orange Forms of a Schiff Base-Oxovanadium(IV) Complex and Interconversion between these Species", *Proc. Japan Acad.* **71B**, 175 (1995).

H. NAKAZAWA and K. MIYOSHI, "Formation of Iron Phosphonate Complexes Containing a Covalent Bond between Iron and Phosphorus and their Reactivity", *Trends Organomet. Chem.* **1**, 295 (1994).

H. OKU, N. UEYAMA, M. KONDO and A. NAKAMURA, "Oxygen Atom Transfer Systems in which the (μ-Oxo) dimolybdenum(V) Complex Formation does not Occur: Syntheses, Structures and Reactivities of Monooxomolybdenum(IV) Benzenedithiolato Complexes as Models of Molybdenum Oxidoreductases", *Inorg. Chem.* **33**, 209 (1994).

H. OKU, N. UEYAMA, A. NAKAMURA, Y. KAI and N. KANEHISA, "The Stablization of Dioxomolybdenum(VI) Dithiolene Complex by the Electron Withdrawing Substituent on the Dithiolene Ligand: Comparison of Reactivities of Monooxomolybdenum (IV) Complex with $R_2S_2C_2$ (R = -CN and -COOMe) Ligands as Models of Molybdenum Oxidoreductases", *Chem. Lett.* 607 (1994).

K. TATSUMI, A. TAHARA and A. NAKAMURA, "Linear vs. Bent M-O-R Bonds in d^0 Metal Alkoxides: X-ray Crystal Structure of $(C_5Me_5)Ta(S^tBu)_3(O^nBu)$ and EHMO Analysis", *J. Organomet. Chem.* **471**, 111 (1994).

K. MASHIMA, Y. NAKAYAMA, A. NAKAMURA, N. KANEHISA, Y. KAI and H. TAKAYA, "A New Convenient Preparation of Monocyclooctatetraenyl-lanthanide Complexes from Metallic Lanthanides and Oxidants", *J. Organomet. Chem.* **473**, 85 (1994).

H. YASUDA, Y. NAKAYAMA, K. TAKEI, A. NAKAMURA, Y. KAI and N. KANEHISA, "Reaction Courses for Formation of Early Transition Metal Phenoxides", *J. Organomet. Chem.* **473**, 105 (1994).

K. MASHIMA, H. SUGIYAMA and A. NAKAMURA, "Diene Complex of Lanthanum: The Crystal Structure of a Diene-Bridged Dilanthanum Complex, $[LaI_2(thf)_3(\mu\text{-}\eta^4\text{:}\eta^4\text{-PhCH=CHCH=CHPh})LaI_2(thf)_3]$", *J. Chem. Soc., Chem. Commun.* 1581 (1994).

N. UEYAMA, M. KONDO, H. OKU and A. NAKAMURA, "Structure and Properties of $(NEt_4)_2[Mo^{IV}O(\alpha,2\text{-}$ toluenedithiolato$)_2]$", *Bull. Chem. Soc. Jpn.* **67**, 1840 (1994).

K. MASHIMA, S. FUJIKAWA, H. URATA, E. TANAKA and A. NAKAMURA, "Polyethylene with Extremely Narrow Polydispersity Obtained from the New Catalyst Systems $Nb(\eta^5\text{-}C_5Me_5)(\eta^4\text{-diene})Cl_2$-MAO and $Nb(\eta^5\text{-}C_5Me_5)(\eta^4\text{-diene})_2$-MAO", *J. Chem. Soc., Chem. Commun.* 1623 (1994).

K. MASHIMA, H. SUGIYAMA, N. KANEHISA, Y. KAI, H. YASUDA and A. NAKAMURA, "Diene Complexes of Calcium and Strontium: First Crystal Structures of Calcium- and Strontium-Diene Complexes, M(2,3-dimethyl-1,4-diphenyl-1,3-butadiene)$(THF)_4$(M= Ca and Sr)", *J. Am. Chem. Soc.*, **116**, 6977 (1994).

K. MASHIMA, Y. NAKAYAMA, H. FUKUMOTO, N. KANEHISA, Y. KAI and A. NAKAMURA, "Formation of Lanthanoid(II) and Lanthanoid(III) Thiolate Complexes Derived from Metals and Organic Disulfides: Crystal Structures of $[\{Ln(SAr)(\mu\text{-}SAr)(thf)_3\}_2]$(Ln = Sm, Eu), $[Sm(SAr)_3(py)_2(thf)]$ and $[Yb(SAr)_3(py)_3]$ (Ar = 2,4,6-Triisopropylphenyl; py = Pyridine)", *J. Chem. Soc., Chem. Commun.* 2523 (1994).

N. UEYAMA, H. OKU, T. OKAMURA, A. NAKAMURA, A. KAJIWARA and M. KAMACHI, "ESR Study of $(Mo^VO)^{3+}$ and $(W^VO)^{3+}$ Thiolate or Selenolate Complexes", *Magnetic Resonance in Medicine* **6**, 216 (1995).

H. KAWAGUCHI, K. TATSUMI and A. NAKAMURA, "A Zigzag Chain Structure of a 3-Thiapentane-1,5-dithiolato Vanadium Complex Linked by Lithium Ions", *J. Chem. Soc., Chem. Commun.* 111 (1995).

W. -Y. SUN, T. UENO, N. UEYAMA and A. NAKAMURA, "^{19}F NMR Investigations of Cobalt(II) Complexes with Cysteine-Containing Peptide Ligands", *Magnetic Resonance in Chemistry,* **33**, 174 (1995).

A. NAKAMURA and N. UEYAMA, "Chemical Functions of Single and Double NH---S Hydrogen Bond in Iron-Sulfur Metalloproteins; Model Ligands with Cys-containing Peptide and Simple Acylaminobenzenethiolate", *Nuclear Magnetic Resonance of Paramagnetic Macromolecules* 265 (1995).

H. ZAIMA, N. UEYAMA, H. ADACHI and A. NAKAMURA, "^{1}H-, ^{13}C- and ^{113}Cd-NMR Study of the Cd (II) Complex of a Blocked Peptide, Z-Cys-Ala-Pro-His-OMe, in Organic Solvents", *Biopolymers* **35**, 319 (1995).

A. NAKAMURA, "Organometallic π-Conjugated Systems", *Bull. Chem. Soc. Jpn.* **68**, 1515 (1995).

H. OKU, N. UEYAMA and A. NAKAMURA, "Thiolato-Activated Oxo–Metal Bond Features in Molybdenum and Tungsten Oxidoreductase Models as Revealed by Raman Spectroscopy", *Inorg. Chem.* **34**, 3667 (1995).

K. MASHIMA, S. FUJIKAWA, Y. TANAKA, H. URATA, T. OSHIKI, E. TANAKA and A. NAKAMURA, "Living Polymerization of Ethylene Catalyzed by Diene Complexes of Niobium and Tantalum, $M(\eta^5\text{-}C_5Me_5)(\eta^4\text{-diene})X_2$ and $M(\eta^5\text{-}C_5Me_5)(\eta^4\text{-diene})_2$ (M=Nb and Ta), in the Presence of Methylaluminoxane", *Organometallics* **14**, 2633 (1995).

K. UNOURA, R. KIKUCHI, A. NAGASAWA, Y. KATO and Y. FUKUDA, "Correlation between ^{95}Mo NMR Chemical Shifts and Rate Constants of Various cis-Dioxobis(dithiocarbamato)molybdenum(VI) Complexes with PPH_3", *Inorg. Chim. Acta* **228**, 89 (1995).

H. KAMBAYASHI, J. YUZURIHARA, Y. MASUDA, H. NAKAGAWA, W. LINERT and Y. FUKUDA, "4- and 5-Coordinate Dinuclear Copper(II) Complexes with the Tetraacetylethanediide and an N-Alkylated Diamine or a Triamine", *Z. Naturforsch.* **50b**, 536 (1995).

T. YOSHIDA, M. OGUNI, Y. MORI and Y. FUKUDA, "Thermo-Analytical and X-Ray Diffractometric Observations of a Plastically Crystalline Phase in Molecular Mixed-Ligand Complex", *Solid State Commun.* **93**, 159 (1995).

F. JALILEHVAND, Y. ISHII, M. HIDAI and Y. FUKUDA, "Copper(II) Mixed Ligand Complex with an N-alkylated Diamine and a New β-Diketonate", *Chem. Lett.* 743 (1995).

Y. KUSHI, H. NAGAO, T. NISHIOKA, K. ISOBE and K. TANAKA, "Remarkable Decrease in Overpotential of Oxalate Formation in Electrochemical CO_2 Reduction by Metal-Sulfide Cluster", *J. Chem. Soc., Chem. Commun.* 1223 (1995)

H. NAKAJIMA, T. MIZUKAWA, H. NAGAO and K. TANAKA, "Catalytic Formation of Ketones via Double Alkylation of Carbon Monoxide Resulting from Reductive Disproportionation of Carbon Dioxide by $[Ru(bpy)_2(qu)(CO)]^{2+}$ (bpy = 2,2'-bipyridine, qu=quinoline)", *Chem. Lett.* 251 (1995).

Y. KUSHI, H. NAGAO, T. NISHIOKA, K. ISOBE and K. TANAKA, "Oxalate Formation in Electrochemical CO_2 Reduction Catalyzed by Rhodium-Sulfur Cluster", *Chem. Lett.* 2175 (1994).

N. KOMEDA, H. NAGAO, Y. KUSHI, G. ADACHI, M. SUZUKI, A. UEHARA and K. TANAKA, "Molecular Structure of Nitro- and Nitrito-Copper Complexes as Reaction Intermediates in Electrochemical Reduction of Nitrite to Dinitrogen Oxide", *Bull. Chem. Soc. Jpn.* **68**, 581 (1995).

T. TAKAHASHI, M. KOTORA and K. KASAI, "Zirconium Mediated or Catalyzed Highly Stereoselective Cyclization of 1,4,7-Trienes", *J. Chem. Soc., Chem. Commun.* 2693 (1994).

Y. MIZOBE, Y. YOKOBAYASHI, H. OHSHITA, T. TAKAHASHI and M. HIDAI, "Preparation of Heterobimetallic Complexes with a Bridging Dinitrogen Ligand, $[WX(PMe_2Ph)_4(\mu\text{-}N_2)MCp_2Cl]$ (M=Ti, X=Cl, M=Zr, Hf, X=I) and X-ray Structure of $[WI(PMe_2Ph)_3(py)(\mu\text{-}N_2)ZrCp_2Cl]$ (py=pyridine)", *Organometallics* **13**, 3764 (1994).

K. KASAI, M. KOTORA, N. SUZUKI and T. TAKAHASHI, "Chemoselective C-C Bond Formation Reaction of

Zirconacyclopentenes", *J. Chem. Soc., Chem. Commun.* 109 (1995).

T. TAKAHASHI, T. ISHIDA and Y. NISHIHARA, "Practical and Selective Method for Preparation and Reactions of Cp_2HfRCl and Cp_2HfRR'", *Chem. Lett.* 159 (1995).

T. TAKAHASHI, K. KASAI, Z. XI and V. DENISOV, "Reaction of Zirconocene Ethylene Complex with Diynes: Formation of Bridged Zirconacyclopentenes", *Chem. Lett.* 347 (1995).

T. TAKAHASHI, M. KOTORA and Z. XI, "Cycloaddition of Zirconacyclopentadienes to Alkynes Using Copper Salts: Formation of Benzene Derivatives", *J. Chem. Soc., Chem. Commun.* 361 (1995).

T. TAKAHASHI, M. KOTORA and Z. XI, "Formation of Five-Membered Carbocyclic Ring by Reaction of Zirconacyclopentane with RCOCl (R = Ph, Pr^i, Et) ", *J. Chem. Soc. Chem. Commun.* 1503 (1995).

T. TAKAHASHI, Z. XI, Y. OBORA and N. SUZUKI, "Intramolecular Coupling of Alkynyl Groups of Bis(alkynyl)silane Mediated by Zirconocene Compounds: Formation of Silacyclobutene Derivatives", *J. Am. Chem. Soc.* **117,** 2665 (1995).

Z. XI, R. HARA and T. TAKAHASHI, "Highly Selective and Practical Alkyne-Alkyne Cross-Coupling Using Cp_2ZrBu_2 and Ethylene", *J. Org. Chem.* **60,** 4444 (1995).

N. SUZUKI, D. Y. KONDAKOV, R. HARA, M. KAGEYAMA, M. KOTORA and T. TAKAHASHI, "Novel Type of Carbozirconation Reaction of Alkynes", *Tetrahedron,* 4519 (1995).

T. TAKAHASHI, D. Y. KONDAKOV, Z. XI and N. SUZUKI, "A Vinylzirconation of Alkynes", *J. Am. Chem. Soc.* **117,** 5871 (1995).

T. KURODA-SOWA, M. MUNAKATA, H. MATSUDA, S. AKIYAMA and M. MAEKAWA, "Syntheses, Structures and Properties of Copper(I) Coordination Polymers with Bridging Phenazine: Construction of One- and Two-Dimensional Structures with π-π Stacking of Phenazine", *J. Chem. Soc. Dalton Trans.* 2201 (1995).

T. KURODA-SOWA, M. MUNAKATA, M. MIYAZAKI and M. MAEKAWA, "Synthesis and Structures of Tetranuclear and Hexanuclear Copper(I) Complexes with Iminomethanethiolate Bridges Derived from Isothiocyanate", *Polyhedron* **14,** 1003 (1995).

X. GAN, M. MUNAKATA, T. KURODA-SOWA, M. MAEKAWA and Y. MISAKI, "Syntheses and Characterization of One- and Two-Dimensional Copper(I) Coordination Polymers with Tetrakis(ethylthio) tetrathiafulvalene and the Properties of their Iodine-Doped Compounds", *Polyhedron* **14,** 1413 (1995).

X. GAN, M. MUNAKATA, T. KURODA-SOWA, M. MAEKAWA and M. YAMAMOTO, "Syntheses, Structures and Properties of a Linear Copper(I) Coordination Polymers with Tetrakis(ethylthio)tetrathiafulvalene", *Polyhedron* **14,** 1647 (1995).

S. KITAGAWA, M. KONDO, S. KAWATA, S. WADA, M. MAEKAWA and M. MUNAKATA, "Molecular Cavity for Tetrahedral and Y-Shaped Anions. Synthetic and Structural Studies of Macrocyclic Dicopper(I) and Disilver(I) Compounds of 1,6-Bis(diphenylphosphino)hexane", *Inorg. Chem.* **34,** 1455 (1995).

M. MUNAKATA, T. KURODA-SOWA, M. MAEKAWA, A. HIROTA and S. KITAGAWA, "Building of 2D Sheet of Tetrakis(methylthio)tetrathiafulvalenes Coordinating to Copper(I) Halides with Zigzag and Helical Frames and the 3D Network through the S···S Contacts", *Inorg. Chem.* **34,** 2705 (1995).

M. MAEKAWA, M. MUNAKATA, T. KURODA-SOWA and K. HATIYA, "Formation of Metallocycle by Dimerization of Acrylonitrile. Crystal Structure of Hexakis(1,4-dicyanobutane-1,4-diyl)nickel(II) Complex", *Inorg. Chim. Acta* **230,** 249 (1995).

M. MAEKAWA, M. MUNAKATA, T. KURODA-SOWA and K. HATIYA, "Synthesis and Crystal Structure of Tetranuclear Nickel(0) Complex with 1,4-Diphenylbutadiene in the η^2, η^2-Bridging Mode", *Inorg. Chim. Acta* **231,** 213 (1995).

M. MAEKAWA, M. MUNAKATA, T. KURODA-SOWA and K. HATIYA, "Synthesis and Crystal Structure of Mono- and Dinickel(0) Ethylene Complex with 4, 4'-Bipyridine: $[Ni(4,4'\text{-bpy})(C_2H_4)_2]_2[Ni_2(4,4'\text{-bpy})(C_2H_4)_4]$", *Inorg. Chim. Acta* **232,** 231 (1995).

T. TAKAMI, "Semiclassical Study of Avoided Crossings", *Phys. Rev. E* **52,** 2434 (1995).

K. ONO, S. TANAKA AND Y. YAMASHITA, "Benzobisthiadiazoles Containing Hypervalent Sulfur Atoms: Novel Heterocycles with High Electron Affinity and Short Interheteroatom Contacts", *Angew. Chem. Int. Ed. Engl.* **33,** 1977 (1994).

K. SAITO, C. SUGIURA, E. TANIMOTO, K. SAITO and Y. YAMASHITA, "Synthesis and Properties of Tetrathiafulvalene Derivatives Containing Quinoid Structures: Novel Electron Donors of Organic Conductors", *Heterocycles* **38,** 2153 (1994).

A. OHTA and Y. YAMASHITA, "Preparation and Properties of Tris(1,3-dithiole) Donors Containig Thiophene Spacer Units", *Heterocycles* **40,** 123 (1995).

A. OHTA and Y. YAMASHITA, "Preparation and Properties of Bis[5-(6-methyl-1,4-dithiaflven-6-yl)-2-thienyl] methanes Affording Near-Infrared Absorbing Cations by Oxidation", *J. Chem. Soc., Chem. Commun.* 557 (1995).

S. TANAKA and Y. YAMASHITA, "Syntheses of Narrow Bandgap Heterocyclic Copolymers of Aromatic-Donor and Quinonoid-Acceptor Units", *Synth. Met.* **69,** 599 (1995).

Y. YAMASHITA, S. TANAKA and K. IMAEDA, "Organic Metals Based on Butterfly-Shaped Donor Molecules", *Synth. Met.* **71,** 1965 (1995).

M. KARIKOMI, C. KITAMURA, S. TANAKA and Y. YAMASHITA, "New Narrow-Bandgap Polymer Composed of Benzobis(1,2,5-thiadiazole) and Thiophenes", *J. Am. Chem. Soc.* **117,** 6791 (1995).

M. HIRAYAMA, M. ITASAKA, T. SUZUKI, Y. YAMASHITA and T. MIYASHI, "The π-Trianion Radical of 2,3,6,7-Tetracyanobenzo[1,2-b:4,5-b']bisdithiole-4,8-dione. Observation of ESR with ^{13}C-Satellites in Natural Abun-

dance", *Chem. Lett.* 511 (1995).
A. HOSHINO, S. ISODA, H. KURATA, T. KOBAYASHI and Y. YAMASHITA, "Prediction of the Epitaxial Orientaion of Ultrathin Organic Films on Graphite", *Jpn. J. Appl. Phys.* **34**, 3858 (1995).
M. SANEKATA, F. MISAIZU, K. FUKE, S. IWATA and K. HASHIMOTO, "Reaction of Singly Charged Alkaline-earth Metal Ions with Water Clusters: Characteristic Size Distribution of Product Ions", *J. Am. Chem. Soc.* **117**, 747 (1995).
F. MISAIZU, K. TSUKAMOTO, M. SANEKATA and K. FUKE, "Photoelectron Spectroscopy of Mass-Selected Copper-Water Cluster Negative Ions", *Laser Chem.* **15**, 195 (1995).
H. WATANABE, S. IWATA, H. NAKAMURA, K. HASHIMOTO, F. MISAIZU and K. FUKE, "Molecular Orbital Studies of the Structures and Reactions of Magnesium-Water Cluster Ions $Mg^+(H_2O)_n$", *J. Am. Chem. Soc.* **117**, 755 (1995).
K. FUKE and R. TAKASU, "Ultrafast Photochemistry of Ammonia Clusters: Formation and Decay of Hypervalent Molecular Clusters Containing the NH_4 Radical", *Bull. Chem. Soc. Jpn.* **68**, 3532 (1995).
K. KIMURA and S. BANDOW, "Isolation and Agglomeration of Zinc Nanocolloids Observed by ESR Spectroscopy", *J. Colloid Interface Sci.* **171**, 356 (1995).
D. KUWAHARA, "Simulation of Homonuclear Two Spin-1/2 Systems under Sample Spinning. Effects of Jump Motions on NMR Line Shapes", *Chem. Phys. Lett.* **231**, 414 (1994)
M. A. TEREKHIN, A. N. VASILEV, M. KAMADA, E. NAKAMURA and S. KUBOTA, "Effects of Quenching Processes on Fluorescence Decay Curves of Barium Fluoride Excited by VUV Synchrotron Radiation", *Phys. Rev. B* **52**, 3117 (1995).
M. A. TEREKHIN, N. YU. SVECHNIKOV, V. G. STANKEVITCH, A. A. KOLMAKOV, V. A. STEPANOV, V. N. BEZMELNITSIN, M. KAMADA and K. KAN'NO, "Radiative Transitions in C_{60} thin Films under UV Laser and SR Excitations", *Optics and Spectroscopy* **78**, 75 (1995).
M. KAMADA and H. HAMA, "Status of the UVSOR Facility -1994-", *Rev. Sci. Instrum.* **66**, 2362 (1995).
M. KAMADA, K. SAKAI, S. TANAKA, S. OHARA, S. KIMURA, A. HIRAYA, M. HASUMOTO, K. NAKAGAWA, K. ICHIKAWA, K. SODA, K. FUKUI, Y. FUJII and E. ISHIGURO, "Monochromator for Circularly Polarized Synchrotron Radiation in the Energy Range of 5-250 eV", *Rev. Sci. Instrum.* **66**, 1537 (1995).
H. HAMA, J. YAMAZAKI, T. KINOSHITA, K. KIMURA and G. ISOYAMA, "Observation of Micro-Macro Temporal Structure and Saturation Mechanism on the UVSOR Free Electron Laser", *Nucl. Instr. and Meth. A* **358**, 365 (1995).
N. KANAYA, H. HAMA, J. YAMAZAKI, O. MATSUDO and G. ISOYAMA, "Gracefully-Degraded Operationable Control System for the UVSOR Synchrotron Radiation Source and its Operational Experience", *Nucl. Instr. and Meth. A* **352**, 166 (1994).
T.K. SHAM, I. COULTHARD, J.W. LORIMER, A. HIRAYA and M. WATANABE, "Reductive Deposition of Cu on Porous Silicon from Aqueous Solutions: An X-Ray Absorption Study at The Cu $L_{3,2}$-edge", *Chem. Mater.* **6**, 2085 (1994).
A. J. YENCHA, A. HOPKIRK, A. HIRAYA, G. DUAJARDIN, A. KVARAN, L. HELLNER, M. J. BESNARD-RAMAGE, R. J. DONOVAN, J. G. GOODE, R. R. J. MAIER, G. C. KING and S. SPYROU, "Threshold Photoelectron Spectroscopy of CF_4 up to 60.5 eV", *J. Electron Spectrosc. Rel. Phenom.* **70**, 29 (1994).
A. J. YENCHA, A. HOPKIRK, A. HIRAYA, R. J. DONOVAN, J. G. GOODE, R. R. J. MAIER, G. C. KING and A. KVARAN, "Threshold Electron Spectroscopy of Cl_2 and Br_2 up to 35 eV", *J. Phys. Chem.* **99**, 7231 (1995).
A. HIRAYA, M. WATANABE and T. K. SHAM, "Electron and X-Ray Fluorescence Yield Measurements of the Cu $L_{2,3}$-Edge X-Ray Absorption Fine Structures: A Comparative Study", *Rev. Sci. Instrum.* **66**, 1528 (1995).
A. HIRAYA, K. MATSUDA and M. WATANABE, "Performance Check of β -Alumina as a Soft X-Ray Monochromator Crystal", *Rev. Sci. Instrum.* **66**, 2102 (1995).
A. HIRAYA, E. NAKAMURA, M. HASUMOTO, T. KINOSHITA, K. SAKAI, E. ISHIGURO and M. WATANABE, "Construction of Constant-Deviation Constant-Length Spherical Grating Monochromator at UVSOR", *Rev. Sci. Instrum.* **66**, 2104 (1995).
H. OHTA, S. KIMURA, E. KULATOV, S. V. HALILOV, T. NANBA, M. MOTOKAWA, M. SATO and K. NAGASAKA, "Optical Measurements and Band Calculations of FeSi", *J. Phys. Soc. Jpn.* **63**, 4206 (1994).
S. KIMURA, Y. SATO, T. SUZUKI and M. IKEZAWA, "Magnetic Polaron of Gd_2S_3 Studied by Infrared Spectroscopy under Magnetic Field", *J. Phys. Soc. Jpn.* **64**, 200 (1995).
S. KIMURA, F. ARAI, Y. HAGA, T. SUZUKI and M. IKEZAWA, "Optical Spectra of CeAs and LaAs", *Physica B* **206&207**, 780 (1995).
S. KIMURA, Y. SATO, T. SUZUKI and M. IKEZAWA, "Deep Magnetic Polaron State in Gd_2S_3", *Physica B* **206&207**, 786 (1995).
Y. S. KWON, T. S. PARK, J. M. KIM, K. S. AN, I. S. JEON, C. Y. PARK, S. KIMURA, T. NANBA, T. MATSUMURA and T. SUZUKI, "Far Infrared Transmission of SmTe under High Pressure", *Physica B* **206&207**, 389 (1995).
T. SUZUKI, Y. HAGA, D. X. LI, T. MATSUMURA, E. HOTTA, A. UESAWA, M. KOHGI, T. OSAKABE, S. TAKAGI, H. SUZUKI, T. KASUYA, Y. CHIBA, T. GOTO, S. NAKAMURA, R. SETTAI, S. SAKATSUME, A. OCHIAI, K. SUZUKI, S. NIMORI, G. KIDO, K. OHYAMA, M. DATE, Y. MORII, T. TERASHIMA, S. UJI, H. AOKI, T. NAKA, T. MATSUMOTO, Y. OHARA, H. YOSHIZAWA, Y. OKAYAMA, Y. OKUNUKI, A. ICHIKAWA, H. TAKAHASHI, N. MORI, T. INOUE, T. KURODA, K. SUGIYAMA, K. KINDO, A. MITSUDA, S. KIMURA, S. TAKAYANAGI, N. WADA, A. OYAMADA, K. HASHI, S. MAEGAWA, T. GOTO, Y. S. KWON, E.

VINCENT and P. BONVILLE, "Anomalous Physical Properties of the Low Carrier Concentration State in f-Electron Systems", *Physica B* **206&207**, 771 (1995).
H. OHTA, S. KIMURA, E. KULATOV, S. V. HALILOV, T. NANBA and M. MOTOKAWA, "The Investigation of Electronic Structure in FeSi by Optical Measurements", *J. Magn. Magn. Mater.* **140-144**, 121 (1995).
K. OZAWA, T. ANAZAWA, S. TOKUMITSU, R. SEKINE, E.MIYAZAKI, K. EDAMOTO, S. TANAKA and S. OTANI, "Adsorption of K on NbC(100):Photoemission and Thermal Desorption Study", *Surf. Sci.* **336**, 93 (1995).

Review Articles and Textbooks

S. LEE, M. IWAI and H. NAKAMURA, "Charactrstics and Dynamics of Doubly Excited States of Molecules", Molecules in Laser Fields, ed. by A. D. Bandrauk, (M. Dekker), p217-286 (1994).
H. NAKAMURA, "Characteristics and Dynamics of Superexcited States of Molecules", *J. Chinese Chem. Soc.* (Special issue of 10th anniversary of IAMS) **42,** p359-366 (1995).
A. SHUDO, "Pseudointegrable Systems and Level Statistics", *Suri-Kagaku* (in Japanese) **376,** 36 (1994).
A. SHUDO, "Level Statistics and Semiclassical Periodic-Orbit Expansion for Polygonal Billiards", *Kokyu-Roku in Res. Inst. of Math. Sci.* (in Japanese) **863,** 67(1994).
S. SAITO, "Carbon Chain Molecules in Space", Kagaku(in Japanese) **49,** 685(1994).
S. SAITO, "Molecular World in Sapce", The 44th Science Lecture(Toray Science Foundation), Abstract, pp. 1-10(1994).
S. SAITO, "Probing the Space with Molecules", J. Visual. Soc. Japan (in Japanese) **15,** No. 59,13(1995).
N. MORITA, R.S. HAYANO and T. YAMAZAKI, "Laser Spectroscopy of Antiprotonic Helium Atoms", *Buturi* (in Japanese) **49,** 827 (1994).
N. MORITA and R.S. HAYANO, "Laser-Induced Annihilation Spectroscopy of Antiprotonic Helium Atoms", *Solid State Physics* (in Japanese) **30,** 118 (1995).
T. KITAGAWA and Y. MIZUTANI, "Resonance Raman Spectra of Highly Oxidized Metalloporphyrins and Heme Proteins.", *Coord. Chem. Rev.* **685-735,** 135/136 (1994).
K. YOSHIHARA, "Solvent and Nuclear Dynamics of Ultrafast Intermolecular Electron Transfer", in "Ultrafast Processes in Chemistry and Biology, International Union of Pure and Applied Chemistry Monograph Series on Chemistry for the 21st Century", M.A. El-Sayed, I. Tanaka and Yu Molin Eds. Chapter 4, Blackwell Science Publisher, p.105 (1995).
K. YOSHIHARA, K. TOMINAGA and Y. NAGASAWA, "Effects of the Solvent Dynamics and Vibrational Motions in Electron Transfer"(Accounts), *Bull. Chem. Soc. Jpn.* **68,** 696 (1995).
Y. MATSUMOTO, "Dynamics of Photo-Induced Desorption and Dissociation", *J. Surf. Sci. Soc. Japan* (in Japanese), **16,** 557 (1995).
M. TAKAYANAGI and I. HANAZAKI, "Applications of the Hole-Burning Spectroscopy in Molecular-Beam Experiments", *Bunko-Kenkyu* (in Japanese) **43,** 347 (1994).
K. KANODA, "Metal-Insulator Transition and Strong Electron Correlation in BEDT-TTF compounds", *Solid State Physics* (in Japanese) **30,** 240 (1995).
S. MIYAJIMA and H. OGATA, "Molecular Dynamics Probed by NMR -Case of C_{60}-", *J. Crystallographic Society of Japan* (in Japanese) **37,** 10 (1995).
K. SHOBATAKE and H. OHASHI, "Applications of Molecular Beam Techniques to the Studies of Surface Reaction Dynamics", *J. Surf. Sci. Soc. Jpn.* (in Japanese) **16,** 544(1995).
S. HASEGAWA, H. ISHII and N. UENO, "Angle-Resolved Ultraviolet Photoemission Spectroscopy for the Thin Films of Functional Organic Molecules", *Hyoumen Kagaku* (in Japanese) **15,** 573 (1994).
K. TORIUMI, "Crystal Structures and State Properties of Halogen-Bridged Metal Complexes with One-dimensional Chain Structures", *J. Cryst. Jpn.* (in Japanese) **37,** 76 (1995).
Y. NARUTA, "Manganese-Containing Peptide (Modeling Systems)", (in Japanese) in "Recent Progress in Bioinorganic Chemistry", *Kikan Kagaku Sousetsu,* No. 24, Chemical Society of Japan, Ed. Gakkai Shuppan Center (Tokyo) pp.133-146 (1995).
J. ADACHI and N. KOSUGI, "Vibrational Spectroscopy and Fragmentation Dynamics of Inner-shell Excited Molecules", *Nippon Houshakou Gakkaishi* (in Japanese) **8,** 164 (1995).
K. MITSUKE, "Ion-Pair Formation from Superexcited Molecules", *J. Jpn. Soc. Synchrotron Radiation Res.* (in Japanese) 7, 309 (1994).
K. HARADA and Y. FUKUDA, "Chromotropism of Coordination Compounds", *Shigen-to-Sozai (J. Mining Materials Processing Institute of Jpn.)* (in Japanese) **111,** 523 (1995).

AUTHOR INDEX-RESEARCH ACTIVITIES AND SPECIAL RESEARCH PROJECTS

Abo, Munehide 111
Achiba, Yohji 89
Adachi, Jun-ichi 102, 103, 171
Akasaka, Takeshi 40
Akiyama, Shin-ichi 133
Akhter, Farooque Md. 118, 119
Amano, Shin-ichi 97
Anraku, Yasuhiro 36
Aoyagi, Katsuhiro 38
Aoyagi, Mutsumi 143
Appelman, Evan H. 164
Arai, Fumitaka 159
Arai, Takeshi 166
Arakawa, Ichiro 111
Araki, Hisashi 69
Asada, Toshio 14
Asaka, Shuji 156, 165, 171
Akakura, Kiyotaka 94
Asano-Someda, Motoko 38
Asao, Naoki 101
Bandow, Shunji 153, 154
Barber, James 46
Bell, Rew J. 48
Bisht, Prem B. 41, 48
Bontuyan, Lizla S. 60, 170
Brion, C. E. 113, 114
Cai, Jianping 101
Carter, C. C. 14
Cassoux, Patrick 79
Chainani, Ashish 90
Chiba, Hiroshi 103
Chiba, Tomonori 64
Choi, Young S. 48
Christensen, Ronald L. 48
Chujo, Takayuki 65
Crystall, Ben 46
Daniel, H. 32, 33
Denisov, V. N. 68
Denisov, Victor 132
Dong, Jian 68, 69, 171
Durrant, James R. 46
Eades, J. 32, 33
Egidy, von.T. 32
Eguchi, Shingo 140, 141
Enoki, Toshiaki 82, 91
Fang, Shaoli 77, 166
Fischer, Reinald 131
Floriani, Carlo 138, 140
Francis, James T. 103
Frankevich, Eugene 69, 78
Fujii, Masaaki 18
Fujii, Toshiaki 17
Fujikawa, S. 125
Fujimoto, Hitoshi 87
Fujita, Junnosuke 121
Fujiwara, Hideo 31, 32
Fuke, Kiyokazu 148, 149, 151, 152, 165
Fukuda, Yutaka 126, 127
Fukuhara, Koichi 65
Fukui, Jun-ichi 135
Fukutome, Hideo 25
Fukuyama, Hidetoshi 95, 96
Funasaka, Hideyuki 40
Gallo, Emma 140
Gan, Xinmin 134, 135
Gandhi, Suketu R. 54, 55
Gejo, Tatsuo 52
Gennis, Robert B. 36
Gerson, G. 103
Gheyas, Syed Irfan 108, 115, 116
Gomei, Motoki 15, 16
Goodman, Frank O. 23
Gorecki, Jerzy 58
Goto, Masa-oki 99
Goto, Masahiro 29
Goto, Yoshio 167
Grigoryan, L. 68
Gruzdkov, Yuri A. 50, 51, 164
H.Mies, Frederick 22
Hachiya, Koji 137
Hama, Hiroyuki 158, 171
Hamano, Hideaki 120, 167
Hamatani, Yukiko 117
Hanazaki, Ichiro 53, 54, 55, 56, 57, 58, 59, 165
Hansmann, Ulrich H.E. 19, 169
Hara, Ryuichiro 131, 168
Harada, Kazumasa 127
Harada, Yoshiya 88
Harayama, Takahisa 20
Harima, Yutaka 117, 172
Hartmann, F.J. 32, 33
Hasegawa, Shinji 87, 88, 89, 117, 172
Haegawa, Tatsuo 83
Hashimoto, Nobuhisa 62, 170
Hashimoto, Yuzo 140
Hasumi, Ryouji 14
Hatherly, Paul A. 103
Hattori, Hideo 108, 109
Hayano, R.S. 32, 33
Hayashi, Michiro 30
Hayashi, Takashi 47, 170
Hayashi, Yoshihito 37
Hidai, Masanobu 126
Hiejima, Toshihiro 67, 166
Hikida, Takumi 109
Hikosaka, Yasumasa 109
Hino, Shojun 89
Hiraki, Ko-ichi 76, 77, 172
Hirano, M. 14
Hirano, Shinya 116
Hirao, Tsuyoshi 30
Hiraya, Atsunari 102, 107, 114, 165, 171
Hirayama, Takato 111
Hirose, Sayumi 159
Hirota, Akihiro 133
Hirota, Shun 34, 36, 37, 164
Hirotsu, Masakazu 118, 119
Hiruta, Ken-ichi 65
Hitchcock, Adam P. 103
Hiyama, Miyabi 23, 169
Holden, J. M. 153
Honma, Kenji 114
Hori, Hiroshi 36
Hori, M. 33
Horie, Yasuhiko 114
Horigome, Toshio 156, 171
Horiki, Yasuhiro 63
Horvath, D. 32, 33
Hoshi, Hajime 77, 166
Hoshi, Toshihiko 126
Hoshino, Kuniyoshi 15
Hosono, Hideo 112, 113
Ibaraki, Akito 97
Ibuki, Toshio 113, 114, 171
Ichihara, Kanako 99
Ichikawa, Akimasa 86
Ichikawa, Taroh 93
Ichikawa, Tetsuya 26
Ichimura, Kenji 90
Ichimura, Satoshi 122

Ida, Takashi 97
Iitaka, Toshiaki 19
Ikawa, Akira 25
Ikeda, Kensuke S. 19, 20
Ikeda, Takuya 124
Ikegami, Isamu 170
Ikegami, Tsutomu 16, 169
Ikejiri, Makoto 115
Ikezawa, Mikihiko 159
Ikuno, Takayuki 97
Imaeda, Kenichi 68, 89, 90, 145
Imai, Kiyohiro 36
Imaizumi, Yoshiaki 106
Inada, Naomi 30
Inatani, Junji 31
Inokuchi, Hiroo 68, 87, 88, 89, 90
Ishida, Toyohisa 132
Ishiguro, Eiji 83, 171
Ishii, Hisao 88, 89, 117
Ishii, Youichi 126, 127
Ishikawa, T. 32, 33
Ishimori, Koichiro 94
Isobe, Kiyoshi 94, 95, 129
Ito, Osamu 63
Itoh, Koichi 66
Itoh, Shigeru 170
Ivlev, A. N. 68
Iwaki, Masayo 170
Iwamoto, Satoshi 101
Iwasa, Yoshihiro 83
Iwasaki, Kentaro 89
Iwata, Suehiro 13, 14, 15, 16, 17, 18, 19, 169
Jalilehvand, Farideh 126
Johnson, Alan E. 41
Joseph, D. Melissa 46
Kageyama, Motohiro 168
Kagoshima, Seiichi 83
Kaifu, Norio 31
Kamada, Masao 49, 107, 156, 159
Kamalov, Valey F. 44, 48, 170
Kambayashi, Hide 126, 127
Kaminaga, Akiko 58, 165
Kaminaka, Shouji 36
Kamiuchi, Akira 114
Kamiya, Koji 88
Kamogawa, Keiji 36
Kang, Tai Jong 164
Kanno, Minoru 111
Kanoda, Kazushi 70, 71, 72, 73, 74, 75, 76, 77, 172
Karikomi, Michinori 145
Kasai, Kayoko 132, 133
Kasaya, Mitsuo 159
Kashino, Setsuo 118, 121
Kataoka, Daisuke 120
Katayanagi, Hideki 61, 62, 170
Kato, Hajime 17
Kato, Hiroyuki 49, 164
Kato, Masako 39
Kato, Shinobu 65
Kato, Tatsuhisa 39, 40, 164
Katoh, Kenichi 159
Katsumata, Koichi 86
Kawada, Satoshi 136
Kawamoto, Atsushi 70, 71, 72, 73, 75, 76, 172
Kawamoto, Ikuko 117
Kawano, Koichi 80
Kawata, Satoshi 137
Kawazoe, Hiroshi 112, 113
Kaya, Koji 14, 15, 16
Kayama, misa 105
Kayatani, Takayuki 37
Keogh, Gary P. 43, 164
Ketzer, B. 32, 33
Kikuchi, Ko-ichi 89
Kim, Hong-Lae 53
Kimura, Eiichi 124, 125
Kimura, Kazuhiko 158
Kimura, Keisaku 97, 153
Kimura, Shin-ichi 158, 159
Kino, Hiori 95, 96
Kinoshita, Takamasa 66
Kinoshita, Toshio 158, 171
Kinoshita, Toyohiko 107, 158
Kishi, Reiko 15, 16
Kitagawa, Hiroshi 86
Kitagawa, Susumu 133, 136, 137
Kitagawa, Teizo 34, 35, 36, 37, 38, 39, 92, 93
Kitagishi, Yuichi 66
Kitahara, Kazuo 58
Kitajima, Yoshinori 102
Kitamura, Chitoshi 145
Klug, David R. 46
Kobayashi, Akiko 79
Kobayashi, Hayao 79
Kobayashi, Kaori 29
Kobayashi, Kaoru 40
Kobayashi, Y. 170
Kobuke, Yoshiaki 136
Kodama, Takeshi 39
Kohama, Keiichi 77, 166
Kohata, Susumu 141
Koike, Tsuneaki 88
Kojima, Masaaki 118, 119, 121
Kokka, Michiyo 167
Kokubo, Katuaki 136
Kondakov, Denis Y. 131, 168
Kondo, Mitsuru 136
Konishi, Yuji 15
Konno, Shin-ichi 120, 167
Kono, Mitsuhiko 114
Kono, Takumi 52
Kosugi, Nobuhiro 102, 103, 104
Kotora, Martin 131, 132, 133, 168
Kotuki, Hiyoshizo 95
Kozlov, Mikhail E. 70
Kruglik, Sergei 38, 39
Kubota, Sinzo 159
Kubozono, Yoshihiro 120
Kumakura, Mitsutaka 33, 163
Kumashiro, Ryotaro 120, 167
Kumazaki, Shigeichi 41, 46, 47, 170
Kurihara, Masato 168
Kurikawa, Tsuyoshi 15
Kuroda, Yasushige 120, 167
Kuroda-sowa, Takayoshi 133, 134, 135, 136, 137
Kushi, Yoshinori 127, 129
Kuwahara, Daisuke 155
Lablanquie, Pascal 103
Lavollée, Michel 103
Lee, Duckhwan 13
Lee, Jihwa 49
Li, Yumin 17
Lin, M.C. 164
Linert, Wolfgang 126
Liu, Hong Ling 118
Ma, Jangseok 43, 44
Maas, F.E. 32, 33
Machii, Kenji 92
Maeda, Hironobu 120, 167
Maeda, Yonezo 37
Maekawa, Masahiko 133, 134, 135, 136, 137
Mago, Genjin 140, 141
Manabe, Toshio 85
Maruyama, Yusei 40, 69, 77,

78, 166
Masatoki, Sei 36
Mase, Kazuhiko 106, 107, 170
Mashima, K. 125
Masuda, Yuichi 126
Matsuda, Hajime 133
Matsui, Toshitaka 94, 167
Matsumoto, Naohide 140, 141
Matsumoto, Yoshiyasu 49, 50, 51, 164
Matsunami, Noriaki 112
Matsuo, Shigeki 105
Matsushita, Michio 40, 164
Matsutsuji, Kazuto 82
Matsuura, Hiroatsu 65
Matsuzaki, Akiyoshi 63, 64
Matsuzawa, Hidenori 18
Matuura, Hiruatsu 36
Mavrin, Boris N. 68
Meech, Steve R. 170
Mekaru, Harutaka 154, 156, 157
Mekawa, Masahiko 134
Mies, Frederick H. 22
Miller, T. A. 14
Minamino, Satoshi 143
Misaizu, Fuminori 148, 165
Misaki, Yoshiharu 134
Mitani, Tadaoki 84, 85, 86, 156, 157
Mitsuke, Koichiro 108, 109, 110, 111, 165
Mitsutake, Ayori 19, 169
Miura, Yuzo 66
Miyagawa, Kazuya 70, 71, 72, 73, 76, 172
Miyahara, Takashi 47
Miyajima, Naomi 141
Miyajima, Seiichi 80, 82, 166
Miyamae, Hiroshi 86
Miyamae, Takayuki 88
Miyasaka, Hitoshi 140, 141
Miyazaki, Makoto 134
Miyazaki, Takafumi 88, 89, 117, 172
Miyoshi, Eisaku 26
Miyoshi, Katsuhiko 122, 123, 167
Mizukawa, Tetsunori 127, 128, 168
Mizuno, Yuri 119
Mizuta, Tsutomu 122, 123, 167
Mizutani, Masakazu 165
Mizutani, Yasuhisa 36, 37, 38, 39, 93
Mo, Yuxiang 61, 170
Mochida, Tomoyuki 166
Mogi, Tatsushi 36
Momose, Masahiro 88
Mori, Takehiko 90
Mori, Toshinori 120
Mori, Yoshihito 55, 59, 165
Mori, Yukie 126
Moribayashi, Kengo 21, 169
Morimoto, Tetsuo 120
Morimoto, Yoshikazu 114
Morin, Paul 103
Morishima, Isao 92, 93, 94
Morita, Norio 32, 33, 163
Moriwaki, Yoshiki 163
Moriya, Narimasa 95
Mukamel, Shual 24, 25
Munakata, Megumu 133, 134, 135, 136, 137
Murakami, Tatsuya 92
Nagai, Masako 36
Nagai, Toshiki 111
Nagano, Shingo 94
Nagao, Hirotaka 127, 128, 129, 130
Nagao, Mahiko 120, 167
Nagasawa, Yutaka 41, 42
Nagase, Shigeru 40
Nagasono, Mitsuru 106, 107
Naito, Toshio 79, 80
Naitoh, Yukito 43, 45, 164, 170
Nakagaki, Ryoichi 65
Nakagawa, Hiroko 126
Nakagawa, Y. 106
Nakagawa, Yuichi 95
Nakai, Toshihito 82, 155, 166
Nakajima, Atsushi 14, 15, 16
Nakajima, Hiroshi 127, 128, 130
Nakajima, Kiyohiko 119, 121, 131
Nakamura, A 125
Nakamura, Eiken 107, 159
Nakamura, Hiroki 21, 22, 23, 169
Nakamura, Hiroyuki 101
Nakamura, Motohiko 104
Nakano, Chikako 91
Nakao, Kojiro 15
Nakashima, Satoru 92
Nakashima, Toshio 140
Nakayoshi, K. 32
Nakazawa, Hiroshi 122, 123, 167
Nakazawa, Takashi 169
Nakazawa, Yasuhiro 70, 71, 72, 73, 74, 75, 172
Namiki, Kei-ichi 29
Nanbu, Shinkoh 23, 143
Narioka, Satoru 89, 117
Naruta, Yoshinori 97, 98, 99, 100
Nemoto, Hisao 101
Niestroj, A. 32
Nikitin, Evgueni E. 23
Nishihara, Yasushi 131, 132
Nishio, Mitsuhiro 108, 115, 116
Nishio, Satoru 63, 64
Nishioka, Takanori 129
Nomura, Sachiyo 156, 157
Noro, Takeshi 26
Nozaki, Takeshi 140, 141
Obora, Yasushi 130
Ochi, Masamitu 95
Ochiai, Yuichi 78
Ogata, Hironori 78, 82, 166
Ogata, Toshihiro 108, 115
Ogawa, Hiroshi 108, 115, 116
Ogino, T. 170
Ogo, Seiji 94
Ogoshi, Hisanobu 47, 170
Oguni, Masaharu 126
Ogura, Takashi 34, 35, 36, 37
Ohashi, Haruhiko 83
Ohba, Shigeru 121
Ohishi, Masatoshi 31
Ohishi, Tachi 86
Ohmo, Kenji 103
Ohmori, Yasuharu 118
Ohta, Akira 144, 145
Ohta, Toshiaki 89
Oishi, Osamu 80, 166
Oka, Yasuo 84
Okada, Akira 25
Okada, Kazutoshi 17
Okada, Norio 156
Okamoto, Hiroshi 84, 85
Okamoto, Yuko 19, 169
Okano, Akihiro 123
Okawa, Hisashi 140, 141
Okazaki, Noriaki 59, 165
Okumura, Ko 24, 25
Okunishi, Misaki 103
Olney, Terry N. 113, 114
Omata, Takahisa 112

Ono, Katsuhiko 144
Orlovich, Valentin 39
Ouchi, Yukio 88, 89, 117, 172
Oura, Masaki 103
Ozawa, Shinji 92, 93
Ozawa, Yoshiki 96, 97
Ozeki, Hiroyuki 30, 31, 32, 163
Pal, Haridas 41, 42
Petek, Hrvoje 48
Pohl, R. 33
Porter, George 46
Proshlyakov, Denis A. 34, 35, 164
Rao, Apparao M. 153
Re, Nazzareno 140
Rábai, Gyula 55, 56, 58, 165
Sadayori, Naoki 101
Saiki, E. 69
Saito, Gunzi 91
Saito, Katsuhiro 144
Saito, Katsushi 144
Saito, Ko 30
Saito, Shuji 29, 30, 31, 32, 163
Saito, Taro 79
Saitow, Ken-ichi 45
Sakai, Yoshiko 26
Sakamoto, Eigo 93
Sakurai, Makoto 111
Sanekata, Masaomi 148
Sanematsu, Kouji 26
Saraoka, Isao 65
Sasai, Masaki 27, 170
Sasaki, Takao 97, 100
Sasano, Tomohiko 83
Sasayama, Masa-aki 97, 98
Sato, Hirohiko 73
Sato, Hiroyasu 63, 64, 65
Sato, Noriko 127
Sato, Shin-ichiro 38
Sato, Yasuhiko 159
Sato, Yukinori 103
Sawabe, Kyoichi 49, 50, 51, 156, 164
Schmid, S. 32
Schmid, W. 32
Sei, Masaki 89, 117, 172
Seki, Kazuhiko 87, 88, 89, 117, 172
Sekiguchi, Tetsuo 55
Sekimoto, Yutaro 31
Shi, Zurong 91
Shibata, Takeshi 170
Shigemasa, Eiji 102, 103
Shimada, Takashi 101
Shimizu, Akiko 72
Shimizu, Yasushi 20, 21
Shinohara, Hisanori 63
Shinzawa-Itoh, Kyoko 34, 35, 37
Shionoiri, Y. 78
Shionoya, Mitsuhiko 124, 125, 168
Shiratani, Eli 27
Shiro, Motoo 124
Shirota, Hideaki 42
Shirotani, Ichimin 74
Shobatake, Kosuke 83, 114
Shudo, Akira 19, 20, 21
Simon, Mark 103
Slobodchikov, Eugene V. 44
Someda, Kiyohiko 22
Sone, Nobuhito 164
Souza, B. De 103
Steimle, Timothy C. 29
Stein, Jugen 21
Struganova, Irina A. 48
Sudo, Yuzo 26
Sugai, I. 32, 33
Suganuma, Akiomi 121
Sugimoto, Hideki 37
Sugimoto, Isamu 118
Sugiura, Chikayuki 144
Sugiura, Sadaki 83
Sugiyama, H. 125
Sugiyama, Masanori 125
Sumi, Tomonari 26
Suzui, Mitsukazu 156, 157
Suzuki, Atsushi 78, 166
Suzuki, Kazuya 154
Suzuki, Masatatsu 37
Suzuki, Noriyuki 130, 131, 133, 168
Suzuki, Tadayoshi 18
Suzuki, Takayoshi 94, 95
Suzuki, Toshinori 60, 61, 62, 170
Suzuki, Toshiyasu 40, 78, 166
Tachi, Kenji 74
Tada, Kazuya 69
Taguwa, Tetsuya 15
Tahara, Tahei 105
Tajima, Yuko 66
Takada, Shoji 22
Takahashi, Hiroaki 89
Takahashi, Takashi 90
Takahashi, Takeshi 40
Takahashi, Tamotsu 130, 131, 132, 133, 168
Takahira, Osamu 65
Takami, Toshiya 143
Takamura, Motoumu 36
Takano, Shiro 171
Takasu, Ryozo 148, 149, 151, 152
Takata, Yasutaka 102, 104
Takayanagi, Masao 51, 53, 55
Takeda, Keiki 74
Takeuchi, Satoshi 105
Takeuchi, Tetsuya 86
Takui, Takeji 66
Tamura, H. 32
Tanaka, Akinori 90
Tanaka, Chizuko 88
Tanaka, E 125
Tanaka, Hideki 100
Tanaka, Hisashi 79
Tanaka, Jiro 88
Tanaka, Kenichiro 114
Tanaka, Koji 127, 128, 129, 130, 168
Tanaka, Motomasa 93
Tanaka, Nobuaki 53, 55
Tanaka, Shin-ichiro 49, 159
Tanaka, Shoji 89, 144, 145, 146, 147, 166
Tang, Jian 30, 31
Taniguchi, Hiromi 73, 74, 172
Tanimoto, Emi 144
Tanimura, Yoshitaka 18, 24, 25, 169
Tanoue, H. 112
Tasaka, Motoyuki 118
Tateishi, Hirotaka 95
Teki, Yoshio 66
Telekhin, M. A. 159
Ten-no, Seiichiro 13
Tinnone, Marcia C. K. 114
Todo, Sakae 74
Tominaga, Keisuke 41, 42, 43, 44, 45, 164, 170
Tomita, Norikazu 18, 25
Tomura, Masaaki 69, 146, 147, 166
Tonokura, Kenichi 60, 61, 62, 170
Torii, H.A. 32, 33
Toriumi, Koshiro 84, 96, 97
Tounge, Brett A. 48
Toyoda, Tomonori 157

Toyohara, Kiyotuna 127, 128, 129
Toyota, Kouichirou 123
Treichel, Paul M. 121
Tsubaki, Motonari 36
Tsuchimoto, Masanobu 121
Tsuda, Ken-ichiro 21
Tsuge, Kiyoshi 128, 168
Tsukada, Naofumi 101
Tsunekawa, Makoto 64
Tsusaka, Yoshiyuki 106, 107, 170
Turci, Cassia C. 103
Tyliszczak, Tolek 103
Ueda, Kiyoshi 103
Ueda, Naoyuki 112, 113
Uehara, Akira 37
Ueno, Nobuo 87, 88
Ueno, Sadaharu 66
Unno, H. 112
Urata, H. 125
Urisu, Tsuneo 106, 107, 108, 156, 170
Uruichi, Mikio 69, 171
Utsuno, Shunji 118, 121
Vanag, Vladimir K. 57, 165
Vasil'ev, A. N. 159
Wada, Senji 167
Wada, Shigetoshi 136
Wada, Yoshiki 84, 85
Watanabe, Hidekazu 13, 14
Watanabe, Katsura 15
Watanabe, Kazuo 50, 51, 164
Watanabe, Michio 171
Watanabe, Yoshihito 92, 93, 94, 167
Weibel, Daniel E. 111
Whitehead, Roger 166
Widmann, E. 32, 33
Williams, K. 153
Williamson, J. M. 14
Wu, Liang Ping 135, 136, 137
Xi, Zhenfeng 130, 131, 132
Yabushita, Satoshi 27
Yagi, Shinya 158
Yagi, Takehiko 74
Yagishita, Akira 102, 103
Yakushi, Kyuya 67, 68, 69, 70, 90, 156, 166, 171
Yamada, Yasunori 126
Yamaguchi, Yoshitaka 122, 123
Yamamoto, K. 78
Yamamoto, Katsuya 123
Yamamoto, Kazunori 40
Yamamoto, Mikiko 135, 136, 137
Yamamoto, Satoshi 29, 31
Yamamoto, Takakazu 88
Yamamoto, Yoshinori 101
Yamasaki, H. 78
Yamasaki, Nobuo 69
Yamasaki, Tomoaki 123
Yamashita, Kazuo 117, 172
Yamashita, Masahiro 84, 85, 86
Yamashita, Yoshiro 68, 69, 89, 144, 145, 146, 147, 166, 171
Yamazaki, Jun-ichiro 158, 171
Yamazaki, T. 32, 33
Yartsev, Arkadiy P. 41
Yasukawa, Masahiro 113
Yokoya, Takayoshi 90
Yonekura, Nobuaki 60, 62, 170
Yoshida, Hiroaki 110
Yoshida, Hisashi 32, 156, 157
Yoshida, Taturu 86
Yoshida, Tomoko 126
Yoshigoe, A. 106, 170
Yoshihara, Keitaro 41, 42, 43, 44, 45, 46, 47, 48, 164, 170
Yoshii, Toshihito 119
Yoshikawa, Kenichi 58
Yoshikawa, Shinya 34, 35, 37
Yoshikawa, Yuzo 118, 119, 120, 121, 167
Yoshimura, Daisuke 88, 117
Yoshino, Katsumi 69
Yuto, Koji 119
Yuzurihara, Junko 126, 127
Zakhidov, Anvar A. 69
Zhan, Chang-Guo 16, 19
Zhou, Shuqin 90
Zhu, Chaoyuan 22, 23, 169
Šeba, Petr 21
Życzkowski, Karol 21

Institute for Molecular Science, Myodaiji, Okazaki 444, Japan